*Reviews in Computational Chemistry, Volume 18*
Edited by Kenny B. Lipkowitz and Donald B. Boyd

ISBN: 0-471-21576-7

# Reviews in Computational Chemistry Volume 18

# Reviews in Computational Chemistry Volume 18

Edited by

**Kenny B. Lipkowitz and Donald B. Boyd**

WILEY-VCH

Kenny B. Lipkowitz
Department of Chemistry
Indiana University–Purdue University
at Indianapolis
402 North Blackford Street
Indianapolis, Indiana 46202–3274,
U.S.A.
lipkowitz@chem.iupui.edu

Donald B. Boyd
Department of Chemistry
Indiana University–Purdue University
at Indianapolis
402 North Blackford Street
Indianapolis, Indiana 46202–3274,
U.S.A.
boyd@chem.iupui.edu



Published by John Wiley & Sons, Inc., Hoboken, New Jersey.
Published simultaneously in Canada.



*Library of Congress Cataloging in Publication Data:*

ISBN 0-471-21576-7
ISSN 1069-3599

Printed in the United States of America

10 9 8 7 6 5 4 3 2 1

# Preface

After our first publisher produced our first volume and we were in the process of readying manuscripts for Volume 2, the publisher's executive editor innocently asked us if there was anything in the field of computational chemistry that we had not already covered in Volume 1. We assured him that there was much. The constancy of change was noted centuries ago when Honorat de Bueil, Marquis de Racan (1589–1670) observed that "Nothing in the world lasts, save eternal change." Science changes too. As stated by Emile Duclaux (1840–1904), French biologist and physician and successor to Louis Pasteur in heading the Pasteur Institute, "It is because science is sure of nothing that it is always advancing." Science is able to contribute to the well-being of mankind because it can evolve. Topics in a number of important areas of computational chemistry are the substance of this volume.

Cheminformatics, a term so new that scientists have not yet come to an agreement on how to spell it, is a facet of computational chemistry where the emphasis is on managing digital data and mining the data to extract knowledge. Cheminformatics holds a position at the intersection of several traditional disciplines including chemical information (library science), quantitative structure-property relationships, and computer science as it pertains to managing computers and databases. One powerful way to extract an understanding of the contents of a data set is with clustering methods, whereby the mutual proximity of data points is measured. Clustering can show how much similarity or diversity there is in a data set. Chapter 1 of this volume is a tutorial on clustering methods. The authors, Drs. Geoff M. Downs and John M. Barnard, were educated at the University of Sheffield—the veritable epicenter and fountainhead of cheminformatics. Each clustering method is described along with its strengths and weaknesses. As frequent consultants to pharmaceutical and chemical companies, the authors can knowledgeably point to published examples where real-world research problems were aided by one or more of the clustering methods.

The previous volume of our series, Volume 17, included a chapter on the use of docking for discovery of pharmaceutically interesting ligands. Employed in structure-based ligand design, docking requires a

three-dimensional structure of the receptor, which can be obtained from experiment or modeling. Docking also requires computational techniques for assessing the affinity of small organic molecules to a receptor. These techniques, collectively called scoring functions, attempt to quantitate the favorability of interaction in the ligand–receptor complex. In Chapter 2 of the present volume, Drs. Hans-Joachim Böhm and Martin Stahl give a tutorial on scoring functions. The authors share their considerable experience using scoring functions in drug discovery research at Roche, Basel. Scoring functions can be derived in different ways; they can be (1) based directly on standard force fields, (2) obtained by empirically fitting parameters in selected force field terms to reproduce a set of known binding affinities, or (3) derived by an inverse formulation of the Boltzmann law whereby the frequency of occurrence of an interatomic interaction is presumed to be related to the strength of that interaction. As with most modern computational methods used in pharmaceutical research, viable scoring functions must be quickly computable so that large numbers of ligand–receptor complexes can be evaluated at a speed comparable to the rate at which compounds can be synthesized by combinatorial chemistry. Despite efforts at numerous laboratories, the "perfect" scoring function, which would be both extremely accurate and broadly applicable, eludes scientists. Sometimes, several scoring functions can be tried on a given set of molecules, and then the computational chemist can look for a consensus in how the individual molecules are ranked by the scores.* A ligand structure having good scores does not guarantee that the compound will have high affinity when and if the compound is actually synthesized and tested. However, a structure with high rankings (i.e., fits the profile) is more likely to show binding than a randomly selected compound. Chapter 2 summarizes what has been learned about scoring functions and gives an example of how they have been applied to find new ligands in databases of real and/or conceivable (virtual) molecular structures stored on computers.

In the 1980s when computers were making molecular simulation calculations more feasible, computational chemists readily recognized that accounting for the polarizability of charge distribution in a molecule would become increasingly important for realistically modeling molecular systems. In most force fields, atomic charges are assigned at the beginning of the calculation and then are held fixed during the course of the minimization or simulation. However, we know that atomic charges vary with the electric field produced by the surrounding atoms. Each atom of a molecular system is in the field of all the other atoms; electrostatic interactions are long range (effective to as much as 14 Å), so a change in the molecular geometry will affect atomic charges,

*Such a consensus approach is reminiscent of what some computational chemists were doing in the the 1970s and 1980s when they were treating each molecule by not one, but several available semiempirical and ab initio molecular orbital methods, each of which gave different—and less than perfect—predictions of molecular properties.

especially if polar functional groups are present. In Chapter 3, Professors Steven W. Rick and Steven J. Stuart scrutinize the methods that have been devised to account for polarization. These methods include point dipole models, shell models, electronegativity equalization models, and semiempirical models. The test systems commonly used for developing and testing these models have been water, proteins, and nucleic acids. This chapter's comparison of computational models gives valuable guidance to users of molecular simulations.

In Chapter 4, Professors Dmitry V. Matyushov and Gregory A. Voth present a rigorous frontier report on the theory and computational methodologies for describing charge-transfer and electron-transfer reactions that can take place in condensed phases. This field of theory and computation aims to describe processes occurring, for instance, in biological systems and materials science. The chapter focuses on analysis of the activation barrier to charge transfer, especially as it relates to optical spectroscopy. Depending on the degeneracy of the energy states of the donor and acceptor, electron tunneling may occur. This chapter provides a step-by-step statistical mechanical development of the theory describing charge-transfer free energy surfaces. The Marcus–Hush mode of electron transfer consisting of two overlapping parabolas can be extended to the more general case of two free energy surfaces. In the last part of the chapter, the statistical mechanical analysis is applied to the calculation of optical profiles of photon absorption and emission, Franck–Condon factors, intensities, matrix elements, and chromophores.

In Chapter 5, Dr. George R. Famini and Professor Leland Y. Wilson teach about linear free energy relationships (LFERs) using molecular descriptors derived from—or adjuncts to—quantum chemical calculations. Basically, the LFER approach is a way of studying quantitative structure-property relationships (QSPRs). The property in question may be a physical one, such as vapor pressure or solvation free energy, or one related to biological activity (QSAR). Descriptors can be any numerical quantity—calculated or experimental—that represents all or part of a molecular structure. In the LFER approach, the number of descriptors used is relatively low compared to some QSPR/QSAR approaches that involve throwing so many descriptors into the regression analysis that the physical significance of any of these is obscured. These latter approaches are somewhat loosely referred to as "kitchen sink" approaches because the investigator has figuratively thrown everything into the equation including objects as odd as the proverbial kitchen sink. In the LFER approach, the descriptors include quantities that measure molecular dimensions (molecular volume, surface area, ovality), charge distributions (atomic charges, electrostatic potentials), electronic properties (ionization potential, polarizability), and thermodynamic properties (heat of formation). Despite use of the term "linear" in LFER, not all correlations encountered in the physical world are linear. QSPR/QSAR approaches based on regression analysis handle this situation by simply squaring—or taking some other power of—the values of

some descriptors and including them as separate independent variables in the regression equation. In this chapter, the authors discuss statistical procedures and give examples covering a wide variety of LFER applications. Quantum chemists can learn from this chapter how their methods may be employed in one of the most rapidly growing areas of computational chemistry, namely, QSAR.

In the nineteenth century, the world powerhouses of chemistry were Britain, France, and Germany. In Germany, Justus Liebig founded a chemistry research laboratory at the University of Giessen in 1825. At the University of Göttingen in 1828, Friedrich Wöhler was the first to synthesize an organic compound (urea) from inorganic material. In Karlsruhe, Friedrich August Kekulé organized the first international meeting on chemistry in 1860. Germany's dominance in the chemical and dye industry was legend well into the twentieth century. In the 1920s, German physicists played central roles in the development of quantum mechanics. Erwin Schrödinger formulated the wave function (1926). Werner Heisenberg formulated matrix mechanics (1925) and the uncertainty principle (1927). The German physicist at Göttingen, Max Born, together with the American, J. Robert Oppenheimer, published their oft-used famous approximation (1927). With such a strong background in chemistry and physics, it is not surprising that Germany was a fertile ground where computational chemistry could take root. The first fully automatic, programmable, digital computer was developed by an engineer in Berlin in 1930 for routine numerical calculations. After Germany was liberated from control of the National Socialist German Workers' Party (''Nazi''), peaceful scientific development could be taken up again, notwithstanding the enormous loss of many leading scientists who had fled from the Nazis. More computers were built, and theoretical chemists were granted access to them. In Chapter 6, Professor Dr. Sigrid D. Peyerimhoff masterfully traces the history of computational chemistry in Germany. This chapter complements the historical accounts covering the United States, Britain, France, and Canada, which were covered in prior volumes of this book series.

Finally, as a bonus with this volume, we editors present a perspective on the employment situation for computational chemists. The essay in the appendix reviews the history of the job market, uncovers factors that have affected it positively or negatively, and discusses the current situation. We also analyze recent job advertisements to see where recent growth has occurred and which skills are presently in greatest demand.

We invite our readers to visit the *Reviews in Computational Chemistry* website at http://chem.iupui.edu/rcc/rcc.html. It includes the author and subject indexes, color graphics, errata, and other materials supplementing the chapters. We are delighted to report that the Google search engine (http://www.google.com/) ranks our website among the top hits in a search on the term ''computational chemistry''. This search engine is becoming popular because it ranks hits in terms of their relevance and frequency of visits. Google

also is very fast and appears to provide a quite complete and up-to-date picture of what information is available on the World Wide Web.

We are also glad to note that our publisher has plans to make our most recent volumes available in an online form through Wiley InterScience. Please check the Web (http://www.interscience.wiley.com/onlinebooks) or contact reference@wiley.com for the latest information. For readers who appreciate the permanence and convenience of bound books, these will, of course, continue.

We thank the authors of this volume for their excellent chapters. Mrs. Joanne Hequembourg Boyd is acknowledged for editorial assistance.

Donald B. Boyd and Kenny B. Lipkowitz
Indianapolis
January 2002

# Epilogue and Dedication

My association with Ken Lipkowitz began a couple of years after he arrived in Indianapolis in 1977. Ken, trained as an synthetic organic chemist, was a new young assistant professor at Indiana University–Purdue University Indianapolis, and I was a research scientist at Eli Lilly & Company, where I, a quantum chemist by training, had been working in the field of computer-aided drug design for nine years. Ken approached me to learn about computational chemistry. I was glad to help him, and he was an enthusiastic "student". Our first paper together was published in 1980. Unsure whether his career as a fledging computational chemist would lead anywhere, he made a distinction in this and other papers he wrote between his organic persona (Kenneth B. Lipkowitz) and his computational persona (Kenny B. Lipkowitz). Over the subsequent years, he focused his career more and more on computational chemistry and established himself as a highly productive and creative scientist. He has always been a hard-working, amiable, and obliging collaborator and friend.

In the late 1980s, Ken had the idea of initiating a book series on computational chemistry. The field was starting to come into full blossom, but few books for it were being published. Whereas review series on other subjects tended to be of mainly archival value and to remain on library shelves, his inspiration for *Reviews in Computational Chemistry* was to include as many tutorial chapters as possible, so that the books would be more used for teaching and individual study. The chapters would be ones that a professor could give new graduate students to bring them up to speed in a particular topic. The chapters would also be substantive, so that the books would not be just a journal with hard covers. As much as possible, the contents of the books would be material that could not be found in any other source. Ken persuaded me to join him in this endeavor.

I have viewed an editor's prime duties to set high standards and to heed the needs of both readers and authors. Hence, every effort has been made to produce volumes of the highest quality. It has been a keen pleasure working with authors who take exceptional pride in their workmanship. The expertise and hard work of many authors have been essential for producing books of

sustained usefulness in learning, teaching, and research. With this volume, the eighteenth, more than 7300 pages have been published since the series began in 1990. More than 200 authors have contributed the chapters. Appreciating the value of these chapters, scientists and libraries around the world have purchased more than 13,000 copies of the books since the series began.

My vision of computational chemistry, as embodied in this book series as well as in the Gordon Conference on Computational Chemistry that I initiated, was that there were synergies to be gained by juxtaposing all the various methodologies available to computational chemists. Thus, computational chemistry is more than quantum chemistry, more than molecular modeling, more than simulations, more than molecular design. Versatility is possible when scientists can draw from their toolbox the most appropriate methodologies for modeling molecules and data. Important goals of this book series have been to nurture the development of the field of computational chemistry, advance its recognition, strengthen its foundations, expand its dimensions, aid practitioners working in the field, and assist newcomers wanting to enter the field.

However, it is now time for me to rest my keyboard-weary hands. I wish Ken and his new co-editors every success as the book series continues. Ken could not have paid me a higher compliment than by enlisting not one, but two, excellent people to carry on the work I did. I have every confidence that as computational chemistry continues to evolve, its spectrum of methods and applications will further expand and increase in brilliance.

## Dedication

With completion of this, my final, volume, I am reminded of my blessings to live in a country conceived by the Founding Fathers of the United States of America. Nothing would have been possible for me without the selflessness and devotion of Howard Milton Boyd, Ph.G., B.S., M.S. Nothing would have been worthwhile without the following:

Andy
Cynthia
Douglas
Drew
Elisabeth
Emma
Joanne
Mary
Richard
Susanne

Donald B. Boyd
Indianapolis
January 2002

# Contents

# Contributors

**John M. Barnard,** Barnard Chemical Information Ltd., 46 Uppergate Road, Stannington, Sheffield S6 6BX, United Kingdom (Electronic mail: barnard@bci.gb.com)

**Hans-Joachim Böhm,** F. Hoffmann-La Roche AG, Pharmaceuticals Division, Chemical Technologies, CH-4070 Basel, Switzerland (Electronic mail: hans-joachim.boehm@roche.com)

**Donald B. Boyd,** Department of Chemistry, Indiana University–Purdue University at Indianapolis (IUPUI), 402 North Blackford Street, Indianapolis, Indiana 46202-3274, U.S.A. (Electronic mail: boyd@chem.iupui.edu)

**Geoff M. Downs,** Barnard Chemical Information Ltd., 46 Uppergate Road, Stannington, Sheffield S6 6BX, United Kingdom (Electronic mail: geoff@bci.gb.com)

**George R. Famini,** RDA International Cooperative Programs Division, United States Army Soldier and Biological Chemical Command, 5183 Blackhawk Road, Aberdeen Proving Ground, Maryland 21010-5424, U.S.A. (Electronic mail: george.famini@sbccom.apgea.army.mil)

**Kenny B. Lipkowitz,** Department of Chemistry, Indiana University–Purdue University at Indianapolis (IUPUI), 402 North Blackford Street, Indianapolis, Indiana 46202-3274, U.S.A. (Electronic mail: lipkowitz@chem.iupui.edu)

**Dmitry V. Matyushov,** Department of Chemistry and Biochemistry, Arizona State University, P. O. Box 871604, Tempe, Arizona 85287-1604, U.S.A. (Electronic mail: dmitrym@asu.edu)

**Sigrid D. Peyerimhoff,** Institut für Physikalische und Theoretische Chemie, Universität Bonn, Wegelerstrasse 12, D-53115 Bonn, Germany (Electronic mail: unt000@uni-bonn.de)

**Steven W. Rick,** Department of Chemistry, University of New Orleans, New Orleans, Louisiana 70148, U.S.A. (Electronic mail: srick@uno.edu)

**Martin Stahl,** F. Hoffmann-La Roche AG, Pharmaceuticals Division, Chemical Technologies, CH-4070 Basel, Switzerland (Electronic mail: martin.stahl@roche.com)

**Steven J. Stuart,** Department of Chemistry, Hunter Laboratory, Clemson University, Clemson, South Carolina 29634-0973, U.S.A. (Electronic mail: ss@clemson.edu )

**Gregory A. Voth,** Department of Chemistry and Henry Eyring Center for Theoretical Chemistry, University of Utah, 315 South 1400 East, Salt Lake City, Utah 84112-0850, U.S.A. (Electronic mail: voth@chemistry.utah.edu)

**Leland Y. Wilson,** Department of Chemistry and Biochemistry, La Sierra University, Riverside, California 92515, U.S.A. (Electronic mail: hlwilson@urs2.net)

# Contributors to Previous Volumes*

## Volume 1 (1990)

**David Feller** and **Ernest R. Davidson,**[†] Basis Sets for Ab Initio Molecular Orbital Calculations and Intermolecular Interactions.

**James J. P. Stewart,**[‡] Semiempirical Molecular Orbital Methods.

**Clifford E. Dykstra,**[¶] **Joseph D. Augspurger, Bernard Kirtman,** and **David J. Malik,** Properties of Molecules by Direct Calculation.

**Ernest L. Plummer,** The Application of Quantitative Design Strategies in Pesticide Design.

**Peter C. Jurs,** Chemometrics and Multivariate Analysis in Analytical Chemistry.

**Yvonne C. Martin, Mark G. Bures,** and **Peter Willett,** Searching Databases of Three-Dimensional Structures.

**Paul G. Mezey,** Molecular Surfaces.

**Terry P. Lybrand,**[§] Computer Simulation of Biomolecular Systems Using Molecular Dynamics and Free Energy Perturbation Methods.

**Donald B. Boyd,** Aspects of Molecular Modeling.

---

*Where appropriate and available, the current affiliation of the senior or corresponding author is given here as a convenience to our readers.

[†]Current address: Department of Chemistry, University of Washington, Seattle, Washington 98195.

[‡]Current address: 15210 Paddington Circle, Colorado Springs, Colorado 80921-2512 (Electronic mail: jstewart@fai.com).

[¶]Current address: Department of Chemistry, Indiana University–Purdue University at Inidanapolis, Indianapolis, Indiana 46202 (Electronic mail: dykstra@chem.iupui.edu).

[§]Current address: Department of Chemistry, Vanderbilt University, Nashville, Tennessee 37212 (Electronic mail: lybrand@structbio.vanderbilt.edu).

**Donald B. Boyd,** Successes of Computer-Assisted Molecular Design.

**Ernest R. Davidson,** Perspectives on Ab Initio Calculations.

## Volume 2 (1991)

**Andrew R. Leach,*** A Survey of Methods for Searching the Conformational Space of Small and Medium-Sized Molecules.

**John M. Troyer** and **Fred E. Cohen,** Simplified Models for Understanding and Predicting Protein Structure.

**J. Phillip Bowen** and **Norman L. Allinger,** Molecular Mechanics: The Art and Science of Parameterization.

**Uri Dinur** and **Arnold T. Hagler,** New Approaches to Empirical Force Fields.

**Steve Scheiner,**† Calculating the Properties of Hydrogen Bonds by Ab Initio Methods.

**Donald E. Williams,** Net Atomic Charge and Multipole Models for the Ab Initio Molecular Electric Potential.

**Peter Politzer** and **Jane S. Murray,** Molecular Electrostatic Potentials and Chemical Reactivity.

**Michael C. Zerner,** Semiempirical Molecular Orbital Methods.

**Lowell H. Hall** and **Lemont B. Kier,** The Molecular Connectivity Chi Indexes and Kappa Shape Indexes in Structure–Property Modeling.

**I. B. Bersuker**‡ and **A. S. Dimoglo,** The Electron-Topological Approach to the QSAR Problem.

**Donald B. Boyd,** The Computational Chemistry Literature.

---

*Current address: GlaxoSmithKline, Greenford, Middlesex, UB6 0HE, U.K. (Electronic mail: arl22958@ggr.co.uk).

†Current address: Department of Chemistry and Biochemistry, Utah State University, Logan, Utah 84322 (Electronic mail: scheiner@cc.usu.edu).

‡Current address: College of Pharmacy, The University of Texas, Austin, Texas 78712 (Electronic mail: bersuker@eeyore.cm.utexas.edu).

## Volume 3 (1992)

**Tamar Schlick,** Optimization Methods in Computational Chemistry.

**Harold A. Scheraga,** Predicting Three-Dimensional Structures of Oligopeptides.

**Andrew E. Torda** and **Wilfred F. van Gunsteren,** Molecular Modeling Using NMR Data.

**David F. V. Lewis,** Computer-Assisted Methods in the Evaluation of Chemical Toxicity.

## Volume 4 (1993)

**Jerzy Cioslowski,** Ab Initio Calculations on Large Molecules: Methodology and Applications.

**Michael L. McKee** and **Michael Page,** Computing Reaction Pathways on Molecular Potential Energy Surfaces.

**Robert M. Whitnell** and **Kent R. Wilson,** Computational Molecular Dynamics of Chemical Reactions in Solution.

**Roger L. DeKock, Jeffry D. Madura, Frank Rioux,** and **Joseph Casanova,** Computational Chemistry in the Undergraduate Curriculum.

## Volume 5 (1994)

**John D. Bolcer** and **Robert B. Hermann,** The Development of Computational Chemistry in the United States.

**Rodney J. Bartlett** and **John F. Stanton,** Applications of Post-Hartree–Fock Methods: A Tutorial.

**Steven M. Bachrach,*** Population Analysis and Electron Densities from Quantum Mechanics.

---

*Current address: Department of Chemistry, Trinity University, San Antonio, Texas 78212 (Electronic mail: steven.bachrach@trinity.edu).

**Jeffry D. Madura,*** **Malcolm E. Davis, Michael K. Gilson, Rebecca C. Wade, Brock A. Luty,** and **J. Andrew McCammon,** Biological Applications of Electrostatic Calculations and Brownian Dynamics Simulations.

**K. V. Damodaran** and **Kenneth M. Merz Jr.,** Computer Simulation of Lipid Systems.

**Jeffrey M. Blaney**† and **J. Scott Dixon,** Distance Geometry in Molecular Modeling.

**Lisa M. Balbes, S. Wayne Mascarella,** and **Donald B. Boyd,** A Perspective of Modern Methods in Computer-Aided Drug Design.

## Volume 6 (1995)

**Christopher J. Cramer** and **Donald G. Truhlar,** Continuum Solvation Models: Classical and Quantum Mechanical Implementations.

**Clark R. Landis, Daniel M. Root,** and **Thomas Cleveland,** Molecular Mechanics Force Fields for Modeling Inorganic and Organometallic Compounds.

**Vassilios Galiatsatos,** Computational Methods for Modeling Polymers: An Introduction.

**Rick A. Kendall,**‡ **Robert J. Harrison, Rik J. Littlefield,** and **Martyn F. Guest,** High Performance Computing in Computational Chemistry: Methods and Machines.

**Donald B. Boyd,** Molecular Modeling Software in Use: Publication Trends.

**Eiji Ōsawa** and **Kenny B. Lipkowitz,** Appendix: Published Force Field Parameters.

---

*Current address: Department of Chemistry and Biochemistry, Duquesne University, Pittsburgh, Pennsylvania 15282-1530 (Electronic mail: madura@duq.edu).

†Current address: Structural GenomiX, 10505 Roselle St., San Diego, California 92120 (Electronic mail: jeff_blaney@stromix.com).

‡Current address: Scalable Computing Laboratory, Ames Laboratory, Wilhelm Hall, Ames, Iowa 50011 (Electronic mail: rickyk@scl.ameslab.gov).

## Volume 7 (1996)

**Geoffrey M. Downs** and **Peter Willett,** Similarity Searching in Databases of Chemical Structures.

**Andrew C. Good*** and **Jonathan S. Mason,** Three-Dimensional Structure Database Searches.

**Jiali Gao,**† Methods and Applications of Combined Quantum Mechanical and Molecular Mechanical Potentials.

**Libero J. Bartolotti** and **Ken Flurchick,** An Introduction to Density Functional Theory.

**Alain St-Amant,** Density Functional Methods in Biomolecular Modeling.

**Danya Yang** and **Arvi Rauk,** The A Priori Calculation of Vibrational Circular Dichroism Intensities.

**Donald B. Boyd,** Appendix: Compendium of Software for Molecular Modeling.

## Volume 8 (1996)

**Zdenek Slanina,**‡ **Shyi-Long Lee,** and **Chin-hui Yu,** Computations in Treating Fullerenes and Carbon Aggregates.

**Gernot Frenking, Iris Antes, Marlis Böhme, Stefan Dapprich, Andreas W. Ehlers, Volker Jonas, Arndt Neuhaus, Michael Otto, Ralf Stegmann, Achim Veldkamp,** and **Sergei F. Vyboishchikov,** Pseudopotential Calculations of Transition Metal Compounds: Scope and Limitations.

**Thomas R. Cundari, Michael T. Benson, M. Leigh Lutz,** and **Shaun O. Sommerer,** Effective Core Potential Approaches to the Chemistry of the Heavier Elements.

---

*Current address: Bristol-Myers Squibb, 5 Research Parkway, P.O. Box 5100, Wallingford, Connecticut 06492-7660 (Electronic mail: andrew.good@bms.com).

†Current address: Depertment Chemistry, University of Minnesota, 207 Pleasant St. SE, Minneapolis, Minnesota 55455-0431 (Electronic mail: gao@chem.umn.edu).

‡Current address: Institute of Chemistry, Academia Sinica, Nankang, Taipei 11529, Taiwan, Republic of China (Electronic mail: zdenek@chem.sinica.edu.tw).

**Jan Almlöf** and **Odd Gropen,*** Relativistic Effects in Chemistry.

**Donald B. Chesnut,** The Ab Initio Computation of Nuclear Magnetic Resonance Chemical Shielding.

## Volume 9 (1996)

**James R. Damewood Jr.,** Peptide Mimetic Design with the Aid of Computational Chemistry.

**T. P. Straatsma,** Free Energy by Molecular Simulation.

**Robert J. Woods,** The Application of Molecular Modeling Techniques to the Determination of Oligosaccharide Solution Conformations.

**Ingrid Pettersson** and **Tommy Liljefors,** Molecular Mechanics Calculated Conformational Energies of Organic Molecules: A Comparison of Force Fields.

**Gustavo A. Arteca,** Molecular Shape Descriptors.

## Volume 10 (1997)

**Richard Judson,**† Genetic Algorithms and Their Use in Chemistry.

**Eric C. Martin, David C. Spellmeyer, Roger E. Critchlow Jr.,** and **Jeffrey M. Blaney,** Does Combinatorial Chemistry Obviate Computer-Aided Drug Design?

**Robert Q. Topper,** Visualizing Molecular Phase Space: Nonstatistical Effects in Reaction Dynamics.

**Raima Larter** and **Kenneth Showalter,** Computational Studies in Nonlinear Dynamics.

**Stephen J. Smith** and **Brian T. Sutcliffe,** The Development of Computational Chemistry in the United Kingdom.

---

*Address: Institute of Mathematical and Physical Sciences, University of Tromsø, N-9037 Tromsø, Norway (Electronic mail: oddg@chem.uit.no).

†Current address: Genaissance Pharmaceuticals, Five Science Park, New Haven, Connecticut 06511 (Electronic mail: r.judson@genaissance.com).

## Volume 11 (1997)

**Mark A. Murcko,** Recent Advances in Ligand Design Methods.

**David E. Clark,*** **Christopher W. Murray,** and **Jin Li,** Current Issues in De Novo Molecular Design.

**Tudor I. Oprea**† and **Chris L. Waller,** Theoretical and Practical Aspects of Three-Dimensional Quantitative Structure–Activity Relationships.

**Giovanni Greco, Ettore Novellino,** and **Yvonne Connolly Martin,** Approaches to Three-Dimensional Quantitative Structure–Activity Relationships.

**Pierre-Alain Carrupt, Bernard Testa,** and **Patrick Gaillard,** Computational Approaches to Lipophilicity: Methods and Applications.

**Ganesan Ravishanker, Pascal Auffinger, David R. Langley, Bhyravabhotla Jayaram, Matthew A. Young,** and **David L. Beveridge,** Treatment of Counterions in Computer Simulations of DNA.

**Donald B. Boyd,** Appendix: Compendium of Software and Internet Tools for Computational Chemistry.

## Volume 12 (1998)

**Hagai Meirovitch,**‡ Calculation of the Free Energy and the Entropy of Macromolecular Systems by Computer Simulation.

**Ramzi Kutteh** and **T. P. Straatsma,** Molecular Dynamics with General Holonomic Constraints and Application to Internal Coordinate Constraints.

**John C. Shelley**¶ and **Daniel R. Bérard,** Computer Simulation of Water Physisorption at Metal–Water Interfaces.

---

*Current address: Computer-Aided Drug Design, Argenta Discovery Ltd., 8/9 Spire Green Centre, Flex Meadow, Harlow, Essex, CM19 5TR, United Kingdom (Electronic mail: david.clark@argentadiscovery.com).

†Current address: Office of Biocomputing, University of New Mexico School of Medicine, 915 Camino de Salud NE, Albuquerque, New Mexico 87131 (Electronic mail: toprea@salud.unm.edu).

‡Current address: Department of Molecular Genetics & Biochemistry, School of Medicine, University of Pittsburgh, Pittsburgh, Pennsylvania 15213 (Electronic mail: hagaim@pitt.edu).

¶Current address: Schrödinger, Inc., 1500 S.W. First Avenue, Suite 1180, Portland, Oregon 97201 (Electronic mail: jshelley@schrodinger.com).

**Donald W. Brenner, Olga A. Shenderova,** and **Denis A. Areshkin,** Quantum-Based Analytic Interatomic Forces and Materials Simulation.

**Henry A. Kurtz** and **Douglas S. Dudis,** Quantum Mechanical Methods for Predicting Nonlinear Optical Properties.

**Chung F. Wong,*** **Tom Thacher,** and **Herschel Rabitz,** Sensitivity Analysis in Biomolecular Simulation.

**Paul Verwer** and **Frank J. J. Leusen,** Computer Simulation to Predict Possible Crystal Polymorphs.

**Jean-Louis Rivail** and **Bernard Maigret,** Computational Chemistry in France: A Historical Survey.

## Volume 13 (1999)

**Thomas Bally** and **Weston Thatcher Borden,** Calculations on Open-Shell Molecules: A Beginner's Guide.

**Neil R. Kestner** and **Jaime E. Combariza,** Basis Set Superposition Errors: Theory and Practice.

**James B. Anderson,** Quantum Monte Carlo: Atoms, Molecules, Clusters, Liquids, and Solids.

**Anders Wallqvist**† and **Raymond D. Mountain,** Molecular Models of Water: Derivation and Description.

**James M. Briggs** and **Jan Antosiewicz,** Simulation of pH-dependent Properties of Proteins Using Mesoscopic Models.

**Harold E. Helson,** Structure Diagram Generation.

## Volume 14 (2000)

**Michelle Miller Francl** and **Lisa Emily Chirlian,** The Pluses and Minuses of Mapping Atomic Charges to Electrostatic Potentials.

---

*Current addrress: Howard Hughes Medical Institute, School of Medicine, University of California at San Diego, 9500 Gilman Drive, La Jolla, California 92093-0365 (Electronic mail: c4wong@ucsd.edu).

†Current address: National Cancer Institute, P.O. Box B, Frederick, Maryland 21702 (Electronic mail: wallqvist@ncifcrt.gov).

**T. Daniel Crawford*** and **Henry F. Schaefer III,** An Introduction to Coupled Cluster Theory for Computational Chemists.

**Bastiaan van de Graaf, Swie Lan Njo,** and **Konstantin S. Smirnov,** Introduction to Zeolite Modeling.

**Sarah L. Price,** Toward More Accurate Model Intermolecular Potentials for Organic Molecules.

**Christopher J. Mundy,†** **Sundaram Balasubramanian, Ken Bagchi, Mark E. Tuckerman, Glenn J. Martyna,** and **Michael L. Klein,** Nonequilibrium Molecular Dynamics.

**Donald B. Boyd** and **Kenny B. Lipkowitz,** History of the Gordon Research Conferences on Computational Chemistry.

**Mehran Jalaie** and **Kenny B. Lipkowitz,** Appendix: Published Force Field Parameters for Molecular Mechanics, Molecular Dynamics, and Monte Carlo Simulations.

## Volume 15 (2000)

**F. Matthias Bickelhaupt** and **Evert Jan Baerends,** Kohn–Sham Density Functional Theory: Predicting and Understanding Chemistry.

**Michael A. Robb, Marco Garavelli, Massimo Olivucci,** and **Fernando Bernardi,** A Computational Strategy for Organic Photochemistry.

**Larry A. Curtiss, Paul C. Redfern,** and **David J. Frurip,** Theoretical Methods for Computing Enthalpies of Formation of Gaseous Compounds.

**Russell J. Boyd,** The Development of Computational Chemistry in Canada.

## Volume 16 (2000)

**Richard A. Lewis, Stephen D. Pickett,** and **David E. Clark,** Computer-Aided Molecular Diversity Analysis and Combinatorial Library Design.

---

*Current address: Department of Chemistry, Virginia Polytechnic Institute and State University, Blacksburg, Virginia 24061-0212 (Electronic mail: crawdad@vt.edu).

†Current address: Computational Materials Science, L-371, Lawrence Livermore National Laboratory, Livermore, California 94550 (Electronic mail: mundy2@llnl.gov).

**Keith L. Peterson,** Artificial Neural Networks and Their Use in Chemistry.

**Jörg-Rüdiger Hill, Clive M. Freeman,** and **Lalitha Subramanian,** Use of Force Fields in Materials Modeling.

**M. Rami Reddy, Mark D. Erion,** and **Atul Agarwal,** Free Energy Calculations: Use and Limitations in Predicting Ligand Binding Affinities.

## Volume 17 (2001)

**Ingo Muegge** and **Matthias Rarey,** Small Molecule Docking and Scoring.

**Lutz P. Ehrlich** and **Rebecca C. Wade,** Protein–Protein Docking.

**Christel M. Marian,** Spin-Orbit Coupling in Molecules.

**Lemont B. Kier, Chao-Kun Cheng,** and **Paul G. Seybold,** Cellular Automata Models of Aqueous Solution Systems.

**Kenny B. Lipkowitz** and **Donald B. Boyd,** Appendix: Books Published on the Topics of Computational Chemistry.

# Topics Covered in Volumes 1–18*



*This brief index lists topics and volume numbers.

# Reviews in Computational Chemistry Volume 18

*Reviews in Computational Chemistry, Volume 18*
Edited by Kenny B. Lipkowitz and Donald B. Boyd

ISBN: 0-471-21576-7

CHAPTER 1

# Clustering Methods and Their Uses in Computational Chemistry

**Geoff M. Downs and John M. Barnard**

*Barnard Chemical Information Ltd., 46 Uppergate Road, Stannington, Sheffield S6 6BX, United Kingdom*

## INTRODUCTION

Clustering is a data analysis technique that, when applied to a set of heterogeneous items, identifies homogeneous subgroups as defined by a given model or measure of similarity. Of the many uses of clustering, a prime motivation for the increasing interest in clustering methods is their use in the selection and design of combinatorial libraries of chemical structures pertinent to pharmaceutical discovery.

One feature of clustering is that the process is unsupervised, that is, there is no predefined grouping that the clustering seeks to reproduce. In contrast to supervised learning, where the task is to establish relationships between given inputs and outputs to enable prediction of the output from new inputs, in unsupervised learning only the inputs are available and the task is to reveal aspects of the underlying distribution of the input data. Clustering is thus complemented by the related supervised process of classification, in which items are assigned labels applied to predefined groups: examples include recursive partitioning, naïve Bayesian analysis, and K nearest-neighbor selection. Clustering is a technique for exploratory data analysis and is used increasingly in preliminary analyses of large data sets of medium and high dimensionality as a method of selection, diversity analysis, and data reduction. This chapter reviews the main clustering methods that are used for analyzing chemical

data sets and gives examples of their application in pharmaceutical companies. Compared to the other costs of drug discovery, clustering can add significant value at minimal cost. First, we provide an outline of clustering as a discipline and define some of the terminology. Then, we give a brief tutorial on clustering algorithms, review progress in developing the methods, and offer some example applications.

Clustering methodology has been developed and used in a variety of areas including archaeology, astronomy, biology, computer science, electronics, engineering, information science, and medicine. Good, general introductory texts on the topic of clustering include those by Sneath and Sokal,[1] Kaufmann and Rousseeuw,[2] Everitt,[3] and Gordon.[4] The main text that is devoted to clustering of chemical data sets is by Willett,[5] with review articles by Bratchell,[6] Barnard and Downs,[7] and Downs and Willett.[8] The present chapter is a complement and update to the latter article. In a previous volume of this series, Lewis, Pickett, and Clark[9] reviewed the use of diversity analysis techniques in combinatorial library design.

As will be shown in the section on Chemical Applications, the current main uses of clustering for chemical data sets are to find representative subsets from high throughput screening (HTS) and combinatorial chemistry, and to increase the diversity of in-house data sets through selection of additional compounds from other data sets. Methods suitable for compound selection are the main focus of this chapter. The methods must be able to handle large data sets of high-dimensional data. For small, low-dimensional data sets, most clustering methods are applicable, and descriptions in the standard texts and implementations available in standard statistical software packages[10,11] suffice. Implementations designed for use on chemical data sets are available from most of the specialist software vendors,[12–17] the majority of which were reviewed by Warr.[18]

The overall process of clustering involves the following steps:

1. Generate appropriate descriptors for each compound in the data set.
2. Select an appropriate similarity measure.
3. Use an appropriate clustering method to cluster the data set.
4. Analyze the results.

This chapter focuses on step 3. For step 1, descriptors may include property values, biological properties, topological indexes, and structural fragments. The performance of these descriptors and forms of representation have been analyzed by Brown[19] and Brown and Martin.[20,21] Similarity searching for step 2 has been discussed by Downs and Willett;[22] characteristics of various similarity measures have been discussed by Barnard, Downs, and Willett.[23,24] For step 4, little has been published specifically about visualization and analysis of results for chemical data sets. However, most publications that focus on implementing systems that utilize clustering do provide details of how the results were displayed or analyzed.

The terminology associated with clustering is extensive, with many terms used to describe the same thing (reflecting the separate development of clustering methods within a multitude of disciplines). Clusters can be *overlapping* or *nonoverlapping*; if a compound occurs in more than one cluster, the clusters are overlapping. At one extreme, each compound is a member of all clusters to a certain degree. An example of this is *fuzzy* clustering in which the degree of membership of an individual compound is in the range 0 to 1, and the total membership summed across all clusters is normally required to be 1. This scheme contrasts with *crisp* clustering in which each compound's degree of membership in any cluster is either 0 or 1. At the other extreme, is the situation wherein each compound is a member of exactly one cluster, in which case the clusters are said to be nonoverlapping. Intermediate situations sometimes occur, where compounds can be members of several, though not of all, clusters. The majority of clustering methods used on chemical data sets generate crisp, nonoverlapping clusters, because analysis of such clusters is relatively simple.

If a data set is analyzed in an iterative way, such that at each step a pair of clusters is merged or a single cluster is divided, the result is *hierarchical*, with a parent–child relationship being established between clusters at each successive level of the iteration. The successive levels can be visualized using a dendrogram, as shown in Figure 1. Each level of the hierarchy represents a partitioning of the data set into a set of clusters. In contrast, if the data set is analyzed to produce a single partition of the compounds resulting in a set of clusters, the result is then *nonhierarchical*. Note that the term *partitioning*

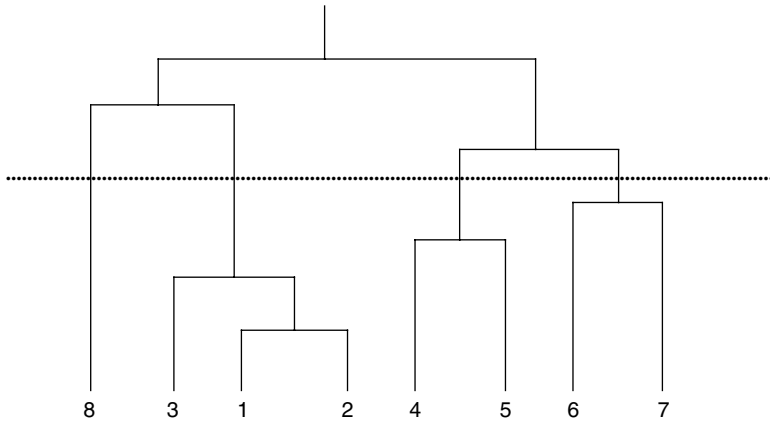


**Figure 1** An example of a hierarchy (dendrogram) generated from the clustering of eight items (shown numbered 1–8 across the bottom). The top (root) is a single cluster containing all eight items. The vertical positions of the horizontal lines joining pairs of items or cluster indicate the relative similarities of those pairs. Items 1 and 2 are the most similar and clusters [8,3,1,2] and [4,5,6,7] are the least similar. The dotted horizontal line represents a single partition containing the four clusters [8], [3,1,2], [4,5], and [6,7].

in this context is different from the technique of partitioning (otherwise known as cell-based partitioning). The latter technique is a method of classification rather than of clustering, and a useful review of it, as applied to chemical data sets, is given by Mason and Pickett.[25] A broad classification of the most common clustering methods is shown in Figure 2. Note that, with the wide range of clustering methods devised, some can be placed in more than one of the given categories.

If a hierarchical method starts with all compounds as *singletons* (in clusters by themselves) and the latter are merged iteratively until all compounds are in a single cluster, the method is said to be *agglomerative*. With respect to the dendrogram in Figure 1, it is a bottom-up approach. If the hierarchical method starts with all compounds in a single cluster and iteratively splits one cluster into two until all compounds are singletons, the method is *divisive*, that

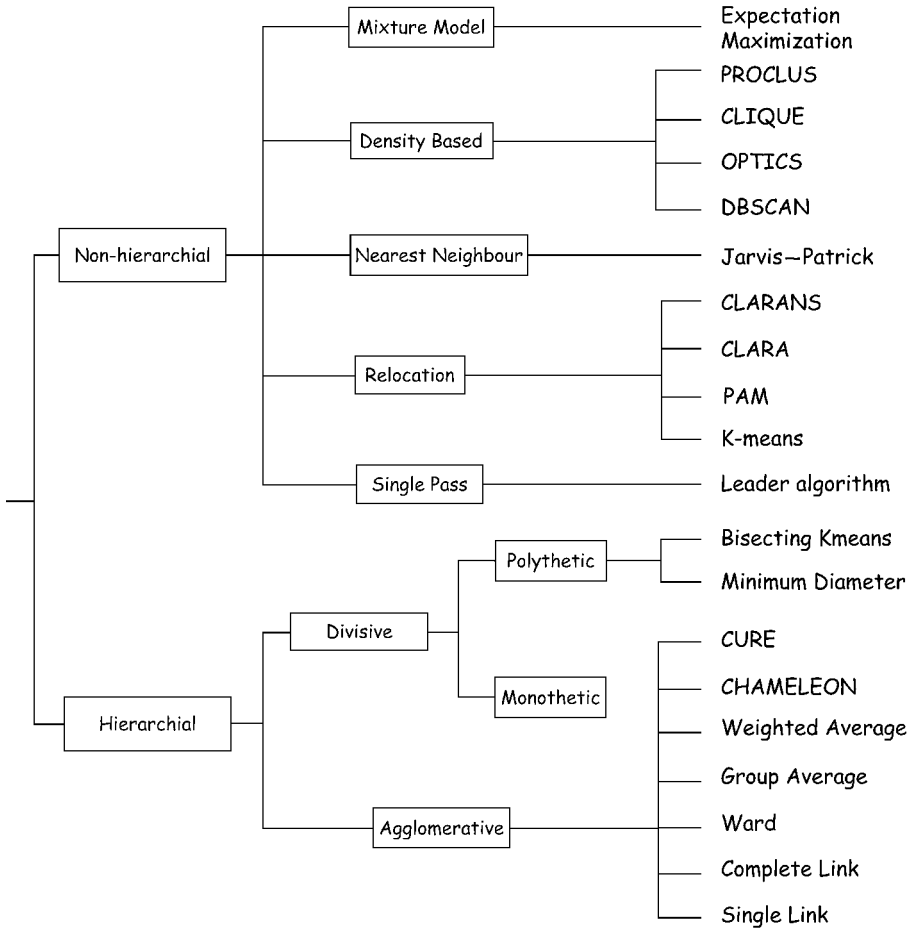


**Figure 2** A broad classification of the most common clustering methods.

is, it is a top-down approach. If, at each split, only one descriptor is used to determine how the cluster is split, the method is *monothetic*; otherwise, more descriptors (typically all available) are used, and the method is *polythetic*.

Nonhierarchical methods encompass a wide range of different techniques to build clusters. A *single-pass* method is one in which the partition is created by a single pass through the data set or, if randomly accessed, in which each compound is examined only once to decide which cluster it should be assigned to. A *relocation* method is one in which compounds are moved from one cluster to another to try to improve on the initial estimation of the clusters. The relocating is typically accomplished based on improving a cost function describing the "goodness" of each resultant cluster. The *nearest-neighbor* approach is more compound centered than are the other nonhierarchical methods. In it, the environment around each compound is examined in terms of its most similar neighboring compounds, with commonality between nearest neighbors being used as a criterion for cluster formation. In *mixture model* clustering the data are assumed to exist as a mixture of densities that are usually assumed to be Gaussian (normal) distributions, since their densities are not known in advance. Solutions to the mixture model are derived iteratively in a manner similar to the relocation methods. *Topographic* methods, such as use of Kohonen maps, typically apply a variable cost function with the added restriction that topographic relationships are preserved so that neighboring clusters are close in descriptor space. Other nonhierarchical methods include *density-based* and *probabilistic* methods. Density-based, or mode-seeking, methods regard the distribution of descriptors across the data set as generating patterns of high and low density that, when identified, can be used to separate the compounds into clusters. Probabilistic clustering generates nonoverlapping clusters in which a compound is assigned a probability, in the range 0 to 1, that it belongs to the chosen cluster (in contrast to fuzzy clustering in which the clusters are overlapping and the degree of membership is not a probability).

Having now provided a broad overview of clustering methodology, we next focus on the "classical" methods, which include hierarchical and single-pass, relocation, and nearest-neighbor nonhierarchical techniques. The classification we have described in Figure 2 is one that is commonly used by many scientists; however, it is just one of many possible classifications. Another way to differentiate between clustering techniques is to consider *parametric* and *nonparametric* methods. Parametric methods require distance-based comparisons be made. Here access to the descriptors is required (typically given as Euclidean vectors), rather than just a proximity matrix derived from the descriptors. Parametric methods can be further organized into *generative* and *reconstructive* methods. Generative methods, including mixture model, density-based, and probabilistic techniques, try to match parameters (e.g., cluster centers, variances within and between clusters, and mixing coefficients for the descriptor distributions) to the distribution of descriptors within the data set. Reconstructive methods, such as relocation and topographic, are

based upon improving a given cost function. Nonparametric methods make fewer assumptions about the underlying data; they do not adapt given parameters iteratively and, in general, need only a matrix of pairwise proximities (i.e., a distance matrix).

The term proximity is used here to include similarity and dissimilarity coefficients in addition to distance measures. Individual proximity measures are not defined in this review; full definitions can be found in standard texts and in the articles by Barnard, Downs, and Willett.[23,24] We now define the terms *centroid* and *square-error*, because they will be used throughout this chapter. For a cluster of $s$ compounds each represented by a vector, let $\mathbf{x}(r)$ be the $r$th vector. The vector of the cluster centroid, $\mathbf{x}(c)$, is then defined as

$$\mathbf{x}(c) = \left(\frac{1}{s}\right) \sum_{r=1}^{s} \mathbf{x}(r) \qquad [1]$$

Note that the centroid is the simple arithmetic mean of the vectors of the cluster members, and this mean is frequently used to represent the cluster as a whole. In situations where a mean is not applicable or appropriate, the median can be used to define the cluster *medoid* (see Kaufman and Rousseeuw[2] for details). The square-error (also called the *within-cluster variance*), $e^2$, for a cluster is the sum of squared Euclidean distances to the centroid or medoid for all $s$ items in that cluster:

$$e^2 = \sum_{r=1}^{s} [\mathbf{x}(r) - \mathbf{x}(c)]^2 \qquad [2]$$

The square-error across all $K$ clusters in a partition is the sum of the square-errors for each of the $K$ clusters. (Note also that the standard deviation would be the square root of the square-error.)

## CLUSTERING ALGORITHMS

This chapter concentrates on the "classical" clustering methods, because they are the methods that have been applied most often in the chemical community. Standard reference works devoted to clustering algorithms include those by Hartigan,[26] Murtagh,[27] and Jain and Dubes.[28]

### Hierarchical Methods

#### *Hierarchical Agglomerative*

The most commonly implemented hierarchical clustering methods are those belonging to the family of *sequential agglomerative hierarchical non-overlapping* (SAHN) methods. These are traditionally implemented using

what is known as the *stored-matrix* algorithm, so named because the starting point is a matrix of all pairwise proximities between items in the data set to be clustered. Each cluster initially corresponds to an individual item (singleton). As clustering proceeds, each cluster may contain one or more items. Eventually, there evolves one cluster that contains all items. At each iteration, a pair of clusters is merged (agglomerated) and the number of clusters decreases by 1. The stored-matrix algorithm proceeds as follows:

1. Calculate the initial proximity matrix containing the pairwise proximities between all pairs of clusters (singletons) in the data set.
2. Scan the matrix to find the most similar pair of clusters, and merge them into a new cluster (thus replacing the original pair).
3. Update the proximity matrix by inactivating one set of entries of the original pair and updating the other set (now representing the new cluster) with the proximities between the new cluster and all other clusters.
4. Repeat steps 2 and 3 until just one cluster remains.

The various SAHN methods differ in the way in which the proximity between clusters is defined in step 1 and how the merged pair is represented as a single cluster in step 3. The proximity calculation in step 3 typically uses the Lance–Williams matrix-update formula:[29]

$$\mathrm{d}[k,(i,j)] = \alpha_{\mathrm{i}}\,\mathrm{d}[k,i] + \alpha_{\mathrm{j}}\,\mathrm{d}[k,j] + \beta\,\mathrm{d}[i,j] + \gamma\left|\mathrm{d}[k,i] - \mathrm{d}[k,j]\right| \qquad [3]$$

where $\mathrm{d}[k,(i,j)]$ is the proximity between cluster $k$ and the cluster $(i, j)$ formed from merging clusters $i$ and $j$. Different values for $\alpha_{\mathrm{i}}$, $\alpha_{\mathrm{j}}$, $\beta$, and $\gamma$ define various SAHN methods, some of which are shown in Table 1 and described below.

In *single-link* clustering, the proximity between two clusters is the minimum distance between any pair of items (one from each cluster), that is, the closest pair of points between each cluster. In contrast, in *complete-link* clustering, the proximity between two clusters is the maximum distance between any pair of items, that is, the farthest pair of points between each cluster. Single-link and complete-link represent the extremes of SAHN clustering. In

**Table 1** Parameter Values for Some Common SAHN Methods Defined by the Lance–Williams Matrix Update Formula[a]

| SAHN Method | $\alpha_i$ | $\alpha_j$ | $\beta$ | $\gamma$ |
|---|---|---|---|---|
| Single-link | 0.5 | 0.5 | 0 | −0.5 |
| Complete-link | 0.5 | 0.5 | 0 | 0.5 |
| Group-average | $\frac{N_i}{N_i+N_j}$ | $\frac{N_j}{N_i+N_j}$ | $\frac{-N_i \times N_j}{(N_i+N_j)^2}$ | 0 |
| Ward | $\frac{N_i+N_k}{N_i+N_j+N_k}$ | $\frac{N_j+N_k}{N_i+N_j+N_k}$ | $\frac{-N_k}{N_i+N_j+N_k}$ | 0 |

[a] The parameters $N_i$, $N_j$, and $N_k$ = number of compounds in clusters $i$, $j$, and $k$, respectively.

the middle is *average-link* clustering in which the proximity between two clusters is the arithmetic average of distances between all pairs of items. Also in the middle is *Ward's* method[30] in which the proximity is the variance between the clusters (where variance is defined as the sum of square-errors of the clusters; see Eq. [2]). At each iteration, the pair of clusters chosen is that whose merger produces the minimum change in square-error (or within-cluster variance; hence the method is also known as the *minimum-variance* method). As the number of clusters decreases, the square-error across all clusters increases. Ward's method minimizes the square-error increase and minimizes the intracluster variance while maximizing the intercluster variance. Because a cluster is represented by its centroid, Ward's method is classified as a *geometric* or *cluster-center* method. Other methods such as the single-link, complete-link, and group-average methods are classified as *graph-theoretic* or *linkage methods*. Murtagh[27] introduced the concept of a *reducibility property* that is applicable to geometric methods. The reducibility property states that for the merger of two clusters, a and b, to form cluster c, there cannot be another cluster, d, that is closer to c than to a or b. If the method satisfies the reducibility property, agglomerations can be performed in localized areas of the proximity space and then amalgamated to produce the full hierarchy. Ward's method, implemented using the Euclidean distance as the proximity measure, is one of the few geometric methods satisfying the reducibility property. Voorhees[31] subsequently showed that if the cosine coefficient of similarity is used as the proximity measure, the group-average method can be implemented as a geometric method, and it satisfies the reducibility property.

For a data set of $N$ compounds, the stored-matrix algorithm for SAHN methods requires $O(N^2)$ time and $O(N^2)$ space for creation and storage of the proximity matrix while requiring $O(N^3)$ time for the clustering. This algorithm is thus very demanding of resources for anything other than small data sets. The importance of the reducibility property is that it enables the stored-matrix algorithm to be replaced by the more efficient *reciprocal nearest-neighbor* (RNN) algorithm that requires only $O(N^2)$ time and $O(N)$ space. Because agglomerations can be performed in localized areas of the proximity space, the RNN algorithm works by tracing paths through proximity space from one point to its nearest neighbor until a point is reached whose nearest neighbor is the previous point in the path, that is, a pair of points that are reciprocal nearest neighbors. These points represent a pair that should be merged into a single point as one of the agglomerations of the full hierarchy. The RNN algorithm is carried out using the following steps:

1. Mark all points as "unused."
2. Begin at an unused point and trace a path of unused nearest neighbors until a reciprocal nearest neighbor pair is found.
3. Add the pair of points to the list of RNNs along with the proximity between them; mark one of the pair of points as "used" (to inactivate it and

its centroid) and replace the centroid of the other point by the centroid of the merged pair.
4. Continue the path tracing from the penultimate point in the path if one exists; otherwise start path tracing from a new, unused starting point.
5. Repeat steps 2–4 until only one unused point remains.
6. Sort the list of RNNs by decreasing proximity values; the sorted list represents the agglomerations needed to construct the hierarchy.

Because path tracing moves from one nearest neighbor to the next, random access to each point is required.

***Hierarchical Divisive***

Most hierarchical divisive methods are monothetic, meaning that each split is determined on the basis of a single descriptor. The methods differ in how the descriptor is chosen with one possibility being to select the descriptor that maximizes the distance between the resultant clusters. Monothetic divisive methods are usually faster than the SAHN methods described above and have found utility in biological classification. However, for chemical applications, monothetic division often gives poor results when compared to polythetic division or SAHN methods, even though the closely related classification method of recursive partitioning can be very effective in chemical applications (e.g., see the article by Chen, Rusinko, and Young[32]). Unfortunately, most polythetic divisive methods are very resource demanding (more so than for SAHN methods), and accordingly they have not been used much for chemical applications. One exception is the *minimum-diameter* method published by Guenoche, Hansen, and Jaumard;[33] it requires $O(N^2 \log N)$ time and $O(N^2)$ space. This method is based on dividing clusters at each iteration in such a way as to minimize the cluster diameter. The cluster diameter is defined as the largest dissimilarity between any pair of its members, with singleton clusters having a diameter of zero. The minimum-diameter algorithm accomplishes its task by carrying out the following steps:

1. Generate a sorted list of all $N(N-1)/2$ dissimilarities, with the most dissimilar pairs listed first.
2. Perform an initial division by selecting the first pair from the sorted list (i.e., the most dissimilar points in the data set); assign every other point to the closest of the pair.
3. Choose the cluster with the largest diameter and divide it into two clusters so that the larger cluster has the smallest possible diameter.
4. Repeat step 3 for a maximum of $N-1$ divisions.

## Nonhierarchical Methods

***Single-Pass***

Methods that cluster data on the basis of a single scan of the data set are referred to as single-pass. A proximity threshold is typically used to decide

whether a compound is assigned to an existing cluster (represented as a centroid) or if it should be used to start a new cluster. The first compound selected becomes the first cluster; a single sequential scan of the data set then assigns the remaining compounds, and cluster centroids are updated as each compound is assigned to a particular cluster. The most common single-pass algorithm is called the *leader algorithm*. The leader algorithm carries out the following steps to provide a set of nonhierarchical clusters:

1. Set the number of existing clusters to zero.
2. Use the first compound in the data set to start the first cluster.
3. Calculate the similarity, using some appropriate measure, between the next compound and all the existing clusters. If its similarity to the most similar existing cluster exceeds some threshold, assign it to that cluster; otherwise use it to start a new cluster.
4. Repeat step 2 until all compounds have been assigned.

This method is simple to implement and very fast. The major drawback is that it is order dependent; if the compounds are rearranged and scanned in a different order, then the resulting clusters can be different.

*Nearest Neighbor*

A simple way to isolate dense regions of proximity space is to examine the nearest neighbors of each compound to determine groups with a given number of mutual nearest neighbors. Although several nearest-neighbor methods have been devised, the *Jarvis–Patrick method*[34] is almost exclusively used for chemical applications. The method proceeds in two stages.

The first stage generates a list of the top $K$ nearest neighbors for each of the $N$ compounds, with proximity usually measured by the Euclidean distance or the Tanimoto coefficient;[23] $K$ is typically 16 or 20. The Tanimoto coefficient has been found to perform well for chemical applications where the compounds are represented by fragment screens (bit strings denoting presence/absence of structural features). For finding nearest neighbors with Tanimoto coefficients as a proximity measure, one can use an efficient inverted file approach described by Perry and Willett[35] to speed up the creation of nearest-neighbor lists.

The second stage scans the nearest-neighbor lists to create clusters that fulfill the three following *neighborhood conditions*:

1. Compound i is in the top $K$ nearest-neighbor list of compound j.
2. Compound j is in the top $K$ nearest-neighbor list of compound i.
3. Compounds i and j have at least *Kmin* of their top $K$ nearest neighbors in common, where *Kmin* is user-defined and lies in the range 1 to $K$.

Pairs of compounds that fail any of the above conditions are not put into the same cluster.

To scan the nearest-neighbor lists and create the clusters in this stage of nonhierarchical clustering, the following three steps are carried out:

1. Tag each compound with a sequential cluster label so that each is a singleton.
2. For each pair of compounds, i and j ($i < j$), compare the nearest-neighbor lists on the basis of the three neighborhood conditions. If the three conditions are passed, replace the cluster label for compound j with the cluster label for compound i. Then, scan all previously processed compounds and replace any occurrences of the cluster label for compound j by the cluster label for compound i.
3. Scan to extract clusters by retrieving all compounds assigned the same cluster label.

The Jarvis–Patrick method requires $O(N^2)$ time and $O(N)$ space.

***Relocation***

Relocation methods start with an initial guess as to where the centers of clusters are located. The centers are then iteratively refined by shifting compounds between clusters until stability is achieved. The resultant clustering is reliant upon the initial selection of seed compounds that serve as cluster centers. Hence, relocation methods can be adversely affected by outlier compounds. [An *outlier* is a cluster of one item (a singleton or noise). It is on its own, and the clustering method has not put it with anything else because it is not similar enough to anything else.] The iterative refinement seeks an optimal partitioning of the compounds but would likely find a suboptimal solution because it would require the analysis of all possible solutions to guarantee finding the global optimum. Nevertheless, the computational efficiency and mathematical foundation of these methods have made them very popular, especially with statisticians.

The best-known relocation method is the *k-means* method, for which there exist many variants and different algorithms for its implementation. The k-means algorithm minimizes the sum of the squared Euclidean distances between each item in a cluster and the cluster centroid. The basic method used most frequently in chemical applications proceeds as follows:

1. Choose an initial set of $k$ seed compounds to act as initial cluster centers.
2. Assign each compound to its nearest cluster centroid (classification step).
3. Recalculate each cluster centroid (minimization step).
4. Repeat steps 2 and 3 for a given number of iterations or until no compounds are moved from one cluster to another.

In step 1, the initial compounds are usually selected at random from the data set. Random selection is quick and, for large heterogeneous data sets, likely to provide a reasonable initial set. Steps 2 and 3 can be performed separately or in combination. If done separately, the classification (step 2) is performed on

all compounds before recalculation of each cluster centroid (step 3). This approach is referred to as *noncombinatorial* (or *batch update*) classification. If steps 2 and 3 are done in combination, moving a compound from its current cluster to a new cluster (step 2) immediately necessitates recalculation of the affected cluster centroids (step 3). This latter approach is called *combinatorial* or *online update* classification. Most implementations for chemical applications use noncombinatorial classification. In step 4, convergence to a point where no further compounds move between clusters, is usually rapid, but, for safety, a maximum number of iterations can be specified. k-Means clustering requires $O(Nmk)$ time and $O(k)$ space. Here, $m$ is the number of iterations to convergence, and $k$ is the number of clusters. Because $m$ is typically much smaller than $N$ and the effect of $k$ can be reduced substantially through efficient implementation, k-means algorithms essentially require $O(N)$ time.

*Mixture Model*

Clustering can be viewed as a density estimation problem. The basic premise used in such an estimation is that in addition to the observed variables (i.e., descriptors) for each compound there exists an unobserved variable indicating the cluster membership. The observed variables are assumed to arrive from a mixture model, and the mixture labels (cluster identifiers) are hidden. The task is to find parameters associated with the mixture model that maximize the likelihood of the observed variables given the model. The probability distribution specified by each cluster can take any form. Although mixture model methods have found little use in chemical applications to date, they are mentioned here for completeness and because they are obvious candidates for use in the future.

The most widely used and most effective general technique for estimating the mixture model parameters is the expectation maximization (EM) algorithm.[36] It finds (possibly suboptimally) values of the parameters using an iterative refinement approach similar to that given above for the k-means relocation method. The basic EM method proceeds as follows:

1. Select a model and initialize the model parameters.
2. Assign each compound to the cluster(s) determined by the current model (expectation step).
3. Reestimate the parameters for the current model, given the cluster assignments made in step 2, and generate a new model (maximization step).
4. Repeat steps 2 and 3 for $n$ iterations or until the $n$th and $(n-1)$th model are sufficiently close.

This method requires prior specification of a model and typically takes a large number of iterations to converge.

Note that the k-means relocation method is really a special case of EM that assumes: (1) each cluster is modeled by a spherical Gaussian distribution, (2) each data item is assigned to a single cluster, and (3) the mixture weights

are equal. Assignment of each compound to the closest-cluster centroid is the expectation step; recalculation of the cluster centroids (model parameters) after assignment is the maximization step.

***Topographic***

Topographic clustering methods attempt to preserve the proximities between clusters, thus facilitating visualization of the clustering results. For k-means clustering, the cost function is invariant, whereas in topographic clustering it is not, and a predefined neighborhood is imposed on the clusters to preserve the proximities between them. The Kohonen, or self-organizing, map,[37,38] apart from being one of the most commonly used types of neural network, is also a topographic clustering method. A *Kohonen network* uses an unsupervised learning technique to map higher dimensional spaces of a data set down to, typically, two or three dimensions (2D or 3D), so that clusters can be identified from the neurons' coordinates (topological position); the values of the output are ignored. Initially, the neurons are assigned weight vectors with random values (weights). During the self-organization process, the data vectors of the neuron having the most similar weight vector to each data vector and its immediately adjacent neurons are updated iteratively to place them closer to the data vector. The *Kohonen mapping* thus proceeds as follows:

1. Initialize each neuron's weight vector with random values.
2. Assign the next data vector to the neuron having the most similar weight vector.
3. Update the weight vector of the neuron of step 2 to bring it closer to the data vector.
4. Update neighboring weight vectors using a given updating function.
5. Repeat steps 2–4 until all data vectors have been processed.
6. Start again with the first data vector, and repeat steps 2–5 for a given number of cycles.

The iterative adjustment of weight vectors is similar to the iterative refinement of k-means clustering to derive cluster centroids. The main difference is that adjustment affects neighboring weight vectors at the same time. Kohonen mapping requires $O(Nmn)$ time and $O(N)$ space, where $m$ is the number of cycles and $n$ the number of neurons.

***Other Nonhierarchical Methods***

We have delineated the main categories of clustering methods applicable to chemical applications above. We have also provided one basic algorithm as an example of each. Researchers in other disciplines sometimes use variants of these main categories. The main categories that have been used by those researchers but omitted here include density-based clustering and graph-based clustering techniques. These will be mentioned briefly in the next section.

## PROGRESS IN CLUSTERING METHODOLOGY

The representations used for chemical compounds are typically "*data-prints*" (tens or hundreds of real number descriptors, such as topological indexes and physicochemical properties) or *fingerprints* (thousands of binary descriptors indicating the presence or absence of 2D structural fragments or 3D pharmacophores). These numbers can be compared to the tens or hundreds of descriptors typically encountered in data mining and the thousands of descriptors encountered in information retrieval. We now outline the development of clustering methods that are suited to handling these representations and that have been, or in the near future are likely to be, used for chemical applications. Specific examples of chemical applications are given later in the section entitled Chemical Applications.

### Algorithm Developments

Having briefly outlined the basic algorithms that are implemented in many of the standard clustering methods, we now set the algorithms in context by reviewing their historical development, discuss the characteristics of each method, and then highlight some of the variants that have been developed for overcoming certain limitations. Clustering is now such a large area of research and everyday use that this chapter must be selective rather than comprehensive in scope. The interested reader can access further details from the references cited throughout this chapter and from the recent review by Murtagh.[39]

Most of the development of hierarchical clustering methods occurred from the 1960s through the mid-1980s, after which there was a period of consolidation, with little new development until recently. From this developmental period, two key publications were those of Lance and Williams[29] in 1967 and the review of hierarchical clustering methods by Murtagh[27] in 1985. Following this developmental period, a few variations have been proposed. Matula[40] developed algorithms that implemented both divisive and agglomerative average-linkage methods, but with high computational costs for processing large data sets. That same year, Jain, Indrayan, and Goel[41] compared single and complete linkage, group and weighted average, centroid, and median agglomerative methods and concluded that complete linkage performed best in failing to find clusters from random data. Podani[42] produced a useful classification of agglomerative methods, in which the standard Lance–Williams update recurrence formula[29] is split into two formulas. He also introduced three new parameter variations, that is, three new agglomerative methods were defined, but these seem to represent more of an inclusion for the sake of completeness than a significant alternative to previously defined parameter variations. Roux[43] recognized the complexity problems in Matula's implementations[40] and mentioned restrictions that could be applied to

overcome them for a polythetic divisive implementation. Unfortunately, no algorithmic details were given.

Overall, the Lance–Williams recurrence formula, and its subsequent extensions, provides a consolidating basis for the implementation of hierarchic agglomerative methods. However, the standard ways of implementation, that is, by generating, storing, and updating the full distance matrix, or by generating distances as required, tend to be very demanding of computational resources. The review by Murtagh[39] explained how substantial reductions in the computational requirements for some of these methods could be achieved by using the reciprocal nearest neighbor approach. El-Hamdouchi and Willett[44] described the use of this approach for the implementation of the Ward method for document clustering. That same year (1989) Rasmussen and Willett[45] discussed parallel implementation of single-link and Ward methods for both document and chemical structure clustering. The RNN approach and single-link clustering have the additional advantage of only requiring a list of descriptor vectors and a function to return the nearest neighbor of any input vector, rather than a full proximity matrix. Downs, Willett, and Fisanick[46] used RNN implementations of the Ward and group-average methods in a comparison of methods for clustering compounds on the basis of property data (see section below on Comparative Studies on Chemical Data Sets). These two agglomerative methods have been used successfully in comparative studies covering a wide range of nonchemical applications, and they have been shown to provide consistently reasonable results. However, centroid- and medoid-based methods, such as Ward (and k-means nonhierarchical), and the group-average and complete-link methods tend to favor similarly sized hyperspherical clusters (i.e., clusters that are shaped like spheres in a space of more than three dimensions), and they can fail to separate clusters of different shapes, densities, or sizes. Single-link is not a centroid method; it uses just the pairwise similarities and is more analogous to density-based methods. Accordingly, it can find clusters of different shapes and sizes, but it is very susceptible to noise, such as outliers, and artifacts, and it has a tendency to produce straggly clusters (an effect known as *chaining*). The development of traditional hierarchical methods largely ignored the issues of noise, and, although the abilities of different methods to separate clusters were noted, little was done about this problem other than to advise users to adopt more than one method so that different types of clusters could be revealed.

Recent developments in the data mining community have produced methods better suited to finding clusters of different shapes, densities, and sizes. For example, Guha, Rastogi, and Shim[47,48] developed an algorithm called ROCK (RObust Clustering using linKs) that is a sort of hybrid between nearest-neighbor, relocation, and hierarchical agglomerative methods. Although more expensive computationally than RNN implementations of the Ward method, the algorithm is particularly well suited to nonnumerical data (of which the Boolean fingerprints used for chemical data sets are a

special case, although they can also be represented as binary, a special case of numeric). The same authors developed another algorithm called CURE (Clustering Using REpresentatives).[49] Here centroid and single-link-type approaches are combined by choosing more than one representative point from each cluster. With CURE, a user-specified number of diverse points is selected from a cluster, so that it is not represented by just the centroid (which tends to lead to hyperspherical clusters). To avoid the problem of influence from selected points that might be outliers, which can result in a chaining effect, the selected points are shrunk toward the cluster centroid by a specified proportion. This results in a computationally more expensive procedure, but the separation of differently shaped and sized clusters is better. Karypis, Han, and Kumar[50] also addressed the problems of cluster shapes and sizes in their Chameleon algorithm. These authors provide a useful overview of the problems of other clustering methods in their summary. Chameleon measures similarity on the basis of a dynamic model, which is to be contrasted with the fixed model of traditional hierarchical methods. Two clusters are merged only if their interconnectivity and closeness is high relative to the internal interconnectivity and closeness within the two clusters. The characteristics of each cluster are thus taken into account during the merging process rather than assuming a fixed model that, if the clusters do not conform to it, can result in inappropriate merging decisions that cannot be undone subsequently. In a different study, Karypis, Han, and Kumar[51] evaluated the use of multilevel refinement methods to detect and correct inappropriate merging decisions in a hierarchy. Fasulo[52] reviewed some of the other recent developments in the area of data mining with World Wide Web search engines. The developments cited in that review describe work that reassesses the manner in which clustering is performed; a range of methods, which are more flexible in their separation of clusters, were evaluated. It is further pointed out that problems still remain when scaling-up hierarchical clustering methods to the very high dimensional spaces characteristic of many chemical data sets. Other fundamental issues remain, such as the problem of tied proximities in hierarchical clustering.[53] This problem was mentioned many years earlier by Jain and Dubes,[28] among others. Tied proximities occur when the proximities between two different pairs of data items are equal, and result in ambiguous decision points when building the hierarchy, effectively leading to many possible hierarchies of which only one is chosen. MacCuish, Nicolaou, and MacCuish[53] show tied proximities to be surprisingly common with the types of fingerprints commonly used in chemical applications, and the problem increases with data set size. What is not clear is whether such ties have a major deleterious effect on the overall clustering and whether the chosen hierarchy is significantly different from any of the others that might have been chosen.

There has been little development of polythetic divisive methods since the publication of the minimum-diameter method[33] in 1991. Garcia et al.[54] developed a path-based approach with similarities to single-link. The method

has time requirements of $O(MN^2)$ for $M$ clusters and $N$ compounds, making the method particularly suitable for finding a small number of clusters. Wang, Yan, and Sriskandarajah[55] updated the single criterion minimum-diameter method with a multiple criteria algorithm that considers both maximum split (intercluster separation) and minimum diameter in deciding the best bipartition. Their algorithm reduces the *dissection* effect (similar items forced into different clusters because doing so reduces the diameter) associated with the minimum-diameter criterion and the chaining effect associated with the maximum-split criterion. More recently, Steinbach, Karypis, and Kumar[56] reported an interesting variant of k-means that is actually a hierarchical polythetic divisive method. At each point where a cluster is to be split into two clusters, the split is determined by using k-means, hence the name "bisecting k-means." The results for document clustering, using keywords as descriptors, are shown to be better than standard k-means, with cluster sizes being more uniform, and better than the agglomerative group-average method.

Monothetic divisive clustering has largely been ignored, although there have been applications and development of a classification method closely related to monothetic divisive clustering. This classification is recursive partitioning, a type of decision tree method.[57–60]

Nonhierarchical algorithms that cluster the data set in a single pass, such as the leader algorithm, have had little development, except to identify appropriate ways of preordering the data set so as to get around the problem of dependency on processing order (work on this is discussed in the Chemical Applications section). For multipass algorithms, however, efforts have been made to minimize the number of passes required, in some cases reducing them to single-pass algorithms. In the area of data mining, this work has resulted in a method that does not fit neatly into the categorization used in this review. Zhang, Ramakrishnan, and Livny[61] developed a program called BIRCH (Balanced Iterative Reducing and Clustering using Heuristics), an $O(N^2)$ method that performs a single scan of the data set to sort items into a cluster features (CF) tree. This operation has some similarity with the leader algorithm; the nodes of the tree store summary information about clusters of dense points in the data so that the original data need not be accessed again during the clustering process. Clustering then proceeds on the in-memory summaries of the data. However, the initial CF tree building requires the maximum cluster diameter to be specified beforehand, and the subsequent tree building is thus sensitive to the value chosen. Overall, the idea of BIRCH is to bring together items that should always be grouped together, with the maximum cluster diameter ensuring that the cluster summaries will all fit into available memory. Ganti et al.[62] outlined a variant of BIRCH called BUBBLE. It does not rely on vector operations but builds up the cluster summaries on the basis of a distance function that obeys the triangle inequality, an operation that is more CPU demanding than operations in coordinate space.

Nearest-neighbor nonhierarchical methods have received much attention in the chemical community because of their fast processing speeds and ease of implementation. The comparative studies outlined in the next section (Comparative Studies on Chemical Data Sets) led to the widespread adoption of the Jarvis–Patrick nearest-neighbor method for clustering large chemical data sets. To improve results obtained by the standard Jarvis–Patrick implementation, several extensions have been developed. The standard implementation tends to produce a few large heterogeneous clusters and an abundance of singletons, which is hardly surprising because the method was originally designed to be space distorting,[34] that is, contraction of sparsely populated areas clusters and splitting of densely populated areas. Attempts to overcome these tendencies include the use of variable-length nearest-neighbor lists,[12,20] reclustering of singletons,[63] and the use of fuzzy clustering.[64] For variable-length nearest-neighbor lists, the user specifies a proximity threshold so that the lists will contain all neighbors that pass the threshold test rather than a fixed number of nearest neighbors. During clustering, the comparison between nearest-neighbor lists is made on the basis of a specified minimum percentage of the neighbors in the shorter list being in common. These modifications help prevent true outliers from being forced to join a cluster while preventing the arbitrary splitting of large clusters arising from the limitations imposed by fixed length lists. When using fingerprints for clustering chemical data sets, Brown and Martin[20] showed improved results compared with the standard implementation, whereas Taraviras, Ivanciuc, and Cabrol-Bass[65] show contrary results when clustering descriptors.

The reclustering of singletons is used in the "cascaded clustering" method of Menard, Lewis, and Mason.[63] This method applies the standard Jarvis–Patrick clustering iteratively, removes the singletons, and reclusters them using less strict parameters until fewer than a specified percentage of singletons remain. The fuzzy Jarvis–Patrick method outlined by Doman et al.[64] is the most radical Jarvis–Patrick variant. In the fuzzy method, clusters in dense regions are extracted using a similarity threshold and the standard crisp method. The compounds are then assigned probabilities of belonging to each of the crisp clusters. Any previously unclustered compounds not exceeding a specified threshold probability of belonging to any of the crisp clusters are regarded as outliers and remain as singletons.

Other nearest-neighbor methods include the agglomerative hierarchical method of Gowda and Krishna,[66] which uses the position of nearest neighbors, rather than just the number, in a measure called the *mutual neighborhood value* (MNV). Given points $i$ and $j$, if $i$ is the $p$th neighbor of $j$ and $j$ is the $q$th neighbor of $i$, then the MNV is $(p + q)$. Smaller values of MNV indicate greater similarity, and a specified threshold MNV is used to determine whether points should be merged. Dugad and Ahuja[67] extended the MNV concept to include the density of two clusters that are being considered for merger. In addition to the threshold MNV, if there exists a point $k$ with

MNV (*i,k*) less than MNV (*i,j*) but distance (*i,k*) greater than or equal to distance (*i,j*), then *i* is not a valid neighbor of *j*, and *j* is not a valid neighbor of *i*. The neighbor validity check can result in many small clusters, but these clusters can be merged afterward by relaxing the reciprocal nature of the check.

Relocation algorithms are widely used outside of chemical applications, largely because of their simplicity and speed. The original k-means noncombinatorial methods, such as that by Forgy,[68] and the combinatorial methods, such as that by MacQueen,[69] have been modified into different versions for use in many disciplines, a few of which are mentioned here. Efficient implementations of k-means include those by Hartigan and Wong[70] and Spaeth.[71] A variation of the k-means algorithm, referred to as the *moving method*, looks ahead to see whether moving an item from one cluster to another will result in an overall decrease in the square error (Eq. [2]); if it does, then the moving is carried out. Duda and Hart[72] and Ismail and Kamel[73] originally outlined this variant, while Zhang, Wang, and Boyle[74] further developed the idea and obtained better results than a standard noncombinatorial implementation of k-means. Because the method relies on the concept of a centroid, it is usually used with numerical data. However, Huang[75] reported variants that use k-modes and k-prototypes that are suitable for use with categorical and mixed-numerical and categorical data, respectively.

The main problems with k-means are (1) the tendency to find hyperspherical clusters, (2) the danger of falling into local minima, (3) the sensitivity to noise, and (4) the variability in results that depends on the choice of the initial seed points. Because k-means (and its fuzzy equivalent, c-means) is a centroid-based method, nothing much can be done about the tendency to produce hyperspherical clusters, although the CURE methodology mentioned above might alleviate this tendency somewhat. Falling into local minima cannot be avoided, but rerunning k-means with different seeds is a standard way of producing alternative solutions. After a given number of reruns, the solution is chosen that has produced the lowest square-error across the partition. An alternative to this is to perturb an existing solution, rather than starting again. Zhang and Boyle[76] examined the effects of four types of perturbation on the moving method and found little difference between them. Estivell-Castro and Yang[77] suggested that the problem of sensitivity to noise is due to the use of means (and centroids) rather than medians (and medoids). These authors proposed a variant of k-means based on the use of medoids to represent each cluster. However, calculation of a point to represent the medoid is more CPU-expensive [$O(n \log n)$ for each cluster of size $n$] than that required for the centroid, resulting in a method that is slightly slower than k-means (but faster than EM algorithms[36]). A similar variant based on medoids is the PAM (Partitioning Around Medoids) method developed by Kaufman and Rousseeuw.[2] This method is very time consuming, and so the authors developed CLARA (Clustering LARge Applications), which takes a sample of a data

set and applies PAM to it. An alternative to sampling the compounds has been developed by Ng and Han.[78] Their CLARANS (Clustering Large Applications based on RANdomized Search) method samples the neighbors, rather than the compounds, to make PAM more efficient.

The most common way of choosing seeds for k-means is by random selection, which is statistically reasonable given a large heterogeneous data set. Alternatively, a set of $k$ diverse seeds could be selected using, for example, the MaxMin subset selection method.[79,80] Diverse seeds have been shown to give better clustering results by Fisher, Xu, and Zard.[81] One of the early suggestions, by Milligan,[82] was that a partition resulting from hierarchical agglomerative clustering should be used as the initial partition for k-means to refine. It may seem counterproductive to initialize an $O(N)$ method by first running an $O(N^2)$ method, because it means that very large data sets cannot be processed, but k-means is then effectively being used to refine individual partitions and to correct inappropriate assignments made by the hierarchical method. An iterative method for refining an entire hierarchy has been discussed by Fisher.[83] The iterative method starts at the root (i.e., the top of the hierarchy, with all compounds in one cluster), recursively removes each cluster, resorts it into the hierarchy, and continues iterating until no clusters are moved, other than moving individual items from one cluster to another.

Of the mixture model methods, the expectation maximization (EM) algorithm[36] is the most popular because it is a general and effective method for estimating the model parameters and for fitting the model to the data. Though now quite old, the method was relatively unused until a surge of recent interest has propelled its further development and implementation for data mining applications.[84] As mentioned earlier, k-means is a special case of EM. However, because standard k-means uses the Euclidean metric, it is not appropriate for clustering discrete or categorical data. The EM algorithm does not have these limitations, and, since the mixture model is probabilistic, it can also effectively separate clusters of different sizes, shapes, and densities. A major contribution to the development of the EM algorithm came from Banfield and Raftery[85] who reparameterized the standard distributions to make them more flexible and include a Poisson distribution to account for noise. Various models were developed and compared using the approximate weight of evidence (AWE) statistic, which estimates the Bayesian posterior probability of the clustering solution. Fraley and Raftery[86] subsequently replaced AWE by the more reliable Bayesian information criterion (BIC), which enabled them to produce an EM algorithm that simultaneously yields the best model and determines the best number of clusters. One other interesting aspect of their work is that the EM algorithm is seeded with the clustering results from hierarchical agglomerative clustering. It is not clear whether, by using a less expensive seed selection, the EM algorithm will scale to the very large, high-dimensional data sets of chemical applications, or if the necessary parameterization will be acceptable in practice.

The use of a fixed model in a clustering method favors retrieval of clusters of certain shapes (as exemplified by the hyperspherical clusters retrieved by centroid-based methods). An alternative is to use a density-based approach, in which a cluster is formed from a region of higher density than its surrounding area. The clustering is then based on local criteria, and it can pick out clusters of any shape and internal distribution. Such approaches are typically not applicable directly to high dimensions, but progress is being made in that direction within the data mining community. An example is the DBSCAN (Density-Based Spatial Clustering of Applications with Noise) method of Ester et al.[87] that was subsequently extended by Ankerst et al.[88] to give the OPTICS (Ordering Points To Identify the Clustering Structure) method. These two methods work on a principle that each point of a cluster must have at least a given number of other points within a specified radius. Points fulfilling these conditions are clustered; any remaining points are considered to be outliers, that is, noise. The OPTICS method has been enhanced by Breunig et al.[89] to identify outliers, and by Breunig, Kriegel, and Sander,[90] who combined it with BIRCH[61] to increase speed.

Other density-based approaches designed for high dimensions include CLIQUE (Clustering In QUEst) by Agrawal et al.,[91] and PROCLUS (PROjected CLUSters), by Aggarwal et al.[92] These two methods recognize that high dimensional spaces are typically sparse so that the similarity between two points is determined by a few dimensions, with the other dimensions being irrelevant. Clusters are thus formed by similarity with respect to subspaces rather than full dimensional space. In the CLIQUE algorithm, dense regions of data space are determined by using cell-based partitioning, which are then used as initial bases for forming the clusters. The algorithm works from lower to higher dimensional subspaces by starting from cells identified as dense in $(k-1)$-dimensional subspace and extending them into $k$-dimensional subspace. The result is a set of overlapping dense regions that are extracted as the clusters. Research into improving grid-based methods is continuing, as demonstrated by the variable grid method of Nagesh.[93] In contrast, the PROCLUS program generates nonoverlapping clusters by identifying potential cluster centers (medoids) using a MaxMin subset selection procedure. The best medoids are selected from the initial set by an iterative procedure in which data items within the locality of a medoid (i.e., within the minimum distance between any two medoids) are assigned to that cluster. Rather than using all dimensions, the dimensions associated with each cluster are used in the Manhattan segmental distance[92] to calculate the distance of an item from the cluster. The Manhattan segmental distance is a normalized form of the Manhattan distance that enables comparison of different clusters with varying numbers of dimensions. (The Manhattan, or city-block, or Hamming, distance is the sum of absolute differences between descriptor values; in contrast, the Euclidean distance is the square root of the sum of squares differences between descriptor values.) Once the best medoids have been

selected, a final single pass over the data set assigns each item to its nearest medoid.

Graph-theoretic algorithms have seen little use in chemical applications. The basis of these methods is some form of a graph in which the vertices are the items in the data set and the edges are the proximities between them. Early methods created clusters by removing edges from a minimum spanning tree or by constructing a Gabriel graph, a relative neighborhood graph, or a Delauney triangulation, but none of these graph-theoretic methods are suitable for high dimensions. Reviews of these methods are given by Jain and Dubes[28] and Matula.[94] Recent advances in computational biology have spurred development of novel graph-theoretic algorithms based on isolating areas called cliques or "almost cliques" (i.e., highly connected subgraphs) from the graph of all pairwise similarities. Examples include the algorithms by Ben-Dor, Shamir, and Yakhini,[95] Hartuv et al.,[96] and Sharan and Shamir[97] that find clusters in gene expression data. Jonyer, Holder, and Cook[98] developed a hierarchical graph-theoretic method that begins with the graph of all pairwise similarities and then iteratively finds subgraphs that maximally compress the graph. The time consumption of these graph-theoretic methods is currently too great to apply to very large data sets.

One way to speed up the clustering process is to implement algorithms on parallel hardware. In the 1980s Murtagh[27,99] outlined a parallel version of the RNN algorithm for hierarchical agglomerative clustering. Also in that decade, Rasmussen, Downs, and Willett[45,100] published research on parallel implementations of Jarvis–Patrick, single-link, and Ward clustering for both document and chemical data sets, and Li and Fang[101] developed parallel algorithms for k-means and single-link clustering. In 1990, Li[102] published a review of parallel algorithms for hierarchical clustering. This in turn elicited a classic riposte from Murtagh[103] to the effect that the parallel algorithms were no better than the more recent $O(N^2)$ serial algorithms. Olson[104] presented $O(N)$ and $O(N \log N)$ algorithms for hierarchical methods using $N$ processors. For chemical applications, in-house parallel implementations include the leader algorithm at the National Cancer Institute[105] and k-means at Eli Lilly[79] (both discussed in the section on Chemical Applications), and commercially available parallel implementations include the highly optimized implementation of Jarvis–Patrick by Daylight[14] and the multiprocessor version of the Ward and group-average methods by Barnard Chemical Information.[12]

Another way of speeding up clustering calculations is to use a quick and rough calculation of distance to assess an initial separation of items and then to apply the more CPU-expensive, full-distance calculation on only those items that were found to cluster using the rough calculation. McCallum, Nigam, and Ungar[106] exploited this idea by using the rough calculation to divide the data into *canopies* (roughly overlapping clusters). Only items within the same canopy, or canopies, were used in the subsequent full-distance calculations to determine nonoverlapping clusters (using, e.g., a hierarchical agglomerative, EM,

or k-means method). The nature of the rough-distance measure used can guarantee that the canopies will be sufficiently broad to encompass all candidates for the ensuing full-distance measure. These ideas to speed up nearest-neighbor searches are similar to the earlier use of bounds on the distance measure, as discussed by Murtagh.[27]

## Comparative Studies on Chemical Data Sets

Much of the use of clustering for chemical applications is based on the *similar property principle*.[107] This principle, which holds in many, but certainly not all, structure–property relationships, states that compounds with similar structure are likely to exhibit similar properties. Clustering on the basis of structural descriptors is thus likely to group compounds having similar properties. However, there exist many different clustering methods, each having its own particular characteristics that are likely to affect the composition of the resultant clusters. Consequently, there have been several comparative studies on the performance of different clustering methods when applied to chemical data sets. The first such studies were conducted by Willett and Rubin[5,108–110] in the early 1980s. These studies were highly influential in the subsequent implementation of clustering methods in commercial and in-house software systems used by the pharmaceutical industry. Over 30 hierarchical and nonhierarchical methods were tested on 10 small data sets for which certain properties were known. Clustering was conducted using 2D fingerprints as compound representations. The leave-one-out approach (based on the similar property principle) was used to compare the results of different clustering methods by predicting the property of each compound (as the average of the property of the other members of the cluster) and correlating it with the actual property. High correlations indicate that compounds with similar properties have been clustered together. The results indicated that the Ward hierarchical method gave the best overall performance. But, this method was not well suited to processing large data sets due to the requirement for random access to the fingerprints. The Jarvis–Patrick nonhierarchical method results were almost as good and, because it does not require the fingerprints to be in memory, it became the recommended method.

In the early 1990s, a subsequent study by Downs, Willett, and Fisanick[46] compared the performance of the Ward and group-average agglomerative methods, the minimum-diameter divisive hierarchical method, and the Jarvis–Patrick nonhierarchical method when using dataprints of calculated physicochemical properties. In this assessment, a data set was used that was considerably larger than those used in the original studies.[108–110] The results highlighted the poor performance of the Jarvis–Patrick method in comparison with the hierarchical methods. The hierarchical methods all had similar levels of performance with the minimum-diameter method being slightly better for small numbers of clusters. Brown and Martin[20] then investigated the same

clustering methods to compare their performance for compound selection, using various 2D and 3D fingerprints. Active/inactive data was available for the compounds in the data sets used, so assessment was based on the degree to which clustering separated active from inactive compounds (into nonsingleton clusters). Although the Jarvis–Patrick method was the fastest of the methods, it again gave the poorest results. The results were improved slightly by using a variant of the Jarvis–Patrick method that uses variable rather than fixed-length nearest-neighbor lists.[12] Overall, the Ward method gave the best and most consistent results. The group-average and minimum-diameter methods were broadly similar and only slightly worse in performance than the Ward method.

The influence of the studies summarized above can be seen in the methods subsequently implemented by many other researchers for their applications (see the section on Chemical Applications). One method that was included in the original assessment studies, but not in the later assessments, is k-means. This method did not perform particularly well on the small data sets of the original studies, and the resultant clusters were found to be very dependent on the choice of initial seeds; hence it was not included in the subsequent studies. However, k-means is computationally efficient enough to be of use for very large data sets. Indeed, over the last decade k-means and its variants have been studied extensively and developed for use in other disciplines. Because it is being increasingly used for chemical applications, any future comparisons of clustering methods should include k-means.

## How Many Clusters?

A problem associated with the k-means, expectation maximization, and hierarchical methods involves deciding how many ''natural'' (intuitively obvious) clusters exist in a given data set. Determining the number of ''natural'' clusters is one of the most difficult problems in clustering and to date no general solution has been identified. An early contribution from Jain and Dubes[28] discussed the issue of *clustering tendency*, whereby the data set is analyzed first to determine whether it is distributed uniformly. Note that randomly distributed data is not generally uniform, and, because of this, most clustering methods will isolate clusters in random data. To avoid this problem, Lawson and Jurs[111] devised a variation of the Hopkins' statistic that indicates the degree to which a data set contains clusters. McFarland and Gans[112] proposed a method for evaluating the statistical significance of individual clusters by comparing the within-cluster variance with the within-group variance of every other possible subset of the data set with the same number of members. However, for large heterogeneous chemical data sets it can be assumed that the data is not uniformly or randomly distributed, and so the issue becomes one of identifying the most natural clusters.

Nonhierarchical methods such as k-means and EM need to be initialized with $k$ seeds. This presupposes that $k$ is a reasonable estimation of the number

of natural clusters and that the seeds chosen are reasonably close to the centers of these clusters. Epter, Krishnamoorthy, and Zaki[113] published one of the few papers addressing these issues for large data sets. Their solution is applicable to distance-based clustering and involves analysis of the histogram of pairwise distances between data items. For small data sets, all pairwise distances can be used, whereas for large data sets, random sampling (up to 10% of the data set) can be used to lessen the quadratic increase in time needed to generate the distances. For the distances calculated, the corresponding histogram is generated and then scanned to find the first spike (a large maximum followed by a large minimum). This point is used as the threshold for intracluster distance. The graph containing distances within this threshold contains connected components used to determine both the number of clusters present in the data set and the initial starting points from within these clusters. Assuming that a reasonable value for $k$ is known, Fayyad, Reima, and Bradley[114,115] showed that one can minimize the problem of poor initial starting points by sampling the data set to derive a better set of starting points. A series of randomly selected subsets, larger than $k$, are extracted, clustered by k-means, amalgamated, and then clustered again using each solution from the subsets. The starting points from the subset giving the best clustering of the amalgamated subset are then chosen as the set of refined points for the main clustering, where "best" means the clustering that gives the minimal "distortion," that is, minimum error across the amalgamated subset. The method aims to avoid selecting outliers, which may occur with other selection methods such as MaxMin.

In hierarchical clustering, each level defines a partition of the data set into clusters. However, there is no associated information indicating which level is best in terms of splitting the data set into the "natural" number of clusters present and with each cluster containing the most appropriate compounds. Many methods and criteria have been proposed to try to derive such information from the hierarchy so that the "best" level is selected. Milligan and Cooper[116] published the first comprehensive comparison of hierarchy level selection methods, using psychology data. Thirty methods were tested for their ability to retrieve the correct number of clusters from several small data sets containing from 2 to 5 "natural" clusters. Fifteen years later, Wild and Blankley[117] published a major comparison of hierarchy level selection methods using chemical data sets. As part of that study, Ward clustering with 2D fingerprints was used to evaluate the performance of nine hierarchy level selection methods. The methods chosen were those that would be easy to implement and that did not require parameters. Eight of those methods were ones that Milligan and Cooper had previously examined; the ninth was a more recent method published by Kelley, Gardner, and Sutcliffe.[118] The study by Wild and Blankley concluded that the point biseral,[119] variance ratio criterion,[120] and Kelley methods gave the best overall results, with the Kelley method being more computationally efficient than the others [scaling at less

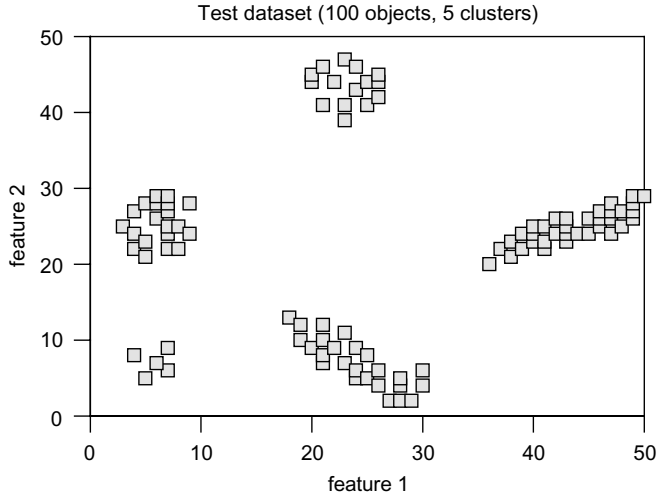


**Figure 3** An example data set of 100 objects, represented by 2 features, that fall into 5 natural clusters.

than $O(N^2)$]. A test data set of 100 objects, represented by 2 features and grouped into 5 natural clusters, is shown in Figure 3. The corresponding plot of penalty values (calculated using the Kelley method) against the number of clusters (Figure 4) shows a clear minimum at 5 clusters.

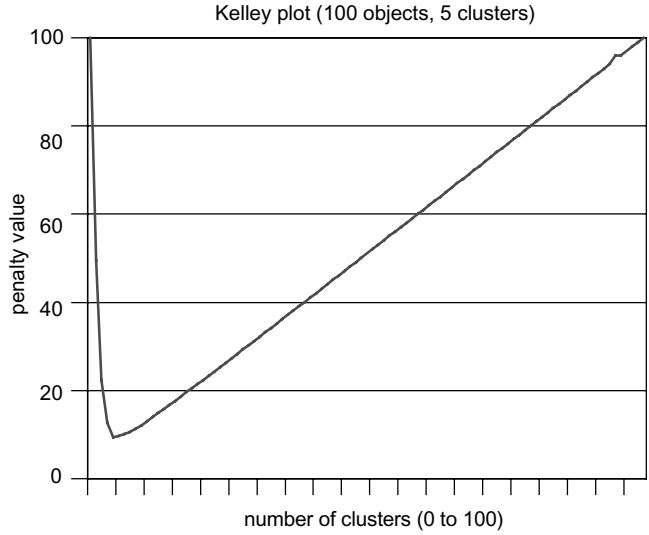


**Figure 4** Kelley plot of the penalty value against number of clusters for the data set of 100 items in Figure 3, showing the minimum at 5 clusters.

Hierarchy level selection methods provide useful guidance in selecting reasonable partitions from hierarchies where the underlying structure of the data set is unknown. They are, however, a compromise in that they compare entire partitions with each other rather than individual clusters. In disciplines outside of chemistry, there is an increasing awareness that such global comparisons can mask comparative differences in local densities. For example, the situation in Figure 5 shows three clusters (below the dendrogram) that cannot be retrieved by using a conventional straight horizontal line across the dendrogram (such as that shown in Figure 1). Using a straight line can include either item 8 with cluster [3,1,2] but merge [4,5] with [6,7], or keep [4,5] and [6,7] separate but maintain 8 as a singleton. What may be required for the selection of the "best," nonoverlapping clusters from different partitions is a *stepped* (or *segmental*) horizontal line, which is illustrated by the dotted line across the dendrogram in Figure 5. No solution to deciding which is the best selection of nonoverlapping clusters appears to have been published to date, but there are examples of methods that are moving toward a solution. One such example

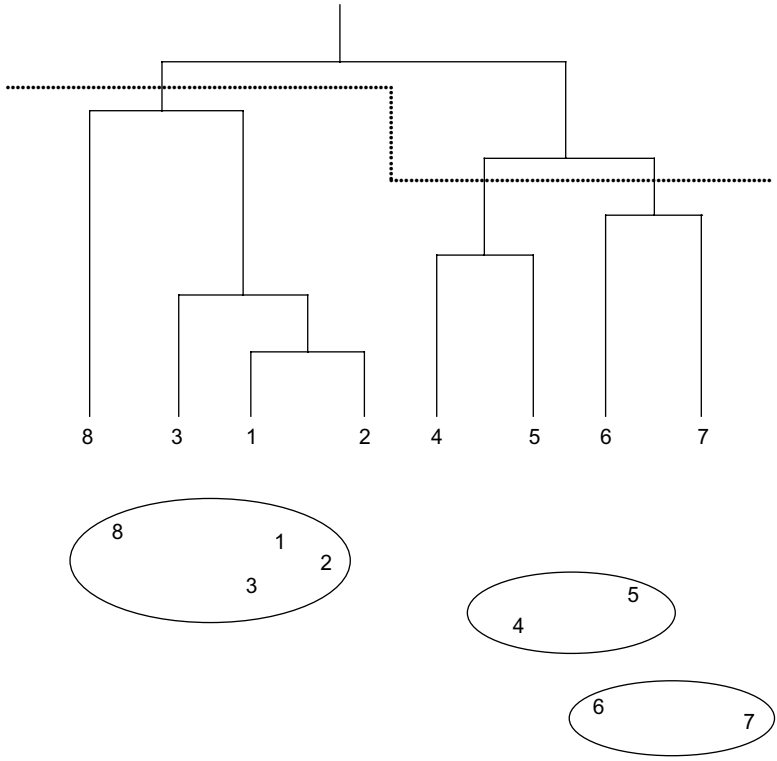


**Figure 5** An illustration of how a stepped hierarchy partition can extract particular clusters (clusters [8,1,2,3], [4,5], and [6,7], as shown below the hierarchy).

is the OPTICS method that orders items in a data set in terms of local criteria, thus providing an equivalent to a density-based analysis.

A variety of different requirements exist for chemical applications. These requirements dictate whether it is important to address the issues of how many clusters exist, what the best partition is, and which the best clusters are. When using representative sampling, for example, for high-throughput screening in pharmaceutical research, the number of required clusters is usually set beforehand. Hence, it is necessary to generate only a reasonable partition from which to extract the required number of representative compounds. For analysis of an unknown data set in, say, a list of vendor compounds, the number of clusters is unknown. Hierarchical clustering with optimum level analysis should provide suitable results for this scenario since the actual composition of each cluster is not critical. For analysis of quantitative structure–activity relationships (QSAR), the number of clusters is unknown, and the quality of the clusters becomes an important issue since complete clusters are required for further analysis. It may be that recent developments[87–93] related to density-based clustering will help in this circumstance.

## CHEMICAL APPLICATIONS

Having introduced and described the various kinds of clustering methods used in chemistry and other disciplines, we are in a position to present some illustrative examples of chemical applications. This section reviews a representative selection of publications that have reported or analyzed the use of clustering methods for processing chemical data sets, largely from groups of scientists working within pharmaceutical companies. The main applications for these scientists are high-throughput screening, combinatorial chemistry, compound acquisition, and QSAR. The emphasis is on pharmaceutical applications because these workers tend to process very large and high dimensional data sets. This section is presented according to method, starting with hierarchical and then moving to nonhierarchical methods.

Little has been reported on the use of hierarchical divisive methods for processing chemical data sets (other than the inclusion of the minimum-diameter method in some of the comparative studies mentioned above). Recursive partitioning, which is a supervised classification technique very closely related to monothetic divisive clustering, has, however, been used at the GlaxoSmithKline[57,58] and Organon[59] companies.

There is, however, widespread use of hierarchical agglomerative techniques, particularly the Ward method. At Organon, Bayada, Hamersma, and van Geerestein[121] compared Ward clustering with the MaxMin diversity selection method, Kohonen maps, and a simple partitioning method to help select diverse yet representative subsets of compounds for further testing. The data came from HTS or combinatorial library results. Ward clustering

was the only method that gave results consistently better than random selection of compounds. It was also found that the standard technique of selecting the compound closest to the centroid to serve as the representative for a cluster tends to result in the selection of the smallest compound or the one with the fewest features. This finding is not surprising because the centroid is the arithmetic average of items in a cluster and hence the representative will be the most common denominator. Users should be aware of this tendency toward biased selection of a representative compound, since such a compound could be less interesting as a drug-like molecule than others in the data set. This effect was not observed when the clustering was done using the first 10 principal components of the descriptor set rather than relying directly on the descriptors (such as fingerprints) themselves.

Van Geerestein, Hamersma, and van Helden[122] used Ward clustering to show that cluster representatives provide a significantly better sampling of activity space than random selection. This key paper shows how clustering can separate actives from inactives in a data set, so that a cluster containing at least one active will contain more than an average number of other actives. The introduction to their article also gives a succinct summary of why diversity analysis (such as clustering) is of use as a lead finding strategy.

At Parke-Davis (now Pfizer), Wild and Blankley[123] incorporated Ward clustering and level selection (by the Kelley function[118]) into a program called VisualiSAR, which supports structure browsing and the development of structure–activity relationships in HTS data sets. At the Janssen unit of the Johnson and Johnson company, Engels et al.[124] have similarly incorporated Ward clustering and the Kelley function into a system (called CerBeruS) that is used for analysis of their corporate compound database. The clustering was used to produce smaller, more homogeneous subsets from which one representative compound was selected as a screening candidate using the Kelley function to determine the optimal clustering level(s). Engels et al.[124] noted two further advantages of a cluster-based approach. First, if a hit was found, related compounds could be tested subsequently by extracting other possible candidates from the cluster containing the hit, and, second, analyses of structure–activity relationships (SAR) could be formulated by linking the results of all the screening runs so as to examine the cluster hierarchy at different levels. Engels and Venkatarangan[125] subsequently developed a two-stage sequential screening procedure supported by clustering to make HTS more efficient.

Stanton et al.[126] reported the use of complete-link clustering in the HTS system at the Proctor & Gamble company. In situations where the screening produces large numbers of hits, clustering was used to determine which compound classes were present so that representatives could be taken. The amount of follow-up analysis was reduced by an order of magnitude while still evaluating which classes of compounds were present in the hits, thus increasing the efficiency of selecting potential leads. The clusters also provided sets of compounds to build preliminary SAR models. Furthermore, the clustering was

found useful in the detection of false positives, especially from combinatorial libraries. In these cases, the structural similarity between the hits was low and their biological activity was subsequently attributed to a common side product. Clustering was performed by Stanton[127] using BCUT (Burden–CAS–University of Texas) descriptors,[128] with the optimum hierarchy level determined visually from the dendrogram. Visual selection was possible because the hit sets were typically a few hundred compounds.

The most significant application of a nonhierarchical single-pass method was for screening antitumor activity at the National Cancer Institute. A variant of the leader algorithm was developed[129] in which the descriptors were weighted by occurrence in each compound, size of the fragment, and frequency of occurrence in the data set. Because of the use of these weighted descriptors, an asymmetric coefficient[129] was used to determine similarity, rather than the more usual Tanimoto coefficient. The data set was then ordered by the increasing sum of fragment weights to remove the order dependency associated with the leader algorithm (or at least, to have a reasonable basis for choosing a particular order) and to enable the use of heuristics to reduce the number of similarity calculations. Compounds were then assigned to any existing cluster for which they exceeded the given similarity threshold, thus creating overlapping clusters. The algorithm was implemented on parallel hardware,[105] and the results from clustering several data sets were presented with a discussion on the large number of singleton clusters produced.[130] Another variant on the leader algorithm was proposed by Butina.[131] In his approach, the compounds are first sorted by decreasing number of near neighbors (within a specified threshold similarity), thus again removing the order dependence of the basic algorithm. Of course, identifying the number of near neighbors for each compound introduces an $O(N^2)$ step, which in turn obviates the single-pass algorithm's primary advantage of linear speed.

At Rohm and Haas Company, Reynolds, Drucker, and Pfahler[132] developed a two-pass method similar to the initial assignment stage of k-means. In the first pass, a similarity threshold is specified, and then the sphere exclusion diverse subset selection method[80] is used to select the cluster seeds (referred to as *probes*). In the second pass, all other compounds are assigned to the most similar probe (the published version unnecessarily performs this in two stages). Clark and Langton[133] adopted a similar methodology in the Tripos OptiSim fast clustering system for selecting diverse yet representative subsets. OptiSim works by selecting an initial seed at random, selecting a random sample of size $K$, analyzing the random sample by choosing the most dissimilar member of the sample from existing seeds, and, if the minimum similarity threshold, $R$, to all existing seeds is exceeded, adding it to the seed set. This operation continues until the specified number of seeds, $M$, has been selected or no more candidates remain. All other compounds are then assigned to their nearest seed (which is equivalent to the initial assignment stage of k-means, with no refinement). OptiSim is an obvious amalgam of the MaxMin and sphere

exclusion subset selection methods[80] and the Reynolds system mentioned above. It also bears similarities with other methods, particularly the clustering of merged multiple random samples reported by Bradley and Fayyad.[115]

The widespread application of the Jarvis–Patrick nonhierarchical method exists in part because of the influence of the publications by Willett et al.[5,108–110] but also because of the availability of the efficient commercial implementation from Daylight[14] for handling very large data sets. The first publication on the use of Jarvis–Patrick clustering for compound selection from large chemical data sets was from researchers who implemented it at Pfizer Central Research (UK).[134] Clustering was done using 2D fragment descriptors, with calculation of the list of 20 nearest neighbors using the efficient Perry–Willett inverted file approach.[35] After clustering the data set of about 240,000 compounds, singletons were moved to the most similar nonsingleton cluster, and representative compounds were then extracted by generating cluster centroids and selecting the compound closest to each centroid.

Earlier in this chapter, we mentioned the cascaded Jarvis–Patrick[63] and fuzzy Jarvis–Patrick[64] variants. The cascaded Jarvis–Patrick method was implemented at Rhone-Poulenc Rorer (RPR) based on using Daylight 2D structural fingerprints and Daylight's Jarvis–Patrick program. With this variant, singletons are reclustered using less strict parameters so that the singletons do not dominate the set of representative compounds selected. The applications reported by the RPR researchers[63] include selection of compounds from the corporate database for HTS and comparison of the corporate database with external databases, such as the Available Chemicals Directory, to assist in compound acquisition. The fuzzy Jarvis–Patrick variant was developed and implemented at G. D. Searle and Company for analysis of their compound database to help support their screening program. The Searle researchers[64] initially used the Daylight implementation but found the chaining and singleton characteristics of the standard method to be significant drawbacks. This in turn prompted them to develop a variant with different characteristics.

McGregor and Pallai[135] discussed an in-house implementation of the standard Jarvis–Patrick algorithm at Procept Inc. They used the MDL 2D structural descriptors to compare and analyze external databases for efficient compound acquisition. Shemetulskis et al.[136] also reported the use of Jarvis–Patrick clustering to assist in compound acquisition at Parke-Davis, giving results from analysis and comparison of the CAST3D and Maybridge compound databases with the corporate database. In a two-stage process, representatives, comprising about a quarter of the compounds, were selected from each data set by clustering on the basis of 2D fingerprints. Each data set was then merged with the corporate database, and the clustering run again on the basis of calculated physicochemical property descriptors. Clusters containing only CAST3D or Maybridge compounds were tagged as highest priority for acquisition. Dunbar[137] summarized the compound acquisition

report,[135] discussed the use of clustering methods to assist in HTS, and then outlined the use at Parke-Davis of Jarvis–Patrick clustering to assist traditional, low-throughput screening. The aim of the Parke-Davis group was to generate a representative subset of no more than 2000 compounds selected from about 126,000 compounds in the Parke-Davis corporate database so that they could be used in a particularly labor-intensive cell-based assay. Jarvis–Patrick clustering was run to generate an initial set of 25,000 nonsingleton clusters. The compounds closest to the centroids were reclustered to give about 2,300 clusters. The compounds closest to these centroids were then analyzed manually providing a final selection of about 1,400 compounds. An interesting feature of this process was that singletons were rejected at each stage, rather than being assigned to the nearest nonsingleton cluster (as at Pfizer, UK) or being reclustered separately (as in the cascaded clustering method used at Rhone-Poulenc Rorer).

Jarvis–Patrick clustering has also been used to support QSAR analysis in a system developed at the European Communities Joint Research Center.[7,138–140] The EINECS (European Inventory of Existing Chemical Substances) database contains more than 100,000 compounds and has been clustered using 2D structural descriptors. That database also has associated physicochemical properties and activities, but the data is very sparse. Jarvis–Patrick clustering was used to extract clusters containing sufficient compounds with measured data for an attempt to be made to estimate the properties of members of the cluster lacking the data. For a few clusters, it was used to develop reasonable QSAR models.

An example of how use of k-means clustering can be used for QSAR analysis of small data sets is that by Lawson and Jurs[141] who clustered a set of 143 acrylates from the ToSCA (Toxic Substances Control Act) inventory. For large chemical data sets, the seminal paper is that published by Higgs et al.,[79] at Eli Lilly and Company. These authors examined three methods of subset selection to assist their HTS and development of combinatorial libraries. The three methods were k-means, MaxMin, and D-optimal design. Seed compounds were selected by the MaxMin method, and the k-means algorithm was implemented on parallel hardware. This research was part of the compound acquisition strategy to support HTS. The Lilly group used an extensive system of filters to ensure that selected compounds were pharmaceutically acceptable. No recommendations were offered in the paper as to the best method.

The use of a topographic clustering method for chemical data sets is exemplified by the work of Sadowski, Wagener, and Gasteiger.[142] The authors compared three combinatorial libraries using Kohonen mapping. Each compound within a library was represented by a 12-element autocorrelation vector (a sort of 3D-QSAR descriptor). The vectors were used as input to a $50 \times 50$ Kohonen network. Mapping the combinatorial libraries onto the same network placed each compound from the library at a particular node in the network. A 2D display of the positions of each compound revealed the degree of

overlap between the libraries. Two very dissimilar libraries formed two distinct clusters with little overlap, whereas two very similar libraries showed no distinction.

The use of mixture-model or density-based clustering has not yet been reported for processing chemical data sets. An interesting application of these techniques is their use to group the compound descriptors so as to obtain a set of orthogonal descriptors. Up to this point, the clustering that we have discussed has been applied to the patterns (fingerprints or dataprints) characterizing each compound; this is the "*Q-mode clustering*" referred to by Sneath and Sokal.[1] One can also cluster the features (the descriptors used in the fingerprints or dataprints) to highlight groups of similar descriptors. Sneath and Sokal call this "*R-mode clustering*." The similar property principle, upon which structure–property relationships depend, assumes that the compound descriptors are independent of each other. Reducing the number of descriptors can thus help in subsequent Q-mode clustering by reducing the dimensionality. Clustering the descriptors, so that a subset of orthogonal descriptors can be extracted, is an alternative to factor analysis and principal components analysis. Using an orthogonal subset of descriptors has the benefit that the result is a set of individual descriptors rather than composite descriptors. Taraviras, Ivanciuc, and Cabrol-Bass[65] applied the single-link, group-average, complete-link, and Ward hierarchical methods, along with Jarvis–Patrick, variable-length Jarvis–Patrick, and k-means nonhierarchical methods to a set of 240 topological indices in an attempt to reveal any "natural" clusters of the descriptors. Descriptors that were found to exist in the same clusters across all seven methods were regarded as being strongly clustered. Reducing the number of methods that needed to be in agreement revealed progressively weaker clusters. Overall, it was found that the strategy of using multiple clustering methods for R-mode clustering could be used to provide representative sets of orthogonal descriptors for use in QSAR analysis.

## CONCLUSIONS

Clustering methodology has been developed over many decades. The application of clustering to chemical data sets began in the 1980s, coinciding with the increasing size of in-house compound collections having their information contained in structural databases and with advances made by the information retrieval community to analyze large document collections. In the 1990s the advent of high-throughput screening, combinatorial libraries, and commercially available external chemical inventories placed a greater emphasis on rational compound selection. The demands of clustering data sets of several million compounds with high-dimensional representations led to the widespread adoption of a few inherently efficient and optimally implemented methods, namely, the Jarvis–Patrick, Ward, and k-means methods.

Acceptance of these methods—and inclusion of them as routine operations within such applications as lead-finding strategies, QSAR analyses, and compound acquisition—has been a gradual process rather than an abrupt revolution. The current decade should see this process continue as the methodologies are refined. The push for such advancement appears to be coming again from the information retrieval community but also from the data mining community, which has made significant progress. The emphasis of current research is turning toward the quality of the resultant clusters. It has been shown that, using representatives selected from clusters for lead-finding can increase the active hit rate significantly and consistently.

The results so far in chemistry are promising, but research in other areas outside of chemistry suggests that clustering is still a blunt instrument that can be sharpened by refinements. An example of this refinement is to be able to handle mixed or nonnumerical data, and another example is to take more consideration of cluster sizes, shapes, and distribution. The existing methods and implementations used to analyze chemical data sets do an impressive job when compared with the situation a decade ago. What is exciting is the number of new ideas that are being generated that should result in significant advances in the next decade.

## REFERENCES

1. P. H. A. Sneath and R. R. Sokal, *Numerical Taxonomy,* W. H. Freeman, San Francisco, CA, 1973.
2. L. Kaufman and P. J. Rousseeuw, *Finding Groups in Data: An Introduction to Cluster Analysis,* Wiley-Interscience, New York, 1990.
3. B. S. Everitt, *Cluster Analysis,* 3rd ed., Edward Arnold, London, 1993.
4. A. D. Gordon, *Classification,* 2nd ed., Chapman and Hall, London, 1999.
5. P. Willett, *Similarity and Clustering in Chemical Information Systems,* Research Studies Press, Letchworth, UK, 1987.
6. N. Bratchell, *Chemom. Intell. Lab. Systems,* **6**, 105 (1989). Cluster Analysis.
7. J. M. Barnard and G. M. Downs, *J. Chem. Inf. Comput. Sci.,* **32** (6), 644 (1992). Clustering of Chemical Structures on the Basis of Two-Dimensional Similarity Measures.
8. G. M. Downs and P. Willett, in *Advanced Computer-Assisted Techniques in Drug Discovery,* H. van de Waterbeemd, Ed., VCH Publishers, Weinheim, 1994, pp. 111–130. Clustering of Chemical Structure Databases for Compound Selection.
9. R. A. Lewis, S. D. Pickett, and D. E. Clark, in *Reviews in Computational Chemistry,* K. B. Lipkowitz and D. B. Boyd, Eds., Wiley-VCH, New York, 2000, Vol. 16, pp. 1–51. Computer-Aided Molecular Diversity Analysis and Combinatorial Library Design.
10. Clustan Ltd., 16 Kingsburgh Road, Edinburgh, UK. http://www.clustan.com.
11. SAS Institute Inc., SAS Campus Drive, Cary, NC 27513, USA. http://www.sas.com.
12. Barnard Chemical Information Ltd., 46 Uppergate Road, Stannington, Sheffield S6 6BX, UK. http://www.bci.gb.com.
13. Chemical Computing Group Inc., 1010 Sherbrooke Street West, Suite 910, Montreal, Quebec H3A 2R7, Canada. http://www.chemcomp.com.

14. Daylight Chemical Information Systems Inc., 441 Greg Avenue, Santa Fe, NM 87501, USA. http://www.daylight.com.
15. MDL Information Systems, Inc., 14600 Catalina Street, San Leandro, CA 94577, USA. http://www.mdl.com.
16. Accelrys (formerly Molecular Simulations Inc.), 9685 Scranton Road, San Diego, CA 92121-3752, USA. http://www.accelrys.com.
17. Tripos Inc., 1699 South Hanley Road, St. Louis, MO 63144, USA. http://www.tripos.com.
18. W. A. Warr, in *Computational Methods for the Analysis of Molecular Diversity,* P. Willett, Ed., *Perspectives in Drug Discovery and Design,* Vol. 7/8, Kluwer/ESCOM, Dordrecht, The Netherlands, 1997, pp. 115–130. Commercial Software Systems for Diversity Analysis.
19. R. D. Brown, in *Computational Methods for the Analysis of Molecular Diversity,* P. Willett, Ed., *Perspectives in Drug Discovery and Design,* Vol. 7/8, Kluwer/ESCOM, Dordrecht, The Netherlands, 1997, pp. 31–49. Descriptors for Diversity Analysis.
20. R. D. Brown and Y. C. Martin, *J. Chem. Inf. Comput. Sci.,* **36** (*3*), 572 (1996). Use of Structure–Activity Data to Compare Structure-Based Clustering Methods and Descriptors for Use in Compound Selection.
21. R. D. Brown and Y. C. Martin, *J. Chem. Inf. Comput. Sci.,* **37** (*1*), 1 (1997). The Information Content of 2D and 3D Structural Descriptors Relevant to Ligand-Receptor Binding.
22. G. M. Downs and P. Willett, in *Reviews in Computational Chemistry,* K. B. Lipkowitz and D. B. Boyd, Eds., VCH Publishers, New York, 1995, Vol. 7, pp. 1–66. Similarity Searching in Databases of Chemical Structures.
23. P. Willett, J. M. Barnard, and G. M. Downs, *J. Chem. Inf. Comput. Sci.,* **38** (*6*), 983 (1998). Chemical Similarity Searching.
24. J. M. Barnard, G. M. Downs, and P. Willett, in *Virtual Screening for Bioactive Molecules,* H.-J. Böhm and G. Schneider., Eds., Wiley, New York, 2000, pp. 59–80. Descriptor-Based Similarity Measures for Screening Chemical Databases.
25. J. S. Mason and S. D. Pickett, in *Computational Methods for the Analysis of Molecular Diversity,* P. Willett, Ed., *Perspectives in Drug Discovery and Design,* Vol. 7/8, Kluwer/ESCOM, Dordrecht, The Netherlands, 1997, pp. 85–114. Partition-Based Selection.
26. J. A. Hartigan, *Clustering Algorithms,* Wiley, New York, 1975.
27. F. Murtagh, *COMPSTAT Lectures,* **4,** (1985). Multidimensional Clustering Algorithms.
28. A. K. Jain and R. C. Dubes, *Algorithms for Clustering Data,* Prentice Hall, Englewood Cliff, NJ, 1988.
29. G. N. Lance and W. T. Williams, *Computer J.,* **9,** 373 (1967). A General Theory of Classificatory Sorting Strategies. 1. Hierarchical Systems.
30. J. H. Ward, *J. Am. Stat. Assoc.,* **58,** 236 (1963). Hierarchical Grouping to Optimize an Objective Function.
31. E. M. Voorhees, *Inf. Processing Management,* **22** (*6*), 465 (1986). Implementing Agglomerative Hierarchic Clustering Algorithms for Use in Document Retrieval.
32. X. Chen, A. Rusinko III, and S. S. Young, *J. Chem. Inf. Comput. Sci.,* **38** (*6*), 1054 (1998). Recursive Partitioning Analysis of a Large Structure-Activity Data Set Using Three-Dimensional Descriptors.
33. A. Guenoche, P. Hansen, and B. Jaumard, *J. Classification,* **8,** 5 (1991). Efficient Algorithms for Divisive Hierarchical Clustering with the Diameter Criterion.
34. R. A. Jarvis and E. A. Patrick, *IEEE Trans. Computers,* **C-22** (*11*), 1025 (1973). Clustering Using a Similarity Measure Based on Shared Near Neighbors.
35. S. A. Perry and P. Willett, *J. Inf. Sci.,* **6,** 59 (1983). A Review of the Use of Inverted Files for Best Match Searching in Information Rretrieval Systems.
36. A. P. Dempster, N. M. Laird, and D. B. Rubin, *J. Royal Stat. Soc.,* **B39,** 1 (1977). Maximum Likelihood from Incomplete Data via the EM Algorithm.
37. T. Kohonen, *Self-organizing Maps,* Springer-Verlag, Berlin, 1995.

38. J. Zupan and J. Gasteiger, *Neural Networks for Chemists, An Introduction,* VCH, Weinheim, 1993. See also, K. L. Peterson, in *Reviews in Computational Chemistry,* K. B. Lipkowitz and D. B. Boyd, Eds., Wiley-VCH, New York, 2000, Vol. 16, pp. 53–140. Artificial Neural Networks and Their Use in Chemistry.
39. F. Murtagh, in *Handbook of Massive Data Sets,* J. Abello, P. M. Pardalos, and M. G. C. Reisende, Eds., Kluwer, Dordrecht, The Netherlands, 2001, pp. 401–545. Clustering in Massive Data Sets.
40. D. W. Matula, in *Classification as a Tool of Research,* W. Gaul and M. Schader, Eds., Elsevier Science (North-Holland), Amsterdam, 1986, pp. 289–301. Divisive vs. Agglomerative Average Linkage Hierarchical Clustering.
41. N. C. Jain, A. Indrayan, and L. R. Goel, *Pattern Recognition,* **19** (*1*), 95 (1986). Monte Carlo Comparison of Six Hierarchical Clustering Methods on Random Data.
42. J. Podani, *Vegetatio,* **81,** 61 (1989). New Combinatorial Clustering Methods.
43. M. Roux, in *Applied Multivariate Analysis in SAR and Environmental Studies,* J. Devillers and W. Karcher, Eds., Kluwer, Dordrecht, The Netherlands, 1991, pp. 115–135. Basic Procedures in Hierarchical Cluster Analysis.
44. A. El-Hamdouchi and P. Willett, *Computer J.,* **32,** 220 (1989). Hierarchic Document Clustering using Ward's Method.
45. E. M. Rasmussen and P. Willett, *J. Doc.,* **45** (*1*), 1 (1989). Efficiency of Hierarchical Agglomerative Clustering Using the ICL Distributed Array Processor.
46. G. M. Downs, P. Willett, and W. Fisanick, *J. Chem. Inf. Comput. Sci.,* **34** (*5*), 1094 (1994). Similarity Searching and Clustering of Chemical-Structure Databases Using Molecular Property Data.
47. S. Guha, R. Rastogi, and K. Shim, Technical Report, Bell Laboratories, Murray Hill, NJ, 1997. A Clustering Algorithm for Categorical Attributes.
48. S. Guha, R. Rastogi, and K. Shim, *Inf. Systems,* **25** (*5*), 345 (2000). ROCK: A Robust Clustering Algorithm for Categorical Attributes.
49. S. Guha, R. Rastogi, and K. Shim, in *Proceedings of the ACM SIGMOD International Conference on Management of Data,* Seattle, WA, 1998, pp. 73–84. CURE: An Efficient Clustering Algorithm for Large Datasets.
50. G. Karypis, E.-H. Han, and V. Kumar, *IEEE Computer: Special Issue on Data Analysis and Mining,* **32** (*8*), 68 (1999). Chameleon: A Hierarchical Clustering Algorithm Using Dynamic Modeling.
51. G. Karypis, E.-H. Han, and V. Kumar, *Technical Report No. 99-020,* Department of Computer Science & Engineering, University of Minnesota, Minneapolis, MN, 1999. Multilevel Refinement for Hierarchical Clustering.
52. D. Fasulo, *Technical Report No. 01-03-02,* Department of Computer Science & Engineering, University of Washington, Seattle, WA, 1999. An Analysis of Recent Work on Clustering Algorithms.
53. J. MacCuish, C. Nicolaou, and N. E. MacCuish, *J. Chem. Inf. Comput. Sci.,* **41** (*1*), 134 (2001). Ties in Proximity and Clustering Compounds.
54. J. A. Garcia, J. Fdez-Valdivia, J. F. Cortijo, and R. Molina, *Signal Processing,* **44** (*2*), 181 (1994). A Dynamic Approach for Clustering Data.
55. Y. Wang, H. Yan, and C. Sriskandarajah, *J. Classification,* **13,** 231 (1996). The Weighted Sum of Split and Diameter Clustering.
56. M. Steinbach, G. Karypis, and V. Kumar, *Technical Report 00-034,* Department of Computer Science & Engineering, University of Minnesota, Minneapolis, MN, 2000. A Comparison of Document Clustering Techniques.
57. D. M. Hawkins, S. S. Young, and A. Rusinko, *Quant. Struct.–Act. Relat.,* **16,** 396 (1997). Analysis of a Large Structure–Activity Data Set Using Recursive Partitioning.
58. X. Chen, A. Rusinko, and S. S. Young, *J. Chem. Inf. Comput. Sci.,* **38** (*6*), 1054 (1998). Recursive Partitioning Analysis of a Large Structure–Activity Data Set Using Three-Dimensional Descriptors.

59. M. Wagener and V. J. van Geerestein, *J. Chem. Inf. Comput. Sci.,* **40** (*2*), 280 (2000). Potential Drugs and Nondrugs: Prediction and Identification of Important Structural Features.

60. D. W. Miller, *J. Chem. Inf. Comput. Sci.,* **41** (*1*), 168 (2001). Results of a New Classification Algorithm Combining K Nearest Neighbors and Recursive Partitioning.

61. T. Zhang, R. Ramakrishnan, and M. Livny, *ACM SIGMOD Record,* **25** (*2*), 103 (1996). BIRCH: An Efficient Data Clustering Method for Very Large Databases.

62. V. Ganti, R. Ramakrishnan, J. Gehrke, A. Powell, and J. French, *Proceedings of the 15th International Conference on Data Engineering,* Sydney, Australia, 1999, pp. 502–511. Clustering Large Datasets in Arbitrary Metric Spaces.

63. P. R. Menard, R. A. Lewis, and J. S. Mason, *J. Chem. Inf. Comput. Sci.,* **38** (*3*), 379 (1998). Rational Screening Set Design and Compound Selection: Cascaded Clustering.

64. T. N. Doman, J. M. Cibulskis, M. J. Cibulskis, P. D. McCray, and D. P. Spangler, *J. Chem. Inf. Comput. Sci.,* **36** (*6*), 1195 (1996). Algorithm5: A Technique for Fuzzy Clustering of Chemical Inventories.

65. S. L. Taraviras, O. Ivanciuc, and D. Cabrol-Bass, *J. Chem. Inf. Comput. Sci.,* **40** (*5*), 1128 (2000). Identification of Groupings of Graph Theoretical Descriptors Using a Hybrid Cluster Analysis Approach.

66. K. C. Gowda and G. Krishna, *Pattern Recognition,* **10** (*2*), 105 (1978). Agglomerative Clustering Using the Concept of Mutual Nearest Neighborhood.

67. R. Dugad and N. Ahuja, *IEEE International Conference on Acoustics Speech and Signal Processing,* **5,** 2761 (1998). Unsupervised Multidimensional Hierarchical Clustering.

68. E. Forgy, *Biometrics,* **21,** 768 (1965). Cluster Analysis of Multivariate Data: Efficiency vs. Interpretability of Classifications.

69. J. MacQueen, in *Proceedings of the 5th Berkeley Symposium on Mathematical Statistics and Probability,* University of California Press, Berkeley, CA, 1967, Vol. 1, pp. 281–297. Some Methods for Classification and Analysis of Multivariate Observations.

70. J. A. Hartigan and M. A. Wong, *Appl. Stat.,* **28,** 100 (1979). A K-Means Clustering Algorithm.

71. H. Spaeth, *Eur. J. Operat. Res.,* **1,** 23 (1977). Computational Experiences with the Exchange Method.

72. R. O. Duda and P. E. Hart, *Pattern Classification and Scene Analysis,* Wiley, New York, 1973.

73. M. A. Ismail and M. S. Kamel, *Pattern Recognition,* **22,** 75 (1989). Multidimensional Data Clustering Utilizing Hybrid Search Strategies.

74. Q. Zhang, Q. R. Wang, and R. D. Boyle, *Pattern Recognition,* **24** (*4*), 331 (1991). A Clustering Algorithm for Datasets with a Large Number of Classes.

75. Z. Huang, *Int. J. Data Mining Knowledge Disc.,* **2** (*3*), 283 (1998). Extensions to the K-Means Algorithm for Clustering Large Data Sets with Categorical Values.

76. Q. Zhang and R. D. Boyle, *Pattern Recognition,* **24** (*9*), 835 (1991). A New Clustering Algorithm with Multiple Runs of Iterative Procedures.

77. V. Estivell-Castro and J. Yang, *Technical Report No. 99-03,* Department of Computer Science & Software Engineering, University of Newcastle, Callaghan, NSW 2308, Australia. A Fast and Robust General Purpose Clustering Algorithm.

78. R. T. Ng and J. Han, in *Proceedings of the 20th International Conference on Very Large Data Bases,* Santiago, Chile, 1994, pp. 144–155. Efficient and Effective Clustering Methods for Spatial Data Mining.

79. R. E. Higgs, K. G. Bemis, I. A. Watson, and J. H. Wikel, *J. Chem. Inf. Comput. Sci.,* **37** (*5*), 861 (1997). Experimental Designs for Selecting Molecules from Large Chemical Databases.

80. M. Snarey, N. K. Terrett, P. Willett, and D. J. Wilton, *J. Mol. Graphics Modell.,* **15,** 372 (1997). Comparison of Algorithms for Dissimilarity-Based Compound Selection.

81. D. Fisher, L. Xu, and N. Zard, in *Proceedings of the 6th International Workshop on Machine Learning,* Morgan Kaufmann, Aberdeen, UK, 1992, pp. 163–168. Ordering Effects in Clustering.

82. G. W. Milligan, *Psychometrika,* **45** (*3*), 325 (1980). An Examination of the Effect of Six Types of Error Perturbation on Fifteen Clustering Algorithms.

83. D. Fisher, *J. Artif. Intell. Res.,* **4,** 147 (1996). Iterative Optimization and Simplification of Hierarchical Clusterings.

84. G. J. McLachlan and T. Krishnan, *The EM Algorithm and Extensions,* Wiley, New York, 1997.

85. J. D. Banfield and A. E. Raftery, *Biometrics,* **49,** 803 (1993). Model-Based Gaussian and Non-Gaussian Clustering.

86. C. Fraley and A. E. Raftery, *Computer J.,* **41** (*8*), 578 (1988). How Many Clusters? Which Clustering Method? Answers via Model-Based Cluster Analysis.

87. M. Ester, H.-P. Kriegel, J. Sander, and X. Xu, in *Proceedings of the 2nd International Conference on Knowledge Discovery and Data Mining,* Portland, OR, 1996, pp. 226–231. A Density-Based Algorithm for Discovering Clusters in Large Spatial Databases with Noise.

88. M. Ankerst, M. M. Breunig, H.-P. Kriegel, and J. Sander, in *Proceedings of the ACM SIGMOD International Conference on Management of Data,* Philadelphia, PA, 1999, pp. 49–60. OPTICS: Ordering Points to Identify Clustering Structure.

89. M. M. Breunig, H.-P. Kriegel, R. T. Ng, and J. Sander, *Proceedings of the Conference on Data Mining and Knowledge Discovery,* Prague, Czech Repub., 1999, in *Lecture Notes in Computer* Science, Springer, **1704,** 262–270 (1999). OPTICS-OF: Identifying Local Outliers.

90. M. M. Breunig, H.-P. Kriegel, and J. Sander, in *Proceedings of the European Conference on Principles and Practice of Knowledge Discovery in Databases,* Lyon, France, 2000. Fast Hierarchical Clustering Based on Compressed Data and OPTICS.

91. R. Agrawal, J. Gehrke, D. Gunopulos, and P. Raghavan, in *Proceedings of the ACM SIGMOD International Conference on Management of Data,* Seattle, WA, 1998, pp. 94–105. Automatic Subspace Clustering of High Dimensional Data for Data Mining Applications.

92. C. C. Aggarwal, C. Procopiuc, J. L. Wolf, P. S. Yu, and J. S. Park, in *Proceedings ACM SIGMOD International Conference on Management of Data,* Philadelphia, PA, 1999, pp. 61–72. Fast Algorithms for Projected Clustering.

93. H. S. Nagesh, M.Sc. Thesis, Northwestern University of Illinois, Evanston, IL, 1999. High Performance Subspace Clustering for Massive Data Sets.

94. D. W. Matula, in *Classification and Clustering,* J. van Ryzin, Ed., Academic Press, 1977, pp. 95–129. Graph Theoretic Techniques for Cluster Analysis Algorithms.

95. A. Ben-Dor, R. Shamir, and Z. Yakhini, *J. Comput. Biol.,* **6** (*3/4*), 281 (1999). Clustering Gene Expression Patterns.

96. E. Hartuv, A. Schmitt, J. Lange, S. Meier-Ewart, H. Lehrach, and R. Shamir, in *Proceedings 3rd International Conference on Computational Molecular Biology (RECOMB 99),* Lyon, France, 1999. An Algorithm for Clustering cDNAs for Gene Expression Analysis.

97. R. Sharan and R. Shamir, in *Proceedings of the 8th International Conference on Intelligent Systems for Molecular Biology,* AAAI Press, Menlo Park, CA, 2000, pp. 307–316. CLICK: A Clustering Algorithm with Application to Gene Expression Analysis.

98. I. Jonyer, L. B. Holder, and D. J. Cook, in *Proceedings of the 13th Annual Florida AI Research Symposium,* pp. 91–95, 2000 (http://www-cse.uta.edu/~cook/pubs). Graph-Based Hierarchical Conceptual Clustering.

99. F. Murtagh, *Computer J.,* **26** (*4*), 354 (1983). A Survey of Recent Advances in Hierarchical Clustering Algorithms.

100. E. M. Rasmussen, G. M. Downs, and P. Willett, *J. Comput. Chem.,* **9** (*4*), 378 (1988). Automatic Classification of Chemical Structure Databases Using a Highly Parallel Array Processor.

101. X. Li and Z. Fang, *Parallel Computing,* **11,** 275 (1989). Parallel Clustering Algorithms.

102. X. Li, *IEEE Trans. Pattern Anal. Machine Intelligence,* **12** (*11*), 1088 (1990). Parallel Algorithms for Hierarchical Clustering and Cluster Validity.

103. F. Murtagh, *IEEE Trans. Pattern Anal. Machine Intelligence,* **14** (*10*), 1056 (1992). Comments on "Parallel Algorithms for Hierarchical Clustering and Cluster Validity".

104. C. F. Olson, *Technical Report CSD-94-786,* University of California, Berkeley, CA, 1994. Parallel Algorithms for Hierarchical Clustering.

105. R. Whaley and L. Hodes, *J. Chem. Inf. Comput. Sci.,* **31** (*2*), 345 (1991). Clustering a Large Number of Compounds. 2. Using a Connection Machine.

106. A. McCallum, K. Nigam, and L. H. Ungar, in *Advances in Knowledge Discovery and Data Mining,* MIT Press, Cambridge, MA, 2000. Efficient Clustering of High Dimensional Data Sets with Application to Reference Matching.

107. M. A. Johnson and G. M. Maggiora, *Concepts and Applications of Molecular Similarity,* Wiley, New York, 1990.

108. P. Willett, *Anal. Chim. Acta,* **136,** 29 (1982). A Comparison of Some Hierarchical Agglomerative Clustering Algorithms for Structure–Property Correlation.

109. V. Rubin and P. Willett, *Anal. Chim. Acta,* **151,** 161 (1983). A Comparison of Some Hierarchical Monothetic Divisive Clustering Algorithms for Structure–Property Correlation.

110. P. Willett, *J. Chem. Inf. Comput. Sci.,* **24** (*1*), 29 (1984). Evaluation of Relocation Clustering Algorithms for the Automatic Classification of Chemical Structures.

111. R. G. Lawson and P. C. Jurs, *J. Chem. Inf. Comput. Sci.,* **30** (*1*), 36 (1990). New Index for Clustering Tendency and Its Application to Chemical Problems.

112. J. W. McFarland and D. J. Gans, *J. Med. Chem.,* **29,** 505–514 (1986). On the Significance of Clusters in Graphical Display of Structure–Activity Data.

113. S. Epter, M. Krishnamoorthy, and M. Zaki, *Technical Report No. 99-6,* Computer Science Department, Rensselaer Polytechnic Institute, Troy, NY, 1999. Clusterability Detection and Initial Seed Selection in Large Data Sets.

114. U. M. Fayyad, C. A. Reima, and P. S. Bradley, in *Proceedings of the 4th International Conference on Knowledge Discovery and Data Mining,* R. Agrawal, P. Stolorz, and G. Piatetsky-Shapiro, Eds., AAAI Press, Menlo Park, CA, 1998, pp. 194–198. Initialization of Iterative Refinement Clustering Algorithms.

115. P. S. Bradley and U. M. Fayyad, in *Proceedings of the 15th International Conference on Machine Learning,* Morgan Kaufmann, San Francisco, 1998, pp. 91–99. Refining Initial Points for K-Means Clustering.

116. G. W. Milligan and M. C. Cooper, *Psychometrika,* **50** (*2*), 159 (1985). An Examination of Procedures for Determining the Number of Clusters in a Data Set.

117. D. J. Wild and C. J. Blankley, *J. Chem. Inf. Comput. Sci.,* **40** (*1*), 155 (2000). Comparison of 2D Fingerprint Types and Hierarchy Level Selection Methods for Structural Grouping Using Ward's Clustering.

118. L. A. Kelley, S. P. Gardner, and M. J. Sutcliffe, *Protein Eng.,* **9,** 1063 (1996). An Automated Approach for Clustering an Ensemble of NMR-Derived Protein Structures into Conformationally-Related Subfamilies.

119. G. W. Milligan, *Psychometrika,* **46** (*2*), 187 (1981). A Monte Carlo Study of Thirty Internal Criterion Measures for Cluster Analysis.

120. T. Calinski and J. Harabasz, *Commun. Stat.,* **3** (*1*), 1 (1974). A Dendrite Method for Cluster Analysis.

121. D. M. Bayada, H. Hamersma, and V. J. van Geerestein, *J. Chem. Inf. Comput. Sci.,* **39** (*1*), 1 (1999). Molecular Diversity and Representativity in Chemical Databases.

122. V. J. van Geerestein, H. Hamersma, and S. P. van Helden, in *Computer-Assisted Lead Finding and Optimization* (Proceedings 9th European QSAR Meeting, Lausanne, Switzerland, 1996), H. van de Waterbeemd, B. Testa, and G. Folkers, Eds., Wiley-VCH, Basel, Switzerland, 1997, pp. 159–178. Exploiting Molecular Diversity: Pharmacophore Searching and Compound Clustering.

123. D. J. Wild and C. J. Blankley, *J. Mol. Graphics Modell.,* **17** (*2*), 85 (1999). VisualiSAR: A Web-Based Application for Clustering, Structure Browsing, and Structure–Activity Relationship Study.

124. M. F. M. Engels, T. Thielmans, D. Verbinnen, J. P. Tollenaere,, and R. Verbeeck, *J. Chem. Inf. Comput. Sci.,* **40** (*2*), 241 (2000). CerBeruS: A System Supporting the Sequential Screening Process.

125. M. F. M. Engels and P. Venkatarangan, *Curr. Opin. Drug Discovery Dev.,* **4** (*3*), 275 (2001). Smart Screening: Approaches to Efficient HTS.

126. D. T. Stanton, T. W. Morris, S. Roychoudhury, and C. N. Parker, *J. Chem. Inf. Comput. Sci.,* **39** (*1*), 21 (1999). Application of Nearest-Neighbor and Cluster Analyses in Pharmaceutical Lead Discovery.

127. D. T. Stanton, *J. Chem. Inf. Comput. Sci.,* **39** (*1*), 11 (1999). Evaluation and Use of BCUT Descriptors in QSAR and QSPR Studies.

128. R. S. Pearlman and K. M. Smith, *J. Chem. Inf. Comput. Sci.,* **39** (*1*) 28–35 (1999). Metric Validation and the Receptor-Relevant Subspace Concept.

129. L. Hodes, *J. Chem. Inf. Comput. Sci.,* **29** (*2*), 66 (1989). Clustering a Large Number of Compounds. 1. Establishing the Method on an Initial Sample.

130. R. Whaley and L. Hodes, *J. Chem. Inf. Comput. Sci.,* **31** (*2*), 347 (1991). Clustering a Large Number of Compounds. 3. The Limits of Classification.

131. D. Butina, *J. Chem. Inf. Comput. Sci.,* **39** (*4*), 747 (1999). Unsupervised Data Base Clustering Based on Daylight's Fingerprint and Tanimoto Similarity a Fast and Automated Way to Cluster Small and Large Data Sets.

132. C. H. Reynolds, R. Druker, and L. B. Pfahler, *J. Chem. Inf. Comput. Sci.,* **38** (*2*), 305 (1998). Lead Discovery Using Stochastic Cluster Analysis (SCA): A New Method for Clustering Structurally Similar Compounds.

133. R. D. Clark and W. J. Langton, *J. Chem. Inf. Comput. Sci.,* **38** (*6*), 1079 (1998). Balancing Representativeness Against Diversity Using Optimizable K-dissimilarity and Hierarchical Clustering.

134. P. Willett, V. Winterman, and D. Bawden, *J. Chem. Inf. Comput. Sci.,* **26** (*3*), 109 (1986). Implementation of Nonhierarchic Cluster-Analysis Methods in Chemical Information Systems; Selection of Compounds for Biological Testing and Clustering of Substructure Search Output.

135. M. J. McGregor and P. V. Pallai, *J. Chem. Inf. Comput. Sci.,* **37** (*3*), 443 (1997). Clustering Large Databases of Compounds: Using the MDL "Keys" as Structural Descriptors.

136. N. E. Shemetulskis, J. B. Dunbar, B. W. Dunbar, D. W. Moreland, and C. Humblet, *J. Comput.-Aided Mol. Design,* **9,** 407 (1995). Enhancing the Diversity of a Corporate Database using Chemical Database Clustering and Analysis.

137. J. B. Dunbar, in *Computational Methods for the Analysis of Molecular Diversity,* P. Willett, Ed., *Perspectives in Drug Discovery and Design,* Vol. 7/8, Kluwer/ESCOM, Dordrecht, The Netherlands, 1997, pp. 51–63. Cluster-Based Selection.

138. G. M. Downs and P. Willett, in *Applied Multivariate Analysis in SAR and Environmental Studies,* J. Devillers and W. Karcher, Eds., Kluwer, Dordrecht, The Netherlands, 1991, pp. 247–279. The Use of Similarity and Clustering Techniques for the Prediction of Molecular Properties.

139. J. Nouwen and B. Hansen, *SAR and QSAR in Environmental Research,* **4,** 1 (1995). An Investigation of Clustering as a Tool in Quantitative Structure–Activity Relationships (QSARs).

140. J. Nouwen, F. Lindgren, B. Hansen, W. Karcher, H. J. M. Verhaar, and J. L. M. Hermens, *J. Chemometrics,* **10,** 385 (1996). Fast Screening of Large Databases Using Clustering and PCA based on Structure Fragments.

141. R. G. Lawson and P. C. Jurs, *J. Chem. Inf. Comput. Sci.,* **30** (*2*), 137 (1990). Cluster Analysis of Acrylates to Guide Sampling for Toxicity Testing.

142. J. Sadowski, M. Wagener, and J. Gasteiger, *Angew. Chem., Int. Ed. Engl.,* **34** (*23/24*), 2674 (1995/1996). Assessing Similarity and Diversity of Combinatorial Libraries by Spatial Autocorrelation Functions and Neural Networks.

*Reviews in Computational Chemistry, Volume 18*
Edited by Kenny B. Lipkowitz and Donald B. Boyd

ISBN: 0-471-21576-7

CHAPTER 2

# The Use of Scoring Functions in Drug Discovery Applications

**Hans-Joachim Böhm and Martin Stahl**

*F. Hoffmann-La Roche AG, Pharmaceuticals Division, Chemical Technologies, CH-4070 Basel, Switzerland*

## INTRODUCTION

Structure-based design has become a mature and integral part of medicinal chemistry. It has been convincingly demonstrated for a large number of targets that the three-dimensional (3D) structure of a protein can be used to design small molecule ligands binding tightly at this target. Indeed, several marketed compounds can be attributed to a successful structure-based design.[1–4] Several reviews summarize these results.[5–9]

Since the introduction of molecular modeling and structure-based design into the drug discovery process in the 1980s, there has been a significant change in the role these computational techniques are playing. Early molecular modeling work concentrated on the manual design of protein ligands using the 3D structure of a target. Usually, the creativity of the designer was used to build a novel putative ligand using computer graphics followed by a molecular mechanics calculation of the resulting protein–ligand complex. A geometric and energetic analysis of the energy-minimized complex was then used to assess the putative ligand. A good complementarity of the shape and surface properties between the protein and ligand was used as an indication that the ligand might indeed bind to the protein with high affinity.

However, designing a single, active, synthetically accessible compound turned out to be a greater challenge than expected. It is still difficult to computationally predict induced-fit phenomena and binding affinities for new ligand candidates. But while existing modeling tools are certainly not suitable to design the one perfect drug molecule, they can help to *enrich* sets of molecules with greater numbers of biologically active candidates, even though the rates of false positives (and false negatives) are still high. Thus, an important current goal of molecular design is to increase the hit rate in biological assays compared to random compound selections, which means that structure-based design approaches now focus on the processing of large numbers of molecules. These "virtual libraries" of molecules can consist of either existing molecules (e.g., the compound collection of a pharmaceutical company) or of putative novel structures that could be synthesized via combinatorial chemistry. The computational goal is to rapidly assess millions of possible molecules by filtering out the majority that are predicted to be extremely unlikely to bind, and then to prioritize the remaining ones. This approach is, in fact, a successful strategy, and several recent publications have demonstrated impressive enrichment of active compounds.[10–15] The change of focus from individual compounds to compound libraries has been supported by three major developments that have taken place since the early days of molecular design:

1. An exponentially growing number of 3D protein structures is available in the public domain. Consequently, the number of projects relying on structural information has increased, and structure-based ligand design is nowadays routinely carried out at all major pharmaceutical companies. The amount of structural knowledge is so large that automated methods are needed to make full use of it.
2. High throughput screening (HTS) has become a well-established process. Large libraries of several hundred thousand compounds are routinely tested against new targets. This biological testing can, in many cases, be carried out in less than one month.
3. Synthetic chemistry has undergone a major change with the introduction of combinatorial and parallel chemistry techniques. There is a continuous trend to move away from the synthesis of individual compounds toward the synthesis of compound libraries, whose members are accessible through the same chemical reaction using different chemical building blocks.

To offer a competitive advantage, structure-based design tools must now be fast enough to prioritize thousands of compounds per day. Several algorithms have been developed that allow for de novo design[16,17] or for flexible docking[18] of hundreds to thousands of small molecules into a protein binding site per day on a single CPU computer. Essential components of all these structure-based design software tools are scoring functions that translate computationally determined protein–ligand interactions into approximate

estimations of binding affinity. These scoring functions guide the conformational and orientational search of a ligand within the binding site and ultimately provide a relative ranking of putative ligands with respect to a target. The purpose of this chapter is to describe some of these functions, discuss their strengths and weaknesses, explain how they are used in practical applications, and present selected results to highlight the current status of the field.

## The Process of Virtual Screening

In this section, we discuss a general strategy of virtual screening based on the 3D structure of a target. Typically, the following steps are typically taken.

1. Analysis of the 3D protein structure.
2. Selection of one or more key interactions that need to be satisfied by all candidate molecules.
3. Computational search (by docking and/or pharmacophore queries) in chemical databases for compounds that fit into the binding site and satisfy key interactions.
4. Analysis of the retrieved hits and removal of undesirable compounds.
5. Synthesis or purchase of the selected compounds.
6. Biological testing.

The first step is usually a careful analysis of available 3D protein structures. If possible, highly homologous structures will also be analyzed, either to generate additional ideas about possible ligand structural motifs or to gain some insight on how to achieve selectivity relative to other proteins of the same class. A superposition of different protein–ligand complexes can provide some indication about key interactions that are repeatedly found in tight binding protein–ligand complexes. Such an overlay will also highlight flexible parts of the protein. Programs like GRID[19] or LUDI[20,21] are frequently used to visualize potential interaction sites (hot spots) in the binding site of the protein. If there are conserved water molecules in the binding site mediating hydrogen bonds between the protein and the ligand, and if these water molecules cannot be replaced, then including them in the docking process can dramatically improve the hit rate.[13–15]

An important result from the aforementioned 3D structure analysis is usually the identification of one or more key interactions that all ligands should satisfy. An example of such a binding hypothesis is that aspartic protease inhibitors should form at least one hydrogen bond to the catalytic Asp side chains. Although it could be left to the computational algorithm using a good scoring function to pick molecules, experience indicates that the percentage of active compounds in a designed library can be significantly increased if a good binding hypothesis is used as filter. In addition, part of a known ligand may be used as a starting scaffold, and virtual screening techniques can then be used to select side chains.

Once a reasonable binding hypothesis has been generated, the next step is the actual virtual screening. Whether one uses databases of commercially available compounds or "virtual" libraries of hypothetical chemical structures, it makes sense to dock not just any compound, but only those that pass a number of simple property filters. Such filters remove

1. Compounds with reactive functional groups. Reactive groups such as $-SO_2Cl$ and $-CHO$ cause problems in some biological assays due to nonspecific covalent binding to the protein.
2. Compounds with a molecular weight below 150 or above 500. Very small molecules like benzene are known to bind to proteins in a rather nonspecific manner and at several sites. Very large molecules (like polypeptides) are difficult to optimize subsequently because bioavailability is usually low for compounds with a molecular weight above 500.
3. Compounds that are not "drug-like" according to criteria that have been derived from sets of known drugs.[22,23]

Each remaining compound is then docked into the binding site and scored. The docking process is the most demanding step computationally and is usually carried out on multiprocessor computers. Depending on the docking algorithm and the scoring function, this step may easily take several days of CPU time. The result is a list of several hundred to a few thousand docked small molecule structures each with a computed score, which is further analyzed to weed out undesirable structures. Selection criteria could be

1. Lipophilicity, if not addressed before. Highly lipophilic molecules are difficult to test because of their low solubility in water.
2. Structural class. If 50% of the docked structures belong to a single chemical class, it is probably unnecessary to test all of them.
3. Improbability of docked binding mode. Fast docking tools cannot produce reasonable solutions for all compounds. Often even some high-scoring compounds are found to be docked to the outer surface of the protein. Computational filters help to detect such situations.

Finally, the selected compounds are purchased or synthesized and then tested. If the goal is to identify weakly binding small molecules, it is important to ensure that the biological assay is sensitive and robust enough to pick up these molecules. Measurements using 100–1000 μM concentration of the ligand frequently cause problems due to the limited solubility of the ligands in water. To compensate for this, the assay is often carried out in the presence of 1–5% dimethyl sulfoxide (DMSO) (see, e.g., Ref. 14).

Note that the process of virtual screening still involves manual interventions at various stages. In principle, the whole process can be carried out in a fully automated manner, but in practice visual inspection and manual selection are still very useful.

## Major Contributions to Protein–Ligand Interactions

The selective binding of a low molecular weight ligand to a specific protein is determined by the structural and energetic recognition of those two molecules. For ligands of pharmaceutical interest, the protein–ligand interactions are usually noncovalent in nature. The binding affinity can be determined from the experimentally measured binding constant $K_i$

$$\Delta G = -RT \ln K_i = \Delta H - T\Delta S \qquad [1]$$

The experimentally determined binding constants $K_i$ are typically in the range of $10^{-2}$ to $10^{-12}$ mol/L, corresponding to a Gibbs free energy of binding $\Delta G$ between $-10$ and $-70$ kJ/mol in aqueous solution.[6,24]

There exists a growing body of experimental data on 3D structures of protein–ligand complexes and binding affinities.[25] These data indicate that several features can be found in almost all complexes of tightly bound ligands. These features include

1. A high steric complementarity between the protein and the ligand. This observation is consistent with the long established lock-and-key paradigm.
2. A high complementarity of the surface properties. Lipophilic parts of the ligands are most frequently found to be in contact with lipophilic parts of the protein. Polar groups are usually paired with suitable polar protein groups to form hydrogen bonds or ionic interactions.
3. The ligand usually adopts an energetically favorable conformation.

Generally speaking, direct interactions between the protein and the ligand are essential for binding. The most important types of direct interactions are depicted in Figure 1.

Structural data on unfavorable protein–ligand interactions are sparse. The scarcity of such complexes is due, in part, to the fact that structures of weakly binding ligands are more difficult to obtain and they are usually considered less interesting by many drug discovery chemists and structural biologists. However, weak binding data are vital for the development of scoring functions. What data are available indicate that unpaired buried polar groups at the protein–ligand interface are strongly adverse to binding. For example, few buried CO and NH groups in folded proteins fail to form hydrogen bonds.[26] Therefore, in the ligand design process, one has to ensure that polar functional groups, either of the protein or the ligand, will find suitable counterparts if they become buried upon ligand binding. Another situation that can lead to diminished binding affinity is imperfect steric fitting, which leads to holes at the protein–ligand interface.

The enthalpic and the entropic component of the binding affinity can be determined experimentally, for example, by isothermal titration calorimetry

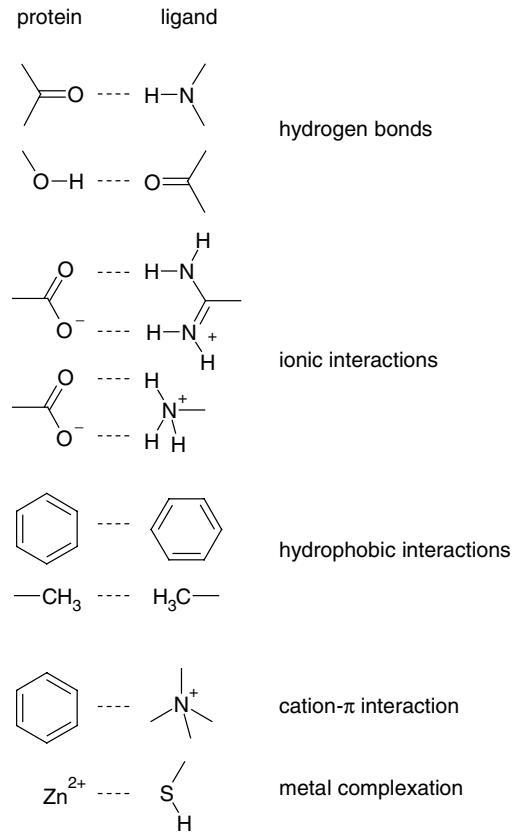


**Figure 1** Typical interactions found in protein–ligand complexes. Usually, the lipophilic part of the ligand is in contact with the lipophilic parts of the protein (side chains of Ile, Val, Leu, Phe, Trp, perpendicular contact to amide bonds). In addition, hydrogen bonds are often involved. Some interactions can be charge assisted. Cation–π interactions and metal complexation can also play a significant role in individual cases.

(ITC). Unfortunately, these data are still sparse and are difficult to interpret.[27] Existing thermodynamic data indicate that there is always a substantial compensation between enthalpic and entropic contributions.[28–30] The data also show that the binding may be enthalpy-driven (e.g., streptavidin–biotin, $\Delta G = -76.5\,\text{kJ/mol}, \Delta H = -134\,\text{kJ/mol}$) or entropy-driven (e.g., streptavidin–2-(4′-hydroxy-azobenzene)benzoic acid (HABA), $\Delta G = -22.0\,\text{kJ/mol}$, $\Delta H = +7.1\,\text{kJ/mol}$).[31] Data from protein mutants yield estimates of $5 \pm 2.5\,\text{kJ/mol}$ for the contribution from individual hydrogen bonds to the binding affinity.[32–34] Similar values have been obtained for the contribution of an intramolecular hydrogen bond to protein stability.[35–37] The consistency of experimental values derived from different proteins suggests some degree of additivity in the hydrogen-bonding interactions.

The contribution of hydrogen bonds to the binding affinity strongly depends on solvation and desolvation effects. Here lies the biggest challenge

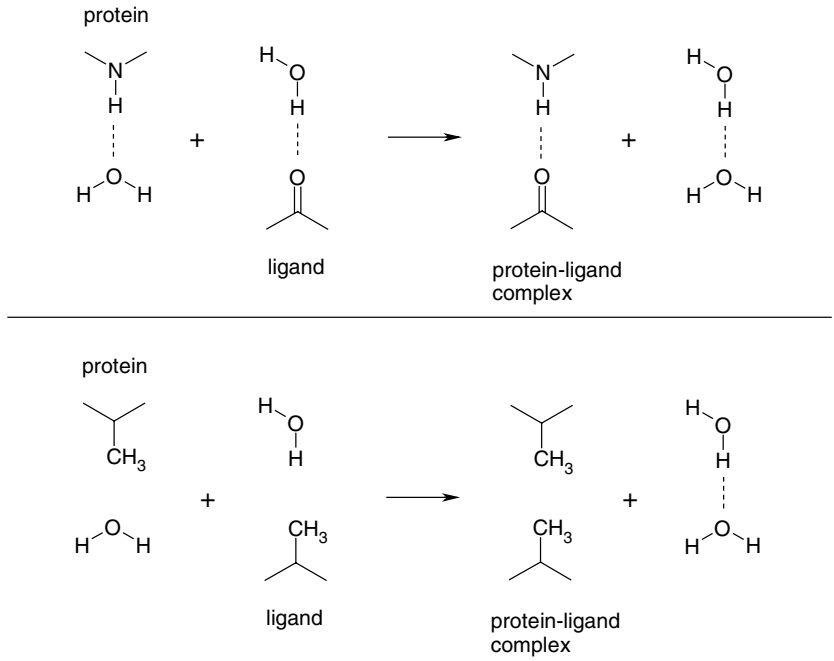


**Figure 2** Role of water molecules in hydrogen bonds (upper part) and lipophilic interactions (lower part). In the unbound state (left side), the polar groups of the ligand and the protein form hydrogen bonds to water molecules. These water molecules are replaced upon complex formation. The hydrogen-bond inventory (total number of hydrogen bonds) does not change. In contrast, the formation of lipophilic contact increases the total number of hydrogen bonds due to the release of water molecules from the unfavorable lipophilic environment.

in the quantitative treatment of protein–ligand interactions: providing an accurate description of the role of water molecules (Figure 2). It has been shown, by comparing the binding affinities of ligand pairs differing by just one hydrogen bond, that the existence of an individual hydrogen bond can even be adverse to binding.[38] Charge-assisted hydrogen bonds are stronger than neutral ones, but this enhancement in binding is paid for by higher desolvation penalties. The electrostatic interaction of an exposed salt bridge is worth as much as a neutral hydrogen bond ($5 \pm 1$ kJ/mol according to Ref. 39), and the same interaction in the interior of a protein can be significantly larger.[40]

The experimental determination of $\Delta H$ and $\Delta S$ sometimes yields surprising results, as, for example, in the thermodynamics of hydrogen-bond formation in the complex of FK506 or rapamycin with FK506-binding protein (FKBP).[34] Binding to the wild-type and to the mutant Tyr 82 $\rightarrow$ Phe 82 was

studied. From X-ray studies, it was known that the side chain hydroxyl of Tyr 82 forms a hydrogen bond with the ligand. If Tyr 82 is replaced by Phe, then one hydrogen bond is lost. As expected, the ligand-binding affinity was slightly reduced. The free enthalpy difference is $4 \pm 1.5$ kJ/mol. Somewhat unexpectedly, however, this destabilization is due to an entropy loss. In other words, the formation of this particular hydrogen bond is enthalpically unfavorable but entropically favorable. The entropy gain appears to be mainly due to the replacement of two water molecules by the ligand.[41]

Lipophilic interactions are essentially contacts between apolar parts of the protein and the ligand. The generally accepted view is that lipophilic interactions are mainly the result of the replacement and release of ordered water molecules and thus are entropy-driven processes.[42,43] The entropy gain is due to the fact that the water molecules are no longer positionally confined. There are also enthalpic contributions to lipophilic interactions. Water molecules occupying lipophilic binding sites are unable to form hydrogen bonds with the protein. If they are released, they can form strong hydrogen bonds with bulk water. It has been shown in many cases that the lipophilic contribution to the binding affinity is proportional to the lipophilic surface area buried from the solvent and typically has values in the range of 80–200 J/(mol Å$^2$).[44–46]

Conformational flexibility is another factor influencing the binding affinity. Usually, a ligand binds in a single conformation and therefore loses much of its conformational flexibility upon binding. Greater binding affinities have been observed for cyclic derivatives of ligands that otherwise adopt the same binding mode.[47,48] The entropic cost of freezing a single rotatable bond has been estimated to be 1.6–3.6 kJ/mol at 300 K.[49,50] Recent estimates derived from nuclear magnetic resonance (NMR) shift titrations of open-chain dications and dianions are much lower (0.5 kJ/mol),[51] but in those systems the conformational restriction may not have been as high as in a protein-binding site. The entropic cost of the external (translational and orientational) degrees of freedom has been estimated to be around 10 kJ/mol.[52,53]

In spite of many inconsistencies and difficulties in interpretation, most of the experimental data suggests that simple additive models for the protein–ligand interactions might be a good starting point for the development of empirical scoring functions. Indeed, the first published scoring functions were actually built based on experimental work that was published by about 1992, including studies on thermolysin[54] and vancomycin.[50,55]

Figure 3 summarizes some of the interactions that play a role in receptor–ligand binding. Binding involves a complex equilibrium between ensembles of solvated species. In the next section, we will discuss various approaches that are used to capture essential elements of this equilibrium in computationally efficient scoring functions. The discussion focuses on general approaches rather than individual functions. The reader is referred to Table 1 for original references to the most important scoring functions.[56–114]

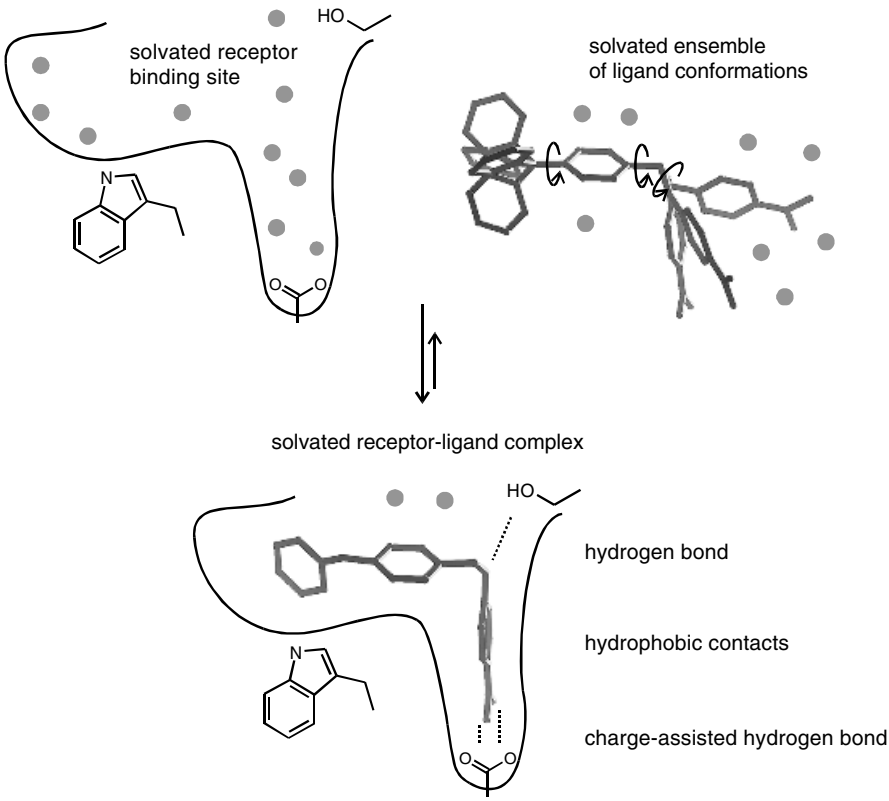


**Figure 3** Overview of the receptor–ligand binding process. All species involved are solvated by water (symbolized by gray spheres). The binding free energy difference between the bound and unbound state is a sum of enthalpic components (breaking and formation of hydrogen bonds, formation of specific hydrophobic contacts), and entropic components (release of water from hydrophobic surfaces to solvent, loss of conformational mobility of receptor and ligand).

## DESCRIPTION OF SCORING FUNCTIONS FOR RECEPTOR–LIGAND INTERACTIONS

A rigorous theoretical treatment of reversible receptor–ligand binding requires full consideration of all species involved in the binding equilibrium. In the unbound state, both the ligand and the receptor are separately solvated and do not interact. In the bound state, both partners are partially desolvated and form interactions with each other. Since it is the free energy of binding one is interested in determining, the energies of the solvated receptor, the solvated ligand, and the solvated complex should be calculated as ensemble averages.

**Table 1** Reference List for the Most Important Published Scoring Functions[a]

| Type of Function | Name | Year Published | Original References | Selected References to Applications |
|---|---|---|---|---|
| Empirical | | 1989–1993 | 115–117 | GRID[19] |
| | SCORE1 (the LUDI scoring function) | 1994 | 56 | LUDI[20,21], e.g. 57,58 |
| | | 1994 | 59 | FLOG[59] |
| | GOLD score | 1995 | 60, 61 | GOLD[60,61] |
| | PLP | 1995, 2000 | 62, 63 | |
| | FlexX score | 1996 | 64 | FlexX[64–67] |
| | VALIDATE | 1996 | 68 | |
| | | 1996 | 69 | Hammerhead[70] |
| | ChemScore | 1997 | 71 | 72 |
| | SCORE2 | 1998 | 73 | |
| | | 1998 | 74 | |
| | SCORE | 1998 | 75 | |
| | Fresno | 1999 | 76 | 77 |
| | ScreenScore | 2001 | 78 | |
| Desolvation terms | HINT | 1991 | 79 | 80 |
| | | 1997 | 81 | |
| Knowledge-based | SMOG | 1996 | 82 | SMOG[83] |
| | BLEEP | 1999 | 84, 85 | |
| | PMF | 1999 | 86 | 87–91 |
| | DrugScore | 2000 | 92 | 93 |
| Force field | AMBER | 1992 | 94 | DOCK[94–99] |
| | CHARMM | 1998 | 100 | |
| Force field + desolvation | | 1998 | 101 | |
| | | 1999 | 102 | |
| | AMBER + desolvation | 1999 | 103 | |
| | CHARMM + PB | 1999 | 104 | |
| | AMBER + desolvation | 1999 | 105 | |
| | MM PB/SA | 1999 | 106 | 107, 108 |
| Linear response simplified free energy perturbation | OWFEG[113] Grid | 1994 | 109 | 110–112 |
| | | 2001 | 114 | |

[a]Where force fields are used, the entry in "Original Reference" column refers to the use as a scoring function, not to the force field itself.

The appropriate statistical mechanics treatment has been reviewed elsewhere[118] and is not the topic of this chapter. Large-scale Monte Carlo or molecular dynamics (MD) simulations are necessary to derive reasonably accurate values of binding free energies. These computational methods are only suitable for small sets of compounds, since they require large amounts of computational resources. Moreover, even the most advanced techniques are reliable only for calculating binding free energy differences between closely related ligands.[119–122] However, a number of less rigorous but faster scoring schemes have been developed that should be amenable to larger numbers of ligands. For example, recent experience has shown that continuum solvation models can replace explicit solvent molecules, at least in the final energy evaluation of the simulation trajectory.[123] Another less expensive alternative for computing binding free energies is the use of linear reponse theory[109,110] in conjunction with a surface term.[112]

Scoring functions that can be evaluated quickly enough to be practical in docking and virtual screening applications are very crude approximations to the free energy of binding. They usually take into account only one receptor–ligand complex structure and disregard ensemble averaging and properties of the unbound state of the binding partners. Furthermore, all scoring methods have in common the fact that the free energy is obtained from a sum of terms. In a strict physical sense, this is not possible, since the free energy of binding is a state function, but its components are not.[124] Furthermore, simple additive models cannot describe subtle cooperativity effects.[125] Nevertheless, it is often useful to interpret receptor–ligand binding in an additive fashion,[126–128] and estimates of binding free energy are available in this way at very low computational cost. Fast scoring functions can be categorized into three main classes: (1) force field-based methods, (2) empirical scoring functions, and (3) knowledge-based methods. Each of these is now discussed.

## Force Field-Based Methods

An obvious idea to circumvent parameterization efforts for scoring is to use nonbonded energies of existing, well-established molecular mechanics force fields for the estimation of binding affinity. In doing so, one substitutes estimates of the free energy of binding in solution by an estimate of the gas-phase enthalpy of binding. Even this crude approximation can lead to satisfying results. A good correlation was obtained between nonbonded interaction energies calculated with a modified MM2 force field and $IC_{50}$ values of 33 inhibitors of human immunodeficiency virus (HIV)-1 protease.[129] Similar results were reported in a study of 32 thrombin–inhibitor complexes with the CHARMM force field.[130] In both studies, however, experimental data represented rather narrow activity ranges and little structural variation.

The AMBER[131,132] and CHARMM[133] nonbonded terms are used as a scoring function in several docking programs. Protein terms are usually

precalculated on a cubic grid, such that for each ligand atom only the interactions with the closest grid points have to be evaluated.[94] This leads to an increase in speed of about two orders of magnitude compared to traditional atom-by-atom evaluation. Distance-dependent dielectric constants are usually employed to approximate the long-range shielding of electrostatic interactions by water.[100] However, compounds with high formal charges still obtain unreasonably high scores due to overestimated ionic interactions. For this reason, it has been common practice in virtual screening to separate databases of compounds into subgroups according to their total charge and then to rank these groups separately.

When electrostatic interactions are complemented by a solvation term calculated by the Poisson–Boltzmann equation[134] or faster continuum solvation models (as in Ref. 135), the deleterious effects of high formal charges are diminished. In a validation study on three protein targets, Shoichet et al.[103] observed a significantly improved ranking of known inhibitors after correction for ligand solvation. The current version of the docking program DOCK calculates solvation corrections based on the generalized Born[136] solvation model.[105] The method has been validated in a study where several peptide libraries were docked into various serine protease active sites.[137]

In the context of scoring, the van der Waals term of force fields is mainly responsible for penalizing docking solutions with steric overlap between receptor and ligand atoms. The term is often omitted when only the binding of experimentally determined complex structures is analyzed.[102,138,139]

A recent addition to the list of force field-based scoring methods has been developed by Charifson and Pearlman. Their so-called OWFEG (one window free energy grid) method[114] is an approximation to the expensive first-principles method of free energy perturbation (FEP).[140] For the purpose of scoring, an MD simulation is carried out with the ligand-free, solvated receptor site. The energetic effects of probe atoms on a regular grid are collected and averaged during the simulation. Three simulations are run with three different probes: a neutral methyl-like atom, a negatively charged atom, and a positively charged atom. The resulting three grids contain information on the score contributions of neutral, positively, and negatively charged ligand atoms located in various positions of the receptor site and can thus be used in a straightforward manner for scoring. The OWFEG approach seems to be successful for $K_i$ prediction as well as for virtual screening applications.[113] Its conceptual advantage is the implicit consideration of entropic and solvent effects and the inclusion of some protein flexibility in the simulations.

The calculation of ligand strain energy traditionally lies in the realm of molecular mechanics force fields. Although effects of strain energy have rarely been determined experimentally,[141] it is generally accepted that high-affinity ligands bind in low-energy conformations.[142,143] If a compound must adopt a strained conformation to fit into a receptor pocket, a less negative binding free energy should result. Strain energy can be estimated by calculating the

difference in conformational energy between the global minimum structure and the current conformation of the ligand in the complex. However, force field estimates of energy differences between individual conformations are not reliable for all systems. In practice, better correlations with experimental binding data are obtained when strain energy is used as a filter to weed out unlikely binding geometries rather than when strain energy is added to the final score. Estimation of ligand strain energy based on force fields can be time consuming, and so alternatives such as empirical rules derived from small-molecule crystal structure data are often employed.[144] Conformations generated by such programs are, however, often not strain free, because only one torsional angle is treated at a time. Some strained conformations can be excluded when two consecutive dihedral angles are simultaneously taken into account, however.[78]

## Empirical Scoring Functions

The underlying idea of empirical scoring functions is that the binding free energy of a noncovalent receptor–ligand complex can be interpreted as a sum of localized, chemically intuitive interactions. Such energy decompositions can be a useful tool to understand binding phenomena even without analyzing 3D structures of receptor–ligand complexes. Andrews, Craik, and Martin[126] calculated average functional group contributions to binding free energy from a set of 200 compounds whose affinity to a receptor had been experimentally determined. These average functional group contributions can then be used to estimate a receptor-independent binding energy for a compound that can be compared to experimental values. If the experimental value is approximately the same as or higher than the calculated value, one can infer a good fit between receptor and ligand and essentially all functional groups of the ligand are involved in protein interactions. If the experimental energy is significantly lower, one can infer that the compound can not fully form its potential interactions with the protein. Experimental binding affinities have also been analyzed on a per atom basis in quest of the maximal binding affinity of noncovalent ligands.[145] It was concluded that for the strongest binding ligands, each nonhydrogen atom on average contributes 1.5 kcal/mol to the total binding energy.

With 3D structures of receptor–ligand complexes at hand, the analysis of binding phenomena can of course be much more detailed. The binding affinity $\Delta G_{\text{binding}}$ can be estimated as a sum of interactions multiplied by weighting coefficients $\Delta G_i$

$$\Delta G_{\text{binding}} \approx \sum_i \Delta G_i f_i(r_l, r_p) \qquad [2]$$

where each $f_i$ is a function of the ligand coordinates $r_l$ and the protein receptor coordinates $r_p$, and the sum is over all atoms in the complex. Scoring schemes

that use this concept are called "empirical scoring functions." Several reviews summarize details of individual parameterizations.[17,146–151] The individual terms in empirical scoring functions are usually chosen so as to intuitively cover important contributions of the total binding free energy. Most empirical scoring functions are derived by evaluating the functions $f_i$ for a set of protein–ligand complexes and fitting the coefficients $\Delta G_i$ to experimental binding affinities of these complexes by multiple linear regression or by supervised learning techniques. The relative weight of the individual contributions depends on the training set. Usually, between 50 and 100 complexes are used to derive the weighting factors, but in a recent study it was shown that many more than 100 complexes were needed to achieve convergence.[75] The reason for this large number is probably due to the fact that the publicly available protein–ligand complexes fall in a few heavily populated classes of proteins, such that in small sets of complexes few interaction types dominate.

Empirical scoring functions usually contain individual terms for hydrogen bonds, ionic interactions, hydrophobic interactions, and for binding entropy. Hydrogen bonds are typically scored by simply counting the number of donor–acceptor pairs falling within a given distance and angle range considered to be favorable for hydrogen bonding, weighted by penalty functions for deviations from preset ideal values.[56,71,73] The amount of error-tolerance in these penalty functions is critical to the success of scoring methodology. When large deviations from ideality are tolerated, the scoring function may be unable to discriminate between different orientations of a ligand. Contrarily, small tolerances lead to situations where many structurally similar complex structures result in very similar scores. Attempts have been made to reduce the localized nature of such interaction terms by using continuous modulating functions on an atom-pair basis.[69] Other workers have avoided the use of penalty functions altogether and introduced separate regression coefficients for strong, medium, and weak hydrogen bonds.[75] For example, at Agouron a simple four-parameter potential, which is called the piecewise linear potential (PLP), was developed that is an approximation of a potential well without angular terms.[62] Most empirical scoring functions treat all types of hydrogen-bond interactions equally, but some attempts have been made to distinguish between different donor–acceptor functional group pairs. Hydrogen-bond scoring in the docking program GOLD,[60,61] for example, is based on a list of hydrogen-bond energies for all combinations of 12 defined donor and 6 acceptor atom types derived from ab initio calculations of model systems incorporating those atom types. A similar differentiation of donor and acceptor groups is made in the hydrogen-bond functions in the program GRID,[152] a program commonly used for the characterization of binding sites.[115–117] The inclusion of such lookup tables in scoring functions is presumed to avoid errors originating from the oversimplification of individual interactions.

Reducing the weight of hydrogen bonds formed at the outer surface of the binding site is a useful measure for reducing the number of false positive

hits in virtual screening applications. Reducing the weight can be done by reducing charges of surface residues when explicit electrostatic terms are used[100] or by multiplying the hydrogen-bond by a factor that depends on the accessibility of the protein-bonding partner[91] in empirical scoring functions.

Ionic interactions are treated in a similar manner as hydrogen bonds. Long-distance charge–charge interactions are usually disregarded, and so it is more appropriate to refer to salt bridges or charged hydrogen bonds here. The SCORE1 function by Boehm implemented in LUDI[56] gives greater weight to salt bridges than to neutral hydrogen bonds. This function was found to be useful in scoring several series of thrombin inhibitors.[57,72] But just as with force field scoring functions, this weighting introduces the danger of giving unreasonably high scores to highly charged molecules. Our experience with the docking program FlexX,[64–67] which contains a variant of SCORE1 (the LUDI scoring function), has been that better results are generally obtained when charged and uncharged hydrogen are treated equally in virtual screening applications. This observation is also the case for the ChemScore function by Protherics.[71]

Hydrophobic interaction energies are usually estimated by the size of the contact surface at the receptor–ligand interface. A reasonable correlation between experimental binding energies can often be achieved with a surface term alone (see, e.g., Refs. 24,153,154 and the discussion in the earlier section on Major Contributions to Protein–Ligand Interactions). Various approximations for surface terms have been used, such as grid-based methods[56] and volume-based methods (see especially the discussion in Ref. 101). Many functions employ distance-scaled sums over neighboring receptor–ligand atom pairs. Distance cutoffs for these functions have been chosen to be short[64] or to be longer to include atom pairs that do not form direct van der Waals contacts.[62,71] The assignment of the weighting factor $\Delta G_i$ for the hydrophobic term depends strongly on the training set. Its value might have been underestimated in most derivations of empirical scoring functions,[155] because most training sets contain an overly large proportion of ligands containing an excessive number of donor and acceptor groups (many peptide and carbohydrate fragments).

In most existing empirical scoring functions, a number of atom types are defined as being hydrophobic, and all their contributions are treated in the same manner. Alternatively, the propensity of specific atom types to be located in the solvent or in the interior of a protein can be assessed by so-called "atomic solvation parameters" that can be derived from experimental data such as octanol–water partition coefficients[156,157] or from structural data.[81,158] Atomic solvation parameters are used in the VALIDATE scoring function,[68] and they have been tested in DOCK.[80] Entropy terms in empirical scoring functions account for the restriction of conformational degrees of freedom of the ligand upon complex formation. A crude but useful estimate of this entropy contribution is the number of freely rotatable bonds of a ligand.

This simple measure has the advantage of being a function of the ligand only.[56,73] Since it is argued that purely hydrophobic contacts allow more residual motion in the ligand fragments, more elaborate estimates try to take into account the nature of each ligand fragment on either side of a flexible bond and the interactions they form with the receptor.[68,71] Such penalty terms are also robust with respect to the distribution of rotatable bonds in the ligands of the training set, but they offer little or no advantage in the virtual screening of compound databases. The group at Agouron has further used an entropy penalty term that is proportional to the score[159] to account for entropy–enthalpy compensation.[28–30,160]

## Knowledge-Based Methods

Empirical scoring functions "see" only those interactions that are part of the model. Many less common interactions are usually disregarded, even though they can be strong and specific, as exemplified, for example, by NH–π hydrogen bonds. It would become a difficult task to generate a comprehensive and consistent description of all these interactions within the framework of empirical scoring functions. But there exists a growing body of structural data on receptor–ligand complexes that can be used to detect favorable binding geometries. "Knowledge-based" scoring functions try to capture the knowledge about receptor–ligand binding hidden in the Protein Data Bank[161] (PDB) by means of statistical analysis of structural data alone—and they do so without referring to inconsistent experimentally determined binding affinities.[162] They have their foundation in the inverse formulation of the Boltzmann law:

$$E_{ij} = -kT \ln(p_{ijk}) + kT \ln(Z) \qquad [3]$$

The energy function $E_{ij}$ is called a potential of mean force for a state defined by three variables $i, j$, and $k$; $p_{ijk}$ is the corresponding probability density, and $Z$ is the partition function. The second term of Eq. [3] is constant at constant temperature $T$ and does not need to be considered, because $Z = 1$ can be chosen by definition of a suitable reference state leading to normalized probability densities $p_{ijk}$. The inverse Boltzmann technique has been applied to derive potentials for protein folding from databases of protein structures.[163] For the purpose of deriving scoring functions, the variables $i, j$, and $k$ are chosen to be protein atom types, ligand atom types, and their interatomic distance. The frequency of occurrence of individual contacts is presumed to be a measure of their energetic contribution to binding. When a specific contact occurs more frequently than that from a random or average distribution, this indicates an attractive interaction. When it occurs less frequently, it is interpreted as being a repulsive interaction between those two atom types. The frequency

distributions for a data set of interacting molecules can thus be converted to sets of atom-pair potentials that are straightforward to evaluate.

The first applications of knowledge-based scoring functions in drug research[164–166] were restricted to small data sets of HIV protease–inhibitor complexes and did not result in generally applicable scoring functions. Recent publications[82–86,92,93] have shown that useful general scoring functions can be derived with this method. The de novo design program SMoG[82,83] contained the first general-purpose implementation of such a potential.

The "PMF" function by Muegge[86] consists of a set of distance-dependent atom-pair potentials $E_{ij}(r)$ that are written as

$$E_{ij}(r) = -kT \ln[f_j(r)\rho^{ij}(r)/\rho^{ij}] \quad [4]$$

Here, $r$ is the atom pair distance, and $\rho^{ij}(r)$ is the number density of pairs ij that occur in a given radius range around $r$. The term $\rho^{ij}$ in the denominator is the average density of receptor atoms j in the whole reference volume. The number density is calculated in the following manner. A maximum search radius is defined. This radius describes a reference sphere around each ligand atom j, in which receptor atoms of type i are searched, and which is divided into shells of a specified thickness. The number of receptor atoms i found in each spherical shell is divided by the volume of the shell and averaged over all occurrences of ligand atoms i in the database of protein–ligand complexes. Muegge argues that the spherical reference volume around each ligand atom needs to be corrected by eliminating the volume of the ligand itself, because ligand–ligand interactions are not regarded. This correction is done by the volume correction factor $f_j(r)$ that is a function of the ligand atom only and gives a rough estimate of the preference of atom j to be solvent exposed rather than buried within the binding pocket. Muegge could show that the volume correction factor contributes significantly to the predictive power of the PMF function.[90] Also, a relatively large reference radius of at least 7–8 Å must be applied to implicitly include solvation effects, particularly the propensity of individual atom types to be located inside a protein cavity or in contact with solvent.[89] For docking calculations, the PMF scoring function is evaluated in a grid-based manner and combined with a repulsive van der Waals potential at short distances and minima extended slightly toward shorter distances.

The DrugScore function created by Gohlke, Hendlich, and Klebe[92] is based on roughly the same formalism, albeit with several differences in the derivation leading to different potential forms. Most notably, the statistical distance distributions $\rho^{ij}(r)/\rho^{ij}$ for the individual atom pairs ij are divided by a common reference state that is simply the average of the distance distributions of all atom pairs $\rho(r) = \sum_i \sum_j \rho^{ij}(r)/i_{max}\, j_{max}$, where the product in the denominator yields the total number of pair functions. Furthermore, no

volume correction term is used, and the sampling cutoff (the radius of the reference sphere) is set to only 6 Å. The individual potentials have the form

$$E_{ij}(r) = -kT(\ln[\rho^{ij}(r)/\rho^{ij}] - \ln[\rho(r)]) \quad [5]$$

The pair potentials in Eq. [5] are used in combination with other potentials, depending on one (protein or ligand) atom type only, that express the propensity of an atom type to be buried within a lipophilic protein environment upon complex formation. Contributions of these surface potentials and the pair potentials are weighted equally in the final scoring function. DrugScore was developed with the aim of differentiating between correctly docked ligand structures versus decoy (arbitrarily placed) structures for the same protein–ligand pair.

A different type of reference state was chosen by Mitchell et al.[85] The pair interaction energy is written as

$$E_{ij}(r) = kT\ln[1 + m^{ij}\sigma] - kT\ln[1 + m^{ij}\sigma\rho^{ij}(r)/\rho(r)]$$

Here, the number density $\rho^{ij}(r)$ is defined as in Eq. [4], but it is normalized by the number density of all atom pairs at this same distance instead of by the number of pairs ij in the whole reference volume. The variable $m^{ij}$ is the number of atom pairs ij found in the data set of protein–ligand complexes, and $\sigma$ is an empirical factor that defines the weight of each observation. This potential is combined with a van der Waals potential as a reference state to compensate for the lack of sampling at short distances and for certain underrepresented atom pairs. Apart from data on 90 protein–ligand complexes used in the original validation, no further application has been published.

## CRITICAL ASSESSMENT OF CURRENT SCORING FUNCTIONS

### Influence of the Training Data

All fast scoring functions share a number of deficiencies that one should be aware of for any application. First, most scoring functions are in some way fitted to or derived from experimental data. The resulting functions necessarily reflect the accuracy of the data that were used in their derivation. A general problem with empirical scoring functions is the fact that the experimental binding energies are compiled from many different sources and therefore form inconsistent data sets containing systematic experimental errors. Scoring functions not only reflect the quality, but also the type of experimental data on which they are based. Most scoring functions are still derived from data on mostly high-affinity receptor–ligand complexes. Moreover, many of these

structures are peptidic in nature, whereas interesting lead molecules in pharmaceutical research are usually nonpeptidic. This influence of peptides is reflected in the relatively high contributions of hydrogen bonds in the total score. The balance between hydrogen bonding and hydrophobic interactions is a critical issue in scoring, and its consequences are especially obvious in virtual screening applications, as will be illustrated in the later section on Hydrogen Bonding versus Hydrophobic Interactions.

## Molecular Size

The simple additive nature of most fast scoring functions often leads to large molecules being assigned high scores. Although it is true that small molecules with a molecular weight below 200–250 are rarely of very high affinity, there is no guarantee that larger compounds are more active. When it comes to comparing scores of two compounds of different size, it therefore makes sense to include a penalty term that diminishes the dependence of the score on molecular size. In some applications, a constant penalty value has been added to the score for each heavy atom.[167] Alternatively, a penalty term proportional to the molecular weight has been used.[168] The scoring function of the docking program FLOG, which contains force field and empirical terms, has been normalized to remove the linear dependence of the crude score on the number of ligand atoms that was found in a docking study of a 7500 compound database.[59] Entropy terms designed to estimate the restriction of conformational mobility upon ligand binding also help to eliminate overly large and flexible molecules, although they were originally introduced to improve the correlation between experimental and calculated affinities.[56,71] The size of the solvent-accessible surface of the ligand within the protein-binding pocket is also a useful penalty term because it helps avoid excessively large ligands that cannot fit completely into the binding site. Note, however, that all these approaches are very pragmatic in nature and do not solve the problem of size dependence, which is closely linked to the understanding of cooperativity effects.[125]

## Other Penalty Terms

Scoring functions in general reward certain favorable interactions such as hydrogen bonds, but rarely penalize unfavorable interactions. Since scoring functions are derived from experimentally determined crystal structures, "unnatural" and energetically unfavorable orientations of a ligand within the receptor cavity are rarely observed and therefore cannot be accounted for by the scoring function. Knowledge-based scoring functions try to capture such effects indirectly by making those interactions repulsive that are not observed in crystal structures. It seems, however, that the statistical difference

between what is not observed and what is to be expected on average is often not significant enough to form reliable repulsive interactions. Furthermore, the neglect of angular terms in the derivation of knowledge-based scoring functions leads to average pair potentials that cannot discriminate well enough between different binding geometries.

In the derivation of regression-based empirical scoring schemes, on the other hand, penalty terms have traditionally not been included. However, some situations like obvious electrostatic and steric clashes can be avoided by guessing reasonable penalty terms or by importing them from molecular mechanics force fields. An example of this is the "chemical scoring" function available in the docking program DOCK.[94–99] This function is a modified van der Waals potential made to be attractive or repulsive between particular groups of donor, acceptor, and lipophilic receptor atoms and ligand atoms.[169,170] Other unacceptable binding orientations cannot be avoided by simple clash terms, but instead require a more refined analysis of binding geometry. Among the causes for poor results are an imperfect steric fit of the ligand within the cavity, an unnaturally high degree of solvent-accessible ligand surface in the complex or the formation of voids at the receptor–ligand interface. Possible remedies are empirical filters that measure such fit parameters and remove docking solutions above a user-specified threshold.[171] A promising approach along these lines is the inclusion of artificially generated, erroneous, decoy solutions in the optimization of scoring functions. In the process of deriving weights for individual terms of the scoring function, the decoy solutions should always obtain lower ranks than the correct solutions, and thus suitable penalty terms could be derived automatically. Such a procedure was first reported for the scoring function of a flexible ligand superposition algorithm.[172,173]

## Specific Attractive Interactions

Another general deficiency of scoring functions stems from the simplified description of attractive interactions. Molecular recognition is not based only on classical hydrogen bonds and hydrophobic contacts. Many researchers, especially those active in host–guest chemistry, are making use of other specific types of interactions. For example, hydrogen bonds that are formed between acidic protons and $\pi$ systems.[174] These bonds can substitute for conventional hydrogen bonds in both strength and specificity, as has been noted, for example, in protein–DNA recognition[175] and as can be observed in serine protease complexes deposited in the PDB.[161] Another class of "unconventional" interactions is the cation–$\pi$ interaction, which is especially important at the surface of proteins.[176,177] Current empirical scoring functions do not model these interactions and mostly disregard the directionality of, for example, interactions between aromatic rings.[178,179] In the derivation of empirical scoring functions, one thus implicitly attributes some of the binding energy arising

from these interactions to conventional interaction terms, which may be one more reason why conventional hydrogen-bond contributions have traditionally been overestimated. One could imagine adding terms to empirical scoring functions that are omitted in the calibration of the functions, but adjusted empirically to reward especially good fits, in a way analogous to penalty terms. Knowledge-based methods would also allow one to incorporate these interactions in a scoring function, again provided that directionality is taken into account, which is not the case in current approaches.

## Water Structure and Protonation State

Uncertainties about protonation states and water structure at the receptor–ligand interface also make scoring difficult. These effects play a role in the derivation as well as in the application of scoring functions. The entropic and energetic contributions of water reorganization upon ligand binding are very difficult to predict (see, e.g., Ref. 180). The only reasonable approach for addressing this problem is to concentrate on conserved water molecules and make them part of the receptor. For example, the docking program FLOG has been applied to the search of inhibitors for a metallo-β-lactamase[13] within the Merck in-house database. Docking was performed with three different configurations of bound water in the active site. The top-scoring compounds showed an enrichment in biphenyl tetrazoles, several of which were found to be active at a concentration below 20 μM. A crystal structure of one tetrazole ($IC_{50} = 1.9\,\mu M$) not only confirmed the predicted binding mode of one of the inhibitors, but also displayed the water configuration that had—retrospectively—been the most predictive one of the three models.

Scoring functions rely on a fixed assignment of a general atom type to each protein and ligand atom. This also implies a fixed assignment of protonation state for each acidic and basic functional group. Even though these assignments can be reliable enough for conditions in aqueous solution, significant $pK_a$ shifts can be witnessed upon ligand binding.[181] This phenomenon can arise from local changes of dielectric conditions inside the binding pocket. The change of a donor to an acceptor functionality due to modified protonation states has important consequences for scoring.[137] Accordingly, improved docking and scoring algorithms will eventually need to have a more detailed and flexible description of protonation states.

## Performance in Structure Prediction

The multitude of different solutions that have been used for receptor–ligand scoring calls for an objective assessment that could help future users to decide which function to use under a given set of circumstances. To do this, one must differentiate between predicting protein–ligand complex structures

(i.e., the scoring function is used as the objective function in docking), rank ordering a set of ligands with respect to the same protein ($K_i$ prediction), and the use of scoring functions to discover weakly binding compounds from a large database of mostly nonbinders (virtual screening). Note that the latter two tasks are indeed very different. In virtual screening, the focus is on elimination of nonbinders, whereas the correct rank order of weakly, medium, and strongly binding molecules is of secondary interest.

Even when the criteria are clear, a comprehensive assessment of scoring functions is difficult because very few functions have been tested on the same data sets. For example, studies where each scoring function is used in conjunction with two different docking algorithms (e.g., Ref. 170) are not meaningful in this context, because each docking algorithm produces different sets of solution structures. For structure prediction, several studies have shown that knowledge-based scoring functions are at least as good as empirical functions. They are somewhat "softer" than empirical functions,[162] meaning that small root-mean-square deviations from the crystal structure usually do not lead to huge changes in score, a fact that can mainly be attributed to the neglect of directionality. The PMF function has been successfully applied to structure prediction of inhibitors of neuraminidase[88] and stromelysin 1 (matrix metalloprotease-3; MMP-3)[182] in the program DOCK, yielding superior results to the DOCK force field and chemical scoring options. The DrugScore function was tested on a large set of PDB complexes and gave significantly better results than the standard FlexX scoring function with FlexX as the docking engine. DrugScore performed as well as the force field score in DOCK, but outperformed chemical scoring. Grueneberg, Wendt, and Klebe[15] used the DrugScore function in a virtual screening study to find novel carbonic anhydrase inhibitors (see the section on Application of Scoring Functions in Virtual Screening later in this chapter). Two of the virtual hits that turned out to be highly active compounds were then examined crystallographically. The docking solution predicted by DrugScore was closer to the experimental structure than that predicted by the FlexX score.

Although the objective function (the function whose global minimum is searched during docking) is used for both structure generation and energy evaluation in many docking programs, better results can often be obtained if different functions are used. More specifically, the docking objective function can be adapted to the docking algorithm used. In a parameter study, Vieth et al.[100] found that by using a soft-core van der Waals potential their MD-based docking algorithm became more efficient. Using FlexX as the docking engine, we observed that when directed interactions (mostly hydrogen bonds) are emphasized in the docking phase, library ranking can be done successfully with the more simple, undirected PLP potential (see the prior section on Empirical Scoring Functions) that emphasizes the general steric fit of receptor and ligand. Results are significantly worse when PLP is used for both docking and energy evaluation.

### Rank Ordering Sets of Related Ligands

For structure prediction, structures of protein–ligand complexes from the PDB can serve as a common pool to test scoring functions. It is more difficult to draw valid conclusions about the relative performance of scoring functions to rank order sets of ligands with respect to their binding to the same target. First, there are few published studies in which different functions have been applied to the same data sets. Second, experimental data are often not measured under the same conditions but collected from various literature references. The latter practice can have especially dramatic effects when inhibitory concentrations for 50% reduction of a biological effect ($IC_{50}$ data) are used instead of $K_i$ values.

On average, empirical scoring functions seem to lead to better correlations between experimental and calculated binding energies than do force field based approaches because the nonbonded interactions in the latter are usually not optimized to reproduce individual intermolecular binding phenomena. However, the only available calculated data for most published functions are those for the complexes used in the derivation of the functions themselves. Very promising results of rank ordering have also been obtained with the knowledge-based functions DrugScore[93] and PMF.[86,88,182]

The task of rank ordering small (ca. 10–100) sets of related ligands with respect to a target can also be accomplished with methods that are computationally more demanding than simple scoring functions. The most generally applicable methods are probably force field scores augmented with electrostatic desolvation and surface area terms. An example is the MM–PBSA method that combines Poisson–Boltzmann electrostatics with AMBER MD calculations.[183] This method has been applied to an increasing number of studies, and it has led to promising results.[106–108,184] Poisson–Boltzmann calculations have been performed on a variety of targets with many related computational protocols.[102,138,139,185–188] Alternatively, extended linear response protocols[112] can be used. The OWFEG grid method by Pearlman has also shown promising results.[114]

## APPLICATION OF SCORING FUNCTIONS IN VIRTUAL SCREENING

In recent years, virtual screening of large databases has emerged as the central application of scoring functions. In the following sections, we describe special requirements that scoring functions must fulfill for successful virtual screening, and we indicate the level of accuracy that can nowadays be expected from virtual screening.

As discussed in the introductory sections, the goal of virtual screening is to use computational tools together with the known 3D structure of the target to select a subset of compounds from chemical libraries for synthesis and

biological testing. This subset typically consists of ca. 100–2000 compounds selected from libraries containing 100,000–500,000 compounds. Therefore, it is essential that the computational process including the scoring function is fast enough to handle several thousand compounds in a short period of time. Consequently, only the fastest scoring functions are currently used for this purpose. Speed is especially important for those scoring functions used as objective functions during the docking calculations, since they are evaluated several hundred to a thousand or so times during the docking process of a single compound.[18]

Following a successful virtual screening run, the selected subset of compounds contains a significantly enhanced number of active compounds as compared to a random selection. A key parameter to measure the performance of docking and scoring methods is the so-called "enrichment factor." It is simply the ratio of active compounds in the subset selected by docking divided by the number of active compounds in a randomly chosen subset of equal size. In practice, enrichment factors are far from the ideal case, where all active compounds are placed on the top ranks of a prioritized list. Insufficiencies of current scoring functions, as discussed in the previous section, are partly responsible for moderate enrichment rates. Another major reason is the fact that the receptor is still treated as a rigid object in the computational protocols being used. To generate correct binding modes of different molecules, it is necessary to predict induced fit phenomena. Unfortunately, predicting protein flexibility remains extremely difficult and computationally expensive.[189–196]

## Seeding Experiments

Enrichment factors can be calculated only when experimental data are available for the full library. But only a few libraries containing experimental data that have been measured under uniform conditions for all members are available to the public. Several authors have therefore tested the predictive ability of docking and scoring tools by compiling an arbitrarily selected set of diverse, drug-like compounds and then adding to it a number of known active compounds. This "seeded" library is then subjected to the virtual screen, and, for the purpose of evaluation, it is assumed that the added active compounds are the only true actives in the library. Several such experiments have been published. An example is a study performed at Merck with the docking program FLOG.[59] A library consisting of 10,000 compounds including inhibitors of various types of proteases and HIV protease was docked into the active site of HIV protease. This resulted in excellent enrichment of the HIV protease inhibitors: all inhibitors but one were among the top 500 library members. However, inhibitors of other proteases were also considerably enriched.[197]

Seeding experiments allow for comparisons of different scoring functions with respect to their performance for different targets. Seeding experiments

also teach how to recognize typical failure cases. Recent examples of library ranking experiments include those by Charifson et al.,[198] Bissantz, Folkers, and Rognan,[77] and Stahl and Rarey.[78] Charifson and co-workers compiled sets of several hundred active molecules for three different targets: p38 MAP kinase, inosine monophosphate dehydrogenase, and HIV protease. The members of these sets were then docked into the corresponding active sites together with 10,000 randomly chosen, but drug-like, commercial compounds using DOCK[98] and the Vertex in-house docking tool Gambler. Three scoring functions performed consistently well in enriching active compounds, namely, ChemScore,[71,199] the DOCK AMBER force field score, and PLP.[62] The finding that these three scoring functions performed so well was partially attributed to the fact that a rigid-body optimization could be carried out with these functions, because the functions include repulsive terms in contrast to many of the other tested functions. The study by Stahl and Rarey[78] compared the performance of DrugScore[92] and PMF[86] to that of PLP[62] and FlexX score using the docking program FlexX.[64–66] Interestingly, the two knowledge-based scoring functions showed significantly different behavior for extreme cases of active sites. DrugScore coped well with situations where ligands are tightly bound in narrow lipophilic cavities (e.g., COX-2 and the thrombin S1 pocket), whereas PMF did not lead to good enrichment in such cases. Conversely, for the very polar binding site of neuraminidase, PMF gave better enrichment than any other scoring function, whereas DrugScore failed. The description of complexes in which many hydrogen bonds play a role seems to be a general strength of PMF. This has also been noted by Bissantz, Folkers and Rognan,[77] who found PMF to perform well for the polar target thymidine kinase and less well for the estrogen receptor.

## Hydrogen Bonding versus Hydrophobic Interactions

It is of central importance in virtual screening to achieve a balanced description of hydrogen bonding and hydrophobic contributions to the score in order to avoid a bias toward either highly polar or completely hydrophobic molecules. Empirical scoring functions have the advantage that they can be quickly reparameterized to achieve such a balance, whereas such an adjustment is impossible with knowledge-based functions. Because this is such an important topic, we will illuminate it with a number of examples.

Consider the following database ranking experiment. A database of about 7600 compounds was flexibly docked into the ATP binding site of p38 MAP kinase. The database consisted of ca. 7500 random compounds from the World Drug Index (WDI)[200] and 72 inhibitors of p38 MAP kinase, which in turn consisted of 30 inhibitors forming two hydrogen bonds with the receptor and 20 inhibitors forming only one. Both groups covered the same activity range from low micromolar (μM) to about 10 nM. For each of the docked compounds, up to 800 alternative docking solutions were

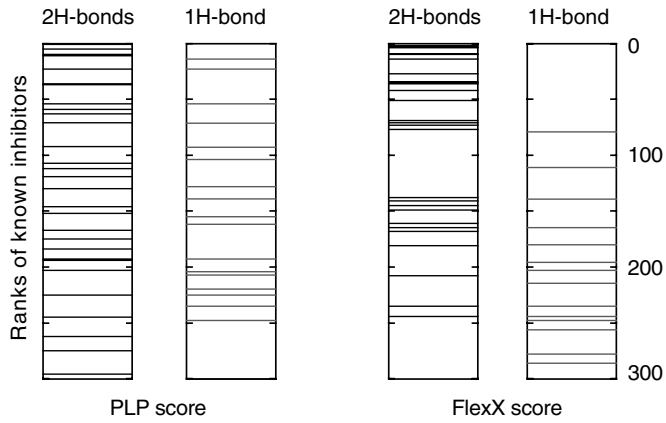


**Figure 4** Results of a seeding experiment. The ranks of known p38 MAP kinase inhibitors are shown as horizontal lines in the four diagrams. Inhibitors have been divided into two classes: those forming one or two hydrogen bonds to the p38 MAP kinase ATP binding site. The FlexX scoring function preferentially enriches those inhibitors that form two hydrogen bonds. This tendency is less pronounced for the PLP scoring function. The inhibitors with the best predicted affinities are at the top. Data is shown for the top 300 compounds in terms of docking scores.

generated by FlexX[64–66] using the FlexX scoring function. These alternative solutions were rescored separately by the FlexX and PLP[62] scoring functions to select the lowest energy docking solution per compound. The compounds in the database were then ranked according to these scores. Figure 4 shows the ranks of the known inhibitors among the top 350 compounds as calculated by both scoring functions. Although the overall performance of both scoring functions in enriching inhibitors is comparable, it is obvious that the FlexX score ''specializes'' on the doubly hydrogen-bonded inhibitors. On the other hand, if one were to select screening candidates from the PLP list, one would most likely select both types of inhibitors.

The PLP function generally emphasizes steric complementarity and hydrophobic interactions with its more far-reaching pair potential, whereas the FlexX score emphasizes hydrogen-bond complementarity. A combination of PLP and FlexX scoring functions called ScreenScore was published recently.[78] It was derived by performing a systematic optimization of library ranking results over seven targets, whose receptor sites cover a wide range of form, size, and polarity. ScreenScore was designed to be a robust and general scoring function that combines the virtues of both PLP and FlexX. Figure 5 shows that this is indeed the case. ScreenScore gives good enrichment values for cyclooxygenase-2 (COX-2 has a highly lipophilic binding site), and neuraminidase (which has a highly polar site), whereas the individual functions fail in one of the two cases. The authors of PLP have recently enhanced their

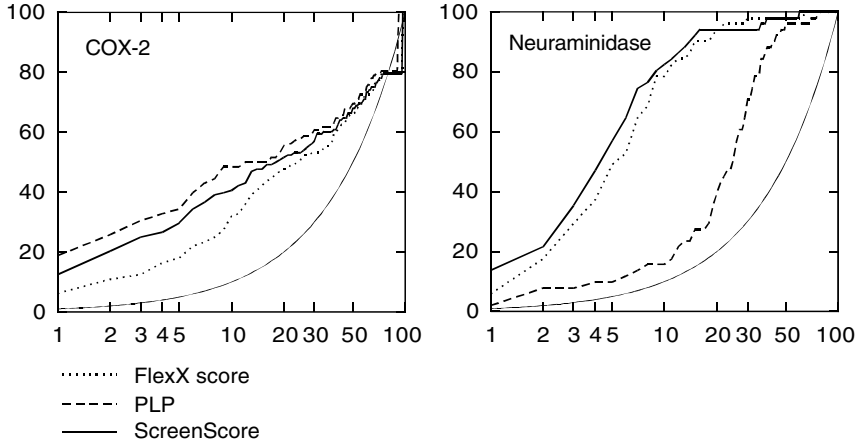


**Figure 5** Results of seeding experiments on two targets with three different scoring functions. In both graphs, the accumulated percentages of active compounds are plotted against the percentage of the total ranked library. The smooth exponential curve in each graph corresponds to the hypothetical case of no enrichment and assumes a random ordering of the database.

scoring function by including directed hydrogen bonding terms,[63] which may lead to a similarly robust scoring function as ScreenScore.

Another example where the balance between H-bonding and hydrophobic contributions is important involves the performance of the knowledge-based scoring function DrugScore.[92] The estrogen receptor binding site is a large lipophilic cavity with acceptor groups at either end that can form hydrogen bonds with ligand hydroxyl groups as present in the agonists **1** and **2** or the antagonists **3** and **4** (Figure 6). The narrow binding pocket and relatively rigid nature of the ligands restrains possible binding modes significantly. Accordingly, it can be assumed that FlexX is capable of generating reasonable solutions likely to be in agreement with experiment. Therefore we can expect the present example to represent a valuable test for scoring functions. For both agonists and antagonists, lipophilic interactions largely determine the binding energy. The majority of antagonists, however, differ from the agonists in an additional side chain bearing a tertiary amino group. This difference is reflected in the bound structures of the receptor. In the agonist-bound state the binding pocket is not accessible to solvent, whereas in the antagonist-bound state it opens up and allows the positively charged antagonist side chain to form a salt bridge with the carboxylate group of Glu 351. Agonists should bind equally well to both forms of the receptor. A 7500 compound subset from the World Drug Index (WDI) and a library of 20 agonists and 16 antagonists were docked into both agonist (PDB code 1ere) and antagonist (PDB code 1err) forms of the receptor. FlexX scores obtained from both structures are plotted against each other in Figure 6(**a**). Due to the large contribution of

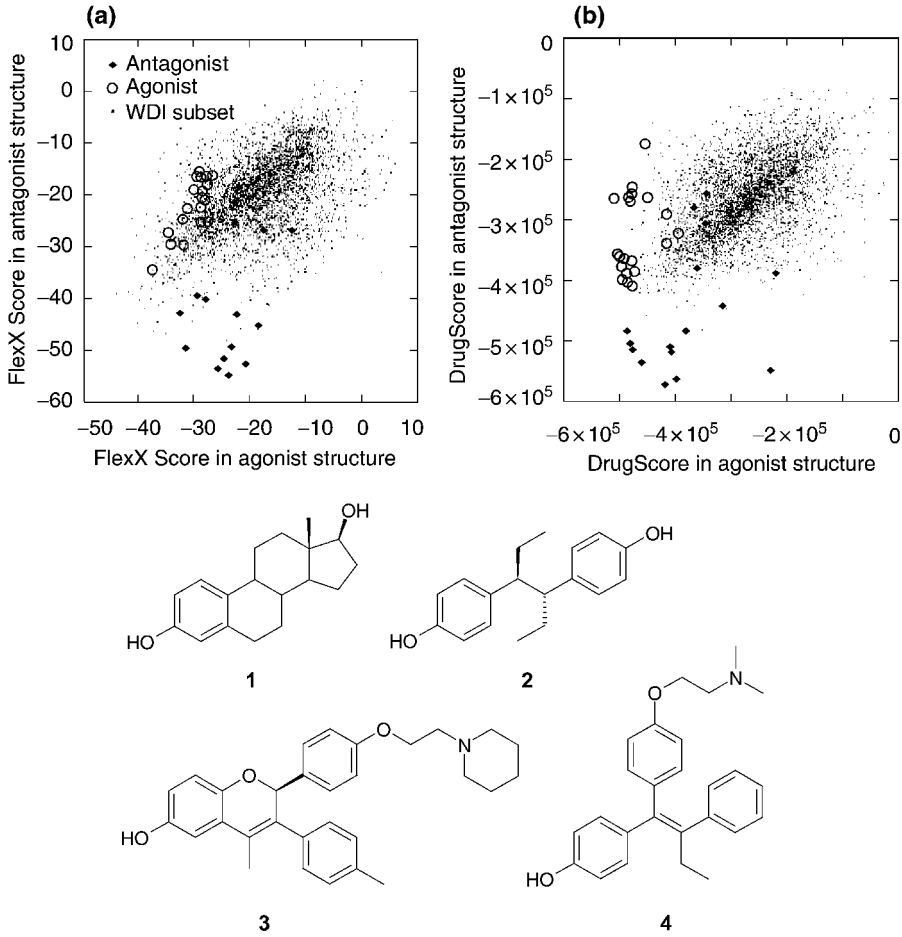


**Figure 6** Docking estrogen receptor agonists and antagonists into two crystal structures of the estrogen receptor, the agonist-bound conformation and the antagonist-bound conformation. Scores for both docking results are plotted against each other. Compounds **1** and **2** are examples of agonists, compounds **3** and **4** are typical antagonists.

the surface-exposed salt bridge formed with Glu 351 to the total score the antagonists are clearly separated from the WDI compounds, whereas the agonists are ranked among the bulk of the WDI entries in the antagonist structure. In the agonist form, the formation of a salt bridge is not possible, resulting in a lower average score for all molecules. Almost the same result as with the FlexX score is obtained with the ChemScore function[71,199] by Protherics.[201] The new DrugScore function[92] performs better in this situation. Using this scoring function, results shown in Figure 6(**b**) are obtained. Not only are the agonists significantly better separated from the WDI subset

when docked into the agonist structure, but more importantly, about half of the agonists are also among the 10% top ranked molecules in the database when docked into the open, antagonist structure, where they have to compete with many structures forming salt bridges.

## Finding Weak Inhibitors

Seeding experiments are often carried out with a handful of active compounds that have already been optimized for binding to a given target. Enrichment factors achieved in this way are often misleading, because finding potent inhibitors from among a number of random molecules is significantly easier than distinguishing weakly binding inhibitors from nonbinders. In practice, virtual screening will find, at best, inhibitors in the low micromolar range, simply because no chemical database will be large enough, diverse enough, and lucky enough to find optimized leads right away.

The difficulties associated with weak binders are illustrated in Figure 7 with thrombin as a target. The 7500 compound subset of the WDI mentioned above was docked into the thrombin active site together with three sets of 100

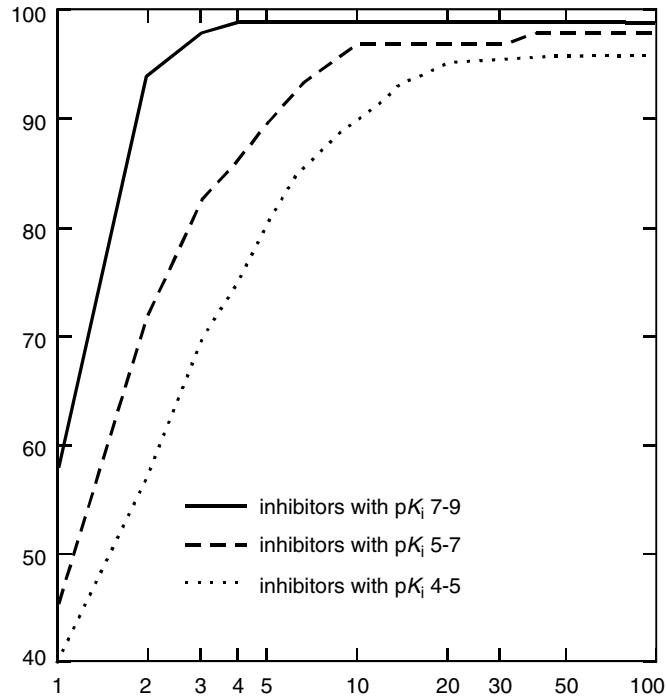


**Figure 7** Enrichment of three sets of 100 thrombin inhibitors that cover different ranges of activity. Less active compounds are more difficult to enrich.

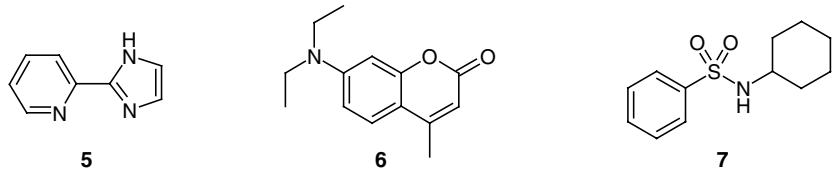

**Figure 8** Weak binders to FKBP.

known inhibitors in different activity ranges. It can be clearly seen in Figure 7 that enrichment decreases as the binding affinity of the active compounds decreases. Note that thrombin is a relatively easy target for most virtual screening methods (at least to identify compounds with charged moieties binding to the S1 subsite), and thus the separation of actives and inactives is still good for the low micromolar inhibitors. According to the authors' experience, the situation is worse for many other targets.

Nevertheless, library ranking can successfully be applied to enrich even very weak ligands. A database of approximately 4000 commercially available compounds was screened against FKBP by means of the SAR-by-NMR technique[202] and was found to contain 31 compounds with activities below 2 mM. Three examples of these compounds are shown in Figure 8. Compounds **5**, **6**, and **7** have measured dissociation constants of 0.1, 0.13 and 0.5 mM, respectively. This set of structures was flexibly docked into the FKBP binding site using DOCK 4.0 in conjunction with the PMF scoring function.[87] For the top 20% of the ranked database, enrichment factors between 2 and 3 were achieved. Enrichment factors were twice as large as those obtained with the standard AMBER score implemented in DOCK.

## Consensus Scoring

Different scoring schemes emphasize different physical phenomena that are important for ligand binding. Differences between scoring schemes might not be obvious in the calculation of binding affinities for known active compounds, but they can be very pronounced in the assessment of nonbinding molecules. The computational group at Vertex has reported good experience with a concept called "consensus scoring," whereby libraries of molecules are docked and assessed with several scoring functions and only those molecules are retained that score well with the majority of those functions. This can lead to a significant decrease in false positives,[198] but invariably a number of true positives is also lost in the process (see, e.g., Ref. 77).

One should keep in mind that in consensus scoring the number of false positives can be reduced, but one runs the risk of eliminating a number of active compounds that only one of the scoring functions has ranked high. Consider the example of the p38 MAP kinase inhibitors in Figure 4: consensus

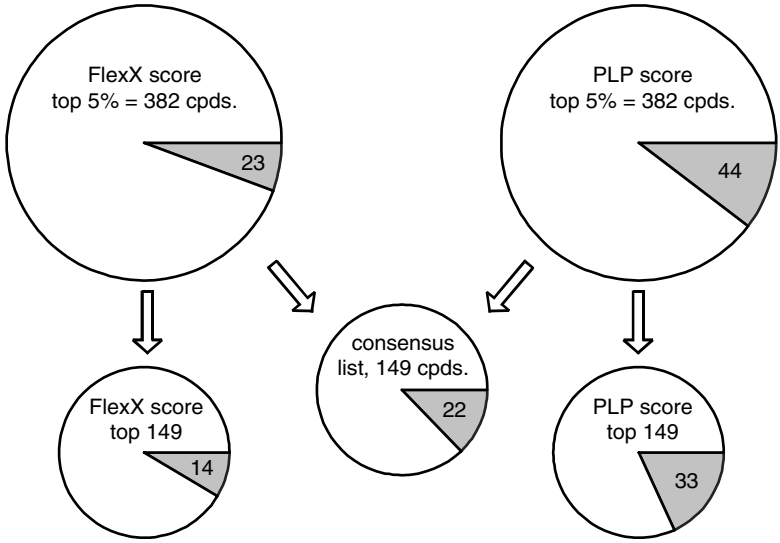


**Figure 9** Analysis of the consensus scoring concept with COX-2 as an example. Numbers in the shaded areas are numbers of active compounds. The larger pie charts at the top show the numbers of inhibitors in the top 5% of the database in terms of scores. The smaller pie charts refer to fewer top ranking compounds for better comparison with the smaller size of the consensus list.

scoring for the top 100 compounds by means of PLP and FlexX scores would eliminate all but one of the singly hydrogen-bonded inhibitors.

Figure 9 shows a worked consensus scoring example for a virtual screening experiment on COX-2. (Figure 5 shows the corresponding FlexX and PLP enrichment curves.) There are 23 inhibitors in the top 5% of the FlexX score rank list and roughly twice as many in the PLP rank list. Consensus scoring retains 22 of the actives. Because many inactive compounds are filtered out, the ratio of actives to false positives increases relative to either of the original lists. A different picture is obtained when one regards only the top 149 compounds from the individual FlexX and PLP rank lists—the same number of compounds that are in the consensus list. It becomes clear that the PLP function alone performs significantly better than does consensus scoring.

Thus, if one does not know in advance which scoring function will work better, more robust results can be obtained with consensus scoring. If one has a rough idea which function works better, one can decrease the number of false positives more effectively by testing fewer compounds from the top of a single rank list. Experience from seeding experiments with known inhibitors or an analysis of the type of binding site of the target can help to identify a suitable scoring function.

## Successful Identification of Novel Leads through Virtual Screening

It has been shown that virtual screening is an efficient way of finding novel leads. The program DOCK, one of the most widely used docking programs, has been applied in many published studies.[101,158,161,163,258,302,316] Usually the DOCK AMBER force field score has been applied. Other docking tools such as GREEN[203] also use the AMBER force field as a scoring function, and a successful screening application has been published.[204] The docking program SANDOCK[205] uses an empirical scoring function that evaluates steric complementarity, hydrophobic contacts, and hydrogen bonding. SANDOCK has been used to find a variety of novel FKBP inhibitors.[12]

Docking routines in the program packages DOCK and ICM[206] have been used to identify novel nuclear hormone receptor antagonists[207] and, for an RNA target, the transactivation response element (TAR) of HIV-1.[208] In both studies, the virtual screening protocol started with 153,000 compounds from the Available Chemicals Directory (ACD),[209] and the researchers employed increasingly elaborate docking and scoring schemes for smaller groups of selected compounds. In the HIV-1 TAR study, the ACD library was first rigidly docked into the binding site with DOCK. Only a simple contact scoring scheme was used in this step. The 20% best-scoring compounds were then subjected to flexible docking with ICM in combination with an empirical scoring function derived specifically for RNA targets, leading to a set of about 5000 compounds. Two more steps of longer sampling for the conformational analysis of these remaining compounds within the binding site led to 350 selected candidates. Two of the compounds that were experimentally tested significantly reduced the binding of the Tat protein to HIV-1 TAR.

A study by Grueneberg, Wendt, and Klebe[15] resulted in subnanomolar inhibitors of carbonic anhydrase II (CAII). The study is a textbook example of virtual screening focusing on successively smaller subsets of the initial database in several steps and employing different methods at each step. Carbonic anhydrase II is a metalloenzyme that catalyzes the reversible hydration of $CO_2$ to $HCO_3^-$.[210] In the human eye, an isoform of the enzyme is involved in water removal. Inhibitors of CAII can thus be used to reduce intraocular pressure in the treatment of glaucoma. The CAII binding site is a rather rigid, funnel-shaped binding pocket. Known inhibitors such as dorzolamide **8** (Figure 10; see also Ref. 8) bind to the catalytic zinc ion via a sulfonamide group.

An initial database of 90,000 entries in the Maybridge[211] and LeadQuest[212] libraries was converted to 3D structures with the 3D structure generation program Corina.[213,214] In a first filtering step, all compounds were passed through a UNITY[215] pharmacophore query. The pharmacophore query was constructed from an analysis of available X-ray structures of the enzyme and incorporated donor, acceptor, and hydrophobic features of the binding site. Compounds passing this filter also had to contain a known zinc-binding

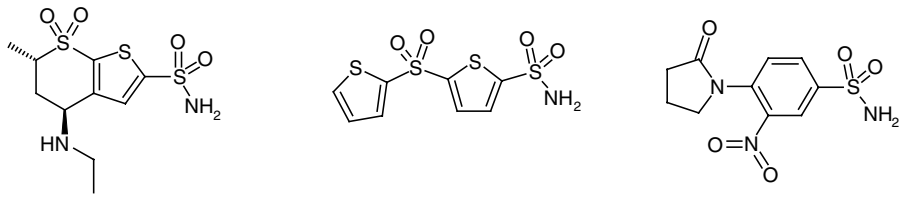

**8** **9** **10**

**Figure 10** Inhibitors of carbonic anhydrase II. Compounds **9** and **10** are subnanomolar inhibitors identified through virtual screening. Compound **8** is the marketed drug dorzolamide.

group. A set of 3314 compounds passed these requirements. In the second filtering step, the known CAII inhibitor dorzolamide **8** was used as a template onto which all potential candidates were flexibly superimposed by means of the program FlexS.[172] The top-ranking compounds from this step were then docked into the binding site with FlexX[64–66] taking into account four conserved water molecules in the active site. The top-ranking 13 hits were chosen for experimental testing. Nine of these compounds showed activities below 1 μM, and the sulfonamides **9** and **10** (Figure 10) have $K_i$ values below 1 nM.

The de novo design of inhibitors of the bacterial enzyme DNA gyrase is another example for a successful application of structure-based virtual screening.[14] DNA gyrase is a well-established antibacterial target.[216] It is an essential, prokaryotic type II topoisomerase with no mammalian counterpart involved in the vital processes of DNA replication, transcription, and recombination. DNA gyrase catalyzes the ATP-dependent introduction of negative supercoils into bacterial DNA as well as the decatenation and unknotting of DNA. The enzyme consists of two subunits A and B with the active enzyme being an $A_2B_2$ complex. Subunit A of DNA gyrase is involved in DNA breakage and reunion, whereas the B subunits catalyze the hydrolysis of ATP. Quinolones (e.g., the now famous ciprofloxacin), which inhibit DNA gyrase by binding to the subunit A, are successfully used as broad-spectrum antibacterial agents in the clinic. Unfortunately, resistance to quinolones emerged some time ago. The two other classes of DNA gyrase inhibitors, cyclothialidines and coumarins (e.g., novobiocin), bind to the ATP binding site of subunit B. Novobiocin was clinically used against *Staphylococcus aureus*, but it suffers from toxicity effects and resistance against it is developing rapidly. As demonstrated by the cyclothialidines, this type of resistance can be overcome. Unfortunately, the cyclothialidines have insufficient in vivo activities due to a class specific rapid and extensive glucuronidation of the essential phenol moiety.

To overcome the limitations of known DNA gyrase inhibitors, a new drug discovery project was inititated at Roche. Searching for novel inhibitors by screening the Roche compound library provided no suitable lead structures.

Therefore, a new rational approach was developed to generate lead structures by using the detailed 3D structural information of the ATP binding site located on subunit B. At the time of project initiation, the X-ray structures of the DNA gyrase subunit B complexed with a nonhydrolyzable ATP analogue, with novobiocin, and with cyclothialidine were available. In the inner part of the pocket they all share a common binding motif: each donates a hydrogen-bond to an aspartic acid side chain (Asp 73) and accepts a hydrogen bond from a conserved water molecule. It was reasoned that a novel inhibitor should have the ability to form these two key hydrogen bonds and a lipophilic part to pick up some lipophilic interactions with the enzyme.

A computational search of the ACD[209] and the Roche Compound Inventory, employing the SCORE1 function also implemented in LUDI, was carried out to identify molecules with a low molecular weight meeting the above criteria. Relying on the results of the in silico screening, just 600 compounds were tested initially. Then, analogues similar to the first hits were assayed. Overall, assay results for 3000 compounds gave rise to 150 hits clustered into 14 chemical classes. Seven of those classes could be validated as true, novel DNA gyrase inhibitors that act by binding to the ATP binding site located on the B subunit. The maximum noneffective concentration (MNEC) was in the 5–64 μg/mL range, that is, two to three orders of magnitude higher than the MNEC of novobiocin or cyclothialidine. Subsequent structure-based optimization of the hits led to compounds with potencies equal or up to 10 times better than novobiocin. Compound **11** (Figure 11; MNEC $< 0.03$ μg/mL) is an example of a novel potent inhibitor of DNA gyrase B resulting from structure-based virtual screening.

An important factor contributing to the success of the project was a new assay that allowed detecting not only highly potent inhibitors but also weak ones, so as to allow testing compounds at high concentrations. Instead of a supercoiling assay usually used to test DNA gyrase inhibitory activity, a coupled spectrophotometric ATPase assay was employed. Compounds could be assayed in concentrations up to 0.5 mM due to a higher tolerance of the solubilizing agent DMSO in this assay.

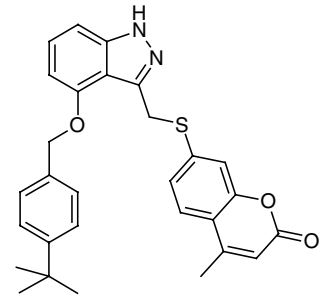


**11**

**Figure 11** An inhibitor of DNA gyrase B, discovered at Roche by means of virtual screening and subsequent structure-based optimization.

## OUTLOOK

The first scoring functions were published about 10 years ago. Since then, much experience has been gained in their application and in assessing their accuracy. Significant progress in the development of better functions has been made over the last few years, and it appears as if there now exist scoring functions that can be applied to a wide range of different proteins and which consistently yield considerable enrichment of active compounds. Consequently, many large and small pharmaceutical companies are increasingly using virtual screening techniques to identify possible leads.

In fact, structure-based ligand design is now seen as a very important approach to drug discovery that nicely complements HTS.[217] High throughout screening has a number of serious disadvantages: it is expensive,[218] and it leads to many false positives and few real leads.[22,219] Furthermore, not all biactivity tests are amenable to HTS techniques. And finally, despite the large size of the chemical libraries available to the pharmaceutical industry, it is far from possible to cover the whole universe of drug-like organic molecules. Because of these limitations, and given the current aggressive patenting strategies, the focused design of novel compounds and compound libraries will continue to gain importance.

Thus, there is every reason to believe that the value of structure-based approaches will continue to grow and become even more embraced by the pharmaceutical, agricultural, and related industries than it now is. The development of improved scoring functions is certainly vital for their success.

The major challenges to be overcome in the further development of scoring functions include

1. Polar interactions are still not treated adequately. It is somewhat strange to find that while the role of hydrogen bonds in biology has been well known for a long time and hydrogen bonds are qualitatively well understood, a quantitative treatment of hydrogen bonds in protein–ligand interactions is still missing. Therefore, hydrogen bonds have been referred to as "the last mystery in structure-based design."[38]
2. All scoring functions are essentially simple analytical functions fitted to experimental binding data. Presently, there exists a heavy bias in the public domain data toward peptidic ligands, which in turn leads to an overestimation of polar interactions in many scoring functions. The development of better scoring function clearly requires access to more data on nonpeptidic, low molecular weight, drug-like ligands.
3. Unfavorable interactions and unlikely docking solutions are not penalized strongly enough. General and robust methods that account for undesired features of complex structures in the derivation of scoring functions are still lacking.

4. So far, fast scoring functions only cover part of the whole receptor–ligand binding process. A more detailed picture could be obtained by taking into account properties of the unbound ligand, that is, solvation effects and energetic differences between the low-energy solution conformations and the bound conformation.

## ACKNOWLEDGMENTS

The authors have benefited from numerous discussions with many researchers active in the field of docking and scoring. We especially thank Holger Gohlke (Marburg), Ingo Muegge (Bayer, U.S.A.), and Matthias Rarey (GMD, St. Augustin). Wolfgang Guba's valuable comments on the manuscript are gratefully acknowledged.

## REFERENCES

1. J. Greer, J. W. Erickson, and J. J. Baldwin, *J. Med. Chem.,* **37,** 1035 (1994). Application of the Three-Dimensional Structures of Protein Target Molecules in Structure-Based Drug Design.
2. M. von Itzstein, W.-Y. Wu, G. B. Kok, M. S. Pegg, J. C. Dyason, B. Jin, T. V. Phan, M. L. Smythe, H. F. White, S. W. Oliver, P. M. Colmant, J. N. Varghese, D. M. Ryan, J. M. Woods, R. C. Bethell, V. J. Hotham, J. M. Cameron, and C. R. Penn, *Nature (London),* **363,** 418 (1993). Rational Design of Potent Sialidase-Based Inhibitors of Influenza Virus Replication.
3. W. Lew, X. Chen, and U. Choung, *Curr. Med. Chem.,* **7,** 663 (2000). Discovery and Development of GS 4104 (Oseltamivir): An Orally Active Influenza Neuraminidase Inhibitor.
4. S. W. Kaldor, V. J. Kalish, J. F. Davies, V. S. Bhasker, J. E. Fritz, K. Appelt, J. A. Burgess, K. M. Campanale, N. Y. Chirgadze, D. K. Clawson, B. A. Dressman, S. D. Hatch, D. A. Khalil, M. B. Kosa, P. P. Lubbehusen, M. A. Muesing, A. K. Patick, S. H. Reich, K. S. Su, and J. H. Tatlock, *J. Med. Chem.,* **40,** 3979 (1997). Viracept (Nelfinavir Mesylate, AG1343): A Potent, Orally Bioavailable Inhibitor of HIV-1 Protease.
5. R. S. Bohacek, C. McMartin, and W. C. Guida, *Med. Res. Rev.,* **16,** 3 (1996). The Art and Practice of Structure-Based Drug Design: A Molecular Modeling Perspective.
6. R. E. Babine and S. L. Bender, *Chem. Rev.,* **97,** 1359 (1997). Molecular Recognition of Protein–Ligand Complexes: Applications to Drug Design.
7. R. E. Hubbard, *Curr. Opin. Biotechnology,* **8,** 696 (1997). Can Drugs Be Designed?
8. D. B. Boyd, in *Rational Molecular Design in Drug Research,* Proceedings of the *Alfred Benzon Symposium No. 42* (Copenhagen, June 8–12, 1997), T. Liljefors, F. S. Jørgensen, and P. Krogsgaard-Larsen, Eds., Munksgaard, Copenhagen, 1998, pp. 15–23. Progress in Rational Design of Therapeutically Interesting Compounds.
9. M. A. Murcko, P. R. Caron, and P. S. Charifson, *Annu. Reports Med. Chem.,* **34,** 297 (1999). Structure-Based Drug Design.
10. D. A. Gschwend, W. Sirawaraporn, D. V. Santi, and I. D. Kuntz, *Proteins: Struct., Funct., Genet.,* **29,** 59 (1997). Specificity in Structure-Based Drug Design: Identification of a Novel, Selective Inhibitor of *Pneumocystis carinii* Dihydrofolate Reductase.
11. E. K. Kick, D. C. Roe, A. G. Skillman, G. Liu, T. J. A. Ewing, Y. Sun, I. D. Kuntz, and J. A. Ellman, *Chem. Biol.,* **4,** 297 (1997). Structure-Based Design and Combinatorial Chemistry Yield Low Nanomolar Inhibitors of Cathepsin D.

12. P. Burkhard, U. Hommel, M. Sanner, and M. D. Walkinshaw, *J. Mol. Biol.,* **287,** 853 (1999). The Discovery of Steroids and Other Novel FKBP Inhibitors Using a Molecular Docking Program.
13. J. H. Toney, P. M. D. Fitzgerald, N. Grover-Sharma, S. H. Olson, W. J. May, J. G. Sundelof, D. E. Vanderwall, K. A. Cleary, S. K. Grant, J. K. Wu, J. W. Kozarich, D. L. Pompliano, and G. G. Hammond, *Chem. Biol.,* **5,** 185 (1998). Antibiotic Sensitation Using Biphenyl Tetrazoles as Potent Inhibitors of *Bacteroides fragilis* Metallo-β-Lactamase.
14. H.-J. Boehm, M. Boehringer, D. Bur, H. Gmuender, W. Huber, W. Klaus, D. Kostrewa, H. Kuehne, T. Luebbers, N. Meunier-Keller, and F. Mueller, *J. Med. Chem.,* **43,** 2664 (2000). Novel Inhibitors of DNA Gyrase: 3D Structure-Based Needle Screening, Hit Validation by Biophysical Methods, and 3D Guided Optimization. A Promising Alternative to Random Screening.
15. S. Grueneberg, B. Wendt, and G. Klebe, *Angew. Chem. Int. Ed.,* **40,** 389 (2001). Subnanomolar Inhibitors From Computer Screening: A Model Study Using Human Carbonic Anhydrase II.
16. M. A. Murcko, in *Reviews in Computational Chemistry,* K. B. Lipkowitz and D. B. Boyd, Eds., Wiley-VCH, New York, 1997, Vol. 11, pp. 1–66. Recent Advances in Ligand Design Methods.
17. D. E. Clark, C. W. Murray, and J. Li, in *Reviews in Computational Chemistry,* K. B. Lipkowitz and D. B. Boyd, Eds., Wiley-VCH, New York, 1997, Vol. 11, pp. 67–125. Current Issues in De Novo Molecular Design.
18. I. Muegge and M. Rarey, in *Reviews in Computational Chemistry,* K. B. Lipkowitz and D. B. Boyd, Eds., Wiley-VCH, New York, 2001, Vol. 17, pp. 1–60. Small Molecule Docking and Scoring.
19. P. J. Goodford, *J. Med. Chem.,* **28,** 849 (1985). A Computational Procedure for Determining Energetically Favored Binding Sites on Biologically Important Macromolecules.
20. H.-J. Boehm, *J. Comput.-Aided Mol. Design,* **6,** 61 (1992). The Computer Program LUDI: A New Method for the De Novo Design of Enzyme Inhibitors.
21. H.-J. Boehm, *J. Comput.-Aided Mol. Design,* **6,** 593 (1992). LUDI: Rule-Based Automatic Design of New Substituents for Enzyme Inhibitor Leads.
22. C. A. Lipinski, F. Lombardo, B. W. Dominy, and P. J. Feeney, *Adv. Drug Delivery Rev.,* **23,** 3 (1997). Experimental and Computational Approaches to Estimate Solubility and Permeability in Drug Discovery and Development Settings.
23. D. E. Clark and S. D. Pickett, *Drug Discovery Today,* **5,** 49 (2000). Computational Methods for the Prediction of "Drug-Likeness."
24. H.-J. Boehm and G. Klebe, *Angew. Chem. Int. Ed.,* 35, 2588 (1996). What Can We Learn from Molecular Recognition in Protein–Ligand Complexes for the Design of New Drugs?
25. O. Roche, R. Kiyama, and C. L. Brooks III, *J. Med. Chem.,* **44,** 3592 (2001). Ligand–Protein Database: Linking Protein–Ligand Complex Structures to Binding Data.
26. I. K. McDonald and J. M. Thornton, *J. Mol. Biol.,* **238,** 777 (1994). Satisfying Hydrogen Bonding Potential in Proteins.
27. M. H. Parker, D. F. Ortwine, P. M. O'Brien, E. A. Lunney, C. A. Banotai, W. T. Mueller, P. McConnell, and C. G. Brouillette, *Bioorg. Med. Chem. Lett.,* **10,** 2427 (2000). Stereoselective Binding of an Enantiomeric Pair of Stromelysin-1 Inhibitors Caused by Conformational Entropy Factors.
28. J. D. Dunitz, *Chem. Biol.,* **2,** 709 (1995). Win Some, Lose Some: Enthalpy–Entropy Compensation in Weak Molecular Interactions.
29. P. Gilli, V. Ferretti, G. Gilli, and P. A. Brea, *J. Phys. Chem.,* **98,** 1515 (1994). Enthalpy–Entropy Compensation in Drug-Receptor Binding.
30. D. H. Williams, D. P. O'Brien, and B. Bardsley, *J. Am. Chem. Soc.,* **123,** 737 (2001). Enthalpy/Entropy Compensation as a Competition Between Dynamics and Bonding: The Relevance to Melting of Crystals and Biological Aggregates.

31. P. C. Weber, J. J. Wendoloski, M. W. Pantoliano, and F. R. Salemme, *J. Am. Chem. Soc.,* **114,** 3197 (1992). Crystallographic and Thermodynamic Comparison of Natural and Synthetic Ligands Bound to Streptavidin.
32. A. R. Fersht, J.-P. Shi, J. Knill-Jones, D. M. Lowe, A. J. Wilkinson, D. M. Blow, P. Brick, P. Carter, M. M. Y. Waye, and G. Winter, *Nature (London),* **314,** 235 (1985). Hydrogen Bonding and Biological Specificity Analysed by Protein Engineering.
33. Y. W. Chen and A. R. Fersht, *J. Mol. Biol.,* **234,** 1158 (1993). Contribution of Buried Hydrogen Bonds to Protein Stability—The Crystal Structure of Two Barnase Mutants.
34. P. R. Connelly, R. A. Aldape, F. J. Bruzzese, S. P. Chambers, M. J. Fitzgibbon, M. A. Fleming, S. Itoh, D. J. Livingston, M. A. Navia, J. A. Thomson, and K. P. Wilson, *Proc. Natl. Acad. Sci. U.S.A.,* **91,** 1964 (1994). Enthalpy of Hydrogen-Bond Formation in a Protein–Ligand Binding Reaction.
35. B. P. Morgan, J. M. Scholtz, M. D. Ballinger, I. D. Zipkin, and P. A. Bartlett, *J. Am. Chem. Soc.,* **113,** 297 (1991). Differential Binding Energy: A Detailed Evaluation of the Influence of Hydrogen Bonding and Hydrophobic Groups on the Inhibition of Thermolysin by Phosphorus-Containing Inhibitors.
36. B. A. Shirley, P. Stanssens, U. Hahn, and C. N. Pace, *Biochemistry,* **31,** 725 (1992). Contribution of Hydrogen Bonding to the Conformational Stability of Ribonuclease T1.
37. U. Obst, D. W. Banner, L. Weber, and F. Diederich, *Chem. Biol.,* **4,** 287 (1997). Molecular Recognition at the Thrombin Active Site: Structure-Based Design and Synthesis of Potent and Selective Thrombin Inhibitors and the X-Ray Crystal Structures of Two Thrombin-Inhibitor Complexes.
38. H. Kubinyi, in *Pharmacokinetic Optimization in Drug Research,* B. Testa, H. van de Waterbeemd, G. Folkers, and R. Guy, Eds., Wiley-VCH, Weinheim, 2001, pp. 513–524. Hydrogen Bonding, the Last Mystery in Drug Design?
39. H.-J. Schneider, T. Schiestel, and P. Zimmermann, *J. Am. Chem. Soc.,* **114,** 7698 (1992). The Incremental Approach to Noncovalent Interactions: Coulomb and van der Waals Effects in Organic Ion Pairs.
40. A. C. Tissot, S. Vuilleumier, and A. R. Fersht, *Biochemistry,* **35,** 6786 (1996). Importance of Two Buried Salt Bridges in the Stability and Folding Pathway of Barnase.
41. J. D. Dunitz, *Science,* **264,** 670 (1994). The Entropic Cost of Bound Water in Crystals and Biomolecules.
42. A. Ben-Naim, *Hydrophobic Interactions,* Plenum Press, New York, 1980.
43. C. Tanford, *The Hydrophobic Effect,* Wiley, New York, 1980.
44. C. Chothia, *Nature (London),* **254,** 304 (1975). Structural Invariants in Protein Folding.
45. F. M. Richards, *Annu. Rev. Biophys. Bioeng.,* **6,** 151 (1977). Areas, Volumes, Packing, and Protein Structure.
46. K. A. Sharp, A. Nicholls, R. Friedman, and B. Honig, *Biochemistry,* **30,** 9686 (1991). Extracting Hydrophobic Free Energies From Experimental Data: Relationship to Protein Folding and Theoretical Models.
47. H. Mack, T. Pfeiffer, W. Hornberger, H.-J. Boehm, and H. W. Hoeffken, *J. Enzyme Inhib.,* **1,** 73 (1995). Design, Synthesis and Biological Activity of Novel Rigid Amidino-Phenylalanine Derivatives as Inhibitors of Thrombin.
48. A. R. Khan, J. C. Parrish, M. E. Fraser, W. W. Smith, P. A. Bartlett, and M. N. G. James, *Biochemistry,* **37,** 16841 (1998). Lowering the Entropic Barrier for Binding Conformationally Flexible Inhibitors to Enzymes.
49. M. S. Searle and D. H. Williams, *J. Am. Chem. Soc.,* **114,** 10690 (1992). The Cost of Conformational Order: Entropy Changes in Molecular Association.
50. M. S. Searle, D. H. Williams, and U. Gerhard, *J. Am. Chem. Soc.,* **114,** 10697 (1992). Partitioning of Free Energy Contributions in the Estimation of Binding Constants: Residual Motions and Consequences for Amide–Amide Hydrogen Bond Strengths.

51. M. A. Hossain and H.-J. Schneider, *Chem. Eur. J.,* **5,** 1284 (1999). Flexibility, Association Constants, and Salt Effects in Organic Ion Pairs: How Single Bonds Affect Molecular Recognition.

52. K. P. Murphy, D. Xie, K. S. Thompson, L. M. Amzel, and E. Freire, *Proteins: Struct., Funct., Genet.,* **18,** 63 (1994). Entropy in Biological Binding Processes: Estimation of Translational Entropy Loss.

53. J. Hermans and L. Wang, *J. Am. Chem. Soc.,* **119,** 2702 (1997). Inclusion of Loss of Translational and Rotational Freedom in Theoretical Estimates of Free Energies of Binding. Application to a Complex of Benzene and Mutant T4 Lysozyme.

54. R. S. Bohacek and C. McMartin, *J. Med. Chem.,* **35,** 1671 (1992). Definition and Display of Steric, Hydrophobic, and Hydrogen-Bonding Properties of Ligand Binding Sites in Proteins Using Lee and Richards Accessible Surface: Validation of a High-Resolution Graphical Tool for Drug Design.

55. D. H. Williams, M. S. Searle, J. P. Mackay, U. Gerhard, and R. A. Maplestone, *Proc. Natl. Acad. Sci. U.S.A.,* **90,** 1172 (1993). Toward an Estimation of Binding Constants in Aqueous Solution: Studies of Associations of Vancomycin Group Antibiotics.

56. H.-J. Boehm, *J. Comput.-Aided Mol. Design,* **8,** 243 (1994). The Development of a Simple Empirical Scoring Function to Estimate the Binding Constant for a Protein–Ligand Complex of Known Three-Dimensional Structure.

57. H.-J. Boehm, D. W. Banner, and L. Weber, *J. Comput.-Aided Mol. Design,* **13,** 51 (1999). Combinatorial Docking and Combinatorial Chemistry: Design of Potent Non-Peptide Thrombin Inhibitors.

58. S.-S. So and M. Karplus, *J. Comput.-Aided Mol. Design,* **13,** 243 (1999). A Comparative Study of Ligand–Receptor Complex Binding Affinity Prediction Methods Based on Glycogen Phosphorylase Inhibitors.

59. M. D. Miller, S. K. Kearsley, D. J. Underwood, and R. P. Sheridan, *J. Comput.-Aided Mol. Design,* **8,** 153 (1994). FLOG: A System to Select "Quasi-Flexible" Ligands Complementary to a Receptor of Known Three-Dimensional Structure.

60. G. Jones, P. Willett, and R. C. Glen, *J. Mol. Biol.,* **245,** 43 (1995). Molecular Recognition of Receptor Sites Using a Genetic Algorithm With a Description of Desolvation.

61. G. Jones, P. Willett, R. C. Glen, A. R. Leach, and R. Taylor, *J. Mol. Biol.,* **267,** 727 (1997). Development and Validation of a Genetic Algorithm for Flexible Docking.

62. D. K. Gehlhaar, G. M. Verkhivker, P. A. Rejto, C. J. Sherman, D. B. Fogel, L. J. Fogel, and S. T. Freer, *Chem. Biol.,* **2,** 317 (1995). Molecular Recognition of the Inhibitor AG-1343 by HIV-1 Protease: Conformationally Flexible Docking by Evolutionary Programming.

63. G. M. Verkhivker, D. Bouzida, D. K. Gehlhaar, P. A. Reijto, S. Arthurs, A. B. Colson, S. T. Freer, V. Larson, B. A. Luty, T. Marrone, and P. W. Rose, *J. Comput.-Aided Mol. Design,* **14,** 731 (2000). Deciphering Common Failures in Molecular Docking of Ligand–Protein Complexes.

64. M. Rarey, B. Kramer, T. Lengauer, and G. Klebe, *J. Mol. Biol.,* **261,** 470 (1996). A Fast Flexible Docking Method Using an Incremental Construction Algorithm.

65. M. Rarey, B. Kramer, and T. Lengauer, *J. Comput.-Aided Mol. Design,* **11,** 369 (1997). Multiple Automatic Base Selection: Protein–Ligand Docking Based on Incremental Construction Without Manual Intervention.

66. M. Rarey, S. Wefing, and T. Lengauer, *J. Comput.-Aided Mol. Design,* **10,** 41 (1996). Placement of Medium-Sized Molecular Fragments into Active Sites of Proteins.

67. M. Rarey, B. Kramer, and T. Lengauer, *Bioinformatics,* **15,** 243 (1999). Docking of Hydrophobic Ligands With Interaction-Based Matching Algorithms.

68. R. D. Head, M. L. Smythe, T. I. Oprea, C. L. Waller, S. M. Green, and G. R. Marshall, *J. Am. Chem. Soc.,* **118,** 3959 (1996). VALIDATE: A New Method for the Receptor-Based Prediction of Binding Affinities of Novel Ligands.

69. A. N. Jain, *J. Comput.-Aided Mol. Design,* **10,** 427 (1996). Scoring Non-Covalent Protein Ligand Interactions: A Continuous Differentiable Function Tuned to Compute Binding Affinities.

70. W. Welch, J. Ruppert, and A. N. Jain, *Chem. Biol.,* **3,** 449 (1996). Hammerhead: Fast, Fully Automated Docking of Flexible Ligands to Protein Binding Sites.

71. M. D. Elridge, C. W. Murray, T. R. Auton, G. V. Paolini, and R. P. Mee, *J. Comput.-Aided Mol. Design,* **11,** 425 (1997). Empirical Scoring Functions. I. The Development of a Fast Empirical Scoring Function to Estimate the Binding Affinity of Ligands in Receptor Complexes.

72. C. W. Murray, T. R. Auton, and M. D. Elridge, *J. Comput.-Aided Mol. Design,* **12,** 503 (1999). Empirical Scoring Functions. II. The Testing of an Empirical Scoring Function for the Prediction of Ligand-Receptor Binding Affinities and the Use of Bayesian Regression to Improve the Quality of the Method.

73. H.-J. Boehm, *J. Comput.-Aided Mol. Design,* **12,** 309 (1998). Prediction of Binding Constants of Protein Ligands: A Fast Method for the Prioritization of Hits Obtained From De Novo Design or 3D Database Search Programs.

74. Y. Takamatsu and A. Itai, *Proteins: Struct., Funct., Genet.,* **33,** 62 (1998). A New Method for Predicting Binding Free Energy Between Receptor and Ligand.

75. R. Wang, L. Liu, L. Lai, and Y. Tang, *J. Mol. Model.,* **4,** 379 (1998). SCORE: A New Empirical Method for Estimating the Binding Affinity of a Protein–Ligand Complex.

76. D. Rognan, S. L. Lauemoller, A. Holm, S. Buus, and V. Tschinke, *J. Med. Chem.,* **42,** 4650 (1999). Predicting Binding Affinities of Protein Ligands from Three-Dimensional Models: Application to Peptide Binding to Class I Major Histocompatibility Proteins.

77. C. Bissantz, G. Folkers, and D. Rognan, *J. Med. Chem.,* **43,** 4759 (2000). Protein-Based Virtual Screening of Chemical Databases. 1. Evaluation of Different Docking/Scoring Combinations.

78. M. Stahl and M. Rarey, *J. Med. Chem.,* **44,** 1035 (2001). Detailed Analysis of Scoring Functions for Virtual Screening.

79. G. E. Kellogg, G. S. Joshi, and D. J. Abraham, *Med. Chem. Res.,* **1,** 444 (1991). New Tools for Modeling and Understanding Hydrophobicity and Hydrophobic Interactions.

80. E. C. Meng, I. D. Kuntz, D. J. Abraham, and G. E. Kellogg, *J. Comput.-Aided Mol. Design,* **8,** 299 (1994). Evaluating Docked Complexes With the HINT Exponential Function and Empirical Atomic Hydrophobicities.

81. C. Zhang, G. Vasmatzis, J. L. Cornette, and C. DeLisi, *J. Mol. Biol.,* **267,** 707 (1997). Determination of Atomic Solvation Energies from the Structure of Crystallized Proteins.

82. R. S. DeWitte and E. I. Shakhnovich, *J. Am. Chem. Soc.,* **118,** 11733 (1996). SMoG: De Novo Design Method Based on Simple, Fast and Accurate Free Energy Estimates. 1. Methodology and Supporting Evidence.

83. R. S. DeWitte, A. V. Ishchenko, and E. I. Shakhnovich, *J. Am. Chem. Soc.,* **119,** 4608 (1997). SMoG: De Novo Design Method Based on Simple, Fast, and Accurate Free Energy Estimates. 2. Case Studies in Molecular Design.

84. J. B. O. Mitchell, R. A. Laskowski, A. Alex, and J. M. Thornton, *J. Comput. Chem.,* **20,** 1165 (1999). BLEEP—A Potential of Mean Force Describing Protein–Ligand Interactions. I. Generating the Potential.

85. J. B. O. Mitchell, R. A. Laskowski, A. Alex, M. J. Forster, and J. M. Thornton, *J. Comput. Chem.,* **20,** 1177 (1999). BLEEP—A Potential of Mean Force Describing Protein–Ligand Interactions. II. Calculation of Binding Energies and Comparison With Experimental Data.

86. I. Muegge and Y. C. Martin, *J. Med. Chem.,* **42,** 791 (1999). A General and Fast Scoring Function for Protein–Ligand Interactions: A Simplified Potential Approach.

87. I. Muegge, Y. C. Martin, P. J. Hajduk, and S. W. Fesik, *J. Med. Chem.,* **42,** 2498 (1999). Evaluation of PMF Scoring in Docking Weak Ligands to the FK506 Binding Protein.

88. I. Muegge, *Med. Chem. Res.,* **9,** 490 (1999). The Effect of Small Changes in Protein Structure on Predicted Binding Modes of Known Inhibitors of Influenza Virus Neuraminidase: PMF-Scoring in DOCK4.

89. I. Muegge, *Perspect. Drug Discovery Design,* **20,** 99 (2000). A Knowledge-Based Scoring Function for Protein–Ligand Interactions: Probing the Reference State.

90. I. Muegge, *J. Comput. Chem.,* **22,** 418 (2001). Effect of Ligand Volume Correction on PMF Scoring.

91. M. Stahl, *Perspect. Drug Discovery Design,* **20,** 83 (2000). Modifications of the Scoring Function in FlexX for Virtual Screening Applications.

92. H. Gohlke, M. Hendlich, and G. Klebe, *J. Mol. Biol.,* **295,** 337 (2000). Knowledge-Based Scoring Function to Predict Protein–Ligand Interactions.

93. H. Gohlke, M. Hendlich, and G. Klebe, *Perspect. Drug Discovery Design,* **20,** 115 (2000). Predicting Binding Modes, Binding Affinities and "Hot Spots" for Protein-Ligand Complexes Using a Knowledge-Based Scoring Function.

94. E. C. Meng, B. K. Shoichet, and I. D. Kuntz, *J. Comput. Chem.,* **13,** 505 (1992). Automated Docking With Grid-Based Energy Evaluation.

95. I. D. Kuntz, J. M. Blaney, S. J. Oatley, R. Langridge, and T. Ferrin, *J. Mol. Biol.,* **161,** 269 (1982). A Geometric Approach to Macromolecule–Ligand Interactions.

96. B. K. Shoichet, D. L. Bodian, and I. D. Kuntz, *J. Comput. Chem.,* **13,** 380 (1992). Molecular Docking Using Shape Descriptors.

97. E. C. Meng, D. A. Gschwend, J. M. Blaney, and I. D. Kuntz, *Proteins: Struct., Funct., Genet.,* **17,** 266 (1993). Orientational Sampling and Rigid-Body Minimization in Molecular Docking.

98. T. J. A. Ewing and I. D. Kuntz, *J. Comput. Chem.,* **18,** 1175 (1997). Critical Evaluation of Search Algorithms for Automated Molecular Docking and Database Screening.

99. S. Makino and I. D. Kuntz, *J. Comput. Chem.,* **18,** 1812 (1997). Automated Flexible Ligand Docking Method and Its Application for Database Search.

100. M. Vieth, J. D. Hirst, A. Kolinski, and C. L. Brooks III, *J. Comput. Chem.,* **19,** 1612 (1998). Assessing Energy Functions for Flexible Docking.

101. G. M. Morris, D. S. Goodsell, R. S. Halliday, R. Huey, W. E. Hart, R. K. Belew, and A. J. Olson, *J. Comput. Chem.,* **14,** 1639 (1998). Automated Docking Using a Lamarckian Genetic Algorithm and an Empirical Binding Free Energy Function.

102. M. Schapira, M. Trotov, and R. Abagyan, *J. Mol. Recognition,* **12,** 177 (1999). Prediction of the Binding Energy for Small Molecules, Peptides and Proteins.

103. B. K. Shoichet, A. R. Leach, and I. D. Kuntz, *Proteins: Struct., Funct., Genet.,* **34,** 4 (1999). Ligand Solvation in Molecular Docking.

104. B. N. Dominy and C. L. Brooks III, *Proteins: Struct., Funct., Genet.,* **36,** 318 (1999). Methodology for Protein–Ligand Binding Studies: Application to a Model for Drug Resistance, the HIV/FIV Protease System.

105. X. Zou, Y. Sun, and I. D. Kuntz, *J. Am. Chem. Soc.,* **121,** 8033 (1999). Inclusion of Solvation in Ligand-Binding Free Energy Calculations Using the Generalized Born Model.

106. I. Massova and P. A. Kollman, *J. Am. Chem. Soc.,* **121,** 8133 (1999). Computational Alanine Scanning to Probe Protein–Protein Interactions: A Novel Approach to Evaluate Binding Free Energies.

107. O. A. T. Donini and P. A. Kollman, *J. Med. Chem.,* **43,** 4180 (2000). Calculation and Prediction of Binding Free Energies for the Matrix Metalloproteinases.

108. B. Kuhn and P. A. Kollman, *J. Am. Chem. Soc.,* **122,** 3909 (2000). A Ligand That is Predicted to Bind Better to Avidin Than Biotin: Insights From Computational Fluorine Scanning.

109. J. Aquist, C. Medina, and J.-E. Samuelsson, *Protein Eng.,* **7,** 385 (1994). A New Method for Predicting Binding Affinity in Computer-Aided Drug Design.

110. T. Hansson, J. Marelius, and J. Aquist, *J. Comput.-Aided Mol. Design,* **12,** 27 (1998). Ligand Binding Affinity Prediction by Linear Interaction Energy Methods.

111. I. D. Wall, A. R. Leach, D. W. Salt, M. G. Ford, and J. W. Essex, *J. Med. Chem.,* **42,** 5142 (1999). Binding Constants of Neuraminidase Inhibitors: An Investigation of the Linear Interaction Energy Method.

112. R. C. Rizzo, J. Tirado-Rives, and W. L. Jorgensen, *J. Med. Chem.,* **44,** 145 (2001). Estimation of Binding Affinities for HEPT and Nevirapine Analogues With HIV-1 Reverse Transcriptase via Monte Carlo Simulations.

113. D. A. Pearlman, *J. Med. Chem.,* **42,** 4313 (1999). Free Energy Grids: A Practical Qualitative Application of Free Energy Perturbation to Ligand Design Using the OWFEG Method.

114. D. A. Pearlman and P. A. Charifson, *J. Med. Chem.,* **44,** 502 (2001). Improved Scoring of Ligand–Protein Interactions Using OWFEG Free Energy Grids.

115. D. N. A. Boobbyer, P. J. Goodford, P. M. McWhinnie, and R. C. Wade, *J. Med. Chem.,* **32,** 1083 (1989). New Hydrogen-Bond Potentials for Use in Determining Energetically Favorable Binding Sites on Molecules of Known Structure.

116. R. C. Wade, K. J. Clark, and P. J. Goodford, *J. Med. Chem.,* **36,** 140 (1993). Further Development of Hydrogen-Bond Functions for Use in Determining Energetically Favorable Binding Sites on Molecules of Known Structure. 1. Ligand Probe Groups With the Ability to Form Two Hydrogen Bonds.

117. R. C. Wade and P. J. Goodford, *J. Med. Chem.,* **36,** 148 (1993). Further Development of Hydrogen Bond Functions for Use in Determining Energetically Favorable Binding Sites on Molecules of Known Structure. 2. Ligand Probe Groups With the Ability to Form More Than Two Hydrogen Bonds.

118. M. K. Gilson, J. A. Given, B. L. Bush, and J. A. McCammon, *Biophys. J.,* **72,** 1047 (1997). The Statistical-Thermodynamic Basis for Computation of Binding Affinities: A Critical Review.

119. T. P. Straatsma, in *Reviews in Computational Chemistry,* K. B. Lipkowitz and D. B. Boyd, Eds., VCH Publishers, New York, 1991, Vol. 9, pp. 81–127. Free Energy by Molecular Simulation.

120. P. A. Kollman, *Acc. Chem. Res.,* **29,** 461 (1996). Advances and Continuing Challenges in Achieving Realistic and Predictive Simulations of the Properties of Organic and Biological Molecules.

121. M. L. Lamb and W. L. Jorgensen, *Curr. Opin. Chem. Biol.,* **1,** 449 (1997). Computational Approaches to Molecular Recognition.

122. M. R. Reddy, M. D. Erion, and A. Agarwal, in *Reviews in Computational Chemistry,* K. B. Lipkowitz and D. B. Boyd, Eds., Wiley-VCH, New York, 2000, Vol. 16, pp. 217–304. Free Energy Calculations: Use and Limitations in Predicting Ligand Binding Affinities.

123. M. K. Gilson, J. A. Given, and M. S. Head, *Chem. Biol.,* **4,** 87 (1997). A New Class of Models for Computing Receptor–Ligand Binding Affinities.

124. A. E. Mark and W. F. van Gunsteren, *J. Mol. Biol.,* **240,** 167 (1994). Decomposition of the Free Energy of a System in Terms of Specific Interactions.

125. D. Williams and B. Bardsley, *Perspect. Drug Discovery Design,* **17,** 43 (1999). Estimating Binding Constants—The Hydrophobic Effect and Cooperativity.

126. P. R. Andrews, D. J. Craik, and J. L. Martin, *J. Med. Chem.,* **27,** 1648 (1984). Functional Group Contributions to Drug–Receptor Interactions.

127. H.-J. Schneider, *Chem. Soc. Rev.,* **227** (1994). Linear Free Energy Relationships and Pairwise Interactions in Supramolecular Chemistry.

128. T. J. Stout, C. R. Sage, and R. M. Stroud, *Structure,* **6,** 839 (1998). The Additivity of Substrate Fragments in Enzyme–Ligand Binding.

129. M. K. Holloway, J. M. Wai, T. A. Halgren, P. M. D. Fitzgerald, J. P. Vacca, B. D. Dorsey, R. B. Levin, W. J. Thompson, L. J. Chen, S. J. deSolms, N. Gaffin, T. A. Lyle, W. A. Sanders, T. J. Tucker, M. Wiggins, C. M. Wiscount, O. W. Woltersdorf, S. D. Young, P. L. Darke, and J. A. Zugay, *J. Med. Chem.,* **38,** 305 (1995). A Priori Prediction of Activity for HIV-Protease Inhibitors Employing Energy Minimization in the Active Site.

130. P. D. J. Grootenhuis and P. J. M. van Galen, *Acta Crystallogr., Sect. D,* **51,** 560 (1995). Correlation of Binding Affinities With Non-Bonded Interaction Energies of Thrombin-Inhibitor Complexes.

131. S. J. Weiner, P. A. Kollman, D. A. Case, U. C. Singh, C. Ghio, G. Alagona, S. Profeta Jr., and P. Weiner, *J. Am. Chem. Soc.,* **106,** 765 (1984). A New Force Field for Molecular Mechanical Simulation of Nucleic Acids and Proteins.

132. S. J. Weiner, P. A. Kollman, D. T. Nguyen, and D. A. Case, *J. Comput. Chem.,* **7,** 230 (1986). An All Atom Force Field for Simulations of Proteins and Nucleic Acids.

133. B. R. Brooks, R. E. Bruccoleri, B. D. Olafson, D. J. States, S. Swaminathan, and M. Karplus, *J. Comput. Chem.,* **4,** 187 (1983). CHARMM: A Program for Macromolecular Energy, Minimization, and Dynamics Calculations.

134. A. Nicholls and B. Honig, *Science,* **268,** 1144 (1995). Classical Electrostatics in Biology and Chemistry.

135. N. Majeux, M. Scarsi, J. Apostolakis, C. Ehrhardt, and A. Caflisch, *Proteins: Struct., Funct., Genet.,* **37,** 88 (1999). Exhaustive Docking of Molecular Fragments with Electrostatic Solvation.

136. W. C. Still, A. Tempczyk, R. C. Hawley, and T. Hendrickson, *J. Am. Chem. Soc.,* **112,** 6127 (1990). Semianalytical Treatment of Solvation for Molecular Mechanics and Dynamics.

137. M. L. Lamb, K. W. Burdick, S. Toba, M. M. Young, A. G. Skillman, X. Zou, J. R. Arnold, and I. D. Kuntz, *Proteins: Struct., Funct., Genet.,* **42,** 296 (2001). Design, Docking and Evaluation of Multiple Libraries Against Multiple Targets.

138. T. Zhang and D. E. Koshland Jr., *Protein Sci.,* **5,** 348 (1996). Computational Method for Relative Binding Free Energies of Enzyme–Substrate Complexes.

139. P. H. Huenenberger, V. Helms, N. Narayana, S. S. Taylor, and J. A. McCammon, *Biochemistry,* **38,** 2358 (1999). Determinants of Ligand Binding to cAMP-Dependent Protein Kinase.

140. H. Meirovitch, in *Reviews in Computational Chemistry,* K. B. Lipkowitz and D. B. Boyd, Eds., Wiley-VCH, New York, 1998, Vol. 11, pp. 1–74. Calculation of the Free Energy and the Entropy of Macromolecular Systems by Computer Simulation.

141. J. Greer, J. W. Erickson, J. J. Baldwin, and M. D. Varney, *J. Med. Chem.,* **37,** 1035 (1994). Application of the Three-Dimensional Structures of Protein Target Molecules in Structure-Based Design.

142. J. Bostrom, P.-O. Norrby, and T. Liljefors, *J. Comput.-Aided Mol. Design,* **12,** 383 (1998). Conformational Energy Penalties of Protein-Bound Ligands.

143. M. Vieth, J. D. Hirst, and C. L. Brooks III, *J. Comput.-Aided Mol. Design,* **12,** 563 (1998). Do Active Site Conformations of Small Ligands Correspond to Low Free-Energy Solution Structures ?

144. G. Klebe and T. Mietzner, *J. Comput.-Aided Mol. Design,* **8,** 583 (1994). A Fast and Efficient Method to Generate Biologically Relevant Conformations.

145. I. D. Kuntz, K. Chen, K. A. Sharp, and P. A. Kollman, *Proc. Natl. Acad. Sci. U.S.A.,* **96,** 9997 (1999). The Maximal Affinity of Ligands.

146. Ajay and M. A. Murcko, *J. Med. Chem.,* **38,** 4953 (1995). Computational Methods to Predict Binding Free Energy in Ligand–Receptor Complexes.

147. J. D. Hirst, *Curr. Opin. Drug Discovery Dev.,* **1,** 28 (1998). Predicting Ligand-Binding Energies.

148. R. M. A. Knegtel and P. D. J. Grootenhuis, *Perspect. Drug Discovery Design,* **9–11,** 99 (1998). Binding Affinities and Non-Bonded Interaction Energies.

149. T. I. Oprea and G. R. Marshall, *Perspect. Drug Discovery Design,* **9–11,** 3 (1998). Receptor-Based Prediction of Binding Activities.

150. J. R. H. Tame, *J. Comput.-Aided Mol. Design,* **13,** 99 (1999). Scoring Functions: A View From the Bench.

151. H.-J. Boehm and M. Stahl, *Med. Chem. Res.,* **9,** 445 (1999). Rapid Empirical Scoring Functions in Virtual Screening Applications.

152. P. J. Goodford, *J. Mol. Graphics,* **3,** 107 (1985). Favored Sites for Drug Design.

153. M. Matsumara, W. J. Becktel, and B. W. Matthews, *Nature (London),* **334,** 406 (1988). Hydrophobic Stabilization in T4 Lysozyme Determined Directly by Multiple Substitutions of Ile 3.

154. V. Nauchatel, M. C. Villaverde, and F. Sussman, *Protein Sci.,* **4,** 1356 (1995). Solvent Accessibility as a Predictive Tool for the Free Energy of Inhibitor Binding to the HIV-1 Protease.

155. A. M. Davis and S. J. Teague, *Angew. Chem. Int. Ed.,* **38,** 736 (1999). Hydrogen Bonding, Hydrophobic Interactions, and Failure of the Rigid Receptor Hypothesis.

156. L. Wesson and D. Eisenberg, *Protein Sci.,* **1,** 227 (1992). Atomic Solvation Parameters Applied to Molecular Dynamics of Proteins in Solution.

157. S. Vajda, Z. Weng, R. Rosenfeld, and C. DeLisi, *Biochemistry,* **33,** 13977 (1994). Effect of Conformational Flexibility and Solvation on Receptor-Ligand Binding Free Energies.

158. S. Miyazawa and R. L. Jernigan, *Macromolecules,* **18,** 534 (1985). Estimation of Effective Interresidue Contact Energies From Protein Crystal Structures: Quasi-Chemical Approximation.

159. P. Rose, Computer Assisted Molecular Design Course, Jan 16–18, 1997, University of California, San Francisco, CA.

160. E. Gallicchio, M. M. Kubo, and R. M. Levy, *J. Am. Chem. Soc.,* **120,** 4526 (1998). Entropy–Enthalpy Compensation in Solvation and Ligand Binding Revisited.

161. F. C. Bernstein, T. F. Koetzle, G. J. B. Williams, E. F. Meyer Jr., M. D. Brice, J. R. Rodgers, O. Kennard, T. Shimanouchi, and M. Tasumi, *J. Mol. Biol.,* **112,** 535 (1977). The Protein Data Bank: A Computer-Based Archival File for Macromolecular Structures. http://www.rcsb.org/pdb.

162. H. Gohlke and G. Klebe, *Curr. Opin. Struct. Biol.,* **11,** 231 (2001). Statistical Potentials and Scoring Functions Applied to Protein–Ligand Binding.

163. M. J. Sippl, *J. Comput.-Aided Mol. Design,* **7,** 473 (1993). Boltzmann's Principle, Knowledge-Based Mean Fields and Protein Folding. An Approach to the Computational Determination of Protein Structures.

164. G. Verkhivker, K. Appelt, S. T. Freer, and J. E. Villafranca, *Protein Eng.,* **8,** 677 (1995). Empirical Free Energy Calculations of Ligand–Protein Crystallographic Complexes. I. Knowledge-Based Ligand Protein Interaction Potentials Applied to the Prediction of Human Immunodeficiency Virus 1 Protease Binding Affinity.

165. A. Wallqvist, R. L. Jernigan, and D. G. Covell, *Protein Sci.,* **4,** 1181 (1995). A Preference-Based Free-Energy Parameterization of Enzyme-Inhibitor Binding. Applications to HIV-1-Protease Inhibitor Design.

166. A. Wallqvist and D. G. Covell, *Proteins: Struct., Funct., Genet.,* **25,** 403 (1996). Docking Enzyme-Inhibitor Complexes Using a Preference-Based Free-Energy Surface.

167. Y. Sun, T. J. A. Ewing, A. G. Skillman, and I. D. Kuntz, *J. Comput.-Aided Mol. Design,* **12,** 579 (1998). CombiDOCK: Structure-Based Combinatorial Docking and Library Design.

168. E. J. Martin, R. E. Critchlow, D. C. Spellmeyer, S. Rosenberg, K. L. Spear, and J. M. Blaney, *Pharmacochem. Libr.,* **29,** 133 (1998). Diverse Approaches to Combinatorial Library Design.

169. DOCK User Manual, Regents of the University of California, San Francisco, CA. http://www.cmpharm.ucsf.edu/kuntz/kuntz.html.

170. R. M. A. Knegtel, D. M. Bayada, R. A. Engh, W. von der Saal, V. J. van Geerestein, and P. D. J. Grootenhuis, *J. Comput.-Aided Mol. Design,* **13,** 167 (1999). Comparison of Two Implementations of the Incremental Construction Algorithm in Flexible Docking of Thrombin Inhibitors.

171. M. Stahl and H.-J. Boehm, *J. Mol. Graphics Modell.,* **16,** 121 (1998). Development of Filter Functions for Protein–Ligand Docking.

172. C. Lemmen, T. Lengauer, and G. Klebe, *J. Med. Chem.,* **41,** 4502 (1998). FlexS: A Method for Fast Flexible Ligand Superposition.

173. C. Lemmen, A. Zien, R. Zimmer, and T. Lengauer, *Abstracts of the Pacific Symposium on Biocomputing,* Big Island, Hawaii, January 4–9, 1999, pp. 482–493. Application of Parameter Optimization to Molecular Comparison.

174. G. R. Desiraju and T. Steiner, *The Weak Hydrogen Bond in Chemistry and Biology,* Oxford University Press, Oxford, UK, 1999.

175. G. Parkinson, A. Gunasekera, J. Vojtechovsky, X. Zhang, T. Kunkel, H. Berman, and R. H. Ebright, *Nature Struct. Biol.,* **3,** 837 (1996). Aromatic Hydrogen Bond in Sequence-Specific Protein DNA Recognition.

176. J. P. Gallivan and D. A. Dougherty, *Proc. Natl. Acad. Sci. U.S.A.,* **96,** 9459 (1999). Cation–π Interactions in Structural Biology.

177. J. P. Gallivan and D. A. Dougherty, *J. Am. Chem. Soc.,* **122,** 870 (2000). A Computational Study of Cation–π Interactions vs. Salt Bridges in Aqueous Media: Implications for Protein Engineering.

178. G. B. McGaughey, M. Gagné, and A. K. Rappé, *J. Biol. Chem.,* **273,** 15458 (1998). π-Stacking Interactions.

179. C. Chipot, R. Jaffe, B. Maigret, D. A. Pearlman, and P. A. Kollman, *J. Am. Chem. Soc.,* **118,** 11217 (1996). The Benzene Dimer: A Good Model for π–π Interactions in Proteins? A Comparison Between the Benzene and the Toluene Dimers in the Gas Phase and in Aqueous Solution.

180. T. G. Davies, R. E. Hubbard, and J. R. H. Tame, *Protein Sci.,* **8,** 1432 (1999). Relating Structure to Thermodynamics: The Crystal Structures and Binding Affinity of Eight OppA-Peptide Complexes.

181. G. Klebe, F. Dullweber, and H.-J. Boehm, in *Drug-Receptor Thermodynamics: Introduction and Applications,* R. B. Raffa, Ed., Wiley, Chichester, UK, 2001, pp. 83–103. Thermodynamic Models of Drug-Receptor Interactions: A General Introduction.

182. S. Ha, R. Andreani, A. Robbins, and I. Muegge, *J. Comput.-Aided Mol. Design,* **14,** 435 (2000). Evaluation of Docking/Scoring Approaches: A Comparative Study Based on MMP3 Inhibitors.

183. I. Massova and P. A. Kollman, *Perspect. Drug Discovery Design,* **18,** 113 (2000). Combined Molecular Mechanical and Continuum Solvent Approach (MM-PBSA/GBSA) to Predict Ligand Binding.

184. B. Kuhn and P. A. Kollman, *J. Med. Chem.,* **43,** 3786 (2000). Binding of a Diverse Set of Ligands to Avidin and Streptavidin: An Accurate Quantitative Prediction of Their Relative Affinities by a Combination of Molecular Mechanics and Continuum Solvent Models.

185. N. Froloff, A. Windemuth, and B. Honig, *Protein Sci.,* **6,** 1293 (1997). On the Calculation of Binding Free Energies Using Continuum Methods: Application to MHC Class I Protein–Peptide Interactions.

186. J. Shen, *J. Med. Chem.,* **40,** 2953 (1997). A Theoretical Investigation of Tight-Binding Thermolysin Inhibitors.

187. C. J. Woods, M. A. King, and J. W. Essex, *J. Comput.-Aided Mol. Design,* **15,** 129 (2001). The Configurational Dependence of Binding Free Energies: A Poisson–Boltzmann Study of Neuraminidase Inhibitors.

188. G. Archontis, T. Simonson, and M. Karplus, *J. Mol. Biol.,* **306,** 307 (2001). Binding Free Energies and Free Energy Components from Molecular Dynamics and Poisson–Boltzmann Calculations. Application to Amino Acid Recognition by Aspartyl–tRNA Synthetase.

189. A. R. Leach, *J. Mol. Biol.,* **235,** 345 (1994). Ligand Docking to Proteins With Discrete Side-Chain Flexibility.

190. R. M. A. Knegtel, I. D. Kuntz, and C. M. Oshiro, *J. Mol. Biol.,* **266,** 424 (1997). Molecular Docking to Ensembles of Protein Structures.

191. C. McMartin and R. S. Bohacek, *J. Comput.-Aided Mol. Design,* **11,** 333 (1997). QXP: Powerful, Rapid Computer Algorithms for Structure-Based Drug Design.

192. J. Apostolakis, A. Plückthun, and A. Caflisch, *J. Comput. Chem.,* **19,** 21 (1998). Docking Small Ligands in Flexible Binding Sites.

193. V. Schnecke, C. A. Swanson, E. D. Getzoff, J. A. Tainer, and L. A. Kuhn, *Proteins: Struct., Funct., Genet.,* **33,** 74 (1998). Screening a Peptidyl Database for Potential Ligands to Proteins With Side-Chain Flexibility.

194. I. Kolossváry, and W. C. Guida, *J. Comput. Chem.,* **20,** 1671 (1999). Low-Mode Conformational Search Elucidated: Application to $C_{39}H_{80}$ and Flexible Docking of 9-Deazaguanine Inhibitors to PNP.

195. H. B. Broughton, *J. Mol. Graphics Modell.,* **18,** 247 (2000). A Method for Including Protein Flexibility in Protein–Ligand Docking: Improving Tools for Database Mining and Virtual Screening.

196. H. Claussen, C. Buning, M. Rarey, and T. Lengauer, *J. Mol. Biol.,* **308,** 377 (2001). FlexE: Efficient Molecular Docking Considering Protein Structure Variations.

197. M. D. Miller, R. P. Sheridan, S. K. Kearsley, and D. J. Underwood, in *Methods in Enzymology,* L. C. Kuo and J. A. Shafer, Eds., Academic Press, San Diego, 1994, Vol. 241, pp. 354–370. Advances in Automated Docking Applied to Human Immunodeficiency Virus Type 1 Protease.

198. P. S. Charifson, J. J. Corkery, M. A. Murcko, and W. P. Walters, *J. Med. Chem.,* **42,** 5100 (1999). Consensus Scoring: A Method for Obtaining Improved Hit Rates from Docking Databases of Three-Dimensional Structures into Proteins.

199. C. A. Baxter, C. W. Murray, D. E. Clark, D. R. Westhead, and M. D. Eldridge, *Proteins: Struct., Funct., Genet.,* **33,** 367 (1998). Flexible Docking Using Tabu Search and an Empirical Estimate of Binding Affinity.

200. WDI: World Drug Index, 1996, Derwent Information. http://www.derwent.com.

201. Protherics PLC, Runcorn, Cheshire, UK. The data set was formerly available at http://www.protherics.com/crunch/.

202. S. B. Shuker, P. J. Hajduk, R. P. Meadows, and S. W. Fesik, *Science,* **274,** 1531 (1996). Discovering High-Affinity Ligands for Proteins: SAR by NMR.

203. N. Tomioka and A. Itai, *J. Comput.-Aided Mol. Design,* **8,** 347 (1994). GREEN: A Program Package for Docking Studies in Rational Drug Design.

204. T. Toyoda, R. K. B. Brobey, G.-I. Sano, T. Horii, N. Tomioka, and A. Itai, *Biochem. Biophys. Res. Commun.,* **235,** 515 (1997). Lead Discovery of Inhibitors of the Dihydrofolate Reductase Domain of *Plasmodium falciparum* Dihydrofolate Reductase–Thymidylate Synthase.

205. P. Burkhard, P. Taylor, and M. D. Walkinshaw, *J. Mol. Biol.,* **277,** 449 (1998). An Example of a Protein Ligand Found by Database Mining: Description of the Docking Method and Its Verification by a 2.3 Å X-Ray Structure of a Thrombin–Ligand Complex.

206. R. Abagyan, M. Trotov, and D. Kuznetsov, *J. Comput. Chem.,* **15,** 488 (1994). ICM—A New Method for Protein Modeling and Design: Applications to Docking and Structure Prediction from the Distorted Native Conformation.

207. M. Schapira, B. M. Raaka, H. H. Samuels, and R. Abagyan, *Proc. Natl. Acad. Sci. U.S.A.,* **97,** 1008 (2000). Rational Discovery of Novel Nuclear Hormone Receptor Antagonists.

208. A. V. Filikov, V. Monan, T. A. Vickers, R. H. Griffey, P. D. Cook, R. A. Abagyan, and T. L. James, *J. Comput.-Aided Mol. Design,* **14,** 593 (2000). Identification of Ligands for RNA Targets via Structure-Based Virtual Screening: HIV-1 TAR.

209. Available Chemicals Directory, MDL Information Systems, Inc., San Leandro, CA, USA. http://www.mdl.com.

210. D. W. Christianson and C. A. Fierke, *Acc. Chem. Res.,* **29,** 331 (1996). Carbonic Anhydrase: Evolution of the Zinc-Binding Site by Nature and by Design.

211. Maybridge Database, Maybridge Chemical Co. Ltd., UK, 1999. http://www.maybridge.com and http://www.daylight.com.

212. LeadQuest Chemical Compound Libraries, Vol. 1–3, 2000, Tripos Inc., St. Louis, MO, USA. http://www.tripos.com.

213. J. Sadowski, C. Rudolph, and J. Gasteiger, *Tetrahedron Comput. Methodol.,* **3,** 537 (1990). Automatic Generation of 3D Atomic Coordinates for Organic Molecules.

214. J. Sadowski, C. H. Schwab, and J. Gasteiger, Corina, 1998, Molecular Networks GmbH Computerchemie, Erlangen, Germany. http://www.mol-net.de/.

215. Unity Chemical Information Software, Version 4.1.1., Tripos, Inc., St. Louis, MO, USA.

216. A. Maxwell, *Biochem. Soc. Trans.,* **27,** 48 (1999). DNA Gyrase as a Drug Target.

217. D. Bailey and D. Brown, *Drug Discovery Today,* **6,** 57 (2001). High-Throughput Chemistry and Structure-Based Design: Survival of the Smartest.

218. R. M. Eglen, G. Scheider, and H.-J. Boehm, in *Virtual Screening for Bioactive Molecules,* G. Schneider and H.-J. Boehm, Eds., Wiley-VCH, Weinheim, 2000, pp. 1–14. High-Throughput Screening and Virtual Screening: Entry Points to Drug Discovery.

219. R. Lahana, *Drug Discovery Today,* **4,** 447 (1999). How Many Leads from HTS?

*Reviews in Computational Chemistry, Volume 18*
Edited by Kenny B. Lipkowitz and Donald B. Boyd

ISBN: 0-471-21576-7

CHAPTER 3

# Potentials and Algorithms for Incorporating Polarizability in Computer Simulations

**Steven W. Rick* and Steven J. Stuart†**

**Department of Chemistry, University of New Orleans, New Orleans, Louisiana 70148 and Chemistry Department, Southern University of New Orleans, New Orleans, Louisiana 70126, and †Department of Chemistry, Clemson University, Clemson, South Carolina 29634*

## INTRODUCTION

Polarization refers to the redistribution of a particle's electron density due to an electric field. In terms of molecular interactions, polarization leads to nonadditivity, since a molecule polarized by another molecule will interact differently with a third molecule than it would if it were not polarized. The change in the electron density can be characterized by changes in the monopole charges, dipole moments, or higher order moments. Methods for treating polarizability in molecular dynamics or Monte Carlo simulations achieve this goal through inducible dipole moments (the polarizable point dipole and shell models) or through fluctuating charges (the electronegativity equalization and semiempirical models). This chapter describes these models, with a focus on those methods that have been developed for molecular dynamics and Monte

Carlo computer simulations, and reviews some of the systems that have been simulated with polarizable potentials.

## NONPOLARIZABLE MODELS

Before discussing polarizable models, a useful starting point is to consider nonpolarizable models. A typical nonpolarizable potential for molecular systems is[1]

$$U = \sum_{\text{bonds}} K_B(r - r_0)^2 + \sum_{\text{angles}} K_\theta(\theta - \theta_0)^2 + \sum_{\text{dihedrals}} \sum_n \frac{V_n}{2}(1 + \cos(n\phi - \gamma)) + \sum_{\text{nonbonded pairs}} \left\{ 4\varepsilon_{ij} \left[ \left(\frac{\sigma_{ij}}{r_{ij}}\right)^{12} - \left(\frac{\sigma_{ij}}{r_{ij}}\right)^{6} \right] + \frac{q_i q_j}{r_{ij}} \right\} \quad [1]$$

where $U$ represents the potential energy of the system. There are terms for the bond length, $r$, with a force constant, $K_B$, and an equilibrium bond length, $r_0$; the bond angle, $\theta$, with a force constant $K_\theta$ and an equilibrium angle, $\theta_0$; and the dihedral angle, $\phi$, with barrier heights, $V_n$, and equilibrium angles, $\gamma$. The intermolecular interactions are described with a Lennard–Jones (LJ) interaction,

$$U_{\text{LJ}}(r) = 4\varepsilon_{ij} \left[ \left(\frac{\sigma_{ij}}{r_{ij}}\right)^{12} - \left(\frac{\sigma_{ij}}{r_{ij}}\right)^{6} \right] \quad [2]$$

in which $\varepsilon$ and $\sigma$ are parameters describing the energy and distance scale of the interactions, respectively, and $r_{ij}$ is the distance between nonbonded atoms $i$ and $j$. The Coulomb interaction between charged atoms is given by $q_i q_j / r_{ij}$, where $q_i$ is the partial charge on atom $i$. These interactions are illustrated in Figure 1.

The Lennard–Jones interaction contains a short-range repulsive part, falling off as $r^{-12}$, and a longer range attractive part, falling off as $r^{-6}$. The attractive part has the same dependence as the (dipole–dipole) London dispersion energy, which for two particles with polarizabilities $\alpha$ is proportional to $-\alpha^2/r^6$ (Ref. 2). The Lennard–Jones parameters are not typically assigned[3] using known values of $\alpha$, but this interaction is one way in which polarizability, in an average sense, is included in nonpolarizable models.

Another way in which polarizability is included implicitly is in the value of the partial charges, $q_i$, that are assigned to the atoms in the model. The charges used in potential energy models for condensed phases are often enhanced from the values that would be consistent with the gas-phase dipole moment, or those that would best reproduce the electrostatic potential (ESP)

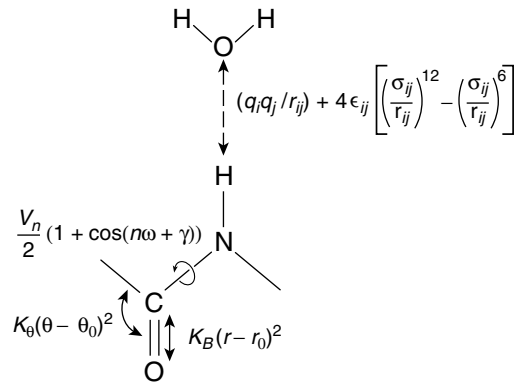


**Figure 1** Schematic of the interactions between an amino group and a water showing the Lennard–Jones and electrostatic nonbonded interactions along with the bond length, bond angle, and dihedral angle (torsional) interactions.

from gas-phase ab initio calculations. Enhanced charge values are a means of accounting for the strong polarization of electron distributions by the electric fields of the other particles in a condensed phase environment. The enhanced charges are obtained either through explicit parameterization[4,5] or by using charges obtained via quantum chemical methods that are known to overestimate charge values.[6] Although the enhanced charge values treat polarization in an effective way, they cannot correctly reflect the dependence of charge distributions on the system's state, nor can they respond dynamically to fluctuations in the electric field due to molecular motion. The average electric field, and therefore the charge distribution and dipole moment, will depend on the physical state and composition of the system. For example, a molecule in a solution with a high ionic strength may feel a field different from a molecule in a pure solvent; even in the bulk liquid state, the polarization of a water molecule will depend on the density, and thus on the system's temperature and pressure. In addition, conformational changes may influence the charge distribution of a molecule.[7–13] Molecular motions in the system will result in conformational changes and fluctuations in the electric field, causing the electrostatic distribution to change on a subpicosecond time scale. Treating these effects requires a polarizable model.

## POLARIZABLE POINT DIPOLES

One method for treating polarizability is to add point inducible dipoles on some or all atomic sites. This polarizable point dipoles (PPD) method has been applied to a wide variety of atomic and molecular systems, ranging from noble gases to water to proteins. The dipole moment, $\boldsymbol{\mu}_i$, induced on a site $i$ is

proportional to the electric field at that site, $\mathbf{E}_i$. The proportionality constant is the polarizability tensor, $\boldsymbol{\alpha}_i$. The dipole feels an electric field both from the permanent charges of the system and from the other induced dipoles. The expression for the $\boldsymbol{\mu}_i$ is

$$\boldsymbol{\mu}_i = \boldsymbol{\alpha}_i \cdot \mathbf{E}_i = \boldsymbol{\alpha}_i \cdot \left[ \mathbf{E}_i^0 - \sum_{j \neq i} \mathbf{T}_{ij} \boldsymbol{\mu}_j \right] \quad [3]$$

where $\mathbf{E}^0$ is the field from the permanent charges. (There also may be permanent dipoles or other multipoles present contributing to $\mathbf{E}^0$.) The induced dipoles interact through the dipole field tensor, $\mathbf{T}_{ij}$,

$$\mathbf{T}_{ij} = \frac{1}{r^3}\mathbf{I} - \frac{3}{r^5} \begin{pmatrix} x^2 & xy & xz \\ yx & y^2 & yz \\ zx & zy & z^2 \end{pmatrix} \quad [4]$$

where $\mathbf{I}$ is the identity matrix, $r$ is the distance between $i$ and $j$, and $x$, $y$, and $z$ are the Cartesian components of the vector between $i$ and $j$.

The energy of the induced dipoles, $U_{\text{ind}}$, can be split into three terms,

$$U_{\text{ind}} = U_{\text{stat}} + U_{\mu\mu} + U_{\text{pol}} \quad [5]$$

The energy $U_{\text{stat}}$ is the interaction energy of the $N$ induced dipoles with the permanent, or static, field

$$U_{\text{stat}} = -\sum_{i=1}^{N} \boldsymbol{\mu}_i \cdot \mathbf{E}_i^0 \quad [6]$$

the energy $U_{\mu\mu}$ is the induced dipole–induced dipole interaction

$$U_{\mu\mu} = \frac{1}{2} \sum_{i=1}^{N} \sum_{j \neq i} \boldsymbol{\mu}_i \cdot \mathbf{T}_{ij} \cdot \boldsymbol{\mu}_j \quad [7]$$

and the polarization energy, $U_{\text{pol}}$,

$$U_{\text{pol}} = \frac{1}{2} \sum_{i=1}^{N} \boldsymbol{\mu}_i \cdot \mathbf{E}_i \quad [8]$$

is that required to distort the electron distribution to create the dipoles.[4,14] Any polarizable model in which dipole moments, charges, or other multipoles

are modified by their environment will have a polarization energy corresponding to $U_{\text{pol}}$. Even nonpolarizable models that are parameterized to have charges enhanced from the gas-phase values should include such a term, and $U_{\text{pol}}$ has been called the "missing term" in many pair potentials.[4,5] By using Eq. [3], the electric field can be replaced by $\boldsymbol{\alpha}^{-1} \cdot \boldsymbol{\mu}_i$ and $U_{\text{pol}}$ can be written as

$$U_{\text{pol}} = \frac{1}{2}\sum_{i=1}^{N} \boldsymbol{\mu}_i \cdot \boldsymbol{\alpha}_i^{-1} \cdot \boldsymbol{\mu}_i \qquad [9]$$

where $\boldsymbol{\alpha}_i^{-1}$ is the inverse of the polarization tensor. If the polarization matrix is isotropic ($\alpha_{xx} = \alpha_{yy} = \alpha_{zz} = \alpha_i$) and diagonal, then

$$U_{\text{pol}} = \sum_{i=1}^{N} \frac{\mu_i^2}{2\alpha_i} \qquad [10]$$

Combining the three energy terms gives

$$U_{\text{ind}} = \sum_{i=1}^{N} \boldsymbol{\mu}_i \cdot \left[ -\mathbf{E}_i^0 + \frac{1}{2}\sum_{j \neq i} \mathbf{T}_{ij} \cdot \boldsymbol{\mu}_j + \frac{1}{2}\mathbf{E}_i \right] \qquad [11]$$

which, using $\mathbf{E}_i = \mathbf{E}_i^0 - \sum \mathbf{T}_{ij} \cdot \boldsymbol{\mu}_j$ (Eq. [3]), reduces to the relationship for the static field, $\mathbf{E}^0$, and

$$U_{\text{ind}} = -\frac{1}{2}\sum_{i=1}^{N} \boldsymbol{\mu}_i \cdot \mathbf{E}_i^0 \qquad [12]$$

Note that the energy is the dot product of the induced dipole and the *static* field, not the total field.[15–19] Without a static field, there are no induced dipoles. Induced dipoles alone do not interact strongly enough to overcome the polarization energy it takes to create them (except when they are close enough to polarize catastrophically).

The static field at site $i$ due to permanent charges is

$$\mathbf{E}_i^0 = \sum_{j \neq i} \frac{q_j \mathbf{r}_{ij}}{r_{ij}^3} \qquad [13]$$

where $q_j$ is the charge at site $j$ and $r_{ij}$ is the distance between $i$ and $j$. A point charge at a site is generally assumed not to contribute to the field at that site. For rigid models of water and other small molecules, charges on the same molecule contribute a constant amount to the electric field at each site

(in internal coordinates). These effects are often incorporated into the fixed charge distribution and are not explicitly included in the static field, which is calculated using only charges from different molecules.[15,19–37]

Some water models use a shielding function, $S(r)$, that changes the contribution to $\mathbf{E}_i$ from the charge at $j$,[20,26,30,31,37]

$$\mathbf{E}_i = \sum_{j \neq i} \frac{S(r_{ij}) q_j \mathbf{r}_{ij}}{|r_{ij}|^3} \qquad [14]$$

The shielding function differs from 1 only at small distances and accounts for the fact that at small separations the electric field will be modified by the spatial extent of the electron cloud. For larger molecules, the interactions from atoms that are directly bonded to atom $i$ and are separated by two bonds or less (termed 1–2 and 1–3 bonded interactions) do not typically contribute to $\mathbf{E}_i$.[32,38]

In the most general case, all the dipoles will interact through the dipole field tensor. The method of Applequist et al.[39,40] for calculating molecular polarizabilities uses this approach. One problem with coupling all the dipoles with the interaction given by Eq. [4] is the "polarization catastrophe". As pointed out by Applequist, Carl, and Fung[39] and Thole,[41] the molecular polarization, and therefore the induced dipole moment, may become infinite at small distances. The mathematical origins of such singularities are made more evident by considering a simple system consisting of two atoms (A and B) with isotropic polarizabilities, $\alpha_A$ and $\alpha_B$. The molecular polarizability, which relates the molecular dipole moment ($\boldsymbol{\mu} = \boldsymbol{\mu}_A + \boldsymbol{\mu}_B$) to the electric field, has two components, one parallel and one perpendicular to the bond axis between A and B,

$$\alpha_{||} = [\alpha_A + \alpha_B + (4\alpha_A\alpha_B/r^3)]/[1 - (4\alpha_A\alpha_B/r^6)] \qquad [15]$$

$$\alpha_{\perp} = [\alpha_A + \alpha_B - (2\alpha_A\alpha_B/r^3)]/[1 - (\alpha_A\alpha_B/r^6)] \qquad [16]$$

The parallel component, $\alpha_{||}$, becomes infinite as the distance between the two atoms approaches $(4\alpha_A\alpha_B)^{1/6}$. The singularities can be avoided by making the polarizabilities sufficiently small so that at the typical distances between the atoms ($>1$ Å) the factor $(4\alpha_A\alpha_B)/r^6$ is always less than one. The Applequist polarizabilities are in fact small compared to ab initio values.[41,42] Applequist's atomic polarizabilities were selected to optimize the molecular polarizabilities for a set of 41 molecules (see Table 1). Note that careful choice of polarizabilities can move the singularities in Eqs. [15] and [16] to small distances, but not eliminate them completely, thus causing problems for simulation techniques such as Monte Carlo (MC), which tend to sample these nonphysical regions of configuration space.

**Table 1** Polarizability Parameters for Atoms

| | Polarizability (Å$^3$) | | |
|---|---|---|---|
| Atom | Applequist et al.[a] | Thole[b] | Experimental or ab initio[c] |
| H (alkane) | 0.135 | 0.514 | 0.667 |
| H (alcohol) | 0.135 | — | — |
| H (aldehyde) | 0.167 | — | — |
| H (amide) | 0.161 | — | — |
| C (alkane) | 0.878 | 1.405 | 1.76 |
| C (carbonyl) | 0.616 | — | — |
| N (amide) | 0.530 | 1.105 | 1.10 |
| N (nitrile) | 0.52 | — | — |
| O (alcohol) | 0.465 | 0.862 | 0.802 |
| O (ether) | 0.465 | — | — |
| O (carbonyl) | 0.434 | — | — |
| F | 0.32 | — | 0.557 |
| Cl | 1.91 | — | 2.18 |
| Br | 2.88 | — | 3.05 |
| I | 4.69 | — | 5.35 |

[a]Ref. 39.
[b]Ref. 41
[c]Ref. 42.

Alternatively, the polarization catastrophe can be avoided by screening (attenuating) the dipole–dipole interaction at small distances.[41] As with the screening of the static field, screening of the dipole–dipole interaction can be physically interpreted as correcting for the fact that the electronic distribution is not well represented by point charges and dipoles at small distances.[39,41,43] Mathematically, screening avoids the singularities such as those in Eqs. [15] and [16]. The Thole procedure for screening is to introduce a scaling distance $s_{ij} = 1.662(\alpha_i\alpha_j)^{1/6}$. This results in a charge density radius of 1.662 Å, for example, between atoms with a polarizability of 1 Å$^3$. The dipole field tensor is thus changed to

$$\mathbf{T}_{ij} = (4v^3 - 3v^4)\frac{1}{r^3}\mathbf{I} - v^4\frac{3}{r^5}\begin{pmatrix} x^2 & xy & xz \\ yx & y^2 & yz \\ zx & zy & z^2 \end{pmatrix} \qquad [17]$$

where $v = r/s_{ij}$. $\mathbf{T}_{ij}$ is unchanged if $r$ is greater than $s_{ij}$. Thole's polarizability parameters, together with the scale factor 1.662, were selected to optimize the molecular polarizabilities for a set of 16 molecules (Table 1). Unlike Applequist, Thole assigns only one polarizability per atom independent of its valence state and does not assign polarizabilities to halide atoms. The Thole parameters are closer to the experimental and ab initio polarizabilities.[42] Although the atomic polarizabilities of Applequist and Thole are different, the resulting

molecular polarizabilities are not that far off, with the Applequist method tending to overestimate the polarization anisotropies.

Various computer simulation models have used either the Applequist parameters and no screening[15,16,24,27,28,32,34] or the Thole parameters and screening of $\mathbf{T}_{ij}$.[19,31,38] Different screening functions have been used as well. A large number of polarizable models have been developed for water, many of them with one polarizable site (with $\alpha = 1.44$ Å$^3$) on or near the oxygen position.[20–23,26,29,30,33,35–37] For these models, the polarizable sites do not typically get close enough for polarization catastrophes $\{(4\alpha\alpha)^{1/6} = 1.4$ Å, see comments after Eq. [16]$\}$, so screening is not as necessary as it would be if polarization sites were on all atoms. However, some water models with a single polarizable site do screen the dipole field tensor.[20,22,37] Another model for water places polarizable sites on bonds.[25] Other polarizable models have been used for monatomic ions and used no screening of $\mathbf{T}$ or $\mathbf{E}^0$.[15,16,27,34] Polarizable models have been developed for proteins as well, by Warshel and co-workers (with screening of $\mathbf{T}$ but not $\mathbf{E}^0$),[44,45] and by Wodak and co-workers (with no screening).[46]

An attractive feature of the dipole polarizable model is that the assignment of electrostatic potential parameters is more straightforward than for nonpolarizable models. Charges can be assigned on the basis of experimental dipole moments or ab initio electrostatic potential charges for the isolated molecule. The polarizabilities can be assigned from the literature (as in Table 1) or calculated. Contrarily, with nonpolarizable models, charges may have some permanent polarization to reflect their enhanced values in the condensed phase.[6,47] The degree of enhancement is part of the art of constructing potentials and limits the transferability of these potentials. By explicitly including polarizability, the polarizable models are a more systematic approach for potential parameterization and are therefore more transferrable.

Using Eqs. [9] and [11], the energy can be rewritten as

$$U_{\text{ind}} = -\sum_{i=1}^{N} \boldsymbol{\mu}_i \cdot \mathbf{E}_i^0 + \frac{1}{2}\sum_{i=1}^{N}\sum_{j\neq i} \boldsymbol{\mu}_i \cdot \mathbf{T}_{ij} \cdot \boldsymbol{\mu}_j + \frac{1}{2}\sum_{i=1}^{N} \boldsymbol{\mu}_i \boldsymbol{\alpha}_i^{-1} \boldsymbol{\mu}_i \qquad [18]$$

and the derivative of $U_{\text{ind}}$ with respect to the induced dipoles is

$$\boldsymbol{\nabla}_{\boldsymbol{\mu}_i} U_{\text{ind}} = -\mathbf{E}_i^0 + \sum_{j\neq i} \mathbf{T}_{ij} \cdot \boldsymbol{\mu}_j + \boldsymbol{\alpha}_i^{-1} \cdot \boldsymbol{\mu}_i = 0 \qquad [19]$$

The derivative in Eq. [19] is zero because $\boldsymbol{\alpha}_i^{-1} \cdot \boldsymbol{\mu}_i = \mathbf{E}_i^0 - \sum \mathbf{T}_{ij} \cdot \boldsymbol{\mu}_j$, according to Eq. [3]. The values of the induced dipoles are therefore those that minimize the energy. Other polarizable models also have auxiliary variables, analogous to $\boldsymbol{\mu}$, which likewise adjust to minimize the energy.

The polarizable point dipole models have been used in molecular dynamics (MD) simulations since the 1970s.[48] For these simulations, the forces, or spatial derivatives of the potential, are needed. From Eq. [18], the force[23] on atomic site $k$ is

$$\mathbf{F}_k = -\nabla_k U_{\text{ind}} = \sum_{i=1}^{N} \boldsymbol{\mu}_i \nabla_k \mathbf{E}_i^0 + \sum_{i \neq k} \boldsymbol{\mu}_k \cdot (\nabla_k \mathbf{T}_{ki}) \cdot \boldsymbol{\mu}_i \qquad [20]$$

All contributions to the forces from terms involving derivatives with respect to the dipoles are zero from the extremum condition of Eq. [19].[23,49]

Finding the inducible dipoles requires a self-consistent method, because the field that each dipole feels depends on all of the other induced dipoles. There exist three methods for determining the dipoles: matrix inversion, iterative methods, and predictive methods. We describe each of these in turn.

The dipoles are coupled through the matrix equation,

$$\mathbf{A} \cdot \boldsymbol{\mu} = \mathbf{E}^0 \qquad [21]$$

where the diagonal elements of the matrix, $A_{ii}$, are $\boldsymbol{\alpha}_i^{-1}$ and the off-diagonal elements $A_{ij}$ are $T_{ij}$. For a system with $N$ dipoles, solving for each of them involves inverting the $N \times N$ matrix, **A**—an $O(N^3)$ operation that is typically too computationally expensive to perform at each step of an $O(N)$ or $O(N^2)$ simulation. Consequently, this method has been used only rarely.[31] Note that since Eq. [21] for $\boldsymbol{\mu}$ is linear, there is only one solution for the dipoles.

In the iterative method, an initial guess for the field is made by, for example, just using the static field, $\mathbf{E}^0$, or by using the dipoles from the previous time step of the MD simulation.[48,49] The dipole moments resulting from this field are evaluated using Eq. [3], which can be iterated to self-consistency. Typical convergence limits on the dipoles range from $1 \times 10^{-2}$ D to $1 \times 10^{-6}$ D.[21,27,34–36,50] Long simulations require very strict convergence limits or mild thermostatting[50] to prevent problems due to poor energy conservation. Alternatively, the energy $U_{\text{pol}}$ can be monitored for convergence.[19,51] The level of convergence, and therefore the number of iterations required, varies considerably. Between 2 and 10 iterations are typically required. For some calculations, including free energy calculations, a high level of convergence may be necessary.[38] The iterative method is the most common method for finding the dipoles.

The predictive methods determine $\boldsymbol{\mu}$ for the next time step based on information from previous time steps. Ahlström et al.[23] used a first-order predictor algorithm, which uses the $\boldsymbol{\mu}$ values from the two previous times steps to predict $\boldsymbol{\mu}$ at the next time step,

$$\boldsymbol{\mu}_i(t) = 2\boldsymbol{\mu}_i(t - \Delta t) - \boldsymbol{\mu}_i(t - 2\Delta t) \qquad [22]$$

where $\Delta t$ is the time step, and $t$ is time. This method is not stable for long times, but can be combined with an iterative solution, either by providing the initial iteration of the electric field values,[52,53] or by allowing the iteration to be performed less frequently than every step.[23,54] Higher-order predictor algorithms have been used as well.[23,52,55]

A different predictive procedure is to use the extended Lagrangian method, in which each dipole is treated as a dynamical variable and given a mass $M_\mu$ and velocity $\dot{\boldsymbol{\mu}}$. The dipoles thus have a kinetic energy, $\frac{1}{2}\sum_i M_\mu \dot{\boldsymbol{\mu}}_i^2$ and are propagated using the equations of motion just like the atomic coordinates.[22,56–58] The equation of motion for the dipoles is

$$M_\mu \ddot{\boldsymbol{\mu}}_i = -\nabla_{\boldsymbol{\mu}_i} U_{\text{ind}} = \mathbf{E}_i - \boldsymbol{\alpha}_i^{-1} \cdot \boldsymbol{\mu}_i \qquad [23]$$

Here $\ddot{\boldsymbol{\mu}}_i$ is the second derivative with respect to time, that is, the acceleration. The dipole mass does not correspond to any physical mass of the system; it is chosen for numerical convenience, by, for example, comparing the trajectories with those from the iterative method.[57] It is desirable to keep the kinetic energy of the dipoles small so that the dipole degrees of freedom are cold and near the potential energy minimum (corresponding to the exact solution of Eq. [3]).

Because this method avoids iterations, which require recalculating $\mathbf{E}_i$ multiple times for every sampled configuration, the extended Lagrangian method is a more efficient way of calculating the dipoles at every time step. But even with methods that allow for only a single evaluation of the energy and force per time step, polarizable point dipole methods are more computationally intensive than nonpolarizable simulations. Evaluating the dipole–dipole interactions in Eqs. [7] and [20] is several times more expensive than evaluating the Coulombic interactions between point charges in Eq. [1]. A widely used rule of thumb is that polarizable simulations based on a point dipole model take roughly four times longer than a nonpolarizable simulation of the same system.

The polarizable point dipole model has also been used in Monte Carlo simulations with single particle moves.[19,21,24,59–62] When using the iterative method, a whole new set of dipoles must be computed after each molecule is moved. These updates can be made more efficient by storing the distances between all the particles, since most of them are unchanged, but this requires a lot of memory. The many-body nature of polarization makes it more amenable to molecular dynamics techniques, in which all particles move at once, compared to Monte Carlo methods where typically only one particle moves at a time. For nonpolarizable, pairwise-additive models, MC methods can be efficient because only the interactions involving the moved particle need to be recalculated [while the other $(N-1)\times(N-1)$ interactions are unchanged]. For polarizable models, all $N \times N$ interactions are, in principle, altered when one particle moves. Consequently, exact polarizable MC calculations can be

two to three orders of magnitude slower than comparable nonpolarizable calculations.[63] Various approximate methods, involving incomplete convergence or updating only a subset of the dipoles, have been suggested.[59] Unfortunately, these methods result in significant errors in computed physical properties.[19,63] Monte Carlo methods are capable of moving more than one particle at a time, with good acceptance ratios,[64,65] using, for example, the hybrid MC technique, but this method has not been applied to polarizable models, as far as we are aware.

One final point concerns the long-range nature of the interactions in dipole-based models. Dipole–dipole and dipole–charge interactions are termed long range because they do not decrease faster than volume grows—that is, as $r^3$. If periodic boundary conditions are used, some treatment of the long-range interactions is needed. The most complete treatment of the long-range forces is the Ewald summation technique.[64,66] All models, whether polarizable or not, face this problem if they have long-range forces, but for polarizable models this is a more significant issue. The use of cut-offs or other truncation schemes will change both the static field and the dipole field tensor. These changes to the electric field will modify the value of the induced dipole, which in turn will change the field at other sites. Accordingly, the treatment of long-range forces feeds back on itself in a way that does not occur with nonpolarizable models. It is thus crucial to treat the long-range interactions as accurately as possible in polarizable simulations. Nevertheless, a large number, if not most, of the simulations using polarizable potentials have not used Ewald sums. Recently, Nymand and Linse[67] showed that different boundary conditions (including Ewald sums, spherical cut-off, and reaction field methods) lead to more significant differences in equilibrium, dynamical, and structural properties for polarizable water models than for nonpolarizable models.

Conventional methods for performing the Ewald sum scale as $O(N^{3/2})$ or $O(N^2)$,[68] and formulations specifically designed to include dipole–dipole interactions[66] are in fairly wide use. Faster scaling methods, such as the fast multipole and particle–mesh algorithms, have also been extended to the treatment of point dipoles.[50,69]

## SHELL MODELS

A defining feature of the models discussed in the previous section, regardless of whether they are implemented via matrix inversion, iterative techniques, or predictive methods, is that they all treat the polarization response in each polarizable center using point dipoles. An alternative approach is to model the polarizable centers using dipoles of finite length, represented by a pair of point charges. A variety of different models of polarizability have used this approach, but especially noteworthy are the shell models frequently used in simulations of solid-state ionic materials.

The shell model has its origin in the Born theory of lattice dynamics, used in studies of the phonon dispersion curves in crystals.[70,71] Although the Born theory includes the effects of polarization at each lattice site, it does not account for the short-range interactions between sites and, most importantly, neglects the effects of this interaction potential on the polarization behavior. The shell model, however, incorporates these short-range interactions.[72,73] The earliest applications of the shell model, as with the Born model, were to analytical studies of phonon dispersion relations in solids.[74] These early applications have been well reviewed elsewhere.[71,75–77] In general, lattice dynamics applications of the shell model do not attempt to account for the dynamics of the nuclei and typically use analytical techniques to describe the statistical mechanics of the shells. Although the shell model continues to be used in this fashion,[78] lattice dynamics applications are beyond the scope of this chapter. In recent decades, the shell model has come into widespread use as a model Hamiltonian for use in molecular dynamics simulations; it is these applications of the shell model that are of interest to us here.

The shell model to be described in detail below is essentially identical to the Drude oscillator model;[79,80] both treat polarization via a pair of charges attached by a harmonic spring. The different nomenclature results largely from the use of these models in recent decades by two different scientific communities. The term *Drude model* is used more frequently in simulations of the liquid state, whereas the term *shell model* is used more often in simulations of the solid state. As polarizable models become more common in both fields, the terms are beginning to be used indistinguishably. In this chapter, we will use the term shell model exclusively to describe polarizable models in which the dipoles are treated adiabatically; they are always at or near their minimum-energy conformation. We reserve the term Drude oscillator specifically for applications where the dipole oscillates either thermally or with a quantum mechanical zero-point energy, and this oscillating dipole gives rise to a dispersion interaction. The literature has not been entirely consistent on this point of terminology, but it is a useful distinction to make.

The shell model describes each polarizable ion or atom as a pair of point charges separated by a variable distance, as illustrated in Figure 2. These charges consist of a positive, "core" charge located at the site of the nucleus, and a negative, "shell" charge. These charges are connected by a harmonic spring. To some extent, these charges can be justified physically as an effective (shielded) nuclear charge and a corresponding effective charge in the valence shell that is responsible for most of the polarization response of the atom. This interpretation should not be taken literally, however; the magnitude of the charges are typically treated as adjustable parameters of the model rather than true shielded charge values. As such, they should be viewed primarily as an empirical method for representing the dipolar polarization of the site.

The magnitudes of both the core and shell charges are fixed in this model. The polarization thus occurs via relative displacement of the core

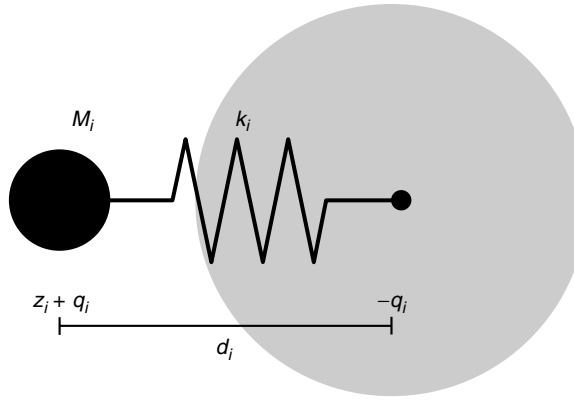


**Figure 2** In the shell model, a "core" charge $z_i + q_i$ is attached by a harmonic spring with spring constant $k_i$ to a "shell" charge $-q_i$. For a neutral atom, $z_i = 0$. The center of mass is at or near the core charge, but the short-range interactions are centered on the shell charge. (Not drawn to scale; the displacement $d_i$ between the charges is much smaller than the atomic radius.)

and shell charges. For a neutral atom $i$ with a core charge of $+q_i$, an equal and opposite shell charge of $-q_i$, and a shell charge that is displaced by a distance $\mathbf{d}_i$ from the core charge, the dipole moment is

$$\boldsymbol{\mu}_i = -q_i \mathbf{d}_i \qquad [24]$$

As with any model involving inducible dipoles, the potential energy of the induced dipoles contains terms representing the interaction with any static field, the interaction with other dipoles, and the polarization energy, that is,

$$U_{\text{ind}} = U_{\text{stat}} + U_{\mu\mu} + U_{\text{pol}} \qquad [25]$$

The polarization energy arises in this case from the harmonic spring separating the two charges,

$$U_{\text{pol}} = \frac{1}{2} \sum_{i=1}^{N} k_i d_i^2 \qquad [26]$$

for a collection of $N$ polarizable atoms with spring constants $k_i$ and charge displacements $d_i = |\mathbf{d}_i|$. Using $\mathbf{d}_i$ from Eq. [24] and comparing it with Eq. [10] for polarizable point dipoles, we see that the polarizability of an isotropic shell model atom can be written as

$$\alpha_i = q_i^2 / k_i \qquad [27]$$

The electrostatic interaction between independent polarizable atoms is simply the sum of the charge–charge interactions between the four charge sites,

$$U_{\mu\mu} = \frac{1}{2}\sum_{i=1}^{N}\sum_{j\neq i} q_i q_j \left[\frac{1}{|\mathbf{r}_{ij}|} - \frac{1}{|\mathbf{r}_{ij} - \mathbf{d}_j|} - \frac{1}{|\mathbf{r}_{ij} + \mathbf{d}_i|} + \frac{1}{|\mathbf{r}_{ij} - \mathbf{d}_j + \mathbf{d}_i|}\right] \quad [28]$$

Typically, no Coulombic interactions are included between the core and shell charges on a single site. Note that the electrostatic interaction in this model is implemented using only the charge–charge terms already present in Eq. [1]. No new interaction types, such as the dipole field tensor $\mathbf{T}_{ij}$ of Eq. [7], are required. The computational advantage of avoiding dipole–dipole interactions is almost exactly nullified by the necessity of calculating four times as many charge–charge interactions, however.

The interaction of the induced dipoles with the static field is the sum of the terms for each individual charge site,

$$U_{\text{stat}} = -\sum_{i=1}^{N} q_i[\mathbf{r}_i \cdot \mathbf{E}_i^0 - (\mathbf{r}_i + \mathbf{d}_i) \cdot \mathbf{E}_i^{0\prime}] \quad [29]$$

where $\mathbf{E}_i^0$ is the static field at the location of the core charge, $\mathbf{r}_i$, and $\mathbf{E}_i^{0\prime}$ is the static field at the location of the shell charge, $\mathbf{r}_i + \mathbf{d}_i$. Note that $\mathbf{E}_i^0 \neq \mathbf{E}_i^{0\prime}$, in general.

Equations [28] and [29] correspond directly to Eqs. [7] and [6], but for the case of dipoles with finite extent. In that sense, models based on point dipoles can be seen as idealized versions of the shell model, in the limit of infinitely small dipoles. That is, the magnitude of the charges $q_i$ and spring constants $k_i$ approach infinity in such a way as to keep the atomic polarizabilities $\alpha_i$ constant. Indeed, in that limit, the displacements will approach zero in the shell model, and the two models will be entirely equivalent.

To the extent that the polarization of physical atoms results in dipole moments of finite length, it can be argued that the shell model is more physically realistic (the section on Applications will examine this argument in more detail). Of course, both models include additional approximations that may be even more severe than ignoring the finite electronic displacement upon polarization. Among these approximations are (1) the representation of the electronic charge density with point charges and/or dipoles, (2) the assumption of an isotropic electrostatic polarizability, and (3) the assumption that the electrostatic interactions can be terminated after the dipole–dipole term.

In describing the shell model, the charge $q$ was described as an effective valence charge of the atom. In some applications of the shell model, the shell charge is indeed interpreted physically in this manner, and $q$ is assigned based

on estimates of shielded charge values. More typically, however, this physical interpretation is relaxed, and $q$ is used as an adjustable parameter in the fitting of the model. Recall that both $q$ and $k$ determine the polarizability of the atom (Eq. [27]). These parameters are often obtained from experimental values for the polarizability, as well as from the elastic and dielectric constants. There is some redundancy in the model, however, as $q$ and $k$ are not independent.[81] In simulations, the shell can either be treated adiabatically (as in the iterative methods) or dynamically (as in the extended Lagrangian method). In the case where the shell is modeled dynamically, the spring constant $k$ affects the characteristic frequency of the spring oscillations, and thus can be chosen from physical arguments or for numerical convenience.[82]

In the model described above, the core and shell charges have equal magnitudes, such that the polarizable atom remains electrically neutral. The original application of the shell model[72,73] and the majority of applications since then[77,83–94] have been to ionic systems. Charged species can easily be accommodated through the introduction of a permanent charge $z_i$ coincident with the core (nuclear) charge (see Figure 2). This permanent charge then contributes to the static electric field experienced by the core and shell charges on other sites. The charge $z_i$ can represent either an integer charge on a simple ion, or the effective partial charge on an atom in a molecular species.[95–100] Assigning charges this way is equivalent to allowing unequal core and shell charges, which is how the model is usually implemented in practice. Conceptually, however, it is useful to consider the permanent charge as a separate component of the model, so that the polarizable component is neutral, and thus has a dipole moment that is independent of the choice of origin.

We should remain cognizant of the fact that there is a conceptual difference between the polarizable point dipole models and the shell model. In the former, the point dipoles can be (and often are) assumed to be merely one term in an infinite series of multipoles that is used in a mathematical expansion of the electric field external to the molecule. In the shell model, on the other hand, the dipole moment is assumed to arise physically from the electron cloud's displacement from the molecular center. Because of the finite length of this dipole, it is important to specify whether the nonelectrostatic interaction centers are located at the cores (nuclei) or the shells (center of electron density). The nonelectrostatic interactions—including short-range repulsion (exchange) and van der Waals terms—are purely electronic in nature. Consequently, these interactions are typically taken to act between the shells, rather than the cores. The specific functional form used for the short-range interactions varies with the implementation, ranging from Buckingham or Born–Mayer potentials for ions to Lennard–Jones potentials for neutral species. Because a steep repulsive potential is an integral part of the shell model, polarization catastrophe is typically not an issue for these models.[91]

Several different methods exist for treating the motion of the polarizable degrees of freedom in dynamic simulations. As with the models based on point

dipoles, there are iterative, adiabatic techniques as well as fully dynamic methods. In the adiabatic methods, the correspondence between the shell charge and the effective electronic degrees of freedom is invoked, along with the Born–Oppenheimer approximation. In this case, the slow-moving nuclei and core charges are said to move adiabatically in the field generated by the shell charges. In other words, the positions of the shell charges are assumed to update instantaneously in response to the motion of the nuclei, and thus always occupy the positions in which they feel no net force (i.e., the positions that minimize the total energy of the system). The forces on the core charges are then used to propagate the dynamics, using standard numerical integration methods. The other alternative is to treat the charges fully dynamically, allowing them to occupy positions away from the minimum-energy position dictated by the nuclei, and thus experience nonzero forces.

When the charges are treated adiabatically, a self-consistent method must be used to solve for the shell displacements, $\{\mathbf{d}_i\}$ (just as with the dipoles $\{\boldsymbol{\mu}_i\}$ in the previous section). Combining Eqs. [26], [28], and [29], we can write the total energy of the shell model system as

$$U_{\text{ind}}(\{\mathbf{r}_i\},\{\mathbf{d}_i\}) = \sum_{i=1}^{N}\left\{\frac{1}{2}k_i d_i^2 + q_i[\mathbf{r}_i\cdot\mathbf{E}_i^0 - (\mathbf{r}_i+\mathbf{d}_i)\cdot\mathbf{E}_i^{0'}] + \left[\frac{1}{2}\sum_{i=1}^{n}\sum_{j\neq i}\left(\frac{1}{r_{ij}} - \frac{1}{|\mathbf{r}_{ij}-\mathbf{d}_j|} - \frac{1}{|\mathbf{r}_{ij}+\mathbf{d}_i|} + \frac{1}{|\mathbf{r}_{ij}-\mathbf{d}_i+\mathbf{d}_j|}\right)\right]\right\} \quad [30]$$

which is the equivalent of Eq. [18] for a model with polarizable point dipoles, but with one important difference: Eq. [18] is a quadratic function of the $\{\boldsymbol{\mu}_i\}$, guaranteeing that its derivative (Eq. [19]) is linear and that a standard matrix method can be used to solve for the $\{\boldsymbol{\mu}_i\}$. Equation [30] is not a quadratic function of the $\{\mathbf{d}_i\}$. Moreover, the dependence of the short-range interactions on the displacements of the shell particles further complicates the matter. Consequently, matrix methods are typically not used to find the shell displacements that minimize the energy.

Iterative methods are used instead. In one such approach,[101] the nuclear (core) positions are updated, and the shell displacements from the previous step are used as the initial guess for the new shell displacements. The net force, $\mathbf{F}_i$, on the shell charge is calculated from the gradient of Eq. [30], together with any short-range interactions. Because the harmonic spring interaction is, by far, the fastest varying component of the potential felt by the shell charge, the incremental shell displacement $\delta\mathbf{d}_i = \mathbf{F}_i/k_i$ represents a very good estimate of the equilibrium (energy minimizing) position of the shells. The forces are recalculated at this position, and the procedure is iterated until a (nearly) force-free configuration is obtained. Alternatively, this steepest descent style

minimization can be replaced by more sophisticated minimization techniques,[102] such as conjugate gradients.[103] Depending on the convergence criterion used, these iterative methods typically require between 3 and 10 iterations.[77,99,101,103]

The dynamic approach to solving for the shell displacements was first proposed by Mitchell and Fincham.[90] In this method, the mass of each atom or ion is partitioned between the core and the shell. The mass of the shell charge is typically taken to be less than 10% of the total particle mass, and often as light as 0.2 amu.[82,90,97,104] No physical significance is attributed to the charge mass, as it is not meant to represent the mass of the electronic degrees of freedom whose polarization the shell charge represents. Rather, it is a parameter chosen solely for the numerical efficiency of the integration algorithm. Choosing a very light shell mass allows the shells (i.e., the dipole moments) to adjust very quickly in response to the electric field generated by the core (nuclear) degrees of freedom. In the limit of an infinitely light shell mass, the adiabatic limit would be recovered. The choice of shell mass also has a direct effect on the characteristic frequency of the oscillating shell model. For a particle with total mass $M$, a fraction $f$ of which is attributed to the shell and $1 - f$ to the core, the reduced mass will be $\mu = f(1 - f)M$, resulting in an oscillation frequency of

$$\omega = \sqrt{\frac{k}{f(1-f)M}} \qquad [31]$$

An overly small shell mass would thus result in high oscillation frequencies, requiring the use of an exceedingly small time step for integration of the dynamics—an undesirable situation for lengthy simulations. In practice, the shell mass is chosen to be (1) light enough to ensure adequate response times, (2) heavy enough that reasonable time steps may be used, and (3) away from resonance with any other oscillations in the system.

The dynamic treatment of the charges is quite similar to the extended Lagrangian approach for predicting the values of the polarizable point dipoles, as discussed in the previous section. One noteworthy difference between these approaches, however, is that the positions of the shell charges are ordinary physical degrees of freedom. Thus the Lagrangian does not have to be "extended" with fictitious masses and kinetic energies to encompass their dynamics.

With an appropriate partitioning of the particle masses between core and shell, this dynamic method for integrating the dynamics of the shell model can become more efficient than iterative methods. The lighter masses in the system require time steps 2–5 times smaller than those required in an iterative shell model simulation (or a nonpolarizable simulation).[82,90,97,99,104] But because the iterative methods require 3–10 force evaluations per time step to achieve

comparable energy conservation,[90,99,101,105] the dynamic methods can have a computational advantage, in some cases by as much as a factor of two to four.[90] Because the shell model represents each polarizable site with two point charges, it replaces the dipole–dipole interactions in the polarizable point dipole models with four charge–charge interactions. The greater number of pair distances largely offsets the computational advantage of the simpler interaction, and energy and force evaluations in the two methods are comparable in speed. Between the reduced time step and the greater number of interactions, shell models typically require 10 times more CPU time than corresponding nonpolarizable simulations.[105,106]

In the shell model, as mentioned above, the short-range repulsion and van der Waals interactions are taken to act between the shell particles. This finding has the effect of coupling the electrostatic and steric interactions in the system: in a solid-state system where the nuclei are fixed at the lattice positions, polarization can occur not only from the electric field generated by neighboring atoms, but also from the short-range interactions with close neighbors (as, e.g., in the case of defects, substitutions, or surfaces). This ability to model both electrical and mechanical polarizability is one reason for the success of shell models in solid-state ionic materials.[73,107]

There exist a variety of extensions of the basic shell model. One variation for molecular systems uses an anisotropic oscillator to couple the core and shell charges,[99,108] thus allowing for anisotropic polarizability in nonspherical systems. Other modifications of the basic shell model that account for explicit environment dependence include a deformable or "breathing" shell[75,76,109] and shell models allowing for charge transfer between neighboring sites.[75,76,110]

Shell models have been used successfully in a wide variety of systems. The greatest number of applications have been in the simulation of ionic materials,[86–88,90,111] especially systems including alkali halides,[83] oxides,[85,89,91,92,112–115] and zeolites.[93,94] The shell model is also commonly used for the simulation of molten salts,[77,84,90,101,116–120] and shell-type models have been developed for various molecular[95–99] and polymeric species.[100,121]

## ELECTRONEGATIVITY EQUALIZATION MODELS

Polarizability can also be introduced into standard potentials (Eq. [1]) by allowing the values of the partial charges to respond to the electric field of their environment. A practical advantage of this approach is that it introduces polarizability without introducing new interactions. And unlike the shell model, this can be accomplished using the same number of charge–charge interactions as would be present in a nonpolarizable simulation. Another more conceptual advantage is that this treats the polarizable and permanent electrostatic interactions with the same multipoles. One way to couple the charges to their environment is by using electronegativity equalization.

The energy required to create a charge, $q$, on an atom can be expressed as a Taylor series expansion,

$$U(q) = E^0 + \chi^0 q + \frac{1}{2} J q^2 \qquad [32]$$

which has been truncated after the second-order terms. If the Taylor series is valid for charges of up to $\pm 1$ $e$, then, because the ionization potential, IP, is equal to $U(1) - U(0)$ and the electron affinity, EA, is $U(-1) - U(0)$, the Taylor series coefficients are

$$\chi^0 = (\mathrm{IP} + \mathrm{EA})/2 \qquad [33]$$

$$J = \mathrm{IP} - \mathrm{EA} \qquad [34]$$

Equation [33] is Mulliken's definition of electronegativity,[122] so the linear coefficient in the Taylor series is the electronegativity of the atom. Mulliken's definition is consistent with other electronegativity scales. The second-order coefficient, $\frac{1}{2}$ $J$, is the "hardness" of the atom, $\eta$.[123] For semiconductors, the hardness is half the band gap, and $\eta$ is an important property in inorganic and acid–base chemistry.[124] Physically, IP − EA is the energy required to transfer an electron from one atom to another atom of the same type,

$$2\mathrm{A(g)} \rightarrow \mathrm{A^+(g)} + \mathrm{A^-(g)} \qquad \Delta E = \mathrm{IP} - \mathrm{EA} \qquad [35]$$

This energy is always positive (in fact, it is positive even if the two atoms are not the same element), so $J \geq 0$. Figure 3 shows $U(q)$ for chlorine and sodium, as calculated from the experimental IP and EA. The energies of the ions, $\chi^0$, and $J$ are all calculated using the experimental IP and EA. Chlorine is more electronegative than sodium ($\chi^0_{\mathrm{Na}} = 2.84$ eV, $\chi^0_{\mathrm{Cl}} = 8.29$ eV) and also harder ($J_{\mathrm{Na}} = 4.59$ eV, $J_{\mathrm{Cl}} = 9.35$ eV). This means that both the slope and the second derivative of $U(q)$ are larger for Cl than for Na.

When atoms are brought together to form molecules, the energy of the charges is described in the EE model as

$$U(\mathbf{q}) = \sum_i \left( E_i^0 + \chi_i^0 q_i + \frac{1}{2} J_{ii} q_i^2 \right) + \sum_i \sum_{j>i} J_{ij}(r_{ij}) q_i q_j \qquad [36]$$

The vector $\mathbf{q}$ represents the set of $q_i$. The second-order coefficient, $J_{ij}(r_{ij})$, depends on the distance between the two atoms $i$ and $j$, and at large distances should equal $1/r_{ij}$. At shorter distances, there may be screening of the interactions, just as for the dipole–dipole interactions in the earlier section on Polarizable Point Dipoles. This screened interaction is typically assumed to arise

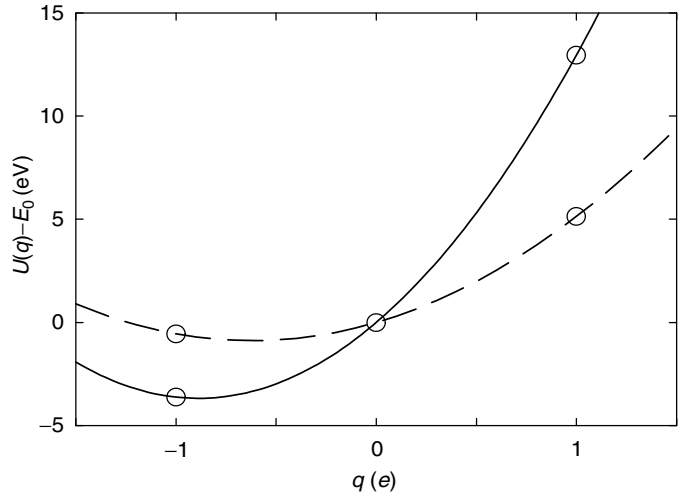


**Figure 3** Energy versus charge for chlorine (solid line) and sodium (dashed line). The lines are a quadratic fit through the energies of the ions relative to the neutral atom.

from the Coulomb interaction between delocalized charge distributions $\rho(\mathbf{r})$, rather than point charges,

$$J_{ij}(\mathbf{r}) = \int \frac{\rho_i(\mathbf{r}_i)\rho_j(\mathbf{r}_j)}{|\mathbf{r}_i - \mathbf{r}_j - \mathbf{r}|} d\mathbf{r}_i \, d\mathbf{r}_j \qquad [37]$$

The charge distributions are frequently assumed to be spherical, for simplicity.[125–128] Directional interactions can be incorporated with nonspherical charge distributions, at some added computational expense.[129–131]

The partial charges on each atom of the molecule are found by minimizing the energy, subject to a constraint that the total charge is conserved.

$$\sum_i q_i = q_{\text{tot}} \qquad [38]$$

The charge conservation constraint can be enforced using an undetermined multiplier,

$$U(\mathbf{q}) = U(\mathbf{q}) - \lambda \left( \sum_i q_i - q_{\text{tot}} \right) \qquad [39]$$

Minimizing this expression for the energy with respect to each of the $q_i$ under the assumption that the molecule in question is neutral ($q_{\text{tot}} = 0$) gives

for all $i$ (i.e., $\forall\, i$):

$$\left(\frac{\partial U}{\partial q_i}\right) - \lambda = 0 \qquad \forall\, i \tag{40}$$

Because $(\partial U/\partial q_i)$ for each atom is equal to the same undetermined multiplier $\lambda$, this quantity must be identical for all atoms in the molecule,[132]

$$\left(\frac{\partial U}{\partial q_i}\right) = \left(\frac{\partial U}{\partial q_j}\right) \qquad \forall\, i, j \tag{41}$$

Through Mulliken's identification of $\partial U/\partial q$ as the electronegativity, we see that minimizing the energy with respect to the charges is equivalent to equalizing the electronegativities,

$$\chi_i \equiv \left(\frac{\partial U}{\partial q_i}\right) = \chi_i^0 + J_{ii} q_i + \sum_{j \neq i} J_{ij}(r_{ij}) q_j \tag{42}$$

for all atoms. Notice that the electronegativity of atom $i$ in a molecule, $\chi_i$, differs from the electronegativity of the isolated atom, $\chi_i^0$, and now depends on its charge, the charge of the other atoms, its hardness, and the interactions with other atoms through $J_{ij}(r_{ij})$. In addition, Parr et al.[132] identified the chemical potential of an electron as the negative of the electronegativity, $\mu = -\partial U/\partial q$. So electronegativity equalization is equivalent to chemical potential equalization. Thus, this model effectively moves charge around a molecule to minimize the energy or to equalize the electronegativity or chemical potential. These interpretations are all equivalent (for a dissenting opinion, see Ref. 133).

Electronegativity equalization (EE) was first proposed by Sanderson.[134] The EE model, with appropriate parameterization, has been successful in predicting the charges of a variety of molecules.[125,135–138] The parameters $\chi^0$ and $J$ are not typically assigned from Eqs. [33] and [34], but instead are taken as parameters to be optimized and can be viewed as depending on the valence state of the atom, as indicated by electronic structure calculations.[139,140] Some models[136] set $J_{\alpha\beta}(r_{ij}) = 1/r_{ij}$, and others use some type of screening.[125,135,137] In addition, some models have an expression for the energy that is not quadratic.[125,135,141] Going beyond the quadratic term in the Taylor expansion of Eq. [32] can possibly extend the validity of the model, but it introduces complications in the methods available for treating the charge dynamics, as will be discussed below.

For a collection of molecules, the overall energy is comprised of the energy given by Eq. [36] for each molecule and an interaction between charge

sites on different molecules,

$$U(\{q\},\{\boldsymbol{r}\}) = \sum_{\alpha}\left(\sum_{i\in\alpha}\chi_i^0 q_i + \frac{1}{2}\sum_{i\in\alpha}\sum_{j\in\alpha} q_i\, q_j\, J_{ij}(r_{ij}) - E_\alpha^{\mathrm{gp}}\right) + \sum_{\alpha}\sum_{\beta>\alpha}\sum_{i\in\alpha}\sum_{j\in\beta} q_i\, q_j\, J_{ij}(r_{ij}) \quad [43]$$

where $\alpha$ and $\beta$ label the molecules, and $i$ and $j$ represent atoms (or other charge sites) in these molecules. The $E_\alpha^{\mathrm{gp}}$ term represents the gas-phase energy of molecule $\alpha$ and defines the zero of energy as corresponding to infinitely separated molecules. The energy given by Eq. [43] replaces the Coulomb energy $q_i q_j / r_{ij}$ in Eq. [1]. The charges $q_i$ are now treated as independent variables, and the polarization response is determined by variations in the charge values. These charges depend on the interactions with other molecules as well as other charge sites on the same molecule, and will change for every time step or configuration sampled during a simulation. The charge values used for each configuration are, in principle, those that minimize the energy given by Eq. [43]. This method for treating polarizability has thus been called the *fluctuating charge* method[126] and has been applied to a variety of systems.[10,82,104,126,142–148] The $J_{ij}(r)$ interaction between different molecules is typically taken to be $1/r$, although the interactions between atoms on the same molecule may be screened. Therefore, this method does not modify the intermolecular interactions.

Charge conservation can be imposed in either of two ways. A charge neutrality constraint can be applied to the entire system, allowing charge to move from atomic site to atomic site until the electronegativities are equal on all the atoms of the system. Alternatively, charge can be constrained independently on each molecule (or other subgroup), so that charge flows only between atoms on the same molecule until the electronegativities are equalized within each molecule, but not between distinct molecules.[126] In most cases, charge is taken to be conserved for each molecule, so there is no charge transfer between molecules.

Variations, including the atom–atom charge transfer (AACT)[149] and the bond-charge increment (BCI)[146,150] model, only allow for charge to flow between two atoms that are directly bonded to each other, guaranteeing that the total charge of each set of bonded atoms is conserved. In some situations, charge transfer is an important part of the interaction energy, so there are reasons to remove this constraint.[151–154] However, this can lead to some nonphysical charge transfer, as illustrated in the simple example of a gas-phase sodium chloride molecule. The energy for one Na atom and one Cl atom is

$$U(q) = E_{\mathrm{Na}}^0 + E_{\mathrm{Cl}}^0 + (\chi_{\mathrm{Na}} - \chi_{\mathrm{Cl}})\, q_{\mathrm{Na}} + \frac{1}{2}\left[\, J_{\mathrm{Na}} + J_{\mathrm{Cl}} - 2\, J_{\mathrm{NaCl}}(r_{\mathrm{NaCl}})\right] q_{\mathrm{Na}}^2 \quad [44]$$

where we have used $q_{Cl} = -q_{Na}$. The charge that minimizes this energy is

$$q_{Na} = \frac{-(\chi_{Na} - \chi_{Cl})}{J_{Na} + J_{Cl} - 2J_{NaCl}(r_{NaCl})} \quad [45]$$

At large distances, $J_{NaCl}(r_{NaCl})$ approaches zero, and, if the $\chi$ and $J$ parameters are taken from Eqs. [33] and [34], then

$$q_{Na} = \frac{-(\chi_{Na} - \chi_{Cl})}{J_{Na} + J_{Cl}} = \frac{-\frac{1}{2}(IP_{Na} + EA_{Na} - IP_{Cl} - EA_{Cl})}{IP_{Na} - EA_{Na} + IP_{Cl} - EA_{Cl}} \quad [46]$$

which gives $q_{Na} = 0.391\ e$. Thus the model predicts a significant amount of charge transfer, even at large distances. Similar errors in the dissociation limit are seen with certain electronic structure methods.[155,156] A significant amount of charge separation, and a consequent overestimation of the dipole moment, can be found for large polymers as well. Reducing this charge transfer along the polymer can be accomplished with the AACT and BCI models.[146,149,150] In addition, when comparing fluctuating charge models with ab initio results for water trimers, agreement was found to be much better for the model without charge transfer, even after the charge-transfer model was reparameterized by fitting to the ab initio three-body energies.[145]

These and associated problems with overestimated charge transfer are a general characteristic of EE-based models. Unfortunately, such errors cannot be eliminated through parameterization; the problem is a side effect of attempting to treat quantum mechanical charge-transfer effects in a purely classical way. As with all empirical potentials, the use of fractional charges is necessary for an accurate description of the electrostatic potential. Yet by allowing fractional charge transfer, the EE model has no means of enforcing the transfer of only an integral number of electrons between distant species. Indeed, the neutral dissociation products for NaCl are correctly predicted by the EE model, if the infinitely separated ions are constrained to have integer charge (see Figure 3). This constraint is difficult to apply in practice, however. As discussed recently by Morales and Martinez,[157] the EE-based models can be viewed as analytically differentiable approximations to a more rigorous statistical interpretation of $U(q)$, which is discontinuous at integer values of charge transfer and correctly predicts zero charge transfer at infinite distance. In chemically bonded systems, the assumption of partial charge transfer is not as unrealistic as in ionic compounds, as electrons are delocalized across covalent bonds. However, in these covalent cases the EE model effectively assumes that the coherence length of a delocalized electron is infinite and does not depend on the surroundings. It is for this reason that the polarizability of polymers, for example, increases too quickly with chain length under the EE model.[149] Molecular charge constraints can avoid problems at the dissociation

limit, and methods constraining the charge based on the bonding network are an extension of EE models that appear to be successful at controlling the coherence lengths.[149] There now exist classical models that can describe the charge transfer reasonably across the full range of a dissociating bond, but these are currently less well developed.[157]

The polarization energy in the EE models can be compared directly to that in the polarizable point dipole and shell models. Consider the first term in Eq. [43],

$$\sum_{i\in\alpha}\chi_i^0 q_i + \frac{1}{2}\sum_{i\in\alpha}\sum_{j\in\alpha} q_i\, q_j\, J_{ij}(r_{ij}) - E_\alpha^{\mathrm{gp}} \qquad [47]$$

This term represents the energy required to induce charges $q_i$ on the atoms of molecule $\alpha$ in the electric field of its neighbors, relative to the energy of the isolated molecule. This quantity is simply the polarization energy of the molecule. The polarization energy of the full system can thus be written

$$U_{\mathrm{pol}} = \sum_{\alpha}\left[\sum_{i\in\alpha}\chi_i^0 q_i + \frac{1}{2}\sum_{i\in\alpha}\sum_{j\in\alpha} q_i\, q_j\, J_{ij}(r_{ij}) - E_\alpha^{\mathrm{gp}}\right] \qquad [48]$$

which can be compared to Eqs. [9] and [26].[10]

There exist other models that treat polarizability using variable charges in a way similar to the fluctuating charge model.[22,53,127,143,158] In the Sprik and Klein[22] model for water, four charge sites are located near the oxygen atom in a tetrahedral geometry, in addition to the three atom-centered permanent charges. The tetrahedron of charges is used to represent an induced dipole moment on the oxygen center. This approach differs from a polarizable point dipole model in using a dipole of finite extent. It also differs from a shell model in that the point charges are fixed in the molecular frame. Consequently, the Sprik–Klein model should perhaps best be considered an entirely different type of model. The model of Zhu, Singh, and Robinson[158] is similar to the Sprik–Klein model, but it has no permanent charges. The four charge sites, two on hydrogen atoms and two on lone-pair positions 1 Å from the oxygen atom, are all variables coupled to the electric field. For both these models, the coupling is described by the polarizability, $\alpha$, just as with other dipole polarizable models. Wilson and Madden[159] described a model for ions in which charge is transferred between ends of a rigid, rotating rod. In the model of Perng et al.,[143] the charge, $q_i$, on an atom is equal to a permanent value, $q_i^0$, plus an induced part, $\delta q_i$. The induced charge is dependent on the electrostatic potential at that site and all the induced charges are coupled through Coulombic interactions, similar to the fluctuating charge models. In the polarizable point charge (PPC) model of Svishchev et al.,[53] charges are coupled directly to the electric field at that site, so this model is slightly different from the fluctuating charge model.

Although a valence-type force field of the type illustrated by Eq. [1] is most suitable for modeling molecular systems, the electronegativity equalization approach to treating polarization can be coupled equally well to other types of potentials. Streitz and Mintmire[127] used an EE-based model in conjunction with an embedded atom method (EAM) potential to treat polarization effects in bulk metals and oxides. The resulting ES + EAM model has been parameterized for aluminum and titanium oxides, and has been used to study both charge-transfer effects and reactivity at interfaces.[127,128,160,161]

In most electronegativity equalization models, if the energy is quadratic in the charges (as in Eq. [36]), the minimization condition (Eq. [41]) leads to a coupled set of linear equations for the charges. As with the polarizable point dipole and shell models, solving for the charges can be done by matrix inversion, iteration, or extended Lagrangian methods.

As with other polarizable models, the matrix methods tend to be avoided by most researchers because of their computational expense. And when they are used, the matrix inversion is typically not performed at every step.[160,162] Some EE applications have relied on iterative methods to determine the charges.[53,127] For very large-scale systems, multilevel methods are available.[161,163] As with the dipole polarizable models, the proper treatment of long-range electrostatic interactions is especially important for fluctuating charge models.[164] Monte Carlo methods have also been developed for use with fluctuating charge models.[162,165] Despite this variety of available techniques, the most common approach is to use a matrix inversion or iterative method only to obtain the initial energy-minimizing charge distribution; an extended Lagrangian method is then used to propagate the charges dynamically in order to take advantage of its computational efficiency.

In the extended Lagrangian method, as applied to a fluctuating charge system,[126] the charges are given a fictitious mass, $M_q$, and evolved in time according to Newton's equation of motion, analogous to Eq. [23],

$$M_q \ddot{q}_i = -\frac{\partial U}{\partial q_i} - \lambda_\alpha \qquad [49]$$

where $\lambda_\alpha$ is the average of the negative of the electronegativity of the molecule $\alpha$ containing atom $i$,

$$\lambda_\alpha = -\frac{1}{N_\alpha} \sum_{i \in \alpha} \chi_i \equiv -\bar{\chi}_\alpha \qquad [50]$$

Here, $N_\alpha$ is the number of atoms in molecule $\alpha$. Combining Eq. [49], [50], and [42], we have

$$M_q \ddot{q}_i = \bar{\chi}_\alpha - \chi_i \qquad [51]$$

In other words, the force experienced by each charge is proportional to the difference between the electronegativity at that site and the average electronegativity in the charge-constrained molecule that contains the charge site.

Equations [50] and [51] assume that the total charge of each molecule is conserved. They also assume that all of the charge masses are identical. If charge is allowed to transfer between molecules, then $\lambda_\alpha$ and $\bar{\chi}_\alpha$ are independent of the molecule, $\alpha$, and are given by[126]

$$\lambda = \frac{1}{N_{\text{mol}}} \sum_{\alpha=1}^{N_{\text{mol}}} \frac{1}{N_\alpha} \sum_{i \in \alpha} \chi_i \equiv -\bar{\chi} \qquad [52]$$

A short trajectory of the fluctuating charge on a water molecule using the TIP4P-FQ model[126] comparing the extended Lagrangian model with the exact minimum energy value is shown in Figure 4. The extended Lagrangian values oscillate around the exact values, until near the end of the interval at which time the two trajectories begin to diverge from each other, due to the chaotic nature of the system. The charges also oscillate with small magnitude around the exact solution, demonstrating that they remain quite close to the true electronegativity equalizing (energy minimizing) values. The small oscillations also imply that the charges are at a much colder temperature ($\approx 1$ K in Figure 4) than the rest of the system. One drawback of the extended Lagrangian method is that it contains an additional parameter, the charge mass. This mass must be chosen to be small enough that the charges respond promptly to changes in the

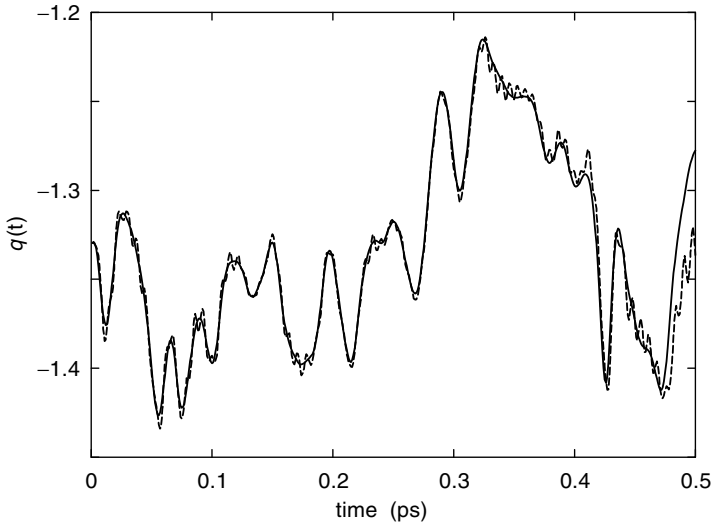


**Figure 4** Negative charge near the oxygen atom versus time for the TIP4P-FQ water model, comparing the exact (solid line) and extended Lagrangian value (dashed line).

electronic potential (i.e., a large frequency for the oscillations about the exact trajectory in Figure 4), but large enough so that reasonable length time steps can still be used. In addition, the mass should be chosen so that the coupling between the charge and nuclear degrees of freedom is relatively weak. Any such coupling enables the cold charges to absorb energy from the rest of the system, eventually reaching equilibrium with the warmer parts of the system. Weak coupling results in relatively slow energy transfer, taking hundreds of picoseconds or longer before the charge temperature and amplitude of the charge oscillations become large enough to require reminimization. For many applications, standard 1 femtosecond time steps can be used, and the charges will remain at a temperature less than 6 K for a 50-ps simulation without thermostatting. Thus EE combined with the extended Lagrangian method is not much more computationally demanding than nonpolarizable simulations.[126,148] Finding the optimum masses can be difficult for systems with many different atom types, each fluctuating on a different time scale.[10] For these cases, different $M_q$ must be used for the different charge masses. The expression for $\lambda_\alpha$ becomes

$$\lambda_\alpha = -\frac{\sum_i \chi_i / M_{q,i}}{\sum_i 1/M_{q,i}} \qquad [53]$$

For more complex systems, thermostatting may be required to keep the charges near 0 K.[10]

Polarizable models based on EE implement the electrostatic interactions using either point or diffuse charges, and can thus be combined quite easily with other methods of treating polarizability to create hybrid models. The EE and the dipole polarizable models have some features in common, but they are not equivalent. They have, for example, different distance dependences and polarizability responses. Some hybrid models have included both dipole polarizability and fluctuating charges.[131,144,150,166] The fluctuating charge model has also been combined with a shell-type model, as a method of allowing polarization in single-atom species such as simple ions, without having to introduce the added complication of the dipole field tensor.[82,104,167]

The $\chi_i$ and $J_{ij}$ parameters for the EE models can be optimized so that the resulting charges match gas-phase values as determined from either ab initio quantum mechanical calculations or the experimental dipole moment.[125,126,136–138,148] Parameters derived along these lines can give accurate gas-phase charge values. Information about many-body interactions can be included in the parameterization in several ways. First, quantities including ESP charges, geometries, and the strength of many-body interactions can be obtained from ab initio calculations on clusters.[142,145,150,166] Second, the polarization response from an applied electric field can be used.[146] Third, one can optimize the parameters to give the optimal charges both in the gas phase and in the presence of a solvent, as modeled using reaction field

methods.[10,168] Finally, the parameters themselves can be directly calculated using density functional theory (DFT) methods.[169,170]

As presented, the EE approach given by Eq. [43] is a simple mathematical model resulting from a Taylor series; it can be given a more rigorous foundation using electronic density functional theory.[169] Using DFT, and making simplifying approximations for the exchange and kinetic energy functionals, expressions analogous to Eq. [43] can be derived.[130,131,171] This approach has been termed chemical potential equalization (CPE).[130] Efforts like CPE or even parameterizations of fluctuating charge models using electronic structure calculations represent a step away from empirical potential models toward ab initio simulation methods. However, even with a sophisticated treatment of the charges, empirical terms in the potential such as the Lennard–Jones interaction still remain. A standard method is to set the Lennard–Jones parameters so that the energies and geometries of important dimer conformations (e.g., hydrogen-bonded dimers) are close to ab initio values.[10,144,145,166] In some cases, the remaining potential parameters have been taken from existing force fields.[146,150] One interesting extension of the fluctuating charge model has been developed by Siepmann and co-workers.[147] In their model, the Lennard–Jones size parameter becomes a variable that is coupled to the charge on a given atom. The size of the atom increases as the atom becomes more negatively charged and obtains greater electronic density. This increase in size is thus consistent with physical intuition. Other models in which some of the remaining potential parameters are treated as variables are described in the next section.

## SEMIEMPIRICAL MODELS

A number of quantum polarizable models have been developed.[144,172–177] These treatments of polarizability represent a step toward full ab initio methods. The models can be characterized by a small number of electronic states or potential energy surfaces, which are coupled to each other. For the purposes of this tutorial, our description is of the method of Gao.[173,174] In his method, molecular orbitals, $\phi_A$, for each molecule are defined as a linear combination of $N_b$ atomic orbitals, $\chi_\mu$,

$$\phi_A = \sum_{\mu=1}^{N_b} c_{\mu A}\chi_\mu \qquad [54]$$

As is standard in semiempirical methods,[178] the molecular orbitals are orthonormal, so the overlap matrix, $S_{AB}$, is assumed to be diagonal. The molecular wave function, $\Psi_a$, is a Hartree[144] or Hartree–Fock[173] product of the molecular orbitals. For a (closed-shell) molecule with $2M$ electrons, there will be $M$ doubly occupied molecular orbitals. The wave function of a system comprised

of $N$ molecules is taken as a Hartree product of the individual molecular wave functions,

$$\Phi = \prod_{i=1}^{N} \Psi_i \qquad [55]$$

The Hartree product neglects exchange correlation interactions between molecules. To include proper exchange would make these models inefficient and impractical.

The Hamiltonian for the system

$$\hat{H} = \sum_{i=1}^{N} \hat{H}_i^0 + \frac{1}{2}\sum_{i=1}^{N}\sum_{j\neq i}^{N} \hat{H}_{ij} \qquad [56]$$

contains the isolated molecular Hamiltonian, $\hat{H}_i^0$, given, in atomic units, by

$$\hat{H}_i^0 = \sum_{a=1}^{2M} \hat{T}_a - \sum_{\alpha=1}^{A}\sum_{a=1}^{2M} \frac{Z_\alpha(i)}{R_{\alpha a}} + \sum_{a=1}^{2M}\sum_{b>a} \frac{1}{r_{ab}} \qquad [57]$$

where $\hat{T}$ is the kinetic energy operator, $Z_\alpha(\mathrm{i})$ is the nuclear charge of atom $\alpha$ on molecule $i$, $R_{\alpha a}$ is the distance between the nucleus of atom $\alpha$ and electron $a$, and $r_{ab}$ is the distance between two electrons. The interaction Hamiltonian between molecules $i$ and $j$, $\hat{H}_{ij}$, is

$$\hat{H}_{ij} = \sum_{a=1}^{2M}\sum_{b=1}^{2M} \frac{1}{r_{ab}} + \sum_{\alpha=1}^{A}\sum_{\beta=1}^{A} \frac{Z_\alpha(i) Z_\beta(j)}{R_{\alpha\beta}} \qquad [58]$$

where $R_{\alpha\beta}$ is the distance between atom $\alpha$ on molecule $i$ and atom $\beta$ on molecule $j$. The interaction energy of the system is

$$E = \langle\Phi|\hat{H}|\Phi\rangle - N\langle\Phi^0|\hat{H}_i^0|\Phi^0\rangle \qquad [59]$$

where $\Phi^0$ is the ground-state wave function of the isolated molecule and $\langle\Phi^0|\hat{H}_{\mathrm{i}}^0|\Phi^0\rangle$ is the energy of the isolated molecule. The polarization energy is

$$E_{\mathrm{pol}} = \sum_{i=1}^{N}(\langle\Phi|\hat{H}_i^0|\Phi\rangle - \langle\Phi^0|\hat{H}_i^0|\Phi^0\rangle) \qquad [60]$$

or, equivalently,

$$E_{\mathrm{pol}} = \sum_{i=1}^{N}(\langle\Psi_i|\hat{H}_i^0|\Psi_i\rangle - \langle\Psi_i^0|\hat{H}_i^0|\Psi_i^0\rangle) \qquad [61]$$

which is the difference between the molecular energy of wave function $\Phi$ (or $\Psi_i$), which is the expectation value of the Hamiltonian in Eq. [56], and the molecular energy of the isolated molecule wave function. This expression for the polarization energy is comparable to Eqs. [9], [26], and [48] for the other models.

To avoid calculating the two-electron integrals in Eq. [59], the assumption is made that no electron density is transferred between molecules. The interaction Hamiltonian is then

$$\hat{H}_{ij}(\Psi_j) = -\sum_{a=1}^{2M} V_a(\Psi_j) + \sum_{\alpha=1}^{A} Z_\alpha(i) V_\alpha(\Psi_j) \qquad [62]$$

where $V_x(\Psi_j)$ is the electrostatic potential[179] from molecule $j$ at the position of electron $a$ or nuclei $\alpha$ of molecule $i$,

$$V_x(\Psi_j) = -\int \frac{\Psi_j^2(\mathbf{r})}{|\mathbf{r}_x - \mathbf{r}|} d\mathbf{r} + \sum_{\beta=1}^{A} \frac{Z_\beta(j)}{|\mathbf{r}_x - \mathbf{R}_\beta|} \qquad [63]$$

If the $V_x(\Psi_j)$ coming from the electrons and nuclei of molecule $j$ is represented just by point charges on atomic sites, then

$$V_x(\Psi_j) = \sum_{\beta=1}^{A} \frac{q_\beta(\Psi_j)}{|\mathbf{r}_x - \mathbf{R}_\beta|} \qquad [64]$$

and

$$\hat{H}_{ij}(\Psi_j) = -\sum_{a=1}^{2M} \sum_{\beta=1}^{A} \frac{q_\beta(\Psi_j)}{r_{a\beta}} + \sum_{\alpha=1}^{A} \sum_{\beta=1}^{A} \frac{Z_\alpha(i) q_\beta(\Psi_j)}{R_{\alpha\beta}} \qquad [65]$$

where $q_\beta(\Psi_j)$ is the partial atomic charge on atom $\beta$ in molecule $j$ derivable from the wave function $\Psi_j$. (Other semiempirical models have charges offset from the atomic sites.)[172,175,176] The energy of molecule $i$ is then changed by the partial charges from the other molecules. Since exchange correlation interactions are neglected as mentioned above in regard to Eq. [55], the short-range repulsive interactions need to be added, which can be done with a Lennard–Jones potential. The interaction energy between molecules $i$ and $j$ is then

$$E_{ij} = \frac{1}{2}(\langle \Psi_i | \hat{H}_{ij} | \Psi_i \rangle + \langle \Psi_j | \hat{H}_{ji} | \Psi_j \rangle) + E_{\mathrm{LJ}} \qquad [66]$$

which is used so that $E_{ij}$ is equal to $E_{ji}$. The interactions between molecules then consist of only Lennard–Jones and Coulombic components. Polarizability

is treated using variable charges. The total energy is then

$$E = E_{\text{pol}} + \frac{1}{2}\sum_{i=1}^{N}\sum_{j\neq i}^{N} E_{ij} \qquad [67]$$

and the forces on the nuclear coordinates are provided by the derivative of $E$ with respect to the positions.

The charges can be found through Mulliken population analysis,[180] which, because the overlap matrix is diagonal, is

$$q_\alpha = K\left(Z_\alpha - 2\sum_{a=1}^{M}\sum_{\mu} c_{\mu a}^2\right) \qquad [68]$$

where the sum over $\mu$ is over atomic orbitals centered on atom $\alpha$, and $K$ is an empirical scaling parameter correcting for errors in the Mulliken charges ($K$ is about 2). The Lennard–Jones parameters are assumed to be independent of the electronic states and all applications to date have been for rigid molecular geometries, so the models do not need to include nonbonded interactions.

The electronic structure of molecules can be described at the semiempirical level using, for example, the Austin model (AM1)[181] or at the ab initio level with a Gaussian basis set.[182] Other quantum theoretical methods can be used, however, as illustrated the method of Kim and co-workers[175,176] who use a ''truncated adiabatic basis'' consisting of the ground and first few excited states of the isolated molecule. For water, these methods introduce about 7–10 basis functions per molecule.[144,176] The wave function coefficients in these models are found using an iterative method.[144,172–176] An interesting variant of the empirical valence bond (EVB) approach has recently been introduced by Lefohn, Ovchinnikov and Voth.[177] In this approach, as applied to water, there are only three EVB states per molecule, and all potential parameters, rather than being derived from ab initio or semiempirical methods, are parameterized against experimental data.

Another method for treating polarizability is to have more than one potential surface with different electronic properties coupled together. This method is applicable to systems that can be represented by a few electronic states, like those with resonance. Each of these states can have its own potential energy parameters. One such model was developed for the peptide bond.[183] The peptide bond can be described as consisting of the resonance structures of two states, one with a N–C single bond and no formal charges and the other with a N=C double bond and formal charges on the nitrogen and oxygen. Each of these states is coupled to the environment, which in turn can shift the energies of the states. The potential parameters for these states can be different, but in the peptide bond model only the charges of the peptide group atoms and the dihedral force constant for rotations about

the peptide bond were taken to be state dependent. All other parameters were taken from existing force fields. Each peptide group, $i$, has a coefficient for each state, $C_{iA}$ and $C_{iB}$, with the constraint that

$$C_{iA}^2 + C_{iB}^2 = 1 \quad [69]$$

The charge for atom $\alpha$ that would go into the potential (e.g., Eq. [1]) is given by

$$q_{i\alpha} = C_{iA}^2 q_{\alpha A} + C_{iB}^2 q_{\alpha B} \quad [70]$$

where $q_{\alpha X}$ is the charge of atom $\alpha$ for state $X$. Similarly, the dihedral force constant (for the $n = 2$ term) is given by

$$V_i = C_{iA}^2 V_A + C_{iB}^2 V_B \quad [71]$$

The charges and dihedral force constants thus vary between the values for state $A$ and the values for state $B$. This model provides a method for treating polarizability in which both the electrostatic parameters and the bonded parameters are coupled to the environment. It would be straightforward to couple the short-range potential to the electrostatic variables, like in the shell models and the fluctuating charge model of Siepmann and co-workers.[147] The two states are coupled with a term, $C_{iA}C_{iB}E_{AB}$. The coefficients for residue $i$ are coupled to those of other residues through the Coulomb interactions. The coefficients are found by minimizing the energy, subject to the constraint of Eq. [69], and they are propagated using the extended Lagrangian method. Since the method treats the bonded parameters as variables too, it can also handle the amino group pyramidalization. In addition, the two-state empirical model enforces a charge conservation constraint on all peptide groups. Consequently, like the AACT and BCI electronegativity equalization models,[146,149,150] it will not overestimate the charge flow along the polymer.

One feature of the semiempirical models is that because the polarization is described by a set of coefficients that have a normalization condition, for example, Eq. [69], there will be no polarization catastrophe like there can be with dipole polarizable or fluctuating charge models. With a finite basis set, the polarization response is limited and can become only as large as the state with the largest dipole moment.

## APPLICATIONS

### Water

Water is the most common substance to be studied with polarizable potentials. An extremely large number of polarizable potentials for liquid

water have been developed, including those that treat the polarizability using polarizable point dipoles,[15,19–21,23–31,33,35,36,52,54,58,184] shell models,[97,99] charge-transfer models,[22,126,130,144,145,147,158,185,186] semiempirical models,[144,172,174,176,177] and hybrid methods.[166] The available literature on the simulation of water is extensive enough to deserve separate reviews.[187,188] Here, we concentrate primarily on general conclusions drawn from polarizable simulations of water.

Considerable latitude exists in choosing the nonelectrostatic features of a water model, including the functional form for the van der Waals interactions, the modeling of the intramolecular bonds and angles (flexible or rigid), and the inclusion or omission of an explicit hydrogen-bonding term. The electrostatic features of the model vary considerably as well. Although many polarizable models are constrained to reproduce the gas-phase dipole, the molecular polarizability, and sometimes the gas-phase quadrupole moment, these replications of the real data can all be accomplished in several ways with different placement of charge sites. Because of this freedom, as well as the facts that different experimental properties were used for the parameterization of the various models and different boundary conditions were used in the various simulations, it is difficult to compare different models on an equal footing. Nevertheless, the large variety of available water models does permit some general conclusions.

One of the principal purposes for using a polarizable model (of any type) is the ability to model a system under a variety of experimental conditions. For water models, a truly transferable model should cover the full range of states from gas phase to condensed phases, including ice, liquid water at ambient conditions, and even the supercritical fluid. It should also be capable of modeling heterogeneous environments by incorporating the varying polarization responses of water at interfaces,[189] around highly charged solutes, and in highly hydrophobic environments (as in the interior of proteins or lipid bilayers). Because water is in fact found under such a wide variety of conditions, and because of its anomalous properties, a fully transferable water model unfortunately remains a holy grail. Nonetheless, polarizable potentials have had considerable success in improving the transferability of water potentials in general.

Most nonpolarizable water models are actually fragile in this regard; they are not transferable to temperatures or densities far from where they were parameterized.[190] Because of the emphasis on transferability, polarizable models are typically held to a higher standard and are expected to reproduce monomer and dimer properties for which nonpolarizable liquid-state models are known to fail. Consequently, several of the early attempts at polarizable models were in fact less successful at ambient conditions than the benchmark nonpolarizable models, SPC[191] (simple point charge) and TIP4P[192] (transferable interaction potential, 4 points). Nonetheless, there is now a large collection of models that reproduce many properties of both the gas phase

(monomer and dimer geometry, dipole moment, and/or polarizability; second virial coefficient) and the bulk liquid (thermodynamic, structural, and dynamic properties).[30,36,52,53,126,166,185] The expectation is typically that such models will also be able to perform well at conditions intermediate between gas and liquid phases, such as clusters and interfaces. It is also assumed that a reasonably correct treatment of polarization will allow for some extrapolation beyond these conditions, so that systems where the electric field is not as homogeneous as in bulk water can be treated.

Even so, there are properties of small clusters and the bulk liquid that remain fairly elusive. For example, many models, both polarizable and nonpolarizable, do a poor job of reproducing the geometry of the water dimer. The methods typically predict a dimer that is too "flat", that is, with too small an angle between the donated O—H bond on the donor and the $C_{2v}$ axis of the acceptor. This lack of tetrahedral coordination at the oxygen acceptor is usually attributed to the lack of lone pairs in the model; the electrostatic potential is insufficiently anisotropic on the oxygen end of the molecule when only atom-centered charges and dipoles are used. Models with off-atom charge sites,[54,166] higher order multipoles,[21,193]or explicitly anisotropic potentials[15,193] can be used to avoid this problem.

For gas-phase properties, the second virial coefficient, $B(T)$, provides one of the most sensitive tests of a water model.[186,194] Both polarizable and nonpolarizable models are capable of reproducing experimental values of $B(T)$, and some models have even been parameterized to do so explicitly.[15,24,29] Polarizable models appear to provide significant improvements in reproducing not only the second virial coefficient,[24,25] but also the third coefficient, $C(T)$.[186,195]

In the liquid phase, calculations of the pair correlation functions, dielectric constant, and diffusion constant have generated the most attention. There exist nonpolarizable and polarizable models that can reproduce each quantity individually; it is considerably more difficult to reproduce all quantities (together with the pressure and energy) simultaneously. In general, polarizable models have no distinct advantage in reproducing the structural and energetic properties of liquid water, but they allow for better treatment of dynamic properties.

It is now well understood that the static dielectric constant of liquid water is highly correlated with the mean dipole moment in the liquid, and that a dipole moment near 2.6 D is necessary to reproduce water's dielectric constant of $\varepsilon = 78$.[4,5,185,196] This holds for both polarizable and nonpolarizable models. Polarizable models, however, do a better job of modeling the frequency-dependent dielectric constant than do nonpolarizable models.[126] Certain features of the dielectric spectrum are inaccessible to nonpolarizable models, including a peak that depends on translation-induced polarization response, and an optical dielectric constant that differs from unity. The dipole moment of 2.6 D should be considered as an optimal value for typical (i.e.,

classical and rigid) water models; it is not necessarily the best estimate of the actual dipole moment. The dipole moment of liquid water cannot be measured experimentally, nor can it even be defined unambiguously, since the electronic density is not zero between molecules.[197,198] Ab initio simulations of liquid water predict that the average dipole moment varies from 2.4 to 3.0 D depending on how the density is partitioned, so a value of 2.6 D is consistent with these studies.[199–201]

Dynamic properties, such as the self-diffusion constant, are likewise strongly correlated with the dipole moment.[5,23] This coupling between the translational motion and the dipole moment is indicated in the dielectric spectrum.[126] Models that are overpolarized tend to undergo dynamics that are significantly slower than the real physical system. The inclusion of polarization can substantially affect the dynamics of a model, although the direction of the effect can vary. When a nonpolarizable model is reparameterized to include polarizability, the new model often exhibits faster dynamics, as with polarizable versions of TIP4P,[202] Reimers–Watts–Klein (RWK),[185,203] and reduced effective representation (RER)[30] potentials. There are exceptions, however, such as the polarizable simple point charge (PSPC)[23,57] and fluctuating charge (FQ)[126] models. The usual explanation for faster dynamics in polarizable models is that given by Sprik.[202] Events governing dynamical properties, such as translational diffusion and orientational relaxation, are activated processes—they depend on relatively infrequent barrier-crossing events. Adiabatic dynamics of the polarizable degrees of freedom allows for relaxation of the polarization at the transition, through means that are inaccessible to nonpolarizable models. This in turn lowers the activation barrier and increases the number of successful transition attempts. The nonunanimity of published simulation results concerning dynamic properties is likely due to such factors as: inconsistent parameterization procedures between the polarizable and nonpolarizable models; a strong dependence of dynamic properties on the system pressure (which is often insufficiently controlled during simulations); and the effects of using point versus diffuse charge distributions.

Transferability to different temperatures is a particularly difficult task for polarizable water models. This statement is illustrated by the problems in predicting the *PVT* and phase coexistence properties. There are a handful of polarizable water models—including both dipole- and EE-based models—that are reasonably successful in predicting some of the structural and energetic changes in liquid water over a range of several hundred degrees.[53,61,204] Many models fail to capture this behavior, however, so temperature transferability is far from an automatic feature of polarizable models.[35,52,61,62] Indeed, it has been demonstrated by several authors[35,52,61] that a point dipole-based model designed specifically to reproduce properties of the gas-phase monomer and the bulk liquid at 298 K is doomed to fail at higher temperatures. This failure could arise from insufficiencies in the Lennard–Jones function typically

used for the short-range repulsion, as well as from the use of point charges or dipoles rather than diffuse charge distributions. Evidence exists showing that diffuse charge distributions are necessary to ensure transferability, in both polarizable and nonpolarizable models.[35,53,205]

Predicting phase coexistence behavior near the critical point seems to be a particularly difficult task, even for the best polarizable models. Almost no existing model that works well at ambient conditions has been demonstrated to predict the critical temperature and density to better than 10% accuracy.[61,206] And those that are specifically designed to work well near the critical point seem to do a poor job of reproducing the liquid structure at lower temperatures.[61] Part of the problem is that the simulations required to measure phase coexistence properties are computationally expensive due to the extensive sampling required. Because of this expense, phase coexistence properties have not typically been included in the list of target properties when parameterizing new water models. Thus, it is only now becoming clear how to construct a model that is transferable across hundreds of degrees, from supercooled liquid to supercritical fluid. It is not yet clear whether one particular type of polarizable model is better able to capture the variation of water properties under varying temperatures and densities than another. However, the current situation clearly underscores the considerable flexibility and ambiguities involved in parameterizing polarizable potentials.

Transferability from the solid state to the liquid state is equally problematic. A truly transferable potential in this region of the phase diagram must reproduce not only the freezing point, but also the temperature of maximum density and the relative stability of the various phases of ice. This goal remains out of reach at present, and few existing models demonstrate acceptable transferability from solid to liquid phases.[33,52,207] One feature of water that has been demonstrated by both an EE model study[207] and an ab initio study[200] is that the dipole moments of the liquid and the solid are different, so polarization is likely to be important for an accurate reproduction of both phases. In addition, while many nonpolarizable water models exhibit a computed temperature of maximum density for the liquid, the temperature is not near the experimental value of 277 K.[53,62,208–215] For example, TIP4P[192] and SPC/E[4] models have a temperature of maximum density, $T_{MD}$, near 248 K.[211,213,215] Several EE models[53,147,207] and one EE–PPD hybrid model[166] yield a $T_{MD}$ right at 277 K, suggesting that polarizability may be an important factor for this property as well. However, PPD models do not reproduce the $T_{MD}$ maximum density very well; one model does not even have a $T_{MD}$[212] and another has a temperature dependence on the density that is much too strong.[62] One nonpolarizable model, the TIP5P model, which includes lone-pair interaction sites, has been successfully constructed to have the correct $T_{MD}$.[216]

The successful transferability of water models from the bulk phases to more heterogeneous conditions is another important goal for scientists

developing polarizable models. A vast literature exists in this area, with applications ranging from the solvation of simple ions[27,82,202,217,218] and biomolecules[10] to hydrophobic hydration and the structure of water at interfaces[104,219,220] and in external electric fields.[206,220] Due to the wide variation in electrostatic environments encountered, it is not surprising to find that polarizable models generally (but not always) provide significant improvements over nonpolarizable models.

## Proteins and Nucleic Acids

For both proteins and nucleic acids, there exist significant structure-determining, hydrogen-bonding interactions between groups with π electrons: the peptide group for proteins and bases for nucleic acids. The extensive network of peptide hydrogen bonds in α-helices and β-sheets in proteins and the base-pair stacking in the double helix of nucleic acids are stablized by polarization of electrons with some π character. This stabilization has been labeled π-bond cooperativity or resonance-assisted hydrogen bonding.[221,222] The polarization of the π electrons in amides can be represented by the usual two dominant resonance structures

and in the nucleic acid bases (shown here for uracil),

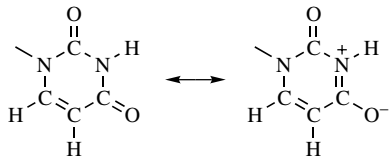

Resonance structures like these are commonly cited as leading to the planar geometry of the peptide bond and nucleic acid bases.

A number of quantum mechanical studies on the molecules *N*-methylactamide (NMA) and *N*-methylformamide (NMF), have addressed the importance of cooperative, or nonadditive, effects on hydrogen-bond formation.[223–225] Aggregates of NMA or NMF may be considered prototypes of the protein backbone. For these systems, the cooperative effects were found to add about 12–20% to the stabilization energy. Most of that energy can be decomposed into the polarization energy, with charge transfer making only a modest contribution, although the size of each component depends on the method of decomposition.[225] Experimental studies on NMA aggregates also

indicate cooperativity in the hydrogen-bond energies,[226] and dielectric measurements on polypeptide chains show an enhancement of the dipole moment of the peptide group in an α-helix.[227] Other quantum mechanical studies have addressed the importance of polarizability on protein folding,[228] enzyme catalysis,[229] DNA base pair stacking,[230] and nucleic acid interactions with ions.[231]

Several polarizable models for proteins and the peptide group have been developed, using polarizable point dipoles,[32,44,45,232] electronegativity equalization models,[10,146] and the two-state empirical model.[183] Simulations using point polarizable dipole models by Warshel and co-workers[44,45] and by Wodak and co-workers[46] examined the role of polarizability on protein stability, dielectric properties, and enzymatic activity. For example, Van Belle et al.[46] found that the helix dipoles are enhanced, in agreement with the dielectric measurements of Wada,[227] and, further, the helix dipoles are enhanced not only through hydrogen bonds to the backbone, but also through association with side chain atoms. Polarization has also been shown to influence the folding time scales for small polypeptides.[183] For nucleic acids, a point polarizable dipole model was recently introduced.[232] Despite these studies and acknowledgment of the importance of polarizability from both electronic structure and experimental studies, not many simulations of proteins or nucleic acids using polarizable models have been done to date.

An implication of resonance-assisted hydrogen bonding is that as the charges are polarized, through hydrogen bonds or other interactions, the hybridization of the atoms involved can change. For example, studies of crystal structures of formamide reveal that the C=O bond length increases and the C–N bond length decreases due to the formation of hydrogen bonded dimers.[233] Other crystal structures and ab initio quantum calculations on amides further validate the fact that hydrogen bonds can change those bond lengths.[234] The hydrogen bonds in these structures are in the amide plane and promote the double bond, zwitterionic state. On the other hand, the interactions in which the amino nitrogen serves as a hydrogen-bond acceptor would stabilize the single bond form. Partial $sp^3$ hybridization of the amino nitrogen leads to pyramidalization. Indeed, nonplanarities of some peptide bonds have been observed in atomic-resolution structures of proteins.[183,235,236] In addition, the planarity of the peptide bond is dependent on a protein's secondary structure, with residues in an α-helix being more planar than elsewhere.[183] For nucleic acids, ab initio calculations indicate that the amino group can be pyramidalized through interactions with neighboring molecules or ions.[237] For both the peptide bond and nucleic acid bases, there is reason to believe that a significant degree of nonplanarity can be induced by the environment. To treat these effects, the polarization of the electrostatic degrees of freedom—charges or dipoles—would have to be coupled to the bonded interactions, as has been developed for the peptide bond.[183]

## COMPARISON OF THE POLARIZATION MODELS

### Mechanical Polarization

One important difference between the shell model and polarizable point dipole models is in the former's ability to treat so-called mechanical polarization effects. In this context, mechanical polarization refers to any polarization of the electrostatic charges or dipoles that result from causes other than the electric field of neighboring atoms. In particular, mechanical interactions such as steric overlap with nearby molecules can induce polarization in the shell model, as further described below. These mechanical polarization effects are physically realistic and are quite important in some condensed-phase systems.

As mentioned earlier, the shell model is closely related to those based on polarizable point dipoles; in the limit of vanishingly small shell displacements, they are electrostatically equivalent. Important differences appear, however, when these electrostatic models are coupled to the nonelectrostatic components of a potential function. In particular, these interactions are the nonelectrostatic repulsion and van der Waals interactions—short-range interactions that are modeled collectively with a variety of functional forms. Point dipole- and EE-based models of molecular systems often use the Lennard–Jones potential. On the other hand, shell-based models frequently use the Buckingham or Born–Mayer potentials, especially when ionic systems are being modeled.

Regardless of the specific potential used, PPD- and EE-based models typically lack coupling between the short-range potential and the long-range electrostatic degrees of freedom. The dipoles and fluctuating charges respond solely to the local electric field (see Eq. [3]), with no regard for local short-range interactions. In other words, the polarizability, $\alpha$, of each point dipole in a PPD model is independent of the local environment. The situation is different for the shell-based models. Because the van der Waals and exchange-repulsion interactions being modeled by the short-range nonelectrostatic part of the potential are electron–electron interactions, the interaction sites are almost always taken to be coincident with the shell (electronic) charge, rather than the core (nuclear) charge or center of mass. The short-range interactions in the shell model couple with only one end of the finite dipole, rather than with both "ends" of the point dipole. Consequently, the shell model includes a coupling between the short-range interactions and the orientation of the dipole—a coupling that is not present in point dipole-based models. The coupling of short-range interactions and dipole orientations is in fact quite realistic physically, and the lack of such a coupling is a disadvantage of the PPD models. One way to better understand this coupling is to recognize that the shell models have two mechanisms for polarization: a purely electrostatic induction effect, governed by the fixed polarizability in Eq. [27], and a

mechanical polarization effect that depends on the specific implementation of the dispersion and short-range repulsive interactions. Thus each polarizable site has an effective polarizability that depends on the local environment. When a shell-model atom is confined in a condensed phase, the steric interactions with neighboring ions will generally reduce the effective polarizability compared to the gas-phase value. In a crystalline environment, there are additional effects to consider: the anions and cations will polarize by different amounts in an applied electric field (due to the more diffuse electron density in the anions). The mechanical polarization effects will act to increase the effective polarizability in cations, and decrease it in anions.[73] These effects are completely realistic; the polarizabilities of atoms and ions do change with their environment in just these ways,[238–240] and shell models have at times been specifically parameterized to include this effect quantitatively.[73,96] Indeed, the inclusion of this mechanical polarizability effect has been shown to be crucial for reproducing condensed-phase properties such as phonon dispersion curves.[74,75]

Another coupling of the short-range repulsive and long-range electrostatic interactions has been developed by Chen, Xing, and Siepmann.[147] In their EE model, the repulsive part of the Lennard–Jones potential is coupled to the charge. This coupling is consistent with ab initio quantum calculations that find that the size of an atom increases with its negative charge.[241] Studies of gas–liquid[61] and solid–liquid[207] coexistence of water also suggest that models that couple the volume of an atom (through the Lennard–Jones interaction) to the size of the atom's charge may be best suited for prediction of molecular properties in the three phases. Empirical and semiempirical methods provide a natural way to link the charges to other parts of the potentials, as is done in the empirical valence bond approach[242] and the two-state peptide bond model.[183]

To further illustrate the importance of coupling the electrostatic and short-ranged repulsion interactions, we consider the example of a dimer of polarizable rare gas atoms, as presented by Jordan et al.[96] In the absence of an external electric field, a PPD model predicts that no induced dipoles exist (see Eq. [12]). But the shell model correctly predicts that the rare gas atoms polarize each other when displaced away from the minimum-energy (force-free) configuration. The dimer will have a positive quadrupole moment at large separations, due to the attraction of each electron cloud for the opposite nucleus, and a negative quadrupole at small separations, due to the exchange-correlation repulsion of the electron clouds. This result is in accord with ab initio quantum calculations on the system, and these calculations can even be used to help parameterize the model.[96]

In essence, this difference between shell models and PPD models arises from the former's treatment of the induced dipole as a dipole of finite length. Polarization in physical atoms results in a dipole moment of a small, but finite, extent. Approximating this dipole moment as an idealized point dipole, as in the PPD models, is an attractive mathematical approximation and produces

negligible errors in such properties as the electric field generated outside the molecule. Unfortunately, there are some physical effects that this idealization obscures, such as the environment-dependent polarizability.

All polarizable models share the ability to polarize, by varying their charge distribution in response to their environment. In addition, shell models and EE models with charge-dependent radii have the ability to modify their polarizability—the magnitude of this polarization response—in response to their local environment. Consequently, it is reasonable to expect that shell models and mechanically coupled EE models may be slightly more transferable to different environments than more standard PPD and EE models. To date, it is not clear whether this expectation has been fully achieved. Although some shell-based models for both ionic and molecular compounds have been demonstrated to be transferable across several phases and wide ranges of phase points,[73,96,99,243] it is not clear that the transferability displayed by these models is better than that demonstrated in PPD- or EE-based models. And even with an environment-dependent polarizability, it has been demonstrated that the basic shell model cannot fully capture all of the variations in ionic polarizabilities in different crystal environments.[85]

## Computational Efficiency

One significant difference between the different methods of incorporating polarization is their computational efficiency. For energy evaluations, the electronegativity equalization-based methods are considerably more efficient than the dipole or shell models. Dipole-based methods require evaluation of the relatively CPU-expensive dipole–dipole interactions (Eq. [7]). The charge–charge interactions used in shell models are much cheaper, by about a factor of three. But this advantage is eliminated by the need to represent each polarizable center by two point charges, thus quadrupling the total number of interactions that need to be computed. Methods based on electronegativity equalization typically represent each polarizable site by a single charge (either point or diffuse), and energy evaluations are thus three-to-four times faster than with the other models, for direct summation. Semiempirical methods have 4–10 basis functions per atom, and each energy evaluation requires solving large matrices, thereby decreasing the computational efficiency of these models.[144,172–176] In the simpler two-state empirical model, the additional computational requirements are comparable to the EE models.[183]

Energy evaluation for any collection of point charges and dipoles can be accelerated significantly by using fast-multipole[244,245] or particle-mesh[246,247] methods. The computational advantages of these methods are proportionally much greater for the dipole-based models, because they avoid the direct evaluation of a more expensive interaction. In large systems, the overhead associated with using dipoles can be reduced to about a third more than the cost of using point charges. Algorithms for performing conventional,[66]

fast-multipole,[69] and particle-mesh Ewald[50] summation on point dipoles are available, and even quite efficient, but are considerably more complex than the comparable methods for monopole charges.[244,247–249]

Regardless of the type of model used, a method must be chosen for the self-consistent solution of the polarizable degrees of freedom. Direct solution via matrix inversion is nearly always avoided by most researchers in the field, because of the prohibitive $O(N^3)$ scaling with system size, $N$. Both iterative and predictive methods reduce the scaling to match that of the potential evaluation [$O(N^2)$ for direct summation; $O(N \ln N)$ for Ewald-based methods;[50,68] $O(N)$ if interactions are neglected beyond some distance cutoff], but the cost of the iterations means that the predictive methods are always more efficient. Extended Lagrangian methods have been implemented for all four types of polarizable potential.[10,22,56–58,82,90,97,99,104,126,148,183] The extended Lagrangian methods are least popular for PPD-based models; as a general rule, simulations with these models still tend to use iterative methods. The extended Lagrangian approach is perhaps most natural for the shell model, for which it is physically reasonable to assign a mass to the polarizable degrees of freedom (the shell charges) and treat them dynamically. However, the small mass of the shell charge usually requires an MD time step smaller than would be chosen in a nonpolarizable simulation.[82,90,97,99,104] The fluctuating charge and PPD models usually do not require a reduction in time step, thus making them somewhat more efficient in this regard.

Multiple time step methods[250,251] can also be used to reduce the computational cost of simulations with polarizable models. Such methods have been used successfully with shell and fluctuating charge models.[82,104] However, it is more problematic to apply these multiple time scale integrators in simulations using iterative integrators. The multiple time scale integrators work by calculating updated values for only a fraction of the system's interactions during some of the time steps; but since all of the interactions are needed in order to provide well-converged values for the polarizable degrees of freedom, the bulk of the expensive electrostatic interactions must still be evaluated at every step.

## Hyperpolarizability

Note that linearly polarizable point dipoles provide only an approximation to the true polarization response in two different ways. First, polarization can include terms that are nonlinear in the electric field. Thus, Eq. [3] represents only the first term in an infinite series,

$$\mu = \alpha \cdot \mathbf{E} + \frac{1}{2}\mathbf{E} \cdot \beta \cdot \mathbf{E} + \cdots \qquad [72]$$

where $\beta$ is a third-rank tensor representing the first hyperpolarizability of the system.[14] In water, for example, the nonlinear polarization effects begin to

become significant at field strengths[252,253] of 2–3 V/Å, which is comparable to the mean field strength in an aqueous solution.[53] This finding indicates that perhaps there are improvements to be made by going beyond the approximation of linear polarization. Only occasional attempts have been made to include these effects.[55]

## Charge-Transfer Effects

The EE-based and semiempirical models implement polarization via charge transfer between atoms on the same molecule. These models are fundamentally different from the treatment of shell and PPD models, which include point polarization but no charge transfer. There are important differences between the two approaches.

As pointed out in the section on Electronegativity Equalization Models, the implementation of charge transfer in current EE models tends to lead to overpolarization in large molecules or when intermolecular charge transfer is allowed. In contrast, the lack of charge transfer in point-polarizable models can sometimes lead to underpolarization. In general, the point-polarizable models predict that the polarizability of a single molecule or a system of molecules will increase linearly with its size, in proportion to the number of (linearly polarizable and weakly interacting) dipoles.[254] This behavior is exactly correct for systems without charge transfer, such as saturated hydrocarbon molecules and most biomolecules. The PPD models severely underpredict, however, the increase of polarization with system size for conductive systems such as unsaturated hydrocarbons. An EE-based model does significantly better at predicting the size-dependent polarization of conductive systems, but exaggerates the polarization in large systems with no charge transfer.[149] Thus we emphasize that it is important to choose the method of treating polarization that is most appropriate for the system being studied. Hybrid models containing both point-polarizable and charge-transfer sites are perhaps the most flexible approach.[145,146,150,166]

Another side effect of the EE and semiempirical models' reliance on charge transfer for treating polarization is a geometry dependence that is absent in point-polarizable models. The charge redistribution in an EE model can arise only as a result of charge transfer from one site to another. Consequently, the polarization response is constrained by the geometry of the charge sites. This constraint is most severe for highly symmetric species. For planar molecules such as benzene and water, the EE model unrealistically predicts that the out-of-plane component of the polarizability tensor is zero. Linear molecules cannot be polarized in the transverse direction. Atomic or ionic species suffer the most dramatic limitation: they have no polarization response at all under the EE approximation. Whereas this can be a severe limitation in some circumstances, an EE model for water with purely planar polarizability somewhat surprisingly performs as well as or better than PPD and shell models

with three-dimensional polarizability tensors.[126] Off-atom charge sites have been successfully used to address this limitation in some cases, as have hybrid models.[82,96,104,145,146,150,166]

## The Electrostatic Potential

In addition to treating the polarization response in different ways, the various methods considered here also provide different levels of approximation to the external electric field. Accurate simulation of intermolecular interactions requires that the electrostatic potential be correctly represented everywhere outside the molecular surface. The correct electrostatic potentials can be reproduced, of course, by the physically correct nuclear and electronic charge distribution. At points outside the molecular surface, however, it can also be reproduced to arbitrary accuracy by a series of point monopoles, dipoles, quadrupoles, and so on. This approach is taken in most computer simulations. The simplest level of approximation is to include point charges (monopoles) at the atomic sites. The accuracy of this approximation can be improved by (1) adding more charge sites (off-atom sites); (2) increasing the number of terms in the series (dipoles, quadrupoles, etc.); and (3) by replacing the point multipoles with delocalized, diffuse charge distributions.

The PPD and shell models are nearly equivalent in this sense, because they model the electrostatic potential via static point charges and polarizable dipoles (of either zero or very small extent). Accuracy can be improved by extending the expansion to include polarizable quadrupoles or higher order terms.[193] The added computational expense and difficulty in parameterizing these higher order methods has prevented them from being used widely. The accuracy of the ESP for dipole-based methods can also be improved by adding off-atom dipolar sites.[96,166]

Because the EE-based methods truncate the series representation of the electrostatic potential one term earlier (i.e., by using only monopole charges), these methods would appear to sacrifice some accuracy in representing the electrostatic potential. It is becoming widely appreciated that models based solely on point charges may require the use of off-atom charge sites to successfully fit the electrostatic potential.[166,255] However, nearly all polarizable simulation methods based on charge-transfer methods have used some sort of delocalized charges, rather than point charges.[22,125,126,130,146,158,171] This approach has been shown to be successful at reproducing the electrostatic potential for most extramolecular sites, although the use of point dipoles can improve the performance for certain conformations (such as bifurcated hydrogen bonds) in which molecular symmetries prevent accurate charge distributions.[146] Indeed, it has been claimed that the better representation of intermolecular interactions due to diffuse charges is as important as the use of polarizability.[205] The chemical potential equalization (CPE) methods are

noteworthy in this regard because they use both diffuse monopoles and dipoles to represent the system's polarization.[130,131,171]

The difference between models having polarizable point dipoles and fixed point charges and those with fluctuating charges and fixed Lennard–Jones interactions reduces to considering which term is static and which is polarizable. For the PPD model, the charge–charge term is static and the induced dipole–induced dipole term is polarizable. For the EE model, the charge–charge term is polarizable and the induced dipole–induced dipole terms (included in the Lennard–Jones $r^{-6}$ interaction) are static. Note that including a Lennard–Jones $r^{-6}$ dispersion term is not redundant for polarizable models because this represents the interaction arising from correlated thermal fluctuations of the induced dipole. With a few exceptions,[22,57,202] most models—whether based on matrix, iterative, or extended Lagrangian algorithms—are adiabatic and do not allow for substantial fluctuations away from the minimum-energy polarization state.

## SUMMARY AND CONCLUSIONS

There are a variety of different models used to treat polarizability in molecular simulations: polarizable point dipoles, shell models, fluctuating charge models, and semiempirical models, along with variations and combinations of these. There are advantages and disadvantages of each model, as discussed in detail in previous sections. These relative merits range from differing computational efficiencies and ease of implementation to different accuracies in representing the external electric field and transferability of parameters. Regardless of the differences in convenience and efficiency, the most important consideration when choosing a polarizable model for a particular problem should be the model's applicability to the system in question.

Despite the many differences between the various polarizable models, it is encouraging to note that the most recent models seem to be converging on the same set of necessary features. A variety of successful models based on different formalisms all share many of the same characteristics.[126,130,131,146,150,166,171,205] Regardless of the direction from which the models evolved, there is a growing consensus that accurate treatment of polarization requires (1) either diffuse charge distributions or some other type of electrostatic screening (2) a mixture of both monopoles and dipoles to represent the electrostatic charge distribution, and (3) only linear polarizability.

Although much work remains to be done before there is a truly accurate, transferable model for a wide range of conditions and systems, it is fair to say that polarizable models have matured considerably since their earliest implementations. Future developments will almost certainly include continued development and parameterization of the more mainstream models, along with their incorporation into commercial and academic simulation software

packages, thereby making these methods much more accessible to the nonspecialist. In particular, we expect polarizable models, and especially polarizable water models, to become more prevalent in biomolecular simulations involving heterogeneous solvent environments. Inclusion of polarizability in the potentials for proteins and other macromolecular systems is also likely to become more common, and hence a careful assessment of the importance of polarizability to these systems is needed. Until the importance of polarizability has been clearly demonstrated, the added computational cost of modeling the polarization makes it is unlikely that polarizable models will displace more traditional models for the bulk of routine simulation, particularly when applied to large systems.

Future directions in the development of polarizable models and simulation algorithms are sure to include the combination of classical or semiempirical polarizable models with fully quantum mechanical simulations, and with empirical reactive potentials. The increasingly frequent application of Car–Parrinello ab initio simulations methods[156] may also influence the development of potential models by providing additional data for the validation of models, perhaps most importantly in terms of the importance of various interactions (e.g., polarizability, charge transfer, partially covalent hydrogen bonds, lone-pair-type interactions). It is also likely that we will see continued work toward better coupling of charge-transfer models (i.e., EE and semiempirical models) with purely local models of polarization (polarizable dipole and shell models).

## REFERENCES

1. J. A. McCammon and S. C. Harvey, *Dynamics of Proteins and Nucleic Acids,* Cambridge University Press, Cambridge, UK, 1987.
2. M. Rigby, E. B. Smith, W. A. Wakeham, and G. C. Maitland, *The Forces Between Molecules,* Oxford Science Publications, Oxford, UK, 1986.
3. T. A. Halgren, *J. Am. Chem. Soc.,* **114,** 7827–7843 (1992). Representation of van der Waals (vdW) Interactions in Molecular Mechanics Force Fields: Potential Form, Combination Rules, and vdW Parameters.
4. H. J. C. Berendsen, J. R. Grigera, and T. P. Straatsma, *J. Phys. Chem.,* **91,** 6269–6271 (1987). The Missing Term in Effective Pair Potentials.
5. K. Watanabe and M. L. Klein, *Chem. Phys.,* **131,** 157–167 (1989). Effective Pair Potentials and the Properties of Water.
6. L. Kuyper, D. Ashton, K. M. Merz Jr., and P. A. Kollman, *J. Phys. Chem.,* **95,** 6661–6666 (1991). Free Energy Calculations on the Relative Solvation Free Energies of Benzene, Anisole, and 1,2,3-Trimethoxybenzene: Theoretical and Experimental Analysis of Aromatic Methoxy Solvation.
7. W. L. Jorgensen and J. Gao, *J. Am. Chem. Soc.,* **110,** 4212–4216 (1988). Cis–Trans Energy Difference for the Peptide Bond in the Gas Phase and in Aqueous Solution.
8. D. E. Williams, *Biopolymers,* **29,** 1367–1386 (1990). Alanyl Dipeptide Potential-Derived Net Atomic Charges and Bond Dipoles, and Their Variation with Molecular Conformation.

9. P. Cieplak and P. Kollman, *J. Comput. Chem.,* **12,** 1232–1236 (1991). On the Use of Electrostatic Potential Derived Charges in Molecular Mechanics Force Field. The Relative Solvation Free Energy of *Cis-* and *Trans-N*-Methyl-Acetamide.
10. S. W. Rick and B. J. Berne, *J. Am. Chem. Soc.,* **118,** 672–679 (1996). Dynamical Fluctuating Charge Force Fields: The Aqueous Solvation of Amides.
11. J. J. Urban and G. R. Famini, *J. Comput. Chem.,* **14,** 353–362 (1993). Conformational Dependence of the Electrostatic Potential-Derived Charges of Dopamine: Ramifications in Molecular Mechanics Force Field Calculation in the Gas Phase and Aqueous Solution.
12. U. Dinur and A. T. Hagler, *J. Comput. Chem.,* **16,** 154–170 (1995). Geometry-Dependent Atomic Charges—Methodology and Application to Alkanes, Aldehydes, Ketones, and Amides.
13. U. Koch, P. L. A. Popelier, and A. J. Stone, *Chem. Phys. Lett.,* **238,** 253–260 (1995). Conformational Dependence of Atomic Multipole Moments.
14. C. J. F. Böttcher, *Theory of Electric Polarization,* 2nd ed., Elsevier, New York, 1973.
15. T. P. Lybrand and P. A. Kollman, *J. Chem. Phys.,* **83,** 2923–2933 (1985). Water–Water and Water–Ion Potential Functions Including Terms for Many Body Effects.
16. P. Cieplak, T. P. Lybrand, and P. A. Kollman, *J. Chem. Phys.,* **86,** 6393–6403 (1987). Calculations of Free Energy Changes in Ion–Water Clusters Using Nonadditive Potentials and the Monte Carlo Method.
17. B. J. Berne and A. Wallqvist, *J. Chem. Phys.,* **88,** 8016–8017 (1988). Comment on: "Water–Water and Water–Ion Potential Functions Including Terms for Many-Body Effects," T. P. Lybrand and P. Kollman, *J. Chem. Phys.* **83,** 2923 (1985), and on "Calculation of Free Energy Changes in Ion–Water Clusters Using Nonadditive Potentials and the Monte Carlo Method," P. Cieplak, T. P. Lybrand, and P. Kollman, *J. Chem. Phys.* **86,** 6393 (1987).
18. P. Kollman, T. Lybrand, and P. Cieplak, *J. Chem. Phys.,* **88,** 8017 (1988). Reply to "Comment on "Water–Water and Water–Ion Potential Functions Including Terms for Many-Body Effects," T. P. Lybrand and P. Kollman, *J. Chem. Phys.* **83,** 2923 (1985), and on "Calculation of Free Energy Changes in Ion–Water Clusters Using Nonadditive Potentials and the Monte Carlo Method," P. Cieplak, T. P. Lybrand, and P. Kollman, *J. Chem. Phys.* **86,** 6393 (1987)".
19. J. A. C. Rullman and P. T. van Duijnen, *Mol. Phys.,* **63,** 451–475 (1988). A Polarizable Water Model for Calculation of Hydration Energies.
20. F. H. Stillinger and C. W. David, *J. Chem. Phys.,* **69,** 1473–1484 (1978). Polarization Model for Water and Its Ionic Dissociation Products.
21. P. Barnes, J. L. Finney, J. D. Nicholas, and J. E. Quinn, *Nature (London),* **282,** 459–464 (1979). Cooperative Effects in Simulated Water.
22. M. Sprik and M. L. Klein, *J. Chem. Phys.,* **89,** 7556–7560 (1988). A Polarizable Model for Water Using Distributed Charge Sites.
23. P. Ahlström, A. Wallqvist, S. Engström, and B. Jönsson, *Mol. Phys.,* **68,** 563–581 (1989). A Molecular Dynamics Study of Polarizable Water.
24. P. Cieplak, P. A. Kollman, and T. P. Lybrand, *J. Chem. Phys.,* **92,** 6755–6760 (1990). A New Water Potential Including Polarization: Application to Gas-Phase, Liquid, and Crystal Properties of Water.
25. U. Niesar, G. Corongiu, E. Clementi, G. R. Kneller, and D. K. Bhattacharya, *J. Phys. Chem.,* **94,** 7949–7956 (1990). Molecular Dynamics Simulations of Liquid Water Using the NCC Ab Initio Potential.
26. S. Kuwajima and A. Warshel, *J. Phys. Chem.,* **94,** 460–466 (1990). Incorporating Electric Polarizabilities in Water–Water Interaction Potentials.
27. J. Caldwell, L. X. Dang, and P. A. Kollman, *J. Am. Chem. Soc.,* **112,** 9144–9147 (1990). Implementation of Nonadditive Intermolecular Potentials by Use of Molecular Dynamics: Development of a Water–Water Potential and Water–Ion Cluster Interactions.
28. L. X. Dang, *J. Chem. Phys.,* **97,** 2659–2660 (1992). The Nonadditive Intermolecular Potential for Water Revised.

29. R. E. Kozack and P. C. Jordan, *J. Chem. Phys.,* **96,** 3120–3130 (1992). Polarizability Effects on a Four-Charge Model for Water.

30. A. Wallqvist and B. J. Berne, *J. Phys. Chem.,* **97,** 13841–13851 (1993). Effective Potentials for Liquid Water Using Polarizable and Nonpolarizable Models.

31. D. N. Bernardo, Y. Ding, K. Krogh-Jespersen, and R. M. Levy, *J. Phys. Chem.,* **98,** 4180–4187 (1994). An Anisotropic Polarizable Water Model: Incorporation of All-Atom Polarizabilities into Molecular Mechanics Force Fields.

32. J. W. Caldwell and P. A. Kollman, *J. Phys. Chem.,* **99,** 6208–6219 (1995). Structure and Properties of Neat Liquids Using Nonadditive Molecular Dynamics: Water, Methanol, and *N*-Methylacetamide.

33. J. Brodholt, M. Sampoli, and R. Vallauri, *Mol. Phys.,* **85,** 81–90 (1995). Parameterizing Polarizable Intermolecular Potentials for Water with the Ice 1h Phase.

34. T. Chang, K. A. Peterson, and L. X. Dang, *J. Chem. Phys.,* **103,** 7502–7513 (1995). Molecular Dynamics Simulations of Liquid, Interface, and Ionic Solvation of Polarizable Carbon Tetrachloride.

35. A. A. Chialvo and P. T. Cummings, *J. Chem. Phys.,* **105,** 8274–8281 (1996). Engineering a Simple Polarizable Model for the Molecular Simulation of Water Applicable over Wide Ranges of State Conditions.

36. L. X. Dang and T. Chang, *J. Chem. Phys.,* **106,** 8149–8159 (1997). Molecular Dynamics Study of Water Clusters, Liquid, and Liquid–Vapor Interface of Water with Many-Body Potentials.

37. L. Ojamäe, I. Shavitt, and S. J. Singer, *J. Chem. Phys.,* **109,** 5547–5564 (1998). Potential Models for Simulations of the Solvated Proton in Water.

38. Y. Ding, D. N. Bernardo, K. Krogh-Jespersen, and R. M. Levy, *J. Phys. Chem.,* **99,** 11575–11583 (1995). Solvation Free Energies of Small Amides and Amines from Molecular Dynamics/Free Energy Perturbation Simulations Using Pairwise Additive and Many-Body Polarizable Potentials.

39. J. Applequist, J. R. Carl, and K.-K. Fung, *J. Am. Chem. Soc.,* **94,** 2952–2960 (1972). An Atom Dipole Interaction Model for Molecular Polarizability. Application to Polyatomic Molecules and Determination of Atom Polarizabilities.

40. J. Applequist, *Acc. Chem. Res.,* **10,** 79–85 (1977). An Atom Dipole Interaction Model for Molecular Optical Properties.

41. B. T. Thole, *Chem. Phys.,* **59,** 341–350 (1981). Molecular Polarizabilities Calculated with a Modified Dipole Interaction.

42. R. C. Weast, Ed., *CRC Handbook of Chemistry and Physics,* CRC Press, Boca Raton, FL, Vol. 66, 1985.

43. F. H. Stillinger, *J. Chem. Phys.,* **71,** 1647–1651 (1979). Dynamics and Ensemble Averages for the Polarization Models of Molecular Interactions.

44. A. Warshel and M. Levitt, *J. Mol. Biol.,* **103,** 227–249 (1976). Theoretical Studies of Enzymic Reactions: Dielectric, Electrostatic and Steric Stabilization of the Carbonium Ion in the Reaction of Lysozyme.

45. S. T. Russell and A.Warshel, *J. Mol. Biol.,* **185,** 389–404 (1985). Calculations of Electrostatic Energies in Proteins. The Energetics of Ionized Groups in Bovine Pancreatic Trypsin Inhibitor.

46. D. Van Belle, I. Couplet, M. Prevost, and S. J. Wodak, *J. Mol. Biol.,* **198,** 721–735 (1987). Calculations of Electrostatic Properties in Proteins. Analysis of Contributions from Induced Protein Dipoles.

47. W. D. Cornell, P. Cieplak, C. I. Bayly, I. R. Gould, K. M. Merz Jr., D. M. Ferguson, D. C. Spellmeyer, T. Fox, J. W. Caldwell, and P. A. Kollman, *J. Am. Chem. Soc.,* **117,** 5179–5197 (1995). A Second Generation Force Field for the Simulation of Proteins, Nucleic Acids, and Organic Molecules.

48. E. L. Pollock and B. J. Alder, *Phys. Rev. Lett.,* **39,** 299–302 (1977). Effective Field of a Dipole in Polarizable Fluids.

49. F. J. Vesely, *J. Comput. Phys.,* **24,** 361–371 (1977). *N*-Particle Dynamics of Polarizable Stockmayer-Type Molecules.

50. A. Toukmaji, C. Sagui, J. Board, and T. Darden, *J. Chem. Phys.,* **113,** 10913–10927 (2000). Efficient Particle-Mesh Ewald Based Approach to Fixed and Induced Dipolar Interactions.

51. R. Kutteh and J. B. Nicholas, *Comput. Phys. Commun.,* **86,** 227–235 (1995). Efficient Dipole Iteration in Polarizable Charged Systems Using the Cell Multipole Method and Application to Polarizable Water.

52. J. Brodholt, M. Sampoli, and R. Vallauri, *Mol. Phys.,* **86,** 149–158 (1995). Parameterizing a Polarizable Intermolecular Potential for Water.

53. I. M. Svishchev, P. G. Kusalik, P. G. Wang, and R. J. Boyd, *J. Chem. Phys.,* **105,** 4742–4750 (1996). Polarizable Point-Charge Model for Water: Results Under Normal and Extreme Conditions.

54. A. Wallqvist, P. Ahlström, and G. Karlstrom, *J. Phys. Chem.,* **94,** 1649–1656 (1990). A New Intermolecular Energy Calculation Scheme: Applications to Potential Surface and Liquid Properties of Water.

55. G. Ruocco and M. Sampoli, *Mol. Phys.,* **82,** 875–886 (1994). Computer Simulation of Polarizable Fluids: A Consistent and Fast Way for Dealing with Polarizability and Hyperpolarizability.

56. M.-L. Saboungi, A. Rahman, J. W. Halley, and M. Blander, *J. Chem. Phys.,* **88,** 5818–5823 (1988). Molecular Dynamics Studies of Complexing in Binary Molten Salts with Polarizable Anions: $MAX_4$.

57. D. van Belle, M. F. G. Lippens, and S. J. Wodak, *Mol. Phys.,* **77,** 239–255 (1992). Molecular Dynamics Simulation of Polarizable Water by an Extended Lagrangian Method.

58. J. W. Halley, J. R. Rustad, and A. Rahman, *J. Chem. Phys.,* **98,** 4110–4119 (1993). A Polarizable, Dissociating Molecular Dynamics Model for Liquid Water.

59. J. M. Goodfellow, *Proc. Natl. Acad. Sci. USA,* **79,** 4977–4979 (1982). Cooperative Effects in Water-Biomolecule Crystal Systems.

60. B. J. Costo, J. L. Rivail, and B. Bigot, *J. Chem. Phys.,* **86,** 1467–1473 (1987). A Monte Carlo Simulation Study of a Polarizable Liquid: Influence of the Electrostatic Induction on Its Thermodynamic and Structural Properties.

61. K. Kiyohara, K. E. Gubbins, and A. Z. Panagiotopoulos, *Mol. Phys.,* **94,** 803–808 (1998). Phase Coexistence Properties of Polarizable Water Models.

62. P. Jedlovszky and R. Vallauri, *Mol. Phys.,* **97,** 1157–1163 (1999). Temperature Dependence of Thermodynamic Properties of a Polarizable Potential Model of Water.

63. M. W. Mahoney and W. L. Jorgensen, *J. Chem. Phys.,* **114,** 9337–9349 (2001). Rapid Estimation of Electronic Degrees of Freedom in Monte Carlo Calculations for Polarizable Models of Liquid Water.

64. M. P. Allen and D. J. Tildesley, *Computer Simulation of Liquids,* Oxford University Press, Oxford, UK, 1987.

65. D. Frenkel and B. Smit, *Understanding Molecular Simulation: from Algorithms to Applications,* Academic Press, San Diego, 1996.

66. W. Smith, *Information Quarterly for Computer Simulation of Condensed Phases,* **4,** 13–25 (1982). Point Multipoles in the Ewald Summation.

67. T. M. Nymand and P. Linse, *J. Chem. Phys.,* **112,** 6386–6395 (2000). Molecular Dynamics Simulations of Polarizable Water at Different Boundary Conditions.

68. D. Fincham, *Information Quarterly for Computer Simulation of Condensed Phases,* **38,** 17–24 (1993). Optimization of the Ewald Sum.

69. R. Kutteh and J. B. Nicholas, *Comput. Phys. Commun.,* **86,** 236–254 (1995). Implementing the Cell Multipole Method for Dipolar and Charged Dipolar Systems.

70. M. Born and T. von Kármán, *Phys. Z.,* **13,** 297–309 (1912). Vibrations in Space Gratings (Molecular Frequencies).
71. M. Born and K. Huang, *Dynamical Theory of Crystal Lattices,* Oxford University Press, Oxford, UK, 1954.
72. B. G. Dick and A. W. Overhauser, *Phys. Rev.,* **112,** 90 (1958). Theory of the Dielectric Constants of Alkali Halide Crystals.
73. J. E. Hanlon and A. W. Lawson, *Phys. Rev.,* **113,** 472–478 (1959). Effective Ionic Charge in Alkali Halides.
74. R. A. Cowley, W. Cochran, B. N. Brockhouse, and A. D. B. Woods, *Phys. Rev.,* **131,** 1030–1039 (1963). Lattice Dynamics of Alkali Halide Crystals. III. Theoretical.
75. W. Cochran, *CRC Crit. Rev. Solid State Sci.,* **2,** 1–44 (1971). Lattice Dynamics of Ionic and Covalent Crystals.
76. A. N. Basu, D. Roy, and S. Sengupta, *Phys. Stat. Sol. A,* **23,** 11–32 (1974). Polarisable Models for Ionic Crystals and the Effective Many-Body Interaction.
77. M. J. L. Sangster and M. Dixon, *Adv. Phys.,* **25,** 247–342 (1976). Interionic Potentials in Alkali Halides and Their Use in Simulations of the Molten Salts.
78. J. Shanker and S. Dixit, *Phys. Status Solidi A,* **123,** 17–50 (1991). Dielectric Constants and Their Pressure and Temperature Derivatives for Ionic Crystals.
79. P. Drude, *The Theory of Optics,* Longmans, Green, and Co., New York, 1901.
80. F. London, *Trans. Faraday Soc.,* **33,** 8–26 (1937). The General Theory of Molecular Forces.
81. W. Cochran, in *Phonons in Perfect Lattices and in Lattices with Point Imperfections,* R. W. H. Stevenson, Ed., Plenum Press, New York, 1966, Vol. 6 of Scottish Universities' Summer School, Chapter 2, pp. 53–72. Theory of Phonon Dispersion Curves.
82. S. J. Stuart and B. J. Berne, *J. Phys. Chem.,* **100,** 11934–11943 (1996). Effects of Polarizability on the Hydration of the Chloride Ion.
83. C. R. A. Catlow, K. M. Diler, and M. J. Norgett, *J. Phys. C,* **10,** 1395–1412 (1977). Interionic Potentials for Alkali Halides.
84. M. Dixon and M. J. Gillan, *Philos. Mag. B,* **43,** 1099–1112 (1981). Structure of Molten Alkali Chlorides I. A Molecular Dynamics Study.
85. G. V. Lewis and C. R. A. Catlow, *J. Phys. C.,* **18,** 1149–1161 (1985). Potential Models for Ionic Oxides.
86. A. M. Stoneham and J. H. Harding, *Annu. Rev. Phys. Chem.,* **37,** 53 (1986). Interatomic Potentials in Solid State Chemistry.
87. C. R. A. Catlow and G. D. Price, *Nature (London),* **347,** 243–248 (1990). Computer Modelling of Solid-State Inorganic Materials.
88. J. H. Harding, *Rep. Progr. Phys.,* **53,** 1403–1466 (1990). Computer Simulation of Defects in Ionic Solids.
89. S. M. Tomlinson, C. R. A. Catlow, and J. H. Harding, *J. Phys. Chem. Solids,* **51,** 477–506 (1990). Computer Modelling of the Defect Structure of Non-Stoichiometric Binary Transition Metal Oxides.
90. P. J. Mitchell and D. Fincham, *J. Phys.: Condens. Matter,* **5,** 1031–1038 (1993). Shell Model Simulations by Adiabatic Dynamics.
91. P. J. D. Lindan, *Mol. Simul.,* **14,** 303–312 (1995). Dynamics with the Shell Model.
92. M. S. Islam, *J. Mater. Chem.,* **10,** 1027–1038 (2000). Ionic Transport in ABO(3) Perovskite Oxides: A Computer Modelling Tour.
93. J.-R. Hill, A. R. Minihan, E. Wimmer, and C. J. Adams, *Phys. Chem. Chem. Phys.,* **2,** 4255–4264 (2000). Framework Dynamics Including Computer Simulations of the Water Adsorption Isotherm of Zeolite Na-MAP. See also J.-R. Hill, C. M. Freeman, and L. Subramanian, in *Reviews in Computational Chemistry,* K. B. Lipkowitz and D. B. Boyd, Eds., Wiley-VCH, New York, 2000, Vol. 16, pp. 141–216. Use of Force Fields in Materials Modeling. The shell model is also discussed by B. van de Graaf, S. L. Njo, and K. S. Smirnov, in *Reviews in*

*Computational Chemistry,* K. B. Lipkowitz and D. B. Boyd, Eds., Wiley-VCH, New York, 2000, Vol. 14, pp. 137–223. Introduction to Zeolite Modeling.

94. J. Sauer and M. Sierka, *J. Comput. Chem.,* **21,** 1470–1493 (2000). Combining Quantum Mechanics and Interatomic Potential Functions in Ab Initio Studies of Extended Systems.
95. H. Saint-Martin, C. Medina-Llanos, and I. Ortega-Blake, *J. Chem. Phys.,* **93,** 6448–6452 (1990). Nonadditivity in an Analytical Intermolecular Potential: The Water–Water Interaction.
96. P. C. Jordan, P. J. van Maaren, J. Mavri, D. van der Spoel, and H. J. C. Berendsen, *J. Chem. Phys.,* **103,** 2272–2285 (1995). Towards Phase-Transferable Potential Functions: Methodology and Application to Nitrogen.
97. N. H. de Leeuw and S. C. Parker, *Phys. Rev. B,* **58,** 13901–13908 (1998). Molecular-Dynamics Simulation of MgO Surfaces in Liquid Water Using a Shell-Model Potential for Water.
98. H. Saint-Martin, J. Hernández-Cobos, M. I. Bernal-Uruchurtu, I. Ortega-Blake, and H. J. C. Berendsen, *J. Chem. Phys.,* **113,** 10899–10912 (2000). A Mobile Charge Densities in Harmonic Oscillators (MCDHO) Molecular Model for Numerical Simulations: The Water–Water Interaction.
99. P. J. van Maaren and D. van der Spoel, *J. Phys. Chem. B,* **105,** 2618–2626 (2001). Molecular Dynamics Simulations of Water with Novel Shell-Model Potentials.
100. N. Karasawa and W. A. Goddard, *Macromolecules,* **25,** 7268–7281 (1992). Force-Fields, Structures, and Properties of Poly(vinylidene Fluoride) Crystals.
101. M. Dixon and M. J. L. Sangster, *J. Phys. C: Solid State Phys.,* **8,** L8–L11 (1975). Simulation of Molten NaI Including Polarization Effects.
102. T. Schlick, in *Reviews in Computational Chemistry,* K. B. Lipkowitz and D. B. Boyd, Eds., VCH Publishers, New York, 1992, Vol. 3, pp. 1–71. Optimization Methods in Computational Chemistry.
103. P. J. D. Lindan and M. J. Gillan, *J. Phys.: Condens. Matter,* **5,** 1019–1030 (1993). Shell-Model Molecular Dynamics Simulation of Superionic Conduction in $CaF_2$.
104. S. J. Stuart and B. J. Berne, *J. Phys. Chem. A,* **103,** 10300–10307 (1999). Surface Curvature Effects in the Aqueous Ionic Solvation of the Chloride Ion.
105. K. F. O'Sullivan and P. A. Madden, *J. Phys.: Condens. Matter,* **3,** 8751–8756 (1991). Light Scattering by Alkali Halides Melts: A Comparison of Shell-Model and Rigid-Ion Computer Simulation Results.
106. J. A. Board and R. J. Elliott, *J. Phys.: Condens. Matter,* **1,** 2427–2440 (1989). Shell Model Molecular Dynamics Calculations of the Raman spectra of Molten NaI.
107. W. Cochran, *Philos. Mag.,* **4,** 1082–1086 (1959). Lattice Dynamics of Alkali Halides.
108. J. Cao and B. J. Berne, *J. Chem. Phys.,* **99,** 2213–2220 (1993). Theory of Polarizable Liquid Crystals: Optical Birefringence.
109. U. Schröder, *Solid State Commun.,* **4,** 347–349 (1966). A New Model for Lattice Dynamics ("Breathing Shell Model").
110. M. P. Verma and R. K. Singh, *Phys. Status Solidi,* **33,** 769 (1969). The Contribution of Three-Body Overlap Forces to the Dynamical Matrix of Alkali Halides.
111. D. K. Fisler, J. D. Gale, and R. T. Cygan, *Am. Mineral.,* **85,** 217–224 (2000). A Shell Model for the Simulation of Rhombohedral Carbonate Minerals and Their Point Defects.
112. R. Ferneyhough, D. Fincham, G. D. Price, and M. J. Gillan, *Model. Simul. Mater. Sci. Eng.,* **2,** 1101–1110 (1994). The Melting of MgO Studied by Molecular-Dynamics Simulation.
113. P. J. D. Lindan and M. J. Gillan, *Philos. Mag. B,* **69,** 535–548 (1994). The Dynamical Simulation of Superionic $UO_2$ Using Shell-Model Potentials.
114. C. Rambaut, H. Jobic, H. Jaffrezic, J. Kohanoff, and S. Fayeulle, *J. Phys.: Condens. Matter,* **10,** 4221–4229 (1998). Molecular Dynamics Simulation of the $\alpha$-$Al_2O_3$ Lattice: Dynamic Properties.

115. M. Baudin and K. Hermansson, *Surf. Sci.,* **474,** 107–113 (2001). Metal Oxide Surface Dynamics from Molecular Dynamics Simulations: The $\alpha$-$Al_2O_3$(0001) Surface.

116. G. Jacucci, I. R. McDonald, and A. Rahman, *Phys. Rev. A,* **13,** 1581–1592 (1976). Effects of Polarization on Equilibrium and Dynamic Properties of Ionic Systems.

117. M. Dixon and M. J. L. Sangster, *J. Phys. C: Solid State Phys.,* **8,** 909–925 (1976). Effects of Polarization on Some Static and Dynamic Properties of Molten NaI.

118. M. Dixon, *Philos. Mag. B,* **47,** 509–530 (1983). Molecular Dynamics Studies of Molten NaI. I. Quasi-Elastic Neutron Scattering.

119. M. Dixon, *Philos. Mag. B,* **47,** 531–554 (1983). Molecular Dynamics Studies of Molten NaI. II. Mass-, Charge- and Number-Density Fluctuations.

120. M. Dixon, *Philos. Mag. B,* **48,** 13–29 (1983). Molecular Dynamics Studies of Molten NaI. III. Longitudinal and Transverse Currents.

121. J. D. Carbeck, D. J. Lacks, and G. C. Rutledge, *J. Chem. Phys.,* **103,** 10347–10355 (1995). A Model of Crystal Polarization in $\beta$-Poly(Vinylidene Fluoride).

122. R. S. Mulliken, *J. Chem. Phys.,* **2,** 782–793 (1934). A New Electronegativity Scale: Together with Data on Valence States and an Ionization Potential and Electron Affinities.

123. R. G. Parr and R. G. Pearson, *J. Am. Chem. Soc.,* **105,** 7512–7516 (1983). Absolute Hardness: Companion Parameter to Absolute Electronegativity.

124. R. G. Pearson, *Inorg. Chem.,* **27,** 734–740 (1988). Absolute Electronegativity and Hardness: Application to Inorganic Chemistry.

125. A. K. Rappé and W. A. Goddard III, *J. Phys. Chem.,* **95,** 3358–3363 (1991). Charge Equilibration for Molecular Dynamics Simulations.

126. S. W. Rick, S. J. Stuart, and B. J. Berne, *J. Chem. Phys.,* **101,** 6141–6156 (1994). Dynamical Fluctuating Charge Force Fields: Application to Liquid Water.

127. F. H. Streitz and J. W. Mintmire, *Phys. Rev. B,* **50,** 11996–12003 (1994). Electrostatic Potentials for Metal-Oxide Surfaces and Interfaces.

128. S. Ogata, H. Iyetomi, K. Tsuruta, F. Shimojo, R. K. Kalia, A. Nakano, and P. Vashista, *J. Appl. Phys.,* **86,** 3036–3041 (1999). Variable-Charge Interatomic Potentials for Molecular-Dynamics Simulations of $TiO_2$.

129. M. Berkowitz, *J. Am. Chem. Soc.,* **109,** 4823–4825 (1987). Density Functional Approach to Frontier Controlled Reactions.

130. D. M. York and W. Yang, *J. Chem. Phys.,* **104,** 159–172 (1996). A Chemical Potential Equalization Method for Molecular Simulations.

131. C. Bret, M. J. Field, and L. Hemmingsen, *Mol. Phys.,* **98,** 751–763 (2000). A Chemical Potential Equilization Model for Treating Polarization in Molecular Mechanics Force Fields.

132. R. G. Parr, R. A. Donelly, M. Levy, and W. E. Palke, *J. Chem. Phys.,* **68,** 3801–3807 (1978). Electronegativity: The Density Functional Viewpoint.

133. L. C. Allen, *Acc. Chem. Res.,* **23,** 175–176 (1990). Electronegativity Scales.

134. R. T. Sanderson, *Science,* **114,** 670–672 (1951). An Interpretation of Bond Lengths and a Classification of Bonds.

135. W. J. Mortier, K. V. Genechten, and J. Gasteiger, *J. Am. Chem. Soc.,* **107,** 829–835 (1985). Electronegativity Equalization: Application and Parameterization.

136. W. J. Mortier, S. K. Ghosh, and S. Shankar, *J. Am. Chem. Soc.,* **108,** 4315–4320 (1986). Electronegativity Equalization: Method for the Calculation of Atomic Charges in Molecules.

137. K. T. No, J. A. Grant, and H. A. Scheraga, *J. Phys. Chem.,* **94,** 4732–4739 (1990). Determination of Net Ionic Charges Using a Modified Partial Equalization of Orbital Electronegativity Method. 1. Application to Neutral Molecules as Models for Polypeptides.

138. K. T. No, J. A. Grant, M. S. Jkon, and H. A. Scheraga, *J. Phys. Chem.,* **94,** 4740–4746 (1990). Determination of Net Atomic Charges Using a Modified Equalization of Orbital Electronegativity Method. 2. Application to Ionic an Aromatic Molecules as Models for Polypeptides.

139. J. Hinze and H. H. Jaffe, *J. Am. Chem. Soc.,* **84,** 540–546 (1962). Electronegativity. I. Orbital Electronegativity of Neutral Atoms.

140. U. Dinur, *J. Mol. Struct. (THEOCHEM),* **303,** 227–237 (1994). A Relationship Between the Molecular Polarizability, Molecular Dipole Moment and Atomic Electronegativities in AB and $AB_n$ Molecules.

141. In Ref. 125, the hardness, $J$, and $J_{\alpha\beta}$ ($r_{\alpha\beta}$) are both characterized by a Slater exponent parameter, $\zeta$. For hydrogen atoms, this parameter is taken to depend on its charge ($\zeta = \zeta_0 + q_H$), introducing nonlinearities in the electronegativities. However, rather than using the Mulliken definition of $\chi$ as $\frac{\partial U}{\partial q}$, Rappé and Goddard use the expression for $\chi$ from Eq. [42] and thereby ignore the nonlinear terms. This means that the charges in this model do not minimize the energy. This fact is not clear from Ref. 125, but it is necessary to use Eq. [42] to reproduce their results.

142. H. Toufar, B. G. Baekelandt, G. O. A. Janssens, W. J. Mortier, and R. A. Schoonheydt, *J. Phys. Chem.*, **99,** 13876–13885 (1995). Investigation of Supramolecular Systems by a Combination of the Electronegativity Equalization Method and a Monte Carlo Simulation Technique.

143. B.-C. Perng, M. D. Newton, F. O. Raineri, and H. L. Friedman, *J. Chem. Phys.,* **104,** 7153–7176 (1996). Energetics of Charge Transfer Reactions in Solvents of Dipolar and Higher Order Multiplier Character. I. Theory.

144. M. J. Field, *Mol. Phys.,* **91,** 835–845 (1997). Hybrid Quantum Mechanical/Molecular Mechanical Fluctuating Charge Models for Condensed Phase Simulations.

145. Y.-P. Liu, K. Kim, B. J. Berne, R. A. Friesner, and S. W. Rick, *J. Chem. Phys.,* **108,** 4739 (1998). Constructing *Ab Initio* Force Fields for Molecular Dynamics Simulations.

146. J. L. Banks, G. A. Kaminski, R. Zhou, D. T. Mainz, B. J. Berne, and R. A. Friesner, *J. Chem. Phys.,* **110,** 741–754 (1999). Parametrizing a Polarizable Force Field from *Ab Initio* Data. I. The Fluctuating Point Charge Model.

147. B. Chen, J. Xing, and J. I. Siepmann, *J. Phys. Chem. B,* **104,** 2391–2401 (2000). Development of Polarizable Water Force Fields for Phase Equilibria Calculations.

148. M. C. C. Ribeiro and L. C. J. Almeida, *J. Chem. Phys.,* **110,** 11445–11448 (1999). Fluctuating Charge Model for Polyatomic Ionic Systems: A Test Case with Diatomic Anions.

149. R. Chelli, P. Procacci, R. Righini, and S. Califano, *J. Chem. Phys.,* **111,** 8569–8575 (1999). Electrical Response in Chemical Potential Equilization Schemes.

150. H. A. Stern, G. A. Kaminski, J. L. Banks, R. Zhou, B. J. Berne, and R. A. Friesner, *J. Phys. Chem. B,* **103,** 4730–4737 (1999). Fluctuating Charge, Polarizable Dipole, and Combined Models: Parameterization from Ab Initio Quantum Chemistry.

151. K. Kitaura and K. Morokuma, *Int. J. Quantum Chem.,* **10,** 325–340 (1976). A New Energy Decomposition Scheme for Molecular Interactions within the Hartee–Fock Approximation.

152. F. Weinhold, *J. Mol. Struct.,* **399,** 181–197 (1997). Nature of H-Bonding in Clusters, Liquids, and Enzymes: An Ab Initio, Natural Bond Orbital Perspective.

153. A. van der Vaart and K. M. Merz Jr., *J. Am. Chem. Soc.,* **121,** 9182–9190 (1999). The Role of Polarization and Charge Transfer in the Solvation of Biomolecules.

154. J. Korchowiec and T. Uchimaru, *J. Chem. Phys.,* **112,** 1623–1633 (2000). New Energy Partitioning Scheme Based on the Self-Consistent Charge and Configuration Method for Subsystems: Application to Water Dimer System.

155. J. P. Perdew, R. G. Parr, M. Levy, and J. L. Balduz Jr., *Phys. Rev. Lett.,* **49,** 1691–1694 (1982). Density-Functional Theory for Fractional Particle Number: Derivative Discontinuities of the Energy.

156. R. Car and M. Parrinello, *Phys. Rev. Lett.,* **55,** 2471–2474 (1985). Unified Approuch for Molecular Dynamics and Density-Functional Theory.

157. J. Morales and T. J. Martinez, *J. Chem. Phys.,* **105,** 2842–2850 (2001). Classical Fluctuating Charge Theories: An Entropy Valence Bond Formalism and Relationships to Previous Models.

158. S.-B. Zhu, S. Singh, and G. W. Robinson, *J. Chem. Phys.,* **95,** 2791–2799 (1991). A New Flexible/Polarizable Water Model.

159. M. Wilson and P. A. Madden, *J. Phys.: Condens. Matter,* **5,** 2687–2706 (1993). Polarization Effects in Ionic Systems from First Principles.

160. T. Campbell, R. K. Kalia, A. Nakano, P. Vashista, S. Ogata, and S. Rodgers, *Phys. Rev. Lett.,* **82,** 4866–4869 (1999). Dynamics of Oxidation of Aluminum Nanoclusters Using Variable Charge Molecular-Dynamics Simulation on Parallel Computers.

161. D. J. Keffer and J. W. Mintmire, *Int. J. Quantum Chem.,* **80,** 733–742 (2000). Efficient Parallel Algorithms for Molecular Dynamics Simulations Using Variable Charge Transfer Electrostatic Potentials.

162. M. Medeiros and M. E. Costas, *J. Chem. Phys.,* **107,** 2012–2019 (1997). Gibbs Ensemble Monte Carlo Simulation of the Properties of Water with a Fluctuating Charges Model.

163. A. Nakano, *Comput. Phys. Commun.,* **104,** 59–69 (1997). Parallel Multilevel Preconditioned Conjugate-Gradient Approach to Variable-Charge Molecular Dynamics.

164. S. W. Rick, in *Simulation and Theory of Electrostatic Interactions in Solution,* L. R. Pratt and G. Hummer, Eds., American Institute of Physics, Melville, NY, 1999, pp. 114–126. The Influence of Electrostatic Truncation on Simulations of Polarizable Systems.

165. B. Chen, J. J. Potoff, and J. I. Siepmann, *J. Phys. Chem. B,* **104,** 2378–2390 (2000). Adiabatic Nuclear and Electronic Sampling Monte Carlo Simulations in the Gibbs Ensemble: Application to Polarizable Force Fields for Water.

166. H. A. Stern, F. Rittner, B. J. Berne, and R. A. Friesner, *J. Chem. Phys.,* **115,** 2237–2251 (2001). Combined Fluctuating-Charge and Polarizable Dipole Models: Application to a Five-Site Water Potential Function.

167. U. Dinur, *J. Phys. Chem.,* **97,** 7894–7898 (1993). Molecular Polarizabilities from Electronegativity Equalization Models.

168. S. W. Rick and B. J. Berne, *J. Phys. Chem. B,* **101,** 10488 (1997). The Free Energy of the Hydrophobic Interaction from Molecular Dynamics Simulations: the Effects of Solute and Solvent Polarizability.

169. R. G. Parr and W. Yang, *Density-Functional Theory of Atoms and Molecules,* Oxford University Press, Oxford, UK, 1989.

170. L. J. Bartolotti and K. Flurchick, in *Reviews in Computational Chemistry,* K. B. Lipkowitz and D. B. Boyd, Eds., VCH Publishers, Vol. 7, pp. 187–216 (1996). An Introduction to Density Functional Theory. A. St-Amant, in *Reviews in Computational Chemistry*, K. B. Lipkowitz and D. B. Boyd, Eds., VCH Publishers, New York, Vol. 7, pp. 217–259. Density Functional Methods in Biomolecular Modeling.

171. P. Itskowitz and M. L. Berkowitz, *J. Phys. Chem. A,* **101,** 5687–5691 (1997). Chemical Potential Equalization Principle: Direct Approach from Density Functional Theory.

172. D. Borgis and A. Staib, *Chem. Phys. Lett.,* **238,** 187–192 (1995). A Semiempirical Quantum Polarization Model for Water.

173. J. Gao, *J. Phys. Chem. B,* **101,** 657–663 (1997). Toward a Molecular Orbital Derived Empirical Potential for Liquid Simulations.

174. J. Gao, *J. Chem. Phys.,* **109,** 2346–2354 (1998). A Molecular-Orbital Derived Polarization Potential for Liquid Water.

175. B. D. Bursulaya and H. J. Kim, *J. Chem. Phys.,* **108,** 3277–3285 (1998). Generalized Molecular Mechanics Including Quantum Electronic Structure Variation of Polar Solvents. I. Theoretical Formulation via a Truncated Adiabatic Basis Set Description.

176. B. D. Bursulaya, J. Jeon, D. A. Zichi, and H. J. Kim, *J. Chem. Phys.,* **108,** 3286–3295 (1998). Generalized Molecular Mechanics Including Quantum Electronic Structure Variation of Polar Solvents. II. A Molecular Dynamics Simulation Study of Water.

177. A. E. Lefohn, M. Ovchinnikov, and G. A. Voth, *J. Phys. Chem. B,* **105,** 6628–6637 (2001). A Multistate Empirical Valence Bond Approach to a Polarizable and Flexible Water Model.

178. J. J. P. Stewart, in *Reviews in Computational Chemistry,* K. B. Lipkowitz and D. B. Boyd, Eds., VCH Publishers, New York, 1990, Vol. 1, pp. 45–81. Semiempirical Molecular Orbital Methods. M. C. Zerner, in *Reviews in Computational Chemistry,* K. B. Lipkowitz and D. B. Boyd, Eds., VCH Publishers, New York, 1991, Vol. 2, pp. 313–365. Semiempirical Molecular Orbital Methods.

179. D. E. Williams, in *Reviews in Computational Chemistry*, K. B. Lipkowitz and D. B. Boyd, Eds., VCH Publishers, New York, 1991, Vol. 2, pp. 219–271. Net Atomic Charge and Multipole Models for the Ab Initio Molecular Orbital Potential.

180. R. S. Mulliken, *J. Chem. Phys.,* **23,** 1833, 1841 (1955). Electronic Population Analysis on LCAO-MO Molecular Wave Functions. I. and II. Overlap Populations, Bond Orders, and Covalent Bond Energies. See also: S. M. Bachrach, in *Reviews in Computational Chemistry,* K. B. Lipkowitz and D. B. Boyd, Eds., VCH Publishers, New York, 1994, Vol. 5, pp. 171–227. Population Analysis and Electron Densities from Quantum Mechanics.

181. M. J. S. Dewar, E. G. Zoebisch, E. F. Healy, and J. J. P. Stewart, *J. Am. Chem. Soc.,* **107,** 3902–3909 (1985). AM1: A New General Purpose Quantum Mechanical Molecular Model.

182. W. J. Hehre, R. F. Stewart, and J. A. Pople, *J. Chem. Phys,* **51,** 2657–2664 (1969). Self-Consistent Molecular-Orbital Methods. I. Use of Gaussian Expansions of Slater-Type Atomic Orbitals. See also: D. Feller and E. R. Davidson, in *Reviews in Computational Chemistry*, K. B. Lipkowitz and D. B. Boyd, Eds., VCH Publishers, New York, 1990, Vol. 1, pp. 1–43. Basis Sets for Ab Initio Molecular Orbital Calculations and Intermolecular Interactions.

183. S. W. Rick and R. E. Cachau, *J. Chem. Phys.,* **112,** 5230–5241 (2000). The Non-Planarity of the Peptide Group: Molecular Dynamics Simulations with a Polarizable Two-State Model for the Peptide Bond.

184. G. Corongiu, *Int. J. Quantum Chem.,* **42,** 1209–1235 (1992). Molecular Dynamics Simulation for Liquid Water Using a Polarizable and Flexible Potential.

185. M. Sprik, *J. Chem. Phys.,* **95,** 6762–6769 (1991). Hydrogen Bonding and the Static Dielctric Constant in Liquid Water.

186. P. G. Kusalik, F. Liden, and I. M. Svishchev, *J. Chem. Phys.,* **103,** 10169–10175 (1995). Calculation of the Third Virial Coefficient for Water.

187. S.-B. Zhu, S. Singh, and G. W. Robinson, *Adv. Chem. Phys.,* **85,** 627–731 (1994). Field-Perturbed Water.

188. A. Wallqvist and R. D. Mountain, in *Reviews in Computational Chemistry,* K. B. Lipkowitz and D. B. Boyd, Eds., Wiley-VCH, New York, 1999, Vol. 13, pp. 183–247. Molecular Descriptions of Water: Derivation and Description.

189. J. C. Shelley and D. R. Bérard, in *Reviews in Computational Chemistry,* K. B. Lipkowitz and D. B. Boyd, Eds., Wiley-VCH, New York, 1998, Vol. 12, pp. 137–205. Computer Simulation of Water Physisorption at Metal–Water Interfaces.

190. A. A. Chialvo and P. T. Cummings, *J. Phys. Chem.,* **100,** 1309–1316 (1996). Microstructure of Ambient and Supercritical Water: Direct Comparison Between Simulation and Neutron Scattering Experiments.

191. H. J. C. Berendsen, J. P. M. Postma, W. F. van Gunsteren, and J. Hermans, in *Intermolecular Forces,* B. Pullman, Ed., Reidel, Dordrecht, The Netherlands, 1981, pp. 331–342. Interaction Models for Water in Relation to Protein Hydration.

192. W. L. Jorgensen, J. Chandrasekhar, J. D. Madura, R. W. Impey, and M. L. Klein, *J. Chem. Phys.,* **79,** 926–935 (1983). Comparison of Simple Potential Functions for Simulating Liquid Water.

193. C. Millot and A. J. Stone, *Mol. Phys.,* **77,** 439–462 (1992). Towards an Accurate Intermolecular Potential for Water.

194. U. Niesar, G. Corongiu, M.-J. Huang, M. Dupuis, and E. Clementi, *Int. J. Quantum. Chem. Symp.,* **23,** 421–443 (1989). Preliminary Observations on a New Water–Water Potential.

195. G. C. Lie, G. Corongiu, and E. Clementi, *J. Phys. Chem.,* **89,** 4131–4134 (1985). Calculation of the Third Virial Coefficient for Water Using Ab Initio Two-Body and Three-Body Potentials.

196. S. L. Carnie and G. N. Patey, *Mol. Phys.,* **47,** 1129–1151 (1982). Fluids of Polarizable Hard Spheres with Dipoles and Tetrahedral Quadrupoles. Integral Equation Results with Application to Liquid Water.

197. E. R. Batista, S. S. Xantheas, and H. Jónsson, *J. Chem. Phys.,* **109,** 6011–6015 (1999). Multipole Moments of Water Molecules in Clusters and Ice Ih from First Principles Calculations.

198. E. R. Batista, S. S. Xantheas, and H. Jónsson, *J. Chem. Phys.,* **112,** 3285–3292 (2000). Electric Fields in Ice and Near Water Clusters.

199. K. Laasonen, M. Sprik, M. Parrinello, and R. Car, *J. Chem. Phys.,* **99,** 9080–9089 (1993). "*Ab Initio*" Liquid Water.

200. L. Delle Site, A. Alavi, and R. M. Lynden-Bell, *Mol. Phys.,* **96,** 1683–1693 (1999). The Electrostatic Properties of Water Molecules in Condensed Phases: An *Ab Initio* Study.

201. P. L. Silvestrelli and M. Parrinello, *J. Chem. Phys.,* **111,** 3572–3580 (1999). Structural, Electronic, and Bonding Properties of Liquid Water from First Principles.

202. M. Sprik, *J. Phys. Chem.,* **95,** 2283–2291 (1991). Computer Simulations of the Dynamics of Induced Polarization Fluctuations.

203. J. R. Reimers, R. O.Watts, and M. L. Klein, *Chem. Phys.,* **64,** 95–114 (1982). Intermolecular Potential Functions and the Properties of Water.

204. N. Yoshii, S. Miura, and S. Okazaki, *Chem. Phys. Lett.,* **345,** 195–200 (2001). A Molecular Dynamics Study of Water from Ambient to Sub- and Supercritical Conditions Using a Fluctuating-Charge Potential Model.

205. B. Guillot and Y. Guissani, *J. Chem. Phys.,* **114**(15), 6720–6733 (2001). How To Build a Better Pair Potential for Water.

206. I. M. Svishchev and T. M. Hayward, *J. Chem. Phys.,* **111,** 9034–9038 (1999). Phase Coexistence Properties for the Polarizable Point Charge Model of Water and the Effects of Applied Electric Field.

207. S. W. Rick, *J. Chem. Phys.,* **114,** 2276–2283 (2001). Simulations of Ice and Liquid Water over a Range of Temperatures Using the Fluctuating Charge Model.

208. F. H. Stillinger and A. Rahman, *J. Chem. Phys.,* **60,** 1545–1557 (1974). Improved Simulation of Liquid Water by Molecular Dynamics.

209. P. H. Poole, F. Sciortino, U. Essman, and H. E. Stanley, *Nature (London),* **360,** 324–328 (1992). Phase Behaviour of Liquid Water.

210. S. R. Billeter, P. M. King, and W. F. van Gunsteren, *J. Chem. Phys.,* **100,** 6692–6699 (1994). Can the Density Maximum of Water Be Found by Computer Simulation?

211. L. A. Báez and P. Clancy, *J. Chem. Phys.,* **101,** 9837–9840 (1994). Existence of a Density Maximum in Extended Simple Point Charge Water.

212. A. Wallqvist and P.-O. Åstrand, *J. Chem. Phys.,* **102,** 6559–6565 (1995). Liquid Densities and Structural Properites of Molecular Models of Water.

213. S. Harrington, P. H. Poole, F. Sciortino, and H. E. Stanley, *J. Chem. Phys.,* **107,** 7443–7450 (1997). Equation of State of Supercooled Water Simulated Using the Extended Simple Point Charge Intermolecular Potential.

214. K. Bagchi, S. Balasubramanian, and M. L. Klein, *J. Chem. Phys.,* **107,** 8561–8567 (1997). The Effects of Pressure on Structural and Dynamical Properties of Associated Liquids: Molecular Dynamics Calculations for the Extended Simple Point Charge Model of Water.

215. W. L. Jorgensen and C. Jensen, *J. Comput. Chem.,* **19,** 1179–1186 (1998). Temperature Dependence of TIP3P, SPC, and TIP4P Water from NPT Monte Carlo Simulations: Seeking Temperatures of Maximum Density.

216. M. W. Mahoney and W. L. Jorgensen, *J. Chem. Phys.,* **112,** 8910–8922 (2000). A Five-Site Model for Liquid Water and the Reproduction of the Density Anomaly by Rigid, Nonpolarizable Potential Functions.

217. M. Sprik, M. L. Klein, and K. Watanabe, *J. Phys. Chem.,* **94,** 6483–6488 (1990). Solvent Polarization and Hydration of the Chlorine Anion.

218. L. Perera and M. L. Berkowitz, *J. Chem. Phys.,* **100,** 3085–3093 (1994). Structures of $Cl^-(H_2O)_n$ and $F^-(H_2O)_n$ $(n = 2, 3, \ldots, 15)$ Clusters. Molecular Dynamics Computer Simulations.

219. P. Jungwirth and D. J. Tobias, *J. Phys. Chem. B,* **104,** 7702–7706 (2000). Surface Effects on Aqueous Ionic Solvation: A Molecular Dynamics Study of NaCl at the Air/Water Interface from Infinite Dilution to Saturation.

220. I.-C. Yeh and M. L. Berkowitz, *J. Chem. Phys.,* **112,** 10491–10495 (2000). Effects of the Polarizability and Water Density Constraint on the Structure of Water Near Charged Surfaces: Molecular Dynamics Simulations.

221. G. Gilli, F. Belluci, V. Ferretti, and V. Berolasi, *J. Am. Chem. Soc.,* **111,** 1023–1128 (1989). Evidence for Resonance-Assisted Hydrogen Bonding from Crystal Structure Correlations on the Enol Form of the β-Diketone Fragment.

222. G. A. Jeffrey and W. Saenger, *Hydrogen Bonding in Biological Structures,* Springer-Verlag, Heidelberg, 1991.

223. H. Guo and M. Karplus, *J. Phys. Chem.,* **98,** 7104–7105 (1994). Solvent Influence on the Stability of the Peptide Hydrogen Bond: A Supramolecular Cooperative Effect.

224. R. Ludwig, F. Weinhold, and T. C. Farrar, *J. Chem. Phys.,* **107,** 499–507 (1997). Theoretical Study of Hydrogen Bonding in Liquid and Gaseous *N*-Methylformamide.

225. H. Guo, N. Gresh, B. P. Rogues, and D. R. Salahub, *J. Phys. Chem. B,* **104,** 9746–9754 (2000). Many-Body Effects in Systems of Peptide Hydrogen- Bonded Networks and Their Contributions to Ligand Binding: A Comparison of DFT and Polarizable Molecular Mechanics.

226. I. M. Klotz and J. S. Franzen, *J. Am. Chem. Soc.,* **84,** 3461–3466 (1962). Hydrogen Bonds Between Model Peptide Groups in Solution.

227. A. Wada, *Adv. Biophys.,* **9,** 1–63 (1976). The α-Helix as an Electric MacroDipole.

228. A. van der Vaart, B. D. Bursulaya, C. L. Brooks III, and K. M. Merz Jr., *J. Phys. Chem. B,* **104,** 9554–9563 (2000). Are Many-Body Effects Important in Protein Folding?

229. H. Guo and D. R. Salahub, *Angew. Chem. Int. Ed.,* **37,** 2985–2990 (1998). Cooperative Hydrogen Bonding and Enzyme Catalysis.

230. J. Šponer, H. A. Gabb, J. Leszczynski, and P. Hobza, *Biophys. J.,* **73,** 76–87 (1997). Base-Base and Deoxyribose-Base Stacking Interactions in B-DNA and Z-DNA: A Quantum-Chemical Study.

231. N. Gresh and J. Šponer, *J. Phys. Chem. B,* **103,** 11415–11427 (1999). Complexes of Pentahydrated $Zn^{2+}$ with Guanine, Adenine, and the Guanine–Cytosine and Adenine–Thymine Base Pairs. Structures and Energies Characterized by Polarizable Molecular Mechanics and Ab Initio Calculations.

232. P. Cieplak, J. Caldwell, and P. Kollman, *J. Comput. Chem.,* **22,** 1048–1057 (2001). Molecular Mechanical Models for Organic and Biological Systems Going Beyond the Atom Centered Two Body Additive Approximation: Aqueous Solution Free Energies of Methanol and *N*-Methyl Acetamide, Nucleic Acid Base, and Amide Hydrogen Hydrogen Bonding and Chloroform/Water Partition Coefficients of the Nucleic Acid Bases.

233. E. D. Stevens, *Acta Crystallogr., Sect. B,* **34,** 544–551 (1978). Low Temperature Experimental Electron Density Distribution in Formamide.

234. G. A. Jeffrey, *An Introduction to Hydrogen Bonding,* Oxford University Press, New York and Oxford, 1997.

235. M. W. MacArthur and J. M. Thornton, *J. Mol. Biol.,* **264,** 1180–1195 (1996). Deviations from Planarity of the Peptide Bond in Peptides and Proteins.

236. E. J. Dodson, G. J. Davis, V. S. Lamzin, G. N. Murshudov, and K. S. Wilson, *Structure,* **6,** 685–690 (1998). Validation Tools: Can They Indicate the Information Content of Macromolecular Crystal Structures?

237. P. Hobza and J. Šponer, *Chem. Rev.,* **99,** 3247–3276 (1999). Structure, Energics, and Dynamics of the Nucleic Acid Base Pairs: Nonempirical *Ab Initio* Calculations.

238. J. N. Wilson and R. M. Curtis, *J. Phys. Chem.*, **74,** 187–196 (1970). Dipole Polarizabilities of Ions in Alkali Halide Crystals.

239. G. D. Mahan, *Solid State Ionics,* **1,** 29–45 (1980). Polarizability of Ions in Crystals.

240. P. W. Fowler and P. A. Madden, *Phys. Rev. B: Condens. Matter,* **29,** 1035–1042 (1984). In-crystal Polarizabilities of Alkali and Halide Ions.

241. J. K. Badenhoop and F. Weinhold, *J. Chem. Phys.,* **107,** 5422–5432 (1997). Natural Steric Analysis: *Ab Initio* van der Waals Radii of Atoms and Ions.

242. A. Warshel and R. M. Weiss, *J. Am. Chem. Soc.,* **102,** 6218–6226 (1980). An Emprical Valence Bond Approach for Comparing Reactions in Solutions and in Enzymes.

243. M. J. L. Sangster, *Solid State Commun.,* **15,** 471–474 (1974). Properties of Diatomic Molecules from Dynamical Models for Alkali Halide Crystals.

244. L. Greengard, and V. Rokhlin, *J. Comput. Phys.,* **73,** 325–348 (1987). A Fast Algorithm for Particle Simulations.

245. H.-Q. Ding, N. Karasawa, and W. A. Goddard III, *J. Chem. Phys.,* **97,** 4309–4315 (1992). Atom Level Simulations of a Million Particles: The Cell Multipole Method for Coulomb and London Nonbond Interactions.

246. R. W. Hockney and J. W. Eastwood, *Computer Simulation Using Particles,* Institute of Physics Publishing, Bristol, UK, 1988.

247. T. Darden, D. York, and L. Pedersen, *J. Chem. Phys.,* **93,** 10089–10092 (1993). Particle Mesh Ewald: An $N\log(N)$ Method for Ewald Sums in Large Systems.

248. P. Ewald, *Ann. Phys.,* **64,** 253–287 (1921). Die Berechnung optischer und elektrostatischer Gitterpotentiale.

249. D. M. Heyes, *J. Chem. Phys.,* **74,** 1924–1929 (1981). Electrostatic Potentials and Fields in Infinite Point Charge Lattices.

250. M. Tuckerman, B. J. Berne, and G. J. Martyna, *J. Chem. Phys.,* **97,** 1990–2001 (1992). Reversible Multiple Time Scale Molecular Dynamics.

251. S. J. Stuart, R. Zhou, and B. J. Berne, *J. Chem. Phys.,* **105,** 1426–1436 (1996). Molecular Dynamics with Multiple Timescales: The Selection of Efficient Reference System Propagators.

252. P. Kaatz, E. A. Donley, and D. P. Shelton, *J. Chem. Phys.,* **180,** 849–856 (1998). A Comparison of Molecular Hyperpolarizabilities from Gas and Liquid Phase Measurements.

253. G. Maroulis, *J. Chem. Phys.,* **94,** 1182–1190 (1991). Hyperpolarizability of $H_2O$.

254. The linear increase in polarization with molecule size assumes that the characteristic polarizability $\alpha$ is small compared to the characteristic volume per polarizable unit: $\alpha \ll r^3$. See Eqs. [15] and [16]. In cases where this approximation does not hold, the polarizability will increase faster than linearly with system size, leading to a polarization catastrophe.

255. B. L. Bush, C. I. Bayly, and T. A. Halgren, *J. Comput. Chem.,* **20,** 1495–1516 (1999). Consensus Bond-Charge Increments Fitted to Electrostatic Potential or Field of Many Compounds: Application to MMFF94 Training Set.

*Reviews in Computational Chemistry, Volume 18*
Edited by Kenny B. Lipkowitz and Donald B. Boyd

ISBN: 0-471-21576-7

CHAPTER 4

# New Developments in the Theoretical Description of Charge-Transfer Reactions in Condensed Phases

**Dmitry V. Matyushov* and Gregory A. Voth†**

**Department of Chemistry and Biochemistry, Arizona State University, Tempe, Arizona 85287-1604, and †Department of Chemistry and Henry Eyring Center for Theoretical Chemistry, University of Utah, 315 South 1400 East, Salt Lake City, Utah 84112*

## INTRODUCTION

Nearly half a century of intense research in the field of electron transfer (ET) reactions in condensed phases has produced remarkable progress in the experimental and theoretical understanding of the key factors influencing the kinetics and thermodynamics of these reactions. The field evolved in order to describe many important processes in chemistry and is actively expanding into biological and materials science applications.[1] Due to its significant experimental background and relative simplicity of the reaction mechanism, the problem of electron transitions in condensed solvents turned out to be a benchmark for testing fundamental theoretical approaches to chemical activation. A number of excellent reviews dealing with various aspects of the field have been written. Two volumes of *Advances in Chemical Physics* (Vols. 106 and 107, 1999) covered much of the progress in the field achieved in recent decades. Therefore, the aim of this chapter is not to replicate these

reviews, but rather to highlight some very recent developments in the field that have not been reviewed. This chapter will provide the reader with a step-by-step statistical mechanical buildup of the theoretical machinery currently employed in ET research. By virtue of the "frontier" nature of this material, many traditional subjects of ET studies are not covered here. The reader will be referred to previous reviews whenever possible, but many excellent contributions are not directly cited.

This chapter concerns the energetics of charge-transfer (CT) reactions. We will not discuss subjects dealing with nuclear dynamical effects on CT kinetics.[2–4] The more specialized topic of employing the liquid-state theories to calculate the solvation component of the reorganization parameters[5] is not considered here. We concentrate instead on the general procedure of the statistical mechanical analysis of the activation barrier to CT, as well as on its connection to optical spectroscopy. Since the very beginning of ET research,[6] steady-state optical spectroscopy has been the major source of reliable information about the activation barrier and preexponential factor for the ET rate. The main focus in this chapter is therefore on the connection between the statistical analysis of the reaction activation barrier to the steady-state optical band shape.

The ET reaction is usually referred to as a process of underbarrier tunneling and subsequent localization of an electron from the potential well of the donor to the potential well of the acceptor (Figure 1). This phenomenon occurs in a broad variety of systems and reactions (see Ref. 1 for a list of

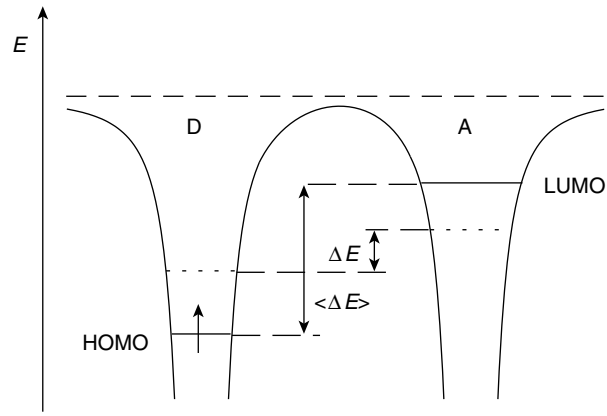


**Figure 1** Potential energy wells for the electron localized on the donor (D) and acceptor (A) sites. The parameter $\langle \Delta E \rangle$ indicates the average energy gap for an instantaneous (Franck–Condon) transfer of the electron from the donor HOMO to the acceptor LUMO. The dotted lines show the electronic energies on the donor and acceptor at a nonequilibrium nuclear configuration with a nonequilibrium energy gap $\Delta E$. The upper dashed horizontal line indicates the bottom of the conduction band of the electrons in the solvent.

applications). For electron tunneling to occur, the electronic states of the donor and acceptor sites must come into resonance (degeneracy) with each other. Degeneracy occurs as a result of thermal nuclear motions of the donor–acceptor complex and the condensed-phase medium. The condition of zero energy gap, $\Delta E = 0$, between the donor and acceptor electronic levels determines the position of the transition state for an ET reaction. The ET rate constant is proportional to the probability of such a configuration

$$k_{\mathrm{ET}} \propto \mathrm{FCWD}(0) \qquad [1]$$

where the *Franck–Condon weighted density* (FCWD), FCWD($\Delta E$), determines the probability of creating a configuration with energy gap $\Delta E$.

Electron transfer refers to the situation when essentially all the electronic density is transferred from the donor to the acceptor. The process of CT, in the present context, refers to basically the same event, but the electron density is not completely relocalized and is distributed between the two potential wells. The key factor discriminating between ET and CT reactions is the ET matrix element,[7] $H_{ab}$, often called the hopping element in solid-state applications. The ET matrix element is the off-diagonal matrix element of the system Hamiltonian taken on the localized diabatic states of the donor and acceptor sites (see below). [The term *diabatic* refers to localized states which do not diagonalize the system Hamiltonian. These localized states are the true states of the donor and acceptor fragments when these fragments are infinitely separated. For covalently bound complexes, diabatic states become just some basis states that allow reasonable localization of the electronic density on the donor and acceptor fragments of the molecule. *Adiabatic* states, in contrast, are actual states of the molecule between which electronic (including optical) transitions occur.]

For long-range electron transitions, the direct electronic overlap, exponentially decaying with distance between the donor and acceptor units, is weak, leading to a small magnitude of the expectation value of $H_{ab}$. Such processes, especially important in biological applications,[8] can be characterized as nonadiabatic ET reactions. The small magnitude of the ET matrix element can be employed to find the transition rate using quantum mechanical perturbation theory. In this theory, the rate constant found by the Golden Rule approximation[9,10] is called the nonadiabatic ET rate constant, and the ET reaction is classified as nonadiabatic ET.[11] (The *Golden Rule formula* is the first-order perturbation solution for the rate of quantum mechanical transitions caused by that perturbation.) The ET rate constant is then proportional to $|H_{ab}|^2$

$$k_{\mathrm{NA}} \propto |H_{ab}|^2 \,\mathrm{FCWD}(0) \qquad [2]$$

Creation of the resonance electronic configuration of the ET transition state, $\Delta E = 0$, is by necessity a many-body event, including complex interactions of the transferred electron with many nuclear degrees of freedom. The

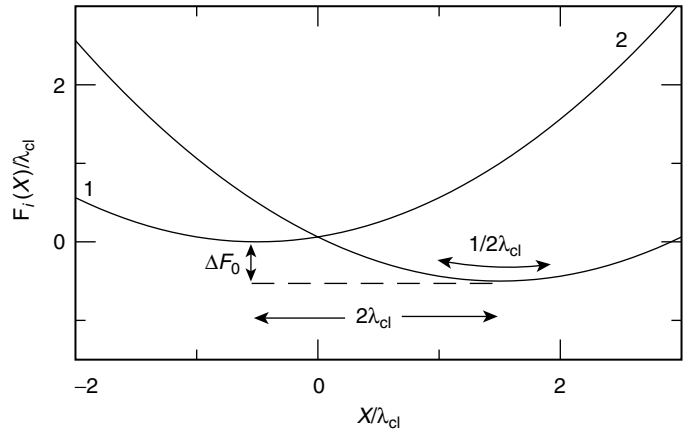


**Figure 2** Two parameters defining the Marcus–Hush model of two intersecting parabolas: the equilibrium free energy gap $\Delta F_0$ and the classical reorganization energy $\lambda_{cl}$. The parabolas curvature is $1/(2\lambda_{cl})$.

great achievement of the Marcus–Hush (MH) model[6,12–14] of ET was to reduce the many-body problem to a one-dimensional (1D) picture of intersecting ET free energy surfaces, $F_i(X)$ ($i = 1$ for the initial ET state, $i = 2$ for the final ET state, Figure 2). Each point on the free energy surface represents the reversible work invested to create a nonequilibrium fluctuation of the nuclei resulting in a particular value of the donor–acceptor electronic energy gap

$$X = \Delta E \qquad [3]$$

The electronic energy gap thus serves as a collective reaction coordinate $X$ reflecting the strength of coupling of the nuclear modes to the electronic states of the donor and acceptor. The point of intersection of $F_1(X)$ and $F_2(X)$ sets up the ET transition state, $X = 0$.

The definition of the ET reaction coordinates according to Eq. [3] allows a direct connection between the activated ET kinetics and steady-state optical spectroscopy. In a spectroscopic experiment, the energy of the incident light with the frequency $\nu$ ($\bar{\nu}$ is used for the wavenumber) is equal to the donor–acceptor energy gap

$$h\nu = X \qquad [4]$$

and monitoring the light frequency directly probes the distribution of donor–acceptor energy gaps. The intensity of optical transitions $I(\nu)$ is then proportional to FCWD$(h\nu)$[15]

$$I(\nu) \propto |m_{12}|^2 \,\mathrm{FCWD}(h\nu) \qquad [5]$$

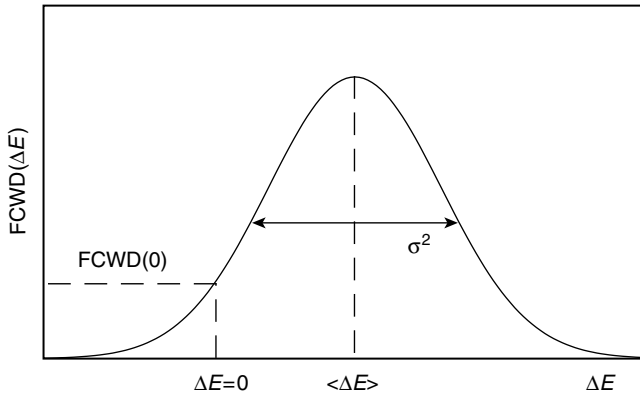


**Figure 3** Franck–Condon weighted density of energy gaps between the donor and acceptor electronic energy levels. The parameters $\langle \Delta E \rangle$ and $\sigma^2$ indicate the first and second spectral moments, respectively. FCWD(0) shows the probability of zero energy gap entering the ET rate (Eq. [2]).

where $m_{12}$ is the adiabatic transition dipole moment. Knowledge of the spectral band shape can in principle provide the activation barrier through FCWD(0) (Figure 3), and the Mulliken-Hush relation connects $|H_{ab}|$ to $|m_{12}|$.[6] (In contrast to Marcus-Hush which refers to the theory of electron transfer activation, the Mulliken-Hush equation describes the preexponential factor of the rate constant. We spell out Mulliken–Hush each place it occurs in this chapter and use the acronym MH to refer to only Marcus–Hush.) In practice, however, FCWD(0) cannot be extracted from experimental spectra, and one needs a theoretical model to calculate FCWD(0) from experimental band shapes measured at the frequencies of the corresponding electronic transitions. This purpose is achieved by a band shape analysis of optical lines.

The two main nuclear modes affecting electronic energies of the donor and acceptor are intramolecular vibrations of the molecular skeleton of the donor–acceptor complex and molecular motions of the solvent. If these two nuclear modes are uncoupled, one can arrive at a set of simple relations between the two spectral moments of absorption and/or emission transitions and the activation parameters of ET. The most transparent representation is achieved when the quantum intramolecular vibrations are represented by a single, effective vibrational mode with the frequency $\nu_v$ (Einstein model).[15–17] If both the forward (absorption) and backward (emission) optical transitions are available, their first spectral moments determine the reorganization energies of quantum vibrations, $\lambda_v$, and of the classical nuclear motions of the donor–acceptor skeleton and the solvent, $\lambda_{cl}$:

$$h(\nu_{abs} - \nu_{em}) = 2(\lambda_{cl} + \lambda_v) \qquad [6]$$

where $\nu_{abs}$ and $\nu_{em}$ are the first spectral moments for absorption and emission, respectively:

$$\nu_{abs/em} = \frac{\int \nu I_{abs/em}(\nu) d\nu}{\int I_{abs/em}(\nu) d\nu} \quad [7]$$

Here $I_{abs/em}(\nu)$ is the transition intensity. The vibrational reorganization energy $\lambda_v$ is defined in terms of force constants, $k_\alpha$, and displacements, $\Delta Q_\alpha$, of the vibrational normal coordinates $Q_\alpha$ as $\lambda_v = \frac{1}{2}\sum_\alpha k_\alpha \Delta Q_\alpha^2$.[15–17] In this chapter, we use $\lambda$ for the solvent component of the classical reorganization energy $\lambda_{cl}$. The subscripts 1 and 2 are used to distinguish between the reorganization energy of the initial ($i = 1$) and final ($i = 2$) ET states when the reorganization energies in these states are different.

The mean of the first two moments gives the equilibrium free energy difference between the final and initial states of the ET reaction

$$h\nu_m = \tfrac{1}{2}h(\nu_{abs} + \nu_{em}) = \Delta F_0 = F_{02} - F_{01} \quad [8]$$

The two parameters, $\lambda_{cl}$ and $\Delta F_0$, actually fully define the parabolic ET free energy surfaces $F_i(X)$ in the MH formulation (Figure 2). Calculation of these two parameters has become the main historical focus of the ET models addressing the thermodynamics of the ET activation barrier. The latter, according to MH theory, can be written in terms of $\Delta F_0$ and $\lambda_{cl}$ as

$$F_i^{act} = \frac{(\lambda_{cl} \pm \Delta F_0)^2}{4\lambda_{cl}} \quad [9]$$

where $i = 1$ and "+" refer to the forward transition, and $i = 2$ and "−" refer to the backward transition.

The second spectral moments of absorption and emission lines

$$\sigma_{abs/em}^2 = \frac{\int \nu^2 I_{abs/em}(\nu) d\nu}{\int I_{abs/em}(\nu) d\nu} - (\nu_{abs/em})^2 \quad [10]$$

are equal in the MH formulation

$$\sigma_{abs}^2 = \sigma_{em}^2 \quad [11]$$

They are related to the classical and vibrational reorganization energies as follows[18]

$$\sigma_{abs/em}^2 = 2k_B T \lambda_{cl} + h\nu_v \lambda_v \quad [12]$$

where $k_B$ is the Boltzmann constant and $T$ is temperature.

Equations [6]–[12] establish a theoretical basis for calculating the activation barrier of ET from spectroscopic observables. This formalism rests on a set of fundamental assumptions of the MH picture that can be summarized as follows: (1) The electronic coupling between the donor and acceptor states is neglected in the calculation of the Franck–Condon weighted density. The latter depends only on electronic energies of localized electronic states and their coupling to the nuclear modes of the solvent and the donor–acceptor complex. (2) A two-state solute is considered. The manifold of the donor and acceptor electronic levels is limited to only two states between which the electron is transferred. (3) The intramolecular vibrations and solvent molecular motions are decoupled. (4) The linear response approximation is used for the interaction of the donor–acceptor complex with the solvent. The linear response approximation assumes that the free energy of solvation of an electric charges localized on the donor–acceptor complex is a quadratic function of this charge.

The neglect of the electronic coupling in the calculation of the FCWD (assumption 1) was adopted in the original Marcus and Hush formulation.[6,12] Within this framework, the ET matrix element does not strongly affect the nuclear fluctuations, although a nonzero value of $|H_{ab}|$ is required for electronic transitions to occur. In other words, the transferred electron is assumed to be fully localized in the calculation of the FCWD. To classify electronic delocalization, Robin and Day distinguished between three classes of symmetrical ($\Delta F_0 = 0$) systems.[19]

- In Class I systems, the coupling is very weak, and there are essentially no electronic transitions.
- Class II systems remain valence-trapped (localized), and $0 < 2|H_{ab}| \leq \lambda_{cl}$.
- In Class III systems, $2|H_{ab}| > \lambda_{cl}$, and the electron is fully delocalized between the donor and acceptor.

The MH formulation is designed to describe the case of intermediate couplings (weak-coupling limit of Class II) when $|H_{ab}|$ can be neglected in the FCWD(0) for activated transitions and the transition moment $m_{12}$ can be neglected in the FCWD($\nu$) for optical transitions. In the absence of a theory incorporating $|H_{ab}|$ and $m_{12}$ into the FCWD, there is no general understanding when this approximation is applicable to particular ET systems or how the relations between optical and activation observables are affected by inclusion of electronic delocalization into the FCWD.[20]

The limitations of the MH picture considerably narrow the range of systems covered by the theory. A considerable range of processes in which the donor–acceptor coupling is strong enough to change the molecular charge distribution under the influence of nuclear fluctuations cannot be treated theoretically. All such processes can be characterized as CT reactions. Weak electronic coupling characteristic of ET exists for intermolecular and

long-distance intramolecular reactions. Many systems with intramolecular electronic transitions over a relatively short distance between the initial and final centers of electron localization have been synthesized in recent years.[21,22] They commonly incorporate the same basic design in which the donor and acceptor units are linked in one molecule through a bridge moiety. In a case of closely separated donor and acceptor units, electronic states on these two sites are strongly coupled, resulting in a substantial delocalization of the electronic density. The electronic density is only partially transferred, and the process can be classified as a CT transition.

The MH formulation for the activation barrier and the related connection between activation ET parameters and optical observables generally do not apply to CT reactions. Hence the researcher is left without a procedure of calculating the activation barrier from spectroscopy. Not being able to calculate the barrier is a deficiency, and this chapter discusses some emerging approaches to develop a theory of CT processes with an explicit account for electronic delocalization effects. In application to optical transitions, this theory should lead to the development of a band shape analysis broadly applicable to Class II and III systems. The effect of electronic delocalization on the solvent component of the FCWD is emphasized here. The previously reviewed problem of delocalization effects on intramolecular vibrations[23] is not included. We also review some new approaches going beyond the two-state approximation in terms of incorporating polarizability of the donor–acceptor complex (assumption 2), and discuss some recent studies on nonlinear solvation effects (assumption 4). There are some very recent indications in the literature pointing to a possibility of an effective coupling between vibrational modes of the donor–acceptor complex and solvent fluctuations (assumption 3), but no consensus on when and why these effects are significant has yet been reached. We briefly discuss the available experimental and theoretical findings.

The first part of this chapter contains an introduction to the statistical mechanical formulation of the CT free energy surfaces. Importantly, it shows how to extend the traditional MH picture of two ET parabolas to a more general case of two CT free energy surfaces of a two-state donor–acceptor complex. The notation we utilize below distinguishes between these two cases in the following fashion: we use the indices 1 and 2 to denote the two ET free energy surfaces, as in Figure 2, and refer to the lower and upper CT free energy surfaces with "−" and "+", respectively. The parameters entering the activation barrier of CT transitions depend on the choice of the basis set of wave functions of the initial and final states of the donor–acceptor complex. The standard MH formulation is based on the choice of a localized, diabatic basis set. When this choice is adopted, we use the superscript "d" to refer to diabatic wave functions. An alternative description is possible in terms of adiabatic wave functions, and this situation is distinguished by the superscript "ad". We also provide a basis-invariant formulation of the theory for a two-state

donor–acceptor complex. A description of CT activation and spectroscopy in terms of two crossing, free energy surfaces (Figure 2) is in fact possible for any choice of the basis set as long as the off-diagonal matrix elements of the solute quantum mechanical operators can be neglected. In cases when a description in both diabatic and adiabatic representations is possible (as it is for the Q-model discussed below), we will not specify the basis by dropping the "d" and "ad" superscripts.

The statistical mechanical analysis of ET and CT free energy surfaces developed in the first part of this chapter is applied to the calculation of optical absorption and emission profiles in the second part. This application of the theory, related to the band shape analysis of optical line shapes, has been a central issue in understanding CT energetics for several decades.[16] The chapter is designed to demonstrate how the extension of the basic models used to describe the thermodynamics of CT is reflected in asymmetry of the energy gap law (dependence of the CT activation barrier on the equilibrium free energy gap) and more complex and structured optical band shapes. The development of a corresponding band shape analysis incorporating these new features is in its infancy, and we will certainly see more activity in this field in the future.

## PARADIGM OF FREE ENERGY SURFACES

The CT/ET free energy surface is the central concept in the theory of CT/ET reactions. The surface's main purpose is to reduce the many-body problem of a localized electron in a condensed-phase environment to a few collective reaction coordinates affecting the electronic energy levels. This idea is based on the Born–Oppenheimer (BO) separation[24] of the electronic and nuclear time scales, which in turn makes the nuclear dynamics responsible for fluctuations of electronic energy levels (Figure 1). The choice of a particular collective mode is dictated by the problem considered. One reaction coordinate stands out above all others, however, and is the energy gap between the two CT states as probed by optical spectroscopy (i.e., an experimental observable).

Our discussion of the CT free energy surfaces involves a hierarchy of reaction coordinates (Figure 4). It starts from the instantaneous free energy surfaces obtained from tracing out (statistical averaging) the electronic degrees of freedom in the system density matrix (i.e., solving the electronic problem for fixed nuclear coordinates). In the case when the direction of electron transfer sets up the only preferential direction in the CT system, one can define a scalar reaction coordinate as the projection of the nuclear solvent polarization on the differential electrical field of the solute. Depending on the basis set employed, this gives the diabatic or adiabatic scalar reaction coordinates, $Y^{d}$ and $Y^{ad}$ (Figure 4). At this step, a reaction coordinate depends on the basis set of solute wave functions employed. This dependence is eliminated when a scalar reaction coordinate is projected on the energy gap between the CT surfaces.

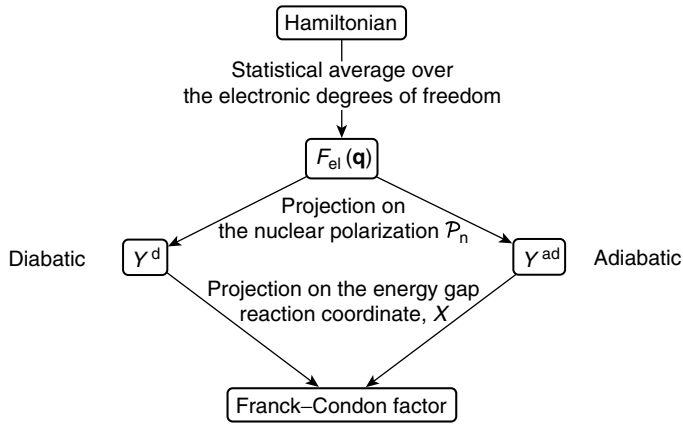


**Figure 4** Hierarchy of reaction coordinates in deriving the Franck–Condon factor from the system Hamiltonian.

The free energy gap, equal to the energy of the incident light, is basis independent. It defines the Franck–Condon factor entering the optical band shapes. The analysis below follows this general scheme (Figure 4).

## Formulation

Electron transfer and, more broadly, CT reactions belong to a general class of problems having a quantum subsystem interacting with a condensed-phase thermal bath. The main challenge in describing such systems is the necessity to treat the quantum subsystem coupled to a wide spectrum of classical and quantum modes of the condensed environment. It implies that the calculation of some property of interest $F$ involves taking a restricted statistical average (trace, Tr) over both the electronic and nuclear modes

$$F(\mathbf{Q},t) = \mathrm{Tr}'_{\mathrm{n}}\mathrm{Tr}_{\mathrm{el}}[\hat{\rho}(t)] \qquad [13]$$

where

$$\hat{\rho}(t) = e^{iHt}\hat{\rho}(0)e^{-iHt} \qquad [14]$$

is the density matrix of the system defined by the Hamiltonian $H$; $\hat{\rho}(0) = \exp(-\beta H)$ and $\beta = 1/k_{\mathrm{B}}T$. The quantity $\mathrm{Tr}_{\mathrm{el}}$ denotes the trace over the electronic degrees of freedom, and $\mathrm{Tr}'_{\mathrm{n}}$ refers to an incomplete or restricted trace over the nuclear degrees of freedom, excluding a manifold of modes $\mathbf{Q}$ that are of interest for some particular problem.

Depending on the order of the statistical average in Eq. [13], there are two basic approaches to calculate $F(\mathbf{Q},t)$. Considerable progress has been

achieved in treating the quantum dynamics in the framework of the functional integral representation of the quantum subsystem.[25,26] In this approach, the electron trace is taken out ($\mathrm{Tr}_{\mathrm{el}}\mathrm{Tr}_{\mathrm{n}}'$) and is represented by a functional integral over the quantum trajectories of the system. The inner trace over the nuclear coordinates is then taken for each point of the quantum path by statistical mechanics methods or by computer simulations of the many-particle system.

The more traditional approach to treat the problem outlined by Eq. [13] goes back to the theory of polarons in dielectric crystals.[27,28] It employs the two-step procedure corresponding to two traces in Eq. [13]: first, the trace over the electronic subsystem is taken with the subsequent restricted trace over the nuclear coordinates. This approach, basic to the MH theory of ET, turns out to be very convenient for a general description of several quantum dynamical problems in condensed phases. It is currently widely used in steady-state[29] and time-resolved[2] spectroscopies and in theories of proton transfer,[30] dissociation reactions,[31] and other types of reactions in condensed media. The central feature of the approach is the intuitively appealing and pictorially convenient representation of the activated electron transition as dynamics on the free energy surface of the reaction. Here, we start with outlining the basic steps and concepts leading to the *paradigm of the free energy surfaces*. In this section, we confine the discussion only to classical modes of the solvent. The results obtained here are then used to discuss the construction of the Franck–Condon factor of optical transitions, including quantum intramolecular excitations of the donor–acceptor complex.

The first step of the derivation involves the BO approximation separating the characteristic timescales of the electronic and nuclear motions in the system. In this step, the instantaneous free energy depending on the system nuclear coordinates $\mathbf{q}$ is defined by

$$e^{-\beta F_{\mathrm{el}}(\mathbf{q})} = \mathrm{Tr}_{\mathrm{el}}\left[e^{-\beta H}\right] \qquad [15]$$

For many homogeneous ET reactions, the energies of electronic excitations are much higher than the energy of the thermal motion, which is of the order of $k_{\mathrm{B}}T$. In such cases, the free energy $F_{\mathrm{el}}(\mathbf{q})$ in Eq. [15] can be replaced by the energy, independent of the bath temperature. This does not, however, happen for electrochemical discharge where states of conduction electrons form a continuum with thermal excitations between them. Entropic effects then gain importance, and the free energy $F_{\mathrm{el}}(\mathbf{q})$ should be considered in Eq. [15] (see below).

The instantaneous free energy $F_{\mathrm{el}}(\mathbf{q})$ is the equilibrium free energy, implying equilibrium populations of the electronic states in the system. It is not suitable for describing nonequilibrium processes with nonequilibrium populations of the ground and excited states of the donor–acceptor complex.

In such cases, the instantaneous eigenvalues $E_i(\mathbf{q})$ of the solute electronic Hamiltonian that form the free energy $F_{\mathrm{el}}(\mathbf{q})$

$$\sum_i e^{-\beta E_i(\mathbf{q})} = e^{-\beta F_{\mathrm{el}}(\mathbf{q})} \qquad [16]$$

should be considered as the basis for building the ET free energy surfaces. The energies $E_i(\mathbf{q})$ can be used for nonequilibrium dynamics, since the population of each surface is not limited by the condition of equilibrium as it is the case in Eq. [16].

An electron is transferred between its centers of localization as a result of underbarrier tunneling when the instantaneous electronic energies $E_i(\mathbf{q})$ come into resonance due to thermal fluctuation or radiation of the medium (Figure 1). The difference between the energies $E_i(\mathbf{q})$ thus makes a natural choice for the ET reaction coordinate (cf. to Eq. [3])

$$X = \Delta E(\mathbf{q}) = E_2(\mathbf{q}) - E_1(\mathbf{q}) \qquad [17]$$

as first suggested by Lax[15] and then utilized in many ET studies.[5,17,32,33] The reversible work necessary to achieve a particular magnitude of the energy gap $X$ defines the free energy profile of CT in terms of a Dirac delta function

$$e^{-\beta F_i(X)+\beta F_{0i}} = \beta^{-1}\mathrm{Tr}_{\mathrm{n}}[\delta(X - \Delta E(\mathbf{q}))e^{-\beta E_i(\mathbf{q})}]/\mathrm{Tr}_{\mathrm{n}}[e^{-\beta E_i(\mathbf{q})}] \qquad [18]$$

The partial trace in nuclear degrees of freedom in Eq. [13] is replaced in Eq. [18] by the constraint imposed on the collective reaction coordinate $X$ representing the energy gap between the two levels involved in the transition. This reduces the many-body problem of calculating the activation dynamics in the coordinate space $\mathbf{q}$ to the dynamics over just one coordinate $X$. As we show in the discussion of optical transition below, the same Boltzmann factor as in Eq. [18] comes into expressions for optical profiles of CT bands. The solvent component of the FCWD then becomes

$$\mathrm{FCWD}_i^{\mathrm{s}}(X) = \beta e^{-\beta F_i(X)+\beta F_{0i}} \qquad [19]$$

A more general definition of the FCWD includes overlap integrals of quantum nuclear modes.[15,17] The definition given by Eq. [19] includes only classical solvent modes (superscript "s") for which these overlap integrals are identically equal to unity. An extension of Eq. [19] to the case of quantum intramolecular excitations of the donor–acceptor complex is given below in the section discussing optical Franck–Condon factors.

In Eqs. [18] and [19], $F_{0i}$ is the equilibrium free energy of the system in each CT state

$$e^{-\beta F_{0i}} = \mathrm{Tr}_n[e^{-\beta E_i(\mathbf{q})}] \quad [20]$$

Although the free energy profile $F_i(X)$ and the free energy $F_{0i}$ are combined in one equation (Eq. [18]), they have a somewhat different physical meaning. The free energy $F_{0i}$ is the total, equilibrium free energy of the system calculated for all its configurations. The difference of $F_{02}$ and $F_{01}$ makes the free energy gap $\Delta F_0$ entering the MH theory of ET (Figure 2). Thus

$$\Delta F_0 = F_{02} - F_{01} \quad [21]$$

On the other hand, $F_i(X)$ is the *constrained*, incomplete free energy implying that some of the configurations of the system separated by the δ-function in Eq. [18] are not included in the calculation of $F_i(X)$.[33] The phase space of the system is not completely sampled in defining $F_i(X)$, in contrast to the complete sampling for $F_{0i}$. Using molecular dynamics simulations and explicit atomistic models, the free energy in Eq. [18] can be explicitly mapped out. This kind of calculation has become fairly routine (see, e.g., Refs. 32 and 33). It should be noted, however, that such simulations usually neglect the electronic polarizability of both the CT complex and the solvent. These effects may be large (cf. Ref. 32 and the later discussion in this chapter).

When the number of electronic states can be limited to two (two-state model), the analytic properties of the generating function for the two CT free energy surfaces can be used to establish a linear relation between them.[32] The δ-function in Eq. [18] can be represented as a Fourier integral that allows one to rewrite the CT free energy in the integral form

$$e^{-\beta F_i(X)+\beta F_{0i}} = \int_{-\infty}^{\infty} \frac{d\xi}{2\pi} \mathcal{G}_i(\xi, X) \quad [22]$$

The integral is taken over one of the variables of the generating function

$$\mathcal{G}_i(\xi, X) = e^{i\xi\beta X}\mathrm{Tr}_n\left(e^{-i\xi\beta\Delta E-\beta E_i}\right)/\mathrm{Tr}_n\left[e^{-\beta E_i}\right] \quad [23]$$

Analytic properties of $\mathcal{G}_i(\xi, X)$ in the complex ξ-plane then allow one to obtain a linear connection between the free energy surfaces

$$F_2(X) = F_1(X) + X \quad [24]$$

as first established by Warshel.[32,34] This relation is based on the transformation of the integral

$$\int_{-\infty}^{\infty} \frac{d\xi}{2\pi} \mathcal{G}_2(\xi, X) = e^{\beta(\Delta F_0 - X)} \int_{-i-\infty}^{-i+\infty} \frac{d\xi}{2\pi} \mathcal{G}_1(\xi, X) \quad [25]$$

that leads to Eq. [24] provided the integrals over the segments $(-i-\infty, -i+\infty)$ and $(-\infty, +\infty)$ are equal. This happens when $\mathcal{G}_1(\xi, X)$ is analytic in $\xi$ inside the closed contour with the two segments as its boundaries. The linear relation between $F_2(X)$ and $F_1(X)$ breaks down when the generating function is not analytic inside this contour.

## Two-State Model

The two-state model (TSM) provides a very basic description of quantum transitions in condensed-phase media. It limits the manifold of the electronic states of the donor–acceptor complex to only two states participating in the transition. In this section, the TSM will be explored analytically in order to reveal several important properties of ET and CT reactions. The gas-phase Hamiltonian of the TSM reads

$$H_0 = \sum_{i=a,b} I_i a_i^+ a_i + H_{ab}\left(a_a^+ a_b + a_b^+ a_a\right) \qquad [26]$$

where $I_i$ are diagonal gas-phase energies, and $H_{ab}$ is the off-diagonal Hamiltonian matrix element usually called the ET matrix element.[7] In Eq. [26], $a_i^+$, $a_i$ are the fermionic creation and annihilation operators in the states $i = a, b$.

The Hamiltonian in Eq. [26] is usually referred to as the diabatic representation, employing the diabatic basis set $\{\phi_a, \phi_b\}$ in which the Hamiltonian matrix is not diagonal. There is, of course, no unique diabatic basis as any pair $\{\tilde{\phi}_a, \tilde{\phi}_b\}$ obtained from $\{\phi_a, \phi_b\}$ by a unitary transformation can define a new basis. A unitary transformation defines a linear combination of $\phi_a$ and $\phi_b$ which, for a two-state system, can be represented as a rotation of the $\{\phi_a, \phi_b\}$ basis on the angle $\psi$

$$\begin{aligned} \tilde{\phi}_a &= \cos\psi\,\phi_a + \sin\psi\,\phi_b \\ \tilde{\phi}_a &= -\sin\psi\,\phi_a + \cos\psi\,\phi_b \end{aligned} \qquad [27]$$

One such rotation is usually singled out. A unitary transformation $\{\phi_a, \phi_b\} \rightarrow \{\phi_1, \phi_2\}$ diagonalizing the Hamiltonian matrix

$$H_0 = \sum_{i=1,2} E_i a_i^+ a_i \qquad [28]$$

generates the adiabatic basis set $\{\phi_1, \phi_2\}$. The adiabatic gas-phase energies are then given as

$$E_i = \tfrac{1}{2}(I_a + I_b) \pm \tfrac{1}{2}\sqrt{(I_b - I_a)^2 + 4H_{ab}^2}, \qquad \Delta E_{12} = E_2 - E_1 \qquad [29]$$

where "+" and "−" correspond to $i = 1$ and $i = 2$, respectively. Here, we outline the procedure of building the CT free energy surfaces in the diabatic representation and then discuss advantages of using the adiabatic representation.

When the donor–acceptor complex is placed in a solvent, its Hamiltonian changes due to the solute–solvent interaction

$$H_{\text{int}} = -\hat{\mathcal{E}} \cdot \mathcal{P} \qquad [30]$$

Here, the dot product of two calligraphic letters stands for an integral over the solvent volume $V$

$$\hat{\mathcal{E}} \cdot \mathcal{P} = \int_V \hat{\mathbf{E}} \cdot \mathbf{P}\, d\mathbf{r} \qquad [31]$$

and $\hat{\mathcal{E}}$ is the electric field operator of the transferred electron coupled to the polarizability of the solvent $\mathcal{P}$. The system Hamiltonian then becomes

$$H = H_{\text{B}} + \sum_{i=a,b} (I_i - \mathcal{E}_i \cdot \mathcal{P}) a_i^+ a_i + (H_{ab} - \mathcal{E}_{ab} \cdot \mathcal{P})\left(a_b^+ a_a + a_a^+ a_b\right) \qquad [32]$$

where $H_{\text{B}}$ refers to the Hamiltonian of the solvent (thermal bath); $\mathcal{E}_i = \langle \phi_i | \hat{\mathcal{E}} | \phi_i \rangle$ and $\mathcal{E}_{ab} = \langle \phi_a | \hat{\mathcal{E}} | \phi_b \rangle$.

The solvent Hamiltonian $H_{\text{B}}$ includes two components. The first one is an intrinsically quantum part that describes polarization of the electronic clouds of the solvent molecules. This polarization is given by the electronic solvent polarization, $\mathcal{P}_{\text{e}}$. The second part is due to thermal nuclear motions that can be classical or quantum in character. Here, to simplify the discussion, we consider only the classical spectrum of nuclear fluctuations resulting in the classical field of nuclear polarization, $\mathcal{P}_{\text{n}}$. Fluctuations of the solvent polarization field are usually well described within the Gaussian approximation,[35] leading to the quadratic solvent Hamiltonian

$$H_{\text{B}} = H_{\text{B}}[\mathcal{P}_{\text{n}}] + H_{\text{B}}[\mathcal{P}_{\text{e}}] = \tfrac{1}{2} \mathcal{P}_{\text{n}} \cdot \chi_{\text{n}}^{-1} \cdot \mathcal{P}_{\text{n}} + \tfrac{1}{2}\left(\omega_{\text{e}}^{-2} \dot{\mathcal{P}}_{\text{e}} \cdot \dot{\mathcal{P}}_{\text{e}} + \mathcal{P}_{\text{e}} \cdot \chi_{\text{e}}^{-1} \cdot \mathcal{P}_{\text{e}}\right) \qquad [33]$$

Here, $\chi_{\text{e}}$ and $\chi_{\text{n}}$ are the Gaussian response functions of the electronic and nuclear solvent polarization, respectively; $\dot{\mathcal{P}}_{\text{e}}$ is the time derivative of the electronic polarization field entering the corresponding kinetic energy term. In terms of the Gaussian solvent model,[35] the nuclear response function is defined through the correlator of corresponding polarization fluctuations (high-temperature limit of the fluctuation–dissipation theorem[36])

$$\chi_{\text{n}}(\mathbf{r} - \mathbf{r}') = \beta \langle \delta P_{\text{n}}(\mathbf{r})\, \delta P_{\text{n}}(\mathbf{r}') \rangle \qquad [34]$$

In Eq. [33], $\omega_{\text{e}}$ denotes a characteristic frequency of the optical excitations of the solvent. The kinetic energy of the nuclear polarization $\mathcal{P}_{\text{n}}$ is left out in

Eq. [33] according to the assumption of the classical character of this collective mode. Depending on the form of the coupling of the electron donor–acceptor subsystem to the solvent field, one may consider linear or nonlinear solvation models. The coupling term $-\mathcal{E}_i \cdot \mathcal{P}$ in Eq. [32] represents the linear coupling model (L model) that results in a widely used linear response approximation.[37] Some general properties of the bilinear coupling (Q model) are discussed below.

Equations [32] and [33] represent the system Hamiltonian that can be used to build the CT free energy surfaces. According to the general scheme outlined above, the first step in this procedure is to take the average over the electronic degrees of freedom of the system. This implies integrating over the electronic polarization $\mathcal{P}_e$ and the fermionic populations $a_i^+ a_i$. The trace $\mathrm{Tr}_{el}$ can be taken exactly, resulting in two instantaneous energies[38]

$$E_\pm[\mathcal{P}_n] = \tilde{I}_{av}[\mathcal{P}_n] \pm \tfrac{1}{2}\sqrt{(\Delta\tilde{I}[\mathcal{P}_n])^2 + 4(H_{ab}^{eff}[\mathcal{P}_n])^2} \qquad [35]$$

where $\tilde{I}_{av} = (\tilde{I}_a + \tilde{I}_b)/2$ and $\Delta\tilde{I} = \tilde{I}_b - \tilde{I}_a$. For $i = a, b$

$$\tilde{I}_i[\mathcal{P}_n] = I_i - \mathcal{E}_i \cdot \mathcal{P}_n - \tfrac{1}{2}(\mathcal{E}_i \cdot \chi_e \cdot \mathcal{E}_i + \mathcal{E}_{12} \cdot \chi_e \cdot \mathcal{E}_{12}) \qquad [36]$$

The effective ET matrix element has the form

$$\tilde{H}_{ab}^{eff}[\mathcal{P}_n] = e^{-S_e/2}[H_{ab} - \mathcal{E}_{ab} \cdot \mathcal{P}_n - \mathcal{E}_{av} \cdot \chi_e \cdot \mathcal{E}_{ab}] \qquad [37]$$

with $\mathcal{E}_{av} = (\mathcal{E}_a + \mathcal{E}_b)/2$. The matrix element $\tilde{H}_{ab}^{eff}[\mathcal{P}_n]$ depends on the solvent through two components: (1) interaction of the off-diagonal solute electric field with the nuclear solvent polarization (second term) and (2) solvation of the off-diagonal field by the electronic polarization of the solvent (third term). The former component leads to solvent-induced fluctuations of the ET matrix element, which represent a non-Condon effect[39] of the dependence of electron coupling on nuclear degrees of freedom of the system. This effect is commonly neglected in the Condon approximation employed in treating nonadiabatic ET rates.[11]

Equation [37] is derived within the assumption that both the electronic polarization and the donor–acceptor complex are characterized by quantum excitation frequencies,[38] $\beta\hbar\omega_e \gg 1$, $\beta\Delta E_{12} \gg 1$, where $\Delta E_{12} = E_2 - E_1$ is the gas-phase adiabatic energy gap in Eq. [29]. The derivation does not assume any particular separation of these two characteristic time scales. The traditional formulation[27] assumes $\Delta E_{12} \ll \hbar\omega_e$ that eliminates the electronic Franck–Condon factor $\exp(-S_e/2)$ in Eq. [37]. The parameter[38,40]

$$S_e = \Delta\mathcal{E}_{ab} \cdot \chi_e \cdot \Delta\mathcal{E}_{ab}/2\hbar\omega_e \qquad \Delta\mathcal{E}_{ab} = \mathcal{E}_b - \mathcal{E}_a \qquad [38]$$

is, however, small for the usual conditions of CT reactions and will be neglected throughout the discussion below.

The energies $E_{\pm}[\mathcal{P}_{\mathrm{n}}]$ in Eq. [35] depend on the nuclear solvent polarization that serves as a three-dimensional (3D) nuclear reaction coordinate driving electronic transitions. The two-state model actually sets up two directions: the vector of the differential field $\Delta\mathcal{E}_{ab}$ and the off-diagonal field $\mathcal{E}_{ab}$. Therefore, only two projections of $\mathcal{P}_{\mathrm{n}}$ need to be considered: the longitudinal field parallel to $\Delta\mathcal{E}_{ab}$ and the transverse field perpendicular to $\Delta\mathcal{E}_{ab}$. In the case when the directions of the differential and off-diagonal fields coincide, one needs to consider only the longitudinal field, and the theory can be formulated in terms of the scalar reaction coordinate

$$Y^{\mathrm{d}} = \Delta\mathcal{E}_{ab} \cdot \mathcal{P}_{\mathrm{n}} \qquad [39]$$

The superscript "d" in the above equations refers to "diabatic" since the diabatic basis set is used to define the electric field difference $\Delta\mathcal{E}_{ab}$. The corresponding free energy profile is obtained by projecting the nuclear polarization $\mathcal{P}_{\mathrm{n}}$ on the direction of the solute field difference

$$e^{-\beta F_{\pm}(Y^{\mathrm{d}})} = \int \mathcal{D}\mathcal{P}_{\mathrm{n}}\delta(Y^{\mathrm{d}} - \Delta\mathcal{E}_{ab} \cdot \mathcal{P}_{\mathrm{n}})e^{-\beta E_{\pm}[\mathcal{P}_{\mathrm{n}}]} \qquad [40]$$

where $\mathcal{D}\mathcal{P}_{\mathrm{n}}$ denotes a functional integral[41] over the field $\mathbf{P}_{\mathrm{n}}(\mathbf{r})$.

The integration in Eq. [40] generates the upper and lower CT free energy surfaces that, after the shift in the reaction coordinate $Y^{\mathrm{d}} \rightarrow Y^{\mathrm{d}} + \Delta\mathcal{E}_{ab} \cdot \chi_{\mathrm{n}} \cdot \mathcal{E}_{\mathrm{av}}$, take the following form[42]

$$F_{\pm}(Y^{\mathrm{d}}) = \frac{(Y^{\mathrm{d}})^2}{4\lambda^{\mathrm{d}}} \pm \frac{\Delta E(Y^{\mathrm{d}})}{2} + C \qquad [41]$$

with

$$\Delta E(Y^{\mathrm{d}}) = [(\Delta F_0^{\mathrm{d}} - Y^{\mathrm{d}})^2 + 4(H_{ab} + \alpha_{ab}(\Delta F_{\mathrm{s}}^{\mathrm{d}} - Y^{\mathrm{d}}))^2]^{1/2} \qquad [42]$$

and

$$C = \frac{F_{0a}^{\mathrm{d}} + F_{0b}^{\mathrm{d}}}{2} + \frac{\lambda^{\mathrm{d}}}{4} \qquad [43]$$

The constant $\alpha_{ab}$ in Eq. [42] represents the ratio of the collinear difference and off-diagonal fields of the solute

$$\alpha_{ab} = \mathcal{E}_{ab}/\Delta\mathcal{E}_{ab} \qquad [44]$$

The diabatic solvent reorganization energy is defined by the nuclear response function $\chi_n$ and by the diabatic field difference

$$\lambda^d = \tfrac{1}{2}\Delta\mathcal{E}_{ab} \cdot \chi_n \cdot \Delta\mathcal{E}_{ab} \quad [45]$$

The free energy gap

$$\Delta F_0^d = F_{0b}^d - F_{0a}^d = \Delta I_{ab} + \Delta F_s^d \quad [46]$$

is composed of the gas-phase splitting $\Delta I_{ab} = I_b - I_a$ and the solvation free energy

$$\Delta F_s^d = -\mathcal{E}_{av} \cdot \chi \cdot \Delta\mathcal{E}_{ab} \quad [47]$$

where $\chi = \chi_e + \chi_n$ is the total response function of the solvent.

Projection on the energy gap reaction coordinate in Eq. [18] is simple to perform for the scalar reaction coordinate $Y^d$

$$\mathrm{FCWD}_{\pm}^{s}(X) = \sum_k (\beta Q_{\pm} \Delta E'[Y^{(k)}])^{-1} e^{-\beta E_{\pm}[Y^{(k)}]} \quad [48]$$

where

$$Q_{\pm} = \int e^{-\beta E_{\pm}(Y^d)} dY^d \quad [49]$$

and $Y^{(k)}$ are all the roots of the equation

$$X = \Delta E[Y^d] \quad [50]$$

In Eq. [48], $\Delta E'[Y^{(k)}]$ denotes the derivative

$$\Delta E'\left[Y^{(k)}\right] = \left.\frac{d\Delta E(Y^d)}{dY^d}\right|_{Y^d = Y^{(k)}} \quad [51]$$

where $Y^d = Y^{(k)}$ indicates that the derivative is taken at the coordinate $Y^{(k)}$ obtained as a solution of Eq. [50].

Equations [41]–[50] provide an exact solution for the CT free energy surfaces and Franck–Condon factors of a two-state system in a condensed medium with quantum electronic and classical nuclear polarization fields. The derivation does not make any specific assumptions about the off-diagonal matrix elements of the Hamiltonian. It, therefore, includes the off-diagonal

solute–solvent coupling through the off-diagonal matrix element of the electric field of the solute.[40] This coupling represents a non-Condon dependence of the ET matrix element on the nuclear solvent polarization (this contribution is commonly neglected in MH theory[13]). In the case of weak electronic overlap, all off-diagonal matrix elements are neglected in the free energy surfaces, and the above equations are transformed to the well-known case of two intersecting parabolas (Figure 2) representing the diabatic ET free energy surfaces

$$F_i(Y^{\mathrm{d}}) = F_{0i} + \frac{(Y^{\mathrm{d}} \pm \lambda^{\mathrm{d}})^2}{4\lambda^{\mathrm{d}}} \qquad [52]$$

The reaction rate constant is then given by the Golden Rule perturbation expansion in the solvent-dependent ET matrix element $H_{ab}^{\mathrm{eff}}[\mathcal{P}_{\mathrm{n}}]$.[43] Careful account for non-Condon solvent dependence of the ET matrix element generates the Mulliken-Hush matrix element in the rate preexponent (see below). In the opposite case of strong electronic overlap, the off-diagonal matrix elements cannot be neglected, and one should consider the CT free energy surfaces, instead of ET free energy surfaces, with partial transfer of the electronic density. The free energy surfaces are then substantially nonparabolic; we discuss this case in the section on Electron Delocalization Effect.

## Heterogeneous Discharge

The diabatic two-state representation for homogeneous CT can be extended to heterogeneous CT processes between a reactant in a condensed-phase solvent and a metal electrode. The system Hamiltonian is then given by the Fano–Anderson model[44,45]

$$H = H_{\mathrm{B}} + [E - \mathcal{D}_{\mathrm{e}} \cdot \mathcal{P}_{\mathrm{n}}]c^{+}c + \sum_{\mathbf{k}} \epsilon_{\mathbf{k}}\, c_{\mathbf{k}}^{+} c_{\mathbf{k}} + \sum_{\mathbf{k}} (H_{\mathbf{k}} c_{\mathbf{k}}^{+} c + \mathrm{h.c.}) \qquad [53]$$

where $\mathbf{k}$ is the lattice reciprocal vector, the two summations are over the wave vectors of the electrons of a metal, $\varepsilon_{\mathbf{k}}$ is the kinetic energy of the conduction electrons (hence $\varepsilon_{\mathbf{k}} = \mathbf{k}^2/2\mathrm{m_e}$, with $\mathrm{m_e}$ being the electron mass), and "h.c." designates the corresponding Hermetian conjugate. In Eq. [53], $c^{+}$ and $c$ are the Fermionic creation and annihilation operators of the localized reactant state. $c_{\mathbf{k}}^{+}$ and $c_{\mathbf{k}}$ are the creation and annihilation operators, respectively, for a conduction electron with momentum $\mathbf{k}$, and $H_{\mathbf{k}}$ is the coupling of this metal state to the localized electron state on the reactant. The energy of the localized reactant state includes solvation by the solvent electronic polarization (included in $E$) and the interaction of the electron electric field $\mathcal{D}_{\mathrm{e}}$ with the nuclear solvent polarization $\mathcal{P}_{\mathrm{n}}$. The transferred electron is much faster than the ions dissolved in the electrolyte. Therefore, on the time scale of charge

redistribution, no screening of the electron field by rearrangement of the electrolyte ions occurs, and the electron field includes the field of the image charge on the metal surface

$$\mathbf{D}_e(\mathbf{r}) = e\int |\Psi_e(\mathbf{r}')|^2 \nabla\left(\frac{1}{|\mathbf{r}-\mathbf{r}'|} - \frac{1}{|\mathbf{r}-\mathbf{r}'_{im}|}\right) d\mathbf{r}' \qquad [54]$$

where $\mathbf{r}'_{im}$ is the mirror image of the electron at the point $\mathbf{r}'$ relative to the electrode plane, $\Psi_e(\mathbf{r})$ is the wave function of the localized electron, and $e$ is the electron charge. (In Eq. [54], $e$ appears because we are not using atomic units. Thoughout this chapter, the energies are generally in electron volts.) The off-diagonal solute–solvent coupling is dropped in the off-diagonal part of the system Hamiltonian in Eq. [53] as no experimental or theoretical information is currently available about the strength of the off-diagonal solute field in the near-to-electrode region.

The free energy surface for the electron heterogeneous discharge can be directly written as

$$e^{-\beta F(Y^d)} = (\beta Q_B)^{-1} \mathrm{Tr}_n \mathrm{Tr}_{el}[\delta(Y^d - \mathcal{D}_e \cdot \mathcal{P}_n)\hat{\rho}] \qquad [55]$$

where $Q_B$ refers to the partition function of the pure solvent and the Dirac delta function is invoked. In electrochemical discharge, the reactant is coupled to a macroscopic bath of metal electrons. The total number of electrons in the system is thus not conserved, and the grand canonical ensemble should be considered for the electronic subsystem. The density matrix in Eq. [55] then reads

$$\hat{\rho} = e^{\beta(\mu_e N - H)} \qquad [56]$$

Here, $\mu_e$ is the chemical potential of the electronic subsystem containing

$$N = c^+ c + \sum_{\mathbf{k}} c^+_{\mathbf{k}} c_{\mathbf{k}} \qquad [57]$$

electrons.

The path-integral formulation of the trace in Eq. [55] allows us to take it exactly. This leads to the following expression for the free energy surface[46]

$$F(Y^d) = \frac{(Y^d)^2}{4\lambda^d} + \frac{\epsilon(Y^d)}{2} + \beta^{-1}\ln\left[\left|\Gamma\left(\frac{\beta\tilde{\Delta}}{2\pi} - i\frac{\beta\epsilon(Y^d)}{2\pi}\right)\right|^2\right] \qquad [58]$$

Here, $Y^d$ is the classical reaction coordinate, $\Gamma(x)$ is the gamma function, and

$$\epsilon(Y^d) = E - \mu_e - Y^d = \lambda^d + e\eta - Y^d \qquad [59]$$

where $\eta$ is the electrode overpotential. Equation [58] presents the exact solution for the free energy surface of an electrochemical system along the classical reaction coordinate $Y^{d}$. It includes the free energy of a classical Gaussian solvent fluctuation (the first term) and the free energy of charge redistribution between the localized reactant state and the continuum of delocalized conduction states of the metal (the second and the third terms). Delocalization effectively proceeds on the range of reaction coordinates given by the effective width

$$\tilde{\Delta} = \Delta + \pi\beta^{-1} \qquad [60]$$

built on the direct electron overlap

$$\Delta = \pi \sum_{\mathbf{k}} \rho_{F} |H_{\mathbf{k}}|^{2} \qquad [61]$$

and the width of the thermal distribution of the conductance electrons on the metal Fermi level ($\pi\beta^{-1}$); $\rho_{F}$ is the electron density of states of the metal on its Fermi level. In the limit

$$\beta\tilde{\Delta} \gg 1 \qquad [62]$$

Eq. [58] reduces to the free energy

$$F(Y^{d}) = \frac{(Y^{d})^{2}}{4\lambda^{d}} + \frac{\epsilon(Y^{d})}{\pi}\cot^{-1}\frac{\epsilon(Y^{d})}{\tilde{\Delta}} + \frac{\tilde{\Delta}}{2\pi}\ln\left[(\beta\tilde{\Delta})^{2} + (\beta\epsilon(Y^{d}))^{2}\right] \qquad [63]$$

The overlap $\tilde{\Delta}$ can be replaced by $\Delta$ when $\Delta \gg \pi\beta^{-1}$. Equation [63] then leads to the ground-state energy $E(Y^{d})$ (zero temperature for the electronic subsystem) often used to describe adiabatic heterogeneous CT.[45]

Equations [58] and [63] indicate an important point concerning the instantaneous energies obtained by tracing out (integrating) the electronic degrees of freedom of the system (Eq. [15]). When the separation of electronic states is much higher than the thermal energy $k_{B}T$, the free energies can be replaced by energies. This does not happen for heterogeneous discharge where thermal excitations of the conductance electrons lead to entropic effects embodied in the temperature-dependent summand in $\tilde{\Delta}$ (Eq. [60]).

## BEYOND THE PARABOLAS

The paradigm of free energy surfaces provides a very convenient and productive conceptual framework to analyze the thermodynamics and dynamics of electronic transitions in condensed phases. It, in fact, replaces the complex dynamics of a quantum subsystem interacting with a many-body

thermal bath with the motion of a classical representative particle over the activation barrier.[47] The MH solution gives the barrier as the vertical gap between the bottom of the initial free energy surface and the intersection point. The problem of finding the activation barrier then reduces to two parameters: the free energy equilibrium gap, $\Delta F_0$, and the classical nuclear reorganization energy, $\lambda_{cl}$ (Figure 2). From a broader perspective, as surprising as it seems, the MH model for classical nuclear modes and its extension to quantum intramolecular skeletal vibrations[17] presents the only exact, closed-form solution for $F_i(X)$ available currently in the field of ET.

The success of the MH theory can also, to a large degree, be attributed to the fact that the parameters of the model are connected to spectroscopic observables. The first spectral moments for absorption and emission transitions $\nu_{abs/em}$ fully define the classical reorganization energy $\lambda_{cl}$ and the equilibrium free energy gap $\Delta F_0$ through the mean energy and the Stokes shift (Eqs. [6] and [8])

$$h\Delta\nu_{st} = h(\nu_{abs} - \nu_{em}) = 2\lambda_{cl} \qquad [64]$$

Clearly, the MH description does not capture all possible complicated mechanisms of ET activation in condensed phases. The general question that arises in this connection is whether we are able to formulate an extension of the mathematical MH framework that would (1) exactly derive from the system Hamiltonian, (2) comply with the fundamental linear constraint in Eq. [24], (3) give nonparabolic free energy surfaces and more flexibility to include nonlinear electronic or solvation effects, and (4) provide an unambiguous connection between the model parameters and spectroscopic observables. In the next section, we present the bilinear coupling model (Q model), which satisfies the above requirements and provides a generalization of the MH model.

It has in fact been anticipated for many years that the CT free energy surfaces may deviate from parabolas. A part of this interest is provoked by experimental evidence from kinetics and spectroscopy. First, the dependence of the activation free energy, $F_i^{act}$, for the forward ($i = 1$ ) and backward ($i = 2$) reactions on the equilibrium free energy gap $\Delta F_0$ (ET energy gap law) is rarely a symmetric parabola as is suggested by the Marcus equation,[48] Eq. [9]. Second, optical spectra are asymmetric in most cases[17] and in some cases do not show the mirror symmetry between absorption and emission.[49] In both types of experiments, however, the observed effect is an ill-defined mixture of the intramolecular vibrational excitations of the solute and thermal fluctuations of the solvent. The band shape analysis of optical lines does not currently allow an unambiguous separation of these two effects, and there is insufficient information about the solvent-induced free energy profiles of ET.

Nonlinear solvation (breakdown of assumption 4 in the Introduction) has long been considered as the main possible origin of nonparabolic free

energy surfaces of ET.[33,50–56] It turns out, however, that equilibrium solvation of fixed solute charges in dense liquids is well described within the linear response approximation,[37] which leads to parabolic free energy surfaces. When the distribution of fixed molecular charges changes with excitation, the equilibrium solvation is still linear and deviations from the linear dynamic response are well described by linear solvation with a time-varying force constant of the Gaussian fluctuations of the medium.[57] The situation changes, however, when the model of fixed charges is replaced by a more realistic model of a distributed electronic density that can be polarized by an external field. The solute free energy then gains the energy of self-polarization that is generally quadratic in the field of the condensed environment.[58] When this self-polarization energy changes with electronic transition, the solute–solvent coupling becomes a bilinear function of solvent nuclear modes instead of a linear function incorporated in the MH model of parabolic ET surfaces. This bilinear coupling model (Q model) produces some very generic types of behavior that are substantially different from what is predicted by the MH model. We thus start our discussion of nonparabolic CT surfaces with a general analysis of the Q model.

## Bilinear Coupling Model

The MH description is isomorphic to the two-state (TS) model with a linear coupling of the solute to a classical harmonic oscillator (L model). Since the earliest days of the theory of radiationless transitions, a possibility of a bilinear solute–solvent coupling (Q model) has been anticipated.[38,59,60] This problem can be interpreted as a TS solute linearly coupled to a harmonic solvent mode with force constants different in the initial and final electronic states (Duschinsky rotation of normal modes[38]). Although a general quantum solution of the Q model exists,[59] no closed-form, analytical representation for $F_i(X)$ was given. The model hence has not received wide application to ET reactions. Instead, nonlinear solute–solvent coupling has been modeled by two displaced free energy parabolic surfaces $F_i(X)$ with different curvatures.[50,53] This approach, advanced by Kakitani and Mataga,[50] was designed to represent nonlinear solvation effects on the ET energy gap law. However, the approximation of the ET energy surfaces by two displaced parabolas with different curvatures suffers from a general drawback of not complying with the exact linear relationship between the free energy surfaces in Eq. [24].

The Q model allows an exact formulation for $F_i(X)$ for classical solvent modes.[61] The instantaneous energy in this case is given by the bilinear form

$$E_i(q) = I_i - C_i q + \tfrac{1}{2}\kappa_i q^2 \qquad [65]$$

where $q$ is a collective nuclear mode driving electron transitions (the longitudinal projection of the nuclear polarization $\mathcal{P}_n$ is an example of such a

collective mode). In Eq. [65], both the linear coupling constant, $C_i$, and the *harmonic force constant*, $\kappa_i$, change with the transition. The MH L model is recovered when $\kappa_1 = \kappa_2$. Note, that since the off-diagonal matrix elements of the Hamiltonian are excluded from consideration, the formalism described here may apply to any choice of wave functions for which such an approximation is warranted. We therefore do not specify the basis set here, and the indices $i = 1, 2$ refer to any basis set in which the energies $E_i(q)$ are obtained.

The calculations of the diabatic (no off-diagonal matrix elements) free energy surfaces in Eq. [18] can be performed exactly for $E_i(q)$ given by Eq. [65]. This procedure yields the closed-form, analytical expressions for the free energies $F_i(X)$. It turns out that the solution exists only in a limited, one-sided band of the energy gaps $X$.[61] Specifically, an asymptotic expansion of the exact solution leads to a simple expression for the free energy

$$F_i(X) = F_{0i} + \left(\sqrt{|\alpha_i||X - X_0|} - |\alpha_i|\sqrt{\lambda_i}\right)^2 \qquad [66]$$

within a one-sided band of reaction coordinate $X$ and

$$F_i(X) = \infty \qquad [67]$$

outside the band.

The parameter $X_0$ establishes the boundary of the energy gaps for which a finite solution $F_i(X)$ exists. The band definition and its boundary

$$X_0 = \Delta I - \frac{\Delta C^2}{2\Delta\kappa} \qquad [68]$$

both depend on the sign of the variation of the force constant $\Delta\kappa$. The one-sided band is defined as (Figure 5):

$$\text{fluctuation band} = \begin{cases} X < X_0 & \text{at} \quad \Delta\kappa < 0 \\ X > X_0 & \text{at} \quad \Delta\kappa > 0 \end{cases} \qquad [69]$$


**Figure 5** Upper energy ($\Delta\kappa > 0$) and lower energy ($\Delta\kappa < 0$) fluctuations boundaries in the Q model.

This result indicates a fundamental distinction between the Q and L models. In the latter, the band of the energy gap fluctuations is not limited, leading to a finite, even small, probability to find a fluctuation of any magnitude of the energy gap. On the contrary, the Q model suggests a limited band for the energy gap fluctuations. The gap magnitudes achievable due to the nuclear fluctuations are limited by a low-energy boundary for $\Delta\kappa > 0$ and by a high-energy boundary for $\Delta\kappa < 0$. The probability of finding an energy gap fluctuation outside these boundaries is identically zero because there is no real solution of the equation

$$X = \Delta E(q) = E_2(q) - E_1(q) \qquad [70]$$

The absence of a solution is the result of a bilinear dependence of the energy gap $\Delta E(q)$ on the driving nuclear mode $q$ (Figure 6).

The other model parameters entering Eq. [66] are the nuclear reorganization energies defined through the second cumulants of the reaction coordinate

$$\lambda_i = \tfrac{1}{2}\beta\langle(\delta X)^2\rangle_i = \tfrac{1}{2\kappa_i}(C_i/\alpha_i - \Delta C)^2 \qquad [71]$$

and the relative changes in the force constants

$$\alpha_i = \frac{\kappa_i}{\Delta\kappa} \qquad [72]$$

The two sets of parameters defined for each state are not independent because of the following connections between them

$$\alpha_1^3\lambda_1 = \alpha_2^3\lambda_2 \qquad [73]$$

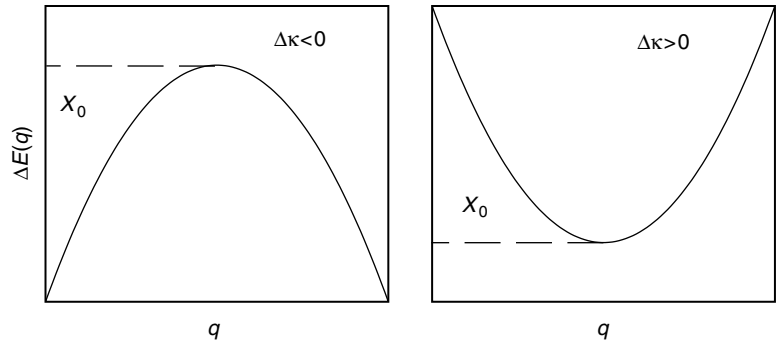


**Figure 6** The origin of the upper energy ($\Delta\kappa < 0$) and lower energy ($\Delta\kappa > 0$) fluctuation boundaries due to a bilinear dependence of $\Delta E$ on $q$.

and

$$\alpha_2 = 1 + \alpha_1 \qquad [74]$$

An additional constraint on the magnitudes of the parameter $\alpha_1$ comes from the condition of the thermodynamic stability of the collective solvent mode in both states, $\kappa_i > 0$, resulting in two inequalities

$$\alpha_1 > 0 \qquad \text{or} \qquad \alpha_1 < -1 \qquad [75]$$

The inequalities in Eq. [75] also define the condition for the generating function (Eq. [23]) to be analytic in the integration contour in Eq. [25]. This condition is equivalent to the linear connection between the diabatic free energy surfaces, Eq. [24]. The Q model solution thus explicitly indicates that the linear relation between the diabatic free energy surfaces is equivalent to the condition of thermodynamic stability of the collective nuclear mode driving ET.

Equations [73] and [74] reduce the number of independent parameters of the Q model to three: $\Delta F_0$, $\lambda_1$, and $\alpha_1$. Here, $\Delta F_0$ (Eq. [21]) is the free energy gap between equilibrium configurations of the system (Figure 2). The fluctuation boundary $X_0$ is connected to $\Delta F_0$ by the relation

$$X_0 = \Delta F_0 + \lambda_1 \alpha_1^2 / \alpha_2 \qquad [76]$$

Compared to the two-parameter MH theory ($\lambda$ and $\Delta F_0$),[12] the Q model introduces an additional flexibility in terms of the relative variation of the fluctuation force constant through $\alpha_1$. The MH theory is recovered in the limit $\alpha_1 \to \infty$.

Importantly, the new free energy surfaces lead to qualitatively new features for the activated ET kinetics. The standard high-temperature limit of two diabatic ET free energy surfaces

$$F_i(X) = F_{0i} + \frac{(X - \Delta F_0 \mp \lambda_i)^2}{4\lambda_i} \qquad [77]$$

is reproduced when $\alpha_i \gg 1$ (the driving mode force constants $\kappa_i$ in the two states are similar) and, additionally, $|X - \Delta F_0 \mp \lambda_i| \ll |\alpha_i|\lambda_i$. Here, "$-$" and "$+$" correspond to $i = 1$ and $i = 2$, respectively. The second requirement implies that the reaction coordinate should be not too far from the free energy minimum to preserve its parabolic form. By contrast, in the limit $|X - X_0| \gg \lambda_i|\alpha_i|$, the linear dependence wins over the parabolic law

$$F_i(X) = F_{0i} + |\alpha_i| \left| X - \Delta F_0 + \lambda_1 \frac{\alpha_1^2}{\alpha_2} \right| \qquad [78]$$

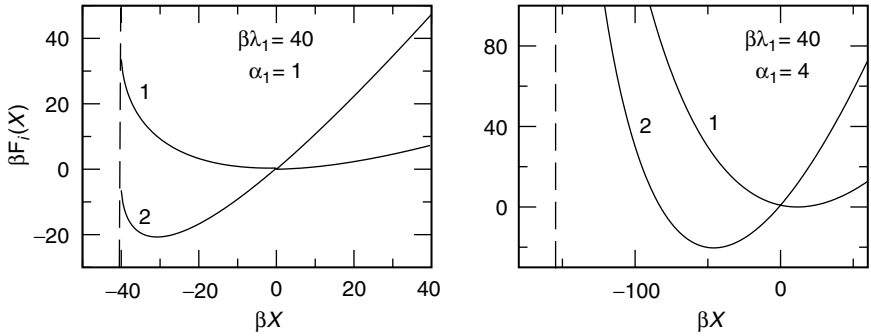


**Figure 7** The free energy surfaces $F_1(X)$ (1) and $F_2(X)$ (2) at various $\alpha_1$; $\Delta I = 0$. The dashed line indicates the position of the fluctuation boundary $X_0$.

As a combination of these two effects, plus the existence of the fluctuation boundary, the free energy surfaces are asymmetric with a steeper branch on the side of the fluctuation boundary $X_0$. The other branch is less steep tending to a linear dependence at large $X$ (Figure 7). The minima of the initial and final free energy surfaces get closer to each other and to the band boundary with decreasing $\alpha_1$ and $\lambda_1$. The crossing point then moves to the inverted ET region where the free energies are nearly linear functions of the reaction coordinate.

The ET activation energy follows from Eq. [66]

$$\begin{aligned} F_i^{\text{act}} &= F_i(0) - F_{0i} \\ &= |\alpha_i| \left( \sqrt{|\Delta F_0 - \lambda_1 \alpha_1^2/\alpha_2|} - \sqrt{|\alpha_i|\lambda_i} \right)^2 \end{aligned} \qquad [79]$$

Equation [79] produces the MH quadratic energy gap law at small $|\Delta F_0| \ll |\alpha_1 \lambda_1|$ and yields a linear dependence of the activation energy on the equilibrium free energy gap at $|\Delta F_0 - \lambda_1 \alpha_1^2/\alpha_2| \gg |\alpha_i|\lambda_i$.

A linear energy gap law is by no means unusual in ET kinetics. It is quite often encountered at large equilibrium energy gaps. Experimental observations of the linear energy gap law are made for intermolecular[62] as well as intramolecular[63] organic donor–acceptor complexes, in binuclear metal–metal CT complexes,[16] and in CT crystals.[64] It is commonly explained in terms of the weak coupling limit of the theory of vibronic band shapes yielding the linear-logarithmic dependence proportional to $\Delta F_i \ln \Delta F_i$ on the vertical energy gap $\Delta F_i$.[17] On the contrary, a strictly linear dependence proportional to $\Delta F_i$ arises from the Q model.

To complete the Q model, one needs to relate the model parameters to spectral observables. Already, the reorganization energies $\lambda_i$ are directly related to the solvent-induced inhomogeneous widths of absorption ($i = 1$)

and emission ($i = 2$)

$$\lambda_i = \tfrac{1}{2}\beta h^2 \langle \delta\nu^2 \rangle_i = \tfrac{1}{2}\beta\sigma_i^2 \qquad [80]$$

where the Gaussian spectral width $\sigma_i$ is experimentally defined through the half-intensity width $\Gamma_i$ as

$$\sigma_i^2 = \Gamma_i^2/(8\ln 2) \qquad [81]$$

As is easy to see from Eq. [80] and Figure 7, the Q model predicts the breaking of the symmetry between the absorption and emission widths (Eq. [11]) generated by a statistical distribution of solvent configurations around a donor–acceptor complex (inhomogeneous broadening). This fact may have a significant application to the band shape analysis of optical transitions since unequal absorption and emission width are often observed experimently.[65,66]

The parameter $\alpha_1$ is defined through the Stokes shift and two reorganization energies from optical widths

$$\alpha_1 = -\Delta\lambda^{-1}(h\Delta\nu_{st} + \lambda_2) \qquad \Delta\lambda = \lambda_2 - \lambda_1 \qquad [82]$$

Similarly, the equilibrium energy gap is (cf. to Eq. [8])

$$\Delta F_0 = h\nu_m - \frac{\lambda_1}{2}\frac{\alpha_1}{\alpha_2^2} \qquad [83]$$

which is equivalent to

$$\Delta F_0 = h\nu_m + \frac{\lambda_1\Delta\lambda}{2}\frac{h\Delta\nu_{st} + \lambda_2}{(h\Delta\nu_{st} + \lambda_1)^2} \qquad [84]$$

The Stokes shift and two second spectral moments fully define the parameters of the model. In addition, they should satisfy Eqs. [73] and [74]. The latter feature establishes the condition of model consistency that is important for mapping the model onto condensed-phase simulations that we discuss below.

The connection of the model parameters to the first and second spectral cumulants enables one to build global, nonequilibrium free energy surfaces of ET based on two cumulants obtained at equilibrium configuration of the system. This allows one to apply the model to equilibrium computer simulations data or to spectral modeling. Compared to the MH picture of intersecting parabolas, the Q model predicts a more diverse pattern of possible system regimes including (1) an existence of a one-sided band restricting the range of permissible reaction coordinates, (2) singular free energies outside the fluctuation band, and (3) a linear energy gap law at large activation barriers. The main features of the Q and L models are compared in Table 1.

**Table 1** Main Features of the Two-Parameter L Model (MH) and the Three-Parameter Q Model

| | L Model | Q Model |
|---|---|---|
| Parameters | $\Delta F_0,\ \lambda$ | $\Delta F_0,\ \lambda_1,\ \alpha_1$ |
| Reaction coordinate | $-\infty < X < \infty$ | $X > X_0$ at $\alpha_1 > 0$<br>$X < X_0$ at $\alpha_1 < 0$ |
| Spectral moments | $\Delta F_0 = h\nu_m$<br>$\lambda = \frac{1}{2}h\Delta\nu_{st}$ | $\Delta F_0 = h\nu_m - [\lambda_1\alpha_1/2(1+\alpha_1)^2]$<br>$\lambda_1 = \frac{1}{2}\beta h^2\langle(\delta\nu)^2\rangle_1$<br>$\alpha_1 = (h\Delta\nu_{st} + \lambda_2)/(\lambda_1 - \lambda_2)$ |
| Energy gap law | | |
| $\Delta F_0 + \lambda_1 \ll \lambda_1$ | $F_1^{act} \propto (\Delta F_0 + \lambda)^2$ | $F_1^{act} \propto (\Delta F_0 + \lambda_1)^2$ |
| $\lvert\Delta F_0\rvert \gg \lambda_1$ | $F_1^{act} \propto \Delta F_0^2$ | $F_1^{act} \propto \lvert\Delta F_0\rvert$ |

## Electron Transfer in Polarizable Donor–Acceptor Complexes

The mathematical model incorporating the bilinear solute–solvent coupling considered above can be realized in various situations involving nonlinear interactions of the CT electronic subsystem with the condensed-phase environment. The most obvious reason for such effects is the coupling of the two states participating in the transition to other excited states of the donor–acceptor complex. These effects bring about polarizability and electronic delocalization in CT systems. The instantaneous energies obtained for a two-state donor–acceptor complex contain a highly nonlinear dependence on the solvent field through the instantaneous adiabatic energy gap. Expansion of the energy gap in the solvent field truncated after the second term generates a state-dependent bilinear solute–solvent coupling characteristic of the Q model. The second derivative of the energy in the external field is the system's polarizability. It is therefore hardly surprising that models incorporating the polarizability of the solute[67] turn out to be isomorphic to the Q model.[61] Here, we focus on some specific features of polarizable CT systems.

The common starting point to build a theoretical description of the thermodynamics and dynamics of the condensed environment response to an electronic transition is to assume that the transition alters the long-range solute–solvent electrostatic forces. This change comes about due to the variation of the electronic density distribution caused by the transition. The combined electron and nuclear charge distributions are represented by a set of partial charges that are assumed to change when the transition occurs. Actually, a change in the electronic state of a molecule changes not only the electronic charge distribution, but also the ability of the electron cloud to polarize in the external field. In other words, the set of transition dipoles to other electronic states is individual for each state of the molecule, and the dipolar (and higher order) polarizability changes with the transition.

Optical excitations quite often generate considerable changes in fixed partial charges, usually described in terms of the difference solute dipole $\Delta m_0$ ("0" refers here to the solute). Chromophores with high magnitudes of the ratio $\Delta m_0/R_0^3$, where $R_0$ is the effective solute radius, are often used as optical probes of the local solvent structure and solvation power.[68] High polarizability changes are also quite common for optical chromophores,[69] as is illustrated in Table 2. Naturally, the theory of ET reactions and optical transitions needs extension for the case when the dipole moment and polarizability both vary with electronic transition:

$$\mathbf{m}_{01} \rightarrow \mathbf{m}_{02} \qquad \alpha_{01} \rightarrow \alpha_{02} \tag{85}$$

To derive the instantaneous free energies $E_i$, one needs an explicit model for a dipolar polarizable solute in a dipolar polarizable solvent. This need is addressed by the Drude model for induced solute and solvent dipole moments.[70] The Drude model represents the induced dipoles as fluctuating vectors: $\mathbf{p}_j$ for the solvent molecules and $\mathbf{p}_0$ for the solute. The potential energy of creating a fluctuating induced dipole $\mathbf{p}$ is given by that of a harmonic oscillator, $\mathbf{p}^2/2\alpha$, with the polarizability $\alpha$ appearing as the oscillator mass. The system Hamiltonian $H_i$ is the sum of the solvent–solvent, $H_{ss}$, and solute–solvent, $H_{0s}^{(i)}$, parts, giving

$$H_i = H_{0s}^{(i)} + H_{ss} \tag{86}$$

In $H_i$, the permanent and induced dipoles add up resulting in the solute–solvent and solvent–solvent Hamiltonians in the form

$$H_{0s}^{(i)} = I_i + U_{0s}^{\text{rep}} - \sum_j (\mathbf{m}_{0i} + \mathbf{p}_0) \cdot \mathbf{T}_{0j} \cdot (\mathbf{m}_j + \mathbf{p}_j) + (1/2\alpha_{0i})[\omega_0^{-2}\dot{\mathbf{p}}_0^2 + \mathbf{p}_0^2] \tag{87}$$

**Table 2** Ground-State Polarizability ($\alpha_1$) and Trace of the Tensor of Polarizability Variation (1/3)Tr[$\Delta\boldsymbol{\alpha}$] for Several Optical Dyes and Charge Transfer Complexes

| Chromophore | $\alpha_1$/Å$^3$ | (1/3)Tr[$\Delta\boldsymbol{\alpha}$]/Å$^3$ |
|---|---|---|
| Anthracene | 25 | 17 |
| 2,2′-Bipyridine-3,3′diol | 21 | 11 |
| Bis(adamantylidene) | 42 | 29 |
| 1-Dimethylamino-2,6-dicyano-4-methylbenzene | 22 | 35 |
| Tetraphenylethylene | 50 | 38 |
| $[(NC)_5Fe^{II}CNOs^{III}(NH_3)_5]^-$ | | 57 |
| $[(NC)_5Os^{II}CNRu^{III}(NH_3)_5]^-$ | | (190) 317[a] |

[a]For two different CT transitions.

and

$$H_{ss} = U_{ss}^{\text{rep}} - \tfrac{1}{2}\sum_{j,k}(\mathbf{m}_j + \mathbf{p}_j)\cdot\tilde{\mathbf{T}}_{jk}\cdot(\mathbf{m}_k + \mathbf{p}_k) + \left(\tfrac{1}{2\alpha}\right)\sum_j[\omega_e^{-2}\dot{\mathbf{p}}_j^2 + \mathbf{p}_j^2] \qquad [88]$$

Here, $\mathbf{T}_{jk}$ is the dipole–dipole interaction tensor, and $\tilde{\mathbf{T}}_{jk} = \mathbf{T}_{jk}(1 - \delta_{jk})$; $U_{0s}^{\text{rep}}$ and $U_{ss}^{\text{rep}}$ stand for repulsion potentials, and $\omega_0 = \Delta E_{12}/\hbar$, where $\Delta E_{12}$ is the adiabatic gas-phase energy gap (Eq. [29]).

The statistical average over the electronic degrees of freedom in Eq. [15] is equivalent, in the Drude model, to integration over the induced dipole moments $\mathbf{p}_0$ and $\mathbf{p}_j$. The Hamiltonian $H_i$ is quadratic in the induced dipoles, and the trace can be calculated exactly as a functional integral over the fluctuating fields $\mathbf{p}_0$ and $\mathbf{p}_j$.[39,67] The resulting solute–solvent interaction energy is[67]

$$E_{0s,i} = I_i + U_{0s}^{\text{rep}} + U_{0s,i}^{\text{disp}} - a_e f_{ei}\mathbf{m}_{0i}^2 - f_{ei}\mathbf{m}_{0i}\cdot\mathbf{R}_p - \tfrac{1}{2}\alpha_{0i}f_{ei}\mathbf{R}_p^2 \qquad [89]$$

Here, $\mathbf{R}_p$ is the reaction field of the solvent nuclear subsystem, and the factor

$$f_{ei} = [1 - 2a_e\alpha_{0i}]^{-1} \qquad [90]$$

describes an enhancement of the condensed-phase solute dipole and polarizability by the self-consistent field of the electronic polarization of the solvent.

For the statistical average over the nuclear configurations, generating the distribution over the solute energy gaps (Eq. [18]), one needs to specify the fluctuation statistics of the nuclear reaction field $\mathbf{R}_p$. A Gaussian statistics of the field fluctuations[35] implies using the distribution function

$$P(\mathbf{R}_p) = \left(4\pi a_p k_B T\right)^{-1/2}\exp[-\beta\,\mathbf{R}_p^2/4a_p] \qquad [91]$$

where $a_p$ is the response coefficient of the nuclear solvent response. Combined with the Gaussian function $P(\mathbf{R}_p)$, Eq. [89] is essentially equivalent to the Q model (Eq. [65]). The vector of the nuclear reaction field plays the role of the nuclear collective mode driving activated transitions ($q$). One can then directly employ the results of the Q model to produce the diabatic free energy surfaces of polarizable donor–acceptor complexes or to calculate the spectroscopic observables.

The reorganization energies follow from Eq. [71] and take the following form for polarizable chromophores:

$$\lambda_i = (a_p f_i/f_{ei})\left(\Delta\tilde{\mathbf{m}}_0 + 2a_p f_i\Delta\tilde{\alpha}_0\mathbf{m}_{0i}\right)^2 \qquad [92]$$

The parameter $f_{ei}$ is defined by Eq. [90]. It scales the solute dipole moment and the polarizability yielding the effective difference values

$$\Delta\tilde{\mathbf{m}}_0 = f_{e2}\mathbf{m}_{02} - f_{e1}\mathbf{m}_{01} \qquad \Delta\tilde{\alpha}_0 = f_{e2}\alpha_{02} - f_{e1}\alpha_{01} \tag{93}$$

The parameter

$$f_i = [1 - 2a\,\alpha_{0i}]^{-1} \tag{94}$$

represents the self-consistent reaction field of the solvent including both the electronic and nuclear polarization components; $a = a_e + a_p$, where $a_e$ is the solvent response coefficient of the solvent electronic polarization. The electronic and total solvent response coefficients can be evaluated from the dielectric cavity or explicit solvent models.[5,71,72] The dielectric continuum estimate for a spherical solute yields

$$a_e = \frac{1}{R_0^3}\frac{\epsilon_\infty - 1}{2\epsilon_\infty + 1} \qquad a = \frac{1}{R_0^3}\frac{\epsilon_s - 1}{2\epsilon_s + 1} \tag{95}$$

where $\epsilon_\infty$ and $\epsilon_s$ are the high frequency and static dielectric constants of the solvent. When the solute polarizability is constant, the reorganization energy is the same in both reaction states ($f = f_1 = f_2$; $f_e = f_{e1} = f_{e2}$) and is given by the well-known relation[73]

$$\lambda = (af - a_e f_e)\Delta\mathbf{m}_0^2 \tag{96}$$

A polarizability change leads to a significant variation of the reorganization energy, which is illustrated in Figure 8, where $\lambda_i$ are plotted against $\alpha_{02}$. As can be seen, the reorganization energy approximately doubles with excitation when the excited-state polarizability is about 50% higher than the ground-state value. Such polarizability differences are not uncommon for optical chromophores (Table 2). The effect of the negative polarizability variation is much weaker, and $\lambda_2$ is only slightly smaller than $\lambda_1$.

From the Q model, the solvent-induced shift of the equilibrium free energy gap $F_{0i} = I_i + \Delta F_{s,i}$ is given by the following relation:

$$\Delta F_{s,i} = -2a_p f_i\left[\Delta\tilde{\mathbf{m}}_0 \cdot \mathbf{m}_{0i} + a_p f_i \Delta\tilde{\alpha}_0\,\mathbf{m}_{0i}^2\right] \tag{97}$$

Also, the solvent-induced Stokes shift between the absorption and emission first spectral moments is

$$\begin{aligned} h\Delta\nu_{st} &= h\nu_{abs} - h\nu_{em} \\ &= 2a_p\Delta\tilde{\mathbf{m}}_0 \cdot [f_2\mathbf{m}_{02} - f_1\mathbf{m}_{01}] + 2a_p^2\Delta\tilde{\alpha}_0[(f_2 m_{02})^2 - (f_1 m_{01})^2] \end{aligned} \tag{98}$$

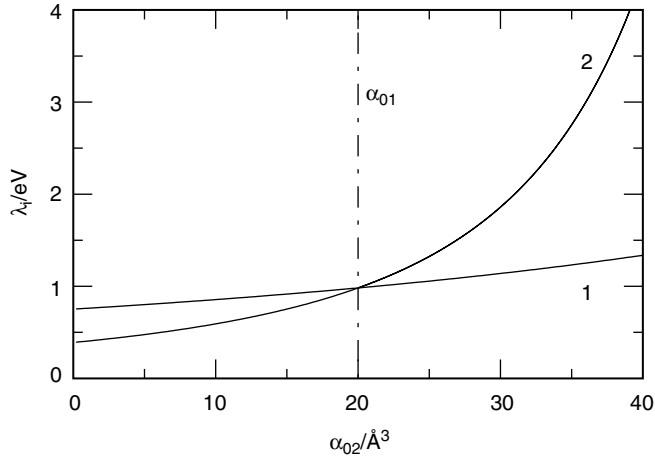


**Figure 8** Dependence of the solvent reorganization energy in the neutral (1, $m_{01}$) and charge-separated (2, $m_{02}$) states on the polarizability of the final state $\alpha_{02}$. The solvent response coefficients are estimated from the continuum dielectric model (Eq. [95]). Solute and solvent parameters are $m_{01} = 0$, $m_{02} = 15$ D, $\alpha_{01} = 20$ Å$^3$, $R_0 = 4$ Å, $\epsilon_\infty = 2$, $\epsilon_s = 30$. In this and subsequent figures, some of the axes are labeled as the ratios shown in order to make the quantities dimensionless. For example, the ordinate in this plot is in units of electron volts, and the abscissa is in units of cubic angstroms.

Both the free energy gap and the Stokes shift include two contributions: one arising from the variation of the solute dipole (the first term) and one due to the polarizability change (the second term). The Stokes shift is hence nonzero even if the charge distribution does not change in the course of the transition ($m_{02} = m_{01}$).

The polarizability difference determines the relative change in the frequency of the solvent driving mode given by the parameter $\alpha_1$ of the $Q$ model

$$\alpha_1 = -\frac{f_{e1}}{2a_p f_1 \Delta\tilde{\alpha}_0} \qquad [99]$$

The fact that the parameter $\alpha_1$ is connected to spectroscopic moments for absorption and emission transitions opens an interesting opportunity to derive the polarizability change of optical chromophores from spectroscopic first and second moments. The equation for the polarizability change is as follows:

$$\Delta\tilde{\alpha}_0 = \frac{1}{2\lambda_1}\frac{\Delta\lambda}{h\Delta\nu_{st} + \lambda_2}\left(\tilde{\mathbf{m}}_{02} - \tilde{\mathbf{m}}_{01}\frac{h\Delta\nu_{st} + \lambda_1}{h\Delta\nu_{st} + \lambda_2}\right)^2 \qquad [100]$$

In many practical cases, the factors $f_{ei}$ are very close to unity and can be omitted. The parameters $\tilde{\alpha}_{0i}$ and $\tilde{\mathbf{m}}_{0i}$ are then equal to their gas-phase values $\alpha_{0i}$ and $\mathbf{m}_{0i}$. Equation [100] then gives the polarizability change in terms of spectroscopic moments and gas-phase solute dipoles. Experimental measurement and theoretical calculation of $\Delta\alpha_0 = \alpha_{02} - \alpha_{01}$ is still challenging. Perhaps the most accurate way to measure $\Delta\alpha_0$ presently available is that by Stark spectroscopy,[74–76] which also gives $\Delta m_0$. Equation [100] can therefore be used as an independent source of $\Delta\alpha_0$, provided all other parameters are available, or as a consistency test for the band shape analysis.

One of the consequences of a nonzero $\Delta\alpha_0$ is that the relation between the solvent-induced Stokes shift and the corresponding spectral width ($\lambda_v = 0$)

$$h\Delta\nu_{st} = \beta\sigma^2 \qquad [101]$$

which is valid for linear solvation response and $\Delta\alpha_0 = 0$, does not hold any more. In Figure 9, the widths $\beta\sigma_i^2$ are plotted versus the Stokes shift obtained by varying the static dielectric constant of the solvent in the range $\epsilon_s = 3 - 65$. The aborption width deviates downward from the unity slope line predicted by Eq. [101], and the emission width goes upward. The opposite behavior follows from nonlinear solvation effects:[77] the absorption width deviates upward from Eq. [101], and the emission width goes downward. This situation arises because nonlinear solvation results in narrowing of emission lines in contrast to the broadening effect of $\Delta\alpha_0 > 0$. The two effects, therefore, tend to compensate each other for $\Delta\alpha_0 > 0$ and to enforce each other for $\Delta\alpha_0 < 0$.

Both the inequality of the charge separation (CS) and charge recombination (CR) reorganization energies ($\lambda_1 \neq \lambda_2$, Figure 8) and the deviation from

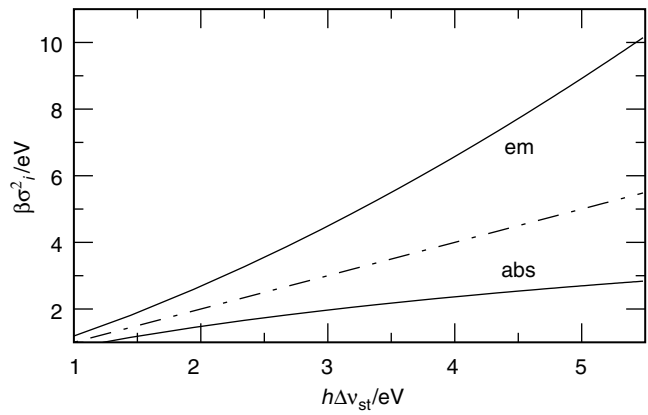


**Figure 9** Absorption (abs.) and emission (em.) widths obtained by changing the static solvent dielectric constant in the range $\epsilon_s = 3 - 65$ versus the Stokes shift; $\epsilon_\infty = 2.0$. The dash–dotted line indicates the equality $h\Delta\nu_{st} = \beta\sigma^2$ is valid for $\Delta\alpha_0 = 0$.

the width/Stokes shift relation (Eq. [101], Figure 9) are indicators of a non-parabolic form of the CS and CR free energy surfaces. Another indication of this effect is the energy gap law. The *energy gap law* refers to the dependence of the activation energy of a reaction on the difference in the Gibbs energy between the products and reactants.[34,38,50] The Marcus equation, Eq. [9], is an example of the energy gap law. Experimentally, the energy gap law is monitored by changing the gas-phase component of $\Delta F_0$ through chemical substitution of the donor and/or acceptor units.[48] The solvent component of $\Delta F_i$ is usually assumed to be reasonably constant. Figure 10 shows the activation energy of the forward (charge separation, CS) reaction plotted against $\Delta F_{CS} = \Delta F_0$ and backward (charge recombination, CR) reaction plotted against $\Delta F_{CR} = -\Delta F_0$ for the transition $m_{01} = 0 \rightarrow m_{02} = 15$ D and $\alpha_{01} = 20$ Å$^3 \rightarrow \alpha_{02} = 40$ Å$^3$. Two important effects of nonzero $\Delta\alpha_0$ manifest themselves in Figure 10. First, in contrast to the case of zero $\Delta\alpha_0$, the maxima of the CS and CR curves do not coincide, as is suggested by Eq. [9]. Second, the CR curve is broader and shallower from the side of negative energy gaps compared to the CS curve.

The energy gap law for thermally activated ET reactions is often obtained by superimposing CS and CR data on a common scale of $\Delta F_0$.[78] For such a procedure, depending on the energy range studied, two outcomes can be predicted. For a narrow range of $\Delta F_{CS}$ and $\Delta F_{CR}$ values close to zero,

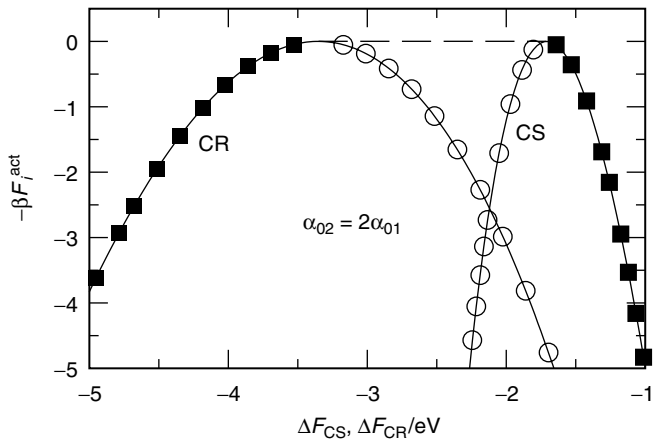


**Figure 10** ET energy gap law for the charge separation (CS, $m_{01} \rightarrow m_{02}$, $\Delta F_{CS} = \Delta F_0$) and charge recombination (CR, $m_{02} \rightarrow m_{01}$, $\Delta F_{CR} = -\Delta F_0$) reactions at $\alpha_{01} = 20$ Å$^3$ and $\alpha_{02} = 40$ Å$^3$. Parameters are as in Figure 8. The points and dashed line are drawn to illustrate two possible outcomes of combining CS and CR experimental data in one plot with a common energy gap scale (see the text). The open circles correspond to crossing curves, whereas the solid squares correspond to a single curve bridged by the dashed line.

intersection of the two curves (illustrated by circles in Figure 10) may occur. Such a behavior was indeed observed in Ref. 78 for a series of porphyrin–quinone diads in tetrahydrofuran. Maxima of the CS and CR curves get closer to each other with decreasing solvent polarity, and, in fact, no curve crossing was seen for the same systems in benzene as a solvent.[78] When the normal region of CS is combined with the inverted region for CR, another scenario is possible. The two branches (shown by squares in Figure 10) fitted by a single curve (the dashed line in Figure 10) result in a plateau in the energy gap law (a picture reminiscent of this behavior can be seen in Figure 4 of Ref. 79).

## Nonlinear Solvation Effects

Experiment provides very limited evidence whether the free energy surfaces of ET should be calculated invoking the linear or nonlinear solvent response. In the absence of direct experimental evidence, the problem of nonlinear solvation effects on the ET free energy surfaces has been approached by computer simulations[33,51–53] and liquid-state solvation theories (integral equations[80] and perturbation techniques[81]). In computer simulations, the free energy surfaces are calculated either directly by umbrella sampling techniques[82] or indirectly by generating a few equilibrium cumulants. In both cases, the lack of a general analytical framework to generate global free energy surfaces from limited data available from simulations considerably impedes the application of the simulation results to generate optical band shapes or to make predictions concerning the ET energy gap law.

The Q model considered above may provide enough flexibility to be used as an analytical background to analyze condensed-phase simulations of the ET energetics. The great advantage of the model is that it requires only two first equilibrium cumulants of the energy gap fluctuations for each electronic state to generate $F_i(X)$ in the whole range of $X$ values in the permissible fluctuation band. The applicability of the model to mapping the simulations can be tested on the consistency requirement given by Eq. [73]. Rewritten in terms of the moments of the reaction coordinate $X$, this requirement implies that the factor

$$\gamma = \frac{\langle(\delta X)^2\rangle_1}{\langle(\delta X)^2\rangle_2}\left(\frac{\langle(\delta X)^2\rangle_2 + 2k_B T\Delta\langle X\rangle}{\langle(\delta X)^2\rangle_1 + 2k_B T\Delta\langle X\rangle}\right)^3 \qquad [102]$$

($\Delta\langle X\rangle = \langle X\rangle_2 - \langle X\rangle_1$) should obey the condition

$$\gamma = 1 \qquad [103]$$

Table 3 lists the parameters $\gamma$ extracted from simulations available in the literature. The condition of Eq. [103] holds very well indeed, which allows one

**Table 3** Mapping of the Q Model on Simulation Data for Charge Separation Reactions (Energies are in kcal/mole)

| Solvent | $h\Delta\nu_{st}$[a] | $\lambda_1$ | $\lambda_2$ | $\alpha_1$ | $\gamma$ | Reference |
|---|---|---|---|---|---|---|
| Lattice of point dipoles | 157 | 121.1 | 48.3 | 2.82 | 1.01 | 54 |
| Lattice of point dipoles | 14.3 | 9.1 | 5.6 | 5.6 | 1.00 | 61 |
| Dipolar liquid | 20.3 | 10.5 | 8.7 | 14 | 1.01 | 61 |
| Polar liquid | 50 | 27.0 | 17.4 | 7.04 | 1.04 | 53 |
| Polar liquid | 267 | 231.5 | 67.1 | 2.03 | 1.04 | 55 |
| Water | 421 | 164.4 | 181.2 | −35.8 | 0.99 | 56 |

[a] $h\Delta\nu_{st} = \langle X\rangle_1 - \langle X\rangle_2$.

to apply the Q model to generating $F_i(X)$ from equilibrium simulations. Figure 11 (left panel) compares the results of the analytical Q model with simulated free energy surfaces for a dipolar solute in a lattice of dipolar hard spheres (DHS) (the two sets of curves coincide on the plot scale). A dipolar lattice as a solvent is chosen because it generates a far larger nonlinear solvation effect than nonpolarizable and polarizable liquids of the same polarity (Figure 11). The parameter

$$\alpha_1 = -\frac{2k_B T\Delta\langle X\rangle + \langle(\delta X)^2\rangle_2}{\langle(\delta X)^2\rangle_2 - \langle(\delta X)^2\rangle_1} \qquad [104]$$

of the Q model serves as an indicator of the strength of nonlinear solvation effects (the linear response is recovered in the limit $\alpha_1 \to \infty$). The right panel

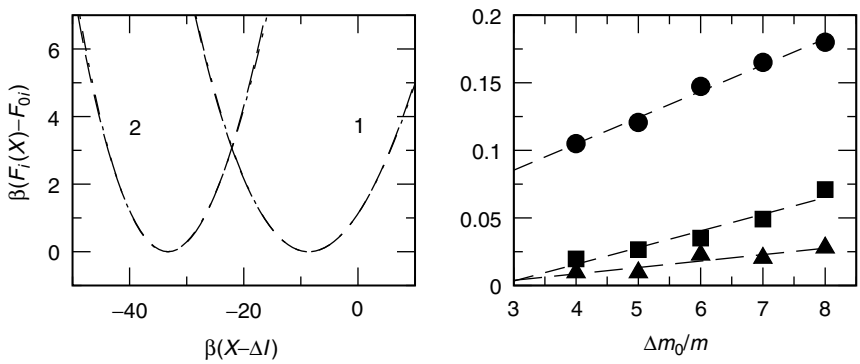


**Figure 11** Left panel: $F_1(X)$ (1) and $F_2(X)$ (2) from the analytical Q model (dashed lines) and from simulations (dash–dotted lines) at $m_{01}/m = 2$ and $m_{02}/m = 10$ in the dipolar lattice with $\beta m^2/\sigma^3 = 1.0$; $R_0/\sigma = 0.9$; $\sigma$ is the hard-sphere diameter of the solvent molecules; $m$ is the solvent dipole moment. The dashed and dash–dotted curves essentially superimpose. Right panel: $1/\alpha_1$ versus $\Delta m_0/m$. Circles indicate the lattice DHS solvent, squares correspond to a liquid DHS solvent, and triangles indicate a nonpolarizable solute in a polarizable DHS liquid; $\beta m^2/\sigma^3 = 1$, $\alpha/\sigma^3 = 0.05$, $\alpha$ is the solvent polarizability.

in Figure 11 shows the dependence of $\alpha_1$ on the magnitude of solute's dipole. The dipolar lattice demonstrates a considerably higher extent of nonlinear solvation compared to dipolar liquids. The reason for this effect is that the lattice dipoles are immobilized and the orientational saturation is not compensated by local density compression as happens in liquid solvents.[83]

## Electron Delocalization Effects

Equations [41]–[42] give a general, exact solution for the free energy surfaces of a two-level system characterized by two collinear vectors: differential, $\Delta\mathcal{E}_{ab}$, and off-diagonal, $\mathcal{E}_{ab}$, electric fields of the donor–acceptor complex. When the off-diagonal matrix elements are nonnegligible, the free energy surfaces are substantially nonparabolic. They are defined by five parameters: $\lambda^{d}$, $\Delta F_{s}^{d}$, $\Delta I_{ab}$, $H_{ab}$, and $\alpha_{ab}$. A careful choice of the basis set allows the elimination of one parameter. Two approaches can be employed. In the adiabatic basis set, $\{\phi_1, \phi_2\}$, the gas-phase ET matrix element is zero, $H_{12} = 0$. Alternatively, one can define the basis set by demanding the off-diagonal matrix element of the solute electric field be zero, $\alpha_{ab} = 0$. This choice sets up the generalized Mulliken–Hush (GMH) basis.[7] These two approaches are essentially equivalent in terms of building the CT free energy surfaces,[42] but the adiabatic basis may be more convenient for practical applications. The reason is that most quantum chemical software packages are designed to diagonalize the gas-phase Hamiltonian matrix, thus generating the adiabatic basis and corresponding adiabatic matrix elements of the solute electric field.

There are several fundamental reasons why the GMH and adiabatic formulations are to be preferred over the traditionally employed diabatic formulation. The definition of the diabatic basis set is straightforward for *intermolecular* ET reactions when the donor and acceptor units are separated before the reaction and form a donor–acceptor complex in the course of diffusion in a liquid solvent. The diabatic states are then defined as those of separate donor and acceptor units. The current trend in experimental design of donor–acceptor systems, however, has focused more attention on intramolecular reactions where the donor and acceptor units are coupled in one molecule by a bridge.[22] The direct donor–acceptor overlap and the mixing to bridge states both lead to electronic delocalization,[75,76] with the result that the centers of electronic localization and localized diabatic states are ill-defined. It is then more appropriate to use either the GMH or adiabatic formulation.

There is an additional, more fundamental, issue involved in applying the standard diabatic formalism. The solvent reorganization energy and the solvent component of the equilibrium free energy gap are bilinear forms of $\Delta\mathcal{E}_{ab}$ and $\mathcal{E}_{\mathrm{av}}$ (Eqs. [45] and [47]). A unitary transformation of the diabatic basis (Eq. [27]), which should not affect any physical observables, then changes $\Delta\mathcal{E}_{ab}$ and $\mathcal{E}_{\mathrm{av}}$, affecting the reorganization parameters. The activation parameters of ET consequently depend on transformations of the basis set!

This situation is of course not satisfactory as observable quantities should be invariant with respect to unitary basis transformations.[84] Here, we outline the adiabatic route to a basis-invariant formulation of the theory.[42]

In the adiabatic gas-phase basis, the number of independent parameters drops to four: $\lambda^{ad}$, $\Delta F_s^{ad}$, $\Delta E_{12}$, and $\alpha_{12}$, where the superscript "ad" refers to the adiabatic representation in which $\Delta E_{12}$ is the gas-phase gap between the eigenenergies, Eq. [29]. The equation for the free energy surfaces can then be rewritten in the basis-invariant form

$$F_{\pm}(Y^{ad}) = \frac{(Y^{ad})^2}{4\Delta e^2 \lambda^I} \pm \tfrac{1}{2}\Delta E(Y^{ad}) + C \qquad [105]$$

with

$$\Delta E(Y^{ad}) = \left[\Delta E_{12}^2 + 2\Delta E_{12}(\Delta e \Delta F_s^I - Y^{ad}) + [\Delta F_s^I - (Y^{ad}/\Delta e)]^2\right]^{1/2} \qquad [106]$$

and

$$\Delta e = \left[1 + 4\alpha_{12}^2\right]^{-1/2} \qquad [107]$$

The reaction coordinate is now a projection of the nuclear solvent polarization on the adiabatic differential solute field

$$Y^{ad} = \Delta \mathcal{E}_{12} \cdot \mathcal{P}_n \qquad [108]$$

Both the solvent reorganization energy

$$\lambda^I = \tfrac{1}{2}\left(\Delta \mathcal{E}_{12}^2 + 4\mathcal{E}_{12}^2\right)^{1/2} \cdot \chi_n \cdot \left(\Delta \mathcal{E}_{12}^2 + 4\mathcal{E}_{12}^2\right)^{1/2} \qquad [109]$$

and the solvent component of the free energy gap

$$\Delta F_s^I = -\tfrac{1}{2}\left(\Delta \mathcal{E}_{12}^2 + 4\mathcal{E}_{12}^2\right)^{1/2} \cdot \chi \cdot (\mathcal{E}_1 + \mathcal{E}_2) \qquad [110]$$

are invariants of unitary basis transformations (Eq. [27]) and have the same magnitude in the GMH and any diabatic basis set. This follows from the invariance property of the matrix trace

$$\sum_i A_{ii} = \text{inv} \qquad [111]$$

and the expression

$$\Delta A_{12}^2 + 4A_{12}^2 = \Delta A_{ab}^2 + 4A_{ab}^2 = \text{inv} \qquad [112]$$

Here "inv" stands for an invariant in respect to transformation consistent with the symmetry of the system. For quantum mechanical operators, this means unitary transformations. The parameter $\Delta e$ in Eq. [107] quantifies the extent of mixing between two adiabatic gas-phase states induced by the interaction with the solvent. For a dipolar solute, it is determined through the adiabatic differential and the transition dipole moments

$$\Delta e = \left[1 + \frac{4m_{12}^2}{\Delta m_{12}^2}\right]^{-1/2} \qquad [113]$$

The differential and transition dipoles can be determined from experiment: the former from the Stark spectroscopy[75,76] and the latter from absorption or emission intensities (see below).

The parameter $\Delta e$ should not be confused with the actual difference in electronic occupation numbers of the two CT states. When the eigenfunctions $\{\tilde{\phi}_+(Y^{ad}), \tilde{\phi}_-(Y^{ad})\}$ corresponding to the eigenstates $F_\pm(Y^{ad})$ are represented as a linear combination of the wave functions of the adiabatic basis, $\{\phi_1, \phi_2\}$,

$$\begin{aligned} \tilde{\phi}_+(Y^{ad}) &= \sqrt{1 - f(Y^{ad})}\phi_1 + \sqrt{f(Y^{ad})}\phi_2 \\ \tilde{\phi}_-(Y^{ad}) &= -\sqrt{f(Y^{ad})}\phi_1 + \sqrt{1 - f(Y^{ad})}\phi_2 \end{aligned} \qquad [114]$$

then the parameter $f(Y^{ad})$ defines the occupation number of the adiabatic state 1 on the lower CT free energy surface at the reaction coordinate $Y^{ad}$. For CT transitions in the normal region, two equilibrium minima are located on the lower CT free energy surface. The occupation number difference in the final and initial states can thus be defined as

$$\Delta z = |1 - f(Y_1^-) - f(Y_2^-)| \qquad [115]$$

where $Y_1^-$ and $Y_2^-$ are two minima positioned on the lower CT surface (Figure 12). In contrast, when transitions between the lower and upper CT surfaces occur in the inverted CT region, the occupation number difference becomes

$$\Delta z = |f(Y^+) - f(Y^-)| \qquad [116]$$

where now $Y^+$ and $Y^-$ define the positions of equilibrium on the upper and lower CT surfaces, respectively (Figure 13). Figure 14 illustrates the difference in the dependence of the occupation number difference on $\Delta e$ in the normal and inverted CT regions. The parameter $\Delta z$ is indeed close to $\Delta e$ for reactions with $|\Delta F_s^I| \ll \lambda^I$. As the absolute value of the equilibrium energy gap increases,

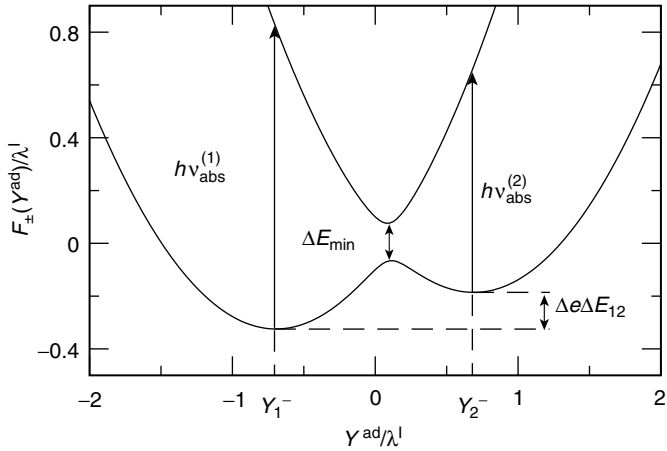


**Figure 12** The CT adiabatic free energy surfaces in the normal CT region. The labels $h\nu_{abs}^{(1)}$ and $h\nu_{abs}^{(2)}$ indicate two adiabatically split absorption transitions corresponding to two minima of the lower surface with the coordinates $Y_1^-$ and $Y_2^-$; $\Delta e = 0.7$, $\Delta F_s^I = 0$, $\Delta E_{12}/\lambda^I = 0.2$. The gap $\Delta E_{min}$ is the minimum splitting between the upper and lower CT surfaces (Eq. [149]).

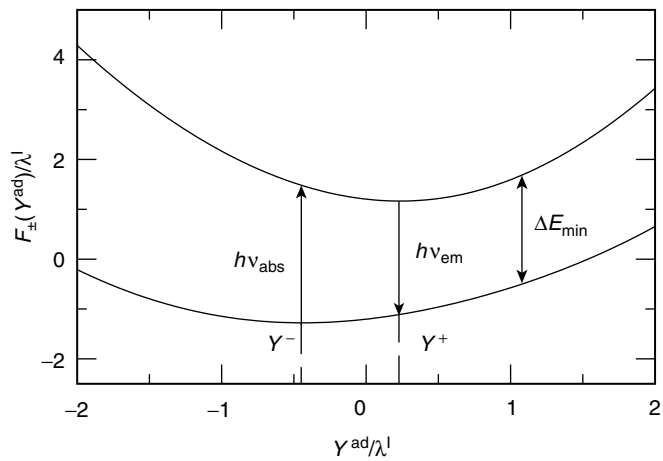


**Figure 13** The CT adiabatic free energy surfaces in the CT inverted region; $\Delta e = 0.7$, $\Delta F_s^I/\lambda^I = -1.0$, $\Delta E_{12}/\lambda^I = 3.0$. The points $Y^-$ and $Y^+$ indicate the minima of the lower and upper adiabatic surfaces, respectively. The labels $h\nu_{abs/em}$ are absorption and emission energies, and $\Delta E_{min}$ is the minimum energy gap between the free energy surfaces (Eq. [149]).

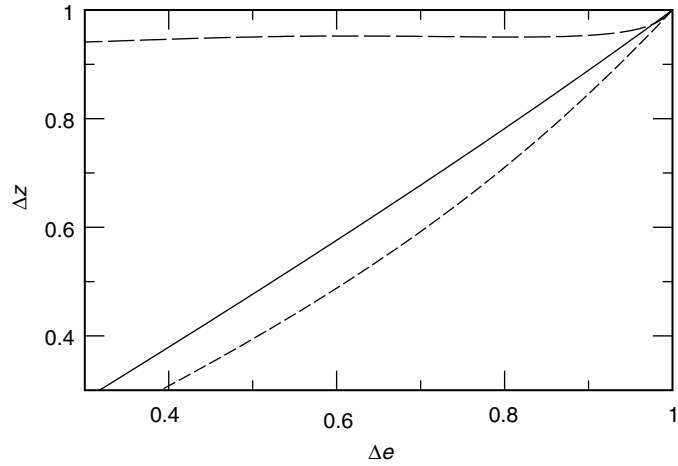


**Figure 14** Dependence of the occupation number difference $\Delta z$ on the mixing parameter $\Delta e$ at $\Delta E_{12}/\lambda^I = 0.2$, $\Delta F_s^I = 0$ (solid line); $\Delta E_{12}/\lambda^I = 0.5$, $\Delta F_s^I = 0$ (dot–dashed line); $\Delta E_{12}/\lambda^I = 3.0$, $\Delta F_s^I/\lambda^I = -1.0$ (dashed line).

$\Delta z$ increasingly deviates from $\Delta e$. In the inverted region, $\Delta z$ is nearly 1 and is almost independent of $\Delta e$.

The establishment of the invariant reorganization energy $\lambda^I$ allows one to use electrostatic models for the reorganization energy based on solvation of fixed charges located at molecular sites[5] instead of using a more complicated algorithm through the delocalized electronic density.[84] This ability to use electrostatic fixed charge models instead of distributed density of quantum mechanics is permitted because the invariant reorganization energy sets up the characteristic length between centers of charge localization to be used in electrostatic models of solvent reorganization[7]

$$r_{CT} = e^{-1}\left[\Delta m_{12}^2 + 4m_{12}^2\right]^{1/2} \qquad [117]$$

For self-exchange transitions, due to the relation $2m_{12} = \Delta m_{ab}$, one gets

$$r_{CT} = \left[r_{12}^2 + r_{ab}^2\right]^{1/2} \qquad [118]$$

where $r_{ab}$ is the distance between the centers of electron localization in the diabatic representation.

The mixing parameter $\Delta e$ makes the CT free energy surfaces dependent on the gas-phase, adiabatic transition dipole moment. The standard extension of the MH theory on the case of strong electronic overlap[85] assumes a nonzero ET matrix element $H_{ab}$, but neglects the diabatic transition dipole (or eliminates

it by choosing the GMH basis set[7]). In this case, the CT free energy surface is defined by Eq. [41] with the following energy gap:

$$\Delta E^{\mathrm{d}}(Y^{\mathrm{d}}) = [\Delta E_{12}^2 + 2\Delta I_{ab}(\Delta F_{\mathrm{s}}^{\mathrm{d}} - Y^{\mathrm{d}}) + (\Delta F_{\mathrm{s}}^{\mathrm{d}} - Y^{\mathrm{d}})^2]^{1/2} \qquad [119]$$

The diabatic and adiabatic formulations can be compared when the condition $\mathcal{E}_{ab} = 0$ is imposed. Then, one obtains $Y^{\mathrm{ad}} = \Delta e Y^{\mathrm{d}}$, $\lambda^I = \lambda^{\mathrm{d}}$, $\Delta F_{\mathrm{s}}^I = \Delta F_{\mathrm{s}}^{\mathrm{d}}$.

Figure 15 compares the free energy surfaces given by Eqs. [105] and [106] to those from Eqs. [41] and [119] for self-exchange CT ($\Delta I_{ab} = 0$, $\Delta F_{\mathrm{s}}^{\mathrm{d}} = \Delta F_{\mathrm{s}}^I = 0$). Several important distinctions between the two formulations can be emphasized. (1) The positions of transition points do not coincide. The maximum of $F_-(Y^{\mathrm{ad}})$ in the present formulation deviates from the position of the resonance of the diagonal elements of the two-state Hamiltonian matrix, $Y^{\ddagger} = 0$, and is approximately equal to $Y^{\ddagger} = (\Delta e)^2 \Delta E_{12}$ when $\Delta E_{12}/\lambda^I \ll 1$ and $\Delta F_{\mathrm{s}}^I = 0$. (2) The splitting of the lower and upper adiabatic surfaces is larger in the MH formulation than in the basis-invariant formulation. For self-exchange CT, the splitting is $2|H_{ab}| = \Delta E_{12}$ in the former case and $\Delta E_{12}\sqrt{1 - \Delta e^2}$ in the latter case. (3) The MH formula involves the diabatic equilibrium free energies $F_{0i}^{\mathrm{d}}$ without donor–acceptor overlap. The gap $\Delta F_0^{\mathrm{d}}$ is therefore zero for self-exchange reactions. The adiabatic representation includes explicitly the donor–acceptor overlap that results in a symmetry-breaking splitting of the gas-phase electronic states to the energy $\Delta E_{12}$.

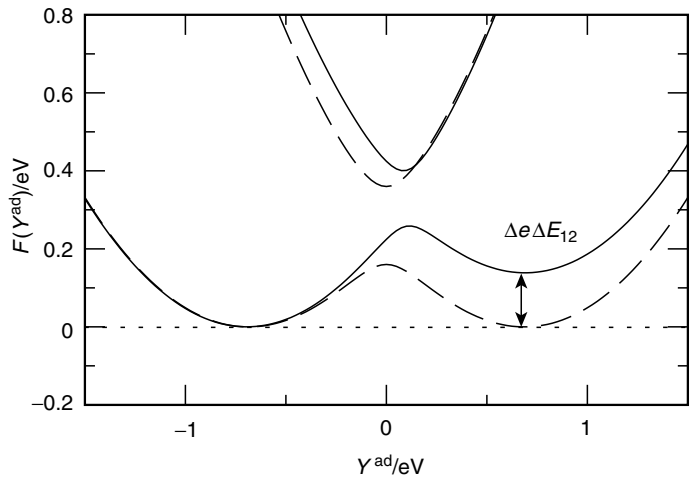


**Figure 15** Adiabatic free energy surfaces $F_{\pm}(Y^{\mathrm{ad}})$ in the present model (solid lines, Eqs. [105] and [106]) and in the Marcus–Hush formulation (long-dashed lines, Eqs. [41] and [119]) for self-exchange CT with $\Delta F_{\mathrm{s}}^I = \Delta F_{\mathrm{s}}^{\mathrm{d}} = 0$, $\lambda^I = \lambda^{\mathrm{d}} = 1$ eV, $\Delta E_{12} = 0.2$ eV, and $\Delta e = 0.7$. All free energy surfaces are vertically shifted to have zero value (dotted line) at the position of the left minimum.

Electronic transitions in the gas phase thus proceed from the lower state $E_1$ to the upper state $E_2$. In condensed phases, these states are of course "dressed" by a solvating environment, but at $\Delta F_s^I = 0$ one gets a nonzero equilibrium driving force approximately equal to $\Delta e \Delta E_{12}$ when $\Delta E_{12}/\lambda^I \ll 1$. The factor $\Delta e$ in the *free energy* driving force appears because the free energy represents the work done to transfer the charge $\Delta e$ ($\Delta z \approx \Delta e$ at $\Delta E_{12}/\lambda^I \ll 1$, see Figure 14) over the energy barrier $\Delta E_{12}$ that results in $\Delta e \Delta E_{12}$ for small splittings $\Delta E_{12}$.

Note above that the GMH[7] and adibatic formulations are equivalent in terms of building the CT free energy surfaces. The distinctions seen in Figure 15 may seem to contradict to this statement. The problem is resolved by noting that the requirement $\mathcal{E}_{ab} = 0$ imposed by the GMH formulation makes the diabatic energy gap nonzero for self-exchange transitions:

$$\Delta I_{ab}^{\mathrm{GMH}} = \Delta e \Delta E_{12} \qquad [120]$$

which is indeed the gap shown in Figure 15. The standard MH formulation[85] is then recovered when $m_{12} = 0$ for symmetry reasons and thus $\Delta e = 1$.

## Nonlinear Solvation versus Intramolecular Effects

The origin of nonparabolic free energy surfaces of ET can be divided into two broad categories: (1) intramolecular electronic effects and (2) nonlinear solvation effects. Although these two origins can, at some instances, be treated within the same mathematical framework (Q model), there are substantial differences between them at both the quantitative and qualitative levels. From the quantitative viewpoint, nonlinear solvation produces a much weaker distortion of ET parabolas than do the polarizability change and electronic delocalization. From a qualitative viewpoint, the two categories of effects produce a nonzero nonparabolic distortion in different orders of the expansion of the system Hamiltonian in the driving solvent mode.

The free energy $F(P)$ invested in creation of a nonequilibrium solvent polarization $P$ can be expressed as a series in even powers of $P$ with the two first terms as follows:

$$F(P) = a_1 P^2 + a_2 P^4 \qquad [121]$$

where $a_1, a_2 > 0$. The interaction energy of the solute field with the solvent polarization, $U_{0s}$, is linear in $P$

$$U_{0s} = -bP \qquad b > 0 \qquad [122]$$

For weak solute–solvent interactions, deviations from zero polarization of the solvent are small, and one can keep only the first, harmonic, term in Eq. [121].

Anharmonic higher order terms gain importance for stronger solute-solvent couplings requiring $a_2 \neq 0$ in Eq. [121]. The nonequilibrium solvent polarization can be considered as an ET reaction coordinate. The curvature of the corresponding free energy surface is

$$F''(P_0) = 2a_1 + 12a_2P_0^2 \qquad [123]$$

at the minimum point $P_0$ defined by the condition $F'(P_0) = b$. Equation [123] indicates that nonlinear solvation effects, usually associated with dielectric saturation, enhance the curvature compared to the linear response result $F'' = 2a_1$. This enhancement of curvature leads to a decrease in the solvent reorganization energy. The effect is, however, relatively small as it arises from anharmonic expansion terms.

When the electron is partially delocalized, one should switch to the adiabatic representation in which the upper and lower CT surface are split by an energy gap depending on $P$. If this energy gap is expanded in $P$ with truncation after the second-order term, we come to the model of a donor–acceptor complex whose dipolar polarizabilities are different in the ground and excited states. The solute–solvent interaction energy then attains the energy of solute polarization that is quadratic in $P$

$$U_{0s} = -bP - cP^2 \qquad c > 0 \qquad [124]$$

The total system energy $F(P) + U_{0s}$ includes, therefore, a quadratic in $P$ term with the coefficient $(a_1 - c)$. This quadratic term initiates a revision of the frequency of solvent fluctuations driving CT. The curvature of harmonic surfaces decreases producing higher reorganization energies. Since the solute polarizability contributes already to the harmonic term, its effect on the reorganization energy is stronger than that of nonlinear solvation.

The revision of characteristic frequencies of nuclear modes is a general result of electronic delocalization holding for both the intramolecular vibrational modes[65] and the solvent modes. The fact that this effect shows up already in the harmonic expansion term makes it much stronger compared to nonlinear solvation in respect to nonparabolic distortion of the free energy surfaces.

## OPTICAL BAND SHAPE

Spectral measurements open a door to access the rate constant parameters of ET. The connection between optical observables and ET parameters can be divided into two broad categories: (1) analysis of the optical band profile (band shape analysis) and (2) the use of integrated spectral intensities (see

below). The former route connects the spectral moments to ET activation parameters (Table 1). The latter is applied to extract off-diagonal matrix elements, most often the ET matrix element and the transition dipole. Band shape analysis of optical spectra has been successfully used in ET research for many years, and our present knowledge about mechanisms and energetics of ET originates largely from spectroscopic measurements.[16] The understanding of electronic and solvent effects on the ET kinetics has been recently supplemented by extensive information about the intramolecular, vibronic envelope from resonance Raman spectroscopy.[86]

The fast growth of the field of ET research and, especially, the design of new bridge-coupled donor–acceptor pairs imposes new demands on the theory of optical spectra. Several major challenges are currently faced by the field. They may be summarized as follows: (1) The presently existing band-shape analysis has been created for ET transitions.[17] It has not anticipated strong electronic coupling and thus fails when applied to transitions with high magnitudes of the ET matrix element.[87] (2) The model is limited to two states only. Mixing to higher excited states, resulting in intensity borrowing, is commonly neglected. Extension to more then two states is especially important for photoinduced CT where a CT state is formed from and is strongly coupled to a locally exited state of either donor or acceptor unit.[17,88] (3) There are indications in the literature that the common assumption of complete decoupling between the intramolecular vibrational modes and solvent thermal motions may fail for some systems.[89,90] Understanding the origin of and full account for these effects should be incorporated into new models of optical bands.

The challenges outlined above still await a solution. In this section, we show how some of the theoretical limitations employed in traditional formulations of the band shape analysis can be lifted. We discuss two extensions of the present-day band shape analysis. First, the two-state model of CT transitions is applied to build the Franck–Condon optical envelopes. Second, the restriction of only two electronic states is lifted within the band shape analysis of polarizable chromophores that takes higher lying excited states into account through the solute dipolar polarizability. Finally, we show how a hybrid model incorporating the electronic delocalization and chromophore's polarizability effects can be successfully applied to the calculation of steady-state optical band shapes of the optical dye coumarin 153 (C153). We first start with a general theory and outline the connection between optical intensities and the ET matrix element and transition dipole.

## Optical Franck–Condon Factors

Absorption of light by molecules, resulting in electronic excitations, is caused by the interaction of the bound molecular electrons with the electric field of the radiation. In the dipolar approximation, the interaction of the dipole operator of the solute $\hat{\mathbf{m}}_0$ with the time-dependent electric field $\mathbf{E}(t)$

of the radiation is the perturbation that drives the electronic excitation. The time-dependent interaction Hamiltonian is

$$-f(n_D)\,\hat{\mathbf{m}}_0 \cdot \mathbf{E}(t) \qquad [125]$$

where the parameter $f(n_D)$ accounts for the deviation of the local field acting on the solute dipole from the external field $\mathbf{E}(t)$; $n_D$ is the solvent refractive index. Dielectric theories[91] predict for spherical cavities

$$f(n_D) = \frac{3n_D^2}{2n_D^2 + 1} \qquad [126]$$

The perturbation given by Eq. [125] mixes the electronic states for which the off-diagonal matrix element of the dipole operator, $m_{jk}$, is nonzero. The latter is called the transition dipole.[49] Mixing of electronic states by a time-dependent external field leads to the dependence of the corresponding electronic state populations on time. The rate constant of the population kinetics is given by the transition probability. Quantum mechanical perturbation theory, limited to the first order in the interaction perturbation, is commonly used to calculate the one-photon transition probability and absorption intensity.[15,92] This formalism, combined with the Einstein relation between absorption intensity and the probability of spontaneous emission,[49,92] leads to experimental observables, the extinction coefficient of absorption, $\epsilon(\nu)$ ($cm^{-1}\ M^{-1}$), and the emission rate, $I_{em}(\nu)$ (number of photons per unit frequency), as functions of the light frequency $\nu$. They are given by the following relations:

$$\frac{\epsilon(\nu)}{\nu} = \frac{8\pi^3 N_A}{3000\,(\ln 10)\,c}\frac{f^2(n_D)}{n_D}G_-(\nu) \qquad [127]$$

and

$$I_{em}(\nu) = \frac{64\pi^4\nu^3}{3c^3}n_D f^2(n_D)G_+(\nu) \qquad [128]$$

In Eq. [127], $N_A$ is the Avogadro number, and $c$ in Eqs. [127] and [128] is the speed of light in vacuum.

The extinction coefficient and emission rate are defined through the spectral density function $G_\pm(\nu)$ that combines the effects of solvent-induced inhomogeneous broadening and vibrational excitations of the donor–acceptor complex. A substantial simplification of the description can be achieved if the two types of nuclear motions are not coupled to each other. The spectral density $G_\pm(\nu)$ is then given by the convolution[17]

$$G_\pm(\nu) = |\tilde{m}_{12}(h\nu)|^2 \int \mathrm{FCWD}_\pm^s(x)\mathrm{FCWD}_\pm^v(\nu - x)dx \qquad [129]$$

of the gas-phase vibronic envelope $\mathrm{FCWD}^{\mathrm{v}}_{\pm}(\nu)$ with the normalized solvent-induced band shape

$$\mathrm{FCWD}^{\mathrm{s}}_{\pm}(\nu) = \langle \delta(\Delta E(\mathbf{q}) - h\nu) \rangle_{\pm} \qquad [130]$$

where the average is taken over the solvent configurations statistically weighted with the Boltzmann factor $\exp(-\beta F_{\pm})$ with "$-$" for absorption and "$+$" for emission.

In Eqs. [129] and [130], $\mathrm{FCWD}^{\mathrm{v}}_{\pm}(\nu)$ and $\mathrm{FCWD}^{\mathrm{s}}_{\pm}(\nu)$ refer to the normalized Franck–Condon weighted density of the vibrational excitations of the solute (including quantum overlap integrals of the vibrational normal modes of the solute coupled to the transferred electron[17]) and the normalized solvent-induced spectral distribution function, respectively. The gap, $\Delta E(\mathbf{q}) = E_{+}(\mathbf{q}) - E_{-}(\mathbf{q})$, in Eq. [130] is defined between the upper adiabatic surface $E_{+}(\mathbf{q})$ and the lower adiabatic surface $E_{-}(\mathbf{q})$ depending on a set of nuclear solvent modes $\mathbf{q}$. Because the transitions occur between the adiabatic free energy surfaces $E_{\pm}(\mathbf{q})$, the unperturbed basis set in the quantum mechanical perturbation theory is built on the wave functions $\{\tilde{\phi}_1(\mathbf{q}), \tilde{\phi}_2(\mathbf{q})\}$ diagonalizing the corresponding two-state Hamiltonian matrix (Eq. [114]). The dependence on the nuclear solvent configuration comes into the transition dipole moment (as calculated within the two-state model, TSM)

$$\begin{aligned} |\tilde{m}_{12}(\mathbf{q})| &= |\langle \tilde{\phi}_1(\mathbf{q}) | \hat{\mathbf{m}}_0 | \tilde{\phi}_2(\mathbf{q}) \rangle| \\ &= |m_{12}| \frac{\Delta E_{12}}{\Delta E(\mathbf{q})} \end{aligned} \qquad [131]$$

only through the energy gap $\Delta E(\mathbf{q})$, which is equal to $h\nu$ according to Eq. [130]. This relationship is the reason for the dependence of the transition dipole on the light frequency in Eq. [129]. Coupling to higher lying excited states modifies Eq. [131], but if the dependence on the solvent field comes into $\tilde{m}_{12}(\mathbf{q})$ only through the instantaneous energy gap, the transition dipole can still be taken out of the solvent average with, however, a more complicated dependence on the frequency of the incident light.[17,93] In the TSM, one has, according to Eq. [131]

$$\tilde{m}_{12}(\nu) = m_{12} \Delta E_{12} / h\nu \qquad [132]$$

where $m_{12}$ is the gas-phase adiabatic transition dipole moment.

The vibronic envelope $\mathrm{FCWD}^{\mathrm{v}}_{\pm}(\nu)$ in Eq. [129] can be an arbitrary gas-phase spectral profile. In condensed-phase spectral modeling, one often simplifies the analysis by adopting the approximation of a single effective vibrational mode (Einstein model) with the frequency $\nu_{\mathrm{v}}$ and the vibrational reorganization energy $\lambda_{\mathrm{v}}$. The vibronic envelope is then a Poisson distribution of

individual vibrational excitations[44]

$$\mathrm{FCWD}^{\mathrm{v}}_{\pm}(\nu) = e^{-S_{\mathrm{v}}} \sum_{m=0}^{\infty} \frac{S_{\mathrm{v}}^{m}}{m!} \delta(h\nu \pm mh\nu_{\mathrm{v}}) \qquad [133]$$

where $S_{\mathrm{v}}$ the Huang–Rhys factor $S_{\mathrm{v}} = \lambda_{\mathrm{v}}/h\nu_{\mathrm{v}}$ (cf. to Eq. [38]). The whole inhomogeneous line shape then takes the form of a weighed sum over the solvent-induced bands, each shifted relative to the other by $\nu_{\mathrm{v}}$

$$G_{\pm}(\nu) = |\tilde{m}_{12}(h\nu)|^2 e^{-S_{\mathrm{v}}} \sum_{m=0}^{\infty} \frac{S_{\mathrm{v}}^{m}}{m!} \mathrm{FCWD}^{\mathrm{s}}_{\pm}(\nu \pm mh\nu_{\mathrm{v}}) \qquad [134]$$

Equation [134], given in the form of a weighted sum of individual solvent-induced line shapes, provides an important connection between optical band shapes and CT free energy surfaces. Before turning to specific models for the Franck–Condon factor in Eq. [134], we present some useful relations, following from integrated spectral intensities, that do not depend on specific features of a particular optical line shape.

## Absorption Intensity and Radiative Rates

Extraction of activation CT parameters requires an analysis of spectral band shapes. One parameter, however, can be obtained from the integrated absorption and emission intensities. Since mixing of the electronic states in the external electric field of radiation is governed by the magnitude of the transition dipole, the transition dipole also defines the intensity of the corresponding optical line. The extinction coefficient or emission rate integrated over light frequencies then allows one to obtain the transition dipole, provided its frequency dependence is known. [Traditionally, the transition dipole is assumed to be frequency independent.[49] This leads, however, to systematic errors in estimates of transition dipoles from optical spectra, see below.] For the TSM, this procedure leads to the gas-phase transition dipole. The transition dipole is important as a parameter quantifying the extent of CT delocalization and to generate CT free energy surfaces in electronically delocalized donor–acceptor complexes. It also has an important implication due to its connection to the ET matrix element (through the Mulliken-Hush relation),[7] which enters the rate constant of nonadiabatic ET reaction rates (Eq. [2]; see below).

Integration of absorption extinction coefficient (Eq. [127]) and emission rate (Eq. [128]) gives two alternative estimates for the adiabatic gas-phase transition dipole $m_{12}$ (in D) within the TSM frequency-dependent $\tilde{m}_{12}(\nu)$ (Eq. [132])

$$m_{12} = 9.585 \times 10^{-2} \frac{\sqrt{n_{\mathrm{D}}}}{\bar{\nu}_0 f(n_{\mathrm{D}})} \left[ \int \bar{\nu} \epsilon(\bar{\nu}) d\bar{\nu} \right]^{1/2} \qquad [135]$$

and

$$m_{12} = 3.092 \times 10^8 [\bar{\nu}_0 \sqrt{n_D} f(n_D)]^{-1} \left[ \int I_{em}(\nu) \nu^{-1} d\nu \right]^{1/2} \quad [136]$$

where $\bar{\nu}$ is the wavenumber ($cm^{-1}$) and $\bar{\nu}_0 = \Delta E_{12}/hc$. When the emission spectrum is not available, the radiative rate[49]

$$k_{rad} = \int I_{em}(\nu) d\nu = \Phi_{em} \tau_{em}^{-1} \quad [137]$$

can be used; $\Phi_{em}$ and $\tau_{em}$ are the quantum yield and emission lifetime. By defining the average frequency

$$\nu_{av} = \int I_{em}(\nu) d\nu \Big/ \int I_{em}(\nu) \nu^{-1} d\nu \quad [138]$$

one gets

$$m_{12} = 1.786 \times 10^3 \left[ \frac{k_{rad}}{\bar{\nu}_{av} \bar{\nu}_0^2 n_D f^2(n_D)} \right]^{1/2} \quad [139]$$

Equation [139] is not very practical because an accurate definition of the average wavenumber, $\bar{\nu}_{av} = \nu_{av}/c$, demands knowledge of the emission spectrum for which Eq. [136] provides a direct route to the transition dipole. But Eq. [139] can be used in approximate calculations by assuming $\bar{\nu}_{av} = \bar{\nu}_{em}$.

Equation [139] is exact for a two-state solute, but differs from the traditionally used connection between the transition dipole and the emission intensity by the factor $\bar{\nu}_0/\bar{\nu}_{av}$.[49] The commonly used combination $m_{12}\bar{\nu}_0/\bar{\nu}_{av}$ appears as a result of neglect of the frequency dependence of the transition dipole $\tilde{m}_{12}(\nu)$ entering Eq. [129]. It can be associated with the condensed-phase transition dipole in the two-state approximation.[43] Exact solution for a two-state solute makes the transition dipole between the adiabatic free energy surfaces inversely proportional to the energy gap between them. This dependence, however, is eliminated when the emission intensity is integrated with the factor $\nu^{-1}$.[93]

The transition dipole $m_{12}$ in Eqs. [136] and [139] is the gas-phase adiabatic transition dipole. Therefore, emission intensities measured in different solvents should generate invariant transition dipoles when treated according to Eqs. [136] and [139]. A deviation from invariance can be used as an indication of the breakdown of the two-state approximation and the existence of intensity borrowing from other excited states of the chromophores (the Murrell mechanism[17,88,94]). Figure 16 illustrates the difference between Eq. [139] and

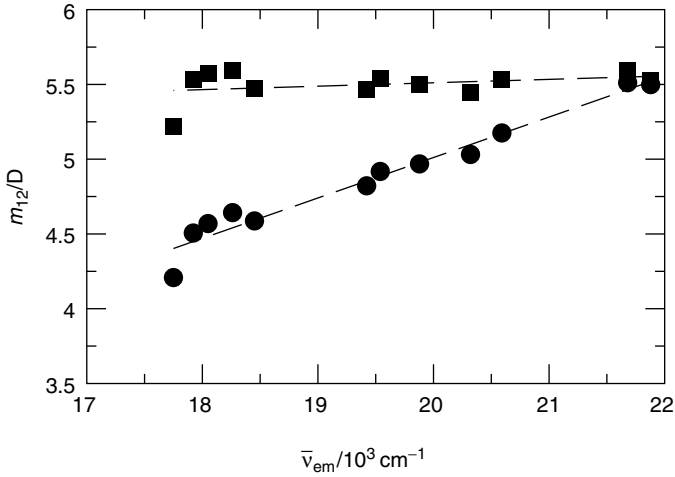


**Figure 16** The transition dipole $m_{12}$ according to Eq. [139] ($\bar{\nu}_{av} = \bar{\nu}_{em}$, circles) and $m_{12}\bar{\nu}_0/\bar{\nu}_{em}$ (squares) versus $\bar{\nu}_{em}$ for emission transitions in C153 in different solvents.[95] The dashed lines are regressions with the slopes 0.02 (squares) and 0.27 (circles).

the traditional formulation. It shows the dependence of $m_{12}$ (circles) and $m_{12}\bar{\nu}_0/\bar{\nu}_{av}$ (squares, $\bar{\nu}_0 = 25{,}400\ cm^{-1}$) on the emission frequency $\bar{\nu}_{em}$ for the dye C153 measured in solvents of different polarity.[95] The two sets of transition dipoles are noticeably divergent in strongly polar solvents.

## Electron-Transfer Matrix Element

The transition dipole between the free energy surfaces $F_{\pm}(X)$ is not the only parameter that depends on the nuclear configuration of the solvent. The effective ET matrix element $H_{ab}^{\text{eff}}[\mathcal{P}_n]$ following from the trace of the two-state Hamiltonian over the electronic degrees of freedom also depends on the nuclear configuration of the solvent (Eq. [37]). In contrast to the case of optical transitions where the dependence on the nuclear solvent configurations is transformed into a frequency dependence of the transition dipole $\tilde{m}_{12}(\nu)$ (Eq. [132]), the dependence of the ET matrix element $H_{ab}^{\text{eff}}[\mathcal{P}_n]$ on the nuclear field $\mathcal{P}_n$ should be fully included into the statistical average over $\mathcal{P}_n$ when the ET rate constant is calculated in the Golden Rule perturbation scheme over $H_{ab}^{\text{eff}}[\mathcal{P}_n]$.[11] The $\mathcal{P}_n$ dependence represents a non-Condon effect of the solvent field on the rate preexponential factor. The result of the calculations[43] is the standard Golden Rule expression[9,11] for the nonadiabatic rate constant

$$k_{NA}^{(i)} = \hbar^{-1}(\pi\beta/\lambda)^{1/2}\left|H^{MH}\right|^2 FCWD_i(0) \qquad [140]$$

with the Mulliken–Hush[6] ET matrix element

$$H^{\mathrm{MH}} = H_{ab} - \frac{(\mathbf{m}_{ab} \cdot \Delta\mathbf{m}_{ab})}{\Delta m_{ab}^2} \Delta I_{ab} \qquad [141]$$

where $\mathbf{m}_{ab}$ and $\Delta\mathbf{m}_{ab}$ refer to, respectively, the gas-phase transition and differential dipole moments calculated in the diabatic basis set; $\Delta I_{ab}$ is the diabatic gas-phase energy gap. The term Mulliken–Hush[6] here refers to the fact that the matrix element in Eq. [141] is related to the projection of the adiabatic transition dipole on the direction of the difference diabatic dipole

$$H^{\mathrm{MH}} = \frac{(\mathbf{m}_{12} \cdot \Delta\mathbf{m}_{ab})}{\Delta m_{ab}^2} \Delta E_{12} \qquad [142]$$

Under the special condition that $\mathbf{m}_{12}$ and $\Delta\mathbf{m}_{ab}$ are parallel, one obtains the MH relation[6,7]

$$H^{\mathrm{MH}} = \frac{m_{12}}{\Delta m_{ab}} \Delta E_{12} \qquad [143]$$

Equations [140]–[143] provide a connection between the preexponential factor entering the nonadiabatic ET rate and the spectroscopically measured adiabatic transition dipole $m_{12}$. It turns out that the Mulliken–Hush matrix element, commonly considered as an approximation valid for $m_{ab} = 0$,[7] enters exactly the rate constant preexponent as long as the non-Condon solvent effects are accurately taken into account.[43] Equation [142] stresses the importance of the orientation of the adiabatic transition dipole relative to the direction of ET set up by the difference diabatic dipole $\Delta\mathbf{m}_{ab}$. The value of $H^{\mathrm{MH}}$ is zero when the vectors $\mathbf{m}_{12}$ and $\Delta\mathbf{m}_{ab}$ are perpendicular.

## Electronically Delocalized Chromophores

Equation [48] gives the Franck–Condon factor that defines the probability of finding a system configuration with a given magnitude of the energy gap between the upper and lower CT free energy surfaces. It can be directly used to define the solvent band shape function[96] of a CT optical transition in Eq. [134]

$$\mathrm{FCWD}_{\pm}^{\mathrm{s}}(\nu \pm mh\nu_{\mathrm{v}}) = Q_{\pm}^{-1} \sum_{k=1,2} |\Delta E'(Y_{km})|^{-1} \exp[-\beta F_{\pm}(Y_{km})] \qquad [144]$$

where

$$Q_{\pm} = \int e^{-\beta F_{\pm}(Y^{\mathrm{ad}})} dY^{\mathrm{ad}} \qquad [145]$$

In Eq. [144], the coordinates $Y_{km}$ $(k = 1, 2)$ are two roots of the quadratic equation

$$\Delta E(Y^{\mathrm{ad}}) = h(\nu \pm m\nu_{\mathrm{v}}) \qquad [146]$$

given by the expression

$$\begin{aligned} Y_{1m} &= Y_{\min} + \Delta e\sqrt{h^2(\nu \pm m\nu_{\mathrm{v}})^2 - \Delta E_{\min}^2} \\ Y_{2m} &= Y_{\min} - \Delta e\sqrt{h^2(\nu \pm m\nu_{\mathrm{v}})^2 - \Delta E_{\min}^2} \end{aligned} \qquad [147]$$

The appearance of the square root in Eq. [147] is an indication of one important feature of delocalized CT systems: the existence of a lower limiting frequency of the incident light that can be absorbed by a donor–acceptor complex. This effect results in asymmetries of CT absorption and emission lines as discussed below.

A real root of Eq. [146] exists only if the following condition holds:

$$h\nu \geq \pm mh\nu_{\mathrm{v}} + \Delta E_{\min} \qquad [148]$$

for a vibronic transition with $m$ phonons of vibrational excitation. The 0–0 transition ($m = 0$) sets up the absolute minimum frequency

$$h\nu_{\min} = \Delta E_{\min} = \sqrt{1 - \Delta e^2}\Delta E_{12} \qquad [149]$$

where $\Delta e$ is the gas-phase mixing parameter (Eq. [107]), and $\Delta E_{12}$ is the gas-phase adiabatic energy gap (Eq. [29]). The energy $\Delta E_{\min}$ corresponds to the minimum splitting between the upper and lower CT free energy surfaces (Figures 12 and 13) that occurs at the coordinate

$$Y_{\min} = \Delta e^2 \Delta E_{12} + \Delta e \Delta F_{\mathrm{s}}^{\mathrm{I}} \qquad [150]$$

The transition intensity is always zero at $\nu < \nu_{\min}$. The existence of the lower transition boundary makes a profound effect on optical band shapes for a large extent of mixing of adiabatic states. The general effect of the existence of the minimum frequency on optical lines is to produce line asymmetry by squeezing its red wing.[20,97] We consider here this effect for the example of transitions in the inverted CT region when both the absorption and emission lines can be observed (Figure 13). For positively solvatochromic dyes with a major multipole higher in the excited state than in the ground state, emission lines are shifted more strongly to the red side of the spectrum than the absorption lines. Therefore, the emission lines are closer to the low-energy boundary $\nu_{\min}$

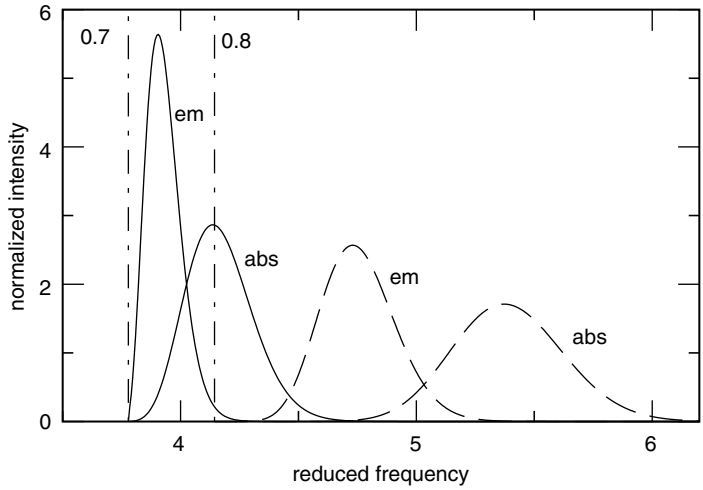


**Figure 17** The normalized absorption (abs.) and emission (em.) intensities at $\Delta e = 0.7$ (solid lines) and $\Delta e = 0.8$ (long-dashed lines) versus the reduced frequency $h\nu/\lambda^I$. The dash–dotted lines indicate the lower boundary for the energy of the incident light $\nu_{min}$ (Eq. [149]).

and get narrower than the absorption lines (Figure 17). The opposite trend holds for negatively solvatochromic dyes with higher major multipoles in their ground states.

The lower free energy surface has two minima in the normal CT region (Figure 12). Two absorption transitions exist in this case, even for self-exchange reactions. The reason is the symmetry breaking induced by a non-zero adiabatic transition dipole leading to $\Delta e < 1$ (the standard MH picture, Figure 15, is recovered when $m_{12} = 0$). The energy splitting between the two minima of the lower free energy surface gives rise to two transition frequencies

$$h\nu_{abs}^{(1)} = \lambda_v + \lambda^I + \Delta F_s^I + \Delta e \Delta E_{12} \qquad [151]$$

and

$$h\nu_{abs}^{(2)} = \lambda_v + \lambda^I - \Delta F_s^I - \Delta e \Delta E_{12} \qquad [152]$$

The combination of Eq. [134] with Eq. [144] provides an effective formalism for the band shape analysis of CT spectra when a substantial degree of electronic delocalization is involved. Equation [134] is exact for a TS donor–acceptor complex and, therefore, can be used for an arbitrary degree of electronic delocalization as long as the assumption of decoupling of the vibrational and solvent modes holds. Figure 18 illustrates the application of the band shape

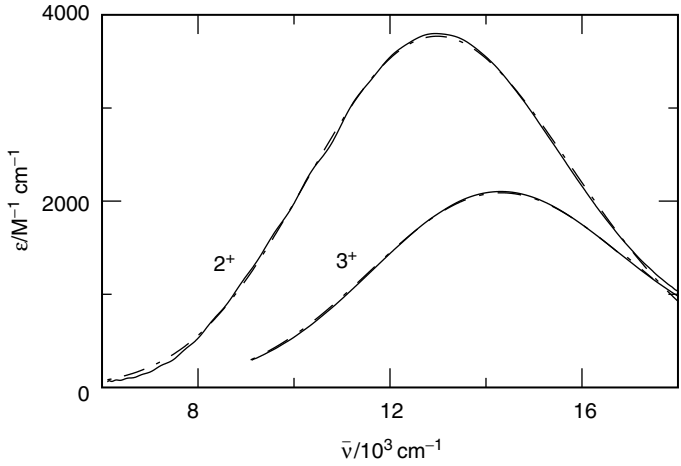


**Figure 18** Fits of experimental spectra in acetonitrile (solid lines)[87] to Eqs. [134] and [144] (dash–dotted lines, almost indistinguishable from the experimental spectra on the graph scale). The labeling of the donor–acceptor complexes is according to Ref. 87.

analysis via Eqs. [134] and [144] to two CT complexes studied in Ref. 87 when the traditional band shape analysis[16,17] fails to fit the experimental spectra. The fitting procedure employs the simulated annealing technique in the space of four parameters: $\lambda^I$, $\lambda_v$, $\nu_v$, and $\Delta E_{12}$.

## Polarizable Chromophores

The model of polarizable dipolar chromophores suggests that the 3D nuclear reaction field of the solvent serves as a driving force for electronic transitions. Even in the case of an isotropic solute polarizability, two projections of the reaction field should be included: the longitudinal (parallel to the difference solute dipole) component and the transverse (perpendicular to the difference dipole) component. The δ function in Eq. [18] eliminates integration over only one of these two field component. The integral still can be taken analytically resulting in a closed-form solution for the Franck–Condon factor

$$\mathrm{FCWD}_i^s(\nu) = \beta A_i \sqrt{\frac{\lambda_i |\alpha_i|^3}{|h\nu - X_0|}} e^{-\beta(|\alpha_i||h\nu - X_0| + \lambda_i \alpha_i^2)} I_1\left(2\beta\sqrt{|\alpha_i|^3 \lambda_i |h\nu - X_0|}\right) \quad [153]$$

where $I_1(x)$ is the first-order modified Bessel function. The normalization factor

$$A_i = (1 - e^{-\beta\lambda_i\alpha_i^2})^{-1} \quad [154]$$

is included to ensure the identity

$$h\int_{-\infty}^{\infty} \mathrm{FCWD}_i^s(h\nu)d\nu = 1 \qquad [155]$$

In Eq. [153], the parameters $\alpha_i$ are given by Eqs. [74] and [99]. The reorganization energies are defined through the second spectral cumulants and are connected to each other according to Eq. [73]. The boundary of the permissible energy gaps between the two-electron states sets up the range of light frequencies for which the transition intensity is nonzero. The magnitude of the spectral boundary is defined for dipolar chromophores through the difference dipole moment and the polarizability difference

$$X_0 = \Delta I + \Delta E^{\mathrm{disp}} + \Delta F^{\mathrm{ind}} - \frac{\Delta\tilde{m}_0^2}{2|\Delta\tilde{\alpha}_0|} \qquad [156]$$

where $\Delta E^{\mathrm{disp}}$ and $\Delta F^{\mathrm{ind}}$ are the differences in dispersion and induction stabilization energies between the two states. When the polarizability does not change with the transition ($\Delta\alpha_0 = 0$), the spectral boundary moves to infinity, $X_0 \to \infty$, and no limiting frequency exists.

The Franck–Condon factors of polarizable chromophores in Eq. [153] can be used to generate the complete vibrational/solvent optical envelopes according to Eqs. [132] and [134]. The solvent-induced line shapes as given by Eq. [153] are close to Gaussian functions in the vicinity of the band maximum and switch to a Lorentzian form on their wings. A finite parameter $\alpha_1$ leads to asymmetric bands with differing absorption and emission widths. The functions in Eq. [153] can thus be used either for a band shape analysis of polarizable optical chromophores or as probe functions for a general band shape analysis of asymmetric optical lines.

## Hybrid Model

Both electronic delocalization and polarizability of the donor–acceptor complex lead to a significant asymmetry between the absorption and emission optical lines as is often observed in experiment.[66,98,99] The importance of this effect can be assessed by comparing the dependence of the observed spectral width on solvent polarity with the prediction of MH theory. Equations [6] and [12] can be combined to give

$$\beta h^2\langle(\delta\nu)^2\rangle_{\mathrm{abs/em}} = h\Delta\nu_{\mathrm{st}} + \lambda_{\mathrm{v}}(\beta h\nu_{\mathrm{v}} - 2) \qquad [157]$$

The MH theory thus predicts that the absorption and emission widths are equal to each other (Eq. [11]) and are linear functions of the Stokes shift

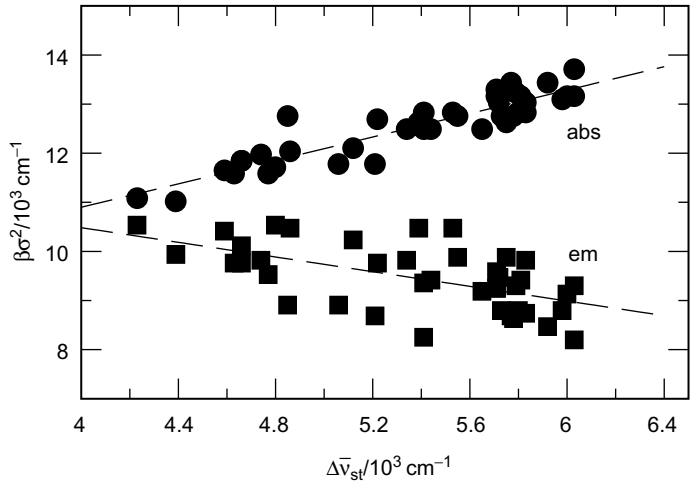


**Figure 19** Absorption (circles) and emission (squares) widths (Eq. [80]) versus the Stokes shift for the coumarin dye C153 in 40 molecular solvents according to Ref. 99. The dashed lines are regressions drawn to guide the eye.

$h\Delta\nu_{st}$ with unit slope. This prediction can be dramatically violated for some optical dyes. An illuminating example of such a breakdown is the steady-state spectroscopy of C153 (Figure 19; data according to Ref. 99). The spectral widths in Figure 19 are obtained from half-intensity widths $\Gamma_{abs/em}$ according to Eq. [81] (in Eq. [81], $i = 1$ and $i = 2$ stand for absorption and emission, respectively). As is seen from Figure 19, not only do the spectral widths differ, but also the slopes of $\sigma^2_{abs/em}$ versus $h\Delta\nu_{st}$ have different signs for absorption and emission transitions. This phenomenon is actually well explained by considering a combined effect of the dye polarizability and the electronic coupling between the ground and excited electronic states on the optical band shape.

Within the TSM, the emission width is lower than the absorption width for electronic transitions with a higher magnitude of the dipole moment in the excited state compared to the ground state, as is seen in Figure 17. This is indeed the feature observed in Figure 19. Despite this qualitative agreement, the TSM is very unrealistic due to the neglect of excited electronic states of the chromophore, leading, for example, to a negative excited state polarizability. The polarizability of the excited state of essentially all known chromophores is, on the contrary, positive, and, in the majority of cases, is higher than that of the ground state.[69] To incorporate correctly the chromophore polarizability on the one hand and generate explicit electronic delocalization on the other, a hybrid model was developed.[100] The two states participating in the transition are explicitly considered. Transitions to all other excited states of the chromophore are assumed to result in polarization of the electron density defined by the dipolar polarizability $\bar{\alpha}_{0i}$ $(i = 1, 2)$. The total vacuum

polarizability of the solute, $\alpha_{0i}$, treated as input available from experiment or independent calculations, is thus split into the polarizability from the $1 \leftrightarrow 2$ transition and the component $\bar{\alpha}_{0i}$ from all other transitions. The solvent effect on the transition between the states 1 and 2 then includes three components: (1) solvation of the fixed charges (dipole moments) of the chromophore, (2) self-polarization of the solute's electronic cloud due to polarizability, and (3) change in the electronic occupation numbers induced by the off-diagonal coupling of the transition dipole to the solvent field.

Figure 20 compares the solvent-induced FCWD calculated in the TSM (dash–dotted lines, Eq. [144]), the polarizable model (dashed line, Eq. [153]), and the hybrid model (solid lines). The latter incorporates the effects of both the electronic delocalization between the ground and excited states and polarizability due to the coupling of these two states to all other excited states of the chromophore. The latter model was called the adiabatic polarizable model (APM).[100] The APM thus includes the linear and all nonlinear polarizabilities arising from transitions between the ground and excited states and only linear polarizability for all other states. The emission line is broader than the absorption line due to a higher excited state polarizability when electron delocalization is neglected (Figure 20, dashed lines). The inclusion of electronic delocalization through the transition dipole narrows the emission line and reduces the maxima separation (APM, solid lines). Finally, the neglect of polarizability from higher lying electronic states in the TSM (dash–dotted lines) generates an even narrower emission band. The line shape is therefore a result of a compensation between the polarizability effect tending to increase both the emission width and the Stokes shift for $\Delta\alpha_0 > 0$ and the opposite effect of electronic delocalization.

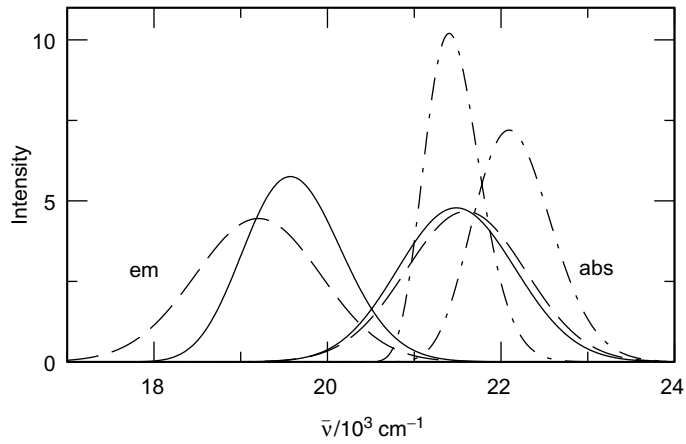


**Figure 20** Absorption (abs.) and emission (em.) solvent-induced FCWD of C153 in acetonitrile calculated according to the APM model (solid lines), the TSM (dash–dotted lines), and the polarizable model (Eq. [153], dashed lines).

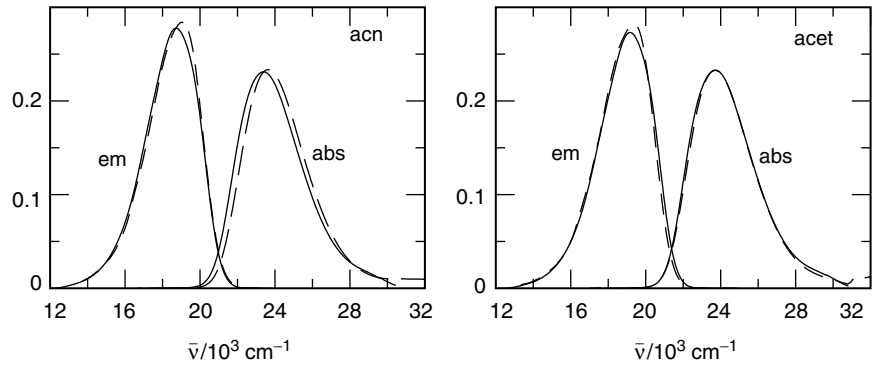


**Figure 21** Normalized experimental (dashed lines) and calculated (solid lines) absorption (abs.) and emission (em.) spectra of C153 in acetonitrile (acn) and acetone (acet).

The application of the APM model to the absorption and emission spectra of C153 gives good agreement with experimentally observed spectra in a broad range of solvent polarities.[100] The quality of the calculations is illustrated in Figure 21 where the experimental (dashed lines) and calculated (solid lines) absorption and emission spectra are compared for acetonitrile and acetone as the solvent. The distinction between the optical band shapes calculated on various levels of the theory shown in Figure 20 and the excellent agreement with the experimental results shown in Figure 21 indicate that transitions to higher excited states (polarizability) and solvent-induced mixing between the adiabatic states (transition dipole) are both crucial for reproducing the optical band shape of C153. For this chromophore, the electronic mixing effect is significant due to its high transition dipole moment, $m_{12} = 5.78$ D, close in magnitude to the difference in the excited- and ground-state dipole moments, $\Delta m_0 \approx 7.5$ D. Depending on the relative magnitudes of the polarizability change, $\Delta\alpha_0$, and the transition dipole, $m_{12}$, polarizability and electronic mixing effects may become more or less important for other optical dyes. For all such cases, the APM provides a general framework for analyzing the FCWD of activated and optical transitions by lifting the two restrictions of the MH theory: the TSM and the neglect of electronic overlap in the FCWD (assumptions 1 and 2 in the Introduction). In fact, the APM also provides a general framework for analyzing the effects of coupling between the vibrational solute modes and the solvent fluctuations (assumption 3),[100] but this problem still requires further studies, both experimental and theoretical.

## SUMMARY

The concept of free energy surfaces has proven its vitality over many years of fruitful applications to electron transfer kinetics. The direct connection

of the ET free energy surfaces to the solvent-induced component of the optical Franck–Condon provides a unique possibility to apply the statistical mechanical analysis of ET and CT energetics and to test it on experiment. The band shape analysis of optical profiles is thus the key factor in a successful interplay between theory and experiment.

This chapter outlines some recent advances in the statistical mechanical analysis of the CT energetics. The basic strategy used in this approach is to introduce new physical features of CT activation into the system Hamiltonian used to build the free energy surfaces. These are then applied to calculate the Franck–Condon factors and determine how the changes in the physics of the problem affect the optical observables. This development highlights two fundamental results. First, the MH model of fixed charges solvated in a dense, condensed-phase environment leads to a very accurate representation of the ET energetics in terms of two intersecting parabolas. The static nonlinear solvation effects are generally weak and do not substantially distort the parabolas. There is, however, ample room to modify the free energy surfaces when changes in the electronic density of the donor–acceptor complex are allowed either through polarizability or electronic delocalization. The CT free energies then inherit nonlinear features, and a number of interesting consequences for optical observables can be anticipated. These fascinating phenomena will be the subject of future research.

## ACKNOWLEDGMENTS

D.V.M. acknowledges the support by the Department of Chemistry and Biochemistry at ASU and partial support by the Petroleum Research Fund, administered by the American Chemical Society, (36404-G6). G.A.V. acknowledges support from the Department of Energy, Basic Energy Sciences Program.

## REFERENCES

1. R. A. Marcus, *Adv. Chem. Phys.,* **106,** 1 (1999). Electron Transfer Past and Future.
2. P. F. Barbara and W. Jarzeba, *Adv. Photochem.,* **15,** 1 (1990). Ultrafast Photochemical Intramolecular Charge and Excited State Solvation.
3. B. Bagchi and N. Gayathri, *Adv. Chem. Phys.,* **107,** 1 (1999). Interplay Between Ultrafast Polar Solvation and Vibrational Dynamics in Electron Transfer Reactions: Role of High-Frequency Vibrational Modes.
4. B. Bagchi and R. Biswas, *Adv. Chem. Phys.,* **109,** 207 (1999). Polar and Nonpolar Solvation Dynamics, Ion Diffusion, and Vibrational Relaxation: Role of Biphasic Solvent Response in Chemical Dynamics.
5. F. O. Raineri and H. L. Friedman, *Adv. Chem. Phys.,* **107,** 81 (1999). Solvent Control of Electron Transfer Reactions.
6. N. S. Hush, *Progr. Inorg. Chem.,* **8,** 391 (1967). Intervalence-Transfer Absorption. Part 2. Theoretical Considerations and Spectroscopic Data. See also, R. S. Mulliken and W. B. Person, *Molecular Complexes,* Wiley, New York, 1969.

7. M. D. Newton, *Adv. Chem. Phys.,* **106,** 303 (1999). Control of Electron Transfer Kinetics: Models for Medium Reorganization and Donor–Acceptor Coupling.
8. J. J. Regan and J. N. Onuchic, *Adv. Chem. Phys.,* **107,** 303 (1999). Electron-Transfer Tubes.
9. L. D. Landau and E. M. Lifshits, *Quantum Mechanics,* Pergamon, Oxford, UK, 1965.
10. A. M. Kuznetsov, *Charge Transfer in Chemical Reaction Kinetics,* Presses Polytechniques et Universitaires Romandes, Lausanne, Switzerland, 1997.
11. J. Ulstrup, *Charge Transfer Processes in Condensed Media,* Springer, Berlin, 1979.
12. R. A. Marcus, *Annu. Rev. Phys. Chem.,* **15,** 155 (1964). Chemical and Electrochemical Electron-Transfer Theory.
13. C. Creutz, *Progr. Inorg. Chem.,* **30,** 1 (1980). Mixed Valence Complexes of $d^5$–$d^6$ Metal Centers.
14. P. F. Barbara, T. J. Meyer, and M. A. Ratner, *J. Phys. Chem.,* **100,** 13148 (1996). Contemporary Issues in Electron Transfer Research.
15. M. Lax, *J. Chem. Phys.,* **11,** 1752 (1952). The Franck–Condon Principle and Its Application to Crystals.
16. P. Chen and T. J. Meyer, *Chem. Rev.,* **98,** 1439 (1998). Medium Effects on Charge Transfer in Metal Complexes.
17. M. Bixon and J. Jortner, *Adv. Chem. Phys.,* **106,** 35 (1999). Electron Transfer–From Isolated Molecules to Biomolecules.
18. R. A. Marcus, *J. Phys. Chem.,* **93,** 3078 (1989). Relation Between Charge Transfer Absorption and Fluorescence Spectra and the Inverted Region.
19. M. B. Robin and P. Day, *Adv. Inorg. Chem. Radiochem.,* **10,** 247 (1967). Mixed Valence Chemistry—A Survey and Classification.
20. S. F. Nelsen, *Chem. Eur. J.,* **6,** 581 (2000). "Almost Delocalized" Intervalene Compounds.
21. M. R. Wasielewski, *Chem. Rev.,* **92,** 435 (1992). Photoinduced Electron Transfer in Supermolecular Systems for Artificial Photosynthesis.
22. J. W. Verhoeven, *Adv. Chem. Phys.,* **106,** 603 (1999). From Close Contact to Long-Range Intramolecular Electron Transfer.
23. K. Y. Wong and P. N. Schatz, *Progr. Inorg. Chem.,* **28,** 369 (1981). A Dynamic Model for Mixed-Valence Compounds.
24. M. Born and K. Huang, *Dynamic Theory of Crystal Lattices,* Clarendon Press, Oxford, UK, 1985.
25. D. Chandler and P. Wolynes, *J. Chem. Phys.,* **74,** 4078 (1981). Exploring the Isomorphism Between Quantum Theory and Classical Statistical Mechanics of Polyatomic Fluids.
26. G. A. Voth, *Adv. Chem. Phys.,* **93,** 135 (1996). Path-Integral Centroid Methods in Quantum Statistical Mechanics and Dynamics.
27. S. I. Pekar, *Research in Electron Theory of Crystals,* United States Atomic Energy Commission, Washington, DC, 1963.
28. A. S. Alexandrov and N. Mott, *Polarons and Bipolarons,* World Scientific, Singapore, 1995.
29. A. B. Myers, *Annu. Rev. Phys. Chem.,* **49,** 267 (1998). Molecular Electronic Spectral Broadening in Liquids and Glasses.
30. K. Ando and J. T. Hynes, *Adv. Chem. Phys.,* **110,** 381 (1999). Acid–Base Proton Transfer and Ion Pair Formation in Solution.
31. H. J. Kim and T. J. Hynes, *Am. Chem. Soc.,* **114,** 10508 (1992). A Theoretical Model for $S_N1$ Ionic Dissociation in Solution. 1. Activation Free Energetics.
32. A. Warshel and W. W. Parson, *Annu. Rev. Phys. Chem.,* **42,** 279 (1991). Computer Simulations of Electron-Transfer Reactions in Solution and in Photosynthetic Reaction Centers.
33. L. W. Ungar, M. D. Newton, and G. A. Voth, *J. Phys. Chem. B,* **103,** 7367 (1999). Classical and Quantum Simulation of Electron Transfer Through a Polypeptide.

34. For a review, see: M. Tachiya, *J. Phys. Chem.,* **93,** 7050 (1989). Relation between the Electron-Transfer Rate and the Free Energy Change of Reaction.
35. D. Chandler, *Phys. Rev. E,* **48,** 2898 (1993). Gaussian Field Model of Fluids with an Application to Polymeric Fluids.
36. C. H. Wang, *Spectroscopy of Condensed Media,* Academic Press, Orlando, FL, 1985.
37. G. van der Zwan and J. T. Hynes, *J. Phys. Chem.,* **89,** 4181 (1985). Time-Dependent Fluorescence Solvent Shift, Dielectric Friction, and Nonequilibrium Solvation in Polar Solvents.
38. D. V. Matyushov and B. M. Ladanyi, *J. Chem. Phys.,* **108,** 6362 (1998). Dispersion Solute–Solvent Coupling in Electron Transfer Reactions. I. Effective Potential.
39. G. Fischer, *Vibronic Coupling,* Academic Press, London, UK, 1984.
40. H. J. Kim and J. T. Hynes, *J. Chem. Phys.,* **96,** 5088 (1992). Equilibrium and Nonequilibrium Solvation and Solvent Electronic Structure. III. Quantum Theory.
41. L. S. Shulman, *Techniques and Applications of Path Integration,* Wiley, New York, 1996.
42. D. V. Matyushov and G. A. Voth, *J. Phys. Chem. A,* **104,** 6470 (2000). Reorganization Parameters of Electronic Transitions in Electronically Delocalized Systems. 1. Charge Transfer Reactions.
43. D. V. Matyushov and B. M. Ladanyi, *J. Phys. Chem. A,* **102,** 5027 (1998). Spontaneous Emission and Nonadiabatic Electron Transfer Rates in Condensed Phases.
44. G. D. Mahan, *Many-Particle Physics,* Plenum Press, New York, 1990.
45. R. J. D. Miller, G. L. McLendon, A. J. Nozik, W. Schmickler, and F. Willig, *Surface Electron Transfer Processes,* VCH Publishers, New York, 1995.
46. A. V. Gorodyskii, A. I. Karasevskii, and D. V. Matyushov, *J. Electroanal. Chem.,* **315,** 9 (1991). Adiabatic Outer-Sphere Electron Transfer Through the Metal–Electrolyte Interface.
47. H. Heitele, *Angew. Chem. Int. Ed. Engl.,* **32,** 359 (1993). Dynamic Solvent Effect on Electron-Transfer Reactions.
48. T. Kakitani, N. Matsuda, A. Yoshimori, and N. Mataga, *Progr. Reaction Kinetics,* **20,** 347 (1995). Present and Future Perspectives of Theoretical Aspects of Photoinduced Charge Separation and Charge Recombination Reactions in Solution.
49. J. B. Birks, *Photophysics of Aromatic Molecules,* Wiley, London, UK, 1970.
50. T. Kakitani and N. Mataga, *J. Phys. Chem.,* **89,** 8 (1985). New Energy Gap Laws for the Charge Separation Process in the Fluorescence Quenching Reaction and the Charge Recombination Process of Ion Pairs Produced in Polar Solvents.
51. J.-K. Hwang and A. Warshel, *J. Am. Chem. Soc.,* **109,** 715 (1987). Microscopic Examination of Free-Energy Relationships for Electron Transfer in Polar Solvents.
52. R. A. Kuharski, J. S. Bader, D. Chandler, M. Sprik, M. L. Klein, and R. W. Impey, *J. Chem. Phys.,* **89,** 3248 (1988). Molecular Model for Aqueous Ferrous–Ferric Electron Transfer.
53. E. A. Carter and J. T. Hynes, *J. Chem. Phys.,* **94,** 5961 (1991). Solvation Dynamics for an Ion Pair in a Polar Solvent: Time-Dependent Fluorescence and Photochemical Charge Transfer.
54. H.-X. Zhou and A. Szabo, *J. Chem. Phys.,* **103,** 3481 (1995). Microscopic Formulation of Marcus' Theory of Electron Transfer.
55. T. Ichiye, *J. Chem. Phys.,* **104,** 7561 (1996). Solvent Free Energy Curves for Electron Transfer Reactions: A Nonlinear Solvent Response Model.
56. R. B. Yelle and T. Ichiye, *J. Phys. Chem. B,* **101,** 4127 (1997). Solvation Free Energy Reaction Curves for Electron Transfer in Aqueous Solutions: Theory and Simulations.
57. P. L. Geissler and D. Chandler *J. Chem. Phys.,* **113,** 9759 (2000). Importance Sampling and Theory of Nonequilibrium Solvation Dynamics in Water.
58. Y.-P. Liu and M. D. Newton, *J. Phys. Chem.,* **99,** 12382 (1995). Solvent Reorganization and Donor/Acceptor Coupling of Electron Transfer Processes: Self-Consistent Reaction Field Theory and Ab Initio Applications.

59. R. Kubo and Y. Toyozawa, *Progr. Theor. Phys.,* **13,** 160 (1955). Application of the Method of Generating Function to Radiative and Non-Radiative Transitions of a Trapped Electron in a Crystal.

60. J. L. Skinner and D. Hsu, *J. Phys. Chem.,* **90,** 4931 (1986). Pure Dephasing of a Two-Level System.

61. D. V. Matyushov and G. A. Voth, *J. Chem. Phys.,* **113,** 5413 (2000). Modeling the Free Energy Surfaces of Electron Transfer in Condensed Media.

62. S. M. Hubig, T. M. Bockman, and J. K. Kochi, *J. Am. Chem. Soc.,* **118,** 3842 (1996). Optimized Electron Transfer in Charge-Transfer Ion Pairs. Pronounced Inner-Sphere Behavior of Olefin Donors.

63. N. Tétreault, R. S. Muthyala, R. S. H. Liu, and R. P. Steer, *J. Phys. Chem. A,* **103,** 2524 (1999). Control of Photophysical Properties of Polyatomic Molecules by Substitution and Solvation: The Second Excited Singlet State of Azulene.

64. T. Asahi, Y. Matsuo, H. Masuhara, H. Koshima, *J. Phys. Chem. A,* **101,** 612 (1997). Electronic Structure and Dynamics of Excited State in CT Microcrystals as Revealed by Femtosecond Diffuse Reflectance Spectroscopy.

65. A. Painelli and F. Terenziani, *J. Phys. Chem. A,* **104,** 11041 (2000). Optical Spectra of Push–Pull Chromophores in Solution: A Simple Model.

66. P. van der Meulen, A. M. Jonkman, and M. Glasbeek, *J. Phys. Chem. A,* **102,** 1906 (1998). Simulation of Solvation Dynamics Using a Nonlinear Response Approach.

67. D. V. Matyushov and G. A. Voth, *J. Phys. Chem. A,* **103,** 10981 (1999). A Theory of Electron Transfer and Steady-State Optical Spectra of Chromophores with Varying Electronic Polarizability.

68. C. Reichardt, *Chem. Rev.,* **94,** 2319 (1994). Solvatochromic Dyes as Solvent Polarity Indicators.

69. W. Liptay, in *Excited States,* E. C. Lim, Ed., Academic Press, New York, 1974, Vol. 1, pp. 129–229. Dipole Moments and Polarizabilities of Molecules in Excited Electronic States.

70. L. R. Pratt, *Mol. Phys.,* **40,** 347 (1980). Effective Field of a Dipole in Non-Polar Polarizable Fluids.

71. P. Vath, M. B. Zimmt, D. V. Matyushov, and G. A. Voth, *J. Phys. Chem. B,* **103,** 9130 (1999). A Failure of Continuum Theory: Temperature Dependence of the Solvent Reorganization Energy of Electron Transfer in Highly Polar Solvents.

72. D. V. Matyushov and G. A. Voth, *J. Chem. Phys.,* **111,** 3630 (1999). A Perturbation Theory for Solvation Thermodynamics: Dipolar-Quadrupolar Liquids.

73. W. Liptay, in *Modern Quantum Chemistry, Part. II,* O. Sinanoğlu, Ed., Academic Press, New York, 1965, pp. 173–198. The Solvent Dependence of the Wavenumber of Optical Absorption and Emission.

74. G. U. Bublitz and S. G. Boxer, *Annu. Rev. Phys. Chem.,* **48,** 213 (1997). Stark Spectroscopy: Applications in Chemistry, Biology, and Materials Science.

75. F. W. Vance, R. D. Williams, and J. T. Hupp, *Int. Rev. Phys. Chem.,* **17,** 307 (1998). Electroabsorption Spectroscopy of Molecular Inorganic Compounds.

76. B. S. Brunshwig, C. Creutz, and N. Sutin, *Coord. Chem. Rev.,* **177,** 61 (1998). Electroabsorption Spectroscopy of Charge Transfer States of Transition Metal Complexes.

77. D. V. Matyushov and B. M. Ladanyi, *J. Chem. Phys.,* **107,** 1375 (1997). Nonlinear Effects in Dipole Solvation. II. Optical Spectra and Electron Transfer Activation.

78. T. Asahi, M. Ohkohchi, R. Matsusaka, N. Mataga, R. P. Zhang, A. Osuka, and K. Maruyama, *J. Am. Chem. Soc.,* **115,** 5665 (1993). Intramolecular Photoinduced Charge Separation and Charge Recombination of the Product Ion Pair States of a Series of Fixed-Distance Dyads of Porphyrins and Quinones: Energy Gap and Temperature Dependences of the Rate Constants.

79. H. Heitele, F. Pöllinger, T. Häberle, M. E. Michel-Beyerle, and H. A. Staab, *J. Phys. Chem.,* **98,** 7402 (1994). Energy Gap and Temperature Dependence of Photoinduced Electron Transfer in Porphyrin–Quinone Cyclophanes.

80. T. Fonseca, B. M. Ladanyi, and J. T. Hynes, *J. Phys. Chem.,* **96,** 4085 (1992). Solvation Free Energies and Solvent Force Constant.

81. D. V. Matyushov and B. M. Ladanyi, *J. Chem. Phys.,* **110,** 994 (1999). A Perturbation Theory and Simulations of the Dipole Solvation Thermodynamics: Dipolar Hard Spheres.

82. H. Meirovitch, in *Reviews in Computational Chemistry,* K. B. Lipkowitz and D. B. Boyd, Eds., Wiley-VCH, New York, 1998, Vol. 12, pp. 1–74. Calculation of the Free Energy and the Entropy of Macromolecular Systems by Computer Simulations.

83. J. Åqvist and T. Hansson, *J. Phys. Chem.,* **100,** 9512 (1996). On the Validity of Electrostatic Linear Response in Polar Solvents.

84. M. V. Basilevsky, G. E. Chudinov, and M. D. Newton, *Chem. Phys.,* **179,** 263 (1994). The Multi-Configurational Adiabatic Electron Transfer Theory and Its Invariance under Transformations of Charge Density Basis Functions.

85. B. S. Brunshwig and N. Sutin, *Coord. Chem. Rev.,* **187,** 233 (1999). Energy Surfaces, Reorganization Energies, and Coupling Elements in Electron Transfer.

86. A. Myers Kelley, *J. Phys. Chem. A,* **103,** 6891 (1999). Resonance Raman Intensity Analysis of Vibrational and Solvent Reorganization in Photoinduced Charge Transfer.

87. S. F. Nelsen, R. F. Ismagilov, K. E. Gentile, and D. R. Powell, *J. Am. Chem. Soc.,* **121,** 7108 (1999). Temperature Effects on Electron Transfer within Intervalence Bis(Hydrazine) Radical Cations.

88. I. R. Gould, R. H. Young, L. J. Mueller, A. C. Albrecht, and S. Farid, *J. Am. Chem. Soc.,* **116,** 8188 (1994). Electronic Structures of Exciplexes and Excited Charge-Transfer Complexes.

89. D. V. Matyushov, R. Schmid, and B. M. Ladanyi, *J. Phys. Chem. B,* **101,** 1035 (1997). A Thermodynamic Analysis of the $\pi^*$ and $E_T(30)$ Polarity Scales.

90. C. Wang, B. K. Mohney, B. B. Akhremitchev, and G. C. Walker, *J. Phys. Chem. A,* **104,** 4314 (2000). Ultrafast Infrared Spectroscopy of Vibrational States Prepared by Photoinduced Electron Transfer in $(CN)_5FeCNRu(NH_3)_5^-$.

91. C. J. F. Böttcher, *Theory of Electric Polarization,* Elsevier, Amsterdam, The Netherlands, 1973.

92. D. P. Craig and T. Thirunamachandran, *Molecular Quantum Electrodynamics. An Introduction to Radiation Molecule Interaction,* Dover, Mineola, NY, 1984.

93. I. R. Gould, D. Noukakis, L. Gomez-Jahn, R. H. Young, G. L. Goodman, and S. Farid, *Chem. Phys.,* **176,** 439 (1993). Radiative and Nonradiative Electron Transfer in Contact Radical-Ion Pairs.

94. R. S. Mulliken and W. B. Person, *Molecular Complexes,* Wiley, New York, 1969.

95. J. L. Lewis and M. Maroncelli, *Chem. Phys. Lett.,* **282,** 197 (1998). On the (Uninteresting) Dependence of the Absorption and Emission Transition Moments of Coumarin 153 on Solvent.

96. D. V. Matyushov and G. A. Voth, *J. Phys. Chem. A,* **104,** 6470 (2000). Reorganization Parameters of Electronic Transitions in Electronically Delocalized Systems. 2. Optical Spectra.

97. C. Lambert and G. Nöll, *J. Am. Chem. Soc.,* **121,** 8434 (1999). The Class II/III Transition in Triarylamine Redox Systems.

98. D. Bingemann and N. P. Ernsting, *J. Chem. Phys.,* **102,** 2691 (1995). Femtosecond Solvation Dynamics Determining the Band Shape of Stimulated Emission from a Polar Styryl Dye.

99. L. Reynolds, J. A. Gardecki, S. J. V. Frankland, M. L. Horng, and M. Maroncelli, *J. Phys. Chem.,* **100,** 10337 (1996). Dipole Solvation in Nondipolar Solvents: Experimental Studies of Reorganization Energies and Solvation Dynamics.

100. D. V. Matyushov and M. D. Newton, *J. Phys. Chem. A,* **105,** 8516 (2001). Understanding the Optical Band Shape: Coumarin-153 Steady-State Spectroscopy.

*Reviews in Computational Chemistry, Volume 18*
Edited by Kenny B. Lipkowitz and Donald B. Boyd

ISBN: 0-471-21576-7

CHAPTER 5

# Linear Free Energy Relationships Using Quantum Mechanical Descriptors

**George R. Famini,* and Leland Y. Wilson†**

**Edgewood Chemical Biological Center, United States Army Soldier and Biological Chemical Command, Aberdeen Proving Ground, Maryland 21010, and †Department of Chemistry and Biochemistry, La Sierra University, Riverside, California 92515*

## INTRODUCTION

The idea that molecular structure is related to a compound's bulk properties is inherent to chemistry. For example, a compound containing a carboxylic group is acidic. This concept leads to a fundamental tenet of computational chemistry: structure–property relationships exist and may be quantified. A natural step is to inquire about using first principles (quantum mechanics) to calculate an appropriate property such as a p$K_a$ value, for example. Quantum mechanical (QM) calculations involving isolated molecules are practical; however, QM calculations for systems involving collections of molecules, such as would be required for p$K_a$ values, are very time consuming.

This chapter provides a tutorial focused on the uses of quantum mechanical descriptors in linear free energy relationships (LFERs). Often, LFERs derived with empirically based (i.e., experimental) descriptors are superior in quality to those derived with quantum mechanical descriptors. However, theoretically based LFERs have some advantages including ease of calculation. The QM

descriptor can be obtained for almost any functional group or combination of atoms, whereas empirical parameters are limited to moieties that have been studied previously. Also, electronic structure is fundamental to other molecular observables. (To understand the material in this chapter, we assume the reader is familiar with QM and its application to chemistry at a level found in undergraduate physical chemistry.)

Once a LFER is established for a given property, the resulting equation is useful for (1) calculating the value for that property for some unmeasured, related compounds and (2) serving as a basis for understanding molecular interactions in the system. This chapter has three goals: (1) to show how LFERs fit into the general scheme for computing properties, (2) to introduce some quantum mechanically derived quantities that have been used in LFERs, and (3) to show how multiple regression analysis is applied to obtain the LFER equations. Achieving these goals will allow you to assess the pertinent literature and work with linear free energy relationships yourself.

To carry out these objectives, the chapter is organized in the following way. The first section briefly describes the overall LFER methodology. The second section provides background information for LFER. The third section discusses descriptors with an emphasis on QM-derived quantities. The fourth section discusses statistical procedures commonly employed to derive LFERs with emphasis on multiple regression analysis. The fifth and final section provides examples taken from seminal papers and recent literature; the citations listed provide leads to earlier work.

Another objective of this chapter is to explain how LFER fits in with respect to linear solvation energy relationships (LSER), quantitative structure–activity relationships (QSAR), and quantitative structure–property relationships (QSPR). Often, these methods are operationally quite similar. Their connection is addressed in the Background section.

## LFER METHODOLOGY

This section provides a concise overview of how an LFER analysis is performed. An LFER analysis involves deriving an equation of the form,

$$Y = \sum_j a_j X_j = a_1 X_1 + a_2 X_2 + a_3 X_3 + \cdots \qquad [1]$$

Equation [1] relates a (macroscopic) bulk, empirical property, $Y$, with some set, $\{X\}$, of (microscopic) molecular structural parameters (descriptors). The equation as shown is linear in that each term involves a first power for its descriptor. Higher order descriptors may also be used. The coefficients, $a_j$, are obtained with the aid of statistical methods, particularly, regression

analysis. The process of determining an LFER involves the following steps.

1. A set of experimental values, ($Y_1$, $Y_2$, . . . , $Y_n$), for a given property are measured or otherwise obtained for each member of a set of $n$ compounds. The experimental values are called the dependent variables of Eq. [1].
2. A set of molecular descriptors, ($X_{j1}$, $X_{j2}$, . . .) is selected and then measured, estimated, or calculated for each compound, $j$, in the data set containing $n$ compounds. The descriptors are the independent variables in statistics.
3. The coefficients in Eq. [1] are determined with the aid of regression analysis by solving a set of $n$ simultaneous equations. In addition to providing coefficient values, $a_j$, these calculations provide statistical parameters that assess the quality of the equation derived.

To quantitate the quality of the equation as a whole, standard statistical parameters are examined. (1) The correlation coefficient, $r$, and the variance, which is the correlation coefficient squared, $r^2$, are measures of "goodness of fit." Values for $r$ range between 0 and 1; $r$ (and $r^2$) values closer to 1 indicate a better correlation. (2) The standard error of the estimate, $s$, also commonly referred to (incorrectly) as the standard deviation, is a measure of the error associated with calculating the $Y$ values from the $X$ values using the derived equation. (3) The $p$ parameter and the $F$ ratio are measures of the statistical significance of the regression equation. A smaller $p$ value indicates a smaller probability of chance correlation, whereas a larger $F$ value implies a lower probability. (4) The cross-validated correlation coefficient squared, $q^2$, is a measure of the ability of the derived equation to predict the value of $Y$ for some as yet unmeasured compound. Similar to $r^2$, values for $q^2$ generally range between 0 and 1; values closer to 1 indicate a better ability to predict. To evaluate the significance of each individual descriptor term in an LFER equation, the following statistical quantities can be invoked. (1) Student's $t$ ratio determines which descriptors should be removed due to nonsignificance; the usual rule of thumb is that independent variables with a $t$ ratio below 2 should be dropped from a regression equation. The larger the better. (2) The variance inflation factor (VIF) is a measure of how a given descriptor correlates with the other descriptors; that is, it indicates the degree of redundancy among the descriptors. More details about these statistical quantities and how they should be used in development of LFERs is given in the section on Statistical Procedures.

Molecular descriptors may suggest some underlying physicochemical concepts involved. The correlation of $Y$ with a particular $X$ descriptor does not necessarily imply causality; it implies only that when $X$ increases, $Y$ may also increase or decrease with it, for whatever reason.

Having put into perspective what an LFER is, how it is derived, and what types of statistical assessments are used to assess its validity, we now provide some additional, detailed background information one would need to be able to carry out such an analysis successfully.

# BACKGROUND

## Computational Methods

This section aims to show how the LFER approach compares to other property calculation methods. Biological, chemical, and physical responses originate from interactions between two or more molecules. Many of these interactions can be looked at as involving a solute molecule surrounded by solvent molecules. The successful application of solute–solvent interaction models to many such properties has been well documented.[1] Examples of these properties include solubility, partition coefficients, rate constants, and biological activities, such as equilibrium binding constants, effective doses, and toxicities, as well as other topics of interest in medicinal chemistry.

There are three approaches to applying QM for predicting and understanding properties. In decreasing order of computational complexity, these may be classified as explicit, implicit, and empirical methods. The LFERs fit in the empirical category.

The explicit modeling approach surrounds a solute molecule with solvent molecules and then examines each molecule in that solvated environment. Quantum chemical methods, both semiempirical[2,3] and ab initio[4] have been used to do this; however, molecular dynamics and Monte Carlo simulations using force fields are used most often.[5–8] Calculations on ensembles of molecules are more complex than those on individual molecules. Dykstra et al. discuss calculations on ensembles of molecules in a chapter in this book series.[9] Because of the many conformations accessible to both solute and solvent molecules, in addition to the great number of possible solute molecule–solvent molecule orientations, such direct QM calculations are very computer intensive. However, the information resulting from this type of calculation is comprehensive because it provides molecular structures of the solute and solvent, and takes into account the effect of the solvent on the solute. This is the method of choice for assessing specific bonding information.

The implicit modeling approach treats solute molecules explicitly but uses a continuum model or potential to represent the solvent.[10] Because solute molecule conformations alone are involved, this approach allows one to use ab initio or semiempirical QM methods more readily than in the explicit approach. Although this implicit solvent modeling strategy does not provide specific solute–solvent or solvent–solvent bonding information, it does give free energies of solvation that have been applied to studies of partition coefficients and solubilities.[10–12] Many of the current quantum chemistry software packages incorporate one or more implicit solvation models.

The empirical modeling approach makes use of existing data to obtain an equation relating that property to molecular parameters. For example, the boiling point could be related to the molecular weight and hydrogen-bonding properties of the compounds. This modeling is in contrast to the

explicit and implicit methods where a property is calculated directly from first principles. In a general sense, empirical modeling may be thought of as involving an interpolation process. For a particular compound, a property value calculated with the derived equation can be expected to be reliable when (1) the compound is structurally related to the molecules employed in deriving that equation, and (2) the calculated value is in the range of the measured values. However, such equations may be used to extrapolate a bit at the ends of the lines and, thus, provide a convenient way to estimate the effect of altering molecular structure.

Disadvantages of the empirical modeling approach include (1) time-consuming experiments must be performed to acquire data on compounds in a data set, (2) the data set must be sufficiently large so that the statistics will be significant, (3) only inferences about the property of the system under study can be made, and (4) the resulting correlation equation is valid primarily for interpolation and might be less valid for extrapolation outside of the data set region. Still, for the study of complex systems such as receptor sites where explicit or implicit methods require prohibitive amounts of computing power, correlation methods using extant data can give useful insights that the other methods cannot. A rationalization for this less rigorous approach was summarized succinctly by Exner in his comment that "any regularity found in nature raises some kind of satisfaction."[13]

The molecular parameters themselves do not have to be empirical; they may have some theoretical basis. Although theoretical descriptors may be used, the bulk property still has to be measured. With the availability of QM programs such as MOPAC,[14] theoretically derived descriptors are particularly convenient to generate. Indeed, these QM-derived descriptors can act as probes for understanding complex interactions similar to the way that the octanol/water partition coefficient[15] was used in QSAR starting in the 1970s.[1,16,17] However, the use of QM to understand structure–property relationships is not new. For example, Kier[18] authored a book in 1971 on using molecular orbitals (MOs) in drug research, and Boyd et al.,[19] published a paper in 1980 correlating antibacterial activity of cephalosporins with a reactivity descriptor obtained from MO calculations.

## Linear Free Energy Relationships

This section provides some historical background for LFER and shows how it compares to similar empirical methods including QSAR. Early contributions to LFER are primarily attributed to the work of Burkhardt[20] and Hammett in the 1930s.[21] Abraham et al.[22] and Reichardt[23] list some even earlier examples of such relationships. The term "linear free energy relationship" stems from the observation that, often, there is a linear relationship between the Gibbs free energy change and the Gibbs free energy of activation

for a series of related reactions.[24,25] With this background in mind, LFER has its basis in physical organic chemistry.

One of the first reaction series studied involved triethylamine reacting with a series of methyl esters of substituted benzoic acids. A plot of the logarithm of the rate constant ($\ln k$) versus the logarithm of the acid equilibrium constant ($\ln K_a$) was linear.[24] In mathematical form, this is Eq. [2] where $m$ is the slope and $b$ the intercept.

$$\ln k = m \ln K_a + b \qquad [2]$$

From a heuristic (suggestive, not rigorous) viewpoint, this linear relationship between $\ln K_a$ and $\ln k$ is not surprising given the relation between the equilibrium constant $K$ for an elementary reaction and its forward and backward rate constants, $k_f$ and $k_b$, respectively,

$$K = k_f/k_b \qquad \text{or} \qquad \ln K = \ln k_f - \ln k_b \qquad [3]$$

The free energy terminology can be interpreted as coming from the familiar relations

$$\Delta G^\circ = -RT \ln K \qquad \Delta G_{af} = -RT \ln k_f \qquad [4]$$

with $\Delta G^\circ$ being the standard state Gibbs free energy and $\Delta G_{af}$ being the Gibbs free energy of activation in the forward direction.

Hammett and Taft[26] took leadership roles in developing descriptor sets that account for the effect of substituents on molecular reaction properties. For a given reaction type, such as ionization, hydrolysis, and so on, for a set of aromatic compounds distinguished by different substituents, $Z$, a plot of the logarithm of the rate constant for each compound versus the corresponding Hammett substituent constant, $\sigma(Z)$, often gives a straight line, that is, it provides a LFER. The $\sigma$ values are obtained from $\log (K_Z/K_H)$, where $K_H$ and $K_Z$ refer to the equilibrium constants for the unsubstituted molecule (benzoic acid) and the $Z$-substituted analogue, respectively. The $\sigma$ values depend on the substituent position, for example, $\sigma_m$ and $\sigma_p$ refer to substituents at the meta and para positions, respectively.

An extension of the LFER concept is the idea that properties (usually the logarithm unless the property is directly related to $\Delta G$) may be modeled by correlation equations (often linear) containing other parameter sets related to molecular structure. As mentioned earlier, many properties may be modeled by an equilibrium or a rate constant. The free energy relationship in the form, $\ln K = -\Delta H^\circ/RT + \Delta S^\circ/R$, suggests an association of bulk properties with molecular interactions contributing to reaction enthalpies and entropies. Heuristically, this leads to the idea that $\ln K$ values may be related to molecular properties affecting molecular interactions such as hydrogen bonding.

In a broader context, LFER and similar approaches are subsets of correlation analyses. Exner defines correlation analysis as "a mathematical treatment starting from experimental data and seeking empirical relationships which can subsequently be interpreted theoretically."[13] Although certainly not restricted to chemistry, correlation analysis has been developed extensively in physical organic chemistry. In addition to LFER, LSER, QSAR, and QSPR involve empirical models and, hence, fall in the category of correlation analysis.

When the investigation of LFERs began (1930s) in the field of physical organic chemistry, equations were generally simple and involved small numbers of descriptors. Later (1960s) the LFER approach was generalized resulting in QSARs and QSPRs. These amount to "uninhibited" LFERs. Rather than being limited to studying a simple process like dissociation, they are employed to correlate a wide range of biological, chemical, and physical properties with a wide variety of descriptors.

From an operational standpoint, the LFER, LSER, QSAR, and QSPR approaches can be quite similar, with distinctions based on their applications. QSAR is usually applied to biological properties, especially those important to pharmacology and toxicology. QSPR usually dwells on physicochemical properties in general. LSER focuses on solute–solvent systems. For organizational purposes, we like to view LSER and some applications of QSAR and QSPR (along with related methods) as subsets of LFER. Each approach typically uses some form of regression analysis (statistics) to help find a mathematical relationship between a property and a set of descriptors.

From another viewpoint, LFER methods tend to be model based. Model-based methods employ sets of descriptors that often (1) model classical chemical concepts, (2) are small in number, and (3) use simple regression analyses. For example, the Hammett equation involving the logarithm of the rate constant as a linear function of the substituent constant, $\sigma$ (mentioned earlier), is model based. Similarly, some QSAR and QSPR studies may be viewed in this manner, and so they are included as LFER subsets in this chapter.

However, many QSAR and QSPR studies also use nonmodel-based approaches. Nonmodel-based studies tend to have the following characteristics: (1) they use large numbers of descriptors (hundreds), (2) many of those descriptors are not readily interpreted in classical chemical terms, and (3) they may use quite complex regression analysis and nonlinear methods. For example, three-dimensional (3D) QSAR[27] and other methods are of the growing importance of biological systems and ligand design. Nonmodel approaches tend to mix many descriptors together in an ad hoc manner resulting in equations that produce good correlations. However, these may sometimes be difficult to interpret in classical chemical terminology.

Bakken and Jurs[28] classify three types of models. A type 1 model uses multiple regression analysis to find a linear equation involving a descriptor set. This is the type we have discussed so far—and focus on—in this chapter. A type 2 model uses neural network analysis[29] to develop a linear/nonlinear

model in terms of the descriptors. A type 3 model uses a genetic algorithm[29] to find the best set of descriptors to form a nonlinear model.

It is helpful to note the complexity of the systems involved when considering property calculations. A physical property of a pure compound involves only interactions between molecules of the same kind. For example, the vaporization process, $R(l) \rightarrow R(g)$ with $K_{vap} = p_{vap}$, ($p_{vap}$ is the vapor pressure) involves $R \cdots R$ intermolecular interactions and possibly a large number of interacting conformations. Solute–solvent processes, such as a solubility distribution, $R(l) \rightarrow R(solvent)$, involve solute–solute, solvent–solvent, and solute–solvent interactions with each species interacting as an assortment of molecular conformations.

Chemical reactions and biological processes involve more complex interactions. These processes may be modeled in similar fashion with substrate or receptor and associated equilibrium or rate constant; $R(aq) \rightarrow R(receptor)$ with $K = 1/[R(aq)]$. Kinetic and binding properties are not distinguished in this representation. Indeed, many biological activities (properties) are expressed as some minimum concentration causing a certain effect; an example is the $LD_{50}$, the dose lethal to 50% of the test animals in an experiment. In much of the following discussion, solute–solvent systems and terminology will be used; however, QSAR and QSPR application can be quite similar.

To reiterate some of the important points covered thus far, LFER equations correlate a physical property, $Y$, with a set of molecular properties, $\{X\}$, often in a linear model (Eq. [1]). A fairly large set of the empirical $Y$ values is required for obtaining statistically meaningful results. The dependent variables are frequently expressed as the logarithm of the property because the range of $Y$ values may vary over several orders of magnitude. Moreover, a logarithmic form is suggested by the expressions relating free energy and equilibrium constant as well as the free energy of activation and rate constant.

Although the terms in Eq. [1] are linear, a nonlinear transformation of one or more "simple" descriptors may also be included. For example, a nonlinear term might be volume squared, polarizability divided by volume, an electrostatic potential times a charge, or some other term involving a product, division, exponentiation, or logarithm of the descriptors. In effect, the nonlinear terms can be introduced into a "linear" regression.

## DESCRIPTORS

### Classifications

Correlation analysis can employ empirical (experimental) descriptors or theoretical descriptors or both. As introduced earlier, theoretical (computational) descriptors offer several advantages over empirical ones. They are

usually more easily obtained, their interpretation is usually straightforward, and they are usually not restricted to a particular compound class. Moreover, the predictive ability of a LFER is especially important when it involves computed descriptors because these can be obtained for structures not yet studied experimentally. Some empirical descriptors will be mentioned later in this chapter for comparative and historical reasons. In fact, the quality of correlation equations using empirical descriptors often provides a standard to which theoretical descriptors are judged.

It is convenient to classify theoretical descriptors into topological, constitutional, geometrical, and quantum mechanical types. Topological descriptors arise from graph theory applied to chemistry, often using atoms (vertices) and bonds (edges), but they also may be geometrical in that they involve distances. Earlier chapters in this series described topological descriptors.[30] Constitutional descriptors include counting descriptors (e.g., numbers of atoms of a certain type), indicator descriptors (e.g., indicating whether a molecule does or does not have some feature), geometrical descriptors, and molecular weight. Counting descriptors could be the number of nitrogen atoms or ring structures in a molecule. Geometrical descriptors might include atom distances, molecular surface areas, and molecular volumes. These geometrical quantities may be calculated with QM or non-QM methods. The latter might be molecular mechanics or simply the use of standard bond lengths and bond angles and van der Waals based atomic radii.

## Quantum Mechanical Descriptors

Quantum mechanical descriptors are those that may be obtained from QM calculations primarily. Although there are empirical methods for estimating values for partial charges, QM calculations yield a wide array of quantities. These descriptors include orbital energies and electron distributions needed to give atomic charges, dipole and higher moments, and polarizabilities, among others. Most solutions of the Schrödinger equation produce a set of MOs, $\{\psi_i\}$, their energies, $\{E_i\}$, and the molecular geometry (distances and angles) corresponding to a local minimum on that molecule's potential energy surface. The MOs are often written as linear combinations of atomic orbitals (LCAO),

$$\psi_i = \sum_r c_{ir}\phi_r = c_{i1}\phi_1 + c_{i2}\phi_2 + c_{i3}\phi_3 + \cdots \qquad [5]$$

where $c_{ir}$ is the coefficient of the $r$th atomic orbital (AO), $\phi_r$, in the $i$th MO. The AOs, $\phi_r$, are the 1s, 2s, 2p, and so on, of appropriate atoms comprising the molecule. The AO coefficients, $c_{ir}$, are related to electron population density which can be used to calculate charges on atoms.

Quantum calculations can be done easily for small systems, but large systems require great computing power; calculation times for $N$ electron systems can scale as much as $N^7$ depending on the level of theory. An alternative way to treat large systems is to use QM solutions for simpler analogues or subspecies. Using quantum mechanics has worked well with gas-phase systems but is far more difficult for condensed phases.

Molecular orbital calculations can be used to generate a large number of descriptors. We will not attempt to list them now; instead, we will organize them in general terms and include specific descriptors in connection with specific examples later in this chapter. Lewis[31] provided a list of some QSAR equations that correlate various biological activities with quantum mechanically derived descriptors. Karelson, Lobanov, and Katritsky[32] provided a summary of QM descriptors used in QSAR and QSPR including: molecular (overall) energies, orbital energies, atomic charges, electron densities, polarizabilities, dipole moments, super-delocalizabilities, and geometrical quantities. Katritsky et al.[33] provided an extensive list of empirical and theoretical descriptors used in QSPR treatments of solvent scales. Solvent scales consist of sets of empirical descriptors designed to help explain and predict the influence of solvents on physicochemical phenomena. For example, some parameters are designed to be a measure of solvent polarity or acidity.

## Quantum Mechanical Calculations

Semiempirical, ab initio (Hartree–Fock), and density functional theory (DFT) QM models may be used to calculate descriptors. Semiempirical methods offer greater computational speed than the others, which is advantageous for large molecules. Based on the neglect of diatomic differential overlap (NDDO) approximation, Dewar et al. developed the modified neglect of differential overlap (MNDO),[34] Austin model 1 (AM1),[35] and parametric model 3 (PM3)[36] semiempirical Hamiltonians commonly used in MO calculations. Chapters in this series by Stewart[2] and Zerner[3] discuss semiempirical methods. These model Hamiltonians are incorporated in commonly used software packages such as MOPAC,[14] AMPAC,[37] and Gaussian,[38] Spartan,[39] and others. A variety of ab initio and, more recently, DFT methods are also being used to calculate descriptors. Again, a number of chapters in this series have covered these methods.[9,40–48]

An essential rule is that descriptors should be calculated by the same level of theory for all molecules in a given data set. Trends in computed quantities have a chance to be consistent within a given computational method but not across different methods. For example, AM1 and MNDO atomic charge values may differ; but within the framework of either method the relative order of numerical values may be similar.

Note that the QM molecular parameters generally apply to the electronic ground state for a single conformation of the isolated system at 0 K. Properties

calculated for such a system in a vacuum do not directly describe bulk phenomena, nor do they usually account for the variety of conformations possible near room temperature. Nevertheless, it is possible for a given property of an isolated molecule to correlate well with a property of the molecule when surrounded by other molecules in the bulk.

Some of the more common descriptors with their common symbols are listed in Tables 1–3. The section on Examples of LFER Equations illustrates and explains some of these. Because of the need for consistency in this chapter, the symbols used here might not always match those used in the original articles. Nonetheless, we have endeavored to retain their meaning as faithfully as possible. Descriptors, along with their symbols, often tend to evolve as their application changes.

### *Atomic Charges*

One component of molecular association involves electrostatic interactions; consequently, it is natural to expect local (atomic and group) electron densities (charges) to be related to properties of compounds and, thus, to be good descriptors. For example, the most negative charge on an oxygen atom could help model hydrogen-bond acceptor (HBA) basicity. Similarly, the most positive charge on a hydroxyl hydrogen could help model hydrogen bond donor (HBD) acidity. Furthermore, charges are incorporated in other descriptors as described below. In most cases, charge, as used here, refers to the Mulliken net atomic charge; it is the number of valence electrons that a given atom should have minus the valence electron population that the atom actually has.

**Table 1** Some QM Terminology and Parameters Used in (and as) Descriptors

| Symbols | Meaning or Definition | Occurs in Equation Number |
|---|---|---|
| $\psi_k$ | $k$th molecular orbital (MO) | |
| $E_k, \varepsilon_k$ | Energy of $k$th MO | |
| $\phi_r$ | $r$th atomic orbital (AO) | |
| $c_{kr}$ | Coefficient of $r$th AO in $k$th MO | |
| HOMO | Highest (in energy) occupied MO | |
| LUMO | Lowest (in energy) unoccupied MO | |
| $E_{\text{HOMO}}, E_{\text{h}}$ | HOMO energy | [23], [24], [46] |
| $E_{\text{hw}}$ | HOMO energy of water | |
| $E_{\text{LUMO}}, E_{\text{l}}$ | LUMO energy | [46] |
| $E_{\text{lw}}$ | LUMO energy of water | |
| $r_{jk}$ | Distance between atoms $j$ and $k$ | |
| $\mathbf{r}$ | Position vector | |
| $S_{rs}$ | Overlap integral of AOs $r$ and $s$ on different centers (atoms) | |
| $q_k$ | Mulliken charge | |

**Table 2** Some QM Descriptors Developed for Model-Based Methods

| Symbol | Name or Description | Occurs in Equation Numbers |
|---|---|---|
| | *General Descriptors* | |
| $\alpha$ | Average molecular polarizability | [31], [32] |
| $\mu$ | Dipole moment | [41], [42], [49] |
| $A, A_d, S$ | Surface area | [42], [43], [49] |
| $V, V_{mc}, V_d$ | Molecular volume | [27], [29a, b], [41], [42] |
| $\Delta H_f$ | Heat of formation | [24] |
| | *TLSER Descriptors* | |
| $\pi_I$ | Polarizability index | [27], [30] |
| $\varepsilon_B$ | Covalent HB acceptor basicity | [27], [30] |
| $\varepsilon_A$ | Covalent HB donor acidity | |
| $q_-$ | Electrostatic HBA basicity | [27], [29b], [30] |
| $q_+$ | Electrostatic HBD acidity | [27], [29a], [30] |
| | *GIPF (MEP) Descriptors* | |
| $A_{\pm s}$ | Positive or negative molecular electrostatic potential (MEP) surface area | [39] |
| $U(\mathbf{r})$ | MEP at point **r** near molecule | |
| $U_{min,max}$ | Most negative or positive MEP | [39] |
| $\sum U_{min,max}$ | Sum of negative or positive MEP | [42] |
| $U_S$ | Average MEP over the surface | |
| $U_{S,max,min}$ | Most positive or negative MEP on surface | [39] |
| $U_{\pm S,avg}$ | Average positive or negative MEP over surface | [39] |
| $U_{-S,\%}$ | Percent of negative electrostatic potential | [42] |
| $\delta U_j$ | MEP deviation | |
| $\Pi$ | Average MEP deviation over surface | |
| $\sigma^2_{\pm}$ | MEP variance for $\pm$ potentials | |
| $\sigma^2_{tot}$ | MEP total variance | [40] |
| $\nu$ | Electrostatic balance parameter | |
| $I(\mathbf{r})$ | Average local ionization energy | |
| $I_{min}$ | Most negative average local ionization energy | |
| $I_{S,min}$ | Most negative average local ionization energy on surface | |
| $[U_{-S,avg}]^2$ | Mean square of negative MEP on surface | [42] |
| $I_-$ | Average of negative MEP over the volume | [42] |

Computed atomic charge is subjective because its value depends on the algorithm used (their values cannot be observed experimentally). Regardless of the algorithm used, however, trends and relative charge values are sometimes useful. To more directly illustrate the relationship between the coefficients, $c_{ir}$, in Eq. [5], and the electron density, we briefly describe Mulliken population

**Table 3** Some QM Descriptors Developed for Nonmodel-Based Methods

| Symbol | Name or Description | Occurs in Equation Numbers |
|---|---|---|
| | *CPSA and Related Descriptors* | |
| DMSI, $A$ | Dispersion molecular surface interaction (MSI) | [43] |
| ENMSI, $A_-$, PNSA3 | Electrostatic negative MSI | [43] |
| EPMSI, $A_+$ | Electrostatic positive MSI | [43] |
| HBMSI, $A_{HB}$ | Hydrogen-bond MSI | [43] |
| PPSA3 | Partial positive atomic charge weighted surface area | |
| PNSA3, ENMSI | Partial negative atomic charge weighted surface area | |
| DPSA | Differential partial surface areas | [44] |
| RPCG | Relative positive charge | [44] |
| $q_D$ | Charge on hydrogen-bond donor (HBD) H atoms | |
| $A_D$ | Exposed surface area of HBD H atoms | |
| HDCA2 | HBD surface area over donor H atoms | [46],[48] |
| HDSA2 | HBD surface area over donor H atoms (modified) | [47] |
| HASA1 | HBA surface area over acceptor atoms | [47] |
| $CSA2_H$ | Charged surface area of H atoms | [47] |
| $CSA2_{Cl}$ | Charged surface area of Cl atoms | [47] |
| $E_A$ | Maximum electrophilic reactivity index of C atom | [48] |
| $Y$ | Maximum AO electronic population | [48] |
| $Q_{min}$ | Most negative charge | |
| $PCWT^E$ | Partial charge weighted topological electronic index | [47] |
| $T_I$ | Topographic electronic index | [47] |
| $G_I$ | Gravitational index | [47] |
| $Q_{O\text{ or }N}$ | Square root of sum of squares of N or O charges | [49] |
| $Q_{ON}$ | Sum of absolute values of N and O charges | [49] |
| ABSQ | Sum of absolute values charges on all atoms | [49] |
| $O$ | Ovality, actual area/area as sphere | [49] |

analysis.[45,49] The integral over all space of the square of the $i$th MO gives the number of electrons associated with that MO (Eq. [6]).

$$\begin{aligned}\langle\psi_i|\psi_i\rangle &= N(i)\left\{\sum_r c_{ir}^2\langle\phi_r|\phi_r\rangle + 2\sum_{r>s} c_{ir}c_{is}\langle\phi_r|\phi_s\rangle\right\}\\ &= N(i)\sum_r c_{ir}^2 + 2N(i)\sum_{r>s} c_{ir}c_{is}S_{rs}\end{aligned} \qquad [6]$$

Here **S** is the AO overlap matrix, and $N(i)$ is the number of electrons occupying MO $\psi_i$. We assume each AO $\phi_i$ is normalized and orthogonal to all other AOs centered on that atom. The sum (Eq. [7]) over all MOs must give the total number, $N$, of electrons in the molecule.

$$N = \sum_{i}^{\text{MOs}} N(i) \sum_{r}^{\text{AOs}} c_{ir}^2 + 2 \sum_{i}^{\text{MOs}} N(i) \sum_{r>s}^{\text{AOs}} c_{ir} c_{is} S_{rs} \qquad [7]$$

Now we can break the two terms in Eq. [7] into sums over specific atoms. Summing over only the AOs centered on atom $k$ in the first term, we obtain the net atomic population $n(k)$, Eq. [8].

$$n(\mathrm{k}) = \sum_{i}^{\text{MOs}} N(i) \sum_{r_k} c_{ir_k}^2 \qquad [8]$$

Similarly, summing over the AOs centered on atom $k$ and the AOs centered on atom $l$ in the second term of Eq. [7], we obtain the total overlap population $N(k,l)$ between the two atoms, Eq. [9].

$$N(k,l) = \sum_{i}^{\text{MOs}} N(i) \sum_{r_k > s_l} c_{ir_k} c_{is_l} S_{r_k s_l} \qquad [9]$$

The net atomic population, $n(k)$, does not include any of the electron density associated with the overlap population, $N(k,l)$. It is clear that some of these electrons in the overlap population belong to atom $k$ and the remaining electrons belong to atom $l$. Furthermore, these should be added to $n(k)$ and $n(l)$ to get the total number of electrons on each atom. Arbitrarily, Mulliken divided this overlap population evenly between the two atoms resulting in the gross atomic population $N(k)$ for atom $k$, Eq. [10].

$$N(k) = \sum_{i}^{\text{MOs}} N(i) \sum_{r_k} c_{ir_k} \left( c_{ir_k} \sum_{s_{k \neq l}} c_{is_l} S_{r_k s_l} \right) \qquad [10]$$

Thus, any differences in the atom types and their electronegativities are ignored. To summarize, Mulliken assigned all electrons associated with an AO centered on that atom to that atom and then split the overlap density evenly between atom pairs. The net charge on an atom, $q_k$, with nuclear charge, $Z_k$, is then given by Eq. [11].

$$q_k = Z_k - N(k) \qquad [11]$$

Many schemes exist for estimating atomic charges that have been derived from MOs. Katritsky and colleagues,[32] for example, have used partial charges calculated with an empirical method by Zefirov et al.[50] The fact remains that charge calculations are usually obtained by MO calculations.

### *Orbital Energy*

In QM theory, covalent interactions arise from orbital overlap. The interaction of two orbitals also depends on their energy eigenvalues. Consequently, energies associated with the highest occupied molecular orbital, $E_{HOMO}$, and lowest unoccupied molecular orbital, $E_{LUMO}$ are often good candidates for descriptors. For example, $E_{HOMO}$ might model the covalent basicity of a hydrogen bond acceptor or the $E_{LUMO}$ might model the covalent acidity of the proton of an H-bond donor. Further interpretation is possible because the HOMO energy is related to the ionization potential and is a measure of the molecule's tendency to be attacked by electrophiles. Correspondingly, the LUMO energy is related to the electron affinity and is a measure of a molecule's tendency to be the attacked by nucleophiles. Furthermore, according to frontier molecular orbital (FMO) theory, transition state formation involves the interaction between the frontier orbitals, HOMO and LUMO, of reacting molecules.

### *Molecular Size*

The molecular volume descriptor, $V$, can be recognized as an important descriptor once one realizes that the free energy of solution is related in part to the size of the cavity that must be carved out of the solvent bath by the solute molecule during the solvation process. The surface area, $A$, of a molecule or a fragment of a molecule may be construed[51,52] as a measure of the region available for interaction with another molecule. For computing $V$ and $A$, one could use a particular electron density contour [45,51] or a non-QM-derived measure of atomic size such as the van der Waals radii available from standard tables in physical chemistry textbooks.

### *Polarizability*

Molecular polarizability, $\boldsymbol{\alpha}$, is a measure of the ability of an external electric field, $\mathbf{E}$, to induce a dipole moment, $\boldsymbol{\mu} = \boldsymbol{\alpha}\mathbf{E}$, in the molecule. As such, it can be viewed as contributing to a model for induced dipole (dispersive) interactions in molecules. Because the polarizability is a tensor (matrix) quantity, there is the question of how to represent this in a scalar form. One approach is to use the average of the diagonal components of the polarizability matrix, $(\alpha_{xx} + \alpha_{yy} + \alpha_{zz})/3$. Since the polarizability increases with size (and has units of volume), it is convenient to define a dimensionless variable, the polarizability index, $\pi_I$, by dividing the quantity $(\alpha_{xx} + \alpha_{yy} + \alpha_{zz})/3$ by the molecular volume, $V$.

*Dipole Moment and Polarity Indexes*

These polarity descriptors combine charge and geometry. Dipole moments are used to model dipole–monopole, dipole–dipole, dipole–induced dipole, and other interactions. Both molecular dipole ($\boldsymbol{\mu}$) as well as bond dipole moments may be defined for neutral molecules. A bond dipole moment due to atoms $k$ and $l$ separated by distance, $r_{kl}$, can be defined as $|q_l - q_k|r_{kl}$. The topographic electronic index defined in Eq. [12] is another measure (index) of polarity.[53] The sum extends over the number of bonded atoms, $N_B$.

$$T_I = \sum_{l<k}^{N_B} |q_l - q_k|/r_{lk}^2 \qquad [12]$$

*Electrostatic Potentials*

The symbol $V$ is often associated with the electrical potential in the literature, but $U$ is employed here so as not to conflict with the volume descriptor. Another aspect of chemical reactivity involves the molecular electrostatic potential (MEP).[54] The MEP is the interaction energy between a unit point charge and the molecular charge distribution produced by the electrons and nuclei. The electrostatic potential, $U(\mathbf{r})$, at a point, $\mathbf{r}$, is defined by Eq. [13].

$$U(\mathbf{r}) = \sum_A (Z_A/|\mathbf{r}_A - \mathbf{r}|) - \int \rho(\mathbf{r}')d\mathbf{r}'/|\mathbf{r}' - \mathbf{r}| \qquad [13]$$

$Z_A$ is the charge on nucleus A located at point $\mathbf{r}_A$, and $\rho(\mathbf{r}')$ is the total electronic density, $\Psi(\mathbf{r}')^*\Psi(\mathbf{r}')$, at each point in space $\mathbf{r}'$, and $\Psi(\mathbf{r}')$ is the molecular wave function. The perturbation caused by the unit test charge is not considered; rather it is simply a hypothetical probe to obtain the relative energy of interaction at points surrounding a molecule.

*Overall Energies*

The parameter $E_T$ is the total (Hartree–Fock) molecular energy; it is listed in the output of most QM programs. The parameter $\Delta H_f$ is the heat of formation for the molecule and also is computed in most semiempirical MO programs.

*Superdelocalizability*

The superdelocalizability of an atom in a molecule provides another measure of the tendency of the molecule to be attacked by an electrophile or nucleophile. It is related to electron density on that atom. The electrophilic superdelocalizability for a given atom $k$ in the molecule may be defined as a sum over occupied MOs (index $i$) and valence AOs (index $r$), Eq. [14].

$$S_{A,k} = 2\sum_i \sum_r (c_{ir,k}^2/\varepsilon_i) \qquad [14]$$

Here $\varepsilon_i$ is the orbital energy of the $i$th occupied MO. Large electron charge densities and low energies would contribute to electrophilic attack near that atom. There is an analogous nucleophilic quantity, $S_{N,k}$, involving the unoccupied MOs.

*Charged Partial Surface Areas*

This is a set of parameters that combine geometry and charge data. The charged partial surface areas (CPSAs), as developed by Stanton and Jurs,[55] model electrostatic interactions at the molecular surface. Some of these descriptors were designed as models for hydrogen bonding.[56] For example, PPSA1 is the partial positive surface area. It is the sum of the surface areas of the positively charged atoms, $\sum A_{+k}$, where $A_{+k}$ is the surface area contribution of the $k$th positive atom. PPSA2 is the total charge weighted PPSA, $Q_{+\text{tot}} \sum A_{+k}$, where $Q_{+\text{tot}}$ is the sum total positive charge on the molecule. PPSA3 is the atomic charge weighted PPSA, $\sum A_{+k} Q_{+k}$. Many other similarly arbitrary descriptors may be defined and used; for example, analogous parameters to these might use negative charges in place of the positive charges. An example is PNSA1, the partial negative surface area, $\sum A_{-k}$, where $A_{-k}$ is the surface area contribution of the $k$th negative atom. Early implementation of CPSA parameters by Stanton and Jurs[55] employed partial atomic charges that were obtained by an empirical (but not experimental) method. The charges were parameterized to reproduce experimental dipole moments.

## STATISTICAL PROCEDURES

The most common statistical procedure for deriving correlations involves regression analysis as mentioned earlier. We discuss it here in some detail. Basically, it is a least-squares method for more than one variable and is suitable for small descriptor sets. Other methods for handling large descriptor sets exist, and some of them are mentioned later along with appropriate references providing more detail. The reader is directed to almost any statistical textbook (e.g., Belesley, Kuh, and Welsh[57]) for further elaboration.

### Multiple Regression Analysis

*General Process*

A bulk property, $Y$, is measured for a set of $n$ compounds leading to a set of values, $\{Y_i\}, 1 \leq i \leq n$. For each of the $n$ compounds, a set of $m$ molecular descriptors, $\{X_j\}, 1 \leq j \leq m$, with the requirements that $(m+1) \leq n$, is obtained by empirical or computational methods. The $(m+1)$ arises because of the possibility of a nonzero intercept appearing in a relationship. A minimum of $m$ measurements are required, one for each parameter. The regression coefficients have greater statistical validity if there exist more measurements than coefficients; a common rule of thumb is $n \geq 5m$ (i.e., at least five

compounds or $Y_i$ values for each descriptor used in the regression equation. To derive a linear correlation, which is the simplest model, the data is then fit to an equation, as in Eq. [1]. Hence, for a given property, $Y$, the coefficients, $a_j$, for each molecular parameter, $X_j$, are determined. There are $(m + 1)$ terms in the summation; the intercept can be associated with $a_0$ by using $X_0 = 1$ for all compounds.

If the relationship between dependent ($Y$) and independent ($X$) variables were perfect, the $Y$ values for any $(m + 1)$ compounds could be used resulting in a square matrix. If the $m$ parameters, $X$, are independent (orthogonal, i.e., have no intercorrelation), the matrix may be inverted and the coefficients, $a_j$, calculated. However, the relationships are seldom perfect so using another set of compounds would lead to another set of coefficients with values different from the previous set. This process could be repeated until all combinations had been tried giving, ultimately, a range of values (a distribution) for each coefficient. For even a medium sized data set, this is a daunting task!

Fortunately, statistical methods exist that may be used to help derive the coefficients, thus minimizing the work. The full data matrix is employed to find the set of coefficient values, $\{a_i\}$, using the requirement that the variance, $s^2$, (Eq. [15]) is a minimum.

$$s^2 = \left(\frac{1}{n}\right) \sum_{i=1}^{n} \delta_i^2 \qquad [15]$$

Here $\delta_i$ is the difference between the observed and calculated values for $Y_i$:

$$\delta_i = Y_i(\text{obs}) - Y_i(\text{calc}) \qquad [16]$$

$Y_i$(calc) is the value obtained by using the correlation equation with the set of coefficients (to be determined) that will minimize $s^2$; this is the least-squares approach. Rather than try all possible coefficient sets, expressions in terms of the $Y$ and $X$ values for the coefficients can be obtained. Differentiation with respect to each of the $a_j$, in turn, leads to $m + 1$ simultaneous equations from which the $m$ coefficient values and intercept are obtained. The resulting equations become more numerous as the number of parameters increase; consequently, calculations must be done by computer. Chemistry is greatly aided through computing.

***Term Significance***

The statistical parameters generated in the process of fitting the data to the equation are also used to determine the significance of the equation. A common criterion is to retain coefficients if their two-tailed probability is less than 0.05; $P(2\text{-tail}) < 0.05$. A two-tailed probability smaller than 0.05 means that the deviation from the ''true'' value lies in the positive or negative regions of the normal error curve corresponding to less than 5% of the area. It

amounts to saying that there is less than 5% probability that the value could occur (be significant) by chance. Small $P$(2-tail) values are associated with large $t$ ratios (Student's $t$ statistic or test).

*Descriptor Orthogonality*

The orthogonality (linear independence, cross-correlation, intercorrelation) of the parameters may be assessed several ways. Nonorthogonal descriptors introduce redundancy into the equation and are therefore undesirable. For example, a descriptor could be expressed as a function of the other descriptors, thus, implying that its term in the correlation equation could be replaced by an expression involving only the other parameters.

One method for measuring the degree of orthogonality is to correlate a particular descriptor, $X_j$, with all other descriptors, thus providing a set of correlation coefficients, $\{r_j\}$. The square of the correlation coefficient, $r_j^2$, may be converted to the tolerance, Tol, by taking $(1 - r_j^2)$ and into the variance inflation factor (VIF) by taking the reciprocal of the tolerance. Adequate orthogonality occurs with $r_j^2$ values $<0.8$, or tolerances $>0.2$ or VIF values $<5$. This latter statistical value means, for example, that if a term's VIF value is greater than 5, that descriptor should not be included in the final equation. (Note that some statistics textbooks suggest that VIF values $<10$ are satisfactory.) It is important to note that a correlation matrix, $r_{jk}$, of descriptors does not provide the same information as the VIF or tolerance, and is not sufficient to determine the orthogonality of the descriptors. The reason for this is that the descriptors may not individually correlate with a fourth descriptor, but the combination of the three descriptors may adequately describe the fourth.

*Equation Significance*

For physicochemical systems, the overall correlation equation is often considered to be acceptable if its Pierson product correlation coefficient, $r$, satisfies $r^2 > 0.8$. The goal is for $r^2$ to be as close to unity as possible with the concomitant standard error of the estimate, *se* or *s*, to be as close to zero as possible. It is common in the literature to find the standard error of the estimate referred to, incorrectly, as the standard deviation, *sd*. A value of 0.10 (10%) or less for the ratio, se/range, (the range is the difference between the highest and lowest values in the data set) is also a good rule of thumb in judging the significance of the equation. One wants the standard error to be small compared to the size (as indicated by the range) of the variable. There often exists some redundancy between $r^2$ and *se*; high values of $r^2$ tend to be associated with low *se* values. In the social sciences, and to a lesser extent biological sciences, correlation equations may be considered significant with smaller $r^2$ values than typically found in physical sciences. Social and biological systems can be exceedingly complex and produce noisy data.

Another commonly used measure of equation significance is the Fisher $F$ ratio. This is the regression mean square divided by the error mean square,

which means, basically, that it is large (better) when the residual mean square error of a regression equation is small and the amount of variance explained by the equation is large.

***Predictive Ability***

The ability of the derived correlation equation to predict values can be measured with the cross-validated $r^2$ value, $q^2$. Values of $q^2$ greater than 0.5 indicate acceptable ability to predict; a $q^2$ of 0.6 is considered quite respectable. Often $q^2$ values are less than $r^2$ values. The simplest cross-validated $r^2$ value is calculated by excluding each point in turn (leave-one-out method) and using the remaining points to calculate a regression equation. The resulting $r^2$ values are averaged to obtain $q^2$.

Other cross-validated correlation coefficient calculation methods are also used. For example, instead of leaving one point out, 20% of the individual cases may be excluded each time. A correlation equation is derived from the remaining set as before, and the resulting equation is used to calculate predicted values for each of the 20% of points omitted in this procedure. The deviations are then accumulated resulting in a $q^2$.

Cross-validation is an internal check on the validity of a correlation equation for a data set. To test for so-called "external" predictive ability, one separates the data into training (larger) and test (smaller) sets. A regression equation is then derived with the training set only, and the resulting equation is used to predict the values for the test set. Deviations for the test set may be accumulated, and $r^2$ and $s$ values calculated. These values are compared to the corresponding $r^2$ and $s$ values for the training set. Typically, the $r^2$ values for the test set are smaller while the $s$ values are larger than the corresponding values for the training set. This indicates that the statistical errors for the test set are larger than those for the training set.

***Outliers***

Compounds with deviations ($\delta_i$ of Eq. [16]) three or more times greater than the standard deviation are considered to be outliers. A case can be made for considering compounds with deviations two or more times larger than the standard deviation as outliers; this can be done at the 95% confidence level. Outliers may be removed from the data set and not used when deriving the final correlation equation. The question naturally arises regarding the number of outliers that can be removed without making the result look fudged. A good rule of thumb is for outliers to constitute no more than 10% of the data.

The presence of outliers is not necessarily bad because they can indicate aberrant behavior where, for example, the compound may undergo a different mechanism than the other compounds in the data set. For example, aldehydes did not fit an otherwise good correlation equation for a toxicity index[58] presumably because of Schiff base formation at membrane surfaces by the aldehyde group with amino groups. Outliers also can be indicative of an

inadequate model in general, or that there may be experimental errors in the input data. The exclusion of outliers should be fully disclosed when a study is published.

***Descriptor Reduction***

To reduce the number of descriptors to only the most relevant ones, one may use a descending regression analysis. Only the first model uses all the descriptors. The statistical parameters resulting from the first iteration are used to accept or reject the least significant term(s); that is, the ones with lowest probability and with $P$(2-tail) $>0.05$. The process is repeated until the remaining terms are significant. The descriptors are then examined for intercorrelation; those with VIF $>5$ are removed because they represent redundancy. Several of the common statistics programs such as JMP[59] and SYSTAT[60] are capable of automating this so-called stepwise regression.

There is also the issue of when to remove outliers. Sometimes removing an insignificant descriptor will result in a compound no longer being considered an outlier. One approach to addressing this issue is to reduce the number of descriptors first and then remove outliers.

Another approach to reducing the number of descriptors is to use an ascending regression analysis. The first step involves generating regressions with individual descriptors. The next step uses the model retaining the most significant descriptor plus the next most significant descriptor. The procedure is continued until each succeeding added descriptor is no longer deemed significant. If the descriptors were truly orthogonal, the final correlation equation would be the same regardless of the pathway followed to derive that equation. This is seldom the case, and accordingly, the resulting equation may not be the optimum least-squares solution. This method for descriptor reduction can only be justified by trying all possible descriptor combinations but is not practical for large descriptor sets.

There exist variations on aforementioned procedures. Equations with parameters raised to a power, such as $X_j^2$, may be considered as linear in a variable $z_j$ ($\equiv X_j^2$). For example, a squared parameter might be used in the case of an extremum occurring in a plot of a property versus some parameter such as the molecular volume. Such a relation might be expected if there exists maximum molecular size for fitting into a receptor cavity. Other mathematical functions of the "primitive" descriptors can likewise be used to generate terms. Linear regression models are preferred because the terms in Eq. [1] have relatively simple physical interpretations.

## EXAMPLES OF LFER EQUATIONS

Representative correlation equations are presented here for illustrative and comparative purposes. For convenience, the examples are classified as

"model based" or "nonmodel based" in keeping with the corresponding definitions in the LFER background section.

Because authors present correlation equations in different ways, a uniform pattern of presentation is employed. For each example given, the following information is provided: the author(s), the bulk property with its units, the number and types of compounds in the data set, the types of descriptors used, and QM methods employed. Computer programs used in molecular model visualization, QM calculation, descriptor calculation, and statistical calculation will be mentioned. More information on some of the computer programs available for these purposes may be found in two chapters in this series.[61,62] A brief explanation of the descriptors will precede the equation and, where possible, units associated with the descriptors will be provided. To avoid conflicts within this chapter, the symbols might not be those used in the original papers. The intercept will be the last term in the equation.

Statistical parameters, when available, indicating the significance of each of the descriptor's contribution to the final regression equation are listed under its corresponding term in the equation. These include the standard errors written as $\pm$ values, the Student $t$ test values, and the VIF. The significance of the equation will be indicated by the sample size, $n$; the variance explained, $r^2$; the standard error of the estimate, $s$; the Fisher index, F; and the cross-validated correlation coefficient, $q^2$. When known, outliers will be mentioned. The equations are followed by a discussion of the physical significance of the descriptor terms.

## Model-Based Methods

### *Empirical Descriptors*

*Classical QSAR* In the "classical" QSAR approach, pioneered by Hansch and Leo,[63] biological properties are usually correlated with a set of descriptors using equations similar to Eq. [17].

$$\log(1/c) = b \log P + c\pi + d\sigma + eE_s + a \qquad [17]$$

Here, $c$ represents a biological activity, often in concentration units, such as an $LD_{50}$. The coefficients, $a$ through $e$, are determined from regression analysis; $a$ is the intercept. Log $P$ is the logarithm of the partition coefficient for R(aq) $\rightleftarrows$ R(octanol); it models lipophilicity of a molecule and is a bulk physicochemical property. The other three terms contain molecular substructural parameters; $\pi$ represents a hydrophobic or lipophilic effect associated with a substituent, the Hammett–Taft substituent constant $\sigma$ models electronic (electron withdrawing or donating) effects of a substituent, and $E_s$ models steric effects of a substituent. Equation [17] is typically applied to a related series of molecules with different substituents.

*LSER General Model* Kamlet, Taft, and their colleagues proposed a type of LFER, called the LSER, which employs a representation for solute–solvent interaction as expressed in general form as Eq. [18].[64,65]

$$\log P = \text{cavity term} + \text{dipole/polarizability terms} + \text{hydrogen-bonding terms} + \text{intercept} \quad [18]$$

The LSER approach relates a bulk property, $P$, to molecular parameters thought to account for cavity formation, dipole moment/polarizability, and hydrogen-bonding effects at the molecular level. The cavity term models the energy needed to provide a solute molecule-sized cavity in the solvent. The dipole moment/polarizability terms model dipole and induced dipole interactions between solute and solvent; these can be viewed as related to dispersion interactions. The hydrogen-bonding terms model HBA basicity and HBD acidity interactions.

Kamlet and Taft recast Eq. [18] in the form of Eq. [19] with a set of empirical parameters designed to model the various terms. This so-called solvatochromic parameter set $(\pi_2^*, \delta_2, \alpha_2, \beta_2)$ was derived from ultraviolet (UV) spectral shifts of solutes in solvents. The subscript 2 refers to solute parameters; solvent parameters may have different values.

$$P = mV_{x2} + s(\pi_2^* - d\delta) + a\alpha_2 + b\beta_2 + P_0 \quad [19]$$

In Eq. [19], $V_{x2}$ is the McGowan volume that models the energy needed to make a solute molecule-sized cavity in the solvent. Again, the subscript 2 denotes a solute molecule. The parameters $\pi_2^*$ and $\delta_2$ account for dipolarity/polarizability, and $\alpha_2$ and $\beta_2$ model hydrogen bond (HB) acidity and basicity, respectively. This parameter set was used to correlate more than 250 biological, chemical, and physical properties successfully.[66]

Abraham[67] built on this approach and developed a new empirical parameter set that provided better correlations, Eq. [20].

$$P = vV_{x2} + rR_2 + s\pi_2^{\mathrm{H}} + a\sum\alpha_2^{\mathrm{H}} + b\sum\beta_2^{\mathrm{H}} + P_0 \quad [20]$$

In Eq. [20], $R_2$ is the excess molar refraction (MR), which is the MR of the solute less the MR of the alkane with the same characteristic volume, $V_{x2}$, as the solute. The $\pi_2^{\mathrm{H}}$ symbol is the dipolarity/polarizability, and $\sum\alpha_2^{\mathrm{H}}$ and $\sum\beta_2^{\mathrm{H}}$ are the so-called overall HB acidity and basicity descriptors, respectively. The summation sign is used to emphasize that these are "overall" HB properties designed to be appropriate to situations where the solute molecule is surrounded by an excess of solvent molecules. These descriptors are in contrast to the HB descriptors $\alpha_2$ and $\beta_2$ employed in Eq. [19], which are derived from 1:1 complexation constants. Equation [20] has also been used with the $V_{x2}$ term replaced by a log $(L^{16})$ term, where $L^{16}$ is the equilibrium constant

for the distribution of solute (gas) $\rightleftarrows$ solute (hexadecane), generally at 25 °C. Such LSER parameters can be determined with chromatographic techniques. For example, an acidic stationary phase in gas–liquid chromatography (GLC) could be used to measure the HB basicity values. Good correlation equations for many properties have been derived with these parameters. Not surprisingly, the chromatographic retention index is one of the properties with good regression equations.[67]

Although the Abraham LSER parameter set produces good correlations for many properties, two questions arise. First, what about compounds for which these empirical parameters have not yet been obtained? Second, can a theoretical, structurally based molecular parameter set be calculated that might model the empirical parameters and/or produce good quality correlation equations? The first question can be answered by noting that already there are methods[68] for estimating empirical parameter values of new functional groups and elements. However, theoretical descriptors would be more convenient. The answer to the second question is affirmative; indeed, it is the reason for this chapter.

Abraham et al.[22] correlated the gas–water [R(g) $\rightleftarrows$ R(aq)] distribution coefficient, $L^{W}$ (unitless), at 298 K in water for a large set of compounds, with the LSER descriptors to obtain Eq. [21].

$$\begin{aligned}&\log L^{W}\\ &= -0.869\,V_x + 0.577\,R_2 + 2.5492\,\pi_2^{H} + 3.813\sum\alpha_2^{H} + 4.841\sum\beta_2^{H} - 0.994\\ &\quad \pm 0.031 \qquad \pm 0.032 \qquad \pm 0.037 \qquad \pm 0.040 \qquad \pm 0.040 \qquad \pm 0.31\end{aligned} \tag{21}$$

$$n = 408 \qquad r^2 = 0.9952 \qquad s = 0.151 \qquad F = 16{,}810$$

The statistical results indicate that the five descriptors give a very good fit of the experimental data. The positive signs for $R_2$ and $\pi_2^{H}$ that suggest that aqueous solubility increases with an increase in the dipolarity/polarizability for each molecule. Similarly, aqueous solubility increases with an increase in HB parameters, while it decreases with an increase in size of the cavity that must be created in water.

In another example, Abraham et al.[69] correlated the nasal pungency thresholds (NPT), in parts per million (ppm), for a set of compounds at 298 K with the LSER parameters to obtain Eq. [22].

$$-\log \mathrm{NPT} = 2.154\,\pi_2^{H} + 3.552\sum\alpha_2^{H} + 1.397\sum\beta_2^{H} + 0.860\log(L^{16}) - 8.519 \tag{22}$$

$$n = 43 \qquad r^2 = 0.955 \qquad s = 0.27 \qquad F = 201$$

The one outlier, acetic acid, was excluded from this equation. The compounds used in this study included esters, aldehydes, ketones, alcohols, carboxylic

acids, aromatics, hydrocarbons, and pyridines. The relationship is both statistically and physically understandable. As expected, NPT values increase with increases in the dipolarity/polarizability, HB acidity and basicity as well as the gas–hexadecane distribution coefficient. From this type of analysis, one can conclude that the nasal receptor has both acidic and basic sites and that the better molecules are at sticking to the nasal tissue, the more pungent they are.

***Quantum Mechanical Descriptors***

*Energy and Charge Descriptors* The introduction commented on the possibility of calculating $pK_a$ values of carboxylic acids starting from molecular structure. Using a set of 32 aliphatic carboxylic acids, Grüber and Buss[70] correlated $pK_a$ values with a set of QM descriptors that were based on the structure of the molecule and its conjugate base anion. These authors used both MNDO and AM1 MO methods with the latter giving slightly (insignificantly) better (0.001 in $r^2$) correlation equations. The $\Delta H_f$ descriptor value (kcal/mol) used refers to the difference in enthalpy of formation for the anion and neutral molecule. It is related to the gas-phase acidity of the compound. This descriptor is not to be confused with the usual $H_f$ values produced in QM output files. The $E_{HOMO}$ (eV) is the energy of the HOMO of the anion. Several atomic charges (acu, atomic charge units) were used in the regression: $q_{11}$ refers to the $RO^-$ oxygen; $q_{12}$ refers to the $COO^-$ carbon. Equation [23] is the regression equation for carboxylic acids; three of the parameters ($E_{HOMO}$, $q_{12}$, and $q_{11}$) pertain to the corresponding carboxylate ion.

$$\begin{array}{ccccccc} pK_a = & -0.06\,\Delta H_f & + 41.70\,q_{12} & - 1.58\,E_{HOMO} & - 51.90\,q_{11} & - 45.28 \\ & \pm 0.03 & \pm 7.47 & \pm 0.35 & \pm 8.47 & \pm 6.76 \end{array} \qquad [23]$$

$$n = 30 \qquad r^2 = 0.86 \qquad s = 0.51 \qquad F = 46.4$$

In this analysis, two outliers were detected, 2,2-dimethylpropanoic acid and 3-sulfopropanoic acid; they were excluded from the final model. The physically reasonable nature of the relation is illustrated by noting that a decrease in $pK_a$ (increase in acidity, less tendency to hold the proton) is associated with a smaller positive charge on the $COO^-$ carbon and less negative charge on the $RO^-$ oxygen.

For a combined set of 183 phenols and aromatic and aliphatic carboxylic acids, in the same paper, Grüber and Buss derived Eq. [24]. Here $q_1$ is the charge on the OH oxygen; the other descriptors were defined in regard to Eq. [23].

$$\begin{array}{ccccccc} pK_a = & 0.16\,\Delta H_f & - 13.01\,q_1 & + 0.12\,E_{HOMO} & + 33.74\,q_{11} \\ & \pm 0.08 & \pm 2.93 & \pm 0.01 & \pm 5.87 \end{array} \qquad [24]$$

$$n = 183 \qquad r^2 = 0.88 \qquad s = 1.01$$

No intercept value was listed, and there were no outliers. It is of interest to note the reversal of signs for $q_{11}$, $\Delta H_f$, and $E_{HOMO}$ when comparing Eq. [24] with Eq. [23] for the aliphatic carboxylic acids. The primary difference is the $q_1$ term suggesting that a decrease in negative charge on the ROH oxygen is associated with an increase in acidity (lower p$K_a$).

*Theoretical Linear Solvation Energy Relationship (TLSER)* With the LSER descriptors of Kamlet and Taft in mind, Famini and Wilson[71] developed QM-derived parameters to model terms in Eq. [18] and dubbed these the TLSER descriptors. Descriptor calculations are done with the MNDO Hamiltonian in MOPAC and AMPAC. MNDO has greater systematic errors than do AM1 and PM3, but the errors tend to cancel out better in MNDO-derived correlation equations. A program called MADCAP was developed[72] to facilitate descriptor calculation from MOPAC output files.

In the work of Famini and Wilson,[71] a molecular volume, $V_{mc}$, (units of 100 Å$^2$) is used to model the cavity term that measures the energy required to create a solute-molecule sized cavity in the solvent. The dipolarity/polarizability term, which attempts to account for dispersion-type interactions, is modeled by the polarizability index, $\pi_I$, (unitless). This index is defined as the average molecular polarizability divided by the molecular volume, $\alpha/V_{mc}$, and helps account for the correlation between polarizability and molecular volume.

Hydrogen bonds are modeled by covalent and electrostatic terms. Covalent HB basicity is accounted for by a linear transformation of the HOMO energy, $\varepsilon_B = 0.30 - 0.01(E_{lw} - E_h)$, in units of 0.01 eV, where $E_{lw}$ is the LUMO energy for water, and $E_h$ is the HOMO energy of the molecule. The particular parameter has been scaled to be similar in magnitude to the other descriptors. Covalent HB acidity is modeled analogously, $\varepsilon_A = 0.30 - 0.01(E_l - E_{hw})$, in units of 0.01 eV, where $E_l$ is the LUMO energy of the molecule, and $E_{hw}$ is the HOMO energy of water. The electrostatic HB basicity descriptor is described by the most negative atomic charge, $q_-$ (acu, atomic charge units). Analogously, the electrostatic acidity descriptor is modeled by the most positive hydrogen-atom charge, $q_+$ (acu).

Two other types of descriptor have been included recently to help describe dipolarity and the possibility of multiple ligands. The molecular dipole moment, μ, has been found to be insignificant in these TLSER correlations; consequently, it was not included in the overall set of descriptors. However, it is possible to define local dipole moments in terms of atomic charges and interatomic distances, Eq. [25].

$$\mu_{tot} = \frac{1}{2}\sum_j \sum_k |q_j - q_k||r_j - r_k| \qquad \mu_{max} = \frac{1}{2}(|q_j - q_k||r_j - r_k|)_{max} \qquad [25]$$

Here the sums are over all pairs, and $n$ is the number of pairs. In addition, the average dipole moment is given by $\mu_{avg} = \mu_{tot}/n$. A more realistic approach might be to sum over the bonded pairs. The units are in acu Å. The second

new descriptor, intended to model multiple ligand possibilities, involves charge variance defined in a manner suggested by the Politzer and Murray electrostatic potential variances.[16] The charge variance (in units of $acu^2$) is defined by Eq. [26] with $q_k$ being the charge on atom k.

$$\delta_{cv}^2 = \frac{1}{n-1}\sum_k (q_k - \langle q \rangle)^2 \qquad [26]$$

Here $n$ is the number of atoms, and $\langle q \rangle$ is the average atomic charge. The latter should be zero for a neutral molecule. Analogous parameters can be defined for negative and positive charge variances separately. Large variation in charge is presumed to model the possibility of multiple ligand sites on a molecule. For example, two amino groups on a molecule would provide two HB proton acceptor (ligand) sites; the N atoms would have similar charges. Such a molecule would have a larger variation in charge across its surface, hence, larger charge variance, than a molecule with only one amino group.

For the same large set of compounds used in deriving Eq. [21], the gas–water distribution coefficient, $L^W$ (unitless), for a set of 423 compounds at 298 K was correlated with the set of TLSER descriptors resulting in Eq. [27].[71] (The subscript 2 refers to solvent parameters.)

$$\log L^W = -0.766\, V_{mc2} + 29.02\, \pi_{I2} + 36.17\, \varepsilon_{B2} + 9.370\, q_{-2} + 12.39\, q_{+2} - 8.706$$

$t$ ratio 4.8 6.1 6.6 21.4 15.7 14.2

VIF 2.20 2.20 1.30 1.48 1.14 [27]

$n = 417 \quad r^2 = 0.810 \quad s = 0.939 \quad F = 352 \quad q^2 = 0.745$

There were six outliers, cyanomethane, cyanoethane, 1-cyanopropane, 1-cyanobutane, *n*-acetyl-pyrrolidine, 3-acetylpyridine, compared to none found in deriving Eq. [21]. The statistical significance of Eq. [27] is given by the correlation coefficient, $r^2$, indicating that it accounts for at least 81% of the variance in the data set. Furthermore the cross-validated correlation coefficient, $q^2$, indicates that the equation has good predicting ability. The *s*/range ratio is on the order of 10% giving a further indication of equation's significance. This suggests that the standard error is small compared to the range of values for the property. The physical significance is indicated by the signs of the coefficients that show the expected increase in solubility in water with increased HB acidity and basicity. In fact, the most statistically significant terms in Eq. [27] (those with the highest $t$ ratios) involve the HB electrostatic models for basicity and acidity. Also, as expected, increased volume, associated with increased dispersion interactions, accompanies decreased water solubility

($\log L^{W}$). Only 6 out of the 423 compounds are outliers; each of them contains nitrogen, with four being CN groups.

When dipole moments and charge variances are incorporated in the descriptor set, the resulting equation contains the same terms as in Eq. [27], but it also contains the total and positive charge variances. The HB electrostatic models for basicity and acidity are still the most significant contributors in that order. There is one more outlier, triethyl phosphate. The statistics are $r^2 = 0.808$, $s = 0.935$, $F = 247$, and $q^2 = 0.754$. The average VIF value, a measure of the intercorrelation or orthogonality of the descriptors in the equation, is higher at 1.73 as compared to 1.66 for Eq. [27]. For this property and this set of compounds, there is little advantage to including the new descriptors.

Debord and colleagues[73] correlated LSER and TLSER parameters with the concentration for 50% inhibition, $C_{50}$ (M), at 298 K for arylesterase by 11 aliphatic alcohols. The LSER parameters gave rise to Eqs. [28a–b], and the TLSER yielded Eqs. [29a–b]. There are two isozymes, A and B; separate equations were derived for each. The intercepts were insignificant in all four equations; so no deviation is listed. Here we use the common transform $pC_{50} = -\log C_{50}$.

$$pC_{50}\ (A) = 10.23\,V_x - 4.61\,V_x^2 - 5.17\,\pi_2^H - 0.44 \qquad [28a]$$
$$\pm 0.97 \quad \pm 0.65 \quad \pm 1.12$$
$$n = 11 \quad r^2 = 0.99 \quad s = 0.12 \quad F = 217$$

$$pC_{50}\ (B) = 10.82\,V_x - 5.02\,V_x^2 - 4.85\,\pi_2^H - 0.73 \qquad [28b]$$
$$\pm 1.24 \quad \pm 0.84 \quad \pm 1.42$$
$$n = 11 \quad r^2 = 0.98 \quad s = 0.15 \quad F = 134$$

$$pC_{50}\ (A) = 11.14\,V_{mc} - 4.61\,V_{mc}^2 - 253.04\,q_+ - 46.22 \qquad [29a]$$
$$\pm 0.94 \quad \pm 0.54 \quad \pm 84.90$$
$$n = 11 \quad r^2 = 0.98 \quad s = 0.16 \quad F = 125$$

$$pC_{50}\ (B) = 11.74\,V_{mc} - 5.05\,V_{mc}^2 - 99.14\,q_- - 28.93 \qquad [29b]$$
$$\pm 1.05 \quad \pm 0.60 \quad \pm 36.88$$
$$n = 11 \quad r^2 = 0.98 \quad s = 0.17 \quad F = 106$$

The empirical LSER parameter set provides slightly better correlation equations. The volume contributions were similar for the LSER and TLSER derived regressions since the empirical (McGowan) and theoretical volume parameters are highly correlated. The inclusion of a volume squared term is consistent with the qualitative observation of an increase with size up to a

certain point (a maximum), hence a parabolic relationship. In Eqs. [22a–b], inhibitory activity is enhanced ($pC_{50}$ made smaller) by greater dipolarity/polarizability suggesting some dipole interaction at the enzyme site. Smaller $pC_{50}$ values, hence smaller concentrations, imply greater effectiveness in inhibiting the enzyme.

The TLSER correlations have charges in place of the LSER dipolarity/polarizability, $\pi_2^H$. The interesting thing to note is that isozyme A involves a positive charge parameter, and isozyme B involves a negative charge parameter. A partial explanation for this peculiarity is that the two charge descriptors happen to correlate with each other ($r = 0.76$).

Famini and Wilson[74] correlated the solubility, $S$ (mol fraction $\times 10^4$), for a set of aromatic compounds in supercritical $CO_2$ at 308 K and 14 megapascal (MPa).

$$\log S = -6.04\,\pi_I + 10.4\,\varepsilon_B - 20.1\,q_- + 24.4\,q_+ - 8.37 \qquad [30]$$

| | | | | |
|---|---|---|---|---|
| $t$ test | 3.4 | 2.4 | 7.6 | 6.2 |
| VIF | 2.4 | 2.6 | 7.0 | 7.1 |

$n = 19 \quad r^2 = 0.861 \quad s = 0.477 \quad F = 22$

Figure 1 displays the relation between the observed and calculated log $S$ values for data used in Eq. [30]. Three compounds were found to be outliers: benzoic acid, phthalic anhydride, and acridine. Their values (not shown in Figure 1)

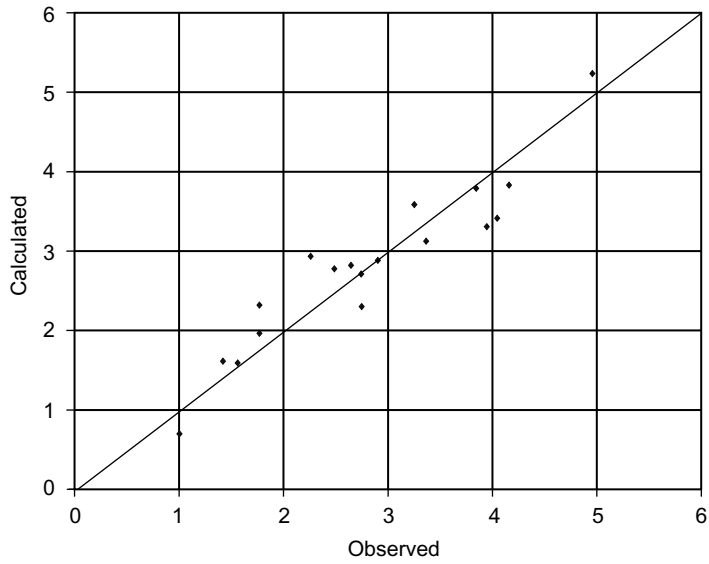


**Figure 1** Plot of calculated versus observed log $S$ values based on Eq. [30]. See Ref. 74. $S$ is the solubility of aromatics in supercritical $CO_2$ at 308 K and 14 MPa.

would have been considerably farther from the line representing perfect correlation than those displayed. The VIF values for Eq. [30] for the charges are a bit high; some references[57] suggest that a VIF value less than 10 is acceptable. However, most publishable TLSER work is limited to VIF values less than 5. The physical significance of Eq. [30] is not obvious. Carbon dioxide is incapable of acting as an acid (except in water as carbonic acid); consequently, the presence of the basicity terms, regardless of sign, is difficult to explain (unless the $CO_2$ were wet). However, the positive sign on the electrostatic acidity term makes sense; it suggests that increased acidity of the solutes would increase their solubility in the base, $CO_2$. The negative sign on the polarizability index, $\pi_{I2}$, is reasonable if one considers $CO_2$ to be a "hard" base.[75] "Hard" solutes would have decreased polarizability indexes and, thus, increased solubility in accord with Eq. [30].

Using a set of 479 compounds, Liang and Gallagher[76] correlated the vapor pressure, $p$ (Torr), at 298 K with the TLSER related descriptors to obtain Eq. [31]. Only a single descriptor was needed to provide a respectable result.

$$\log p = -0.401\,\alpha + 3.940 \qquad [31]$$
$$n = 479 \qquad r^2 = 0.922 \qquad s = 0.745 \qquad q^2 = 0.920$$

Here, $\alpha$ is the polarizability related through TLSER descriptors by $\alpha = \pi_{I2}\, V_{mc}$. The physical meaning of Eq. [31] is indicated by the negative sign on the polarizability term. Increased polarizability would increase the dispersion type intermolecular interactions and, thus, decrease the vapor pressure.

Liang and Gallagher[76] found that the inclusion of counting descriptors for OH, C=O, NH, COOH, $NO_2$, and CN groups improved somewhat the correlation as expressed in Eq. [32].

$$\log p = -0.432\,\alpha - 1.382\,N_{OH} - 0.482\,N_{C=O} - 0.416\,N_{NH} - 2.197\,N_{COOH} - 1.383\,N_{NO_2} - 1.101\,N_{CN} + 4.610 \qquad [32]$$
$$n = 479 \qquad r^2 = 0.960 \qquad s = 0.534 \qquad q^2 = 0.957$$

The negative signs are physically reasonable because these additional parameters would be expected to be associated with increased intramolecular attractions. The authors provided no measure of intercorrelation; indeed, one might expect some correlation of $\alpha$, the average molecular polarizability, with the presence of C=O, COOH, $NO_2$, and CN groups. The counting descriptors are not QM quantities; their inclusion is not philosophically satisfying, but they do improve the fit.

*GIPF (Molecular Electrostatic Potential)* Politzer and Murray[54,77] developed a general interaction property function (GIPF) based on MEP symbolized

here as $U$. The GIPF emanates from the idea that the electrostatic field of a molecule influences its interactions with other molecules. The GIPF descriptors are calculated by ab initio MO methods. Early work was done with Hartree–Fock theory with the STO-3G* basis set for finding the optimized geometry and the STO-5G* for the electrostatic potential. However, for the example to be presented here, the QM calculations were done with DFT using B3P86 functionals with the 6-31+G** basis set option in Gaussian 94.[78]

Early MEP-based parameters considered included surface area ($A$), $\Pi$, $\sigma^2_{tot}$, and $\nu$. Here $\Pi$ is a measure of local polarity, and $\sigma^2_{tot}$ is a measure of electrostatic interaction tendency. Larger values imply larger charge separation leading to greater electrostatic interaction. Electrostatic interactions are also described by $\nu$, which is a measure of electrostatic balance. The three charge related variables are defined in terms of the surface electrostatic potential difference, $\delta U_i$, at the $i$th point, Eq. [33],

$$\delta U_i = [U(\mathbf{r}_i) U_S] \tag{33}$$

where $U_S$ is the average MEP over the surface. The local polarity, $\Pi$, is defined in Eq. [34], where $n$ is the number of surface points used in the summation.

$$\Pi = \frac{1}{n} \sum_{i}^{n} |\delta U_i| \tag{34}$$

The $\sigma^2_{tot}$ descriptor, another measure of local interaction tendency, is defined in Eq. [35]

$$\sigma^2_{tot} = \sigma^2_{+} + \sigma^2_{-} \tag{35}$$

where the individual terms are sums over the positively and negatively charged surface points, respectively, as described in Eq. [36]. These are equivalent to variances in the electrostatic potential difference, $\delta U_i$, for the positive, negative, and total points on the surface.

$$\sigma^2_{\pm} = \frac{1}{n_{\pm}} \sum_{i=1}^{n_{\pm}} |\delta U_i|^2 \tag{36}$$

Finally, the electrostatic balance parameter, which is made up of the parameters defined in Eqs. [35] and [36] and is seen to be dimensionless, is expressed by Eq. [37].

$$\nu = \sigma^2_{+} \sigma^2_{-} / (\sigma^2_{tot})^2 \tag{37}$$

Electrostatic balance can be illustrated by noting that alcohols are more "balanced" between having HB donors and acceptors; that is, they have higher ν values than their structurally isomeric ethers. This correlates with alcohols being relatively strong HB donors and acceptors, whereas the ethers are only HB acceptors.

Another descriptor used in this MEP approach is the average local ionization energy, $I(\mathbf{r})$, defined at some point, **r**, as the following sum, Eq. [38].

$$I(\mathbf{r}) = \sum_i \rho_i(\mathbf{r})|\varepsilon_i|/\rho(\mathbf{r}) \qquad [38]$$

Here $\rho_i(\mathbf{r})$ and $\rho(\mathbf{r})$ are the electron density for the *i*th MO and total electron density at some point **r**, respectively, and $E_j$ is the MO energy. The parameter $I(\mathbf{r})$ models the energy need to remove an electron from that point in the field of the molecule. Consequently, the ionization potential measured at the site with the lowest value, $I_{\min}$, could account for the tendency of a molecule to react with electrophiles. The quantity, $I_{S,\min}$, is evaluated at the surface of lowest potential; $U_{S,\min}$ is the analogous electrostatic potential. Averages over the positive and negative values can also be computed in this way. Other related parameters include $A_{-S}$, the negatively charged surface area, and $U_{-S,\text{avg}}$, the average electrostatic potential over this area. The parameter $U_{\min}$ is the most negative MEP value anywhere around the molecule.

Murray, Abu-Awwad, and Politzer[79] used GIPF descriptors to correlate aqueous solvation Gibbs free energies, $\Delta G_{\text{sol}}$ (kJ/mol), for R(g) $\rightleftarrows$ R(aq) at 298 K.

$$\Delta G_{\text{sol}} = 0.712U_{\min} - 2.6412 \times 10^{-5}(U_{S,\max} - U_{S,\min})^3 + 5.1892 \times 10^{-2}A_{-S}U_{-S,\text{avg}} + 9.7042 \times 10^3(A_{-S}U_{-S,\text{avg}})^{-1} + 46.827 \qquad [39]$$

$$n = 50 \qquad r^2 = 0.976 \qquad s = 1.57$$

The physical significance of Eq. [39] can be interpreted by the negative ($U_{S,\max} - U_{S,\min}$) term. Greater charge variation on the surface of a solute molecule means a greater separation of positive and negative charges on the surface. This variation implies more space for interaction with hydrogen and oxygen atoms on water molecules and, hence, a decrease in $\Delta G_{\text{sol}}$. Decreased (more negative) free energy implies greater tendency to interact (greater "spontaneity"). The increase in free energy with $U_{\min}$ implies that the H atom interactions are more important than oxygen interactions. Terms involving the area multiplied by potential may be viewed as terms describing size effects; these may be associated with dispersion interactions, for example. Larger dispersion interactions would lead to stronger solute–solute attractions and smaller solute-water attraction.

Using the same set of compounds as those for Eq. [30], Politzer et al.[80] correlated the solubility, $S$ (mol fraction $\times 10^4$), in supercritical $CO_2$ at 308 K and 14 MPa with the GIPF descriptors to derive Eq. [40].

$$\log S = 12.321 \times 10^3 (V)^{-1.5} - 2.24 \times 10^{-4} (\sigma_{\text{tot}}^2)^2 - 10.378 \qquad [40]$$

$$n = 21 \qquad r^2 = 0.90$$

Only one compound was an outlier for Eq. [40], whereas there were three for Eq. [30]. As in the case for Eq. [30], the physical significance of Eq. [40] is not readily apparent, although decreased volume could be associated with decreased polarizability and, thus, greater "hardness". This in turn would increase the interaction with "hard" $CO_2$ and, hence, increase the solute solubility. The decrease in solubility associated with the increase in the charge variance might be associated with decreased interaction with the nonpolar $CO_2$ molecule. As with Eq. [39], Eq. [40] has terms raised to unusual powers.

Eisfeld and Maurer[81] correlated the octanol/water partition coefficient, $P_{\text{ow}}$ (unitless), defined as the ratio of the concentration of the solute R in the two phases, [R(octanol)]/[R(aq)], for the process, R(aq) $\rightleftarrows$ R(octanol), to obtain Eq. [41] for a set of about 200 compounds. As mentioned previously, this empirical quantity has been used as a descriptor in the classical Hansch QSAR correlations. In the study of Eisfeld and Maurer, the descriptors were calculated with an ab initio Hartree–Fock model using a 3-21G* basis set and the Gaussian 94 program. The polarity of each molecule is accounted for by terms containing the dipole moment ($\mu$), polarizability ($\alpha$), percentage of negative electrostatic potential ($U_{-\text{S},\%}$), and mean square of the negative electrostatic potential on the surface ($[U_{-\text{S,avg}}]^2$). The influence of $\pi$ bonds in the data set is accounted for by the average of the negative electrostatic potential ($I_-$), which is the negative electrostatic potential summed over the volume divided by the total electrostatic potential summed over the same volume. The delocalized electrons associated with $\pi$ bonds are expected to correspond to a large negatively charged surface area compared to the total area. Hydrogen bonding is modeled by the $\sum U_{\text{min}}$ and $\sum U_{\text{max}}$ terms. The parameter $V$ is the molecular volume. The counting descriptors, $N_{\text{N}}$ and $N_{\text{O}}$, which measure the number of N and O atoms, respectively, were included to improve the overall quality of the correlation. The equation is linear in composite descriptors but not in volume.

$$\begin{aligned} \log P_{\text{ow}} = {} & 3.393\, V + 0.595\, \mu V + 0.739\, \alpha / V^2 - 0.876\, U_{S,\%} - 5.769\, I_- \\ & + 3.393 \sum U_{\text{min}} - 0.586 \sum U_{\text{max}} - 0.034\, [U_{-\text{S,avg}}]^2 V^2 \\ & - 0.259\, N_{\text{N}} - 0.241\, N_{\text{O}} - 0.305 \end{aligned} \qquad [41]$$

$$n = 202 \qquad s = 0.274$$

The only statistical parameter provided was $s$. However, Figure 2, plotted from their data, shows that the data clusters quite well around the line

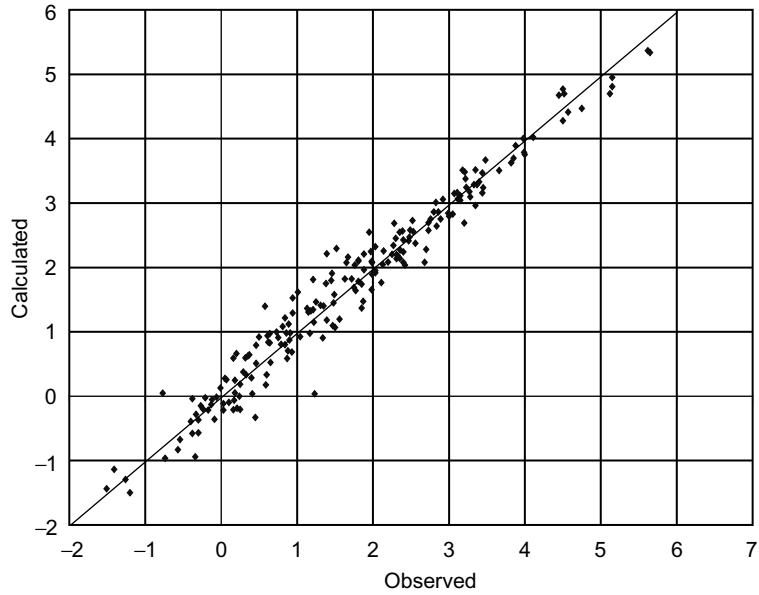


**Figure 2** Plot of calculated versus observed log $P_{ow}$ values based on Eq. [41]. See Ref. 81. $P_{o/w}$ is the octanol/water partition coefficient at 298 K.

corresponding to perfect correlation. The physical meaning of Eq. [41] is difficult to decipher. However, the volume term, $V$, implies an increase in solubility in octanol with increased molecular volume. This trend is reasonable because increased solute size can be associated with increased dispersion interactions, which leads to increased intermolecular interactions with the nonpolar layer and, hence, increased solubility in octanol, leading to increased $P_{o/w}$ values. The negative sign for $\sum U_{max}$, a HBD acidity measure, implies that an increase in solute acidity would lead to increased water solubility and, hence, decreased $P_{o/w}$ values. This trend is reasonable because increased HBD acidity would lead to increased interaction with water as compared to octanol. Analogous reasoning suggests that increased HBA basicity, $\sum U_{min}$, should increase solubility in octanol as compared to water, which implies that the HBA basicity of water contributes more to solute solubility than does its HBD acidity.

Using a smaller (74) set of compounds, Haeberlein and Brinck[82] correlated the log $P_{o/w}$ at 298 K with a set of GIPF related descriptors to obtain Eq. [42]. Calculations were done at the HF/6-31G* ab initio level using Gaussian 94. In Eq. [42], $A$ is the surface area (Å$^2$) defined as the isodensity surface of 0.001 electrons/bohr$^3$; $[U_{-S,avg}]^2$ is the mean of the squares of the negative molecular electrostatic potential points (kJ/mol) on that same surface; $\mu$ is the dipole moment (Debye); $V$ is the molecular volume (Å$^3$); and $\sum U_{min}$ is the sum over the surface of the MEP less than $-147$ kJ/mol with the provision

that, if two minima were 2.1 Å apart, only the lowest would be used.

$$\log P_{o/w} = 0.0290\,A - 9.99 \times 10^{-7} A[U_{-S,\,avg}]^2 + 2.02\,\mu^2/V + 3.81 \times 10^{-3} \sum U_{min} - 0.894 \qquad [42]$$

$$n = 74 \qquad r^2 = 0.966 \qquad s = 0.292 \qquad F = 481$$

The physical meaning of Eq. [42] is tied to the interpretation of some of the terms, some being convoluted. The $A$ term can be associated with dispersion interactions; an increase in surface area suggests an increase in dispersion interactions (attractions) and, thus, increased solubility in octanol that in turn results in enhanced $P_{o/w}$ values. A similar interpretation holds if one associates $\mu^2/V$ with dipolarity/polarizability effects. The positive sign on the HBA term ($\sum U_{min}$) for the solute suggests that the HBD acidity of water is less important than the HBA basicity of water for those molecules partitioning between phases. This implies that increased solute HBD acidity would increase the solute–water interaction.

Grigoras[83] employed the concept of molecular surface interactions (MSI) to propose new descriptors involving areas quite similar to those in the CPSA set that was described in an earlier section. The four descriptors can be calculated with the extended Hückel theory (EHT) method using modified hydrogen parameters. The total molecular surface area, $A$, is the dispersion molecular surface interactions (DMSI) term. The electrostatic negative molecular surface interactions (ENMSI) term, $A_-$, is the sum of surface areas of negatively charged atoms multiplied by their charges, ($\sum A_{-j}\, q_{-j}$). The electrostatic positive molecular surface interactions (EPMSI) term, $A_+$, is analogous to $A_-$ but excludes positive charges on hydrogen atoms H-bonding to oxygen and nitrogen. The HB molecular surface interactions (HBMSI) term, $A_{HB}$, is analogous to $A_-$ but includes positive charges on hydrogens involved with HB to oxygen and nitrogen, only. Care is taken in the latter two descriptors so that charges are not overcounted.

Grigoras[83] correlated the normal boiling point, $T_b$ (K), for a set of 137 compounds, with these MSI descriptors to obtain Eq. [43]. To minimize confusion with the previously defined symbol $A$ for area, the extended symbols are used here.

$$\begin{array}{lllll} T_b = 0.718\ \text{DMSI} - 1.105\ \text{ENMSI} + 0.230\ \text{EPMSI} + 8.800\ \text{HBMSI} + 127.7 \\ \pm 0.038 \qquad \pm 0.030 \qquad \pm 0.024 \qquad \pm 0.225 \qquad \pm 6.1 \end{array} \qquad [43]$$

$$n = 137 \qquad r^2 = 0.958 \qquad s = 14.1 \qquad F = 745$$

The physical meaning of this equation can be discerned by noting the positive signs on the DMSI and HBMSI terms. Increased dispersion interactions increase molecular attractions and, hence, increase the boiling point. Similarly, an increase in H-bonding molecular interactions would have the same result.

## Nonmodel-Based Methods

Nonmodel-based methods use large sets of descriptors and, often, complex methods for regression analysis. The equations from regression analysis have been labeled by Bakken and Jurs as "type 1" equations.[28] The equations are similar in form to those used with small descriptor sets. Type 1 equations rely on QM and other theoretical descriptors.

### *Jurs and Katritsky Methodology*

Stanton and Jurs[55] developed and used large sets of descriptors consisting of charged partial surface area descriptors along with other theoretical descriptors in correlation studies of a wide range of properties. Some of the CPSA descriptors were designed as models representing hydrogen bonding. The Jurs group relied on the PM3 semiempirical Hamiltonian and employed their ADAPT program to generate a large set of descriptors. As mentioned earlier, CPSA QM descriptors involve charges not necessarily found from QM calculations directly.

Using a set of 352 hydrocarbons and halohydrocarbons, Goll and Jurs[84] correlated the vapor pressure, $p$ (Pa), at 298 K with a mixture of the CPSA and indicator descriptors to derive Eq. [44]. These authors used topological (connectivity) parameters (V0 and N3C), three counting descriptors (NF, NSB, NRA), and two QM descriptors (DPSA, RPCG). The parameter V0 is the zero-order molecular connectivity found by a valence molecular connectivity term; N3C is a third-order cluster that involves counting the number of connections or paths. The terms NF, NSB, and NRA are the numbers of fluorine atoms, single bonds, and atoms appearing in rings (saturated or unsaturated), respectively. The DPSA is the difference between the atomic charge weighted partial positive and partial negative surface areas, (PPSA3) − (PNSA3). Table 3 and the subsection on charged partial surface area descriptors help clarify the notation here; PPSA3 refers to atomic charge weighted PPSA, PPSA2 refers to the total charge weighted PPSA, whereas PPSA1 refers to the ordinary (noncharge weighted) PPSA. The RPCG parameter, relative positive charge, is the charge of the most positive atom divided by the summation of positive charges in the molecule.

$$\begin{aligned}\log p = {} & -0.670\,\mathrm{V0} + 0.204\,\mathrm{NF} + 0.0547\,\mathrm{NSB} - 0.121\,\mathrm{NRA} - 0.0635\,\mathrm{DPSA} \\ & \pm 0.00123 \quad \pm 0.018 \quad \pm 0.0072 \quad \pm 0.004 \quad \pm 0.0023 \\ & + 0.117\,\mathrm{N3C} + 0.518\,\mathrm{RPCG} + 8.15 \\ & \pm 0.007 \quad \pm 0.067 \quad \pm 0.05 \\ & n = 352 \quad r^2 = 0.983 \quad s = 0.186\end{aligned} \qquad [44]$$

The interpretation of Eq. [44] is suggested by the negative DPSA term. Decreased DPSA values mean decreased positively charged surface atom area as compared to negatively charged surface atom area. This could be associated with smaller (weaker) intermolecular surface electrostatic interactions which

would make it easier for molecules to enter the gas phase. The increase of vapor pressure with RPCG, the largest fraction of positive charge on an atom, could be attributed to the mutual repulsion by neighboring molecules.

Katritsky, Mu, and Karelson[85] used the same large set of compounds that was used for deriving Eqs. [21] and [27] to correlate the gas–water distribution coefficient, $L^W$ (no units), at 298 K. A mix of CPSA and indicator descriptors were adopted to obtain Eq. [46]. The QM descriptors were calculated with the AM1 Hamiltonian. To facilitate matters, Katritsky and colleagues developed a program they call CODESSA[86] (comprehensive descriptors for structural and statistical analysis) that generates most of the theoretical descriptors automatically from output files of some common QM programs. CODESSA also contains statistical routines. A descriptor labeled HDCA2 is a HBD surface area weighted charge descriptor defined by $\sum q_D(A_D/A_{tot})^{1/2}$, where $q_D$ is the partial charge on atom D (an HBD H atom), $A_D$ is the exposed surface area of atom D, and $A_{tot}$ is the total molecular surface area. The most negative partial charge weighted topological electronic index, $PCWT^E$, is defined by

$$PCWT^E = \left(\frac{1}{Q_{min}}\right) \sum_j \sum_{k \neq j} |q_j - q_k| / r_{jk}^2 \qquad [45]$$

The parameter $q_j$ is the Zefirov[50] partial charge on atom $j$ mentioned earlier, $Q_{min}$ is the most negative partial charge, and $r_{jk}$ is the distance between atoms $j$ and $k$. It would be interesting to use QM calculated partial charges to compare and contrast with the work of Katritzky, Mu, and Karelson.[85] The O and N counting descriptors are combined in a single term in the following equation:

$$\begin{array}{lccc} \log L^W = & 41.61\,\mathrm{HDCA2} & + 0.71\,(N_O + 2 \times N_N) & - 0.17\,(E_{HOMO} - E_{LUMO}) \\ & \pm 1.11 & \pm 0.02 & \pm 0.02 \\ t \text{ ratio} & 37.44 & 28.41 & 9.42 \\ & + 0.13\,PCWT^E & - 2.82 & \\ & \pm 0.01 & \pm 0.22 & \\ t \text{ ratio} & 19.03 & 12.92 & \end{array} \qquad [46]$$

$$n = 406 \qquad r^2 = 0.941 \qquad s = 0.53 \qquad F = 1269 \qquad q^2 = 0.939$$

The physical meaning of Eq. [46] is suggested by the positive sign of the HBD surface area parameter, HDCA2. Increased HDCA2 values implies increased HBD acidity, which then means greater water solubility and, hence, increased $L^W$ values. Furthermore, the high $t$-test value (37.44) for HDCA2 indicates that it is the statistically most significant term. The most negative charge weighted topological electronic index ($PCWT^E$) term, which is a measure of electrostatic solute–solvent interaction, provides more evidence for the physically reasonable nature of Eq. [46]. As expected, an increase in this index results in an increase in $L^W$.

Katritsky, Lobanov, and Karelson[53] correlated the boiling point, $T_b$ (K), for a set of 584 compounds with a very large set (>800) descriptors of various types, including many of those employed by Jurs and colleagues. Equation [47] regresses on eight descriptors. As before, QM descriptors were calculated with the AM1 Hamiltonian and other calculations were done with CODESSA.

Four QM descriptors involved surface areas: (1 and 2) $CSA2_H$ and $CSA2_{Cl}$, the charged surface area of H ($\sum_j A_{Hj}q_{Hj}$) or Cl atoms ($\sum_j A_{Clj}$ $q_{Clj}$); (3) HDSA2, the HB donor surface area, $\sum_j q_D(A_D)^{1/2}/A_{tot}$, with the sum over donor H atoms (similar to HDCA2 in Eq. [46]); (4) HASA1, the HB acceptor surface area, $\sum_j A_{HBAj}$, over acceptor atoms [O atoms in C=O (but not COOR) and OH, N atoms in amino and aromatic groups, and S atoms in SH groups]. The parameter $G_I$ is the gravitational index, $\sum m_j m_k/r_{jk}$, with $m_j$ and $m_k$ being the masses of atoms $j$ and $k$, and the summation ($j<k$) is over the bonded pairs; it is a measure of bulk cohesiveness. The term $T_I$ is the topographic electronic index, $\sum|q_j - q_k|/r_{jk}^2$ (see Eq. [12]), where $q_j$ and $q_k$ are partial charges on atoms $j$ and $k$ also summed ($j<k$) over the bonded pairs. $N_F$, $N$, and $N_{CN}$ are counting descriptors for F atoms, total atoms, and CN groups, respectively.

$$\begin{aligned} T_b = {} & 64.6\, G_I^{1/3} + 536\, \mathrm{HDSA2} - 193.0\, N_F/N - 86.0\, N_{CN} + 0.75\, \mathrm{HASA1} \\ & \pm 0.73 \qquad \pm 16 \qquad\quad \pm 10.8 \qquad\quad \pm 3.0 \qquad\quad \pm 0.04 \\ & - 85.8\, T_I + 10.4\, CSA2_H + 21.9\, CSA2_{Cl} - 166.5 \qquad [47] \\ & \pm 4.7 \qquad \pm 0.68 \qquad\quad \pm 2.1 \qquad\quad\ \pm 5.3 \\ & n = 584 \qquad r^2 = 0.9645 \qquad s = 15.5 \end{aligned}$$

A physical interpretation of Eq. [47] can be made by noting the positive signs on the gravitational and QM descriptors. It is expected that boiling points would increase with increased intermolecular attractions. The gravitational index, $G_I$, is a size dependent descriptor that accounts for dispersion and cavitation effects in the liquid. Hydrogen-bonding donor–acceptor interactions would be expected to increase with increased values for HDSA2, HASA1, and $CSA2_H$.

Following a similar approach but using a smaller data set of 369 compounds, Ivanciuc et al.[87] correlated their liquid viscosity ($10^{-3}$ Pa s) at 298 K with a mixed set of descriptors to obtain Eq. [48]. This involves three QM descriptors, one topological, and one constitutional descriptor. The QM descriptors were calculated with the AM1 Hamiltonian in AMPAC, and CODESSA was used to calculate the descriptors and perform the statistical analyses. The HDCA2 parameter is the same HBD charged surface area used in Eq. [46]. The maximum electrophilic reactivity index, $E_A$, for a carbon atom is defined by $\sum_j c_{LUMO,j}^2/(E_{LUMO}+10)$, with the summation over the valence AOs on a carbon atom in the LUMO. The maximum AO electronic population, $Y$, models the molecular nucleophilicity and is defined by

$2\sum_j c_j^2$, where the sum runs over the occupied MOs for a single AO. The molecular mass is represented by M, and $^3\chi$ is the Randić connectivity index of order 3.

$$\begin{aligned}\ln \eta = {} & +3.387\ \mathrm{HDCA2} + 8.858 \times 10^{-3}\ \mathrm{M} + 0.3919\ {}^3\chi \\ & \pm 0.139 \qquad \pm 0.647 \times 10^{-3} \qquad \pm 0.0303 \\ & -8.486\ \mathrm{E_A} + 0.6684\ \mathrm{Y} - 2.184 \\ & \pm 1.435 \qquad \pm 0.0803 \qquad \pm 0.144 \end{aligned} \quad [48]$$

$$n = 337 \qquad r^2 = 0.846 \qquad s = 0.371 \qquad F = 367$$

The physical meaning of Eq. [48] is indicated by the positive sign on the hydrogen-bonding charged surface parameter, HDSA2. Increased hydrogen bonding would be expected to increase intermolecular attractions and, hence, viscosity. The increase of viscosity with increased molecular mass is also expected; dispersion interactions increase with mass. A similar argument applies to *Y*, which models nucleophilic reactivity.

Bodor and Huang[88] correlated the octanol/water partition coefficient, $P_{\mathrm{o/w}}$ (unitless) at 298 K for a set of 302 compounds with a set of 58 descriptors to obtain Eq. [49]. These parameters include seven QM based descriptors that were calculated with the AM1 method. The dipole moment is μ(D); $Q_{\mathrm{O}}$ and $Q_{\mathrm{N}}$ are the square roots of the sum of the squares of charges on the O and N atoms, respectively. The parameter $Q_{\mathrm{ON}}$ is the sum of absolute values of charges on the O and N atoms, and ABSQ is the sum of the absolute values of the charges on all atoms. In addition to these QM descriptors, the surface area, *A* (Å$^2$) , and the ovality, *O*, were calculated from the QM-optimized geometry. The ovality is defined by actual area/area as a sphere, $O = A/[4\pi(3V/4\pi)^{2/3}]$. The molecular mass, *M*, and two indicator variables, $N_{\mathrm{alk}}$ and $N_{\mathrm{C}}$, for alkanes and carbon atoms, respectively, were also employed.

$$\begin{aligned}\log P_{\mathrm{o/w}} = {} & 0.057261\,\mu + 1.0392\,N_{\mathrm{alk}} - 17.377\,Q_{\mathrm{N}}^4 + 31.243\,Q_{\mathrm{N}}^2 \\ & \pm 0.043557 \quad \pm 0.2198 \qquad \pm 3.843 \qquad \pm 3.443 \\ & - 8.5144\,Q_{\mathrm{N}} - 5.4195\,Q_{\mathrm{O}}^4 + 20.346\,Q_{\mathrm{O}}^2 - 4.6249\,Q_{\mathrm{O}} \\ & \pm 1.3688 \qquad \pm 3.5436 \qquad \pm 3.261 \qquad \pm 1.1402 \\ & - 5.0040\,Q_{\mathrm{ON}} + 0.0052861\,\mathrm{M} - 1.1414 \times 10^{-4} A^2 + 0.059838\,A \\ & \pm 0.7632 \qquad \pm 0.0026608 \qquad \pm 0.1641 \times 10^{-4} \qquad \pm 0.014051 \\ & + 0.083249\,N_{\mathrm{C}} - 0.27406\,\mathrm{ABSQ} - 7.6661\,O - 5.5961\,O^2 \\ & \pm 0.058322 \qquad \pm 0.14935 \qquad \pm 29.1952 \quad \pm 14.6597 \\ & + 2.1059\,O^4 - 9.5524 \\ & \pm 1.0550 \end{aligned} \quad [49]$$

$$n = 302 \qquad r^2 = 0.95656 \qquad s = 0.30579 \qquad F = 367.9$$

This equation is the lengthiest in this chapter. The uncertainties associated with the $O$ and $O^2$ terms are very high; it is not clear why the authors included them. The physical significance of Eq. [49] is hinted at by the signs on the first power $Q_N$ and $Q_O$ terms as well as the ABSQ term. Increasing values of these parameters would accompany increased HB basicity leading to increasing water solubility and, hence, a lower $P_{o/w}$ value. The sign on the surface area parameter, $A$, also is reasonable in that increased molecular surface area is associated with increased dispersion interactions that in turn leads to increased solubility in octanol and, hence, a higher $P_{o/w}$ value.

## CONCLUSIONS

Seeking correlations in a chemical system presumes an inherent relationship between a bulk (macroscopic) property of a compound and its molecular structural (microscopic) properties. Based on the examples given here, QM-derived descriptor sets can provide statistically significant correlation equations for a wide range of properties. However, as mentioned in the Introduction, empirical descriptor sets often provide better quality correlation equations than do the QM sets. Despite this, QM descriptor sets can still provide significant regression equations to go along with the convenience in obtaining the descriptors.

Including counting descriptors (indicator variables) with the QM descriptors tends to improve the quality of some of the theoretical correlation equations. As pointed out by the Katritsky group,[85] the inclusion of the counting descriptors for O and N may be due to a deficiency in calculated charges needed to adequately describe electrostatic and hydrogen-bonding interactions. A possible explanation for this could be defective or inadequate parameterization of the semiempirical QM model Hamiltonians; perhaps inclusion of more oxygen- and nitrogen-containing compounds in the parameterization of the semiempirical methods might have improved the fit. However, the parameterization was done as best as possible at the time of the method development. Interpretation of the regression equations is facilitated when more than one QM descriptor is viewed as contributing to a given classical chemical concept, for example, dispersion interactions, dipolarity–polarizability, and hydrogen bonding, which provide the underpinning for the molecule's observed physical properties.

The examples presented here help us to address the question of whether to use a model-based (small sets of simply interpreted descriptors) or nonmodel-based QSAR/QSPR method (large sets of descriptors). The model-based equations (which includes LFERs) can be used to fairly readily predict the result of changing molecular structure on a property. This is because these equations can often be easily interpreted from a chemical viewpoint. The nonmodel-based equations are frequently not so easily interpreted

in chemical terms. On the other hand, the quality of their statistical parameters suggest that values calculated with nonmodel-based equations might be closer to what would be measured.

Because many chemical (and all biochemical) processes occur in condensed phase, a fruitful approach for improving QM correlation equations might involve QM descriptor calculation with a computational scheme that includes solvation effects.[32] In this connection, it is important to note that a QSPR study of gas/water distribution showed little difference between a regression equation derived with isolated molecule parameters and one calculated with solvated molecular parameters.[85] Since one example does not constitute proof, continued investigation is warranted.

## REFERENCES


1. G. R. Famini and L. Y. Wilson, *Org. Reactivity,* **29,** 117 (1995). Characterizing Solute–Solvent Interactions.
2. J. J. P. Stewart, in *Reviews in Computational Chemistry,* K. B. Lipkowitz and D. B. Boyd, Eds., VCH Publishers, New York, 1990, Vol. 1, pp. 45–81. Semiempirical Molecular Orbital Methods.
3. M. C. Zerner, in *Reviews in Computational Chemistry,* K. B. Lipkowitz and D. B. Boyd, Eds., VCH Publishers, New York, 1991, Vol. 2, pp. 313–365. Semiempirical Molecular Orbital Methods.
4. W. J. Hehre, L. Radom, P. v. R. Schleyer, and J. A. Pople, *Ab Initio Molecular Orbital Theory,* Wiley, New York, 1986.
5. H. Meirovitch, in *Reviews in Computational Chemistry,* K. B. Lipkowitz and D. B. Boyd, Eds., Wiley-VCH, New York, 1998, Vol. 12, pp. 1–74. Calculation of the Free Energy and the Entropy of Macromolecular Systems by Computer Simulation.
6. W. L. Jorgensen and C. J. Ravimohan, *J. Chem. Phys.,* **83,** 3050 (1985). Monte Carlo Simulation of Differences in Free Energies of Formation.
7. W. L. Jorgensen and J. M. Briggs, *J. Am. Chem. Soc.,* **109,** 6857 (1987). A Priori Calculations of p$K_a$ for Organic Compounds in Water. The p$K_a$ of Ethane.
8. A. Wallqvist and R. D. Mountain, in *Reviews in Computational Chemistry,* K. B. Lipkowitz and D. B. Boyd, Eds., Wiley-VCH, New York, 1999, Vol. 13, pp. 183–247. Molecular Models of Water: Derivation and Description.
9. C. E. Dykstra, J. D. Augspurger, B. Kirtman, and D. J. Malik, in *Reviews in Computational Chemistry,* K. B. Lipkowitz and D. B. Boyd, Eds., VCH Publishers, New York, 1990, Vol. 1, pp. 83–118. Properties of Molecules by Direct Calculation.
10. C. J. Cramer and D. G. Truhlar, in *Reviews in Computational Chemistry,* K. B. Lipkowitz and D. B. Boyd, Eds., VCH Publishers, New York, 1995, Vol. 6, pp. 1–72. Continuum Solvation Models: Classical and Quantum Mechanical Implementations.
11. C. J. Cramer and D. G. Truhlar, *Science,* **256,** 213 (1992). An SCF Solvation Model for the Hydrophobic Effect and Absolute Free Energies of Aqueous Solvation.
12. J. Tomasi and M. Persico, *Chem. Rev.,* **94,** 2027 (1994). Molecular Interactions in Solution: An Overview of Methods Based on Continuous Distribution of Solvent.
13. O. Exner, *Correlation Analysis of Chemical Data,* Plenum Press, New York, 1988.
14. MOPAC Program Package: QCPE No. 455. QCPE, Department of Chemistry, Indiana University, Bloomington, IN 47405, e-mail qcpe@ucs.indiana.edu, http://www.qcpe.indiana.edu. For a newer, commercial version of MOPAC, contact Schrödinger, Inc., 1500

SW First Ave., Suite 1180, Portland, OR 97201, e-mail help@schrodinger.com, http://www.schrodinger.com.

15. P.-A. Carrupt, B. Testa, and P. Gaillard, in *Reviews in Computational Chemistry,* K. B. Lipkowitz and D. B. Boyd, Eds., Wiley-VCH, New York, 1997, Vol. 11, pp. 241–315. Computational Approaches to Lipophilicity: Methods and Applications.
16. P. Politzer and J. S. Murray, in *Quantitative Treatments of Solute/Solvent Interactions,* P. Politzer and J. S. Murray, Eds., Elsevier, Amsterdam, The Netherlands, 1994, pp. 243–289. A General Interaction Properties Function (GIPF): An Approach to Understanding and Predicting Molecular Interactions.
17. A. R. Katritzky, M. Karelson, and V. S. Lobanov, *J. Chem. Inf. Comput. Sci.,* **69,** 245 (1997). QSPR as a Means of Predicting and Understanding Chemical and Physical Properties.
18. L. B. Kier, *MO Theory in Drug Research,* Academic Press, New York, 1971.
19. D. B. Boyd, D. K. Herron, W. H. W. Lunn, and W. A. Spitzer, *J. Am. Chem. Soc.,* **102,** 1812 (1980). Parabolic Relationships Between Antibacterial Activity of Cephalosporins and β-Lactam Reactivity Predicted from Molecular Orbital Calculations.
20. G. N. Burkhardt, *Nature (London),* **136,** 684 (1935). Influence of Substituents on Organic Reactions.
21. L. P. Hammett, *J. Am. Chem. Soc.,* **59,** 96 (1937). The Effect of Structure upon the Reactions of Organic Compounds. Benzene Derivatives.
22. M. H. Abraham, J. Andonian-Haftvan, G. S. Whiting, A. Leo, and R. W. Taft, *J. Chem. Soc., Perkin Trans. 2,* 1777 (1994). Hydrogen Bonding. Part 34. The Factors that Influence the Solubility of Gases and Vapours in Water at 298 K, and a New Method for Its Determination.
23. C. Reichardt, *Chem. Rev.,* **94,** 2319 (1994). Solvatochromic Dyes as Solvent Polarity Indicators.
24. L. P. Hammett and H. L. Pfluger, *J. Am. Chem. Soc.,* **55,** 4079 (1933). The Rate of Addition of Methyl Esters to Triethylamine.
25. L. P. Hammett, *Chem. Rev.,* **17,** 125 (1935). Some Relations Between Reaction Rates and Equilibrium Constants.
26. For a review, see: C. Hansch, A. Leo, and R. W. Taft, *Chem. Rev.,* **91,** 165 (1991). A Survey of Hammett Substituent Constants and Resonance and Field Parameters.
27. T. I. Oprea and C. L. Waller, in *Reviews in Computational Chemistry,* K. B. Lipkowitz and D. B. Boyd, Eds., Wiley-VCH, New York, 1997, Vol. 11, pp. 127–182. Theoretical and Practical Aspects of Three-Dimensional Quantitative Structure–Activity Relationships. G. Greco, E. Novellino, and Y. C. Martin, in *Reviews in Computational Chemistry,* K. B. Lipkowitz and D. B. Boyd, Eds., Wiley-VCH, New York, 1997, Vol. 11, pp. 183–240. Approaches to Three-Dimensional Quantitative Structure–Activity Relationships.
28. G. A. Bakken and P. C. Jurs, *J. Chem. Inf. Comput. Sci.,* **39,** 508 (1999). Prediction of Methyl Radical Rate Constants from Molecular Structure.
29. K. L. Peterson, in *Reviews in Computational Chemistry,* K. B. Lipkowitz and D. B. Boyd, Eds., Wiley-VCH, New York, 2000, Vol. 16, pp. 53–140. Artificial Neural Networks and Their Use in Chemistry. R. Judson, in *Reviews in Computational Chemistry,* K. B. Lipkowitz and D. B. Boyd, Eds., VCH Publishers, New York, 1997, Vol. 10, pp. 2–73. Genetic Algorithms and Their Use in Chemistry.
30. L. H. Hall and L. B. Kier, in *Reviews in Computational Chemistry,* K. B. Lipkowitz and D. B. Boyd, Eds., VCH Publishers, New York, 1991, Vol. 2, pp. 367–422. The Molecular Connectivity Chi Indexes and Kappa Shape Indexes in Structure-Property Modeling. I. B. Bersuker and A. S. Dimoglo, in *Reviews in Computational Chemistry,* K. B. Lipkowitz and D. B. Boyd, Eds., VCH Publishers, New York, 1991, Vol. 2, pp. 423–460. The Electron-Topological Approach to the QSAR Problem.
31. D. F. V. Lewis, in *Reviews in Computational Chemistry Toxicity,* K. B. Lipkowitz and D. B. Boyd, Eds., VCH Publishers, New York, 1992, Vol. 3, pp. 173–222. Computer-Assisted Methods in the Evaluation of Chemical Toxicity.

32. M. Karelson, V. S. Lobanov, and A. R. Katritsky, *Chem. Rev.,* **96,** 1027 (1996). Quantum-Chemical Descriptors in QSAR/QSPR Studies.

33. A. R. Katritsky, T. Tamm, Y. Wang, S. Sild, and M. Karelson, *J. Chem. Inf. Comput. Sci.,* **39,** 684 (1999). QSPR Treatment of Solvent Scales.

34. M. J. S. Dewar and W. Thiel, *J. Am. Chem. Soc.,* **99,** 4899 (1977). Ground State of Molecules. The MNDO Method. Approximation and Parameters.

35. M. J. S. Dewar, E. G. Zoebisch, E. F. Healy, and J. J. P. Stewart, *J. Am. Chem. Soc.,* **107,** 3902 (1985). AM1: A New General Purpose Quantum Mechanical Molecular Model.

36. J. J. P. Stewart, *J. Comput. Chem.,* **10,** 209 (1989). Optimization of Parameters for Semi-empirical Methods. I. Method.

37. AMPAC, Semichem, P.O. Box 1649, Shawnee Mission, KS 66222, e-mail info@semichem.com, http://www.semichem.com.

38. Gaussian, Gaussian, Inc., Carnegie Office Park, Building 6, Suite 230, Carnegie, PA 15106, e-mail info@gaussian.com, http://www.gaussian.com.

39. Spartan, Wavefunction, Inc., 18401 Von Karman Ave., Suite 370, Irvine, CA 92612, e-mail support@wavefun.com, http://www.wavefun.com.

40. L. J. Bartolotti and K. Flurchick, in *Reviews in Computational Chemistry,* K. B. Lipkowitz and D. B. Boyd, Eds., VCH Publishers, New York, 1995, Vol. 7, pp. 187–216. An Introduction to Density Functional Theory.

41. A. St-Amant, in *Reviews in Computational Chemistry,* K. B. Lipkowitz and D. B. Boyd, Eds., VCH Publishers, New York, 1995, Vol. 7, pp. 217–259. Density Functional Methods in Biomolecular Modeling.

42. E. R. Davidson, in *Reviews in Computational Chemistry,* K. B. Lipkowitz and D. B. Boyd, Eds., VCH Publishers, New York, 1990, Vol. 1, pp. 373–382. Perspectives on Ab Initio Calculations.

43. J. Cioslowski, in *Reviews in Computational Chemistry,* K. B. Lipkowitz and D. B. Boyd, Eds., VCH Publishers, New York, 1993, Vol. 4, pp. 1–33. Ab Initio Calculations on Large Molecules: Methodology and Applications.

44. R. J. Bartlett and J. F. Stanton, in *Reviews in Computational Chemistry,* K. B. Lipkowitz and D. B. Boyd, Eds., VCH Publishers, New York, 1994, Vol. 5, pp. 65–169. Applications of Post-Hartree–Fock Methods: A Tutorial.

45. S. M. Bachrach, in *Reviews in Computational Chemistry,* K. B. Lipkowitz and D. B. Boyd, Eds., VCH Publishers, New York, 1995, Vol. 5, pp. 171–227. Population Analysis and Electron Densities from Quantum Mechanics.

46. N. R. Kestner and J. E. Combariza, in *Reviews in Computational Chemistry,* K. B. Lipkowitz and D. B. Boyd, Eds., Wiley-VCH, New York, 1999, Vol. 13, pp. 99–132. Basis Set Superposition Errors: Theory and Practice.

47. M. M. Francl and L. E. Chirlian, in *Reviews in Computational Chemistry,* K. B. Lipkowitz and D. B. Boyd, Eds., Wiley-VCH, New York, 2000, Vol. 14, pp. 1–31. The Pluses and Minuses of Mapping Atomic Charges to Electrostatic Potentials.

48. T. D. Crawford and H. F. Schaefer III, in *Reviews in Computational Chemistry,* K. B. Lipkowitz and D. B. Boyd, Eds., Wiley-VCH, New York, 2000, Vol. 14, pp. 33–136. An Introduction to Coupled Cluster Theory for Computational Chemists.

49. D. E. Williams, in *Reviews in Computational Chemistry,* K. B. Lipkowitz and D. B. Boyd, Eds., VCH Publishers, New York, 1991, Vol. 2, pp. 219–271. Net Atomic Charge and Multipole Models for the Ab Initio Molecular Electric Potential.

50. N. S. Zefirov, M. A. Kirpichenok, F. F. Izmailov, and M. I. Trofimov, *Dokl. Akad. Nauk SSSR (Engl. Transl.),* **296,** 440 (1987). Scheme for the Calculation of the Electronegativities of Atoms in a Molecule in the Framework of Sanderson's Principle.

51. P. G. Mezey, in *Reviews in Computational Chemistry,* K. B. Lipkowitz and D. B. Boyd, Eds., VCH Publishers, New York, 1990, Vol. 1, pp. 265–294. Molecular Surfaces.

52. G. A. Arteca, in *Reviews in Computational Chemistry,* K. B. Lipkowitz and D. B. Boyd, Eds., VCH Publishers, New York, 1996, Vol. 9, pp. 191–253. Molecular Shape Descriptors.

53. A. R. Katritsky, V. S. Lobanov, and M. Karelson, *J. Chem. Inf. Comput. Sci.,* **38,** 28 (1998). Normal Boiling Points of Organic Compounds: Correlation and Prediction by a Quantitative Structure–Property Relationship.
54. P. Politzer and J. S. Murray, in *Reviews in Computational Chemistry,* K. B. Lipkowitz and D. B. Boyd, Eds., VCH Publishers, New York, 1991, Vol. 2, pp. 273–312. Molecular Electrostatic Potentials and Chemical Reactivity.
55. D. T. Stanton and P. C. Jurs, *Anal. Chem.,* **62,** 2323 (1990). Development and Use of Charged Partial Surface Area Structural Descriptors in Computer-Assisted Quantitative Structure–Property Relationship Studies.
56. D. T. Stanton, L. M. Egolf, P. C. Jurs, and M. G. Hicks, *J. Chem. Inf. Comput. Sci.,* **32,** 306 (1992). Computer-Assisted Prediction of Normal Boiling Points of Pyrans and Pyrroles.
57. D. A. Belesley, E. Kuh, and R. E. Welsh, *Regression Diagnostics,* Wiley, New York, 1980.
58. H. Köneman, *Toxicity,* **19,** 209 (1981). Industrial Toxicity.
59. JMP Statistical Discovery Software, SAS Institute, Inc., SAS Campus Drive, Cary, NC 27513, http://www.sas.com and www.JMPdiscovery.com.
60. SYSTAT, SPSS Inc., 233 South Wacker Drive, 11th floor, Chicago, IL 60606-6307, e-mail info-usa@systat.com, http://www.spssscience.com/systat, and www.systat.com.
61. D. B. Boyd, in *Reviews in Computational Chemistry,* K. B. Lipkowitz and D. B. Boyd, Eds., VCH Publishers, New York, 1995, Vol. 7, pp. 303–380. Appendix: Compendium of Software for Molecular Modeling.
62. D. B. Boyd, in *Reviews in Computational Chemistry,* K. B. Lipkowitz and D. B. Boyd, Eds., Wiley-VCH, New York, 1997, Vol. 11, pp. 373–399. Appendix: Compendium of Software and Internet Tools for Computational Chemistry.
63. C. Hansch and A. Leo, *Exploring QSAR: Fundamentals and Applications in Chemistry and Biology,* American Chemical Society, Washington, DC, 1995.
64. M. J. Kamlet, M. H. Abraham, P. W. Carr, R. M. Doherty, and R. W. Taft, *J. Chem. Soc., Perkin Trans. 2,* 2087 (1988). Solute–Sovent Interactions in Chemistry and Biology. Part 7. An Analysis of Mobile Phase Effects in High Pressure Liquid Chromatography Capacity Factors and Relationships of the Latter with Octanol–Water Partition Coefficients.
65. M. J. Kamlet and R. W. Taft, *J. Chem. Soc., Perkin Trans. 2,* 337 (1979). Linear Solvation Energy Relationships. 1. Solvent Polarity-Polarizability Effects on Infrared Spectra.
66. M. J. Kamlet, R. W. Taft, G. R. Famini, and R. M. Doherty, *Acta Chem. Scand.,* **41,** 589 (1987). Linear Solvation Energy Relationships. Local Empirical Rules or Fundamental Laws of Chemistry? The Dialogue Continues. A Challenge to the Chemometricians.
67. M. H. Abraham, in *Quantitative Treatments of Solute/Solvent Interactions,* P. Politzer and J. S. Murray, Eds., Elsevier, Amsterdam, The Netherlands, 1994, pp. 83–134. New Solute Descriptors for Linear Free Energy Relationships and Quantitative Structure–Activity Relationships.
68. J. P. Hickey and D. R. Passino-Reader, *Environ. Sci. Technol.,* **25,** 1753 (1991). Linear Solvation Energy Relationships: "Rules of Thumb" for Estimation of Variable Values.
69. M. H. Abraham, R. Kumarsingh, J. E. Commetto-Muniz, and W. S. Cain, *Arch. Toxicol.,* **72,** 227 (1998). An Algorithm for Nasal Pungency Thresholds in Man.
70. C. Grüber and V. Buss, *Chemosphere,* **19,** 1595 (1989). Quantum Mechanically Calculated Properties for the Development of Quantitative Structure–Activity Relationships (QSARs). p$K_a$ Values of Phenols and Aromatic and Aliphatic Carboxylic Acids.
71. G. R. Famini and L. Y. Wilson, *Collect. Czech. Chem. Commun.,* **64,** 1727 (1999). Computational Parameters in Correlation Analysis: Gas–Water Distribution Coefficient.
72. MADCAP (MOPAC Automatic Data Collection and Assembly Program), 1993, Available from G. R. Famini, e-mail grfamini@emh1.apgea.army.mil.
73. J. Debord, T. Dantoine, J.-C. Bollinger, M. H. Abraham, B. Verneuil, and L. Merle, *Chemico-Biological Interactions,* **113,** 105 (1998). Inhibition of Arylesterase by Aliphatic Alcohols.

74. G. R. Famini and L. Y. Wilson, *J. Phys. Org. Chem.,* **6,** 539 (1993). Using Theoretical Descriptors in Structure–Activity Relationships: Solubiluty in Supercritical $CO_2$.

75. R. S. Drago, G. C. Vogel, and T. E. Needham, *J. Am. Chem. Soc.,* **93,** 6014 (1971). Four Parameter Equation for Predicting Enthalpies of Adduct Formation.

76. C. Liang and D. A. Gallagher, *J. Chem. Inf. Comput. Sci.,* **38,** 321 (1998). QSPR Prediction of Vapor Pressure from Solely Theoretically Derived Descriptors.

77. J. S. Murray, T. Brinck, P. Lane, K. Paulsen, and P. Politzer, *J. Mol. Struct. (THEOCHEM),* **307,** 55 (1994). Statistically Based Interaction Indices Derived from Molecular Surface Electrostatic Potentials: A General Interaction Properties Function (GIPF).

78. J. B. Foresman and A. Frisch, *Exploring Chemistry with Electronic Structure Methods,* Gaussian, Inc., Pittsburgh, PA, 1993, p. 119.

79. J. S. Murray, F. Abu-Awwad, and P. Politzer, *J. Phys. Chem. A,* **103,** 1853 (1999). Prediction of Aqueous Solvation Free Energies from Properties of Solute Molecular Surface Electrostatic Potentials.

80. P. Politzer, J. S. Murray, P. Lane, and T. Brinck, *J. Phys. Chem.,* **97,** 729 (1993). Relationship Between Solute Molecular Properties and Solubility in Supercritical $CO_2$.

81. W. Eisfeld and G. Maurer, *J. Phys. Chem. B,* **103,** 5716 (1999). Study on the Correlation of Octanol/Water Partition Coefficients by Quantum Chemical Calculations.

82. M. Haeberlein and T. Brinck, *J. Chem. Soc., Perkin Trans. 2,* 289 (1997). Prediction of Water–Octanol Partition Coefficients Using Theoretical Descriptors Derived from Molecular Surface Area and the Electrostatic Potential.

83. S. Grigoras, *J. Comput. Chem.,* **11,** 493 (1990). A Structural Approach to Calculate Physical Properties of Pure Organic Substances: The Critical Temperature, Critical Volume and Related Properties.

84. E. Goll and P. C. Jurs, *J. Chem. Inf. Comput. Sci.,* **39,** 1081 (1999). Prediction of Vapor Pressures of Hydrocarbons and Halohydrocarbons from Molecular Structure with a Computation Neural Network.

85. A. R. Katritsky, L. Mu, and M. Karelson, *J. Chem. Inf. Comput. Sci.,* **36,** 1162 (1996). A QSPR Study of the Solubility of Gases and Vapors in Water.

86. CODESSA, 1999, Semichem, PO Box 1649, Shawnee Mission, KS 66216, e-mail info@semichem.com, http://www.semichem.com.

87. O. Ivanciuc, T. Ivanciuc, P. A. Filip, and D. Cabrol-Bass, *J. Chem. Inf. Comput. Sci.,* **39,** 515 (1999). Estimation of Liquid Viscosity of Organic Compounds with a Quantitative Structure–Property Model.

88. N. Bodor and M.-J. Huang, *J. Pharm. Sci.,* **81,** 272 (1992). An Extended Version of a Novel Method for the Estimation of Partition Coefficients.

*Reviews in Computational Chemistry, Volume 18*
Edited by Kenny B. Lipkowitz and Donald B. Boyd

ISBN: 0-471-21576-7

CHAPTER 6

# The Development of Computational Chemistry in Germany

**Sigrid D. Peyerimhoff**

*Institut für Physikalische und Theoretische Chemie, Universität Bonn, Wegelerstrasse 12, D-53115 Bonn, Germany*

## INTRODUCTION

Computational chemistry was able to develop thanks to two major advances: first was the understanding and formulation of a mathematical description of the microscopic behavior of matter, and second was the technical development of computers much more powerful than mechanical desk calculators. A large part of the foundation of the mathematical theory was laid by the physics community in Europe in the 1920s. The University of Göttingen in Germany became a center of the new quantum mechanics.

Although various established chemists in Germany had become aware of the amazing explanatory power of the new quantum mechanics by Heisenberg and Schrödinger, they were not yet ready to make use of this tool for chemistry. Very likely they could not imagine that a mathematical theory would be able to describe data and processes that generations of experimentalists had collected and studied. Thus several young people were the first to apply the new theory to chemical problems. In early 1927, two Germans, Walter Heitler (from Karlsruhe) and Fritz London (who had received his Ph.D. degree in München), supported by a Rockefeller fellowship, spent some time in Zürich where Erwin Schrödinger was at that time. Both wanted to work in quantum mechanics. Apparently, Schrödinger was not fond of collaborations,

so Heitler and London decided in Zürich to calculate the van der Waals force between two hydrogen atoms. According to the article of Gavroglu and Simoes[1] on the history of quantum chemistry, "nothing indicates that Schrödinger gave them the problem of the hydrogen molecule or that they talked with him about it." This work culminated in their famous Heitler–London paper[2] as basis for the valence bond approach of chemical binding. Later in 1927, Heitler became Max Born's assistant in Göttingen, and London became the assistant to Schrödinger who had then moved to Berlin as the successor to Max Planck. Heitler and London had to resign their positions in 1933, and both emigrated to England.

Linus Pauling from the United States spent 1926 to 1927 (his postdoctoral year) with Arnold Sommerfeld in München. He was supported by a Guggenheim fellowship and made visits to Göttingen. Pauling used the new quantum mechanics to study the electronic structure and physical properties of complex atoms and atomic ions.[3] The young Robert S. Mulliken, also from the United States, spent 1927–1928 as a postdoctoral fellow in Göttingen where he met Friedrich Hund. They not only had intense scientific discussions with each other, but also became friends and even spent some vacation time hiking together in the Black Forest. Their approach to chemical binding, today referred to as the molecular orbital (MO) method, was derived from the study of molecular spectra.[4,5] It was an exciting time, and Germany was an attractive place for scientific visits, especially for young people.

Still, skepticism remained as to the general power of quantum mechanics applied to complex chemical systems. The situation around 1930 is described by the well-known dictum of Paul Dirac[6] (the Nobel Prize winning physicist at Cambridge): "The underlying physical laws necessary for the mathematical theory of a large part of physics and the whole of chemistry are thus completely known, and the difficulty is only that the exact application of these laws leads to equations much too complicated to be soluble. It therefore becomes desirable that approximate practical methods of applying quantum mechanics should be developed, which can lead to an explanation of the main features of complex atomic systems without too much computation."

Indeed, approximate methods were quickly designed, and during the first years German scientists contributed their share. Erich Hückel[7] developed the very simple but highly successful Hückel method for aromatic π-electron systems, and Hans G. A. Hellmann[8] made important contributions to the methodology of quantum chemistry. These two men may be considered the most prominent German representatives to apply quantum mechanics to chemistry in this era. Starting in 1933, the political influence of Nazi Germany forced many scientists to emigrate, including Hellmann, and Germany lost its lead in the field. It was probably the United States that became the strongest player due to the work and effort of Pauling, Mulliken, and John Slater.[9]

What Dirac did not—and perhaps could not—foresee is the development of computers. The first programmable computer was designed by Konrad

Zuse shortly before and during World War II. Zuse was a young engineer who was tired of all the very similar calculations required in his study and early job; he dreamed of making these steps all automatic. His project was not triggered by military needs unlike some of the computer developments in England and the United States. At least in the United Kingdom, the main impetus for the development of a digital computer[10] came from the need to break the codes of the German forces in World War II.

It is obvious that after World War II the groundwork was prepared so that computational chemistry could develop. This review will start with this period. Because the field of computational chemistry is based on developments in both computer technology and in theoretical methods, these areas and their interplay will be addressed. This essay considers progress in the various decades, although it is clear that such a chronological division has a feature of arbitrariness.

In the first decades after the war, the primary users of computers were quantum chemists. Considering German history, this outcome was logical considering all the work that was stopped in the early 1930s and which was reanimated after the war making use of the new computational tools. For the same historical reason and with the outlook to more computer power, relatively little semiempirical quantum chemical work was developed in Germany. Instead, an emphasis was placed on ab initio quantum chemistry, and, accordingly, only the latter will be discussed in this chapter.

As time went on, computers were used for increasingly complex problems in chemistry, as will be shown. In this process, the early quantum chemistry users received competition from the theoretical chemists oriented toward a broader field of mathematical chemistry. Eventually many experimentalists started to use computational tools for quantum and classical mechanics, statistical mechanics, and database searching. Parallel to these applications, almost every experimental setup had a dedicated computer to run experiments and evaluate data automatically. Laboratory automation will not be treated in this chapter. Likewise, no attempt will be made to cover the impact of computers on experimental structure determination (e.g., X-ray crystallography).

This account is based on my own experience in the quantum chemistry field, which began around 1961, initially still with a desk computer. I received information that I tried to incorporate in this chapter from many colleagues, and I have extracted a number of details from the literature. As a personal review, it will certainly possess a bias, and I apologize to all those German colleagues whose efforts I should have mentioned but have inadvertently overlooked. Nevertheless, I hope that this essay will give an impression of a fascinating era with many challenges and some real pioneers. Finally, for reasons given later, the development of computational chemistry in only what was West Germany will be discussed.

## COMPUTER DEVELOPMENT

### The ZUSE Computers

The first fully automatic digital computer that could be programmed was developed by Konrad Zuse in Berlin during World War II. A description of the years of intense work under very difficult conditions is found in Zuse's book appropriately entitled "Der Computer—Mein Lebenswerk."[11] The first working model was the Z3 introduced in May 1941. It was based on electromagnetic relays: 600 relays in the computing unit and 1400 in the storage unit. It used a binary number system, floating point operation, 22 bit word length and had a storage capacity of 64 words. It required a special keyboard to generate the input via an 8-channel punched tape (i.e., one instruction represented by 8 bits). Most parts of the computer were constructed from used materials because new materials were hardly available during the war. This meant, for example, that the various relays required different voltage, and this had to be considered also. Nevertheless, the machine was apparently relatively stable in its performance. The speed was about 3 seconds for multiplication, division, or taking a square root. The Z3 was used to calculate determinants and, in particular, complex matrices that were important in optimizing the design of airplane wings. Part of the work on the Z3 was financially supported by the Deutsche Versuchsanstalt für Luftfahrt. This first model was completely destroyed in 1944 by Allied bombs, but a replica was reconstructed 1960 and can be seen in the Deutsche Museum in München.

Further development of the Z-series was seriously hampered by the war. The design of a much larger system Z4 started in 1942. The machine was transported in 1944 to Göttingen, which seemed a somewhat safer place than Berlin, but as Zuse writes,[11] it took two weeks for the transport, interrupted by heavy bombing of the trains. Work continued for a while in the building of the Aerodynamische Versuchsanstalt in Göttingen, which is near the center of Germany. From Göttingen, Zuse and some of his friends escaped in 1945 with the Z4 to Hinterstein, a small village close to Hindelang in the German Alps where other scientists such as Wernher von Braun had also found some shelter. In these years, they were entirely isolated from the rest of the world and heard only after the war the details of computer developments in the United States (MARK I, in operation 1944, and ENIAC, operating somewhat later) and in Britain (COLOSSUS, which was a stored program machine to break the code of the German forces in the war). There was no possibility of continuing work on the Z4 until the monetary reform of 1948. Zuse in Germany had been the first with an operational freely programmable digital computer but had lost the competition with other countries due to the war situation in Germany.

In 1949, Zuse started his company ZUSE KG (at Hünfeld in Hessen). The Z22 was his first computer with vacuum tubes (1955), followed by the Z23 with transistors. A small number of German universities was able to

obtain such machines. Personally, I saw a Z22 for the first time in operation at the Technische Hochschule (TH) of Darmstadt (around 1960 in the Institute of Professor Alwin Walther) during an excursion organized by a course in applied mathematics from the University of Giessen, at which I was a student at that time. Around 1962, a Z23 was installed at the University of Giessen, and I was one of the first users. The instruction language was "Freiburger Code," the input by punched paper tape. Each instruction or number had 40 bits. There was a fast storage with 255 words and a magnetic drum with 8191 addresses, of which the first 1052 were used by basic programs. The calculation of a trigonometric function took approximately 0.2 s.

As far as I know, there were no funding programs from the government to support computer development in Germany during the period before 1960. Unlike in the United States, it was impossible for the civilian technical sector to take advantage of products developed for the military. It was the Deutsche Forschungsgemeinschaft (German Science Foundation) that made it eventually possible for computers to be purchased at universities starting in the early 1960s. The ZUSE company was eventually taken over by Brown-Boveri (1964) and has belonged to Siemens AG since 1967.

## The G1, G2, and G3 of Billing in Göttingen

Late in 1947 the building of the Aerodynamische Versuchsanstalt in Göttingen, which had housed the ZUSE Z4 for a short time during the war, became available for new institutions and institutes, including the Kaiser-Wilhelm-Gesellschaft (today called the Max Planck Gesellschaft) with Max Planck and Otto Hahn, and the Institute of Physics with Werner Heisenberg, Max von Laue, and Carl Friedrich von Weizsäcker. The experimental groups had to construct equipment since nearly all laboratory equipment had been destroyed in the war. Heinz Billing[12] started to build a small High-Frequency Lab in the "Institut für Instrumentenkunde" with a few instruments to measure electric currents and with some vacuum tubes left over from the German army. He was fascinated by a very short note on the existence of the ENIAC computer[9] in the United States, a computer containing 18,000 vacuum tubes and with a weight of 30 tons.

At this time, a group of British computer experts from Teddington, who, among others included Alan Turing, J. R. Womersley, and A. Porter, visited the British occupation zone of Germany. They intended to investigate whether there were new developments in Germany and met in Göttingen with selected German scientists, including Heinz Billing of Göttingen, Alwin Walther of the TH Darmstadt who had worked on Hollerith machines, and Konrad Zuse. Another pioneer in the computer development, Professor Friedrich Willers from Dresden was apparently not able to come to this visit because he was in the Soviet occupation zone. Womersley discussed with Billing computer plans in England that led in 1950 to the ACE (Automatic Computing Engine)

machine, and Billing considers this discussion as the basis for his development of the G1 and G2 computers (G stands for Göttingen).

One of the big problems at that time was intermediate storage of numbers with fast access during the calculations. For this reason, great effort was directed toward the development of storage methods. Billing's British colleagues worked with a delay line in which a number is represented as a sequence of impulses continuously circulating around a closed path; their realization were mercury delay lines, that is, the information was represented as a sequence of acoustic pulses traveling round a tube filled with mercury. This general storage idea led Billing to introduce the magnetic drum.[12] Magnetic tapes and magnetic recorders already had been used by him in 1943, and his first successful magnetic drum storage system was in 1948. The drum, which had magnetic tapes glued around, could store 192 dual (20-digit) numbers. The publication describing this device, submitted in July 1948 as "Numerische Rechenmaschinen mit Magnetophonspeicher" in *Zeitschrift für Angewandte Mathematik und Mechanik*, showed, in addition, general aspects of how to construct a computer to solve the Schrödinger equation, $Y'' + F(\mathbf{x})Y + T(\mathbf{x}) = 0$.

Billing's development work was interrupted by the monetary reform of 1948, which caused heavy cuts in the Institute's budget. Billing's engineers took job offers from Argentina, and he himself accepted an offer from Australia in order to develop a computer including his magnetic drum at the University of Sydney. He left a detailed description of the design of his computer in Göttingen, however. Since the astrophysicist Ludwig Biermann in Göttingen was extremely interested in numerical calculations and believed in the future of digital computers, he convinced Heisenberg to bring Billing back. In June 1950, Billing was back in Göttingen and started to work on the computer, and Heisenberg was even able to obtain funds from the Marshall Plan to buy vaccum tubes and resistors.

Since for Biermann the construction of the computer in its original concept would have taken too much time, a smaller model, the G1, was constructed and went into operation by the middle of 1952. This machine was the first programmable computer operating with vacuum tubes in Germany, and it was based on Zuse's programmable relay computer. It made two operations per second, but was, as such, 10–20 times faster than a good mechanical desk calculator. In addition, it could be used 24 hours/day. The magnetic drum had a frequency of 50 revolutions per second; it had 9 tracks and could store four 32-bit numbers per track. Since 10 positions were required for transforming decimal numbers into binaries, only 26 of the 36 positions of the drum remained for the storage of numbers. In spite of this, the machine was used by many scientists from various places in Germany. The first applications included the calculation of the motion of charged cosmic ray particles in the earth's magnetic field, a topic of interest to Biermann. A chemical application involved the electronic structure of the helium atom. Many of the integrals

required in quantum chemical calculations (see the section on Quantum Chemistry, A New Start) were computed on this machine, which remained in operation until 1958 and was operable 82% of the time during its life span. Technical details can be found elsewhere.[12]

The larger model, the G2, with 30 operations per second and a magnetic drum storage of 2048 words at (50+1) bits fixed point, went into operation in the fall of 1954 in Göttingen, two years before the main German competitor PERM in München.

Billing's third machine, the G3, used already existing ferrite kernels as main storage and floating point arithmetic. This storage device had been developed in 1952 in the United States. In 1953 a German company also started to produce such ferrite core storage for the G3. The storage of the G3 had 4096 words at (42+1) bits, that is, it needed 176,000 ferrite kernels, each costing 0.5 Deutsche Mark (DM), which amounted to the large sum of 90,000 DM. The main goal of the G3 was to have a very reliable machine—the speed was of second priority. So, the faster vacuum tubes were replaced as much as possible by more stable germanium diodes (1500 vacuum tubes, 6000 germanium diodes). This G3 model could then perform 5000 operations per second it was very robust and was inoperable only 1.1% of its entire life span from 1960 to 1972. Its operation ended in 1972, some time after it had been moved into the new buildings of the Max Planck Institut für Physik und Astrophysik in München. All three machines were eventually dismantled; only photographs are left of them today.

## Computer Development at Universities

In the 1950s, the design of computers also started at various German universities. These efforts were supported by the German Science Foundation (Deutsche Forschungsgemeinschaft, DFG), which initiated a special committee for this purpose (Kommission für Rechenanlagen). Main competitors to the machine in Göttingen were Professor Walther with Hans-Joachim Dreyer at the TH Darmstadt whose DERA machine went in operation in 1957, Robert Piloty at the Technical University (TU) of München with the PERM (1956), and Friedrich Willers with Joachim Lehmann in Dresden with D1 (1956) and D2 (1957). Even though PERM stands for "Programmgesteuerte Elektronische Rechenmaschine München," some people called it "Piloty's erstes Rechen-Monster". This computer was later put under the guidance of Professor Friedrich L. Bauer at the TU München. More information can be found in Refs. 12 and 13.

Looking back at these early developments at a research institution in Göttingen and at several universities, it is regrettable that the German industry was not able to take advantage of this knowledge and lost out in the internationally fast growing competition in computer technology.

### The Analog Computer in Chemistry

Hans Kuhn at the University of Marburg was interested in the spectra of dyes.[14] Based on the electron gas model, he could understand the quantum mechanical states involved in such light absorption processes in a qualitative way, but he wanted to have quantitative results. So he developed an analog computer to determine stationary wave functions and corresponding energies of a particle ($\pi$ electron) in a one- and two-dimensional (1D and 2D) potential field as given by the Schrödinger equation. The basic idea was put forth[15] in 1951 when he experimentally determined the vibrational frequencies of membranes whose form represented that of certain (planar) molecules. The transition from the mechanical system described by masses and springs to the analogous electrical system replaces masses by self-induction (coils) and springs by capacitances. The potential acting on the site of an atom could be changed by an adjustable capacitor. The entire network was driven by high-frequency voltage that was varied to obtain stationary electric waves. Hence, the actual computer was based on the analogy between oscillatory states of a network of electric circuits and the stationary waves of a corresponding quantum mechanical system. The energies of the stationary states were given by the applied frequencies and the corresponding wave functions by the voltage at each mesh point of the network. The entire network had 4000 resonators; a picture of the size of the installation can be found in Ref. 16 and details to the installation in Ref. 17.

In this way, Kuhn and his co-workers calculated $\pi$ electron distributions in effective potentials of the molecular skeletons of many organic dyes[18] and found that in long polyene chains the alternating bond lengths had analogous values as the C—C single and C=C double bond in butadiene. The treatment of benzene showed equal bond length in such "calculations." Later on, Kuhn was also able to obtain from this analog computer transition moments, and in this way he could determine and explain the location, intensity, and form of absorption bands and even the shift of a phosphorescence band of a dye relative to its fluorescence location.

With the introduction of digital computers to German universities and research institutions in the mid-1960s and ab initio programs for larger polyatomic molecules in the 1970s, the Marburg analog computer reached the end of its service. It should not be forgotten, however, that it was a considerable technical achievement and a very valuable tool during its time, at which time the calculational alternatives were very simple Hückel type (without the possibility of taking into account different nuclear potentials) and semiempirical Pariser–Parr–Pople (PPP)[19] MO treatments.

## QUANTUM CHEMISTRY, A NEW START

After the important work of Heitler and London[2] in 1927 as well as that of Hund[4] and Mulliken,[5] a great interest arose among scientists to apply the

new quantum theory to problems in chemistry, particularly to molecular structure and spectra and to the study of the chemical bond. According to Schwarz et al.,[8] the word "Quantenchemie" was probably used first in 1929 by Arthur Haas in his presentations at the Chemisch-Physikalische Gesellschaft in Vienna. One of the young Germans in this field was Hans G. A. Hellmann in Hannover, close to the center of development of this new theory (Göttingen). His scientific achievements to the further development of quantum chemistry are summarized in a recent article that also contains details of his life.[8] He left Germany in 1934, being married to a Jewish wife and in opposition to the Nazi regime, and found an attractive position at the Karpov Institute in Moscow. Under the Stalin regime, he was arrested and executed in 1938. His heritage is the excellent textbook "*Einführung in die Quantenchemie*,"[20] which appeared in the German language in 1937 and served as a basis to introduce German scientists to this field after World War II.

The first activity after the war seems to have started at Göttingen, again at the Max Planck Institut für Physik, where the G1 computer was also designed. Various publications by H.-J. Kopineck[21] derive analytical expressions for Coulomb and exchange two-center integrals over 2s and 2p Slater-type functions ($e^{-\zeta r}$) required for the quantum chemical calculations of diatomic molecules and give extensive tables of numerical values of such integrals as a function of internuclear separation. Kopineck based some of this work on the tables of auxiliary functions published in 1938 by Kotany, Ameniya, and Simose,[22] but was careful enough to recalculate all those that he specifically needed and found that the Japanese tables were very reliable. Apparently, these latter tables had been overlooked when other work started on the evaluation of integrals for selected applications.[23] In Kopineck's papers,[21,24,25] acknowledgment is expressed to Professor K. Wirtz for suggesting the work, to Professor L. Biermann for support, and to a group of people of the astrophysical section of the institute (director Biermann) for carrying out all the tedious numerical computations. This happened all before the electronic computer G1 became available. A very interesting work on the potential energy curve of $N_2$ as a 6- and 10-electron problem based on the Heitler–London method as described by Hellmann[20] made use of the previous tables of integrals and is among the first German publications[24] in this area. This 1952 paper was dedicated to the 50th birthday of Heisenberg.

While work on the computation of two-center two-electron molecular integrals continued in Göttingen, it became known[25] that Clemens C. J. Roothaan[26] and Klaus Ruedenberg[27] at the University of Chicago had also started a program to evaluate molecular integrals, obviously in connection with the seminal Roothaan article on the self-consistent field (SCF) procedure.[28] In 1952, Heinzwerner Preuß came to the Institute in Göttingen as successor to Kopineck. He already had experience in $H_2$ calculations and integral approximations,[29] performed while at Hamburg, and was the ideal person to continue the work on integral evaluation in Göttingen. He first extended the studies to heteronuclear diatomics, and later on, with the use of the G1 and G2

electronic computers, this work culminated in four books "*Integraltafeln zur Quantenchemie*."[30] These volumes give an excellent introduction to the general problem of quantum chemical calculations and contain many references to historical work in this connection. They are also an excellent dictionary to look up details of the analytical derivations of molecular two-center integrals over Slater functions and their necessary auxiliary functions. The numerical values are tabulated for a small grid so that intermediate values could easily be obtained by interpolation. These tables were used for quantum chemical calculations[31] of diatomics until the beginning of the 1960s.

I used these tables of Preuß for the first part of my doctoral work. The computation of integrals for a valence bond treatment of the H—F molecule on a mechanical desk calculator was greatly simplified by the fact that I could look up values for the required auxiliary functions in these tables. Toward the end of this work (1962–1963), I got access to the electronic computer Z23, which of course could perform the calculations in a much shorter time with much higher accuracy.

Other numerical tables were apparently also produced in 1954–1956 by a Japanese group.[32] One must conclude that at that time it was not widely forseeable that such numerical tables of functions, similar to tables of logarithms, would become obsolete so soon due to the rapid progress in electronic computers.

Parallel to the work on molecular integrals, Preuß also worked on conceptual developments. Boys had introduced Cartesian Gaussian functions[33] as a possible basis for molecular calculations. Preuß was the first to discuss what he called "reine Gaußfunktionen"[34] and what is known today as "floating Gaussians." It is interesting that in Vol. IV of his *Tables of Integrals*[30] Preuß already had a chapter of numerical examples comparing integrals over Gaussians with those over exponential (Slater) functions and concluded that numerical tables for integrals involving pure Gaussians with different origins are not required because integrals over Gaussians are so easy to compute. Calculations with such basis sets were started later on by J. L. Whitten[35] without the knowledge of this part of the work of Preuß. Other important early papers of Preuß treat effective core potentials[36] (kombiniertes Näherungsverfahren nach Hellmann), variational treatments with respect to expectation values other than the energy, and simple building-up principles for the construction of energy hypersurfaces with an arbitrary number of centers. Unfortunately, Preuß's work was not publicized as much as it should have been, simply because all his publications (at least until 1970) were written in the German language and appeared mostly in the journal *Zeitschrift für Naturforschung*. Even though the seminal German publications (e.g., *Zeitschrift für Physik*) of the 1920s were well known, the situation after World War II had changed and publication in the English language seemed to be required to get the work into circulation and the necessary widespread attention.

Even though the incentive to perform quantum chemical ab initio calculations came from the Max Planck Institute at Göttingen, quantum chemistry ideas were also used in other physical chemistry departments of German universities. The work of Hans Kuhn on large π-electron systems with the use of his analog computer has already been mentioned in the previous section. Hermann Hartmann in Frankfurt published his textbook *Theorie der chemischen Bindung*[37] in 1954 and had a great influence for the next 10 years on advertising theoretical chemistry to the chemistry community. Theodor Förster in Stuttgart was also open to quantum chemistry ideas in his investigations of molecular excited states and energy transfer. Bernhard Kockel from the Institute of Theoretical Physics at Leipzig used his book *Darstellungstheoretische Behandlung einfacher wellenmechanischer Probleme*[38] to present numerous examples of how to apply algebraic concepts to the quantum theory of atoms and molecules. As a result of this, he began actual quantum chemical calculations himself. Finally, the textbook by P. Gombas from Budapest *Theorie und Lösungsmethoden des Mehrteilchenproblems der Wellenmechanik*[39] should also be mentioned since it is an excellent introduction to the quantum theory of many-body problems, oriented especially toward experimental physicists and chemists, and which has an appendix with analytical formulas for important molecular one- and two-center integrals.

## THEORETICAL CHEMISTRY 1960–1970

After a slow and almost unnoticed start in the 1950s, the application of quantum mechanics to problems of chemistry received several major boosts in the 1960s. First of all, the isolation of Germany, which was still a problem in the early 1950s, came to an end, and the international exchange of ideas began. Likewise the travel of young Germans to other countries, at that time in particular to the United States, where they found much better working conditions, became very attractive. International summer schools were advertised. In Germany a central computer (Deutsches Rechenzentrum) was installed in 1961, which was open to all German universities. Several chairs in theoretical chemistry were added to the faculty at universities in the latter part of the 1960s to support research and to include at least some theoretical concepts into the teaching and education of chemistry students. Meetings to publicize theoretical chemistry methods and their results were organized and a special priority program to support theoretical chemistry was created by the Deutsche Forschungsgemeinschaft in 1966. At least part of the German organizational support was due to the influence of Professor Hermann Hartmann in Frankfurt. He was also the first (in 1963) to establish a journal devoted specifically to the subject of theoretical and computational chemistry: *Theoretica Chimica Acta*. I personally remember this era as having an atmosphere of great fascination and competition.

On the other hand, one should not forget that at the beginning of this period the Wall went up on August 13, 1961 and separated Germany into two parts. The travel of colleagues from the East (Deutsche Demokratische Republik, DDR) to the West (Bundesrepublik Deutschland, BRD) was severely restricted, and only a very small percentage of the Eastern colleagues received permission to visit institutes or to attend meetings in the BRD. Likewise travel from the BRD to the DDR became more difficult, and even the exchange of letters was controlled. While scientists from the BRD could freely move to almost all countries, the flow of information between the two parts of Germany became very much restricted. Scientists in the DDR became increasingly isolated internationally.

## The Deutsche Rechenzentrum at Darmstadt

The realization of a central German Computer Center (Deutsches Rechenzentrum; DRZ) had been suggested by the Kommission für Rechenanlagen of the Deutsche Forschungsgemeinschaft (DFG) in 1956. It finally came into existence on October 3, 1961. It was accessible to all universities and research institutions in Germany for such jobs that could not be handled on the computer (if there was any at all) of the local institution. The first machine at the DRZ was an IBM 704, which was replaced in June 1963 by an IBM 7090, which was about five times faster than the IBM 704. The front-end was an IBM 1401, financed by the Volkswagen Foundation and the DFG. In 1965, the DFG financed another disk and the total investment amounted to about 18 million DM. The chairman of the scientific board was Professor Walther from Darmstadt, who, as already mentioned, had been involved earlier in computer developments.

The building for this central German computer center had 85 rooms, altogether 2150 $m^2$, and the part of the computer installation plus tape units required air conditioning of 570 $m^2$. The total area of the entire site was 8700 $m^2$. In 1966 the DRZ had a staff of 50 scientific and technical persons, in addition to a number of operators, people to punch cards and handle the program libraries, secretaries, and others.[40] Three technicians from IBM were on site. Details of the installation can be found in Ref. 40. In short, the equipment consisted of a main memory of 32,768 words, 13 magnetic tapes, 1 disk, 1 cardreader, 1 automatic punch, 1 plotter, 1 reader for punched paper tape, 1 sorting machine, 10 card punches for users, 8 card punches for internal use, and 2 teletypes. The cost of one hour of computer time was 240 DM. Starting at the end of 1965, the trade unions did not allow any work on Sunday any more, so that this computer center was shut down on Sundays and on holidays. Office hours were from 8.00 to 17.30 from Monday to Friday.

Looking back from today's standard, where a workstation or a laptop personal computer is more powerful and has more memory than the entire DRZ in 1966, it is almost unbelievable that method developments and actual

calculations could have been performed under the circumstances given. Access to the DRZ was in three ways: either one traveled to Darmstadt by train or car with one or several boxes of punched cards—in case one had a card punch at the home university. This way was probably the "normal" situation. One tried to compile the programs, correct errors and, if fortunate, stored the program somewhere on tape in binary code for further use at the DRZ. Such a procedure worked quite well as long as a friendly person of the DRZ staff took care of the programs and was available for further telephone instructions. We had such a person who had worked at our university for a while, and so we were lucky people. The second way was to send cards by mail to the DRZ, but to debug programs or to run them using this approach was a very slow process. If one was very fortunate, one could use the third way: a teletype (which was the exception at universities), via which one could send input data for programs already stored in binary somewhere in the DRZ and administered by the DRZ personnel. The output was always sent back by regular mail.

From the 1966 annual report,[41] one learns that quantum mechanical calculations used 8% of the total computer time available. Next to Hückel calculations, one finds projects involving linear combination of atomic orbitals–molecular orbitals–self-consistent field (LCAO–MO–SCF) calculations using Gaussian functions, and calculation of natural orbitals using Gaussian functions. I myself was a heavy user, and projects of Martin Klessinger and Reinhart Ahlrichs are also found in that report. The statistics show further that a considerable number of computational projects were in connection with doctoral theses, that is, young people using the modern tool. Within chemistry, the heavy users besides the quantum chemists were those processing measured nuclear magnetic resonance (NMR) data and crystal structure data. The preferred symbolic languages were FORTRAN II and IV, ALGOL (developed in Germany) and COBOL; FAP, MAP, and LISP were also heavily used to optimize computer codes. In 1965, the DRZ had acquired programs from the Quantum Chemistry Program Exchange (QCPE) at Indiana University and was proud that by 1965–1966 they had distributed 65 such programs to researchers outside of Germany such as Great Britain (15), France (13), Sweden (2), Spain (2), Switzerland (3), Italy (1), Denmark (11), Finland (1), Belgium (1), and Romania (1), demonstrating their international visibility.

## Formation of Theoretical Chemistry Groups

Most experimental chemists in Germany in those times did not believe that quantum theory beyond the simple Hückel model had any use for chemistry in the foreseeable future.[42,43] So quantum chemistry had to get its main support from the more optimistic international community. Per-Olov Löwdin's summer schools held in Uppsala (Sweden) were instrumental in getting young researchers interested in quantum molecular science. Since these schools

(lasting 4–5 weeks) had international participation from both teachers and students, they were also a very attractive place to start international contacts. Heinzwerner Preuß was the first German to spend a postdoctoral year in Löwdin's quantum chemistry group in 1958–1959. Werner Kutzelnigg and Martin Klessinger participated in Löwdin's summer school in 1960. My turn came in 1962, together with four other Germans, all of whom later became professors of physical or theoretical chemistry at German universities. Raphael Levine (Jerusalem) was one of the most eager students in my class.

Access to international publications also improved in West Germany. The Technical Reports of the Laboratory of Molecular Science and Spectra in Chicago, which contained reprints and preprints of the work done around Mulliken and Roothaan, got distributed to some of the German scientists[44] (e.g., L. Biermann, G. Briegleb, Th. Förster, H. Hartmann, F. Hund, H. Kuhn, R. Mecke, and Georg Maria Schwab). The results of the 1959 Conference on Molecular Quantum Mechanics held in Boulder, Colorado, were published in *Reviews in Modern Physics*[45] and were extremely exciting. This conference is also discussed in connection with the history of computational chemistry in the United States[9] and the United Kingdom.[10] All of this work offered encouragement, especially for young people.

Nevertheless, progress was very slow. Preuß had moved to the Max Planck Institute (MPI) at München in 1959 after his stay with Löwdin in Sweden and started to build up a group in quantum chemistry—for which he had Heisenberg's support. In Gerd Diercksen, he found an excellent student, and, in the MPI staff, competent help in carrying out computations. Furthermore, the MPI was able to purchase a computer in the first half of the 1960s, so that this group did not have to rely solely on the DRZ in Darmstadt.

Hartmann had his group at the University of Frankfurt, but believed more in models than in ab initio calculations. Nevertheless he tried hard to get students interested in theoretical chemistry and held extra summer courses at Konstanz. Bernhard Kockel, from the University of Leipzig, had been vacationing together with his wife in West Germany (canoeing on the Danube) when the Wall was built (1961); he remained in the BRD upon receiving an offer for the theoretical physics chair at the University of Giessen. He started a small computational group to which I belonged. W. A. Bingel, who was the only German of his generation whose doctoral advisor had been a pioneer in theoretical chemistry (E. Hückel), became professor at the University of Göttingen in 1963. Werner Kutzelnigg joined him in 1964 after his postdoctoral years from 1960 to 1963 (with a NATO fellowship) first in Paris with Bernard Pullman and Gaston Berthier and later on with Per-Olov Löwdin at Uppsala. Kutzelnigg had received his doctorate with Reinhard Mecke in Freiburg and had been so impressed by Bernard Pullman's invited talk in Freiburg that he decided to move into the field of quantum chemistry. Bingel and Kutzelnigg soon attracted the excellent students Reinhart Ahlrichs and Volker Staemmler, most probably because at that time the chair in theoretical physics at Göttingen

was vacant and also because theoretical chemistry seemed to be the closest to the original intention of these two students.

I myself was fascinated from what I heard from Chicago and in 1963 went with a fellowship of the Volkswagen Foundation administered by the Cusanuswerk to join the group of Clemens Roothaan and Robert Mulliken. Then in 1964 I spent several months in the laboratory of Ernest R. Davidson in Seattle. In Chicago, I realized for the first time how important it was to have access to a reasonably-sized computer (IBM 7090) on campus, even if runs could be performed only during the night. And furthermore that a turnaround time of a day or two for computer jobs made all the difference compared to the German situation using a Z23 or sending programs and outputs back and forth to the DRZ in Darmstadt by regular mail. After a short visit back to Germany, I spent another postdoctoral period (1965–1966) with Leland C. Allen at Princeton, where we could use the Gaussian-lobe function SCF program for polyatomics, which was due to J. L. Whitten,[35] also a postdoc at that time in Allen's group. To compute realistic molecular structures and properties, based solely on the Schrödinger equation, was a great challenge to us. I seriously considered staying in the United States. But then the situation for such kind of work had improved drastically in Germany because it had been realized that other countries were far ahead, and for this reason special programs were initiated in Germany to produce top-quality researchers in this field. It was finally realized that state-of-the-art computers were needed at research institutions in addition to the central DRZ and that special support for research in theoretical chemistry was needed.

## Deutsche Forschungsgemeinschaft–Schwerpunktprogramm Theoretische Chemie

In 1966, the DFG decided to initiate a special priority program for theoretical chemistry for the next 5 years in order to support this field on a broad basis.[46] The intention was to support primarily new ideas and the development of methods in theoretical chemistry and to a lesser extent computations.

The DFG had been reestablished after World War II on January 11, 1949, under the name of "Notgemeinschaft der Deutschen Wissenschaft." Its present name came into existence after merging with the Deutsche Forschungsrat in 1951. The DFG is legally registered as a private association based in Bonn. Its members are universities, some research institutions, and academies of science. Member institutions delegate one representative each to a general assembly that meets annually. This general assembly (among other duties) elects the DFG president, vice presidents, and the members of the DFG Senate, and decides on the admission of new members into the DFG. The DFG's mission is according to Article 1 in its statutes: "The Deutsche Forschungsgemeinschaft serves all branches of science and the humanities by financing research projects and by promoting cooperation among researchers.

It advises parliaments and governments on scientific matters and fosters relations between academic research and the private sector as well as research abroad. It devotes particular attention to the education and promotion of young scientists.'' To accomplish this mission, the DFG receives funds from the federal government and from the states (Länder) on a 50:50 basis for regular programs. (For special programs, the formula for funding is somewhat different, i.e., 60:40.) The total amount in the year 2000 was around 2000 million DM.

All research supported by the DFG is investigator initiated. It is the ''bottom-up'' principle. Funds can be granted only on the basis of applications, and the responsibility for all projects for which funds are granted lies with the principal investigator. All applications are subject to peer review, and in all DFG programs the reviewers' evaluation is the basis for the decision on funding. The DFG's peer reviewers work in an honorary capacity. They are elected every four years by direct, secret ballot. Active voting rights are accorded to all scientists who have held a doctorate for at least three years and are working in a university or other publicly funded research institution. In the year 2000, there were 524 elected members of 37 review committees responsible for 186 disciplines.

There are basically two forms of research support under the DFG system: financing of individual research projects (''Normalverfahren'' is the largest in this category) and coordinated, cooperative funding programs with structural effects, among which the most important are the Schwerpunktprogramm (special priority program) and Sonderforschungsbereich (collaborative research centers). Again the initiative for such programs comes from the scientific community. To establish a Schwerpunktprogramm, researchers draft a program, submit it to the DFG Senate, which decides once a year on the adoption of new programs. Within a given scope, participants in such a priority program are free to choose their project, research plan, and methods. Coordination is ensured through a coordinator—generally one of the initiators of the application for such research program—and through annual colloquia.

The priority program in theoretical chemistry in 1966 was one of 14 newly adopted priority programs. It was the only one in chemistry [the others were in medicine (2); biology (3); physics (1), geoscience (2); engineering (3); agriculture (1); and a special project in Mexico, to show the broad range of DFG funding]. Since such priority programs generally run for six years, the priority program in theoretical chemistry was one out of a total of 61 new and continuing programs[47] funded altogether with a total sum of about 55 million DM.

Looking back, this theoretical chemistry program turned out to be one of the most successful priority programs of the DFG. It was adopted immediately and welcome to all researchers in the field. In the first year, there were 29 project proposals, 13 of which were applications to participate in summer schools. The total budget in this first year was 350,000 DM, that is, 0.64%

of the total priority program budget. These funds were used primarily to pay students (60%), but also to pay for computer time at the DRZ or at some other installation (such as the research institution at Jülich), or for short-term visitors. These funds were vital for the work of young scientists, most of whom had become Privatdozent without—or with very little—budget from their own university institution. In the last year of this priority program (1970), the number of accepted research proposals was increased to 45 for which a total sum of 720,000 DM was granted. Fifteen of these proposals were applications to participate in summer schools in Uppsala or in Oxford. This increase in the number of proposals in the course of the program showed the growing acceptance and interest in the field, but also that there was a special need for teaching theoretical chemistry, which at that time had not been introduced into the standard curriculum of chemistry studies in Germany.

The total amount spent in this special priority program over the five-year period (1966–1970) was 2.8 million DM. Even though the success of such a program cannot be measured by simple numbers, the report[46] quotes an impressive number of publications: 7 diploma and 30 doctoral theses, 190 publications in 22 different journals. An increasing tendency for German scientists to become visible in the field was also observed, as measured by the invited talks at international meetings. And finally, the list of applicants in this program includes many names whose carreer in this field is now well known (Werner A. Bingel, Jürgen Brickmann, Gerd Diercksen, Hermann Hartmann, Georg Hohlneicher, Martin Klessinger, Edgar König, Hans Georg Kuball, Werner Kutzelnigg, Jörn Manz, Sigrid Peyerimhoff, Heinzwerner Preuß, Ernst Ruch, and Armin Schweig).

## Theoretical Chemistry Symposia

Professor Hartmann, who had been among the initiators of the DFG special priority program, also organized the first "Symposium für Theoretische Chemie" in Frankfurt in 1965. His goal was to bring experimentalists together with theoreticians in this new field. About 60 scientists participated in this first event[48] coming from the German speaking countries: Germany, Austria, and Switzerland.

The main emphasis of the 1965 symposium[48] was on ligand-field theory, a topic close to Hartmann's interests at that time, and on Kuhn's electron gas model. The organization committee, consisting of Hartmann (Frankfurt), H. Labhart (Zürich), and O. E. Polansky (Vienna)—to which at a later time W. A. Bingel (Göttingen), E. Ruch (Berlin), G. Wagniere (Zürich), and P. Schuster (Vienna) were added—suggested holding an annual symposium with the location rotating between the three countries. These meetings not only provided the opportunity to exchange ideas between experimentalists and theoreticians and to meet with colleagues in a similar field, but were primarily a platform for diploma or doctoral students to present their own results

for the first time to a larger audience in the scientific community without language difficulties.

Attendance grew to 90 participants at the 1966 meeting in Zürich and about 110 at the third symposium in 1967 at Vienna. At Zürich, electron transfer due to excited molecular states (A. Weller), solvation effects in electronic spectra (W. Liptay), and determination of vibrational force constants (W. Zeil) were topics from the experimental side.[48] On the theoretical side, lower limits of eigenvalues (N. Bazley), electron pair approximations (W. Kutzelnigg), and six contributions on ab initio calculations using Gaussian functions of the group around Preuß were presented. Apparently, the SCF computer program based on "pure" Gaussians, as Preuß used to call them, had been finished by G. Diercksen and gave its first results as presented in Zürich.

To some extent, these symposia reflect the state of the art in the field of theoretical quantum chemistry in Germany at a given time. The meetings continue. For many years, W. A. Bingel was the person who selected the next organizer, and this procedure worked quite well. Today, the symposium organizer is selected by the Arbeitsgemeinschaft Theoretische Chemie (AGTC), which was founded in 1992 to give this field a more official status in concert with the established professional organizations of chemistry (Gesellschaft Deutscher Chemiker, GDCh), physical chemistry (Deutsche Bunsengesellschaft für Physikalische Chemie, DBG), and physics (Deutsche Physikalische Gesellschaft, DPG). Initially, experimentalists and theoreticians had about equal weight among the participants, but gradually the theoreticians took the lead. Today the symposium is the annual meeting for German speaking theoretical chemists, even though an increasing number of talks and posters are presented in the English language. For many students, these symposia are still the first opportunity to present their results and to learn about the scientific work and atmosphere in other groups from personal contacts. These contacts on the student level are also very important for the exchange of computer programs or computer information. The location of these meetings varies in the series between Germany–Switzerland–Germany–Austria.

## Scientific Developments

The period of diatomic SCF calculations using Slater functions, which were extensively pursued in the Laboratory of Molecular Structure and Spectra in Chicago,[9] passed by the German scientists. I think I was one of the few Germans who got a glimpse of this fascinating work during my stay at Chicago[49] and less so during my doctoral work on valence bond (VB) calculations of the hydrogen fluoride molecule.[50] Starting in 1966, a large number of polyatomic molecules were treated by the newly written SCF–MO–LC(LCGO) program of Preuß and Diercksen.[51] This program constructed MOs as a linear combination (LC) of another linear combination of

Gaussian orbitals (LCGO). Preuß called this group of pure Gaussians with fixed linear coefficients "LCGO;" these could consist of atom-centered Gaussians or a group of functions representing molecular fragments. Numerous applications including molecules such as $C_6H_6$, $C_5H_5^-$, $C_3H_6$, $C_2H_4$, $CH_4$, $CH_3^+$, and so on[52] were published side by side in the *International Journal of Quantum Chemistry*.

At about the same time, SCF calculations for a series of polyatomic molecules[53] such as $AH_2$ (A = first-row atom) $C_2H_6$, $B_2H_6$, $F_2O$, $CH_2$, $C_2H_4$, $C_2H_6$, and ozone[54] were carried out independently at Princeton, employing the same type of Gaussian functions. In this approach, various Gaussian (lobe) functions were also grouped together in a linear combination with fixed coefficients, referred to as "atomic group orbitals." Later on, the name "contracted Gaussian orbitals" for such groupings or LCGO became more popular. This was the early exciting time of polyatomic ab initio treatments. Relatively soon, however, it became clear that SCF treatments have serious drawbacks if one is interested in relative stabilities, dissociation energies, or electronically excited states. Configuration interaction (CI) calculations, carried out at whatever computer was available in the United States or Germany, started on formate anion and cyclobutadiene,[55] and even systems as large as $C_{10}H_8$ were treated by ab initio methods.[56] Such work was only possible by a combined use of computers in Germany and at various sites in the United States.

Parallel to these endeavors, work started in Germany on new concepts to account for electron correlation. The independent electron pair approach (IEPA) was developed by Ahlrichs and Kutzelnigg,[57] followed a few years later by the CEPA (coupled electron pair approach).[58,59] The relation of these methods to contemporary Møller–Plesset second order (MP2) and coupled cluster treatments is discussed in Ref. 60. Work on circular dichroism by Ruch[46] and on the chemical shift by Voitländer[46] showed the variety of ab initio problems treated. The special priority program of the DFG from 1966–1970 demonstrated the intended impact.

In 1962, the newly established journal *Theoretica Chimica Acta* (TCA; edited by H. Hartmann in Frankfurt) contributed also to the visibility of theoretical chemistry in the German scientific community. It preceded the *International Journal of Quantum Chemistry* (founded in 1967 by Per-Olov Löwdin) by 5 years. TCA welcomed manuscripts from the entire field of theoretical chemistry, and special emphasis was placed on the application of quantum theory and problems of chemical physics. According to Hartmann's philosophy, general and analytical work in the field of quantum chemistry was preferred, and computational work was considered if it concerned new methods and questions of special chemical interest. Articles could be published in English, German, and French, and even articles in the Latin language were allowed, presumably to point to the common background of European languages and the language of erudition for many centuries in Europe. The first volume 1962–1963 had 25 articles in English (from many European countries,

the United States, and Canada), 19 in German, and 5 in the French language. All abstracts—at least for many years to come—appeared trilingually (English, German, French), translated into the corresponding two other languages by the editorial office. This journal showed very distinctly the growth of the field of theoretical chemistry within Europe; but it also made clear that there were still language barriers in international communication. In 1984, the sentence "Papers will preferably be published in English" was added to the stated editorial policy. Shortly before his death (1984), Hartmann turned the editorship of TCA over to an editorial team headed by Klaus Ruedenberg at the Iowa State University in the United States. After Ruedenberg's retirement 1997, the name of *Theoretica Chimica Acta* TCA was broadened to *Theoretical Chemistry Accounts: Theory, Computation, and Modeling*, still keeping its initials TCA, with the new editor Donald G. Truhlar, at the University of Minnesota in the United States.

Before concluding the decade 1960—1970, it should be mentioned that theoretical chemistry started to influence not only chemical research in Germany but slowly became an independent field for which professorships were created at universities. H. Preuß moved from the MPI in Munich to a chair of theoretical chemistry at the University of Stuttgart in 1969, while Diercksen remained at the MPI at München. Ludwig Hofacker, coming from Northwestern University near Chicago, took the chair at the Technical University of Munich, E. Ruch was appointed professor of theoretical chemistry at the Freie Universität of Berlin, and Karl Heinz Hansen became professor of theoretical chemistry at the University of Bonn.

## COMPUTATIONAL CHEMISTRY 1970–1980

Theoretical chemistry, whose major part in the 1960s was quantum chemistry of molecular structure, was now ready to propagate into other areas of chemistry. Work started on the dynamics of chemical reactions, on spectroscopy, on database and expert systems in chemistry, and on synthesis planning. During the 1970s, about 15 chairs in theoretical chemistry at German universities became available in addition to five positions for associate professors. International conferences were organized by Germans and took place in Germany. Germans participated in the design of the European Centre for Atomic and Molecular Calculations (CECAM), which is described later. However, computer time was still a bottleneck since the demand for computer power was much greater than could be financed by the universities or the DFG.

Some of the German universities had been able to obtain International Business Machines and Control Data Corporation machines. (For example, Münster had an IBM 360-50 around 1968, while Mainz and Gießen had

CDC 3300 computers around 1968 and 1970.) But there was a definite tendency from the DFG (in its funding and advisory capacity) to support the German AEG Telefunken company which offered the Telefunken Rechner TR4 and the larger model TR440. The DRZ, for example, had applied for an IBM 360-75 to replace their IBM 7090 hoping for an increase in efficiency of a factor of 10, but the DFG had ordered for them[41] a TR440.

Again, it should be stressed that it was the initiative of the potential scientific users that was the driving force to obtain a computer installation at their university; the proper choice of the director of the computer center and its advisory committee was of great importance. The Kommission für Rechenanlagen (KfR) of the DFG had given general recommendations to the government about the necessity of computational resources, but the negotiation with the various computer companies and the formal application for the computer installation had to be submitted from the universities with a very detailed justification for every item, generally based on the research requirements of the faculty. The KfR reviewed the application, oftentimes made visits to the site, and then gave final recommendation to the Science Council. Because an application had to include comparable offers from three different computer companies, the KfR recommendation (considering a variety of arguments) sometimes took precedence over the specification outlined in the application.

For users, there was always the problem of computer program compatibility between different machines. An IBM 7094 had a word length of 36 bit, a CDC 3300 generally 24 bit, the TR machines 48 bit, and the IBM 360 series had 24 bit. A large problem for quantum chemical calculations was the small main memory. Our CDC 3300 at Mainz had 5 modules at 16 K word memory, which were separated so that one array of floating point numbers (e.g., a matrix) had to fit in a single module; this meant that we could have only symmetric CI matrices up to dimension 178 in core storage. External storage on magnetic tape with 800 bits/inch was extremely slow.

The reason for my accepting a professorship from the University of Bonn (1972) (over that of Berlin and Bochum) was primarily the much better computer installation compared to the other places. With our atomic orbital (AO) integral program (floating point number crunching), the four-index transformation routine (integer arithmetic), SCF program (input/output oriented), and a special integral program testing double precision arithmetic, I compared the running time on the CDC 3300 (Mainz), Siemens S4004/55 (Berlin), TR440 (Bochum) and IBM 370/165 (Bonn). In all cases, the IBM at Bonn was ahead of the others. For number crunching, the relative times were 1.0:1.64:0.43:0.086, for integer arithmetic 1.0:1.15:0.37:0.08, for I/O 1.0: 1.5:0.35:0.1, and for double-precision (DP) arithmetic 1.0:0.24:0.08:0.036. This example also shows that, in spite of commercial benchmarks, computer performance could depend very much on the individual program requirements.

## European Efforts

At the end of the 1960s, the idea arose to create a European Centre for Atomic and Molecular Calculations[61] (Centre Européen pour des Calculs Atomiques et Moléculaires). CECAM opened in Orsay, France, in October 1969 with IBM 360–50-75, CDC, and UNIVAC computers. The main aim of CECAM was not to offer computer time, and simply "cranking away" was not permitted. It was expected that the most original and creative uses of computers must be developed. The lag behind the United States in this field was clearly evident, and it is stated[61] "that the level in many laboratories could be raised by bringing together for short periods of time from these several laboratories scientists who are interested in the same or related problems, so that they could benefit from a mutual stimulation which would lead to a much more rapid development of ideas in the employment of computers." The general hope was expressed that this center would become a driving force for progress in atomic and molecular physics. Carl Moser (France) was the first director, and W. A. Bingel and W. Kutzelnigg from Germany were in the governing body.

The CECAM designed a plan for its future efforts that included the calculation of atomic and molecular wave functions with the inclusion of relativistic and correlation effects, both by perturbation and variational approaches. Fourier transform techniques, crystallography, chemical reactivity at surfaces, statistical mechanics, and information retrieval were major areas of the proposed work. This was certainly an ambitious undertaking. As an example, consider the workshop in 1973 on "Dynamics on Potential Energy Surfaces,"[62] which laid down significant guidelines for further research and influenced a number of European scientists. At this workshop, Jörn Manz from Germany presented exciting investigations of the $H+F_2 \rightarrow HF+F$ and $F+H_2 \rightarrow FH+H$ reactions. As far as I remember, German participation in the interesting workshops of CECAM was infrequent, however, simply because researchers had to provide their own money for travel and accommodation, and Orsay/Paris was not the least expensive place one can think of.

## Computer-Aided Synthesis

The first internationally available computer programs for planning organic syntheses[63] were primarily based on the retrieval and manipulations of filed data on known reactions (reaction library as databases).[64] This approach led to programs such as LHASA,[65] SECS,[66] or SYNCHEM,[67] and Ugi had also his own version for peptide syntheses.[68] These programs are typical expert systems with a large database and a set of rules, and are based on a retrosynthetic approach from which one does not expect totally novel synthetic reactions. A completely different approach to the use of computers in chemistry came from the organic chemist Ivar Ugi at the Technical University of München and the mathematician J. Dugundji.[69]

Ugi, Dugundji, and co-workers conceived a novel mathematical model of constitutional chemistry.[69] It is based on an algebraic model and logical connectivity. It represents reactants with B and R matrices resulting in E matrices for the products. The "chemical distance" between B and E is an important metric and represents something as the minimum number of valence electrons which must be shifted to convert reactants into products. In this approach, it is possible in principle to find entirely novel synthesis routes not based on prior experience stored in databases. The hard part is to cut the branches of the enormous tree of possible reactions. The approach was implemented in a series of computer programs such as CICLOPS,[70] EROS, and IGOR. A detailed discussion of this work is contained in a summarizing article,[64] which presents examples of true novel syntheses and simplifications of syntheses designed earlier by empirical approaches.

## Progress in Quantum Chemical Methods

Even though computers were an essential tool in quantum chemical calculations, the main challenge was the further development of methods and concepts to describe even more facets of chemistry and with higher accuracy. Methods that account for electron correlation were extended to be able to describe energy surfaces more reliably. Several variants of the CEPA Ansatz (CEPA-1, CEPA-2) were developed as well as the method of self-consistent electron pairs (SCEP).[71] Formulations using canonical or localized orbitals (e.g., pair natural orbitals,[72] PNO, as a kind of optimized virtual orbitals) were put forth. These methods were extensively used for two decades, primarily in Germany, until coupled cluster formulations became more popular.[73]

The computation of electronically excited states and hence the interpretation of ultraviolet–visible (UV–vis) spectra saw much activity outside Germany in the postwar years by semiempirical methods such as the Platt perimeter model, the PPP,[19] and the complete neglect of differential overlap (CNDO)[74] approaches. Thus after more than a decade of dealing primarily with ground-state properties of molecular systems, the stage was now set to attack this problem by ab initio methods. The first international discussion meeting, under the auspices of the DFG, was held at Schloß Reisensburg in 1974. The book of abstracts[75] contains many of the ideas that were extended technically to much higher proficiency at a later time. Multireference configuration interaction (MR–CI) was presented for excited states of a number of small diatomic and polyatomic molecules (by Robert J. Buenker and Sigrid D. Peyerimhoff and by Jerry L. Whitten), different ways of configuration selection were discussed (by Isaiah Shavitt and by Buenker and Peyerimhoff), and the choice of orbitals for CI, that is, natural orbitals (Charles F. Bender) and MC–SCF orbitals (Fritz Grein) to improve CI convergence was treated. Ruedenberg presented advantages of the even-tempered orbital basis. Enrico

Clementi showed that adjoined basis sets, used to evaluate less important integrals and matrix elements, could reduce the computation time for 450 primitive Gaussians from 4 h to 35 min without loss of accuracy in the results. The mixing of Rydberg states with valence states was discussed from experimental (Camille Sandorfy) and theoretical (by Robert S. Mulliken, by Helene Lefebvre-Brion, and by Eugen Schwarz) perspectives in great detail. The role of negative ions as interstellar molecules (Jürgen Barsuhn) and responsible for Feshbach resonances (Lefebvre-Brion) was discussed, and suggestions were given for how to compute nonadiabatic couplings in predissociation processes due to avoided crossing of states (Jean-Claude Lorquet). Studies using equation of motion (EOM) methods for excited states and data on photoionization cross sections based on a discrete orbital basis (Vincent McKoy) were shown. Even first results for transition metal compounds (Alain Veillard) were presented. This meeting was remembered by many of the participants for its scientific content, but also because of the beautiful site of this castle, which serves as the guest house of the University of Ulm.

In the middle of the 1970s, experimentalists realized that theoretical treatments had made great progress and renewed their interest in cooperation or in challenging the theoreticians. At the 1976 Theoretical Chemistry Symposium, for example, Christoph Schlier (Freiburg), an expert on molecular beam experiments, presented his talk on "Scattering Collision Experiments—And What We Always Would Have Liked To Know About It from Theoretical Chemistry." Similarly, Peter Toennies (Göttingen) had approached theoretical chemists on this subject before.

In 1976, Paul von Ragué Schleyer moved from Princeton to the University of Erlangen-Nürnberg to accept a professorship in organic chemistry, after he had spent 1974–1975 at the Technical University of München as Senior U.S. Scientist Awardee of the Alexander von Humboldt Stiftung. Trained as an experimental organic chemist, he had become aware of the great potential of computational quantum chemistry for the study of new chemical compounds and reactions. Coming from the same background as other organic chemists, he spoke their language and—after a number of years[76]—was able to convince them of the practicability of this new theoretical tool. In particular, his work on organolithium compounds[77] and carbonium ions, carbanions, and reactive intermediates was essential in this respect. His work certainly had a great impact on the acceptance of computational chemistry within the community of German (experimental) organic chemists.

IBM in Germany organized a symposium on "Computational Methods in Chemistry"[78] at Bad Neuenahr in 1979 with the preface: "According to Graham Richards[79] the 'Third Age of Quantum Chemistry' has started, where the results of quantum chemical calculation can guide the experimentalists in their search for the unknown." One of the examples chosen to underline this statement was the acetylene molecule. In 1970 Kammer[80] had made qualitatively correct predictions for the first cis ($^3B_2$, $^3A_2$) and trans ($^3B_u$, $^3A_u$) bent

electronically excited states of this molecule. In 1975 Demoulin[81] had calculated the corresponding potential energy curves, and in 1978 Wetmore and Schaefer[82] reliably determined the geometry of $C_2H_2$ in these states. With the help of this guidance, Wendt, Hunziker, and Hippler[83] took up the search and succeeded in finding the theoretically predicted near infrared (IR) absorption for the cis conformer. The measured spectrum confirmed all theoretical predictions quantitatively.

This symposium showed very convincingly how theoretical methods had taken up a large variety of different problems and had influenced experimental studies. At the symposium, W. Meyer with co-workers P. Botschwina, P. Rosmus, and H.-J. Werner reported on their work on molecular properties. This group discussed results on spectroscopic data ($R_e$, $\omega_e$, $\omega_e x_e$, $\alpha_e$), ionization energies, electron and proton affinities, dipole moment functions, and static dipole polarizabilities, and even showed results on polarizability anisotropies. In all calculations, they included electron correlation (PNO–CI or PNO–CEPA) and showed the importance of going beyond simple Hartree–Fock calculations. W. von Niessen, L. S. Cederbaum, W. Domcke, and J. Schirmer showed how the Greens function approach,[84,85] which computes energy differences directly, can be used to analyze vibrational structure and vibronic coupling effects in photoelectron spectra (PES). They also discussed complications in inner-shell ionization spectra due to the breakdown of the one-particle picture. Inner-shell phenomena were also discussed by MR–CI methods (Buenker and Peyerimhoff), and it was shown that such methods can reliably predict details of molecular spectra in small polyatomic molecules including vibrational features and intensities. The use of computer chemistry for the study of organic reactions (in particular the Wolff rearrangement which involves isomerization of α-carbonyl carbenes into ketenes) presented by the IBM crew was an excellent example of how quantum chemistry had joined experimental organic chemistry to study chemical reactions. First calculations on silicon clusters prepared the way to investigate problems in surface chemistry.[86] One section of this symposium was devoted to the analysis of molecular spectra (NMR, IR) and the problem of data storage and man–machine communication, and another section was held on computer-aided synthesis, as discussed before. This symposium not only treated quantum chemical methods, but demonstrated further uses of computers in chemistry; its title "Computational Methods in Chemistry" was thus fully justified.

Toward the end of the 1970s, the challenge of Ch. Schlier to describe atom–molecular collisions by quantum chemical methods was met by two young Germans, Jörn Manz and Joachim Römelt for a three-body A+BC reaction. Traditionally, chemical reactions had been treated using the coordinates leading from the reactants to the product,[87] according to chemist's intuition. In accurate quantum calculations, such a scheme excludes the description of branching ratios, dissociative processes, or heavy–light–heavy reactions associated with small skewing angles. The polar Delves or hyperspherical

coordinates, on the other hand, allow the treatment of all such processes (elastic, inelastic, reactive, and dissociative) for all mass combinations. In 1980, Hauke, Manz and Römelt, using such coordinates, published their theory and a first numerical example for a quantum mechanically exact treatment[88] of a collinear reaction, which was followed by applications to H+HI, $H+H_2$, and dissociative collinear reactions.[89] When Römelt saw his third paper in print, he realized that A. Kuppermann and co-workers had thought very much along the same lines.[90]

Work on clusters[91,92] also had its origin in this decade. Initial work led in following years to the production of the well-known Stuttgart pseudopotentials,[93] which enables the realistic calculation of systems containing heavier elements. It also prepared the route to many studies on magic numbers in cluster chemistry and eventually to fullerenes and nanotubes.

Finally, the ground was almost ready for the ab initio calculation of NMR chemical shifts. Kutzelnigg[94] designed the IGLO (individual gauge for localized orbitals) method, and Schindler[95] presented the first systematic application of this method to compute $^{13}C$ chemical shifts of carbocations. The computation of NMR chemical shifts[96] is an ideal link between theory and experiment because calculated shifts can be used in combination with the NMR measurements to differentiate between various structural possibilities of the species under investigation. Hence, IGLO calculations are an ideal tool to give fingerprints to identify transient species with unusual structures.

## BEYOND 1980

The field of computational chemistry found itself in good times by the 1980s, and many young students were fascinated by the combination of computer usage and chemical research. At the 1981 Theoretical Chemistry Symposium, about 160 people participated. Henry Fritz Schaefer III talked about the third age of quantum chemistry. He stated that the Americans had been proud to have the center of gravity of quantum chemical or computational research after World War II. He had to admit that this center had moved—seen from a geographical point of view—at least toward the middle of the Atlantic Ocean, and that German scientists had a heavy weight in this change.

International cooperation had become the rule in universities and research institutions. Computers became cheaper so that it became possible to purchase "minicomputers" such as VAX 11/780 (Digital Equipment Corporation), Perkin-Elmer 8/32, or Convex C220 for dedicated purposes. For a number of theoretical chemistry groups, this helped them to become independent of the long queue of users at their university central computer. In addition, access over a network to machines at a remote site became realistic, even if it was only via a 1200-baud special telephone line. For these reasons the

development of computational chemistry seems to have become very similar in various countries. Applications rather than method development became dominant and many inorganic and organic chemists as well as scientists in molecular physics and pharmaceutical research were no longer hesitant to use the new computational methods. Computer programs for molecular modeling based on quantum chemistry, on classical mechanics, or on empirical force fields became available in international exchange. Monte Carlo simulations became feasable on vector computers and parallel machines, and access to large databases was made possible. The quantum chemistry tools were extended to include relativistic effects,[97] which play an important role in transition metal and heavy-element chemistry. Such efforts were later on supported by a program from the European Science Foundation[98] which gave financial support to a number of European groups working in this field. The possibility to include relativistic effects, either directly or by effective potentials[93] made quantum chemical calculations also interesting for many inorganic chemists and organometallic chemists. Today, theoretical and computational chemists participate in many of the collaborative research centers (Sonderforschungsbereich) at German universities, which are created to support interdisciplinary work in areas expected to have great impact for our future.

In 1981, the computational chemists who are primarily interested in a wide area of applications rather than in developing quantum methods founded their own Fachgruppe (Section) "Chemie-Information-Computer" (CIC) within the Gesellschaft Deutscher Chemiker (GDCh). Of special interest in this Fachgruppe are discussions on the use of computers in all fields of chemistry, development of chemical software, databases, information retrieval systems, computer-aided synthesis, molecular modeling, expert systems, and artificial intelligence. The members have their annual meetings, generally in the frame of the annual meeting of the GDCh. Some of the CIC members participate in the Theoretical Chemistry Symposia, and delegates of the Arbeitsgemeinschaft Theoretische Chemie attend CIC events.

At this point, a look at computational chemistry in German industry is appropriate. An evaluation is somewhat difficult, however, because generally only a few of the industrial computational chemists attend the annual chemistry conferences in Germany, and in addition, these chemists are generally reluctant to talk about details of their work. The main topic in the era 1970–1980 was presumably computer-aided synthesis. It was a joint endeavor of seven companies in Germany and Switzerland (BASF, Bayer, Ciba–Geigy, Hoffmann–LaRoche, Merck, Hoechst, and Sandoz). Pattern recognition was also an important tool to find structurally related compounds that show similar or better molecular properties. Computer programs for the automatic recognition of the maximal common substructures among drug molecules, or computerized systems with graphical and topological information for handling and analysis of large databases were topics at special conferences.[99]

Quantum chemistry played a minor role in these investigations; in industry it was used at most on the semiempirical level in this era.

In the middle of the 1980s, molecular modeling, molecular mechanics (MM), molecular dynamics (MD), and some ab initio quantum chemistry became important tools in industry to study quantitative structure–activity relationships (QSAR). The necessary computer programs were purchased from academic or commercial institutions. A number of young German theoretical chemists accepted job offers from chemical industry in the 1980s in the hope to build up a computational chemistry nucleus within the companies, doing applied but also some basic research. At a special symposium on "Scientific Computing and Modeling in Chemical Industry" at the annual meeting 1994 of the Physical Chemistry Society (Bunsentagung), young computational chemists from seven chemical and pharmaceutical companies in Germany presented already 13 talks. The main topics were QSAR, enzymes, polymers, and databases, and the studies were clearly dominated by applications. The restructuring of chemical companies that took place in the second half of the 1990s under new managements left little room for the development of computational chemistry methods in industry. Invitations for consultants were seldom. The future will show whether the cooperation between German universities and industry in the area of computational chemistry will strengthen.

Fast expansion of the German university system in the 1970s had brought a considerable number of new positions in theoretical and computational chemistry to universities. However, this positive side was turned around in the following 20 years. Financial restrictions lead to a decrease in budgets, and salary lines of postdoctoral positions at universities were often simply cut off. Since many of the professors, who came into office toward the end of the 1970s, were quite young, there was essentially no university post open for young people until the mid 1990s when retirement of this first generation of professors started. In other words, the generation of young scientists who were all well trained in the field could not really use their talents for research at German universities or research centers. Many of those people went into (computer-oriented) industry or took their talents to other countries.

This chapter has dealt almost exclusively with the development of quantum chemistry in the western part of Germany after World War II. In East Germany the situation under a harsh, centralistic regime was vastly different. The ideology of the ruling party reached all facets of society. Thus a top-down philosophy of science administration led to a concentration of a large part of research in the many institutes of the Akademie der Wissenschaften der DDR. It remains for an insider to record the full story. With the fall of the Wall (November 9, 1989) and reunification of Germany (October 3, 1990), the situation has changed drastically, but it appears too early to judge the lasting effects of the new structures or the lingering effects of the old structures.

Looking back, I find it truly amazing with what intensity science in Germany recuperated after the total vacuum caused by the Nazi regime and World War II. If I ask myself what were the main influences on the positive development of computational chemistry in Germany, I see it in our "bottom-up" principle of support. Contrary to some other countries, in which the "top-down" principle is favored, that is, in which research topics that are thought to deserve funding are earmarked from a centralized body, West German support of science wanted to be far away from dictating any route —especially after considering Germany's recent history. Hence, a small number of young energetic people, in competition with each other, fascinated by new tools and methods, were the hard core to develop the field. The first generation was generally trained in physics or mathematics; the second generation originated mostly from chemistry. The foresight of a few senior scientists that digital computers would become an extremely useful tool and should be made available to researchers (recommended by a committee of the DFG) and that it was worthwhile to bring the young German researchers together within a special priority program gave important support to the field. The advance of quantum chemistry and computational chemistry and its introduction into the education of chemistry students occurred without the support of large government contracts from the ministry of education or ministry of research and technology and largely without the support of dedicated research institutions such as the Max Planck Institutes or industry.

It is gratifying to observe that computational chemistry in Germany is again strongly visible internationally. This remarkable development should be kept in mind in the present tendency to favor the support of large scientific centers over modest proposals from young individuals.

## ACKNOWLEDGMENTS

I would like to gratefully acknowledge the help I received from various colleagues. In particular, I want to thank W. Kutzelnigg for information on the Theoretical Chemistry Symposia and for various articles in which he looks back on the history of quantum chemistry. I want to thank H.-W. Preuß for annotated reprints of his early work and H. Kuhn for information on his work with the analog computer. I am also grateful to Frank-Dieter Kuchta who helped to search for essential data in DFG reports.

## REFERENCES

1. K. Gavroglu and A. Simoes, *Hist. Stud. Phys. Biol. Sci.,* **25/1,** 47 (1994). The Americans, the Germans and the Beginning of Quantum Chemistry.
2. W. Heitler and F. London, *Z. Physik,* **44,** 455 (1927). Wechselwirkung neutraler Atome und Homöopolare Bindung nach der Quantenmechanik.
3. L. Pauling, *Proc. R. Soc. London, Ser. A,* **114,** 181 (1927). The Theoretical Prediction of the Physical Properties of Many Electron Atoms and Ions.

4. F. Hund, *Z. Phys.,* **36,** 657 (1926). Zur Deutung einiger Erscheinungen in den Molekülspektren. F. Hund, *Z. Phys.,* **51,** 759 (1928). Zur Deutung der Molekülspektren. IV.
5. R. S. Mulliken, *Phys. Rev.,* **32,** 186 (1928). The Assignment of Quantum Numbers for Electrons in Molecules. R. S. Mulliken, *Phys. Rev.,* **32,** 761 (1928). The Assignment of Quantum Numbers for Electrons in Molecules. II. Correlation of Molecular and Atomic Electron States.
6. P. A. M. Dirac, *Proc. R. Soc. London, Ser. A,* **123,** 714 (1929). Quantum Mechanics of Many-Electron Systems.
7. E. Hückel, *Z. Phys.,* **60,** 423 (1930). Zur Quantenchemie der Doppelbindung. E. Hückel, *Z. Phys.,* **70,** 204 (1931). Quantentheoretische Beiträge zum Benzol-Problem. I. Die Elektronenkonfiguration des Benzols und verwandter Verbindungen. Habilitationsschrift. E. Hückel, *Z. Phys.,* **72,** 310 (1931). Quantentheoretische Beiträge zum Benzol-Problem. II. Quantentheorie der induzierten Polaritäten.
8. W. H. E. Schwarz, D. Andrae, S. R. Arnold, J. Heidberg, H. Hellmann Jr., J. Hinze, A. Karachalios, M. A. Kovner, P. C. Schmidt, and L. Zülicke, *Bunsenmagazin,* **1,** 10 (1999); **2,** 60 (1999). Hans G. A. Hellmann (1903–1938). Ein Pionier der Quantenchemie.
9. J. D. Bolcer and R. B. Hermann, in *Reviews in Computational Chemistry,* K. B. Lipkowitz and D. B. Boyd, Eds., VCH Publishers, New York, 1994, Vol. 5, pp. 1–63. The Development of Computational Chemistry in the United States.
10. S. J. Smith and B. T. Sutcliffe, in *Reviews in Computational Chemistry,* K. B. Lipkowitz and D. B. Boyd, Eds., VCH Publishers, New York 1997, Vol. 10, pp. 271–316. The Development of Computational Chemistry in the United Kingdom.
11. K. Zuse, "*Der Computer–Mein Lebenswerk,*" Springer Verlag, Berlin-Heidelberg, 1984.
12. H. Billing, private communication and *MPG (Max Planck-Gesellschaft)-Spiegel,* **4,** 41 (1982). Die Göttinger Rechenmaschinen G1, G2 und G3.
13. H. Petzold, Rechnende Maschinen, *Technikgeschichte in Einzeldarstellungen,* VDI-Verlag, Düsseldorf, Band 41, 1985.
14. H. Kuhn, in *Selected Topics in the History of Biochemistry: Personal Recollections VI* (Comprehensive Biochemistry, G. Semenza and R. Jaenicke, Eds., Elsevier Science, Amsterdam, The Netherlands, 2000, Vol. 41), pp. 301–362. Fascination in Modeling Motifs.
15. H. Kuhn, *Z. Elektrochem.,* **55,** 220 (1951). Analogieversuche mit schwingenden Membranen zur Ermittlung von Elektronenzuständen in Farbstoffmolekülen mit verzweigtem Elektronengas.
16. H. Kuhn, *Chimica,* **15,** 53 (1961). Analogiebetrachtungen und Analogrechner zur quantenchemischen Behandlung der Lichtabsorption der Farbstoffe.
17. F. P. Schäfer, "Analogrechner und Registrierautomat zur Ermittlung der stationären Wellenfunktionen und Energieniveaus eines Teilchens in einem zweidimensionalen Potentialfeld," Doctoral Thesis, Marburg, Germany, 1960.
18. H. Kuhn, *Angew. Chem.,* **71,** 93 (1959). Neuere Untersuchungen über das Elektronengasmodell organischer Farbstoffe.
19. R. Pariser and R. Parr, *J. Chem. Phys.,* **21,** 466 (1953). A Semi-Empirical Theory of the Electronic Spectra and Electronic Structure of Complex Unsaturated Molecules. I. See also, R. Pariser and R. Parr, *J. Chem. Phys.,* **21,** 767 (1953). A Semi-Empirical Theory of the Electronic Spectra and Electronic Structure of Complex Unsaturated Molecules. II. J. A. Pople, *Trans. Faraday Soc.,* **49,** 1375 (1953). Electron Interactions in Unsaturated Hydrocarbons. J. A. Pople, *J. Phys. Chem.,* **61,** 6 (1957). Application of Self-Consistent Molecular Orbital Methods to π Electrons.
20. H. Hellmann, *Einführung in die Quantenchemie,* Franz Deuticke, Leipzig und Wien, 1937.
21. H.-J. Kopineck, *Z. Naturforsch.* **5a,** 420 (1950). Austausch- und andere Zweizentrenintegrale mit 2s- und 2p-Funktionen. H.-J. Kopineck, *Z. Naturforsch.,* **6a,** 177 (1951). Zweizentrenintegrale mit 2s- und 2p-Funktionen. II, Ionenintegrale.

22. M. Kotani, A. Ameniya, and T. Simose, *Proc. Physico-Math. Soc. Jpn.,* **20,** Extra Nr. 1 (1938); **22,** Extra Nr. 1 (1940).
23. P. J. Wheatley and J. W. Linnett, *Trans. Faraday Soc.,* **45,** 897 (1949). Molecular Force Fields. Part XI. A Wave Mechanical Treatment of the Change with Distortion of the Interaction Energy of Carbon $2p_\pi$ Orbitals. R. G. Parr and B. L. Crawford, *J. Chem. Phys.,* **16,** 1049 (1948). On Certain Integrals Useful in Molecular Orbital Calculations. J. O. Hirschfelder and J. W. Linnett, *J. Chem. Phys.,* **18,** 130 (1950). The Energy of Interaction between Two Hydrogen Atoms.
24. H.-J. Kopineck, *Z. Naturforsch.*, **7a,** 22 (1952). Quantentheorie des $N_2$-Moleküls. I. Problemstellung und Grundlagen der durchzuführenden Untersuchungen. Das $N_2$-Molekül als Sechselektronenproblem. H.-J. Kopineck, *Z. Naturforsch.,* **7a,** 314 (1952). Quantentheorie des $N_2$-Moleküls. II. Behandlung des $N_2$-Moleküls als Zehnelektronenproblem.
25. H.-J. Kopineck, *Z. Naturforsch.,* **7a,** 785 (1952) 785. Zweizentrenintegrale. III. Integrale mit 2p- und wasserstoffähnlichen 2s-Funktionen.
26. C. C. J. Roothaan, *J. Chem. Phys.,* **19,** 1445 (1951). A Study of Two- Center Integrals Useful in Calculations on Molecular Structure. I.
27. K. Ruedenberg, *J. Chem. Phys.,* **19,** 1459 (1951). A Study of Two-Center Integrals Useful in Calculations on Molecular Structure. II. The Two- Center Exchange Integrals.
28. C. C. J. Roothaan, *Rev. Mod. Phys.,* **23,** 69 (1951). New Developments in Molecular Orbital Theory.
29. H. Preuß, *Z. Phys.,* **130,** 239 (1951). Berechnung des $H_2$-Molekül-Grundzustandes. *Z. Naturforsch.,* **8a,** 270 (1953). Abschätzung für Zweizentrenintegrale.
30. H. Preuß, *Integraltafeln zur Quantenchemie,* Springer-Verlag Berlin, Göttingen, Heidelberg, Vol. I, 1956; Vol. II, 1957; Vol. IV, 1960; and Vol. III, 1961.
31. See, for example, B. Kockel, *Z. Naturforsch.,* **16a,** 1021 (1961). Zustandsfunktionen für die Atome Li bis Ne.
32. M. Kotani, A. Amemiya, E. Ishiguro, and T. Kimura, *Tables for Molecular Integrals,* Maruzen, Tokyo, 1955. See also: E. Ishiguro, S. Yuasa, M. Sakamoto, and T. Arai, *Nat. Sci. Rep.,* **5,** 33 (1954).
33. S. F. Boys, *Proc. Roy. Soc. London, Ser. A,* **200,** 542 (1950). Electronic Wave Functions. I. A General Method of Calculation for the Stationary States of Any Molecular System.
34. H. Preuß, *Z. Naturforsch.,* **11a,** 823 (1956). Bemerkungen zum Self-consistent-field-Verfahren und zur Methode der Konfigurationswechselwirkung in der Quantenchemie.
35. J. L. Whitten, *J. Chem. Phys.,* **44,** 359 (1966). Gaussian Lobe Function Expansions of Hartree–Fock Solutions for the First-Row Atoms and Ethylene.
36. H. Preuß, *Z. Naturforsch.,* **10a,** 365 (1955). Untersuchungen zum kombinierten Näherungsverfahren. H Preuß, *Fortschritte Phys.,* **10,** 271 (1962). Die Güte von Näherungslösungen der Schrödingergleichung und die Genauigkeit der Erwartungswerte und Übergangselemente. H. Preuß, *Theor. Chim. Acta,* **6,** 413 (1966). Die Bestimmung der Energiehyperflächen mehratomiger Systeme nach einer Interpolationsmethode mit Hilfe der Vorstellung der Atomassoziationen. Dreizentrensysteme.
37. H. Hartmann, *Theorie der chemischen Bindung auf quantentheoretischer Grundlage,* Springer-Verlag, Berlin, 1954.
38. B. Kockel, *Darstellungstheoretische Behandlung einfacher wellenmechanischer Probleme,* Teubner Verlagsgesellschaft, Leipzig, 1955.
39. P. Gombas, *Theorie und Lösungsmethoden des Mehrteilchenproblems der Wellenmechanik,* Verlag Birkhäuser, Basel, Switzerland, 1950.
40. *Deutsches Rechenzentrum,* Allgemeine Information, Darmstadt, November 1966.
41. Jahresbericht 1966 des Deutschen Rechenzentrums, Darmstadt, 1967.
42. H. Preuß, *Naturwissenschaften,* **11,** 21 (1960). Die gegenwärtige Situation der Quantenchemie.

43. W. Kutzelnigg, *Nachr. Chem. Techn.,* **13,** 351 (1965). Theoretische Chemie in Deutschland.
44. *Technical Report,* Laboratory of Molecular Structure and Spectra, Department of Physics, University of Chicago, Chicago, IL, 1961.
45. *Reviews Modern Physics,* **32,** No. 2, 169–476 (1960). (S. A. Goudsmit and E. U. London, Eds. with an introduction by R. G. Parr. The Conference was held at the University of Colorado, June 21–27, 1959.)
46. *DFG–Jahresberichte* 1966–1970. (Annual Reports of the German Science Foundation, 1966–1970, Kennedyallee 40, D-53170 Bonn, Germany).
47. There were three more in chemistry: analytical chemistry, crystal structure research, and physics and chemistry of interfaces.
48. W. Kutzelnigg, private communication and a preprint "30 Jahre Symposium Theoretische Chemie," presented at the 31st Theoretical Chemistry Symposium, Loccum, Germany, 1995.
49. S. D. Peyerimhoff, *J. Chem. Phys.,* **43,** 998 (1965). Hartree–Fock Roothaan Wavefunctions, Potential Curves and Charge-Density Contours for the $HeH^+$ ($X^1\Sigma^+$) and $NeH^+$ ($X^1\Sigma^+$) Molecule Ions.
50. S. D. Peyerimhoff, *Z. Naturforsch.,* **18a,** 1197 (1963). Berechnungen am HF-Molekül.
51. H. Preuß, *Z. Naturforsch.,* **19a,** 1335 (1964). Das SCF–LCGO–MO–Verfahren. G. Diercksen and H. Preuß, *Z. Naturforsch.,* **21a,** 863 (1966). Erste Mitteilung über Absolutrechnungen nach der neuen SCF–MO–LC(LCGO)-Methode am Benzol und Cyclopentadienylanion.
52. H. Preuß and G. Diercksen, *Int. J. Quantum Chem.,* **1,** 349 (1967). Wellenmechanische Absolutrechnungen an Molekülen und Atomsystemen mit der SCF-MO-LC(LCGO)-Methode. I. Das Cyclopentadienylanion ($C_5H_5^-$). H. Preuß and G. Diercksen, *Int. J. Quantum Chem.,* **1,** 357 (1967). II. Das Benzol ($C_6H_6$). H. Preuß and G. Diercksen, *Int. J. Quantum Chem.,* **1,** 361 (1967). III. Das Cyclopropan ($C_3H_6$). H. Preuß and G. Diercksen, *Int. J. Quantum Chem.,* **1,** 369 (1967). IV. Das Äthylen ($C_2H_4$), and following articles.
53. S. D. Peyerimhoff, R. J. Buenker, and L. C. Allen, *J. Chem. Phys.,* **45,** 734 (1966). Geometry and Molecules. I. Wavefunctions for Some Six- and Eight-Electron Polyhydrides. R. J. Buenker, S. D. Peyerimhoff, L. C. Allen, and J. L. Whitten, *J. Chem. Phys.,* **45,** 2835 (1966). Geometry of Molecules. II. Diborane and Ethane. R. J. Buenker and S. D. Peyerimhoff, *J. Chem. Phys.,* **45,** 3682 (1966). Geometry of Molecules. III. $F_2O$, $Li_2O$, FOH, LiOH.
54. R. J. Buenker, S. D. Peyerimhoff, and J. L. Whitten, *J. Chem. Phys.,* **46,** 2029 (1967). Theoretical Analysis of the Effects of Hydrogenation in Hydrocarbons: Accurate SCF MO Wavefunctions for $C_2H_2$, $C_2H_4$, and $C_2H_6$. S. D. Peyerimhoff and R. J. Buenker, *J. Chem. Phys.,* **47,** 1953 (1967). Geometry of Ozone and Azide Ion in Ground and Certain Excited States.
55. S. D. Peyerimhoff, *J. Chem. Phys.,* **47,** 349 (1967). Relationships Between $AB_2$ and $H_nAB_2$ Molecular Spectra and Geometry: Accurate SCF MO and CI Calculations for Various States of $HCOO^-$. R. J. Buenker and S. D. Peyerimhoff, *J. Chem. Phys.,* **48,** 354 (1968). Ab Initio Study on the Stability and Geometry of Cyclobutadiene.
56. R. J. Buenker and S. D. Peyerimhoff, *Chem. Phys. Lett.,* **3,** 37 (1969). Ab Initio SCF Calculations for Azulene and Naphthalene.
57. R. Ahlrichs and W. Kutzelnigg, *J. Chem. Phys.,* **48,** 1819 (1968). Direct Calculation of Approximate Natural Orbitals and Natural Expansion Coefficients of Atomic and Molecular Electronic Wavefunctions. II. Decoupling of the Pair Equations and Calculation of the Pair Correlation Energies for the Be and LiH Ground States. R. Ahlrichs and W. Kutzelnigg, *Theor. Chim. Acta,* **10,** 377 (1968). Ab initio Calculations on Small Hydrides Including Electron Correlation. I. The $BeH_2$ Molecule in Its Ground State.
58. W. Meyer, *Int. J. Quantum Chem.,* Symp. No. 5, **5,** 341 (1971). Ionization Energies of Water from PNO–CI Calculations. W. Meyer, *J. Chem. Phys.,* **58,** 1017 (1973). PNO–CI Studies of Electron Correlation Effects. I. Configuration Expansion by Means of the Nonorthogonal Orbitals, and Application to the Ground State and Ionized States of Methane.
59. R. Ahlrichs, H. Lischka, V. Staemmler, and W. Kutzelnigg, *J. Chem. Phys.,* **62,** 1225 (1975). PNO–CI (Pair Natural Orbital Configuration Interaction) and CEPA–PNO (Coupled

Electron Pair Approximation with Pair Natural Orbitals) Calculations of Molecular Systems. I. Outline of the Method for Closed-Shell States.

60. W. Kutzelnigg and P. v. Herigonte, *Adv. Quantum Chem.,* **36,** 185 (2000). Electron Correlation at the Dawn of the 21st Century.
61. Centre de Calcul du C.N.R.S., Faculté des Sciences, Orsay, France. (A description of the centre to open October 1969; a booklet of 13 pages.)
62. CECAM Annual Report, C. Moser Ed., CECAM, Batiment 506, 91-Campus Orsay, France, 1973.
63. E. J. Corey and W. T. Wipke, *Science,* **166,** 178 (1969). Computer-Assisted Design of Complex Organic Syntheses. E. J. Corey, W. T. Wipke, R. D. Cramer, and W. J. Howe, *J. Am. Chem. Soc.,* **94,** 421 (1972). Computer-Assisted Synthetic Analysis. Facile Man-Machine Communication of Chemical Structure by Interactive Computer Graphics. E. J. Corey, W. T. Wipke, R. D. Cramer, and H. J. Howe, *J. Am. Chem. Soc.,* **94,** 431 (1972). Techniques for Perception by a Computer of Synthetically Significant Structural Features in Complex Molecules.
64. I. Ugi, J. Bauer, K. Bley, A. Dengler, A. Dietz, E. Fontain, B. Gruber, R. Herges, M. Knauer, K. Reitsam, and N. Stein, *Angew. Chem.,* **105,** 210 (1993). Die Computerunterstützte Lösung Chemischer Probleme—Eine neue Disziplin der Chemie.
65. E. J. Corey and X.-M. Cheng, *The Logic of Chemical Synthesis,* Wiley, New York, 1989.
66. W. T. Wipke and D. Rogers, *J. Chem. Inf. Comput. Sci.,* **24,** 71 (1984). Artificial Intelligence in Organic Synthesis. SST: Starting Material Selection Strategies. An Application of Superstructure Search.
67. H. Gelernter, N. S. Sridharan, A. J. Hart, S.-C. Yen, F. W. Fowler, and H.-J. Shue, *Top. Curr. Chem.,* **41,** 113 (1973). The Discovery of Organic Synthetic Routes by Computer. H. Gelernter, J. R. Rose, and C. Chen. *J. Chem. Inf. Comput. Sci.,* **30,** 492 (1990). Building and Refining a Knowledge Base for Synthetic Organic Chemistry via the Methodology of Inductive and Deductive Machine Learning.
68. I. Ugi, *Record of Chemical Progress,* **30,** 289 (1969). A Novel Synthetic Approach to Peptides by Computer Planned Stereoselective Four Component Condensations of α-Ferrocenyl Alkylamine and Related Reactions.
69. J. Dugundji and I. Ugi, *Top. Curr. Chem.,* **39,** 19 (1973). An Algebraic Model of Constitutional Chemistry as a Basis for Chemical Computer Programs. I. Ugi, *Intra-Sci. Chem. Rep.,* **5,** 229 (1971). The Potential of Four Component Condensations for Peptide Syntheses—A Study in Isonitrile and Ferrocene Chemistry as well as Stereochemistry and Logics of Syntheses.
70. J. Blair, J. Gasteiger, C. Gillespie, P. D. Gillespie, and I. Ugi, in *Computer Representations and Manipulation of Chemical Information,* W. T. Wipke, S. R. Heller, R. J. Feldmann, and E. Hyde, Eds., Wiley, New York, 1974, pp. 129–145. CICLOPS–A Computer Program for the Design of Synthesis on the Basis of a Mathematical Model.
71. W. Meyer, *J. Chem. Phys.,* **64,** 2901 (1976). Theory of Self-Consistent Electron Pairs. An Iterative Method or Correlated Many-Electron Wavefunctions.
72. W. Meyer, *Configuration Expansion by Means of Pseudonatural Orbitals,* Modern Theoretical Chemistry, Vol. 3, H. F. Schaefer III, Ed., Plenum Press, New York, 1977.
73. T. D. Crawford and H. F. Schaefer III, in *Reviews in Computational Chemistry,* K. B. Lipkowitz and D. B. Boyd, Eds., Wiley-VCH, New York, 2000, Vol. 14, pp. 33–136. An Introduction to Coupled Cluster Theory for Computational Chemists.
74. For details, see: J. A. Pople and D. L. Beveridge, *Approximate Molecular Orbital Theory,* McGraw-Hill, New York, 1970.
75. Abstracts, Symposium on Calculation of Electronically Excited States of Molecules by Ab Initio Methods, Schloß Reisensburg, Ulm, Germany, July 2–5, 1974.
76. K. Krogh-Jespersen, D. Cremer, D. Poppinger, J. A. Pople, P. v. R. Schleyer, and J. Chandrasekhar, *J. Am. Chem. Soc.,* **101,** 4843 (1979). Molecular Orbital Theory of the Electronic Structure of Molecules. 39. Highly Unusual Structures of Electron-Deficient Carbon Compounds. Reversal of van't Hoff Stereochemistry in BBC Ring Systems.

K. Raghavachari, R. A. Whiteside, J. A. Pople, and P. v. R. Schleyer, *J. Am. Chem. Soc.,* **103,** 5649 (1981). Molecular Orbital Theory of the Electronic Structure of Organic Molecules. 40. Structures and Energies of C1-C3 Carbocations, Including Effects of Electron Correlation.

77. E. D. Jemmis, J. Chandrasekhar, and P. v. R. Schleyer, *J. Am. Chem. Soc.,* **101,** 2848 (1979). The Unusual Structures, Energies, and Bonding of Lithium-Substituted Allenes, Propynes, and Cyclopropenes. A. J. Kos, T. Clark, and P. v. R. Schleyer, *Angew. Chem.,* **96,** 622, (1984). Die ab initio Berechnung der Struktur von 1,3-Dilithioaceton.
78. J. Bargon, Ed., *Computational Methods in Chemistry,* The IBM Research Symposia Series, Plenum Press, New York, 1980.
79. G. Richards, *Nature (London),* **278,** 507 (1979). Third Age of Quantum Chemistry.
80. W. E. Kammer, *Chem. Phys. Lett.,* **6,** 529 (1970). Ab Initio SCF and CI Calculations of Linear and Bent Acetylene.
81. D. Demoulin, *Chem. Phys.,* **11,** 329 (1975). The Shapes of Some Excited States of Acetylene.
82. R. W. Wetmore and H. F. Schaefer III, *J. Chem. Phys.,* **69,** 1648 (1978). Triplet Electronic States of Acetylene: Cis and Trans Structures and Energetics.
83. H. R. Wendt, H. Hippler, and H. E. Hunziker, *J. Chem. Phys.,* **70,** 4044 (1979). Triplet Acetylene: Near Infrared Electronic Absorption Spectrum of the Cis Isomer and Formation from Methylene.
84. L. S. Cederbaum, *Theor. Chim. Acta,* **31,** 239 (1973). Direct Calculation of Ionization Potentials of Closed-Shell Atoms and Molecules. L. S. Cederbaum *J. Phys. B,* **8,** 290 (1975). One-Body Green's Function for Atoms and Molecules: Theory and Application.
85. L. S. Cederbaum and W. Domcke, *Adv. Chem. Phys.,* **36,** 205 (1977). Outer-Valence Greens' Functions (OVGF).
86. P. S. Bagus, B. Liu, A. D. McLean, and M. Yoshimine, in *Computational Methods in Chemistry,* J. Bargon, Ed., Plenum Press, New York, 1980, pp. 203–237. The Application of Ab Initio Quantum Chemistry to Problems of Current Interest Raised by Experimentalists.
87. G. L. Hofacker, *Z. Naturforsch. A,* **18,** 607 (1963). Quantentheorie chemischer Reaktionen. R. A. Marcus, *J. Chem. Phys.,* **45,** 4493 (1966). On the Analytical Mechanics of Chemical Reactions. Quantum Mechanics of Linear Collisions. R. A. Marcus, *J. Chem. Phys.,* **45,** 4500 (1966). On the Analytical Mechanics of Chemical Reactions. Classical Mechanics of Linear Collisions.
88. G. Hauke, J. Manz, and J. Römelt, *J. Chem. Phys.,* **78,** 5040 (1980). Collinear Triatomic Reactions Described by Polar Delves' Coordinates.
89. J. Römelt, *Chem. Phys. Lett.,* **74,** 263 (1980). The Collinear $H+H_2$ Reaction Evaluated by S-Matrix Propagation along Delves' Radial Coordinate. J. Manz and J. Römelt, *Chem. Phys. Lett.,* **77,** 172 (1981). Dissociative Collinear Reactions Evaluated by S-Matrix Propagation along Delves' Radial Coordinate. J. Manz and J. Römelt, *Chem. Phys. Lett.* **81,** 179 (1981). On the Collinear I+HI and I+MuI Reactions. (Here Mu represents a muonium isotopic variant.)
90. A. Kuppermann, J. A. Kaye, and J. P. Dwyer, *Chem. Phys. Lett.,* **74,** 257 (1980). Hyperspherical Coordinates in Quantum Mechanical Collinear Reactive Scattering.
91. J. Flad, H. Stoll, and H. Preuß, *J. Chem. Phys.,* **71,** 3042 (1979). Calculation of Equilibrium Geometries and Ionization Energies of Sodium Clusters Up to $Na_8$.
92. H.-O. Beckmann, J. Koutecký and V. Bonačić-Koutecký, *J. Chem. Phys.,* **73,** 5182 (1980). Electronic and Geometric Structure of $Li_4$ and $Na_4$ Clusters.
93. H. Stoll, L. v. Szentpály, P. Fuentealba, J. Flad, M. Dolg, F.-X. Fraschio, P. Schwerdtfeger, G. Igel, and H. Preuß. *Int. J. Quantum Chem.,* **26,** 725 (1984). Pseudopotential Calculations Including Core-Valence Correlation: Alkali and Noble-Metal Compounds. M. Dolg, U. Wedig, H. Stoll, and H. Preuß, *J. Chem. Phys.,* **86,** 866 (1987). Energy-Adjusted Ab Initio Pseudopotentials for the First Row Transition Elements. M. Dolg, H. Stoll, A. Savin, and H. Preuß, *Theor. Chim. Acta,* **75,** 173 (1989). Energy-Adjusted Pseudopotentials for the Rare Earth Elements.

94. W. Kutzelnigg, *Isr. J. Chem.*, **19,** 193 (1980). Theories of Magnetic Susceptibilities and NMR Chemical Shifts in Terms of Localized Quantities.

95. M. Schindler and W. Kutzelnigg, *J. Chem. Phys.*, **76,** 1919 (1982). Part II. Applications to Some Simple Molecules. M. Schindler, *J. Am. Chem. Soc.*, **109,** 1020 (1987). Magnetic Properties in Terms of Localized Quantities. 5. Carbocations.

96. See, e.g., D. B. Chesnut, in *Reviews in Computational Chemistry,* K. B. Lipkowitz and D. B. Boyd, Eds., VCH Publishers, New York, 1996, Vol. 8, pp. 245–297. The Ab Initio Computation of Nuclear Magnetic Resonance Chemical Shielding.

97. B. A. Heß, *Phys. Rev. A,* **33,** 3742 (1986). Relativistic Electronic Structure Calculations Employing a Two-Component No-Pair Formalism with External Field Projection Operators.

98. Program of the European Science Foundation, "Relativistic Effects in Heavy-Element Chemistry and Physics," 1992–1998. See http://www.chemie.uni-erlangen.de/hess/html/esf/nl.html.

99. Abstracts of Papers, VIIth International Conference on Computers in Chemical Research and Education, Garmisch-Partenkirchen, Germany, June 10–14, 1985.

*Reviews in Computational Chemistry, Volume 18*
Edited by Kenny B. Lipkowitz and Donald B. Boyd

ISBN: 0-471-21576-7

APPENDIX

# Examination of the Employment Environment for Computational Chemistry

**Donald B. Boyd and Kenny B. Lipkowitz**

*Department of Chemistry, Indiana University–Purdue University at Indianapolis (IUPUI), Indianapolis, Indiana 46202-3274*

*Draw from others the lesson that may profit yourself.*
Publius Terentius Afer (ca. 190–159 B.C.)

## INTRODUCTION

The purpose of this essay is to put into perspective the job market for computational chemists. Professors and career counselors may find the information useful when advising their students. For students thinking about career directions, the data we present give an indication of the growing value of expertise in computational chemistry. The right kinds of computational chemist are needed to meet important economic and societal needs; for example, in designing new materials or in helping to find cures to debilitating diseases. Experienced laboratory chemists who are thinking of reinventing themselves for the information age may find the trends reported here pertinent to their decision making. We are not advocating that everyone should become a computational chemist, but we do point out that job opportunities expand for specialists in other areas of science if those scientists also possess some expertise in computational chemistry.

The last discussion of the job market for computational chemists was a brief one that DBB wrote for Volume 12 of this book series.[1] In the present chapter, the history of the job market is reviewed and brought up to date. We discuss factors that have affected the job market either positively or negatively and look at where recent growth has occurred. We ascertain which skills are currently in greatest demand. We then look at some data on R&D spending, graduation rates, and the number of patents granted, which reveal the broader R&D environment in which many computational chemists work. Lastly, we look at a subject dear to the heart of most everyone: salaries.

## HIRING TRENDS

A barometer of job opportunities for scientists with computational chemistry expertise is the number of relevant positions advertised in *Chemical and Engineering News* (C&EN), the widely-read weekly magazine of the American Chemical Society (ACS). Although many of the world's computational chemists are in the United States, it should be emphasized that advertisements in this one magazine reflect only partially the total number of positions available in any given year. Job opportunities in other nations are not usually advertised in C&EN, unless a search committee is seeking candidates to return to their homeland after having obtained an education in the United States. Still other job openings not appearing in C&EN are those advertised in other magazines or journals, those posted on corporate websites, and those disseminated on the Internet.[2] Many positions are filled by personal contacts and are not publicized. Nevertheless, we think that the C&EN numbers give a good indication of the overall trend in the job market for computational chemists.

Figure 1 shows the number of jobs advertised each year from 1983 through 2001, which spans most of modern era of computational chemistry. For purposes of constructing Figure 1, job openings were put into the following categories: tenure-track academic positions, nontenured academic staff positions, academic postdoctoral research positions, positions in industry (other than at software and hardware companies), positions at software or hardware companies, industrial postdoctoral positions, and positions in government laboratories. About three-quarters of the jobs required a Ph.D. degree, and many employers preferred postdoctoral experience. All the jobs included in Figure 1 required a chemistry degree, rather than a computer science or life science degree, for example.

Looking at the whole period 1983–2001 plotted in Figure 1, three major features are noteworthy. First, looking at the top curve, which is the sum of all categories each year, we see an expansion in the total number of jobs for computational chemists. Second is the interruption of growth in 1992–1994. And third is the high rate of job creation in recent years. We elaborate on these points.

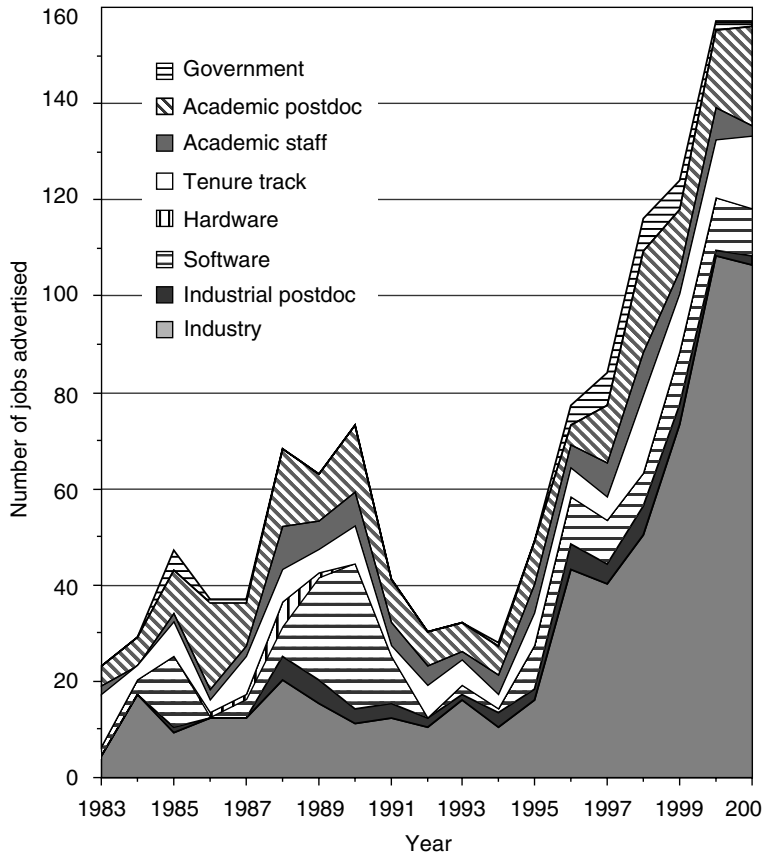


**Figure 1** Annual number of jobs for scientists in the field of computational chemistry that were advertised in *Chemical and Engineering News* for the years 1983–2001. The positions available are categorized as to whether they were for government laboratories, academia (nontenured staff, tenure-track professorial, or postdoctoral appointments), industrial research laboratories (permanent or postdoctoral appointments), software companies, or hardware companies. Having a separate category for hardware companies in our compilations stemmed from when these companies were more numerous in the 1980s, and they were hiring computational chemists primarily for marketing purposes. However, more recently as the hardware companies have had to consolidate, they have done little or no additional hiring. The data for software vendors include some postdoctoral-type positions primarily in the years 1988–1990. In a few cases, jobs advertised near the end of one year were also advertised early in the following year; in these situations the positions are counted in both years. In cases of advertisements for an unspecified number of open positions, an estimate was made. Therefore, the data are approximate, but representative and consistent.

Inspection of the contributory curves shows that the main area of job growth has been in industry. This growth has been at pharmaceutical and biotechnology companies principally, but also some jobs have been created at agrochemical, chemical, petroleum, lubricant, polymer, explosives, flavorings, photographic film, glass and ceramic companies.

The first industrial jobs for computational chemists opened in the early 1960s when such scientists were usually called theoretical chemists or physical chemists.[3] Those early pioneers not only had to prove themselves, they had to prove a whole new approach to answering questions in science, that is, computationally. Human nature being what it is, traditional (experimental) chemists reacted in different ways to computational chemistry: some were curious (some of whom even tried their own hand at calculations but often found the early technology—computer punch cards—too bothersome), some were disinterested, and some felt their prerogatives and perquisites were threatened. At the pharmaceutical companies, many of the medicinal chemists (who far outnumbered the computational chemists) were skeptical, if not resentful, of the upstarts.[4] Because of finite resources, one more person hired as a physical (or analytical) chemist often mean one less organic chemist would be hired.

At pharmaceutical companies in the 1960s through 1980s, each organic chemist could crank out the synthesis of about 50 new compounds per year. The odds of one of these compounds exhibiting all the attributes to become a pharmaceutical product were extremely small (traditionally asserted as approximately 1 in 10,000). No one would have considered organic chemistry a failure because of so many syntheses leading to dead ends. Yet some of the organic chemists of that era would declare computational chemistry totally useless after just one case where a calculated prediction turned out to be inaccurate. Antagonists of an approach are more likely to remember one failed prediction than the cases where the approach gave a useful result.

The obstacles were gradually overcome. The early "successes" were small indeed. To find a simple correlation between experimental results and calculated properties for a few molecules was once a special accomplishment. To correctly predict the biological activity of a proposed structure was even rarer.

Thanks mainly to improved methods and advances in computer technology, but aided by hard work, persistence, adaptability, optimism, and patience, computational chemists became able to answer research questions better and faster. Computers became easier to use, quicker, and capable of handling larger molecules. One of the aspects that experimentalists had a particular trouble accepting was the need for computational chemists to use simplified models of the structures they computed. Computational chemists could readily understand that replacing computationally irrelevant side chains with hydrogens would have no material effect on the outcome of the calculations of, say, the electronic structure of the core of the molecule. However,

experimentalists thought that any simplified model could not possibly represent properties of a molecule that they had made in the laboratory. More powerful computers meant that models closer to the experimentalists' concept of the molecules could be computed in a reasonable time. The computational chemists in industry steadily justified their existence and prevailed in demonstrating the value of their approach.

Enlightened management at companies was necessary in fostering a collaborative environment wherein the computational chemists would be accepted as integral partners in the research projects. Then computer-based ideas, as well as traditionally generated design ideas, could be tested in the iterative process of molecular design. Another key factor in convincing the organic chemists to get on board with molecular modeling was education. Thanks to hands-on training, in some instances pushed by enlightened management, experimentalists learned to do some of the calculations themselves and thus felt less threatened by a computational approach. Also the experimentalists learned that certain calculations were difficult enough that they should trust computational chemistry experts to do them. Despite the field being about 40 years old, clearly defined successes of using computational chemistry to aid drug discovery have become prevalent only in the last ten years.[5]

It should not be thought that difficulties were encountered solely in industry. Similar hurdles were, and still are, faced by some computational chemists trying to expand their presence on the faculties of colleges and universities. A lingering, negative attitude, which seems incongruent with this modern Information Age, is that computer modeling is either not "real" or not "real science". By definition, a model is an approximation to reality, but this does not mean that the results of modeling are useless. Ample evidence exists that computer modeling can and does lead to effective advances in science. In fact, in the so-called real world (industry), modeling is every day proving itself an efficacious partner in research and development.

This evolution to an acceptance of a computational approach to scientific research is an example of the famous observation of the Nobel Laureate physicist Max Planck (1858–1947) as expressed in 1936,[6] "An important scientific innovation rarely makes its way by gradually winning over and converting its opponents .... What does happen is that its opponents gradually die out and that the growing generation is familiarized with the idea from the beginning." This statement might be amended to point out that the naysayers merely needed to retire.

Returning to Figure 1, the job market for computational chemists is not immune to macroeconomic and political factors. In terms of the overall United States economy, the 1970s were characterized by dreary stagflation (no growth accompanied by rapid inflation) due to poor government policies originating in the mid-1960s. Greatly improved government policies in the early 1980s led to a remarkable economic revitalization which was accompanied by a rapidly increasing demand for computational chemists. The number of

computational chemists employed in industry was doubling about every five years.[7] The government policies of the 1980s provided a basis for the economic growth of the 1990s, when even more jobs for computational chemists were created. For the most part, the bursting of the "dot com" bubble at the turn of the century had little impact on computational chemists because their jobs were chiefly in companies with established business models. In contrast to what happened with other high technology businesses, plenty of venture capital continued to flow into businesses with biomedical objectives, so that more computational chemists were needed for the start-up pharmaceutical and biotechnology companies.

It is worth considering what caused the negative period 1992–1994 apparent in Figure 1, so that history might not repeat itself. There are three underlying facts. First, by the early 1990s the pharmaceutical industry was becoming the largest employer of computational chemists. Second, there was a mild economic slowdown, which reduced spending on research and development (R&D) across all industries in the United States, thus shifting the balance in the supply/demand equation for scientific talent. Third, the high profitability and self-supporting character of the pharmaceutical companies allowed them to invest more in R&D than did most other industries.

In the early 1990s, the profitability of the pharmaceutical industry in the United States came under threat from two sources. One was that the rapid transformation of health care delivery in the United States to a system based on health maintenance organizations (HMOs) and pharmacy benefits management (PBM) companies. At pharmaceutical manufacturers, it was feared that the HMOs and PBMs would have more clout to negotiate lower prices charged for prescription drugs. Initial indications were that this fear was justified. The other threat to profitability would have affected the entire health care industry and came from a proposed government plan that was being debated in 1992 and 1993. Under the plan, not only were pharmaceutical companies affected, but also hospitals and physicians. The high profitability of this whole industry was an irresistible target for some politicians who wanted to "reform" it. The scheme was not to nationalize the businesses, but rather to leave them under private ownership, but with prices effectively controlled by new government bureaucracies. Such a plan was reminiscence of what some governments in Europe imposed on their private industries in the 1930s. As expected, prudent pharmaceutical company executives became more cautious about investing in science for future growth. As recorded on the pages of C&EN and in the general press at the time, thousands of jobs at pharmaceutical companies were cut. Fortunately, computational chemists fared better than other pharmaceutical scientists and employees in these restructurings (down-sizings). By retaining the computational chemists, company managers were dramatically acknowledging the value of computational techniques in drug discovery. Additionally, computational chemists were a relatively small percentage of a company's employment

totals and tended to be younger on average than the other employees. The proposed government takeover plan was defeated in the United States Congress, and subsequent experience dealing with the HMOs and PBMs did not turn out to have as large an impact as the pharmaceutical companies originally feared. Confidence in the future was restored, and investment in R&D could takeoff.

Figure 2 shows the combined annual investments in R&D of large pharmaceutical companies in the United States.[8] The slowdown in 1992–1994 is evident. The pharmaceutical industry did not reduce its investment in science, but did temper the rate of increase in 1993 and 1994. Although the inflection in the curve may seem small, comparison with Figure 1 indicates that between 100 and 200 fewer jobs were created for computational chemists as a result.

We can glean other information from Figure 1. The little peak in 1985 and the modest one around 1989–1990 resulted from hiring at software companies catering to the pharmaceutical industry. A lucrative market developed for computational chemistry software[9] written to meet the needs of the

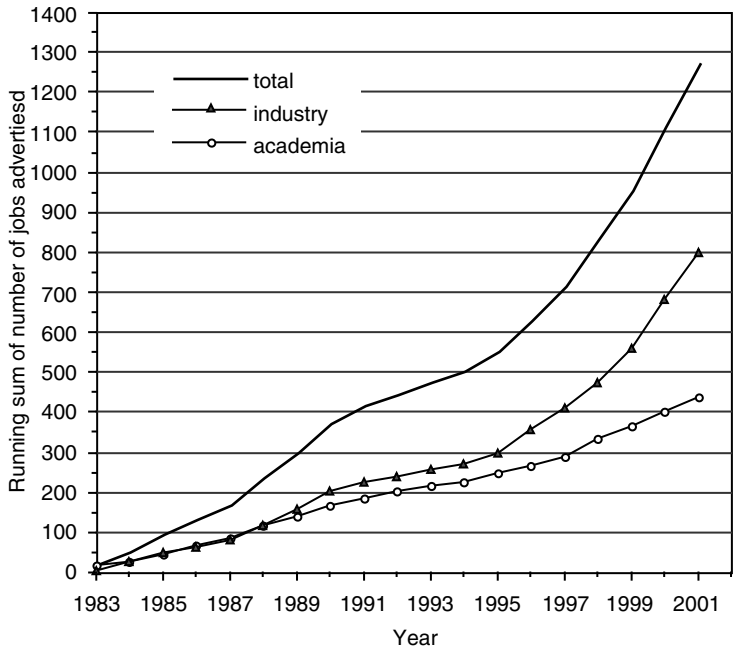


**Figure 2** Sum of annual R&D spending by six large pharmaceutical companies in the United States: Pfizer, Merck, Eli Lilly, Bristol-Myers Squibb, American Home Products (renamed Wyeth in 2002), and Schering-Plough. These companies are listed in descending order of the total amount of their profit spent on R&D. In terms of R&D investment in 2000 as of percentage of sales that year, the order of the companies changes to: Eli Lilly (19%), Pfizer (15%), Schering-Plough (14%), American Home Products (13%), Bristol-Myers Squibb (11%), and Merck (6%). On average, these companies spent almost 12% of their 2000 sales on R&D. Data from Ref. 8.

pharmaceutical industry. Some programs were for molecular modeling and others for management of databases of molecular structures. Although some pharmaceutical companies developed software internally, most companies found it more efficient to buy supported software. As seen in Figure 1, the software vendors essentially stopped hiring during the 1992–1994 downturn, but since 1995 the number of advertised jobs at these companies has been at a fairly steady pace.

The modest peak at 1988 in Figure 1 was due in part to hiring by industry. And most of the growth since 1995 has been in industrial jobs. The rising demand for computational chemists reached a new high in 2000 when about three-quarters of the demand came from industry, principally pharmaceutical and biotechnology. In 2001, hiring by industry slowed a bit, which was offset by an increase in advertised academic positions. A few of the latter were for tenure-track faculty, but most of them were only postdoctoral positions, which tend to be short lived.

Figure 3 compares the number of academic and industrial positions advertised in C&EN. The academic curve combines tenure-track, staff, and postdoctoral data from Figure 1. The industrial curve combines data for the industry, software, and hardware categories of Figure 1. The number of academic job openings has remained fairly steady, with a small peak in the late

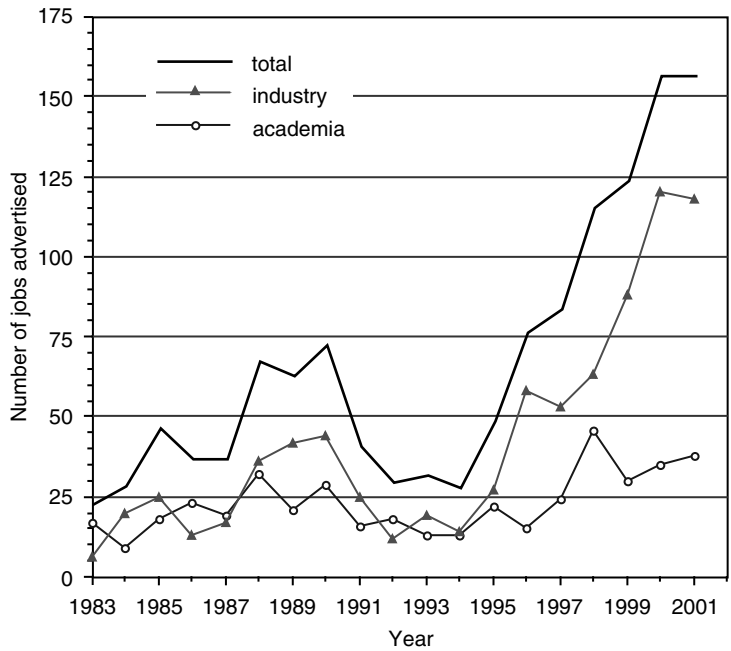


**Figure 3** Comparison of the total number of jobs and the total number of academic jobs for scientists in the field of computational chemistry advertised in C&EN.

1980s and a larger one about ten years later (1998). The last few years have been good for individuals wanting to stay in academia. Generally, academic hiring rises when funding from government and industry increases or when retiring or deceased faculty are being replaced.

Figure 4 shows the running sums for academic and industrial positions advertised in C&EN. The curves are based on the data in Figure 3. It can be seen that the academia and industry curves essentially coincided in the early 1980s. In the late 1980s, the accumulated number of advertisements from industry pulled ahead of the academic ones, but the two curves still paralleled each other in the early 1990s. After 1995, the industry curve accelerated even further ahead. Almost 1300 jobs for computational chemists were advertised in C&EN from 1983 through 2001. On the one hand, it should be realized that not all these jobs advertised in C&EN were new. Work forces have become increasingly fluid. As with other scientists, some computational chemists change jobs every few years. This turnover necessitates further job advertisements to be placed. On the other hand, as we mentioned, not all positions that have been created and filled since 1983 were advertised in C&EN. We do not have an accurate way to estimate the total number of individuals finding jobs as computational chemists since 1983, but it is certainly much greater than 1300. By way of comparison, the Computers in Chemistry (COMP)

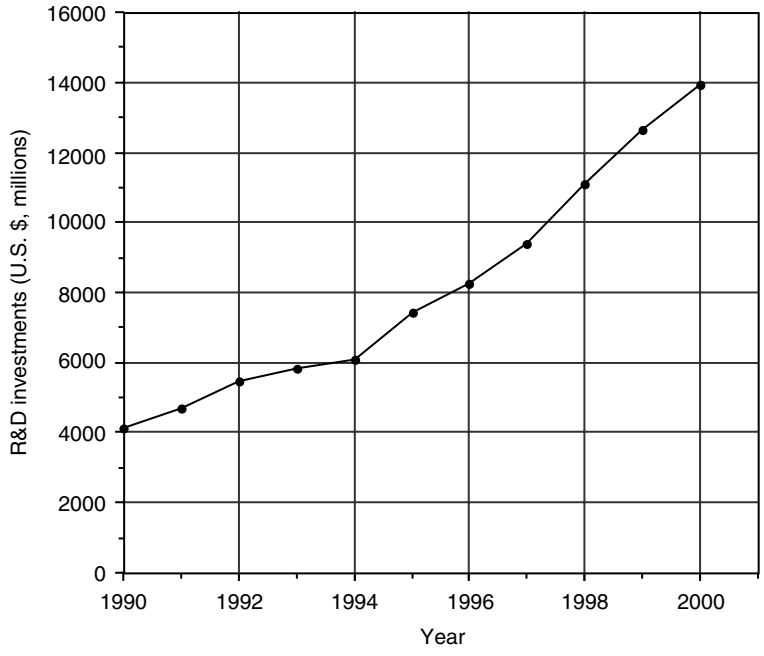


**Figure 4** Running summations of the number of industrial jobs and the number of academic jobs for scientists in the field of computational chemistry advertised in C&EN.

division of the ACS had about 2600 members as of 2001, and this probably represents less than half the total number of computational chemists in the United States.[10]

An overall indication of where computational chemists have found employment is given in Figure 5. The pie chart shows the percentage of jobs in each of the categories of Figure 1. The three largest categories are industry (46%), academic postdoctoral positions (17%), and software companies (13%). A loose comparison can be made to some data from the American Chemical Society. ACS surveys in 1999 and 2000 showed where new chemistry graduates were finding positions and covered all disciplines of chemistry.[11] About 60% of newly graduated chemists in the ACS surveys found jobs in industry; of these, a third (20%) went into the pharmaceutical industry. The ACS found similar percentages for both B.S.- and Ph.D.-level chemists doing so. Roughly 7% of the new chemistry graduates went into the biotechnology industry according to the ACS sampling. From these data, it appears, not surprisingly, that a higher percentage of computational chemists go into the pharmaceutical industry than do chemists in general.

In the United States, pharmaceutical companies are the largest employer of industrial chemists, not just computational chemists.[12] If the pharmaceutical

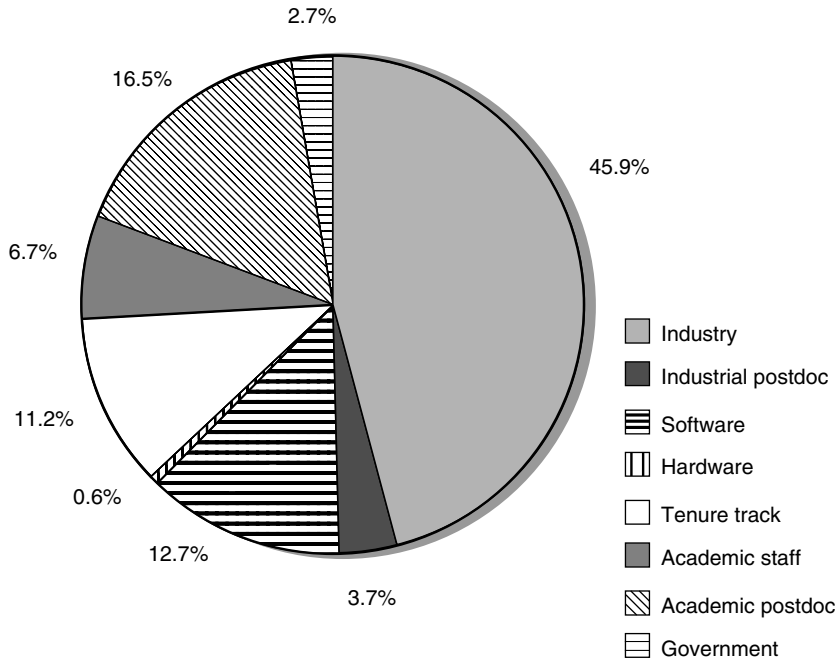


**Figure 5** Pie chart showing the accumulated total distribution of positions advertised in C&EN during the period 1983–2001 for scientists with computational chemistry expertise.

industry suddenly had to shrink because of economic or political adversity, it would affect not only computational chemists, but chemists in general and many kinds of biologists. What happens in this industry would also impact the software vendors that develop and maintain programs for use in molecular design and data management, and it would even affect the universities producing new scientists and performing research. A healthy pharmaceutical industry means a robust job market for computational chemists.

The worldwide market for pharmaceuticals is highly competitive and fragmented. No pharmaceutical company serves more than about 11% of the total worldwide market for prescription drugs, and most serve a much smaller percentage. The expiration of patent coverage on a major product can be a major blow to a company's ability to invest in science. Historically, it has been an exceptionally strong and confident pharmaceutical company that could withstand a patent expiration of a blockbuster drug without resorting to a merger or acquisition. Generic drug manufacturers can rapidly take away the market for a molecule of a research-based company when its patent expires. But the generic manufacturers employ relatively few scientists and no computational chemists to our knowledge. Looking forward, in the next few years, generics could eat away about a quarter of the recent corporate sales of several large pharmaceutical companies, and a few such companies could lose as much as almost half their sales! Thus, scientists at these research-based companies are not necessarily secure in their jobs, although in the short run they are desperately needed to help keep the discovery pipeline from drying out and in the long run will be rewarded if their discovery efforts succeed.

Job insecurity also exists at small companies. At a small pharmaceutical or biotechnology company that is still working to develop its first product, having adequate cash on hand to meet periodic expenses (cash flow) can be a serious problem. The jobs of computational chemists at such company can be in jeopardy if available cash must be devoted to meet current expenses instead of being used for a long-term project such as drug discovery.

## SKILLS IN DEMAND

Further information can be uncovered by looking at the job descriptions in the C&EN advertisements for computational chemists. The chart in Figure 6 lists the types of expertise specified in the advertisements during 2001 and shows the number of advertisements requesting a given expertise. The data are for advertisements appearing in the last complete year for which there is data (2001). Some advertisements were terse, but most advertisements called for several types of expertise, and each of these has been counted for constructing Figure 6. Job advertisements are often created by human resource people who may not be scientifically trained and thus may not fully understand the subtleties of the wording given them by the scientific managers. Hence,

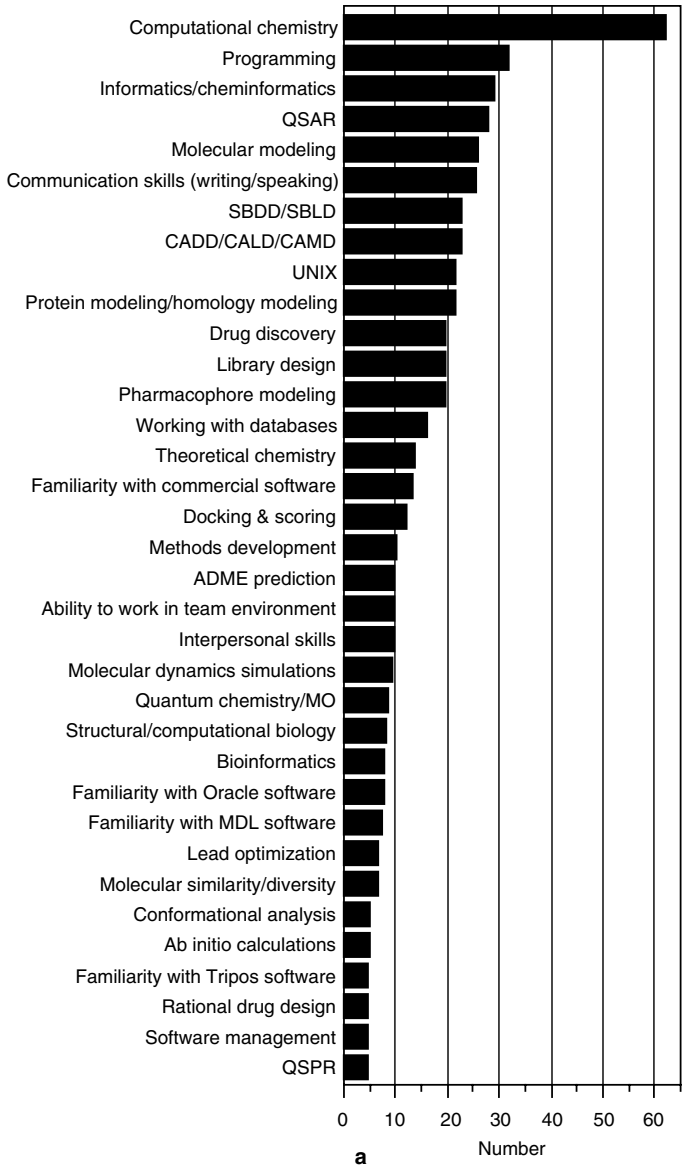


**Figure 6** Number of advertisements in C&EN in the year 2001 that specified the skills desired for job openings. The total number of advertisements was almost 160. (**a**) Frequently mentioned skills. (**b**) Less frequently requested skills. QSAR and QSPR are acronyms for quantitative structure–activity/property relationships. SBDD and SBLD refer to structure-based drug/ligand design. CADD, CALD, and CAMD refer to computer-aided (or -assisted) drug/ligand/molecular design. ADME stands for adsorption, distribution, metabolism, and excretion/elimination. Of MDL software, ISIS was

(*continued*)

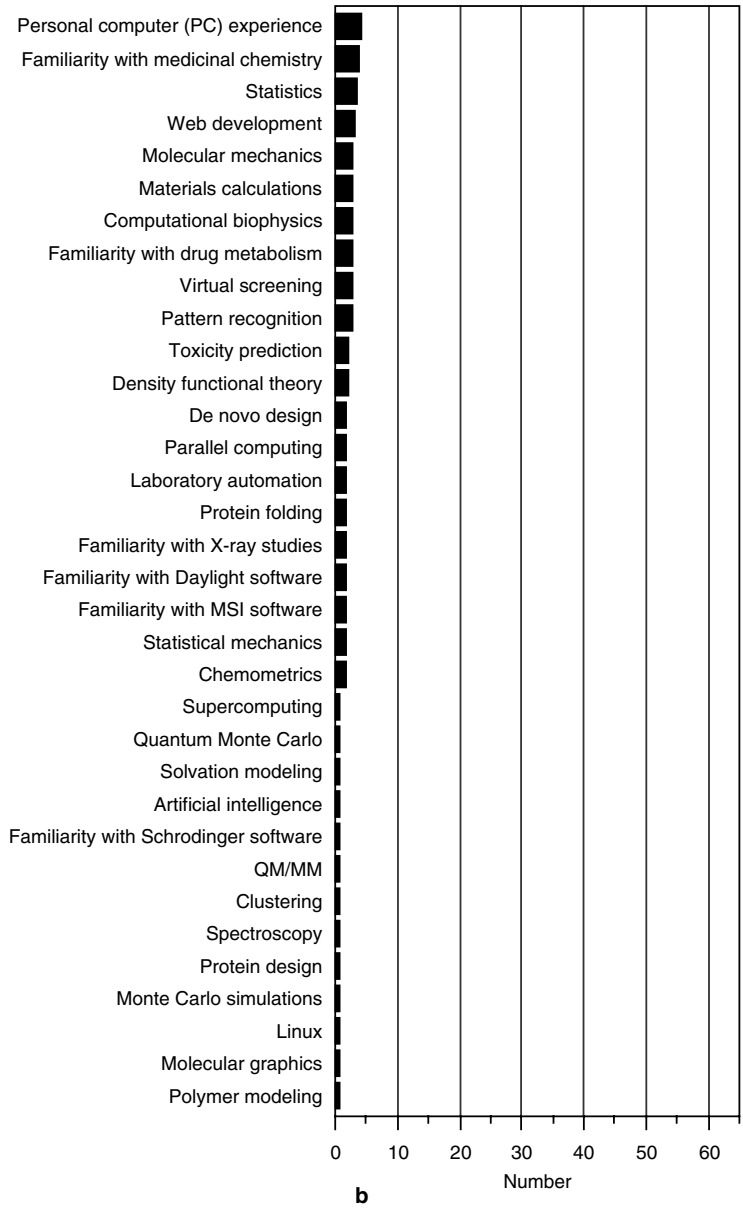


mentioned most frequently. Knowledge of UNIX is mentioned much more frequently than the operating systems of personal computers (PCs), principally Windows. MO refers to doing molecular orbital calculations. MSI abbreviates Molecular Simulations Inc., which was renamed Accelrys Inc. during 2001. QM/MM stands for quantum mechanics/molecular mechanics approaches, whereby the reaction center of a large molecular system is treated quantum mechanically, while the remainder of the molecular system is modeled by molecular mechanics.

different job advertisements use different terms for very similar kinds of expertise. To better represent the data, we have combined closely related terms as shown in Figure 6.

The most general term "computational chemistry" appears in the greatest number of advertisements. However, this term (or computational chemist) is not used in all advertisements. In fact, these terms appear in only about 40% of them.

The second most sought-after expertise is in programming. C++ was the most frequently mentioned programming language; C, FORTRAN, Perl, and Java were among others often mentioned. Knowing how to program not only guarantees intimate familiarity with computers, but also gives a computational chemist extra flexibility in how to attack research problems; preconceived algorithms can be customized and totally new algorithms can be created. Despite the demand for programming skills, many companies use commercially available computational chemistry/molecular modeling software. Company managers commonly reason that commercial software can be learned on the job if a person is not already experienced in its use.

The expertise ranked third in Figure 6 is a relatively new job description: informatics and cheminformatics (informatics as applied to chemical problems). The job description of a cheminformatician is still in a state of flux. Just like "computational chemist" and "molecular modeler" are used interchangeably by some employers, "cheminformatician" apparently is coming to be used synonymously with the other terms, or at least with an overlapping meaning. Advertisements for informatics scientists often specify skill in programming.

The fourth most sought-after expertise is in quantitative structure–activity relationships (QSAR). Once regarded by some scientists as somewhat passé, QSAR has become a hot area because its techniques are applicable to drug discovery, molecular design, and design of combinatorial libraries of compounds. Of all the methods of computational chemistry, QSAR is particularly adept at handling the large volume of data generated by modern drug discovery strategies.

Fifth in rank in Figure 6 is "molecular modeling". This is another general term with multiple meanings and can imply manipulating three-dimensional (3D) structures of molecules on a computer screen, molecular mechanics, and even QSAR and quantum chemistry, which are other ways to model chemical structures.

Ranking sixth is a general skill: the ability to communicate in speaking and writing. This skill is indispensable for most jobs, not just those in computational chemistry. Not too much further down the list in Figure 6 are "ability to work in a team environment" and "interpersonal skills". These general skills reflect how well a person can get along with co-workers and management. The ability to collaborate effectively with experimentalists is important for computational chemists because calculations without connection to

experimental data are difficult to justify. Collaborations between experimentalists and computational chemists can prove synergistic. At pharmaceutical companies, computational chemists must be able to interact with pharmacologists and other biologists, and especially with medicinal chemists. The latter interaction is indeed sensitive and crucial. Medicinal chemists and computational chemists share the objective of designing biologically effective compounds, but only medicinal chemists are equipped to synthesize a new design. In industry, computational chemists must get along with the synthetic chemists in order to have real impact. Management support of the computational chemists is also needed. Depending on management policy, the medicinal chemists and computational chemists could be forced into a situation where they are competing with each other for credit on a discovery of a worthwhile design.[13] Will certain members of a collaborative team have primacy in taking credit for new intellectual property generated? Will some members of the team be regarded as merely service providers? A team environment with shared credit for discoveries obviously facilitates collaboration, but good interpersonal skills are necessary regardless.

Ranked seventh and eighth are "structure-based drug (ligand) design" (SBDD/SBLD) and "computer-aided drug (ligand/molecular) design" (CADD/CALD/CAMD), respectively. The advertisements for a skill in SBDD/SBLD signify modeling of ligands when the 3D structure of a target receptor molecule is known. In Figure 6, we included only those SBDD/SBLD advertisements calling for chemists to do molecular modeling, not those advertisements for crystallographers to solve the structure of receptors. CADD/CALD/CAMD are terms that entail not only the molecular modeling aspect of SBDD, but also imply using techniques for the design of ligands even when the 3D structures of target receptors are unknown.

Not surprisingly, the highest ranking computer operating system mentioned in the advertisements is UNIX. This is the operating system currently used on most workstations. Next in the list of skills is protein homology modeling, which is relevant to drug discovery because if the 3D structure of a receptor molecule is not known experimentally, then the next best thing to do is to create a 3D structure by sequence alignment and molecular modeling techniques.

Continuing down the list of skills in the left-hand panel of Figure 6, we have "drug discovery", another general term indicating the overall goal of the employment opportunity. Library design refers to a rational approach to combinatorial chemistry (which involves combining a large number of reagents to produce an array of products). The modeling of pharmacophores (the minimum structural features required of a drug molecule for eliciting a biological response) and docking and scoring are both interwoven with CALD and SBLD. ADME refers to prediction of the adsorption, distribution, metabolism, and excretion/elimination behavior of compounds administered to a test animal and/or the human body. ADME modeling is a relatively recent area of focus;

pharmaceutical companies have learned that QSAR techniques can help in research areas besides the discovery of ligands. Medicinal chemists have tended to synthesize compounds based on (1) their area of synthetic expertise (and interest) and (2) maximizing potency against a therapeutic target. However, single-minded pursuit of these two factors too often can result in compounds that lack the other properties required of a good candidate pharmaceutical product. But such shortcomings may not become apparent until after much further — and expensive — research. On the other hand, if predictions can be made about the potential for a compound to have good ADME properties and to be clean toxicologically, then much time and money can be saved.

Slightly over fifteen C&EN job advertisements in 2001 requested what we label as "working knowledge of databases". This encompasses database creation, database management, and database mining. It is not surprising that the Oracle and Molecular Design Ltd. (MDL) database management systems are explicitly mentioned in some advertisements covered in Figure 6. Oracle software is for handling general data, whereas MDL software is specifically for handling molecular structures. Slightly under fifteen C&EN job advertisements asked for people familiar with "commercial software", meaning computational chemistry/molecular modeling programs, but without mentioning any specific program. Of C&EN job advertisements explicitly mentioning a program, the most frequently stated was the small-molecule molecular modeling package SYBYL and other software of Tripos Inc. SYBYL is also equipped for 3D-QSAR analyses, another widely used approach for relating bioactivity of a set of molecules to the properties those molecules exhibit in the space around them.[14]

Quantum chemistry, a traditional core area of computational chemistry, was requested in fewer than ten of the C&EN advertisements. Perhaps not surprisingly, most of the jobs requiring an interest in theoretical chemistry or quantum mechanics were in academia. Likewise molecular simulations, another favorite and important field in academia, is not a skill in exceptionally high demand in industry.

As seen in Figure 6, industry currently has the most need for experts in informatics, QSAR, and CALD. There is thus a disconnect between the types of expertise the universities are teaching and the types of expertise needed in commerce. It appears that some university administrators are continuing to think as they did in the 1960s and 1970s rather than keeping up with the evolving nature of computational chemistry. We will leave it to the reader to contemplate what obligations university administrators and faculty have when professors take new graduate students to work in an area of research of interest to the professor, but for which there are poor job prospects. Or is it totally the responsibility of the students to look after their own interests? In any case, it is valuable for the students to learn to gather information, to think, to ask

the right questions, to create, to solve problems, and to communicate, whether they stay in science or become stockbrokers.

Structural biology and computational biology are sometimes used as buzzwords for the specialties of X-ray crystallography and computational chemistry, respectively, when the subject of study are biomolecules. But the terms can also be used to mean molecular modeling. We counted only those job advertisements where it was clear that the main set of skills being sought were those of a computational chemist. Given the proclivity of people to invent new buzzwords, it is not inconceivable that a hybrid of "genomics" and a synonym for "computational chemist" will be appear in future job advertisements. Likewise, "computational proteomics" will probably gain currency. We list bioinformatics as a category in Figure 6; these come from advertisements that wanted a person with computational chemistry skills plus knowledge of bioinformatics. Since all the jobs corresponding to Figure 6 are for individuals with chemistry degrees, we did not count advertisements for bioinformatics specialists with only life science degrees, i.e., those with a molecular biology orientation.

We do not need to elaborate on every skill listed in Figure 6. The low ranking of some topics may result from human resource people or non-technically trained managers not understanding the relationships of the skills. For example, molecular mechanics is the basis of much of ligand and pharmacophore modeling, as well as conformational analysis, and often in the course of modeling, it is necessary to generate reliable new force field parameters. Yet molecular mechanics was not a skill often requested in the job advertisements.

Students training for a career in computational chemistry should realize that the skills being called for in one year may be different from those in use four or five years later. Practicing computational chemists come from many backgrounds, including experimental ones. Regardless of what students concentrate on in their advanced education, be it quantum mechanics, or molecular simulations, or something else, it would be severely limiting to address every research problem they encounter in their career by only one approach. A complete computational chemist should be versatile enough to be able to use a variety of methodologies. Then each research problem can be attacked with the most appropriate tools, and the range of problems that can be tackled will be much wider. As with other scientists, computational chemists must be willing to learn new things and work in new directions.

The walls between traditional disciplines are becoming more porous. Increasingly, chemists need to know biology, and biologists need to know chemistry. Likewise mathematics has long been of value to physical chemists. Now computer science is important to chemists and biologists. A solid grounding in chemistry, physics, biology, mathematics, statistics, and computer science can help prepare the computational chemist for tomorrow. The

ability to communicate in the language of collaborating experimentalists is also vital. For example, if a computational chemist will be working with medicinal chemists, then a good proficiency in the terminology of organic chemistry will prove to be a clear advantage. Likewise, a computational chemist may need to learn the language of biologists or materials scientists.

## THE BROADER CONTEXT

For the edification of our readers, we next briefly present some other data showing the broader scientific R&D environment in the United States. From an international perspective, the United States spends far more on R&D than do other countries.[15] In Figure 7, we plot the annual amount of money spent on R&D by a set of large and medium-sized chemical companies in the United States. Comparable data for the major pharmaceutical companies was shown in Figure 2. Combining the R&D investments at both chemical and pharmaceutical companies gives the top curve in Figure 7. As far as computational chemists are concerned, important conclusions can be drawn from the figure. First, there has been no growth in investing in R&D at the chemical companies. In fact, after correcting the data for inflation, chemical companies were spending less on R&D at the end of the 1990s than they were at the beginning. The total curve shows a steady increase only because pharmaceutical companies invest so much in R&D.

At the bottom of Figure 7 is another important curve worth noting. Government spending in chemistry research is small and not growing. This curve shows the total amount of taxpayer dollars that all the federal agencies are directing to support the discipline of chemistry. Again, after correcting for inflation, the amount the government is directing toward chemistry has declined over the last ten years. The main driver for increasing R&D investment in the United States has been private enterprise[16] seeking new molecules that will increase the health and longevity or improve the quality of life of people.

In Figure 8, we plot the total number of chemistry graduates in the United States. The three curves show the number of individuals earning degrees at the B.S., M.S., and Ph.D. levels.[17] The number of individuals obtaining their first chemistry degree has fluctuated widely with time, but the number of advanced degrees granted has shown remarkably little variation for the last 15 years. There was a slight increase in the number of Ph.D. degrees granted in the early 1990s, reaching a high-water mark in 1994. By comparing Figures 7 and 8, it can be seen that there is little relationship between the amount of R&D money available each year and the number of students being produced by educational institutions. Paradoxically, if there is any correlation at all, it is a rough inverse one, with Ph.D. production decreasing when R&D funding is increasing. Remembering the supply/demand equation, we note that the recent decline

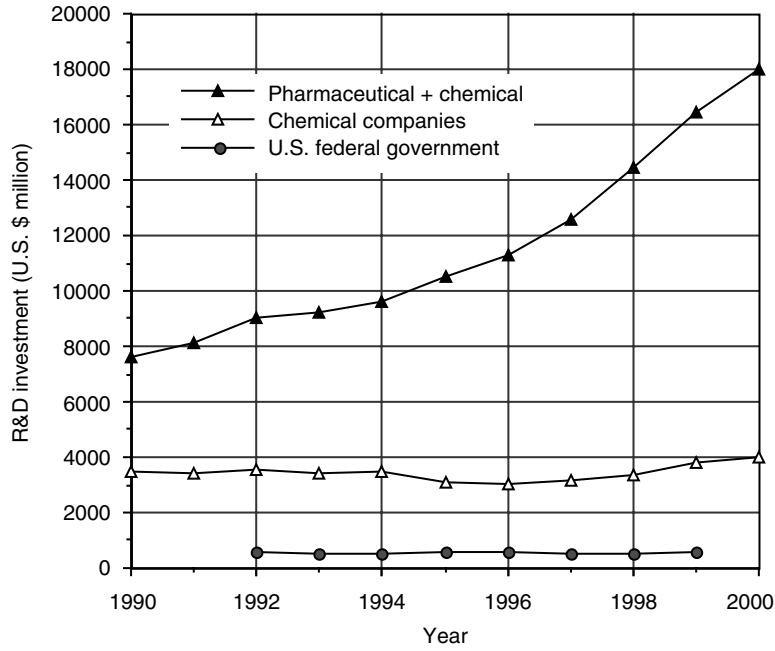


**Figure 7** (Upper curve) Sum of research and development spending at selected pharmaceutical and chemical companies in the United States. The pharmaceutical companies included are Pfizer, Merck, Eli Lilly, Bristol-Myers Squibb, American Home Products, and Schering-Plough. (Middle curve) R&D spending at 17 chemical companies: DuPont, Dow Chemical, Rohm and Haas, Union Carbide (acquired by Dow in 2001), Eastman Chemical, Air Products & Chemicals, International Flavors, Lubrizol, Crompton, Hercules, Solutia, Praxair, W. R. Grace, Ethyl, Cytec Industries, Albemarle, and Cambrex. These companies are listed here in descending order of the total amount they spent on R&D. On average, the chemical companies invest only about 4% of sales in R&D. (Lower curve) Amount of taxpayer dollars allocated by the federal government to chemistry. The federal agencies include the National Science Foundation, National Institutes of Health, Department of Energy, Department of Defense, Department of Agriculture, and others which allocate smaller amounts to chemistry. The government allocations in 1990 and 1991, which are not shown, are not comparable to the plotted data because the government guidelines changed. The federal data for 2000 had not yet been reported when this figure was prepared. Data from Ref. 8.

in Ph.D. production in the face of rising R&D investments bodes well for those individuals presently seeking jobs as well as for pay increases as companies compete for available scientific talent.

In Figure 9, the number of patents awarded in the United States are plotted by year.[18] Two of the curves show the number of patents in chemistry and the other two trace the number of patents in biotechnology. Of each pair of curves, one corresponds to the total number of patents granted, and the other gives the number granted to United States companies. Hence the "total"

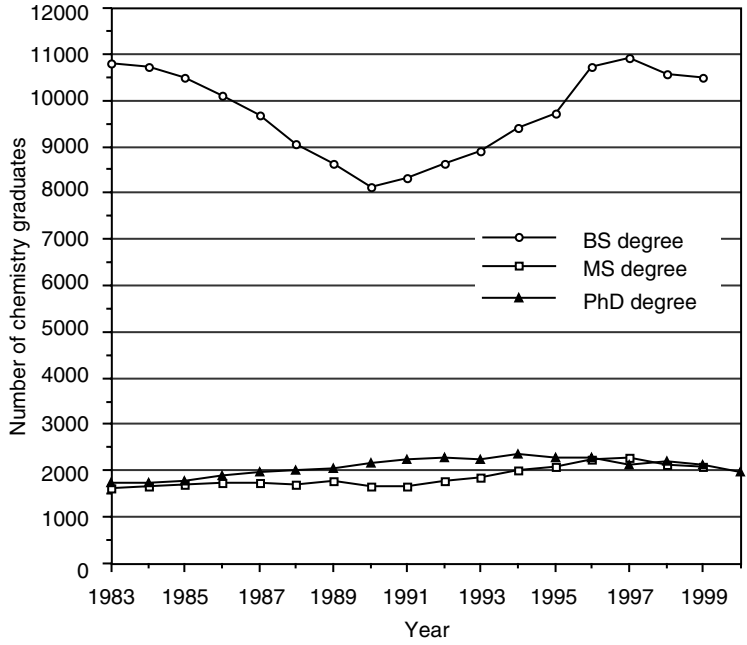


**Figure 8** Annual number of chemistry degrees granted. Data from Ref. 11.

curves has folded in the number of patents granted to educational institutions, nonprofit organizations, individuals, and foreign entities. By comparing Figures 7 and 9, it can be seen that an increase in the amount of R&D spending each year has not led to a proportionate increase in the number of innovations recorded as patentable discoveries. Thus, each patentable invention is costing much more now than ten years ago. One might expect a lag between when R&D money is invested (or when new graduates are hired) and when patentable discoveries are made. Instead, the correlation appears to be weak, except perhaps for the dip in the number of patents in 1995, which one could speculate as arising from the slowing of R&D investments in 1993–1994 or perhaps from scientists in general being distracted by concerns over the security of their jobs. However, the last year for which we have data, 2000, was a great one as far as R&D spending and job stability were concerned, but difficult in terms of generating patentable discoveries. Certainly, pressure to maximize productivity will increase on scientists in the years ahead, even though the pressure is already at an extremely high level.

We do not have data on the number of patents that include the names of computational chemists as discoverers or co-discoverers. Until about ten years ago, a widespread practice at the pharmaceutical companies was to routinely exclude computational chemists from patents. This exclusion stemmed in part from the hegemony of the organic chemists and partly from the legal reasoning

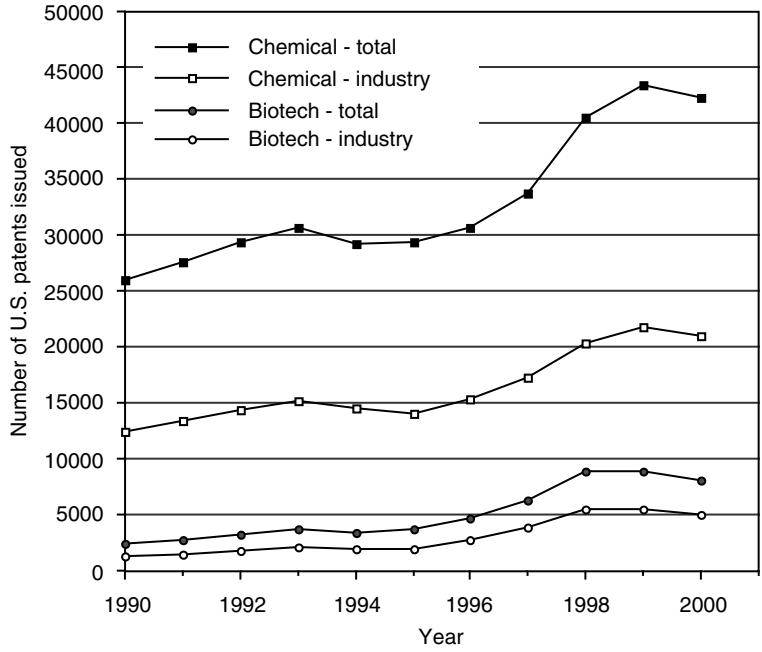


**Figure 9** Annual number of patents in chemistry and biotechnology issued by the United States Patent & Trademark Office. The curves with open symbols correspond to patents owned by companies in the United States. The curves with solid symbols correspond to the total number of patents including those owned by these companies, nonprofit organizations, the government, and individuals in the United States plus patents owned by foreign entities. Data from Ref. 11.

that although computational chemists may have conceived a novel molecular design, but they did not reduce the idea to practice. The synthetic (medicinal) chemists reduced the ideas to practice, so they were often recognized as the sole inventors on any resulting patents. Fortunately, this practice of excluding computational chemists started to die away about ten years ago, and more and more computational chemists are being recognized for their contributions.

In the 1980s, the United States Patent & Trademark Office started treating software for computational chemistry as patentable inventions. One of the earliest such patents, or at least the earliest that generated some debate, described an algorithm for conformational analysis.[19] Prior to this patent, there were three main types of software: (1) freely distributed, (2) commercially available, and (3) closely held (by the developers). If this third type were in industry, it would be called treating the technology as a trade secret. In academia, there have been a number of cases of a quantum chemistry program used in only the laboratory where it was written because the developers wanted to maintain a competitive advantage. Prior to 1989, the concept of obtaining patents in the realm of scientific software was relatively foreign to

most researchers in computational chemistry. Many scientists did not welcome the possibility that patents might interfere with the free flow of scientific progress and exchange of technology. However, software patents are becoming more common.

How large is the job market for chemists in the United States? The National Science Foundation (NSF) has compiled data on the number of chemists employed in the chemical industry in general and the number employed in the pharmaceutical industry specifically. The former number has ranged from 80,000 to 90,000, and the latter from 35,000 to 50,000. However, these data are difficult to analyze because the definitions and standards used by the government have changed over the years.

In the United States, annual reports of corporations commonly give the number of employees. But these simple employment numbers can be misleading because so many companies nowadays use contract workers. The actual number of workers coming to work everyday at a company site may be much higher than reported. The practice of outsourcing is done to reduce overhead expenses because the contract workers usually are paid less and receive fewer benefits than regular employees at those companies. When the trend of using contract workers began in the early 1990s, it was mainly for low-skill jobs, but as the trend accelerated even scientific positions were filled with people hired through contract companies. What seems particularly ugsome are the cases where full-time, long-term contract workers are used to work at the same site and perform comparable tasks as the full-time regular workers, but receive different pay and benefits. Conversely, if a computational chemist chooses part-time work, temporary work, or the freedom to work at home, then a differential in pay and benefits for the contract researchers makes sense.

## SALARIES

Limited data are available on the salaries that computational chemists earn. The ACS conducts an annual survey of a sampling of their membership.[20] The ACS is the world's largest scientific society with more than 163,000 members. Of these, almost 10,000 domestic members respond to the survey; a different random sample is used each year. The ACS reports the data in terms of type of employer, work function, discipline (the major traditional ones, but not computational chemistry), degree level, years of experience, age, and the other orthodox ways of looking at certain groups identified by gender, race, and ethnicity.

Plotted in Figure 10 are starting salaries as reported in the ACS survey.[21] The salaries of Ph.D.-level chemists increased gradually until 1993, then paused, suffered a fairly large dip in 1996, before finally taking off again in

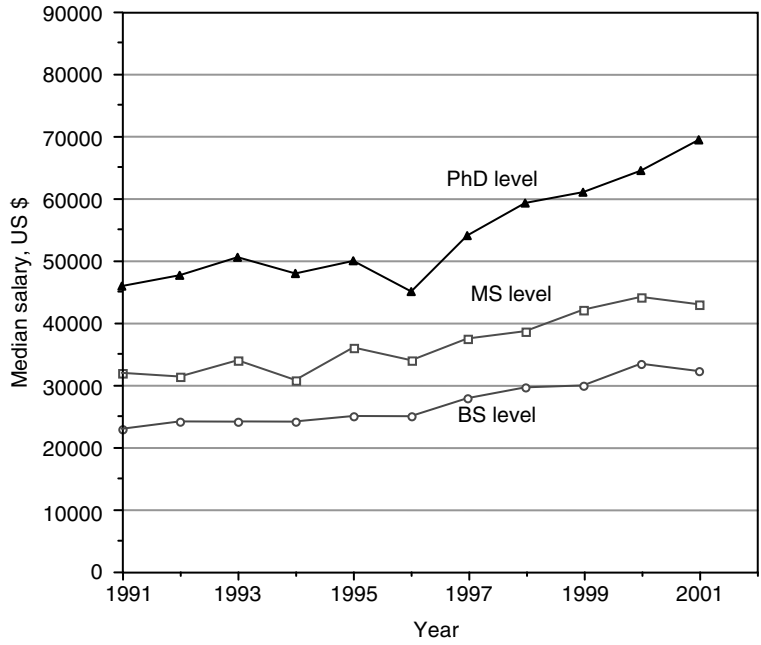


**Figure 10** Median starting salary paid chemists belonging to the American Chemical Society. The salaries are grouped by highest degree held. The ACS survey covered a sampling of all types of employers (academic, industry, and government) and all disciplines of chemistry. The ACS reports medians, rather than averages, in order to suppress the distortion that could result from excessively small or overly large salaries that some respondents might claim. Data from Ref. 21.

the late 1990s. In the last few years, competition among the pharmaceutical companies for the best talent was so fierce that some chemists were being offered signing bonuses, albeit not as large as those awarded sports stars. Similarly, competition between the elite and would-be elite universities for the best academic talent shows up as start-up grants and other perquisites. For chemists whose highest degree was at the B.S. and M.S. degree, there was a decline in starting salaries in the most recent year (2001) for which there is data.

Figure 11 shows the trend in median salaries spanning across the population of chemists in the survey regardless of years of experience, discipline, and type of employers.[20] Growth in salaries at the bachelor's, master's, and doctorate levels has been fairly steady, except for a mild moderation of salary increases in the mid-1990s. The salaries of BS-level chemists paused and actually declined slightly in 1996. Overall, salaries have been increasing faster than the cost of living in the United States, so the relative economic status of chemists is improving.

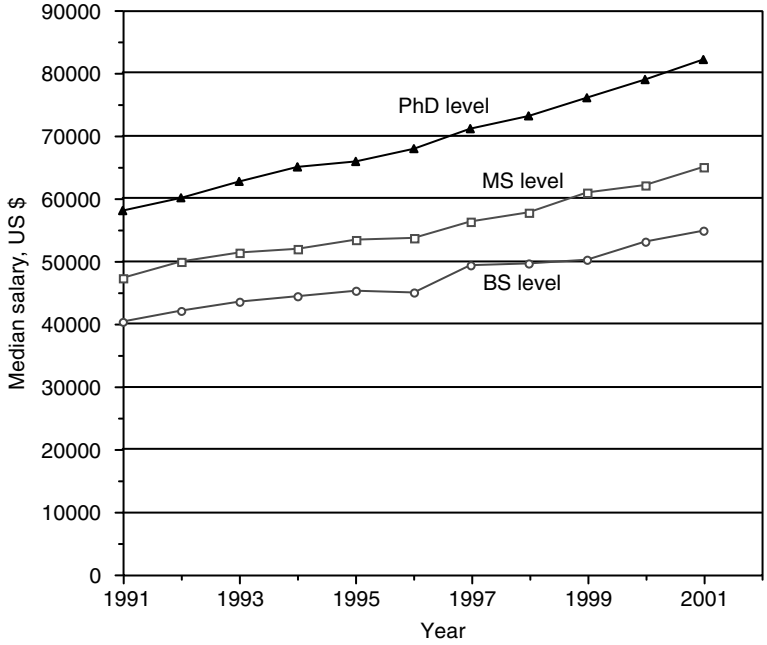


**Figure 11** Median salary received by chemists who belong to the American Chemical Society. The ACS survey covered a sampling of all types of employers (academic, industry, and government) and all disciplines of chemistry. Data from Ref. 20.

The only ACS salary data that deals directly with computational chemists is a category the ACS describes as chemists in industry with a work function of "computers"; the typical Ph.D. in this category earned $84,000 in 2001.[20] Of the various industrial functions, only chemists in analytical services were paid less than computational chemists; Ph.D. analytical chemists received $83,000 in 2001. For all Ph.D. industrial chemists performing basic research, the median salary in 2001 was $89,500. Ph.D. chemists performing a management function in industry were paid more, of course, $110,000 in 2001. Comparing these numbers, the pay for computational chemists appears to be slightly lower than their colleagues in other disciplines. We can only speculate whether this disparity in pay comes from the old hierarchical structure of companies, whereby some disciplines are better represented in management than are other disciplines, or whether the disparity is just a question of supply and demand. The ACS survey did not generate a sufficient number of responses from B.S.- and M.S.-level industrial chemists working with "computers" to compute a statistically meaningful number for them.

The ACS survey also showed that in 2001 the typical Ph.D. chemist (across all disciplines) earned $90,200 in industry, $84,800 in government, and $63,000 in academia. Full professors of chemistry earned a very

respectable $115,000 (for 12 months) at Ph.D.-granting universities in 2001. It would thus be incorrect to think that all academic salaries are lower than those in industry. The elite professors are reaping the rewards of capitalism whereby people are paid based on supply and demand, rather than on need.

Beyond the United States, salaries for computational chemists are generally lower. In countries with markets that are more controlled and less entrepreneurial, workers pay for greater job security with lower income. In the United States, individuals are compensated more because they take greater risk and personal responsibility for their own needs.

## CONCLUSIONS

The pioneering scientists of the 1960s and 1970s created the discipline of computational chemistry and opened up new career paths for thousands of younger scientists. Computational chemists play an important role in advancing scientific discoveries in collaboration with experimentalists. Computational chemists have enjoyed seeing their techniques used to help solve research problems in analytical, biological, environmental, geological, inorganic, materials, medicinal, organic, physical, and polymer chemistry, as well as in branches of biology, biophysics, and physics. Although there are new vistas in many research directions, most of the jobs for computational chemists have been and are still in the area of drug discovery. If society continues to value innovative medicines, free enterprise and free people will seek to discover new and better products, and scientists with computational chemistry expertise will find a place on the research teams of these companies.

Finally, it should be emphasized that not everyone entering the computational chemistry job market will immediately and easily find a secure, high-paying job. Every employer wants to assemble the strongest possible team of scientists (and other employees). Common sense tells us that any employer, whether in industry, academia, or government, will hire only the best candidates from any given pool of job applicants.

## ACKNOWLEDGMENTS

Valuable critiques on an earlier draft of this chapter were provided by Douglas M. Boyd, Robert B. Hermann, who started working as a computational chemist in the pharmaceutical industry in 1964, Max M. Marsh, who had the foresight and faith that computational chemistry would be important in pharmaceutical research, and James T. Metz, who supplied copies of hard-to-locate documents and shared a firsthand perspective of the job market.

## REFERENCES

1. D. B. Boyd and K. B. Lipkowitz, in *Reviews in Computational Chemistry*, K. B. Lipkowitz and D. B. Boyd, Eds., Wiley-VCH, New York, 1998, Vol. 12, pp. *v–xiii*. Preface.

2. See, for example, the websites of the Computational Chemistry List (http://www.ccl.net/chemistry/, e-mail chemistry@ccl.net) and of the QSAR and Modelling Society (http://www.ndsu.nodak.edu/qsar_soc/, e-mail qsar_society@accelrys.com). For other relevant URLs and a brief introductory guide to the use of the World Wide Web, see D. B. Boyd, in *Reviews in Computational Chemistry*, K. B. Lipkowitz and D. B. Boyd, Eds., Wiley-VCH, New York, 1997, Vol. 11, pp. 373–399. Appendix: Compendium of Software and Internet Tools for Computational Chemistry.
3. For those who might be tempted to try, it is not easy to tell from data mining of the chemical literature when theoretical chemistry started to be used for pharmaceutical discovery. This difficulty arises because the early research was sometimes delayed five or more years before it was published, and much work in industry simply goes unpublished because of lack of time to write papers. Because patent lawyers at companies must approve all disclosures and those attorneys (and corporate management) did not always understand the significance and potential utility, if any, of the early calculations, the lawyers tended to be overly cautious. For instance, work on antibacterial agents was performed many years before it was published: R. B. Hermann, *J. Antibiot.*, **26**, 223 (1973). Structure-Activity Correlations in the Cephalosporin C Series Using Extended Hückel Theory and CNDO/2. Some of the pitfalls encountered in data mining the literature were discussed by K. B. Lipkowitz and D. B. Boyd, in *Reviews in Computational Chemistry*, K. B. Lipkowitz and D. B. Boyd, Eds., Wiley-VCH, New York, 2001, Vol. 17, pp. 255–357. Appendix: Books Published on the Topics of Computational Chemistry.
4. Although the problems of working with medicinal chemists have been a standard topic of informal discussion among computational chemists for decades, the subject has been alluded to only infrequently in formal talks and in the literature. An extensive discussion of the problems is in a paper by J. P. Snyder, *Med. Res. Rev.*, **11**, 641 (1991). Computer-Assisted Drug Design. Part I. Conditions in the 1980s. Snyder, based on having seen the problems recurring at two different pharmaceutical companies, recommended more effective means of managing computational chemistry assets in industry. An intended Part II has not been published by Snyder, but his viewpoints and those of computational chemistry leaders at other companies are recorded in two documents. One is a summary of a managerial Workshop on Molecular Design Strategies in New Drug Discovery: The Computer-Aided Drug Discovery – Medicinal Chemistry Partnership, June 27–28, 1992, Mackinac Island, Michigan. The second document is the transcript of a panel discussion on the Medchem–CADD Partnership, J. P. Snyder, G. Maggiora, and P. Gund, Organizers, Symposium on Molecular Design Strategies in New Drug Discovery, Medicinal Chemistry Division, 204th National Meeting of the American Chemical Society, Washington, DC, August 26, 1992. See also: P. Gund, G. Maggiora, and J. P. Snyder, *Chem. Design Automation News*, **7** (11), 30 (1992). Approaches for Integrating CADD Strategies into Pharmaceutical R&D. S. Borman, *Chem. Eng. News*, Oct. 5, 1992, p. 59. Role of Computers in Drug Discovery Analyzed. Three other commentaries can be found: R. W. Counts, *Comput.-Aided Mol. Design*, **5**, 167 (1991). Do You Believe in Wavefunctions? R. W. Counts, *Comput.-Aided Mol. Design*, **5**, 381 (1991). Corporate Structure and Computational Chemistry. D. B. Boyd and K. B. Lipkowitz, in *Reviews in Computational Chemistry*, K. B. Lipkowitz and D. B. Boyd, Eds., VCH Publishers, New York, 1994, Vol. 5, pp. *v–ix*. Preface.
5. D. B. Boyd, in *Rational Molecular Design in Drug Research*, Proceedings of the Alfred Benzon Symposium No. 42 (Copenhagen, June 8–12, 1997), T. Liljefors, F. S. Jørgensen, and P. Krogsgaard-Larsen, Eds., Munksgaard, Copenhagen, 1998, pp. 15–23. Progress in Rational Design of Therapeutically Interesting Compounds. See also update by D. B. Boyd, *Modern Drug Discovery*, November/December, 1998, pp. 41–48. Rational Drug Design: Controlling the Size of the Haystack. In contrast, less than a decade earlier there were relatively few cases of computed-aided molecular design leading to a marketable product, and most of those successes were fruits of QSAR. See: D. B. Boyd, in *Reviews in Computational Chemistry*, K. B. Lipkowitz and D. B. Boyd, Eds., VCH Publishers, New York, 1990, Vol. 1, pp. 355–371. Successes of Computer-Assisted Molecular Design.
6. J. Bartlett, *Bartlett's Familiar Quotations*, 16th ed., J. Kaplan, Ed., Little, Brown, Boston, 1992, p. 575.

7. D. B. Boyd, *Quantum Chemistry Program Exchange (QCPE) Bulletin*, **5**, 85–91 (1985). Profile of Computer-Assisted Molecular Design in Industry.
8. *Chem. Eng. News*, October 29, 2001, pp. 29–58. Facts and Figures for Chemical R&D.
9. D. B. Boyd, in *Reviews in Computational Chemistry*, K. B. Lipkowitz and D. B. Boyd, Eds., VCH Publishers, New York, 1995, Vol. 6, pp. 317–354. Molecular Modeling Software in Use: Publication Trends.
10. D. C. Spellmeyer, personal communication (2002). A. J. Holder, *COMP Newsletter*, Fall 2001, S. Kenner, Ed., published with Abstracts of the Division of Computers in Chemistry, 222nd American Chemical Society National Meeting, Chicago, IL, Aug. 26–30, 2001. See also http://www.chemistry.org, http://membership.acs.org/COMP/, and American Chemical Society Annual Report 2001, Washington, DC.
11. *Chem. Eng. News*, November 12, 2001, pp. 38–63. Employment Outlook 2002.
12. According to American Chemical Society data published in Ref. 8, pharmaceutical companies in the United States employ about 27% of industrial chemists. The National Science Foundation estimates that roughly half the 82,700 R&D scientists and engineers employed in the so-called "chemical sector" of industry in January 2000 were employed by pharmaceutical companies.
13. Whereas scientific progress is certainly driven by altruism and a quest for the eureka moment, it is also driven by cupidity and self-interest.
14. T. I. Oprea and C. L. Waller, in *Reviews in Computational Chemistry*, K. B. Lipkowitz and D. B. Boyd, Eds., Wiley-VCH, New York, 1997, Vol. 11, pp. 127–182. Theoretical and Practical Aspects of Three-Dimensional Quantitative Structure-Activity Relationships. G. Greco, E. Novellino, and Y. C. Martin, in *Reviews in Computational Chemistry*, K. B. Lipkowitz and D. B. Boyd, Eds., Wiley-VCH, New York, 1997, Vol. 11, pp. 183–240. Approaches to Three-Dimensional Quantitative Structure-Activity Relationships.
15. Data from the National Science Foundation, as summarized in Ref. 8.
16. Basic economics: The law of supply and demand is fundamental to an understanding of economics (and human nature). The price of goods or services will increase in proportion to how much demand there is for those items. The price of goods or services will increase inversely proportional to the supply. Thus, in a free market, the price will fall when there is less demand or an oversupply. Unlike a physical law, the law of supply and demand is a rough generality; exceptions occur. The concepts of industry, academia, and government are easily misunderstood. A corporation is just a subset of the world's population working together toward a set of common goals for their mutual benefit. The value of their efforts is measured in large part by the excess of their income (sales) over the cost to produce their goods and services. Money is a measure of value and flows to those companies (or organizations or individuals) who are perceived by others as offering a desirable product or service. (See, e.g., J. P. Jones, *The Scientist*, February 4, 2002, p. 12. Letter to the Editor.). Nonprofit organizations differ from corporations in that the former are usually designed to spend all available funds, so that there is no profit to report. Most economic "organisms", be it a corporation, a nonprofit organization, or government, have a tendency to try to grow. Free competition, where it exists, weeds out those organizations that fail to deliver goods and services efficiently or that fail to offer goods and services that are wanted. Capitalism has proven effective at catalyzing progress because the system is congruent with the human spirit to make individual choices (freedom) and the desire to improve oneself (opportunity).
17. Data from the National Center for Education Statistics, National Science Foundation, and the American Chemical Society, as summarized in Ref. 11.
18. Data from the United States Patent & Trademark Office as summarized in Ref. 11.
19. M. Saunders, U.S. Patent 4,855,931, August 8, 1989. Stochastic Method for Finding Molecular Conformations.
20. *Chem. Eng. News*, August 20, 2001, pp. 51–58. Salary Survey.
21. *Chem. Eng. News*, March, 18, 2002, pp. 51–54. 2001 Starting Salary Survey.

*Reviews in Computational Chemistry, Volume 18*
Edited by Kenny B. Lipkowitz and Donald B. Boyd

ISBN: 0-471-21576-7

# Author Index

*Reviews in Computational Chemistry, Volume 18*
Edited by Kenny B. Lipkowitz and Donald B. Boyd

ISBN: 0-471-21576-7

# Subject Index

Computer programs are denoted in boldface; databases and journals are in italics.